International Journal of Photoenergy

Synthesis, Characterization and Applications of Nanocrystalline Materials in Dye-sensitized Solar Cell Systems

Lead Guest Editor: BR Ramesh Bapu
Guest Editors: T. M. Yunus Khan, V Kirubakaran, and Fayaz Hussain

Synthesis, Characterization and Applications of Nanocrystalline Materials in Dye-sensitized Solar Cell Systems

International Journal of Photoenergy

Synthesis, Characterization and Applications of Nanocrystalline Materials in Dye-sensitized Solar Cell Systems

Lead Guest Editor: BR Ramesh Bapu
Guest Editors: T. M. Yunus Khan, V Kirubakaran, and Fayaz Hussain

Chief Editor

Academic Editors

Contents

Contents

Hindawi
International Journal of Photoenergy
Volume 2023, Article ID 4717110, 17 pages
https://doi.org/10.1155/2023/4717110

Research Article

Application of Deep Learning to the Prediction of Solar Irradiance through Missing Data

R. Girimurugan,[1] P. Selvaraju,[2] Prabahar Jeevanandam,[3] M. Vadivukarassi,[4] S. Subhashini,[5] N. Selvam,[6] S. K. Hasane Ahammad,[7] S. Mayakannan,[8] and Selvakumar Kuppusamy Vaithilingam[9]

[1]*Department of Mechanical Engineering, Nandha College of Technology, Perundurai, Erode, Tamil Nadu, India*
[2]*Department of Mathematics, Rajalakshmi Institute of Technology, Chennai, Tamil Nadu, India*
[3]*Department of Mechanical Engineering, Park College of Engineering and Technology, Kaniyur, Coimbatore 641659, India*
[4]*Department of Computer Science Engineering, St. Martin's Engineering College, Secunderabad, Telangana, India*
[5]*Department of Computer Science and Engineering, B S Abdur Rahman Crescent Institute of Science and Technology, Vandalur, Chennai, Tamil Nadu, India*
[6]*Department of Electrical and Electronics Engineering, M.Kumarasamy College of Engineering, Karur, Tamil Nadu, India*
[7]*Department of Electronics and Communication Engineering, Koneru Lakshmaiah Education Foundation, Guntur, Andhra Pradesh, India*
[8]*Department of Mechanical Engineering, Vidyaa Vikas College of Engineering and Technology, Tiruchengode, Namakkal, Tamil Nadu, India*
[9]*School of Chemical and Bioengineering, Dire Dawa University Institute of Technology, Dire Dawa University, Dire Dawa, Ethiopia*

Correspondence should be addressed to Selvakumar Kuppusamy Vaithilingam; selvakumar.kuppusamy@ddu.edu.et

Received 13 October 2022; Revised 19 June 2023; Accepted 30 August 2023; Published 22 September 2023

Academic Editor: Qiliang Wang

The task of predicting solar irradiance is critical in the development of renewable energy sources. This research is aimed at predicting the photovoltaic plant's irradiance or power and serving as a standard for grid stability. In practical situations, missing data can drastically diminish prediction precision. Meanwhile, it is tough to pick an appropriate imputation approach before modeling because of not knowing the distribution of datasets. Furthermore, not all datasets benefit equally from using the same imputation technique. This research suggests utilizing a recurrent neural network (RNN) equipped with an adaptive neural imputation module (ANIM) to estimate direct solar irradiance when some data is missing. Without imputed information, the typical projects' imminent 4-hour irradiance depends on gaps in antique climatic and irradiation records. The projected model is evaluated on the widely available information by simulating missing data in each input series. The performance model is assessed alternative imputation techniques under a range of missing rates and input parameters. The outcomes prove that the suggested methods perform better than competing strategies when measured by various criteria. Moreover, combine the methodology with the attentive mechanism and invent that it excels in low-light conditions.

1. Introduction

Using solar photovoltaic (PV) electricity instead of fossil fuels is an excellent way to reduce civilization's impact on the environment. Solar photovoltaic (PV) power plants use PV modules and inverters to generate electricity from the sunshine. PV modules, also known as solar panels, are made up of photovoltaic cells that convert sunlight into electricity through the photovoltaic effect. These modules are typically made up of multiple cells that are connected together and mounted onto a support structure to form an array. By 2050, experts anticipate doubling the world's installed PV

capacity [1]. Due to the inherent unpredictability of PV systems, their rapid evolution makes it difficult for us to use them effectively. Predicting irradiance with great precision helps reduce the wasteful use of resources and unnecessary expenditures. Significant progress has been made since then in the field of solar irradiance prediction [2–4]. The output of PV plants can be predicted with high accuracy by focusing on two variables: global horizontal irradiance (GHI) and direct normal irradiance (DNI). Finally, GHI can be calculated using the natural, normal incidence, and solar angles [5].

The three main methods for predicting irradiance are those based on physical mechanisms, classical statistical models, and machine learning. One such physical model is numerical weather prediction (NWP) [6]. In NWP, researchers use complex differential equations to simulate the atmosphere behavior [7]. The findings of such approaches are valid on a regional scale but do not apply to local predictions. Time series data from sources like power plants and weather satellites are crunched by data-driven methods like statistical modeling and machine learning to identify features [8, 9].

One of the most popular statistical models is the autoregressive integrated moving average model (ARIMA), which uses data order determination and optimization techniques to learn the model's parameters. Approaches like this make good use of past data and are far simpler to train than conventional physical models [10]. Priority model templates, such as the linear assumption, introduce bias into learned models that cause them to distort reality. In recent years, there has been a significant uptick in using machine learning (ML) techniques and intense learning in the renewable energy sector. Recurrent neural networks (RNNs) have effectively tackled sequence prediction challenges. Neural networks can theoretically provide approximations for any nonlinear function. Thus, model bias is reduced, and fewer assumptions about the starting model are needed compared to the prior two approaches. However, long historical connections might arise from numerical issues like vanishing gradients [11]. Gate recurrent units (GRUs) and long-short-term memories (LSTMs) are frequently utilized in RNNs to get around this problem. Enhancing the outdated recurrent neural network with forgetting update and output gates makes it possible for the network to capture a wider variety of contexts more accurately. These strategies can reduce the effects of the vanishing gradient problem by extracting more meaningful information from the sequence [12].

All of the following techniques necessitate a substantial quantity of raw data. At PV stations, irradiance data and meteorological parameters can be gathered in two common approaches [13]. Some of the most common methods are ground-based weather stations, satellite-based remote sensing, sky imagers, pyranometers and pyrheliometers, and numerical weather prediction models.

The satellite can first offer approximations of surface irradiation. The data is more comprehensive but too dispersed to be helpful. Therefore, the actual irradiance at a given location can vary. The ground station radiometer can deliver the observed data under various conditions [14]. However, there are significant gaps due to communication and instrumentation breakdowns. Similar openings can be found in the weather records. Around 50% of solar energy is lost in actual circumstances [15].

Research into imputation models used during the preprocessing of data to fill in missing information has been extensively pursued to make algorithms more useful in practice [16]. Random sampling, Kalman filters, weighted moving average (MA), persistence, and interpolation are only some of the 36 imputation methods covered, along with their impacts at various temporal frequencies and their implications for midterm horizontal solar irradiance estimates. Recently, generative adversarial networks (GAN) have been used in unsupervised imputation algorithms for photovoltaic (PV) data [17]. These methods can generate the imputed sequence during the inference phase because they employ generative models to understand the possible distribution of the data.

However, some problems with GAV approaches are challenging to fix. However, PV data is notoriously unreliable and is intricately connected to the weather. Therefore, conventional statistical methods typically only address intermittent missing values and frequently disregard the actual distribution of the data [18]. Moreover, traditional imputation techniques often impute missing values using straightforward changes of the nearest neighbor or history sequence. They will struggle more when the target changes because of the difficulty in accurately representing nonlinear, multidimensional data. However, quick action is essential for short-term irradiance forecasts. Forecasting using an unsupervised technique involves an additional, time-consuming imputation step [19]. Many parameters require specific optimization because of the unpredictable nature of the training process of a generative model, which necessitates a great deal of time and human effort. Overfitting can occur if training data imputation is performed with too much precision, reducing the practical utility of the application.

To include more data and capture any oscillations in the initial difficulty stated above, more dimensional factors and nonlinear norms are frequently employed [20–22]. The second problem necessitates a plan that simplifies the network and the process. To tackle these issues, the researcher suggests an imputed GRU (IGRU), a bidirectional gate recurrent unit that employs an adaptive neural imputation module for DNI prediction. Preimputation network and GRU were combined into a single-stage network [23]. When there are gaps in data, the preimputation network uses positional prior and delay techniques to fill them in. Subsequently, the completed series is directly encoded instead of the raw data to generate summary characteristics. This process culminates in decoding the created features to recover the desired series. During the training procedure, prediction loss is used to fine-tune the GRU and imputation module weights jointly [24, 25]. As a result, the imputation values are based on operational procedures. This is the primary distinction from approaches that fill raw data's gaps before modeling. The researcher also added a novel attention module to IGRU called attention imputed gate recurrent units (AIGRU) to help with the high-frequency volatility of irradiance data. The model now pays more attention to higher-energy information than higher-frequency information.

The following are the most significant contributions of the research:

(i) To avoid time-consuming and inefficient imputation of raw data that may be missing, the researcher suggests a method for forecasting solar irradiance straight from the missing data, which performs well under a wide range of cutting rates. The benefits of preimputation include simplifying the two-stage process into a single step, lowering the model's complexity, and achieving accuracy on par with that of alternative approaches. The two-stage process is simplified into a single step, the model's complexity is lowered, and the resulting accuracy is on par with that of alternative approaches. Second, the network parameters are learned by evaluating the accuracy with which they anticipate future events. In this way, the bias and overfitting phenomena are mitigated by preventing the mistake of an outcome acquired by the imputation technique in preprocessing from being transferred to the learners. The network parameters are learned by evaluating the accuracy with which they anticipate future events, thereby preventing the mistake of an outcome acquired by the imputation technique in preprocessing from being transferred to the learners. Finally, not many hyperparameters are needed to be modified in this method compared to others. KNN's nearest neighbors, Kalman filtering's order, and so on have a significant role in determining performance. Third, more information is required for model-based imputation than for prediction. It is challenging to have amassed enough original data in some industrial contexts to provide high-precision imputation. That is why it is possible to get meaningful findings by imputing during predicting with fewer data than with model-based imputation methods based on a priori assumptions

(ii) Researchers present a neural imputation module that is adaptable and able to produce imputation data from prediction errors. Using this module, the researcher can skip the step of calculating imputation values before making a forecast

(iii) Researchers present a missing data prediction method based on attention, which is more effective under bright light. In irradiance prediction, it aims to address the issue of uneven sample sizes between high and low radiation levels without resampling. An ensemble setting can compensate for the other models

2. Related Works

2.1. Solar Irradiance Forecast/Regression with Missing Value. In the last few years, there has been a lot of focus on missing data radiation and prediction. Since irradiance imputation has many features with more common time series imputation problems, many tried-and-true traditional approaches can be applied with slight modification. While conventional methods relied on the moment and neighborhood information, they often avoided handling missing values. To fill in the gap, the author [26] employs two techniques. For missing time series data, the author [27] uses k-nearest neighbors (KNN). When it comes to characterizing multidimensional inputs; however, these methods fall short, as they do not consider the things like the correlation between irradiance and climatic data.

Several imputations by chained equivalences and regression-built imputation approach, such as multiple linear regression representations and converse distance weightage, are compared and contrasted in the article [28]. Matrix completion is used by the author of [29] to fill in data gaps before making solar radiation predictions for the near future. Several imputation approaches are investigated by the author [30], who concludes that KNN is the best option for day-ahead forecasting of photovoltaic generation. Several publications have appeared recently that attempt to summarize and compare the effectiveness of various imputation approaches. Numerous interpolations and prediction approaches are combined, and their effects are compared by authors [31, 32]. They put each method through its paces under varying time frames for predicting and conclude that Kalman filtering (KF) is the most effective for hourly data. Recent years have seen a rise in interest in using deep learning for imputation and prediction. Generative adversarial network (GAN) is the first unsupervised deep learning model to be employed as an imputation approach in solar irradiance prediction. As with conventional methods, these take two steps—first interpolating, then using the resulting data for prediction to arrive.

2.2. Time Series Imputation. Numerous disciplines, including medicine and traffic, face the age-old challenge of filling in gaps in temporal data. Mean imputation is one type of interpolation still extensively employed because of its simplicity and effectiveness. The primary source of negative consequences brought on by the absence of imputations is the split in the frequency domain [33]. In addition, model noise in the temporal field must be tolerated well. Variational autoencoders and generative adversarial networks are two unsupervised deep-learning methods that apply generative models to uncover the underlying pattern in sequence data. Together, they apply generative models to uncover the underlying pattern in sequence data. The difference between variational autoencoders and generative adversarial networks is that GAN does not aim to maximize the hidden representation in any particular way. Another RNN-based algorithm is the self-learning approach, such as Bayesian regression and inference for time series (BRITS), where the positional information of the missing data is used to dampen the hidden layer information [20].

3. Methodology

3.1. Problem Setting. For a given multivariant time series $X = (x_1, x_n, y_n)$, the research investigates the problem of irradiance Y prediction. Multihorizon forecasting refers to the prediction of multiple future steps in the time series, specifically predicting the next m steps based on the first k steps. The goal is to construct a direct method multihorizon forecasting

model that makes comprehensive, rather than incremental, predictions of all outputs [34, 35]. Researchers have one-time series represented by x_1 and the number of feature dimensions indicated by n. The researcher zeroed down on the challenge of predicting the next m steps based on t.

The first$k$steps, where the input includes previous values for the output, researchers attribute missing data to either a communication breakdown or a malfunctioning sensor. The researcher next proceeds to define several key terms. The letter M represents the positive data for missing values, where 0 indicates no data is missing and one suggests all information is present. Additionally, M states that the missing value's time step from the nearest valid observation is denoted by δt.

3.2. Traditional Imputation Methods. Here are some of the most typical approaches taken to fill in the gap during PV prediction and the methodologies utilized for comparison during the experiments.

3.2.1. Interpolation. Averages are often interpolated by using the k values closest to the gap, and standard deviations are also estimated in this module. This method of interpolation assumes that missing values are typically located near the mean distribution or median if they were lost due to random chance. The original allocation of the variables has been warped.

3.2.2. I Matrix Factorization. A matrix X with a missing value can be broken down into two or three smaller matrices using MF. The original matrix $X\hat{}$ can then be approximated by multiplying the decomposed matrices. To complete the unique matrix $X\hat{}$, the researcher employs the values found in this estimate composites, X. To maximize the loss function J in equation, the decomposition often uses an arithmetical class technique of gradient descent.

$$J = \left\|X - X\hat{}\right\|^2 = X - \mathrm{UV}^{\top 2} = \sum_{i,j,x_i \neq \mathrm{man}} \left(x_{ij} - \sum_{l=1}^{k} u_{il} v_{jl}\right)^2. \tag{1}$$

Regularization methods, as shown in equation (2), can improve estimation accuracy.

$$\begin{aligned} J &= \left\|X - X\hat{}\right\|^2 + \frac{\beta}{2}\left(\|U\|^2 + \|V\|^2\right) \\ &= \sum_{i,j,x_i \neq \neq \mathrm{an}} \left(x_{ij} - \sum_{l=1}^{k} u_{il} v_{jl}\right)^2 + \frac{\beta}{2}\left(\sum_{i,l} u_{il}^2 + \sum_{j,l} v_{jl}^2\right). \end{aligned} \tag{2}$$

3.2.3. K-Nearest Neighbors. The distance between the samples is considered by the nearest neighbor filling concept. When there is a gap in the data, it is filled in by averaging or weighting the nearby observations. KNN is preferable to mean imputation because it is less sensitive to outliers and works better with high-dimensional data. On the downside, it is computationally and spatially intensive and cannot account for sample imbalance. KNN may be computed using

$$\tilde{x}_m = \frac{\sum_i w_l c_l}{\sum_i w_i}, \tag{3}$$

where

$$w_i = \frac{1}{d_i}. \tag{4}$$

Here, $\tilde{x}_m$ indicates the missing data. i indicates the i^{th} of designated k nearest data. d indicates the distance between two specimens.

3.2.4. Multiple Imputation by Chained Equations (MICE). Assume there are n such variables as $(x_1, x_2, ..x_n)$. The variables x_2 through x_k will be used to perform a regression on the missing x_1. In this case, the regressed values are substituted for x_1 in the expression. If x_2 is missing data, the regression model will still use x_1, x_3, and up to x_n as inputs. Later, regression estimates will be substituted for the missing values.

3.2.5. Kalman Filtering. The state space model upon which the Kalman filter is based consists of two equations [36].

$$\begin{aligned} y_t &= H_t \alpha_t + \omega_t, \\ \alpha_{t+1} &= F_t \alpha_t + \varepsilon_t, \end{aligned} \tag{5}$$

where α is for the hidden condition, y stands for the observing data, H stands for the measuring matrix, F stands for the transitional matrix, and ω and ε stand for the noise. Standard practice for interpolation involves two stages. In the first stage, the states and covariances in equation (5) are erudite depending on the observable data. In the second stage, the researcher uses the past data to make an educated guess or smooth the future goal. For this purpose, the researcher employs Kalman filtering's smoothing technique.

3.3. IGRU and AIGRU. Two different approaches are presented here. For starters, the researcher presents the neural imputation module, any predictive model with imputation capabilities. Then, a neural imputation module for GRU and the rationale for employing a bidirectional structure are shown. The paper concludes by introducing an attention-based GRU with a neural imputation module.

3.3.1. Module for Neural Imputation. To better handle missing data, researchers in the current paper develop an adaptive imputation unit in a neural network. When dealing with missing data, researchers presume that the location of the missing data is either known empirically or using techniques like irregularity finding or that the position range is nil. In post-apocalyptic scenarios, for instance, the radiometer readings may show up as long stretches of zeros between sunrise and sunset. For example, suppose raw data are fed into a neural network without preprocessing. In that case,

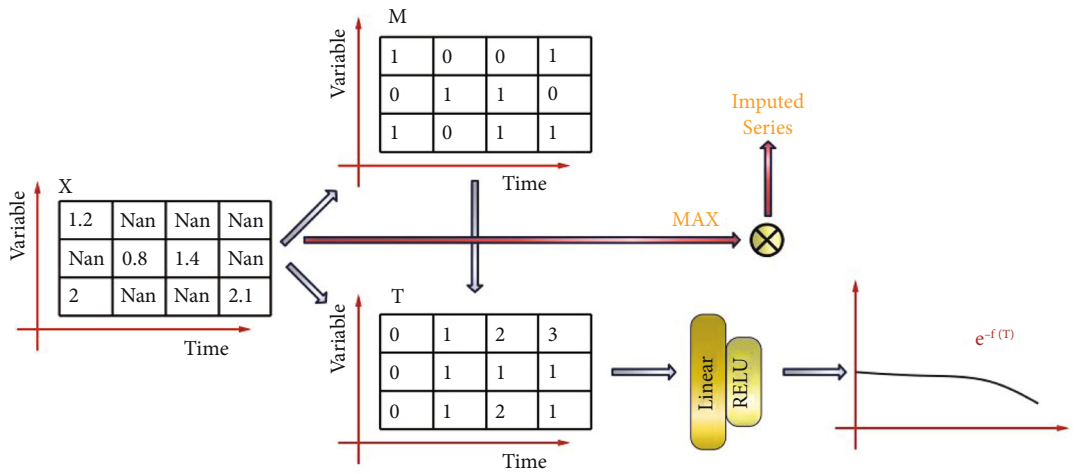

Figure 1: The imputation flow.

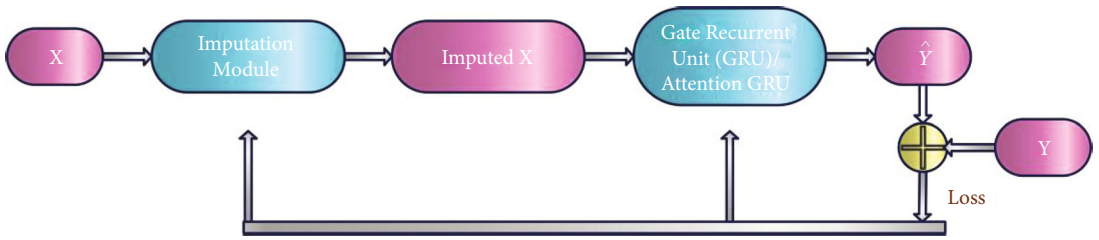

Figure 2: The path of loss.

the model may incorrectly infer features based on a high proportion of missing values in the input and the supervised data.

The law of large numbers states that gaps in data are typically filled in by values close to the most recent measurements. The missing step δ in equation (6) defines the decay coefficient as γ.

$$\gamma_t = \mathbf{exp}\left\{-\mathrm{m}\left(\mathbf{0}, \mathbf{W}_\gamma \boldsymbol{\delta}_t + \mathbf{b}_\gamma\right)\right\}, \tag{6}$$

where the linear coefficient and bias for the missing stage δ are denoted by $\mathbf{W}_\gamma$ and $\mathbf{b}_\gamma$. In the first place, the step size is linearly transformed. Afterward, the activation function places constraints on the altered result, checking that γ is not equivalent to one and is not equal to nil. The process on the right-hand side of this equation does not have to be exponential; rather, it can be any member of a class of monotonically decreasing functions. If the decline is monotonic, then the more significant the δ missing values relative to the last observation, the lesser the γ, and the higher the decay.

$$\mathbf{x}_t = \mathrm{m}_t \odot \mathbf{x}_t + (1 - \mathrm{m}_t) \odot (\gamma_t \bar{x}_t). \tag{7}$$

The estimated, $\mathbf{x}_t$ incorporates both the actual value and the imputed values after missing information has been "filled in." The researcher may generate a new estimate if the researcher knows the time step of the preceding observation and the largest possible range within the observation window. The nearest observation is insufficient since it is not easy to guarantee that the missing value is less than the most relative value. That is why it makes sense to use historical data, like the highest value during the preceding days, by considering the maximum observation inside the period. Looking at Figure 1 shows a simplified version of the imputation procedure.

The revised estimates are fed into the model. All the network weightage, such as the linear factors in the decay coefficients and the missing step coefficients, is learned by backpropagation during the training process. A reliable estimate for the missing data will result from this. The overall algorithm flow and the loss propagation track are displayed in Figure 2.

3.3.2. IGRU. An in-depth description of GRU is provided here. GRU is a type of recurrent neural network, a kind of neural network structure typically employed in sequence modeling. To solve sequence problems, RNNs rely on a crucial component: memory state neurons. These neurons' job is to memorize past events, and the researcher may express them as generalities using equation (8).

$$b_t = f(b_{t-1}, y_t, x_t), \tag{8}$$

where b is the hidden-layer neuron's value and f is the update function that must be memorized.

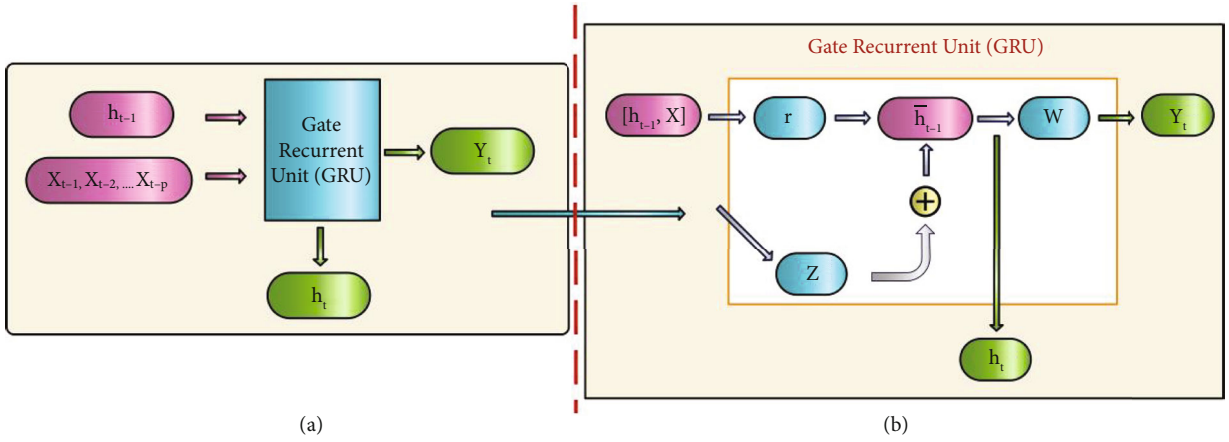

Figure 3: GRU's structural arrangement. (a) The GRU's input and output and (b) the GRU cell's internal structure.

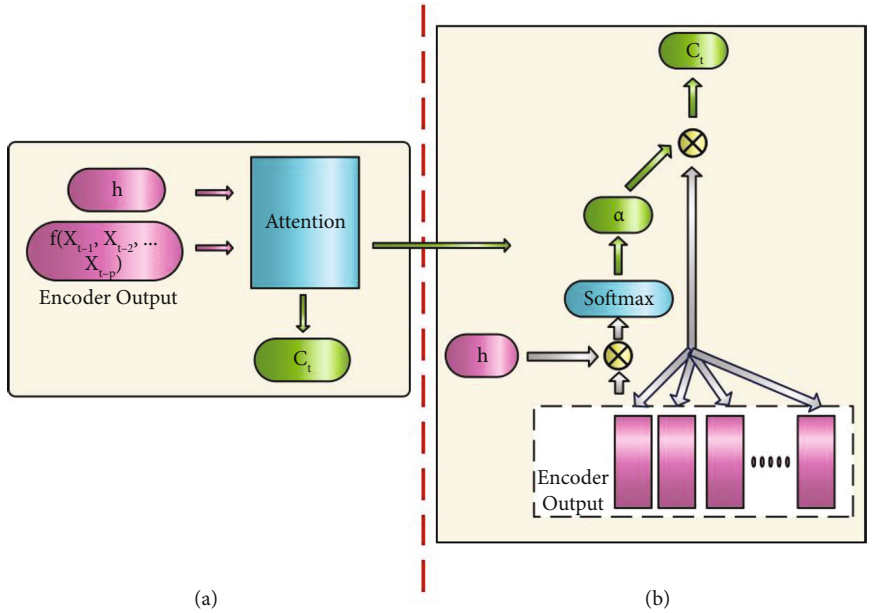

Figure 4: Mechanism for attention. (a) Input(I\P) and output(O/P) of the attention unit and (b) internal structure of the attention unit.

Both an update gate and a reset gate are labeled f in the GRU model. Equated to LSTM, the memory is guaranteed, and gradient disappearance is reduced with fewer parameters and faster training.

$$r_t = \sigma(W_r \cdot [b_{t-1}, x_t]), \tag{9}$$

$$z_t = \sigma(W_z \cdot [b_{t-1}, x_t]), \tag{10}$$

$$\tilde{b}_t = \tanh\,(W_b \cdot [r_t * b_{t-1}, x_t]), \tag{11}$$

$$b_t = (1 - z_t) * b_{t-1} + z_t * \tilde{b}_t, \tag{12}$$

$$y_t = \sigma(W_o \cdot b_t), \tag{13}$$

where r and z stand for the reset and update gates, respectively, and the current hidden layer's information and observations are used by the rearranged gate function to determine the next in-between hidden layer. The update gate determines how much the current weighted average of hidden layer data deviates from the previous value. The input-output relationship and GRU cell architecture are diagrammed in Figure 3.

Table 1: Processing factors.

Factors	Unit
Humidity	%
Temperature	˚C
Wind speed	m/s
Cloud cover	%
DNI	W/m^2

This paper makes use of the bidirectional structure. The two-way recurrent network uses both past information and predictions for the future. Neighboring neurons whose time windows extend beyond the current time step represent

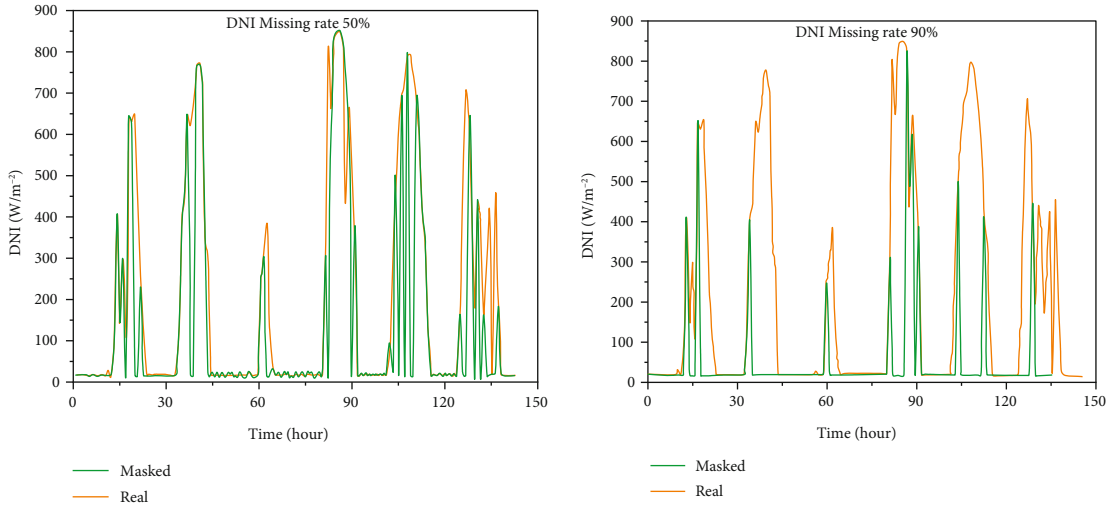

Figure 5: Incomplete data with different missing rate.

information about what will happen in the future without any data loss. Compared to regular GRU, bidirectional GRU is preferable since the factors are instantaneously defined by material from both instructions, making it worthwhile even if the assertion is primarily decided by ancient data (maximum and missing steps).

3.3.3. AIGRU. In this paper, the researcher provides the GRU model based on attention. Natural language processing (NLP) was the first area to make use of the attention mechanism [37, 38]. Its primary purpose is to quantify the degree of association between a source word and the rest of the sentence. Like in equation (9), the final hidden layer is often used as the output source. A linear combination that can be taught is allocated to the hidden layer, even if the network can remember substantial time steps from the past. In equation (14), the researcher finds the updated weights for the hidden layer [39].

$$\alpha_i = p(z = i|X, q) = \text{softmax}(s(x_i, q)) = \frac{\exp\left(s(x_i, q)\right)}{\sum_{j=1}^{N} \exp\left(s\left(x_j, q\right)\right)}. \tag{14}$$

In the interpreter, where the confidential data from the highest-order GRU layer is accessed, q is the number of queries. The weights are normalized from zero to one through the SoftMax function. The internal construction of attention and the link between its inputs and outputs are depicted in Figure 4.

3.4. Performance Evaluation Metrics. Even though RMSE is the utmost popular statistic, it is still insufficient. The following case study uses three evaluation measures, each briefly described below. The number of test samples, m, observation is denoted by y_i, whereas the prediction results are indicated by $\hat{y}_i$.

3.4.1. RMSE. The RMSE formula, equation (15), employs the square of the variation among the predicted and actual values.

$$\text{Root Mean Square Error (RMSE)} = \sqrt{\frac{1}{m}\sum_{i=1}^{m} (y_i - \hat{y}_i)^2}. \tag{15}$$

3.4.2. Mean Absolute Error (MAE). Distinct RMSE, MAE uses absolute error in equation (16). It more accurately depicts the condition of the error in the projected values than RMSE does and is not as susceptible to extreme levels. However, specific gradient optimizers find it inconvenient to utilize because the calculation cannot be distinguished.

$$\text{MAE} = \frac{1}{m}\sum_{i=1}^{m} |(y_i - \hat{y}_i)|. \tag{16}$$

3.4.3. Squared Differences between the True Value and the Mean Value. The numerator in equation (17) is the total of the squares of the discrepancies between the actual and estimated values. In this case, the summation of the squared discrepancies between the actual and the average value is represented in the denominator.

$$R^2 = 1 - \frac{\sum_i (\hat{y}_i - y_i)^2}{\sum_i (\bar{y}_i - y_i)^2}. \tag{17}$$

The reliability of a regression model may often be assessed using the R^2. The improved model estimate is associated with a higher value of R^2.

4. Results and Discussion

4.1. Data. The coordinates 39.8320 (N), 106.210 (W), and 1832.9 (meters) are the center and the edge of the target

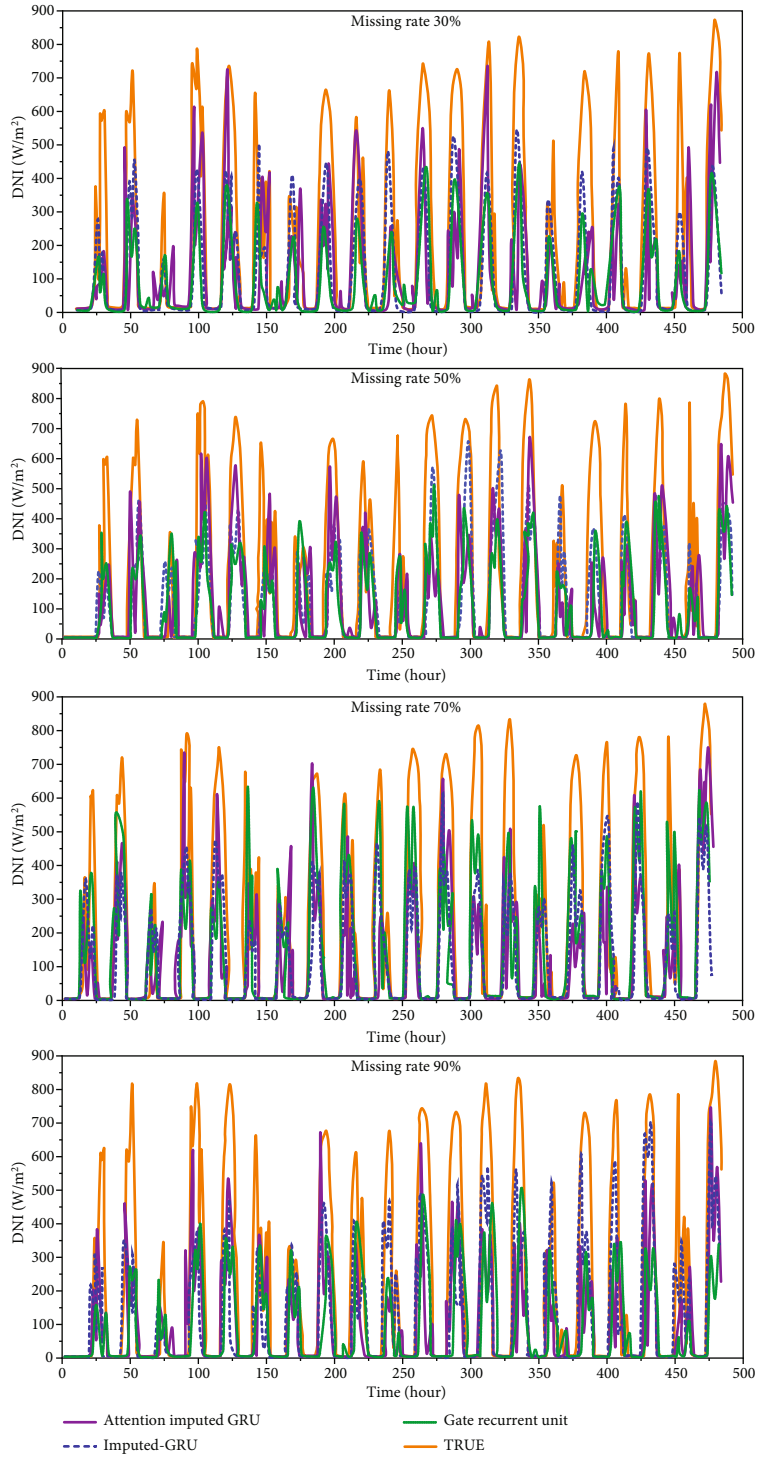

Figure 6: An outcome of AIGRU (purple), IGRU (blue), GRU (green), and observed DNI (orange).

Table 2: Error valuation.

Missing data	AIGRU	GRU	IGRU
0.30	−456.6563	−469.6538	**−407.2598**
0.50	**−391.1825**	−431.3310	−404.1761
0.70	−409.6805	−379.0675	**−329.7932**
0.90	−423.5651	−434.6867	**−348.8767**

region, respectively. The case study makes use of five sets of meteorological data, all of which are listed in Table 1.

Researchers generate the missing data at random to make the model more accurate. Here, the researcher provides a concise introduction of "missing" and its impetus. Radiometers and anemometers are just two examples of meteorological sensors used in PV facilities to measure irradiance and other weather conditions. The two most frequent

Table 3: The results of AIGRU, IGRU, and GRU.

Evaluation technique	Mean absolute error			Masked root mean squared error			Regression			Root mean square error		
	GRU	IGRU	AIGRU	GRU	IGRU	AIGRU	GRU	IGRU	AIGRU	GRU	IGRU	AIGRU
0.30	158.60	132.15	**125.72**	257.24	220.53	**209.97**	0.25	0.45	**0.49**	254.97	**223.91**	227.63
0.50	139.88	**132.28**	138.81	230.31	**220.63**	231.03	0.40	**0.44**	0.39	235.32	**228.38**	236.40
0.70	128.22	**117.81**	124.70	211.09	**199.74**	208.02	0.49	**0.54**	0.51	212.40	**201.58**	228.89
0.90	140.45	**121.46**	126.27	234.33	**200.13**	213.66	0.37	**0.54**	0.48	241.16	**208.15**	231.03

maintenance voids are single-point voids and segmented voids. The most frequent cause of a single missing point is a malfunctioning instrument, while the most frequent reason for a segmented missing is a severed line of communication. Because of the warning systems and routine checks, these outages never last more than a day. In Figure 5, the researcher saw the synthetic DNI researcher generated, with the missing data at varying percentages. When the interest rate is high, the situation is reversed. When there is a lot of missing data, it is not easy to conclude anything, such as when irradiance levels are highest.

4.2. Experimental Setting. The variables used in the experiment are briefly explained below. The researcher begins with a summary of the network's settings. A GRU encoder and two linear layers make up each bidirectional GRU's three-layer structure. At present, each GRU encoder has two hidden layers. There are 32 neurons in each of the hidden layers. The linear layer performs the dimensional translation, ensuring that all networks produce the same results. An early-stopping approach is implemented alongside a prolonged learning rate of 0.001. Once the validation set loss is not minimized after 20 iterations of training, overfitting is prevented by stopping the activity. The current epoch is 100. There is a 90% training ratio, a 16% validation rate, and a 4% testing rate.

4.3. Case Study. During this section, the researcher reclaims the case study. Starting with the past four days of radiation ranges and weather information, our studies use numerous input solitary outputs to predict the next 4 hours of diffuse near-infrared illumination (DNI). Considering the current state of affairs, the lack of irradiance is set at 50%, while the percentage of other meteorological parameters that are absent varies from 30% to 90%. In contrast to imputation tasks, predictions made without sufficient background knowledge are meaningless. There is also little chance of a significant number of missing due to maintenance with the primary variable monitors. Increasing the training sample can overcome the problem of missing data, even if there is a lot of it in a short time.

4.3.1. Evaluation among AIGRU, GRU, and IGRU. The findings are primarily analyzed using the three most typical parameters: temperature, wind speed, and DNI. The outcomes for the 30, 50, 70, and 90% missing rates are depicted in Figure 6. The test sequence is 20 days long, and the vertical axis represents the DNI power (500 W/m^2). If looking for an approach that gets the researcher closer to the actual numbers, IGRU is the best result. In Table 2, the researcher saw the average inaccuracy of the methods when the actual DNI is more significant than 500 W/m^2. Improved results are seen across a range of missing rates when using the proposed strategy.

This suggests that IGRU can improve its predictions. There is no significant difference in performance between the three approaches when the missing data rate is 30%. When the light intensity is high, AIGRU performs well. The most important goal is that the consideration module directs the model's attention to the most important objectives when there is enough accurate data. IGRU outperforms MSE in three additional scenarios with varying missing rates. The three scenarios are (1) evaluating model performance, (2) image processing, and (3) signal processing.

The inaccuracy of three approaches across four evaluation measures is shown in Table 3. Systems that include a neural imputation module improve on average by 4-18% in RMSE compared to methods that do not, with IGRU outperforming the competition. At a 30% missing rate, AIGRU is superior to IGRU in all measures except RMSE. One possible explanation is that the model can better match high-energy data, such as high-irradiance data. However, as the gap grows, the imputation module's estimates become less reliable, and the data becomes more skewed. Despite this, it shows improvement over the original data without losing quality, reassuring the accuracy of the imputed values. Moreover, IGRU improves its performance as the missing rate increases, peaking at a missing rate of 90%. Weaker performance is seen from the initial strategy as the IGRU is raised higher.

The error distribution $(Y - Y^{\wedge})$ is displayed graphically through a histogram, which the researcher uses to compare the two methods. Error distributions for the suggested approaches of AIGRU and IGRU and the baseline GRU model are shown in Figure 7. When plotted, mistakes with the correct DNI are shown along the horizontal axis, while error frequency is shown along the vertical axis in the test dataset. It is generally accepted that both AIGRU and IGRU perform better than the approach without imputation due to their high frequency at zero. The proposed methods focus on the range from 200 W/m^2 to 600 W/m^2, with a greater frequency at low error density and a lower frequency at high error density. Performance-wise, AIGRU is at its finest at 30% and vilest at 70%. In the range from 260 to zero with a 70% missed rate, AIGRU is still somewhat more frequent than GRU.

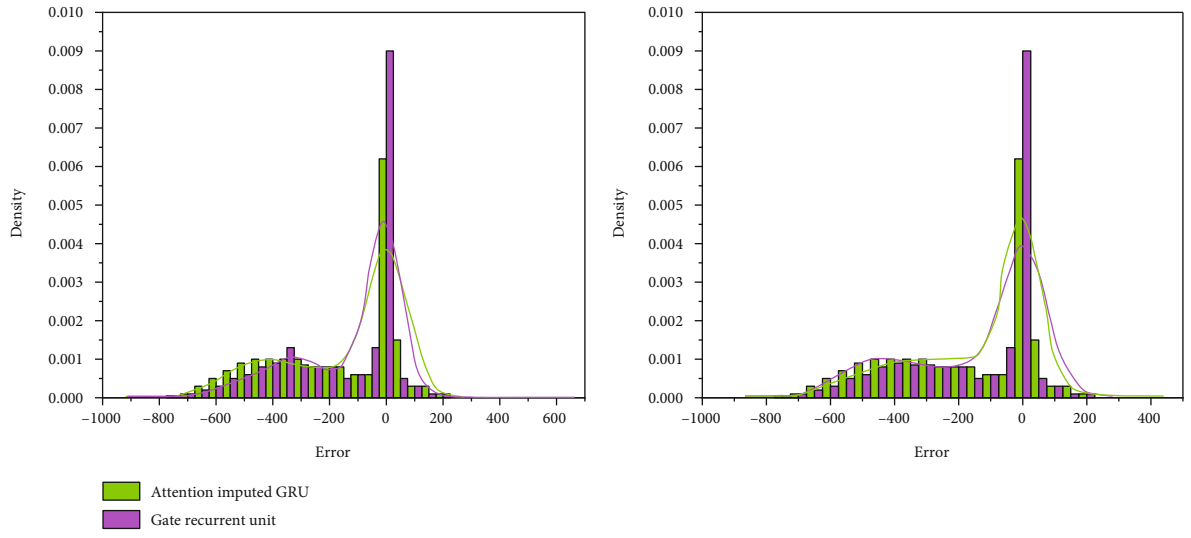

(a) 30% missing rate

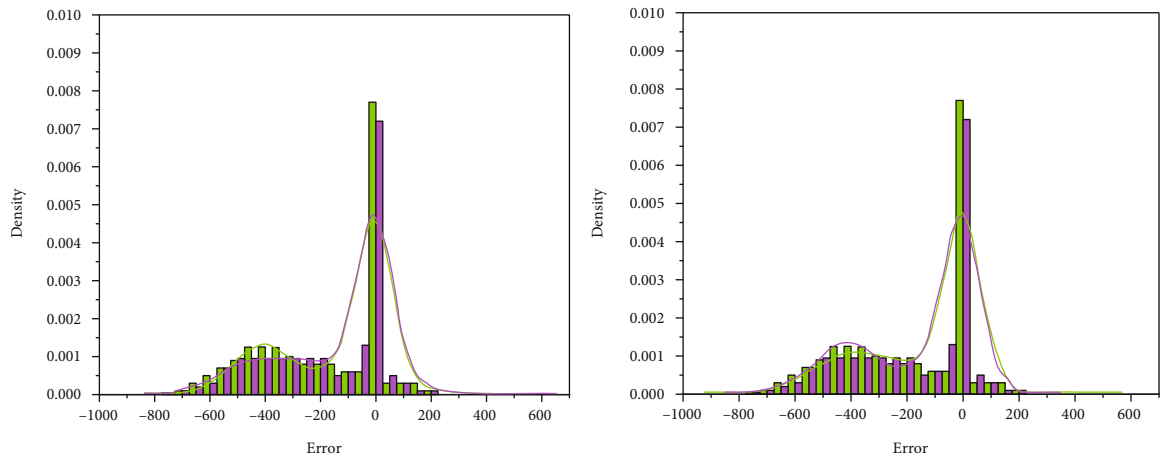

(b) 50% missing rate

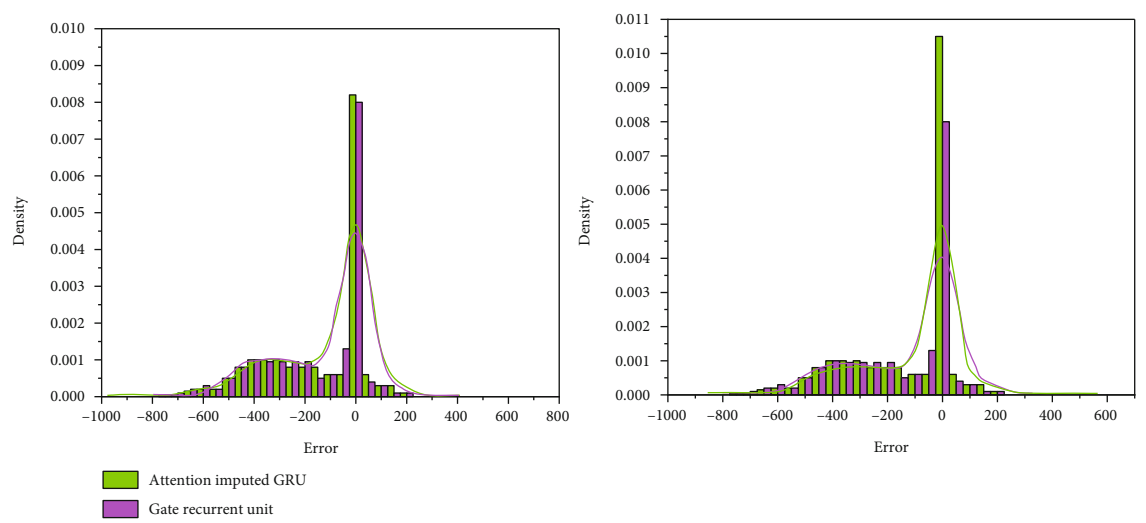

(c) 70% missing rate

Figure 7: Continued.

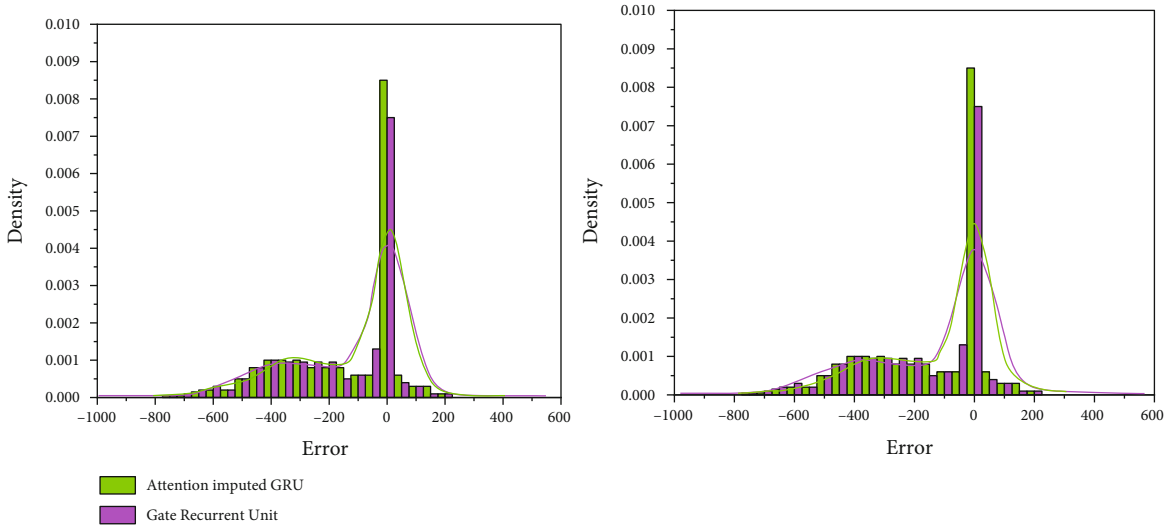

(d) 90% missing rate

Figure 7: Error histogram.

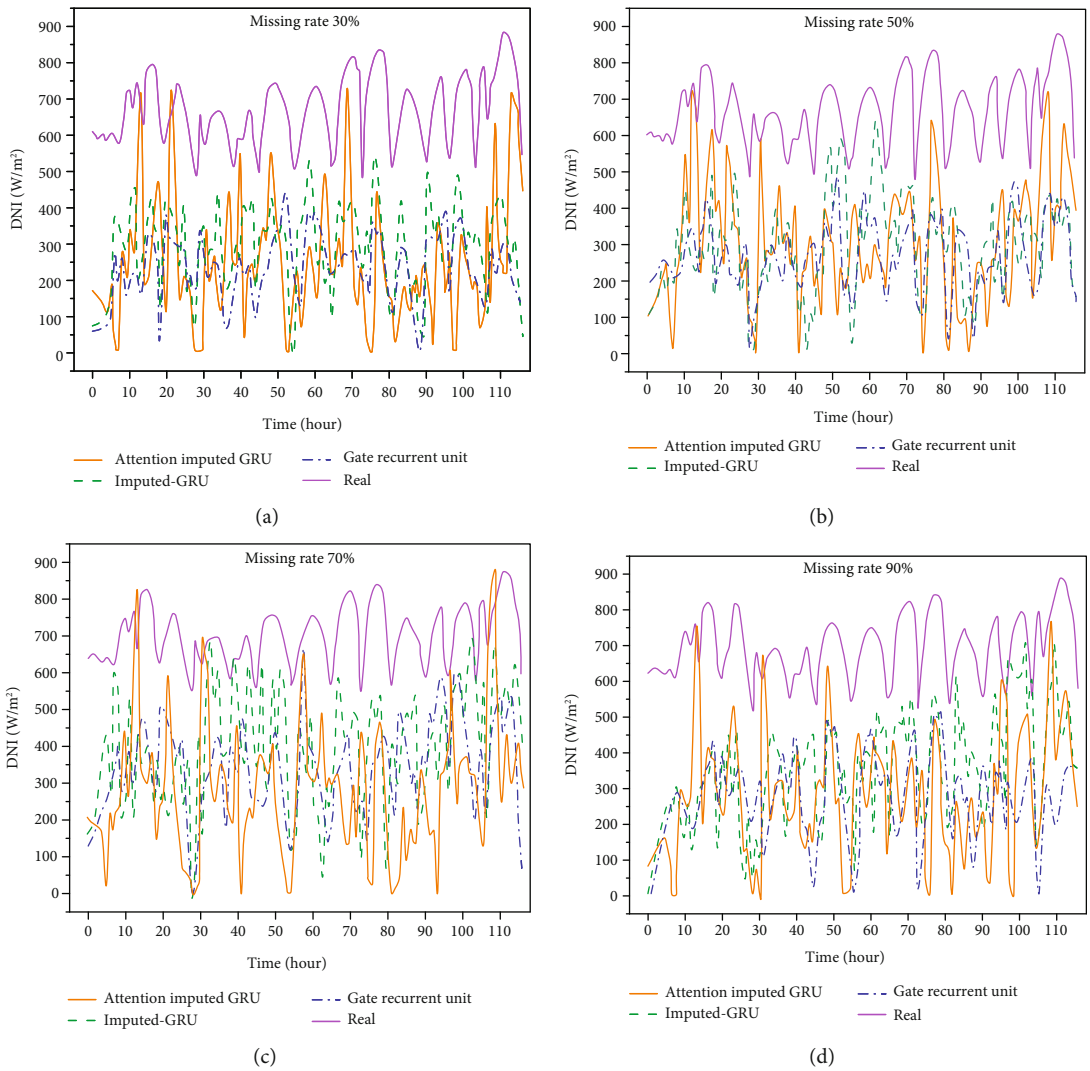

Figure 8: An outcome of AIGRU, IGRU, and GRU at higher irradiance (500 W/m^2).

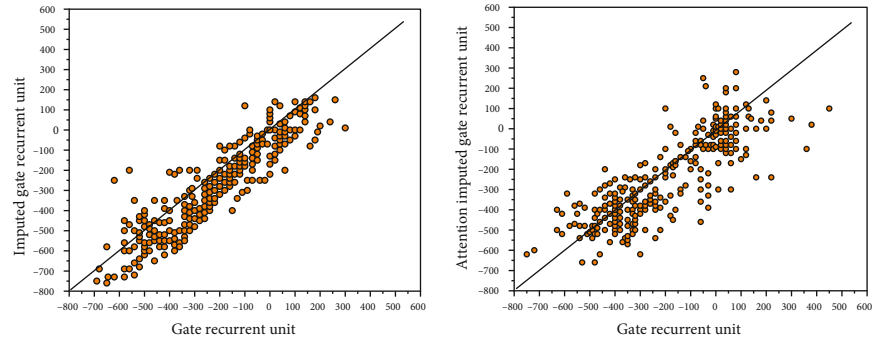

(a) 30% missing rate

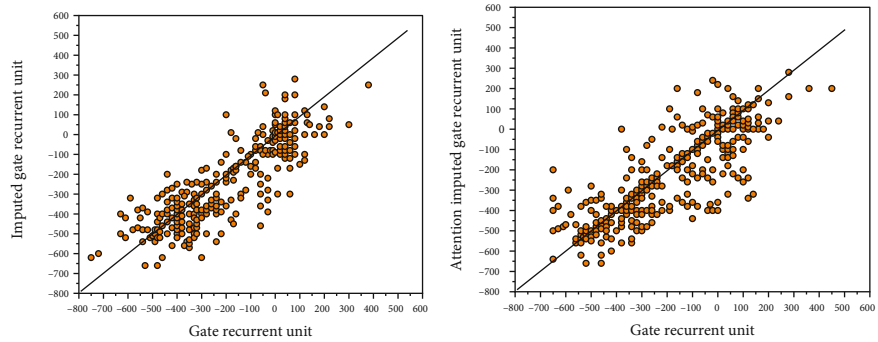

(b) 50% missing rate

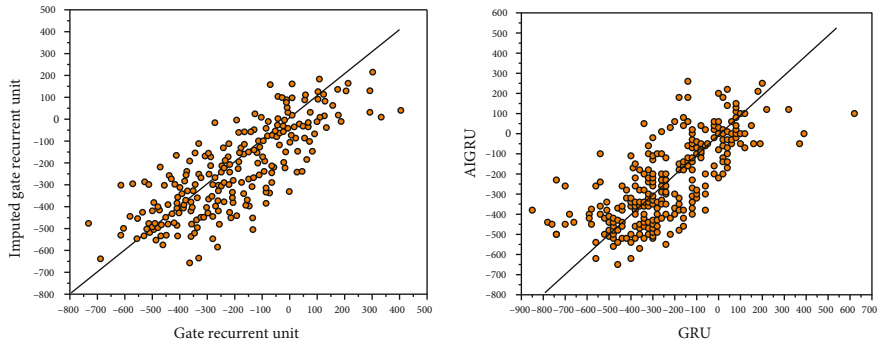

(c) 70% missing rate

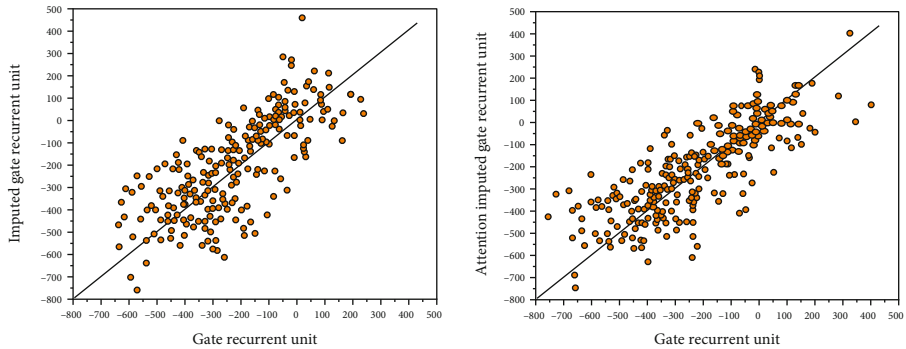

(d) 90% missing rate

Figure 9: The scatter error for various missing rates.

By either metric, AIGRU lags behind IGRU in terms of overall performance, but it pulls ahead by a wide margin when the radiation levels are high. When true DNI is more significant than 500 W/m^2, the results of the three models are shown in Figure 8. For a variety of missing rates, AIGRU is superior.

Scatter plots show the relation between the two approaches; they can be used to check this theory. In Figure 9, the GRU's blunders are shown along the horizontal axis. Possible flaws in the suggested procedures are shown in the vertical axis. Meanwhile, since $Y = X$, the mistakes

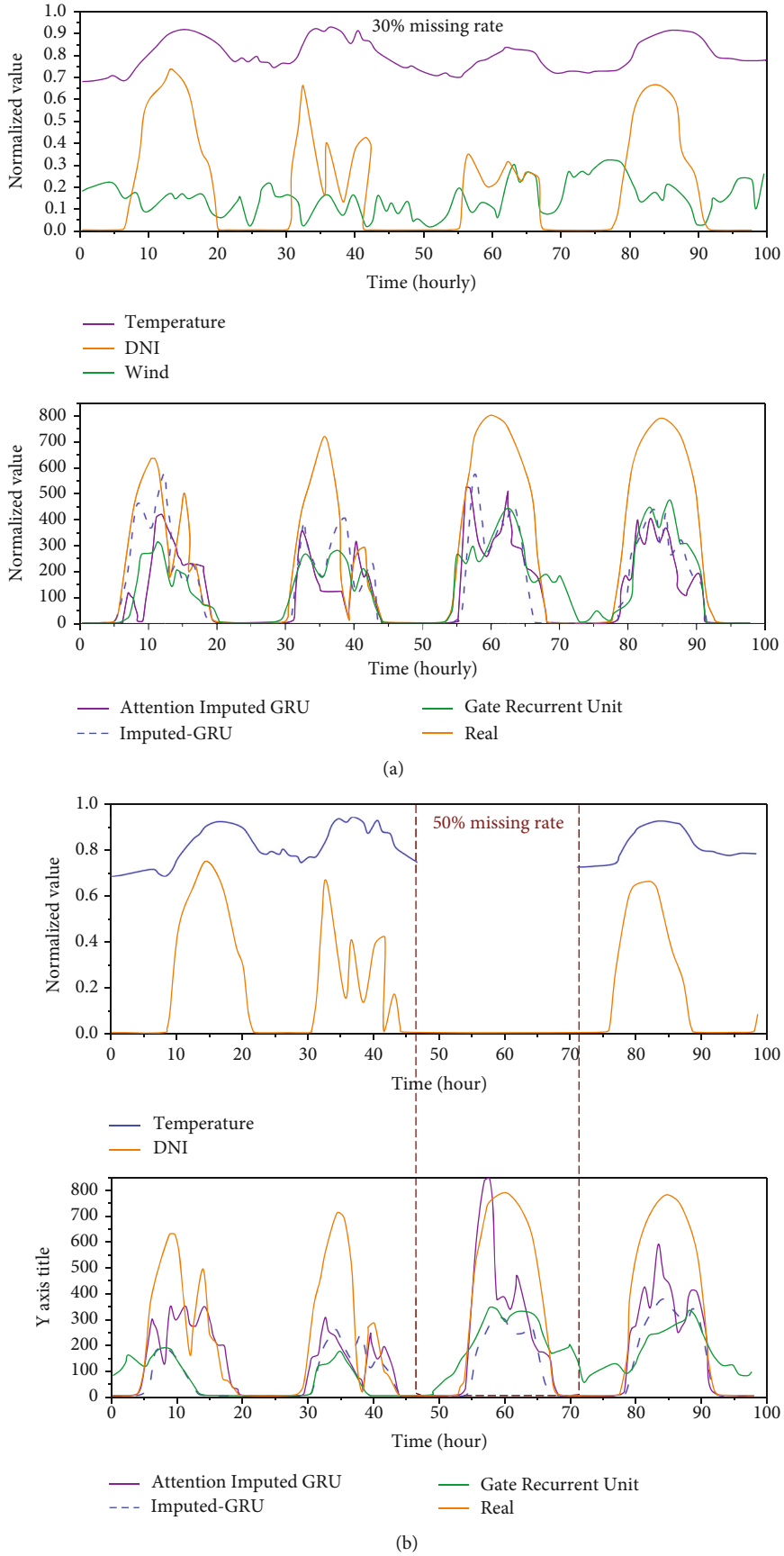

Figure 10: Continued.

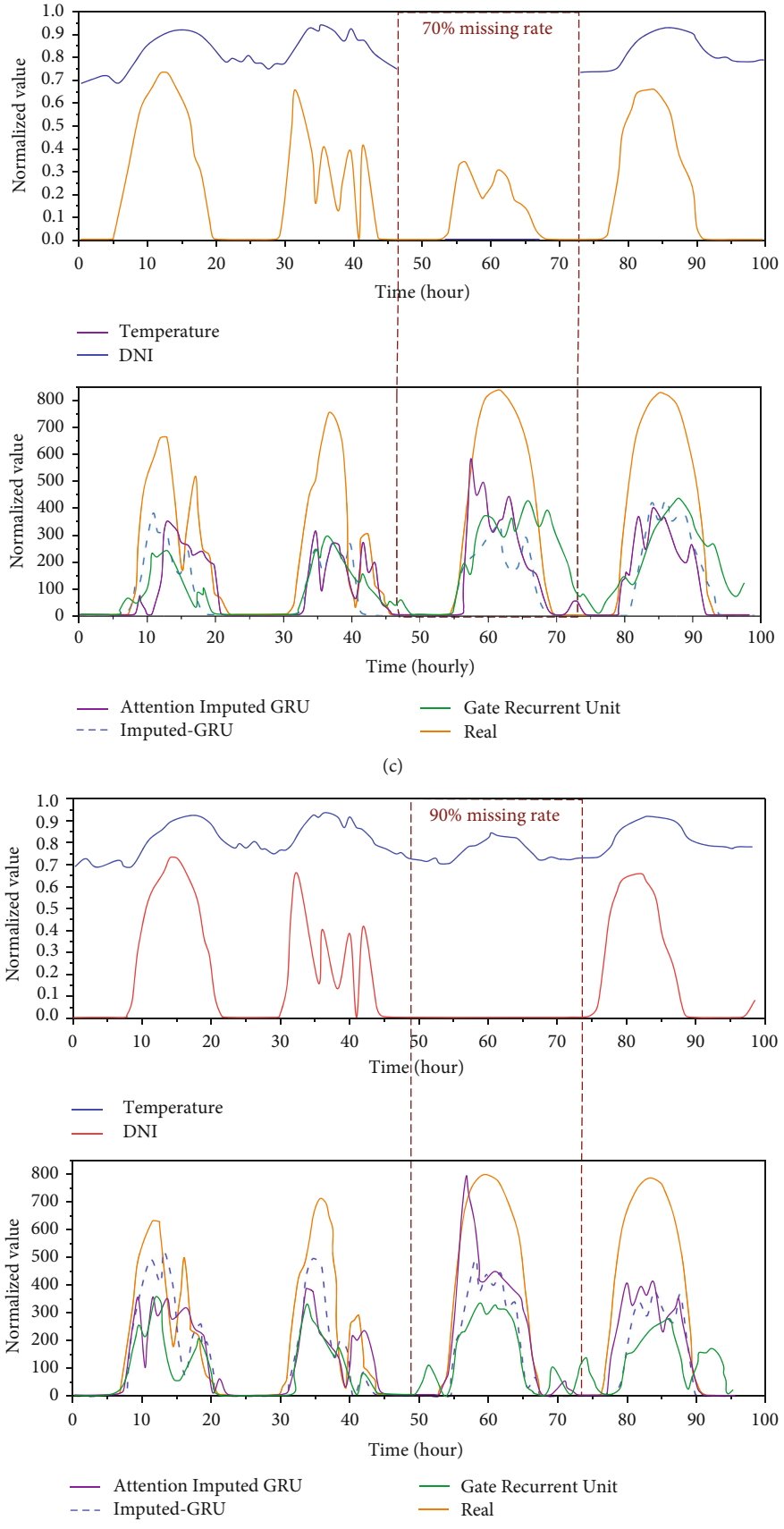

Figure 10: An outcome of variant missing design with 50% missing data.

associated with the two approaches are equivalent. The line's higher portion indicates wherever the GRU performs restored than the proposed approaches, while the line's lower part shows where the GRU serves worse. The smaller the distance between the point and the line, the more similar the two approaches are. The further the moment is from the line, the greater the method's superiority over the alternative. More data points are below the line than above, suggesting that the proposed approaches outperform GRU. When equating AIGRU and gate recurrent unit, the researcher can also see that the data under AIGRU are further spread out, which denotes that AIGRU is more precise than IGRU at forecasting specific values. For instance, in the locations near the right border, the GRU error is about 400 W/m^2, while the error in AIGRU is nearly zero. Errors of over 400 W/m^2 are possible only under extreme illumination conditions.

This finding agrees with the one drawn from the prediction mentioned in the graph. In conclusion, the attention module enables the model to pay closer attention to important details, but at the sacrifice of some average accuracy or the need for tweaks.

4.3.2. Different Missing Patterns. The impact on the model varies depending on the type of missing data. Here, the researcher undertakes tests using three frequently encountered pattern types: (1) sensor noise-related random missing (existence of short segments and sporadic missing) and (2) intervals of missing data for all variables (e.g., an entire day), most often due to technical difficulties with the network. Missing DNI segments (the primary aim), climate factor segments at random, or DNI segments with climate factor missing are all missing data in category three. In Figure 10(a), the researcher saw random missing data; somewhere, 50% of all variables are missing. Since the researcher does not see the whole picture, our model for comparing patterns is a learned one, so the researcher can only make educated guesses about what the missing design might be.

The upper figure depicts the absent Temp and DNI, while the lower figure contrasts the original GRU with the two enhanced approaches based on 96 days of data. The long history of data used and the higher model order prevent the prediction failure caused by the sporadic missing during the model inference process. Similar convincing predictions can be made by the GRU without imputation, albeit with a little lower accuracy. The third type of missing data is segmented missing data, where all input variables are blank for a given period, say, 24 hours. Figure 10(b) demonstrates the two approaches to predicting the DNI. IGRU and GRU suffer performance drops under these conditions, although AIGRU outperforms random missing. Possible explanation: accuracy suffers significantly at the expense of robustness to missing all day when utilizing more extensive historical data. Adverse effects on IGRU and AIGRU are apparent when the weather factor and typical DNI are removed. While the absence of DNI has less impact on both approaches, AIGRU obtains better results in Figures 10(c) and 10(d). Instinctively, as DNI fluctuates, it becomes clear that incorporating the weather factor into the prediction task is essential. Despite the overall decrease in loudness and smoothness of the waveform, GRU remains unaffected by these absences. As with filtering, GRU achieves a desirable smoothing outcome at the expense of precision.

Table 4: Mean absolute error valuation with three characteristics.

Missing data	MICE	Mean	MF	KF	KNN	This study
0.50	161.28	154.26	172.82	138.86	144.17	**131.43**
0.70	156.13	169.34	176.68	129.53	124.12	**118.22**
0.90	164.44	174.12	155.26	126.01	128.42	**121.81**

Table 5: Mean absolute error valuation with five characteristics.

Missing data	MICE	Mean	MF	KF	KNN	This study
0.50	162.63	162.36	187.22	**121.96**	130.31	137.81
0.70	154.57	162.58	157.23	**124.59**	131.24	151.12
0.90	179.78	188.41	140.38	133.63	145.54	**126.24**

4.3.3. Comparison with Other Imputation Techniques. To authenticate that the approaches were as reliable as advertised, the researcher expanded their range from three to five variables and tested each using a variety of interpolation schemes. Using these techniques, the researcher attributes the missing variables and sets GRU to work on the prediction. Mean interpolation, matrix complementarity, minimum irradiance consistent emulation, and K-nearest neighbor are some additional irradiance imputation methods compared in Tables 4 and 5. Two climatic elements, cloud cover and humidity, are added to the three input factors of the other group. To create this approach, the researcher combined the most valuable aspects of both IGRU and AIGRU. Here, MAE is the error of choice.

According to Table 4, the suggested technique is more accurate than the poorest imputation methods by as much as 32% and provides a 4-8% enhancement over the best imputation method. The proposed methods outperform most of the existing techniques in the case study with five contributions. When comparing KF to the suggested approach, KF performs better in the 50% and 70% missing proportion cases. On the other hand, the recommended strategy is the best option when 90% of the data is absent. In conjunction with the trivariate case, it demonstrates that KF and the suggested technique perform well under conditions with an adequate amount of reliable information. However, the proposed method exhibits higher performance with high missing rates, indicating that it is more robust. It also shows that the proposed strategy may be applied to any situation without modifying the model. However, the various data sets will still require different imputation procedures.

As the percentage of missing values rises, the performance of mean interpolation declines compared to the other approaches. In contrast, MICE and MF outcomes are data-driven.

5. Conclusion

With the help of a neural imputation module, this research suggests a new approach to predicting irradiance. In many cases, its performance is superior to the standard method and other well-known imputation techniques. The IGRU benefits from being highly adaptable, requiring no additional imputation step during data pre-processing, and having minimal computational complexity. Additionally, it is an effort to combine the imputation and prediction steps, hoping that incorporating prediction data can improve imputation. Of course, there is still much room for improvement in the field of time series imputation for renewable energy.

Irradiance readings fluctuate wildly and are significantly influenced by weather patterns. This finding demonstrates that the outcomes of various approaches vary among datasets. Traditional methods are effective when the targets are easy to hit. It is still worthwhile to study imputation techniques, especially under challenging conditions like heavy rain or other extreme weather. Because of this, the imputation module can benefit from encoding feature correlations by investigating more explicit model properties, such as fundamental relationships among components and time graph relations among its parts.

For optimal performance in the field, the imputation architecture should be fine-tuned using real-world applications, such as irradiance prediction and missing data states for power prediction in photovoltaic plants. Designing temporal windows with flexibility, interpolating data in real-time, using multiple modalities, and other strategies are all viable alternatives. The model parameters can also be adjusted to make it more generalizable.

Data Availability

All data supporting the findings of this study are included in this article.

Ethical Approval

All procedures performed in this study involving human participants were in accordance with the ethical standards of the institutional and/or national research committee and its later amendments or comparable ethical standards.

Disclosure

The funders had no role in the study design, data collection, and analysis, decision to publish, or manuscript preparation.

Conflicts of Interest

The authors declare that they have no competing financial interest conflicts in this paper.

References

[1] G. Narvaez, L. F. Giraldo, M. Bressan, and A. Pantoja, "Machine learning for site-adaptation and solar radiation forecasting," *Renewable Energy*, vol. 167, pp. 333–342, 2021.

[2] L. S. Hoyos-Gómez, J. F. Ruiz-Muñoz, and B. J. Ruiz-Mendoza, "Short-term forecasting of global solar irradiance in tropical environments with incomplete data," *Applied Energy*, vol. 307, article 118192, 2022.

[3] Q.-T. Phan, Y.-K. Wu, Q.-D. Phan, and H.-Y. Lo, "A study on missing data imputation methods for improving hourly solar dataset," in *2022 8th International Conference on Applied System Innovation (ICASI)*, pp. 21–24, Nantou, Taiwan, 2022.

[4] E. Miranda, J. F. G. Fierro, G. Narváez, L. F. Giraldo, and M. Bressan, "Prediction of site-specific solar diffuse horizontal irradiance from two input variables in Colombia," *Heliyon*, vol. 7, no. 12, article e08602, 2021.

[5] L. Wang and J. Shi, "A comprehensive application of machine learning techniques for short-term solar radiation prediction," *Applied Sciences*, vol. 11, no. 13, 2021.

[6] A. Kocian, G. Carmassi, F. Cela, L. Incrocci, P. Milazzo, and S. Chessa, "Bayesian sigmoid-type time series forecasting with missing data for greenhouse crops," *Sensors*, vol. 20, no. 11, 2020.

[7] D. P. Choudhary, A. C. Cadavid, A. Cookson, and G. A. Chapman, "Variability in irradiance and photometric indices during the last two solar cycles," *Solar Physics*, vol. 295, no. 2, 2020.

[8] M. Alqudah, T. Dokic, M. Kezunovic, and Z. Obradovic, "Prediction of solar radiation based on spatial and temporal embeddings for solar generation forecast," 2022, http://arxiv.org/abs/2206.08832.

[9] C. Rizos-Theodoros and A. F. Bais, "Determination of Uncertainty in Hourly and Daily Averages of Solar Irradiance Due to Missing Measurements," *AIP Conference Proceedings*, vol. 2075, 2019.

[10] M. David, M. A. Luis, and P. Lauret, "Comparison of intraday probabilistic forecasting of solar irradiance using only endogenous data," *International Journal of Forecasting*, vol. 34, no. 3, pp. 529–547, 2018.

[11] H. Alam, M. Y. Mashor, M. Irwanto et al., "Output characteristics of photovoltaic module in Medan based on estimated solar irradiance using hargreaves method for application assessment of transformerless photovoltaic inverter," in *AIP Conference Proceedings*, AIP Publishing, 2016.

[12] T. D. De Wit, "A method for filling gaps in solar irradiance and solar proxy data," *Astronomy & Astrophysics*, vol. 533, p. A29, 2011.

[13] M. Kumar, K. Namrata, and N. Kumari, "Hyper-parametric improved machine learning models for solar radiation forecasting," *Concurrency and Computation: Practice and Experience*, vol. 34, no. 23, 2022.

[14] S. A. Haider, M. Sajid, H. Sajid, E. Uddin, and Y. Ayaz, "Deep learning and statistical methods for short- and long-term solar irradiance forecasting for Islamabad," *Renewable Energy*, vol. 198, pp. 51–60, 2022.

[15] X. Jiao, X. Li, D. Lin, and W. Xiao, "A graph neural network based deep learning predictor for spatio-temporal group solar irradiance forecasting," *IEEE Transactions on Industrial Informatics*, vol. 18, no. 9, pp. 6142–6149, 2022.

[16] Y. Su, N. Li, H. Yang et al., "A feature importance analysis based solar irradiance mapping model using multi-channel satellite remote sensing data," in *2022 IEEE/IAS 58th Industrial and Commercial Power Systems Technical Conference (I&CPS)*, Las Vegas, NV, USA, 2022.

[17] O. Bamisile, A. Oluwasanmi, C. Ejiyi, N. Yimen, S. Obiora, and Q. Huang, "Comparison of machine learning and deep

learning algorithms for hourly global/diffuse solar radiation predictions," *International Journal of Energy Research*, vol. 46, no. 8, pp. 10052–10073, 2022.

[18] B. Brahma and R. Wadhvani, "Visualizing solar irradiance data in ArcGIS and forecasting based on a novel deep neural network mechanism," *Multimedia Tools and Applications*, vol. 81, no. 7, pp. 9015–9043, 2022.

[19] A. Abubakar Mas'ud, "Comparison of three machine learning models for the prediction of hourly PV output power in Saudi Arabia," *Ain Shams Engineering Journal*, vol. 13, no. 4, 2022.

[20] W. Bendali, I. Saber, B. Bourachdi, M. Boussetta, and Y. Mourad, "Deep learning using genetic algorithm optimization for short term solar irradiance forecasting," in *2020 Fourth International Conference On Intelligent Computing in Data Sciences (ICDS)*, Fez, Morocco, 2020.

[21] T.-P. Chu, J.-H. Jhou, and Y.-G. Leu, "Image-based solar irradiance forecasting using recurrent neural networks," in *2020 International Conference on System Science and Engineering (ICSSE)*, Kagawa, Japan, 2020.

[22] S. Shan, X. Xie, T. Fan et al., "A deep-learning based solar irradiance forecast using missing data," *IET Renewable Power Generation*, vol. 16, no. 7, pp. 1462–1473, 2022.

[23] S. Syama and J. Ramprabhakar, "Multistep ahead solar irradiance and wind speed forecasting using Bayesian optimized long short term memory," in *2022 7th International Conference on Communication and Electronics Systems (ICCES)*, Coimbatore, India, 2020.

[24] G. L. Martins, R. A. Campos, M. Braga, and R. Rüther, "Implementing k-Nearest Neighborhood as a forecast method for Intra hour resolution with no exogenous outputs," in *Proceedings of the ISES Solar World Congress 2019*, pp. 2109–2114, Germany, 2020.

[25] H. Farahneh, F. Hussian, and X. Fernando, "De-noising scheme for VLC-based V2V Systems; a machine learning approach," *Procedia Computer Science*, vol. 171, pp. 2167–2176, 2020.

[26] S. Saha, N. Majumder, D. Sangani, and A. Das Bhattacharjee, "Comprehensive forecasting-based analysis using hybrid and stacked stateful/stateless models," *Lecture Notes in Networks and Systems*, vol. 427, pp. 567–579, 2022.

[27] N. P. Sebi, "Intelligent Solar Irradiance Forecasting Using Hybrid Deep Learning Model: A Meta-Heuristic-Based Prediction," *Neural Processing Letters*, vol. 55, no. 2, pp. 1247–1280, 2023.

[28] B. Zhou, S. Du, L. Li, H. Wang, Y. He, and D. Zhou, "An explainable recurrent neural network for solar irradiance forecasting," in *2021 IEEE 16th Conference on Industrial Electronics and Applications (ICIEA)*, pp. 1299–1304, Chengdu, China, 2021.

[29] F. R. Alharbi and D. Csala, "Short-term solar irradiance forecasting model \based on bidirectional long short-term memory deep learning," in *2021 International Conference on Electrical, Communication, and Computer Engineering (ICECCE)*, Kuala Lumpur, Malaysia, 2021.

[30] X. Huang, Q. Li, Y. Tai et al., "Hybrid deep neural model for hourly solar irradiance forecasting," *Renewable Energy*, vol. 171, pp. 1041–1060, 2021.

[31] S. Sharda, M. Singh, and K. Sharma, "RSAM: robust self-attention based multi-horizon model for solar irradiance forecasting," *IEEE Trans Sustain Energy*, vol. 12, no. 2, pp. 1394–1405, 2021.

[32] M. Abdel-Nasser, K. Mahmoud, and M. Lehtonen, "Hifa: promising heterogeneous solar irradiance forecasting approach based on kernel mapping," *IEEE Access*, vol. 9, pp. 144906–144915, 2021.

[33] C. N. Obiora, A. Ali, and A. N. Hasan, "Forecasting hourly solar irradiance using long \short-term memory (LSTM) network," in *2020 11th International Renewable Energy Congress (IREC)*, Hammamet, Tunisia, 2020.

[34] D. Knol, F. de Leeuw, J. F. Meirink, and V. V. Krzhizhanovskaya, "Deep learning for solar irradiance nowcasting: a comparison of a recurrent neural network and two traditional methods," in *Lecture Notes in Computer Science (including subseries Lecture Notes in Artificial Intelligence and Lecture Notes in Bioinformatics), vol. 12746 LNCS*, pp. 309–322, Springer International Publishing, Cham, 2021.

[35] D. Kumar, H. D. Mathur, S. Bhanot, and R. C. Bansal, "Forecasting of solar and wind power using LSTM RNN for load frequency control in isolated microgrid," *International Journal of Modelling and Simulation*, vol. 41, no. 4, pp. 311–323, 2021.

[36] R. A. Rajagukguk, R. A. A. Ramadhan, and H.-J. Lee, "A review on deep learning models for forecasting time series data of solar irradiance and photovoltaic power," *Energies*, vol. 13, no. 24, 2020.

[37] Q. Ashfaq, A. Ulasyar, H. S. Zad, A. Khattak, and K. Imran, "Hour-ahead global horizontal irradiance forecasting using long short term memory network," in *2020 IEEE 23rd International Multitopic Conference (INMIC)*, Bahawalpur, Pakistan, 2020.

[38] B. Brahma and R. Wadhvani, "Solar irradiance forecasting based on deep learning methodologies and multi-site data," *Symmetry*, vol. 12, no. 11, p. 1830, 2020.

[39] H. He, N. Lu, Y. Jie, B. Chen, and R. Jiao, "Probabilistic solar irradiance forecasting via a deep learning-based hybrid approach," *IEEJ Transactions on Electrical and Electronic Engineering*, vol. 15, no. 11, pp. 1604–1612, 2020.

Hindawi
International Journal of Photoenergy
Volume 2023, Article ID 9763709, 1 page
https://doi.org/10.1155/2023/9763709

Retraction

Retracted: Application of Machine Learning in Multi-Directional Model to Follow Solar Energy Using Photo Sensor Matrix

International Journal of Photoenergy

Received 15 August 2023; Accepted 15 August 2023; Published 16 August 2023

This article has been retracted by Hindawi following an investigation undertaken by the publisher [1]. This investigation has uncovered evidence of one or more of the following indicators of systematic manipulation of the publication process:

(1) Discrepancies in scope

(2) Discrepancies in the description of the research reported

(3) Discrepancies between the availability of data and the research described

(4) Inappropriate citations

(5) Incoherent, meaningless and/or irrelevant content included in the article

(6) Peer-review manipulation

The presence of these indicators undermines our confidence in the integrity of the article's content and we cannot, therefore, vouch for its reliability. Please note that this notice is intended solely to alert readers that the content of this article is unreliable. We have not investigated whether authors were aware of or involved in the systematic manipulation of the publication process.

Wiley and Hindawi regrets that the usual quality checks did not identify these issues before publication and have since put additional measures in place to safeguard research integrity.

We wish to credit our own Research Integrity and Research Publishing teams and anonymous and named external researchers and research integrity experts for contributing to this investigation.

The corresponding author, as the representative of all authors, has been given the opportunity to register their agreement or disagreement to this retraction. We have kept a record of any response received.

References

[1] P. Dhanalakshmi, V. Venkatesh, P. S. Ranjit et al., "Application of Machine Learning in Multi-Directional Model to Follow Solar Energy Using Photo Sensor Matrix," *International Journal of Photoenergy*, vol. 2022, Article ID 5756610, 9 pages, 2022.

Hindawi
International Journal of Photoenergy
Volume 2023, Article ID 4705193, 9 pages
https://doi.org/10.1155/2023/4705193

Research Article

Performance Analysis of Solar Still by Using Octagonal-Pyramid Shape in the Solar Desalination Techniques

Bipin Kumar Singh,[1] C. Ramji,[2] P. Ganeshan,[1] V. Mohanavel,[3,4,5] T. Balasundaram,[6] V. Vignesh Kumar,[7] B. Balasubramanian,[8] P. Ramshankar,[9] Adireddy Ramesh,[10] and Subash Thanappan[11]

[1]*Department of Mechanical Engineering, Sri Eshwar College of Engineering, Coimbatore, 641202 Tamil Nadu, India*
[2]*Department of Rubber and Plastic Technology, MIT Campus, Anna University, Chennai, 600 025 Tamil Nadu, India*
[3]*Centre for Materials Engineering and Regenerative Medicine, Bharath Institute of Higher Education and Research, Chennai-600073, Tamil Nadu, India*
[4]*Department of Mechanical Engineering, Chandigarh University, Chandigarh, Mohali-140413, Punjab, India*
[5]*Department of Mechanical Engineering, School of Technology, Glocal University, Delhi-Yamunotri Marg, Uttar Pradesh 247121, India*
[6]*Department of Mechanical Engineering, Medak College of Engineering and Technology, Siddipet, Telangana, India*
[7]*Department of Mechanical Engineering, St. Joseph College of Engineering, Chennai, Tamil Nadu, India*
[8]*Department of Mechanical Engineering, Chettinad College of Engineering and Technology, Karur, 639114 Tamil Nadu, India*
[9]*Department of Civil Engineering, University College of Engineering, Dindgul-624622, India*
[10]*Department of Electrical and Electronics Engineering, Aditya College of Engineering, Surampalem 533437, Andhra Pradesh, India*
[11]*Department of Civil Engineering, Ambo University, Ambo, Ethiopia*

Correspondence should be addressed to Subash Thanappan; subash.thanappan@ambou.edu.et

Received 14 July 2022; Revised 7 September 2022; Accepted 20 September 2022; Published 17 March 2023

Academic Editor: Br Ramesh Bapu

This research work explored and compared the experimental performance of a solar still having novel octagonal-pyramid shape with a single slope solar still. It is found that the novel still provides twice distillation compared with conventional still. The experiments also evaluated the desalination productivity of octagonal-pyramid solar still by varying the depth of saline water inside the basin and angle of inclination of glass cover. It is observed that the optimum condition for high distillation is obtained when depth of water inside the basin is 5 cm with angle of inclination of glass cover which is 30°. Four types of water, i.e., underground borewell water, sea water, leather industry effluent, and plastic industry effluent were also used to see the effect on distillation. Results showed that underground borewell water provides high distillation due to low density. Furthermore, the performance of the octagonal-pyramid solar still is enhanced by adding different latent heat and sensible heat materials in the octagonal-pyramid solar still. Hence, the addition of brick to the octagonal-pyramid still yields the highest productivity compared to incorporation of paraffin wax. Hence, it can be concluded that the octagonal design of the solar still has shown an increased productivity when compared to a single slope solar still (conventional still) under all the conditions.

1. Introduction

The fresh water resources are getting polluted alongside the demand for fresh water which is increasing day by day due to modernization. Water reclamation could bring the complete solution for this problem. There are numerous ways to desalinate sea water and waste water into fresh water [1, 2]. The simplest and cost-effective method is using solar still for distillation. Since the daily productivity of a conventional single slope solar still is very low, hence, in this paper,

modification in design is made to improve the productivity. Various research experiments are being performed to increase the distillate productivity of a solar still. Wind velocity, solar radiation, still basin area, water surface area, and water depth and glass cover temperature are some of the influences that affect the daily efficiency of a solar still [3–5].

Single-basin single-slope solar stills are the conventional stills used for desalination of water which works on the basic condensation principle. Though the construction or design of single-basin solar still is simple and constructive cost is cheap and requires low maintenance cost, with the same setup, the productivity cannot be increased [6]. Hence, in order to increase the quality and quantity of the fresh water, the distilled water for drinking and irrigation purpose single-basin solar still is ministering modifications. With the view to overcome the limitations of a single-basin solar still, various modifications to the solar still have been proposed such as double-slope solar still, multistage solar still, stepped solar still, and wick-type solar still. With a flat plate collector enclosed to a single-basin solar still, an improvement of 52% in the productivity was shown. Double glass cover on a single-slope basin also achieved high productivity by running cool water between the double glass cover. A stepped solar still effectively showed an increase in the daily productivity [7–9]. A stepped solar still with a flashing chamber was constructed and investigated by experimenting on a stepped solar still with and without a reflector to illustrate that there was a 20% increase in the daily efficiency of productivity compared to conventional solar still [10].

Later, researchers improved the work efficiency of the solar still by adding wick, fins, and various thermal energy storage materials into the still. Basin-type stepped solar still with wick-type still showed high efficiency in terms of productivity. The wick-type evaporator collector system showed an increase in overall efficiency when compared to the basin-type system [11–13]. Various types of wick materials to innumerable absorber plate designs discovered the most productive as 4.28 L per day while utilising a wire mesh stepped-type absorber plate made up of coral fleece. The research also developed a multibasin solar still added to thermal storage materials in order to increase the performance of the still even in the absence of sunlight [14]. Sensible heat resources such as sand, cement, and glass, as well as latent heat storage materials like wax, were used and found the increased productivity as 73% when compared to traditional solar panels. Experiments with different water nanofluids in basin also showed remarkable improvement in the performances. Incorporated sensible heat storage materials like cement concrete bits, quartzite rock, washed pebbles, iron scraps, and red brick bits into the still found that adding of an inch quartzite rock showed increased productivity than the other materials [15–18].

In this paper, a novel octagonal-pyramid solar still is developed to improve the desalination productivity of the solar still. The basin of the still is octagonal in shape, and condensing glass covers are slanted over each side of the basin giving it a pyramidal shape. The narrowing effect of the pyramidal glass cover will be an aid in enhancing the laminar flow of water vapour without any disruption [19, 20]. The pyramidal shape of the glass cover circulates the wind around the structure which causes a decrease in glass surface temperature. The difference in temperature between the saline water and the glass cover will enhance the condensation process and thus increase the daily productivity of the still [21]. The hourly desalinate production of the both conventional solar still and the new solar still has been measured. The octagonal-pyramid solar still is erected in the month of May, 2021, in Ramanathapuram, Tamil Nadu, India.

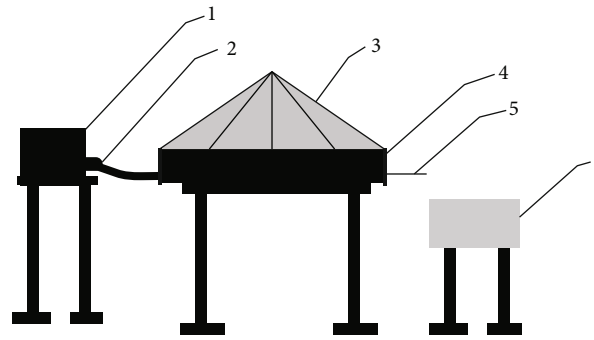

Figure 1: Schematic diagram of the octagonal-pyramid solar still.

Figure 2: Photograph of experimental setup of the octagonal-pyramid solar still.

2. Experimental Setup

A conventional single-slope solar still and an octagonal-pyramid solar still were planned and erected to compare the performance of solar desalination. The base and the side walls are built using galvanized steel sheets of 1.6 mm thickness [22, 23]. The base area of the still is 0.36 m^2 (0.6 m length × 0.6 m breadth). The taller side wall has a

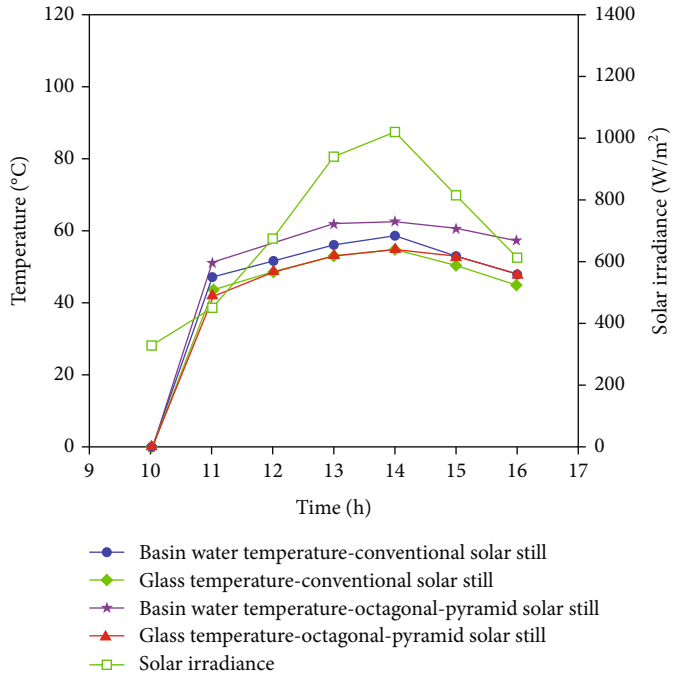

Figure 3: Variation of basin water temperature, glass temperature, and solar radiation of the conventional and octagonal-pyramid solar still.

height of 0.5 m and the shorter side wall has 0.2 m. To increase the absorptive, black paint has been applied to the basin's interior surface [24–26]. The basin is protected with glass which allows the solar radiation to reach the basin plate and also acts as the condensing surface. Tempered glass is used in the experiment as it has a solar transmittance of 91% for the incident solar radiation and has high wet ability. The glass cover is slanted horizontally over the basin at an angle of 30 degrees.

An octagonal-shaped base with each side of length 248.5 mm is cut. The side walls of height 200 mm are fabricated over the base. The base and the side walls are built using galvanized steel sheets of 1.6 mm thickness. Eight sides of the octagonal basin are sealed with a glass cover in the shape of octagonal pyramid as given in Figure 1. The photograph of the complete experimental setup of the octagonal-pyramid solar still is shown in Figure 2.

The water to be desalinated is filled in the basin. On account of incidence of solar radiation, the temperature of the water inside the basin increases and the water evaporates. The water vapour gets condensed on reaching the glass cover. The condensed water was collected in a trough placed at the bottom of the glass cover.

A wired digital thermometer is used to accurately measure the temperature of the water and the glass of ±1°C. Instantaneously, a solarimeter was used to measure the intensity of solar radiation ± 1 W/m^2. A digital vane anemometer is used to measure the wind velocity with an accuracy of ±0.1 m/s. A calibrated measuring jar having 2 L capacity with an accuracy of 5 mL is used to measure the hourly distillate yield.

Experiments were conducted at Ramanathapuram, Tamil Nadu, India, during May 2019. For every one hour, solar radiation, wind velocity, basin plate temperature, water to be treated, glass cover, and distilled water were measured. The experiment was conducted on both the conventional and the octagonal-pyramid solar stills, and the hourly yield is measured. The hourly yield of the octagonal-pyramid solar still was measured by the following:

(i) Varying the depth of saline water inside the basin, h

(ii) Varying the angle of inclination of glass cover, ⊠

(iii) Adding latent heat and sensible heat materials, viz., paraffin wax and brick

(iv) Changing the type of liquid to be distilled, viz., underground borewell water, sea water, leather industrial waste liquid, and plastic industrial waste liquid

3. Results and Discussion

Ambient temperature measured at Ramanathapuram, Tamil Nadu, is varied between 38° and 42°. Wind velocity and solar radiation intensity were measured.

3.1. The Effect of Solar Radiation on the Solar Still's Performance. Basin water temperature and glass temperature are measured for both conventional and octagonal-pyramid solar stills after every hour. Figure 3 demonstrates how the temperature of the basin, temperature of glass, and intensity of solar radiation changed over time. It is experiential that the water temperature increases as solar radiation increases. The temperature of the basin rises till it reaches a maximum value around noon and decreases subsequently as the solar

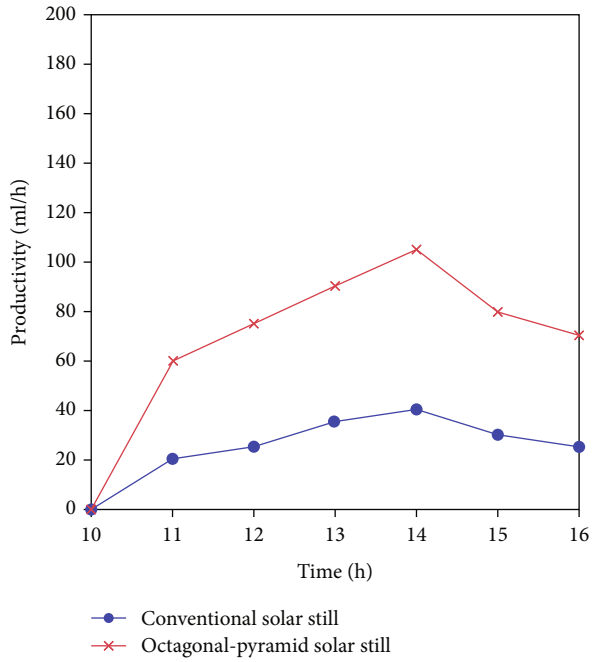

Figure 4: Hourly desalination productivity of the conventional and octagonal-pyramid solar still.

radiation decreases. It is also observed that the octagonal-pyramid still shows a lower glass temperature value than a conventional still. It is to be noted that this decrease in the glass temperature is caused due to its conical shape nearly possessed by octagonal-pyramid still.

3.2. Hourly Desalination Productivity of the Conventional and Octagonal-Pyramid Solar Still. The hourly variation of desalinated water productivity for conventional and octagonal-pyramid stills is shown in Figure 4. In this experiment, underground borewell water is used as saline water in the solar stills. The depth of saline water is 5 cm, and the angle of glass cover is 30 degrees. It is observed that desalinated productivity increases slowly from zero in the early hours and reaches a maximum value around noon. Both the stills take time to increase from value zero because the water takes time to get heated up to transform into vapour state. The productivity in the afternoon decreases gradually as the solar radiation decreases. The octagonal-pyramid still shows a higher productivity than the conventional still. The hourly productivity obtained on using octagonal-pyramid still is more than twice that of the conventional still.

3.3. Performance of the Octagonal-Pyramid Solar Still on Varying Saline Water Depths. The desalination productivity of the octagonal-pyramid solar still at various saline water depths (h) is shown in Figure 5. Borewell water is used as saline water to find the optimum saline water depth in the octagonal-pyramid solar still. The saline water depths are 5 cm, 10 cm, and 15 cm with a fixed glass cover angle of inclination of 30 degrees. It is observed that the increase in water depth decreases the productivity of the still.

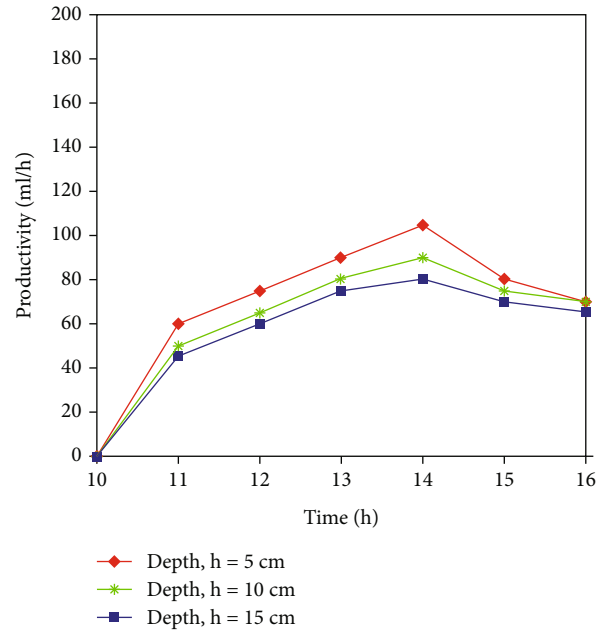

Figure 5: Productivity of various water depths of the octagonal-pyramid solar still.

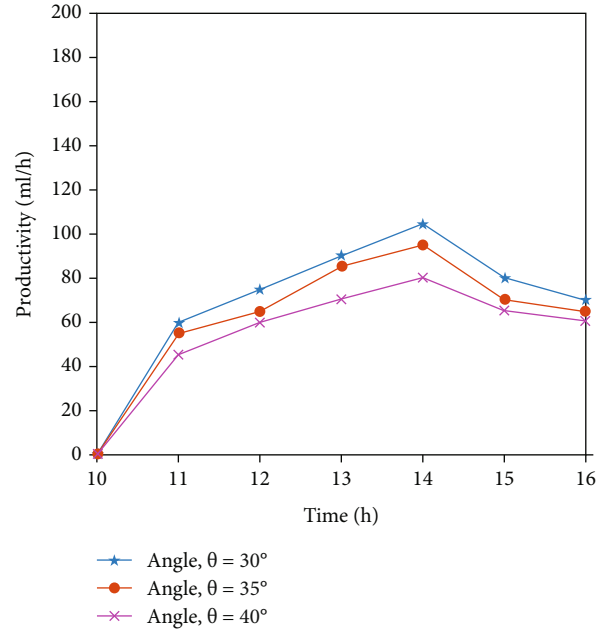

Figure 6: Productivity of various glass cover angles of the octagonal-pyramid solar still.

The highest productivity is achieved at the lowest depth of 5 cm. The factors that contributed to achieve increased productivity are the lower depth of water, decreased mass of the water, and the eventual specific increased heat capacity of the water.

3.4. Performance of the Octagonal-Pyramid Solar Still on Varying the Angle of Inclination of Glass Cover. The variation in desalination productivity is observed by changing

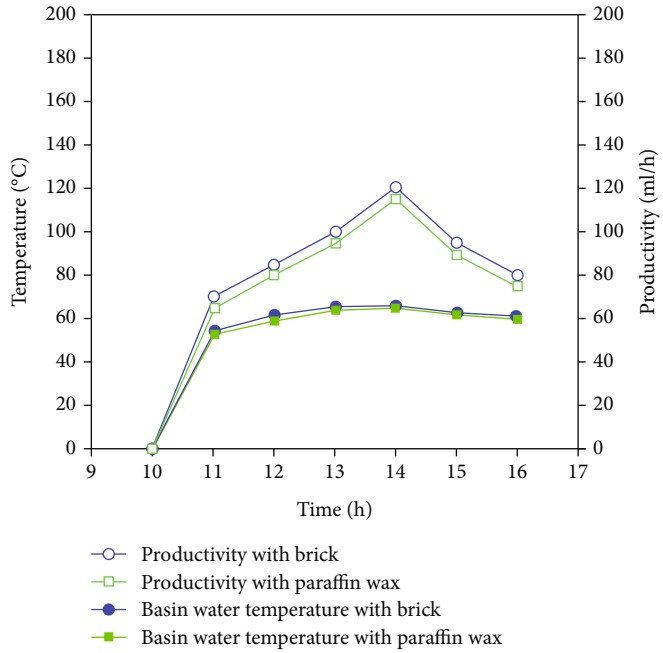

Figure 7: Effect of latent heat and sensible heat materials in the octagonal-pyramid solar still.

the angle of glass cover (θ). The angle of glass cover is varied from 30°, 35° to 40°. Borewell water is used as a saline water, and a uniform saline water depth of 5 cm is used in this experiment. The hourly desalination productivity at various angles of glass cover in the octagonal-pyramid solar still is shown in Figure 6. The experimental results show that the change in angle of inclination affects the desalination productivity of the still. It is seen that the octagonal-pyramid solar still yields the highest cumulative distillate for $\theta = 30°$.

3.5. Performance of the Octagonal-Pyramid Solar Still on Adding Latent Heat and Sensible Heat Materials. Latent heat and sensible heat materials are the thermal storage materials added separately inside the still so that the high heat is maintained inside the basin. The latent heat and sensible heat materials used in the experiment are paraffin wax and brick, respectively. Initially, paraffin wax is stored in a small stainless-steel container which is half-filled and placed in a basin area of the still. As the basin water temperature increases, the paraffin wax absorbs the heat and melts inside the small container and supply heat to the saline water.

After experimenting with paraffin wax, a brick is added in the basin area of saline water. The brick absorbs heat from the saline water and releases additional heat to the saline water inside the still. Underground borewell water is the saline water used in this experiment. The octagonal pyramid maintains an angle of glass cover at 30° and the saline water depth of 5 cm throughout the experiment. The increased desalination productivity due to the addition of latent heat and sensible heat materials is shown in Figure 7. Following the addition of the thermal heat storage materials, the basin water temperature rises in the late afternoon. The addition of brick to the octagonal-pyramid still yields the highest productivity compared to incorporation of paraffin wax.

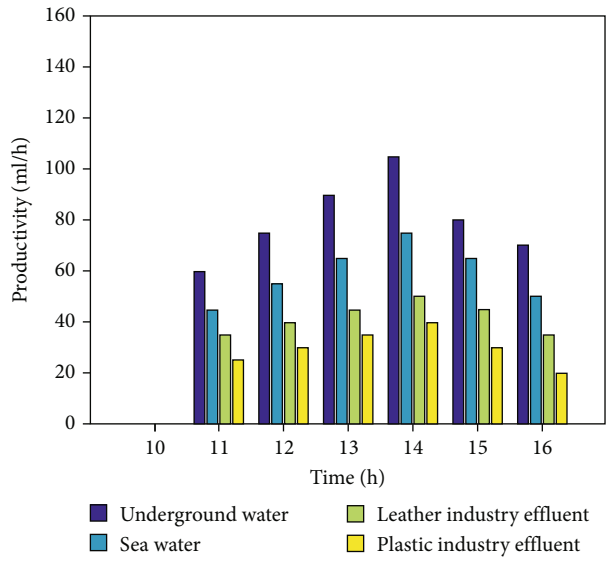

Figure 8: Productivity of underground water, sea water, leather industry waste, and plastic industry waste in the octagonal-pyramid solar still.

3.6. Performance of the Octagonal-Pyramid Solar Still for Different Types of Liquid. In this experiment, four types of saline liquids are used for desalination in the octagonal-pyramid solar still. The four liquids are underground borewell water, sea water, leather industry effluent, and plastic industry effluent. The desalination productivity of four liquids is given in Figure 8. The still shows higher desalination productivity for underground borewell water than other liquids. It is because of low density and low salinity in underground borewell water.

Table 1: Chemical examination of saline water and desalinated water.

Sl. No.	Chemical examination	Permissible limit	Bore water	Desalinated bore water	Sea water	Desalinated sea water	Leather industrial waste	Desalinated leather industrial waste	Plastic industrial waste	Desalinated plastic industrial waste
1	Turbidity (NT units)	5	1	1	2	1	160	3	240	1
2	Total dissolved solids (mg/L)	2000	320	675	33250	1680	5530	1960	23100	1820
3	pH	6.5-8.5	8.1	6.6	7.8	7.4	7.6	7.1	6.8	7.4
4	Total alkalinity as $CaCo_3$ (mg/L)	600	335	100	280	125	800	190	1200	410
5	Total hardness as $CaCo_3$ (mg/L)	600	460	150	8600	320	1300	320	5200	580
6	Calcium as Ca (mg/L)	200	96	32	480	72	420	72	400	120
7	Magnesium as Mg (mg/L)	100	53	16	1776	34	144	34	1008	67
8	Sodium as Na (mg/L)	—	220	130	6500	380	890	520	4600	320
9	Potassium as K (mg/L)	—	16	8	430	24	16	8	240	24
10	Iron as Fe (mg/L)	0.3	0	0	0.2	0	14.0	0.2	22	0
11	Free ammonia as NH_3 (mg/L)	0.5	0	0	0	0	6.8	0	11.9	0.16
12	Nitrite as NO_3 (mg/L)	45	5	0	15	0	30	6	25	12
13	Chloride as CL (mg/L)	1000	380	230	15500	680	2300	820	9400	580
14	Fluoride as F (mg/L)	1.5	0.8	0.2	1.6	0.4	1.6	0.8	1.8	1.0
15	Sulphate as SO_4 (mg/L)	400	40	25	1450	35	145	85	685	60
16	Phosphate as PO_4 (mg/L)	—	0	0	0	0	2.0	0.8	4.0	0.6
17	Tidy's test 4 hrs. as O_2 (mg/L)	—	0.64	0.52	1.12	0.60	1.04	0.51	1.64	0.72

Table 2: Economic analysis and payback period of the still.

Sl. No.	Fabrication cost	Maintenance cost/day	Cost of distilled water	Cost of water produced/day	Net profit/day = cost of water produced − maintenance cost	Payback period
Octagonal-pyramid solar still (cost in rupees)	4,000	0.5	15	15	14.5	40000/14.5 = 276 days

3.7. Chemical Examination. The four types of saline water are tested in the laboratory of Tamil Nadu Water Supply and Drainage board Sivagangai, Tamil Nadu, India. The laboratory results of four types of saline water and their desalinated types are shown in Table 1. The chemical examination of desalinated water shows that it can be used for domestic purpose.

3.8. Economic Analysis. The octagonal-pyramid solar still's economic analysis is calculated and tabulated in Table 2. The payback period of the octagonal-pyramid solar still can be calculated using the fabrication and maintenance cost of the still. The payback period of the octagonal-pyramid solar still has 276 days [27–29].

4. Conclusion

Successful functioning of the octagonal-pyramid solar still has been demonstrated by subjecting it to a series of experimental tests. The performance of the octagonal-pyramid solar still is experimentally compared with a conventional single-slope solar still. The results of experiments showed that the productivity in case of the octagonal-pyramid solar still has increased more than twice than that of the conventional still. The optimum values for maximum productivity are obtained when

(i) the depth of water inside the basin $h = 5\,\text{cm}$

(ii) angle of inclination of glass cover $\theta = 30^{\circ}$

The novel developed solar still also showed better efficiency when coupled with latent heat and sensible heat material, viz., paraffin wax and brick. The comparative analysis showed an increased the productivity of 9.18% by adding a brick. The experimental results also showed that the still is suitable for the desalination of different types of liquid, viz., underground borewell water, sea water, leather industry waste liquid, and plastic industry waste liquid. Among these liquids, the best efficiency is obtained for underground borewell water due to low density.

Data Availability

The data used to support the findings of this study are included within the article. Further data or information is available from the corresponding author upon request.

Conflicts of Interest

The authors declare that there is no conflict of interest regarding the publication of this article.

Acknowledgments

The authors appreciate the supports from Ambo University, Ethiopia, for providing help during the research and preparation of the manuscript. The authors thank Sri Eshwar College of Engineering, Anna University, and Chandigarh University for providing assistance in completing this work.

References

[1] M. Abu-Arabi, Y. Zurigat, H. Al-Hinaib, and S. Al-Hiddabib, "Modeling and performance analysis of a solar desalination unit with double- glass cover cooling," *Desalination*, vol. 143, no. 2, pp. 173–182, 2002.

[2] T. Elango, A. Kannan, and K. KalidasaMurugavel, "Performance study on single basin single slope solar still with different water nanofluids," *Desalination*, vol. 360, pp. 45–51, 2015.

[3] A. M. El-Zahaby, A. E. Kabeel, A. I. Bakry, S. A. El-agouz, and O. M. Hawam, "Augmentation of solar still performance using flash evaporation," *Desalination*, vol. 257, no. 1-3, pp. 58–65, 2010.

[4] R. S. Hansen, C. S. Narayanan, and K. K. Murugavel, "Performance analysis on inclined solar still with different new wick materials and wire mesh," *Desalination*, vol. 358, pp. 1–8, 2015.

[5] M. Balu, K. Lingadurai, P. Shanmugam, K. Raja, N. Bhanu Teja, and V. Vijayan, "Biodiesel production from Caulerpa racemosa (macroalgae) oil," *IJMS*, vol. 49, no. 4, pp. 616–621, 2020.

[6] A. Hanson, W. Zachritz, K. Stevens, L. Mimbela, R. Polka, and L. Cisneros, "Distillate water quality of a single-basin solar still: laboratory and field studies," *Solar Energy*, vol. 76, no. 5, pp. 635–645, 2004.

[7] J. Ganeshkumar, D. Kathirkaman, K. Raja, V. Kumaresan, and R. Velraj, "Experimental study on density, thermal conductivity, specific heat, and viscosity of water-ethylene glycol mixture dispersed with carbon nanotubes," *Thermal Science*, vol. 21, no. 1 Part A, pp. 255–265, 2017.

[8] T. Balasundaram and K. Raja, "Development and morphology of titanium nanotubes anode for new generation solar cell by electrochemical anodizing method," *Journal of Scientific and Industrial Research*, vol. 75, pp. 315–319, 2016.

[9] A. E. Kabeel, Z. M. Omara, and F. A. Essa, "Enhancement of modified solar still integrated with external condenser using nanofluids: an experimental approach," *Energy Conversion and Management*, vol. 78, pp. 493–498, 2014.

[10] K. Raja, V. Srinivasa Raman, R. Parthasarathi, K. Ranjitkumar, and V. Mohanavel, "Performance analysis of DEE-biodiesel blends in diesel engine," *International Journal of Ambient Energy*, vol. 43, no. 1, pp. 1016–1020, 2019.

[11] C. Tiris, M. Tiris, Y. Erdalli, and M. Sohmen, "Experimental studies on a solar still coupled with a flat-plate collector and a single basin still," *Energy Conversion and Management*, vol. 39, pp. 853–856, 1998.

[12] T. Balasundaram and K. Raja, "Growth and characterization of titanium nanotubes anode for solar cell application by electrochemical anodization method," *International Journal of Advanced Engineering Technology*, vol. 7, no. 2, pp. 359–363, 2016.

[13] A. Senthil Rajan, K. Raja, and P. Mari Muthu, "Augmentation of single basin and pyramid still desalination using common biomass heat source and analytical validation using RSM," *Australian Journal of Basic and Applied Sciences*, vol. 8, no. 10, pp. 212–218, 2014.

[14] A. E. Kabeel, Z. M. Omara, and F. A. Essa, "Improving the performance of solar still by using nanofluids and providing vacuum," *Energy Conversion and Management*, vol. 86, pp. 268–274, 2014.

[15] K. Kalidasa Murugavel and K. Srithar, "Performance study on basin type double slope solar still with different wick materials and minimum mass of water," *Renewable Energy*, vol. 36, no. 2, pp. 612–620, 2011.

[16] K. Vikas, "Evaluation of machining performance and multi criteria optimization of novel metal-Nimonic 80A using EDM," *SN Applied Sciences*, vol. 3, no. 3, pp. 1–10, 2021.

[17] A. Pratap, B. K. Singh, and N. Sardana, "Fracture in self-lubricating inserts: a case study," *Materials Today: Proceedings*, vol. 66, pp. 3738–3742, 2022.

[18] A. Pratap, P. Kumar, N. Mandal, and B. K. Singh, "Effect of indentation load on mechanical properties and evaluation of tribological properties for zirconia toughened alumina," *Materials Today: Proceedings*, vol. 26, pp. 2442–2446, 2020.

[19] M. A. S. Malik, G. N. Tiwari, A. Kumar, and M. S. Sodha, *Solar Distillation*, Pergamon Press, Oxford, 1982.

[20] S. M. A. Moustafa, G. H. Brusewitz, and D. M. Farmer, "Direct use of solar energy for water desalination," *Solar Energy*, vol. 22, no. 2, pp. 141–148, 1979.

[21] A. Senthil Rajan, K. Raja, and P. Marimuthu, "Increasing the productivity of pyramid solar still augmented with biomass heat source and analytical validation using RSM," *Desalination and Water Treatment*, vol. 57, no. 10, pp. 4406–4419, 2014.

[22] Z. M. Omara, A. E. Kabeel, and M. M. Younes, "Enhancing the stepped solar still performance using internal and external reflectors," *Energy Conversion Management*, vol. 78, pp. 876–881, 2014.

[23] A. Senthil Rajan, K. Raja, and P. Marimuthu, "Multi basin desalination using biomass heat source and analytical validation using RSM," *Energy Conversion and Management*, vol. 87, pp. 359–366, 2014.

[24] M. Lokeshwari, P. V. Sagar, K. D. Kumar et al., "Optimization and tribological properties of hybridized palm kernel shell ash and nano boron nitride reinforced aluminium matrix composites," *Journal of Nanomaterials*, vol. 2022, Article ID 8479012, 9 pages, 2022.

[25] N. Bhanu Teja, P. Ganeshan, V. Mohanavel et al., "Performance and emission analysis of watermelon seed oil methyl ester and n-butanol blends fueled diesel engine," *Mathematical Problems in Engineering*, vol. 2022, Article ID 2456338, 12 pages, 2022.

[26] N. Mohanraj, N. Mathan Kumar, P. Prathap et al., "Mechanical properties and electrical resistivity of the friction stir spot-welded dissimilar Al–Cu joints," *International Journal of Polymer Science*, vol. 2022, Article ID 4130440, 7 pages, 2022.

[27] V. Velmurugan, S. SenthilKumaran, V. NiranjanPrabhu, and K. Srithar, "Productivity enhancement of stepped solar still – performance analysis," *Thermal Science*, vol. 12, no. 3, pp. 153–163, 2008.

[28] M. K. Patan, K. Raja, M. Azaharahmed, C. D. Prasad, and P. Ganeshan, "Influence of primary regulation on frequency control of an isolated microgrid equipped with crow search algorithm tuned classical controllers," *Journal of Electrical Engineering & Technology*, vol. 16, no. 2, pp. 681–695, 2021.

[29] M. Azaharahmed, K. Raja, M. K. Patan, C. D. Prasad, and P. Ganeshan, "Invasive weed optimized area centralized 2 degree of freedom combined PID controller scheme for automatic generation control," *Journal of Electrical Engineering & Technology*, vol. 16, no. 1, pp. 31–42, 2021.

Hindawi
International Journal of Photoenergy
Volume 2022, Article ID 4493116, 9 pages
https://doi.org/10.1155/2022/4493116

Research Article

Machine Learning Strategy to Achieve Maximum Energy Harvesting and Monitoring Method for Solar Photovoltaic Panel Applications

Bibhu Prasad Ganthia,[1] Sudheer Hanumanthakari,[2] Hemachandra Gudimindla,[3] Harishchander Anandaram,[4] M. Siva Ramkumar,[5] Monalisa Mohanty,[6] S. Raja Gopal,[7] Atul Sarojwal,[8] and Kibrom Menasbo Hadish[9]

[1]*Department of Electrical Engineering, Indira Gandhi Institute of Technology, Sarang, Dhenkanal, Odisha 759146, India*
[2]*Department of Electronics and Communication Engineering, Faculty of Science and Technology, ICFAI Foundation for Higher Education, Hyderabad, Telangana 500029, India*
[3]*Department of Electrical and Electronics Engineering, M S Ramaiah Institute of Technology, Bengaluru, Karnataka 560054, India*
[4]*Centre for Computational Engineering and Networking, Amrita School of Engineering, Amrita Vishwa Vidyapeetham, Coimbatore, Tamil Nadu 641112, India*
[5]*Department of Electrical and Electronics Engineering, Faculty of Engineering, Karpagam Academy of Higher Education, Coimbatore, Tamil Nadu 641021, India*
[6]*Department of Electrical and Electronics Engineering, Siksha 'O' Anusandhan D University, Bhubaneswar, Odisha 751030, India*
[7]*Department of Electronics & Communications Engineering, Koneru Lakshmaiah Education Foundation, Vaddeswaram, Andhra Pradesh 522502, India*
[8]*Department of Electrical Engineering, FET, Mahatma Jyotiba Phule Rohilkhand University, Bareilly, Uttar Pradesh 243006, India*
[9]*Faculty of Mechanical Engineering, Arba Minch University, Arba Minch, Ethiopia*

Correspondence should be addressed to Kibrom Menasbo Hadish; kibrom.menasbo@amu.edu.et

Received 4 June 2022; Revised 2 September 2022; Accepted 7 September 2022; Published 14 October 2022

Academic Editor: Br Ramesh Bapu

The choice of the optimal orientation of the solar panels is by far one of the most important issues in the practical application of solar installations. The use of phase changing materials (PCMs) is an efficient approach of storing solar thermal energy. Because PCMs are isothermal in nature, they provide better density energy storage and the capacity to function across a wide temperature range. Unfortunately, this feature is very rare on various solar power panels; however, ignoring it can reduce the performance of the panels to unacceptable levels. The fact is that the angle of incidence of rays on the surface greatly affects the reflection coefficient and, consequently, the role of unacceptable solar energy. In this paper, a smart energy harvesting model was proposed. In the case of glass, when the angle of incidence varies vertically from its surface to 30, the reflection coefficient is practically unchanged and slightly less than 5%, i.e., more than 95% of the radiation goes inwards. Furthermore, the reflection increase is noticeable, and the area of the reflected radiation by 60 doubles to almost 10%. At an angle of incidence of 70, it reflects 20% of the radiation, and at 80, 40%. For most other objects, the dependence of the reflection magnitude on the angle of incidence is approximately the same.

1. Introduction

Even more important is the so-called effective group area, viz. The intersection of the radiation flow was thereby blocked. This is equal to the actual area of the panel multiplied by the sine of the angle between its plane and the direction of flow (or, equally, perpendicular to the panel and by the cosine of the angle between the direction of flow) [1].

Therefore, if the panel is perpendicular to the flow, its effective area is equal to its actual area, the flow becomes 60% from the vertical—half of the actual area, and if the flow is parallel to the panel, its performance area is zero [2]. Thus, the significant deviation of the flow from the perpendicular to the panel increases the reflection, but reduces its effective area, which causes a more significant drop in output [3–5]. For our purposes, it is obvious that the fixed orientation of the panel perpendicular to the flow of sunlight is the most effective [6]. But this requires changing the position of the panel in two planes, because the position of the sun in the sky depends not only on the time of day but also on the season. Although such a system is certainly technically feasible, it turns out to be very complex, so expensive, and not very reliable [7–9]. Remember that there are many sources of renewable energy. By far, solar and wind are the most efficient, in general shown in Figure 1.

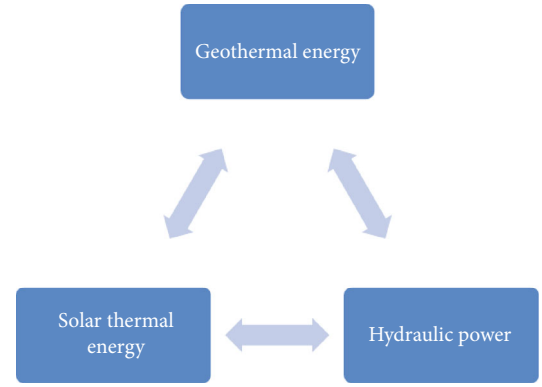

Figure 1: Important resources of renewable energy.

(i) Geothermal energy depends on the location of the tectonic plate on which it is located. Its main use is water heating for residential buildings and hospitals

(ii) On the other hand, we see hydraulic power. Hydraulic power is powered by the falls of the reservoirs. In Spain, due to drought, the amount of hydraulic energy produced is limited

(iii) As for solar thermal energy, the same happens with geothermal energy

However, at angles of occurrence up to 30, keep in mind that the reflection coefficient at the "air-glass" boundary is low and practically unchanged, and the angle of maximum sunrise above the horizon during the year deviates from the mean, not more than ±23. The effective area of the panel with a 23° deviation from the vertical is also very large—at least 92% of its actual area [10–12]. Therefore, one can focus on the average annual height of the maximum rise of the sun and rotate only in one plane, without losing efficiency in practice—at a speed of 1 revolution per day on the polar axis of the earth [13]. The angle of inclination of the axis of such rotation relative to the horizontal is equal to the geographic latitude of the space. For example, for solar panel, located at latitude of 56, the axis of such rotation must be inclined 56° northward (or, equally, deviate by 34% from the vertical) [14]. Such rotation is already very easy to organize, however, and requires a lot of space for a large group to rotate freely. In addition, it is necessary to arrange a sliding connection that allows you to divert all the energy received from the constantly rotating panel or restrict yourself to flexible communications with a fixed connection, but make sure that the panel returns automatically at night; otherwise, the deenergizing communication can be avoided by twisting and breaking [15–18]. Both solutions dramatically increase the problem and reduce the reliability of the system. As the power of the panels (hence their size and weight) increases, the technical issues become exponentially more complex [19]. Even if you just want to put up a few solar panels to save on electricity bills, investing in renewable energy is not cheap. Usually, the money invested pays for itself in the long run. The only positive aspect of renewable energies is that the price of photovoltaic panels has been reduced this year, as it was practically impossible to access them.

In connection with all of the above, the panels of individual solar installations are always mounted seamlessly, which ensures comparative affordability and high reliability of installation. However, here the choice of the angle of the panel space is especially important [20]. If the batteries are installed practically free of natural dust or washed in a timely manner by natural rain, they can work for many years without any maintenance. Another big advantage is the possibility of such a long operation in unattended mode [21]. The solar panels are capable of generating energy even in cloudy weather from dawn to dusk, while thermal solar collectors have slightly different temperatures from ambient temperatures [22]. Of course, compared to a clear sunny day, their productivity decreases many times over, but at least nothing is better than anything! In this regard, it is of particular interest to develop batteries with maximum energy transfer within the minimum solar absorption limits of the clouds [23–25]. In addition, when choosing solar photo converters, one should pay attention to the dependence of the voltage generated by them on the light—it should be as small as possible (when the light decreases, the current should fall first, not the voltage; otherwise at least some useful effect on cloudy days to obtain, expensive additional equipment must be used which forcibly increases the voltage sufficient to charge the batteries and operate the inverters).

2. Literature Review

The most important of the broad and ubiquitous barriers of energy harvesting solar photovoltaic solar panels is their high cost. Solar battery components are currently priced at a minimum amount and are subject to inefficient modifications regardless of the cost of assembling and installing the panels, as well as the cost [1]. The batteries charge controllers and inverters (converting manufactured low-voltage DC current to household or industrial standard). In most cases, for a minimum estimate of the actual cost, these should be multiplied by 3-5 times for self-assembly from

individual photocells and 6-10 times for the purchase of ready-made equipment (plus installation cost) [2]. Every time we have less time. Fossil fuels are reaching their limits which present new demands. We have to think about how severe effects like climate change on a global scale are affected by the cost of excess pollution. This pollution can be reduced if renewable energies are further improved and developed.

The batteries in all components of the PV power supply system have a very short lifespan, but manufacturers of modern nonmaintenance batteries call the buffer mode a discharge of about 10 years (or traditional 1000 cycles working on a strong charge—if you count one cycle per year, in this mode they will last 3 years) [3]. It noticed that the cost of batteries is usually only 10-20% of the total cost of the whole system, and the cost of inverters and charge controllers (both are complex electronics, so there is some probability of their failure) too less. Therefore, taking into account the long service life and the ability to work long hours without maintenance, photo converters can pay more than once in their lives, not only in remote areas, but also in populated areas—continuing to grow at current rates [5]. It is the energy that interferes with the different caloric processes that occur when bodies of different temperatures come into contact. As long as the bodies maintain a friction between them, this energy spreads from one body to another. This is what happens when we place a hand on a surface. The gain or loss of this internal energy during operation is called heat. Thermal energy is derived from a variety of sources. Therefore, there is an internal energy inside everybody that has a certain temperature [6]. Alternative energy is considered capable of generating energy without polluting the environment. Additionally, it can be more efficient if it uses natural energy or waste (like biomass), solar, wind, hydroelectric, wave, geothermal, tidal energy, and others. However, they are not the only alternative energy sources that we can find in the world. In nature, there are sources of energy that we know or are accustomed to exploit. Figure 2 shows photovoltaic solar power generation.

It must think that energy is not created or destroyed, but is transformed. Thermal energy is generated in many ways. It is created by the motion of atoms and molecules of matter like a form of kinetic energy produced by random motions. When there is a large amount of thermal energy in a system, its atoms move faster [10]. Receiving thermal energy causes environmental damage to release carbon dioxide and radioactive waste. It is a kind of renewable energy that does not pollute or damage the environment [24]. Thermal energy can be converted into electrical energy. For example, fossil fuels generate electricity by burning and releasing. Electrical energy is supplied as a result of the potential difference between the two points and allows an electric current to be generated between the two when in contact with an electrical conductor [25, 26]. Thermal energy is a type of energy that is released in the form of heat, which can be obtained by contacting another body with high temperature at low temperature, as well as by different conditions or mechanisms as mentioned earlier [27, 28].

3. Proposed Model

Figure 3 shows the proposed model block. The proposed maximum energy harvesting and monitoring model consists of 4 different levels: level A—when observing the position of the sun around the polar axis (i.e., parallel to the earth's axis); level B—fixed horizontal panel; level C—a fixed vertical panel, facing south; level D—a fixed group sloping south at an angle of 40 to the horizon. The Helioculture is an alternative form of energy. This energy is achieved by creating a hydrocarbon fuel. This is achieved by mixing salt water, photosynthetic organisms, nutrients, carbon dioxide, and sunlight. After mixing all this, the result is a fuel that does not need to be directly refined. The natural process of photosynthesis is used to produce ready-to-use fuels [27]. Let us look at the insulation levels for different panel installation angles. Of course, the spinning team after the sun is out of competition (level A). However, even on long summer days, its efficiency is only about 30% higher than the performance of standard horizontal (level B) and optimally inclined (level C) panels. But there is enough heat and light these days! But during the period of the most energy shortage from October to February, the benefit of the rotary panel over the fixed ones is very small and almost incomprehensible. True, at this point, the organization of the oblique group is not a horizontal one, but a vertical group (level D). This is not surprising—the low rays of the winter sun glide along the horizontal panel, but they are well perceived almost vertically.

The output power is calculated using Kirchhoff's rules, as said in

$$A_a = A_b - A_c\{\exp\left[B(C_a + C_bD_s) - 1\right]\} - \frac{C_a + C_bD_s}{D_s}, \quad (1)$$

$$A = \frac{b}{\alpha * \text{solar power resistance}}, \quad (2)$$

where A_a is the output solar power, A_b is the parallel solar panel link, A_c is the serial solar panel link, and D_s is the serial power resistance.

Therefore, the vertical panel exceeds even the oblique one in its performance and is almost indistinguishable from the rotary one. In March and October, the days are longer, and the rotary panel is already confidently (if not more) starting to perform better than any standard options, but the performance of the sloping and vertical panels is almost identical. Only on long days from April to August, the horizontal panel is more forward than the vertical one and approaches the oblique and slightly higher than that in June, based on the energy obtained. Summer loss of the vertical panel is natural—after all, the day of the summer solstice lasts more than 17 hours, and the sun cannot be more than 12 in the front (working) hemisphere of the vertical panel. At angles of incidence greater than 60, the rate of light reflected from the surface of the panel begins to grow rapidly, and considering that its effective area is reduced by half or more, the effective absorption time for such a panel is no more than 8 hours—i.e., less than 50% of the total length of

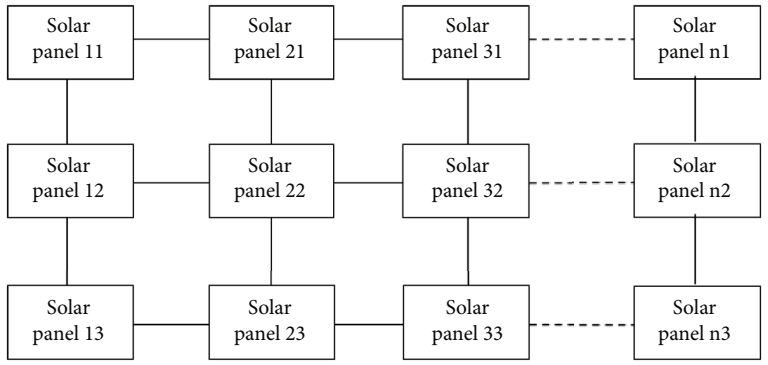

Figure 2: Photovoltaic solar power generation.

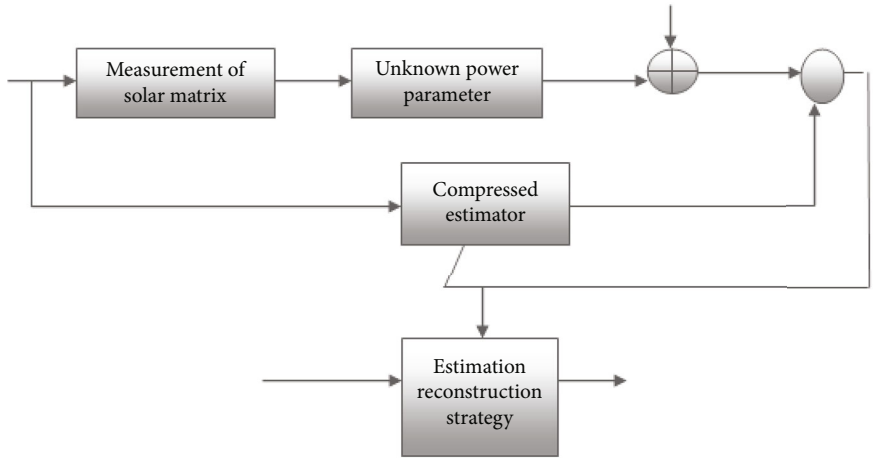

Figure 3: Proposed model block.

the day. The more people we have in the world, the more movements there are on a daily basis. We are continuously more than 7.500 million people. We can harness these human movements and displacements to generate energy. Piezoelectricity is the ability of some materials to generate a type of electric field in response to some mechanical stress [27].

The differences in light-generated solar powerA_a are needy on the experiential and referenced irradiance level parameters as chosen to follow

$$A_a = \left[A_C + R_a(f - f_{\text{ref}})\frac{\mu}{\mu_{\text{ref}}}\right]. \tag{3}$$

It all depends on when you need solar energy. If you want to use it only in hot weather (if, in the country), you should choose the "optimal" inclination angle, which is perpendicular to the average level of the sun between spring and autumn sunrises. It is approximately 10° to 15° lower than the geographical latitude and 40° to 45. If you need energy throughout the year, you should "squeeze" as much as possible during the energy-deficient winter months, which means you should focus on the average level of sun between autumn and spring sunrises and place the panels. Vertically close -5° to 15° higher than the geographical latitude (for solar panel it is 60° to 70°). If the tiles are constructed of materials with piezoelectric properties, they can be attached to heavily traveled paths. This way, we can generate force while walking with the sole friction of the shoes.

Figure 4 shows the proposed maximum energys harvesting and monitoring schematic. The current is flowing in the diode A_c described by the Shockley equations, as shown in formula (3), where A_c indicates the saturation current and is represented by

$$A_a = A_c\left(\frac{f}{f_{\text{ref}}}\right)^3 \exp\left(\frac{sR_G}{d\beta}\left[\frac{1}{f} - \frac{1}{f_{\text{ref}}}\right]\right). \tag{4}$$

This explains the fact that the performance of the vertical panels is stabilized throughout the long days—from March to September. Finally, January is a bit off—this month; the performance of panels of all orientations will be almost identical. The truth is this month in solar panel is very cloudy, and more than 90% of all solar energy comes from scattered radiation, and for such radiation, the orientation of the panel is not so important (the main thing is not to send it to the ground). However, some sunny days, which still occur in

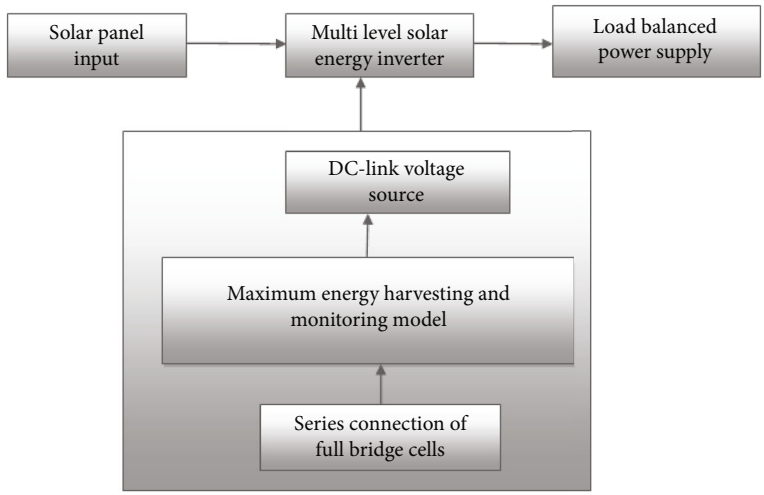

Figure 4: Proposed maximum energy harvesting and monitoring.

January, reduce the output of the horizontal panel by 20% compared to the rest and shown in

$$A_{\mathrm{PV}} = \frac{R_a}{ASD \times \beta_a \times \beta_b}. \quad (5)$$

If, for architectural or structural reasons, this angle cannot be maintained and a slope angle of 40° or less is required to choose between, the vertical position should be preferred. At the same time, the "shortage" of energy during the long summer days is not so significant—there is a lot of natural heat and light during this period, and the need for energy production is usually not as great as winter and winter. This type of energy is a little better known. It is about harnessing energy from hot rocks. It is geothermal energy that is extracted by pumping salt and cold water towards rocks that have high temperatures due to the contribution of heat from the earth's mantle. When water is heated, the steam generated in the process is used to generate electricity in a steam turbine. One advantage of this type of energy is that it can be completely controlled [27]. Naturally, the slope of the panel should be south, although turning 10° to 15° east or west in this direction is slightly different, so this is more acceptable. In addition to the drastic reduction in energy production during the fall-winter period, dust accumulates rapidly on the horizontal panels, and even snow accumulates in the winter, and they can only be removed with the help of specially organized cleaning. If the slope of the panel is greater than 60, the snow does not last on its surface and usually collapses quickly, and the thin layer of dust is well washed away by rain.

4. Results and Discussion

In general, "solar battery" can be understood as identical modules that sense solar radiation and are fully integrated into a single device, including heating devices, but traditionally the term is assigned to panels of energy harvesting solar photovoltaic converters. Therefore, "solar battery" refers to energy harvesting solar photovoltaic device that always converts solar radiation directly into electricity. This technology has been actively developed since the middle of the 20th century. A major impetus for its development was space exploration, where only small-scale nuclear sources could currently compete with solar cells in power generation and duration of operation. During this time, the conversion efficiency of solar cells increased from one or two percent to 17% or more mass in relatively inexpensive models and over 42% in prototypes. Significantly, it increased the service life and reliability. The annual solar power fabrication and utilizations are shown in Table 1.

The main advantage of solar panels is their extreme design simplicity and the complete absence of moving parts. The result is a combination of a small specific weight and high reliability, as well as minimal maintenance requirements during simple installation and operation (usually it is sufficient to remove dirt from the accumulated work surface). This refers to flat elements of small thickness, which are most successfully placed on the slope of the roof facing the sun or on the wall of the house, practically do not require extra space for themselves and build individual bulky structures. The only condition is that nothing should obscure them as much as possible. The sun not only illuminates us within the earth but also illuminates it outside. Outside of earth, solar panels are not affected by day and night cycles. They are not affected by climate or the filters created by clouds or atmospheric gases. The idea is to create solar panels capable of orbiting the earth to continuously harvest solar energy. Table 2 shows annual power loss of solar electrical system.

Calorific value of a gas is the amount of energy released per unit mass or volume upon complete oxidation. This oxidation is not known for iron. This is very common when asking some chemists to think about oxidation. Oxidation is a concept that refers to the loss of electrons from a substance. When this happens, its positive charge increases and it is said to oxidize. This mentioned oxidation takes place in the combustion process. The efficiency of energy harvesting solar photovoltaic converters decreases during their service life. Semiconductor scales, in which solar cells

Table 1: Annual solar power fabrication and utilization.

Production	kWh/ year	Percentage (%)	Consumption	kWh/ year	Percentage (%)
Energy harvesting solar photovoltaic solar system	1882	90%	Demand of AC prime solar panel	488	90%
Overall harvesting	1986	96%	All other solar panels	468	96%

Table 2: Annual power loss of solar electrical system.

Measure	Converter	Rectifier	Component units
Working duration in hours	8457	0	h/annum
Input solar power	547	0	h/annum
Output solar power	482	0	h/annum
Operational solar power loss	54	0	h/annum

are normally formed, degrade and lose their properties over time, resulting in even lower efficiency of already nonexistent solar cells. Prolonged exposure to high temperatures accelerates this process. The proposed maximum energy harvesting and monitoring model (MEHMM) was compared with the existing optimized fuzzy logic control (OFLC), fuzzy logic control of standalone energy harvesting solar photovoltaic system (FLCSP), an improved fuzzy logic controller design (IFLCD), and fuzzy probabilistic-based semi-Markov model (FPSMM).

4.1. Energy Harvesting Solar Photovoltaic Cells. First, it was mentioned that this is a shortcoming of energy harvesting solar photovoltaic batteries; especially those that cannot recover "dead" energy harvesting solar photovoltaic cells are shown in Table 3. However, it is unlikely that any mechanical power generator will be able to demonstrate at least 1% efficiency after 10 years of continuous operation—often due to mechanical wear and, if not the bearings, requiring drastic repairs due to the brushes. And modern photo converters can maintain their performance for decades. According to reliable estimates, in 25 years, the efficiency of the solar battery will be reduced by only 10%, which means that after 100 years almost 2/3 of the original performance will remain if other factors do not intervene.

However, for mass commercial energy harvesting solar photovoltaic cells based on poly- and single-crystal silicon, honest manufacturers and sellers give slightly different aging after 20 years; 20% performance loss is to be expected (then, in theory, after 40 years, performance will initially be 2/3, halved in 60 years, and less than 1/3 of original productivity in 100 years). In general, the normal service life of modern photo converters is at least 25 to 30 years, so degradation is not so important and it is very important to wash the dust from them in a timely manner.

4.2. Performance. The same solar collector, with the right choice of shape and surface material, is capable of absorbing all the solar radiation that falls on it at almost full frequency. Solar cells, on the other hand, selectively convert energy—to stimulate the work of atoms, some photon energies (radiation frequencies) are required so that, at some frequency bands, the transition is very efficient, while at other frequency bands they are ineffective. In addition, the energy of the photons captured by them is used as a scale—its "surplus" exceeds the required level and in this case the harmful photo converter goes to the heat of matter. In many ways, this explains their low efficiency displayed in Table 4.

By the way, choosing the wrong material for the protective coating will significantly reduce the efficiency of the battery. Ordinary glass makes things worse by absorbing the high-energy UV of the range well, and this range is very suitable for certain types of photocells—the energy of the infrared photons is very small for them.

4.3. Sensitivity to High Temperatures. With increasing temperature, the efficiency of solar cells decreases like all other semiconductor devices. At temperatures above 100 to 125°C, they usually temporarily lose their ability to work, and high temperatures threaten them with irreversible damage. In addition, high temperatures accelerate the decay of solar cells shown in Table 5.

Therefore, it is necessary to take all measures to reduce the unavoidable heat under burning direct sunlight. In general, manufacturers limit the nominal operating temperature range of photocells to +70° to +90°C (i.e., heating the cells, and the ambient temperature, of course, must be very low).

4.4. Sensitivity to Random Light. As a rule, photocells are connected in series chains to obtain a battery voltage that is more or less convenient for use (12, 24, or more volts). The current in each such chain, and therefore its power, is determined by the weak connection—a photocell with poor properties or low brightness is shown in Table 6.

Therefore, if at least one element of the chain is in the shade, it significantly reduces the output of the entire chain—the losses are not compatible with the shade (and, in the absence of protective diodes, such an element will begin to scatter power). Unbalanced reduction in output can be avoided only by connecting all the photocells in parallel; however, the battery output will have a higher current at a much lower voltage—typically 0.5 to0.7 V for individual photocells of type and loading.

4.5. Sensitivity to Pollution. Even a delicate layer of dirt on the surface of energy harvesting solar photovoltaic cells or protective glass can absorb a significant amount of sunlight and significantly reduce energy production. In a dusty city,

Table 3: Energy harvesting solar photovoltaic cells.

No. of inputs	OFLC	FLCSP	IFLCD	FPSMM	MEHMM
100	72.93	64.31	69.15	93.49	93.41
200	74.23	65.31	69.85	94.36	93.52
300	75.53	66.31	70.55	95.23	93.63
400	76.83	67.31	71.25	96.10	93.74
500	78.13	68.31	71.95	96.97	93.85
600	79.43	69.31	72.65	97.84	93.96
700	80.73	70.31	73.35	98.71	94.07

Table 4: Performance of solar photovoltaic cells.

No. of inputs	OFLC	FLCSP	IFLCD	FPSMM	MEHMM
100	70.03	61.99	65.69	90.33	91.64
200	71.17	62.37	66.90	91.24	92.60
300	72.22	63.38	68.04	92.16	92.17
400	73.33	63.97	69.23	93.07	92.67
500	74.43	64.67	70.40	93.99	92.93
600	75.52	65.36	71.58	94.90	93.20
700	76.62	66.06	72.75	95.82	93.46

Table 5: Sensitivity to high temperature.

No. of inputs	OFLC	FLCSP	IFLCD	FPSMM	MEHMM
100	68.36	59.38	64.12	87.63	90.47
200	68.69	60.88	64.71	89.50	91.51
300	69.02	62.38	65.30	91.37	92.55
400	69.35	63.88	65.89	93.24	93.59
500	69.68	65.38	66.48	95.11	94.63
600	70.01	66.88	67.07	96.98	95.67
700	70.34	68.38	67.66	98.85	96.71

Table 6: Sensitivity to random light.

No. of inputs	OFLC	FLCSP	IFLCD	FPSMM	MEHMM
100	55.20	58.88	50.37	71.75	90.43
200	54.49	57.95	49.26	70.42	89.23
300	53.19	56.95	48.56	69.55	89.08
400	52.28	56.00	47.59	68.37	88.23
500	51.28	55.03	46.68	67.27	87.56
600	50.27	54.07	45.78	66.17	86.88
700	49.27	53.10	44.87	65.07	86.21

this requires frequent cleaning of the surface of the solar panels, especially those fitted horizontally or at a slight incline. Of course, the same procedure is necessary after every snowstorm and after a dust storm. The sensitivity in pollution is shown in Table 7.

Table 7: Sensitivity to pollution.

No. of inputs	OFLC	FLCSP	IFLCD	FPSMM	MEHMM
100	57.39	60.27	52.72	73.58	90.96
200	56.25	59.89	51.51	72.67	90.00
300	55.11	59.51	50.30	71.76	89.04
400	53.97	59.13	49.09	70.85	88.08
500	52.83	58.75	47.88	69.94	87.12
600	51.69	58.37	46.67	69.03	86.16
700	50.55	57.99	45.46	68.12	85.20

However, in cities, industrial areas, busy roads, and other strong sources of dust at an angle of 45° or more, it will rain. It has the ability to wash natural dust off the surface of the panels, "automatically" keeping them very clean. The snow on such a slope, and moreover facing south, usually does not last long even on very frosty days. So away from sources of air pollution, solar panels can work successfully for many years without any maintenance.

4.6. Solar Collectors. The name "solar collectors" is derived from devices that use direct heat from the sun, single and stackable (modular). A simple example of a thermal solar collector is a black water tank on the roof of the aforementioned country shower (which can significantly increase the efficiency of heating the water in the summer rain by building a mini-greenhouse around the tank, at least from a plastic film, being desirable). The performance of the solar collectors is shown in Table 8.

Burning natural gas provides energy to generate electricity, hot water, etc. Therefore, it is important to know what a gas is capable of producing per unit mass or volume in order to determine its quality. The higher the calorific value, the less gas we use. This includes the importance of the quality of a gas in relation to economic costs.

5. Conclusion

As prices for solar equipment have been declining recently, it may be advantageous to use single panels of solar panels instead of a single field with large total capacities of adjacent (southeast and southwest) and opposite (east and west). It will provide more uniform output on sunny days and higher output on cloudy days, while the rest of the equipment will be uniform, designed for relatively low power, so will be more compact and cheaper. The proposed maximum energy harvesting and monitoring model (MEHMM) was compared with the existing optimized fuzzy logic control (OFLC), fuzzy logic control of standalone energy harvesting solar photovoltaic system (FLCSP), an improved fuzzy logic controller design (IFLCD), and fuzzy probabilistic based semi-Markov model (FPSMM). The proposed model was performed an analysis with the surface not smooth, but has a special relief, senses the side light very efficiently and can transmit it to the working elements of the solar panel. The most optimal is north-south (for vertical panels top to bottom), a type of linear lens (for vertical panels) with ripple

Table 8: Performance of solar collectors.

No. of inputs	OFLC	FLCSP	IFLCD	FPSMM	MEHMM
100	59.06	62.88	54.29	76.28	92.13
200	58.73	61.38	53.70	74.41	91.12
300	58.40	59.88	53.11	72.54	90.11
400	58.07	58.38	52.52	70.67	89.10
500	57.74	56.88	51.93	68.80	88.09
600	57.41	55.38	51.34	66.93	87.08
700	57.08	53.88	50.75	65.06	86.07

relief with orientations of protrusions and depressions. Corrugated glass can increase standard panel output by 5% or more.

Data Availability

The data used to support the findings of this study are included within the article. Further data or information is available from the corresponding author upon request.

Conflicts of Interest

The authors declare that there are no conflicts of interest regarding the publication of this paper.

Acknowledgments

The authors appreciate the supports from Arba Minch University, Ethiopia, for the research and preparation of the manuscript. The authors thank the Indira Gandhi Institute of Technology, ICFAI Foundation for Higher Education, M S Ramaiah Institute of Technology, for providing assistance to this work.

References

[1] S. Singh and S. C. Kaushik, "Optimal sizing of grid integrated hybrid PV-biomass energy system using artificial bee colony algorithm," *IET Renewable Power Generation*, vol. 10, no. 5, pp. 642–650, 2016.

[2] B. Roy, A. K. Basu, and S. Paul, "Techno-economic feasibility analysis of a grid connected solar energy harvesting solar photovoltaic power system for a residential load," in *2014 First International Conference on Automation, Control, Energy and Systems (ACES)*, pp. 1–5, India, February 2014.

[3] L. Karikalan, S. Baskar, N. Poyyamozhi, and K. Negash, "Experimental analysis of heat transfer by using nanofluid and impact of thermophysical properties," *Journal of Nanomaterials*, vol. 2022, Article ID 5119797, 8 pages, 2022.

[4] J. Zhou, S. Tsianikas, D. P. Birnie, and D. W. Coit, "Economic and resilience benefit analysis of incorporating battery storage to photovoltaic array generation," *Renewable Energy*, vol. 135, pp. 652–662, 2019.

[5] L. Ortiz, R. Orizondo, A. Águila, J. W. González, G. J. López, and I. Isaac, "Hybrid AC/DC microgrid test system simulation: grid-connected mode," *Heliyon*, vol. 5, no. 12, article e02862, 2019.

[6] M. A. Omar and M. M. Mahmoud, "Design and simulation of a PV system operating in grid-connected and stand- alone modes for areas of daily grid blackouts," *International Journal of Photoenergy*, vol. 2019, Article ID 5216583, 9 pages, 2019.

[7] V. Karthikeyan, S. Rajasekar, V. Das, P. Karuppanan, and A. K. Singh, "Grid-connected and off-grid solar energy harvesting solar photovoltaic system," in *Smart Energy Grid Design for Island Countries*, F. M. R. Islam, K. A. Mamun, and M. T. O. Amanullah, Eds., pp. 125–157, Springer International Publishing, Cham, 2017.

[8] D. Abdoulaye, Z. Koalaga, and F. Zougmore, "Grid-connected photovoltaic (PV) systems with batteries storage as solution to electrical grid outages in Burkina Faso," *IOP Conference Series: Materials Science and Engineering*, vol. 29, article 012015, 2012.

[9] A. A. Alabi, A. U. Adoghe, O. G. Ogunleye, and C. O. A. Awosope, "Development and sizing of a grid-connected solar PV power plant for Canaanland community," *IJAPE*, vol. 8, no. 1, p. 69, 2019.

[10] S. Deshmukh, Y. Baghzouz, and R. F. Boehm, "Design of grid connected-PV system for a hydrogen refueling station," in *International Solar Energy Conference*, pp. 171–175, Denver, Colorado, USA, January 2006.

[11] K. A. Makinde, O. B. Adewuyi, A. O. Amole, and O. A. Adeaga, "Design of grid-connected and stand-alone photovoltaic systems for residential energy usage: a technical analysis," *Journal of Energy Research and Reviews*, vol. 8, pp. 34–50, 2021.

[12] N. Saxena, B. Singh, and A. L. Vyas, "Single-phase solar PV system with battery and exchange of power in grid-connected and standalone modes," *IET Renewable Power Generation*, vol. 11, no. 2, pp. 325–333, 2017.

[13] K.-C. Chang, N. Hagumimana, J. Zheng et al., "Standalone and minigrid-connected solar energy systems for rural application in Rwanda: an in situ study," *International Journal of Photoenergy*, vol. 2021, Article ID 1211953, 22 pages, 2021.

[14] O. Diouri, N. Es-Sbai, F. Errahimi, A. Gaga, and C. Alaoui, "Modeling and design of single-phase PV inverter with MPPT algorithm applied to the boost converter using back-stepping control in standalone mode," *International Journal of Photoenergy*, vol. 2019, Article ID 7021578, 16 pages, 2019.

[15] H. Lan, S. Wen, Q. Fu, D. C. Yu, and L. Zhang, "Modeling analysis and improvement of power loss in microgrid," *Mathematical Problems in Engineering*, vol. 2015, Article ID 493560, 8 pages, 2015.

[16] Y. Chaibi, M. Salhi, and A. El-jouni, "Sliding mode controllers for standalone PV systems: modeling and approach of control," *International Journal of Photoenergy*, vol. 2019, Article ID 5092078, 12 pages, 2019.

[17] R. Syahputra and I. Soesanti, "Planning of hybrid micro-hydro and solar photovoltaic systems for rural areas of central Java, Indonesia," *Journal of Electrical and Computer Engineering*, vol. 2020, Article ID 5972342, 16 pages, 2020.

[18] H. A. Kazem and T. Khatib, "A novel numerical algorithm for optimal sizing of a photovoltaic/wind/diesel generator/battery microgrid using loss of load probability index," *International Journal of Photoenergy*, vol. 2013, Article ID 718596, 8 pages, 2013.

[19] A. M. Eltamaly and M. A. Mohamed, "A novel design and optimization software for autonomous PV/wind/battery hybrid power systems," *Mathematical Problems in Engineering*, vol. 2014, Article ID 637174, 16 pages, 2014.

[20] J. Logeshwaran, M. J. Rex, T. Kiruthiga, and V. A. Rajan, "FPSMM: fuzzy probabilistic based semi Morkov model among the sensor nodes for realtime applications," in *2017 International Conference on Intelligent Sustainable Systems (ICISS)*, pp. 442–446, Palladam, India, 2017.

[21] A. H. Mutlag, H. Shareef, A. Mohamed, M. A. Hannan, and J. A. Ali, "An improved fuzzy logic controller design for PV inverters utilizing differential search optimization," *International Journal of Photoenergy*, vol. 2014, Article ID 469313, 14 pages, 2014.

[22] A. Abusorrah, M. M. al-Hindawi, Y. al-Turki et al., "Stability of a boost converter fed from photovoltaic source," *Solar Energy*, vol. 98, pp. 458–471, 2013.

[23] K. A. Alboaouh and S. Mohagheghi, "Impact of rooftop photovoltaics on the distribution system," *Journal of Renewable Energy*, vol. 2020, Article ID 4831434, 23 pages, 2020.

[24] Y. Sukamongkol, S. Chungpaibulpatana, and W. Ongsakul, "A simulation model for predicting the performance of a solar photovoltaic system with alternating current loads," *Renewable Energy*, vol. 27, no. 2, pp. 237–258, 2002.

[25] S. Lalouni, D. Rekioua, T. Rekioua, and E. Matagne, "Fuzzy logic control of stand-alone photovoltaic system with battery storage," *Journal of Power Sources*, vol. 193, no. 2, pp. 899–907, 2009.

[26] C. Larbes, S. A. Cheikh, T. Obeidi, and A. Zerguerras, "Genetic algorithms optimized fuzzy logic control for the maximum power point tracking in photovoltaic system," *Renewable Energy*, vol. 34, no. 10, pp. 2093–2100, 2009.

[27] https://www.renovablesverdes.com/en/alternative-energies/.

[28] K. Chen, S. Tian, Y. Cheng, and L. Bai, "An improved MPPT controller for photovoltaic system under partial shading condition," *IEEE Transactions on Sustainable Energy*, vol. 5, no. 3, pp. 978–985, 2014.

Hindawi
International Journal of Photoenergy
Volume 2023, Article ID 9763709, 1 page
https://doi.org/10.1155/2023/9763709

Retraction

Retracted: Application of Machine Learning in Multi-Directional Model to Follow Solar Energy Using Photo Sensor Matrix

International Journal of Photoenergy

Received 15 August 2023; Accepted 15 August 2023; Published 16 August 2023

This article has been retracted by Hindawi following an investigation undertaken by the publisher [1]. This investigation has uncovered evidence of one or more of the following indicators of systematic manipulation of the publication process:

(1) Discrepancies in scope

(2) Discrepancies in the description of the research reported

(3) Discrepancies between the availability of data and the research described

(4) Inappropriate citations

(5) Incoherent, meaningless and/or irrelevant content included in the article

(6) Peer-review manipulation

The presence of these indicators undermines our confidence in the integrity of the article's content and we cannot, therefore, vouch for its reliability. Please note that this notice is intended solely to alert readers that the content of this article is unreliable. We have not investigated whether authors were aware of or involved in the systematic manipulation of the publication process.

Wiley and Hindawi regrets that the usual quality checks did not identify these issues before publication and have since put additional measures in place to safeguard research integrity.

We wish to credit our own Research Integrity and Research Publishing teams and anonymous and named external researchers and research integrity experts for contributing to this investigation.

The corresponding author, as the representative of all authors, has been given the opportunity to register their agreement or disagreement to this retraction. We have kept a record of any response received.

References

[1] P. Dhanalakshmi, V. Venkatesh, P. S. Ranjit et al., "Application of Machine Learning in Multi-Directional Model to Follow Solar Energy Using Photo Sensor Matrix," *International Journal of Photoenergy*, vol. 2022, Article ID 5756610, 9 pages, 2022.

Hindawi
International Journal of Photoenergy
Volume 2022, Article ID 5756610, 9 pages
https://doi.org/10.1155/2022/5756610

Research Article

Application of Machine Learning in Multi-Directional Model to Follow Solar Energy Using Photo Sensor Matrix

P. Dhanalakshmi,[1] V. Venkatesh,[2] P. S. Ranjit,[3] N. Hemalatha,[4] S. Divyapriya,[5] R. Sandhiya,[6] Sumit Kushwaha,[7] Asmita Marathe,[8] and Mekete Asmare Huluka[9]

[1]*Department of Computer Science and Systems Engineering, Sree Vidyanikethan Engineering College (SVEC), Tirupati, Andhra Pradesh 517102, India*
[2]*Department of Electrical and Electronics Engineering, Rajalakshmi Engineering College, Chennai, Tamil Nadu 602105, India*
[3]*Department of Mechanical Engineering, Aditya Engineering College, Surampalem, Andhra Pradesh 533437, India*
[4]*Institute of Electronics and Communication Engineering, Saveetha School of Engineering (SIMATS), Chennai, Tamil Nadu 600124, India*
[5]*Department of Electrical and Electronics Engineering, Karpagam Academy of Higher Education, Eachanari, Tamil Nadu 641021, India*
[6]*Department of Computer Science Engineering, RMK College of Engineering and Technology (RMKCET), Thiruvallur, Tamil Nadu 601206, India*
[7]*Department of Computer Applications, University Institute of Computing, Chandigarh University, Punjab 140413, India*
[8]*Department of Technology, Savitribai Phule Pune University, Pune, Maharashtra 411007, India*
[9]*Department of Electrical and Computer Engineering, Institute of Technology, University of Gondar, Gondar, Ethiopia*

Correspondence should be addressed to Mekete Asmare Huluka; mekete.asmare@uog.edu.et

Received 19 July 2022; Revised 13 September 2022; Accepted 19 September 2022; Published 14 October 2022

Academic Editor: BR Ramesh Bapu

In this paper, we introduce a deep neural network (DNN) for forecasting the intra-day solar irradiance, photovoltaic PV plants, regardless of whether or not they have energy storage, can benefit from the work being done here. The proposed DNN utilises a number of different methodologies, two of which are cloud motion analysis and machine learning, in order to make forecasts regarding the climatological conditions of the future. In addition to this, the accuracy of the model was evaluated in light of the data sources that were easily accessible. In general, four different cases have been investigated. According to the findings, the DNN is capable of making more accurate and reliable predictions of the incoming solar irradiance than the persistent algorithm. This is the case across the board. Even without any actual data, the proposed model is considered to be state-of-the-art because it outperforms the current NWP forecasts for the same time horizon as those forecasts. When making predictions for the short term, using actual data to reduce the margin of error can be helpful. When making predictions for the long term, however, weather information can be beneficial.

1. Introduction

Researchers in the field of meteorology have been interested in solar radiation for centuries. Irradiance forecasting has produced precise and accurate results in a number of recently conducted studies as a result of a variety of recently developed technologies [1]. PV is a technology that has been steadily increasing its share in the global power generation industry, which has made it a key player in the global energy market. This industry has experienced consistent growth over the past ten to twelve years, with more than one hundred gigawatts of new grid-connected capacity being added in just the year 2018 [2]. As a consequence of this, a significant number of PV deployments that are currently taking place and those that are anticipated to take place in the near future imply significant levels of PV penetration

in a variety of power systems. Power can be obtained directly from the sun. But it can get little power when it is surrounded by rain. Solar energy is used all over the world. Also, the use of solar energy to generate electricity or heat and convert seawater into fresh water is becoming increasingly popular. Because of the inherently intermittent nature of PV production, for instance, the casuistic threat to the grid stability that is posed by passing clouds is made significantly worse. PV power plants are unable to provide accurate forecasts regarding their future output, which makes it difficult for grid operators and PV owners to manage the system and sell their output on the market for electricity. As a consequence of these constraints, multiple photovoltaic (PV) plants located in different parts of the country have traditionally been combined [3]. More recently, however, a variety of energy storage systems, primarily batteries, have been installed in close proximity to PV plants [4]. PV plants are subject to significant costs in the form of batteries, which are prone to experiencing accelerated wear and tear in the event that operating conditions are not properly monitored [5].

In this setting, the capacity to accurately forecast irradiance and, as a consequence, PV output is absolutely necessary. Irradiance forecasting improves the reliability of operation of photovoltaic (PV) systems, also known as dispatch ability [6]. The integration of batteries into photovoltaic plants makes it possible to use smaller batteries, which is necessary for hybrid power plants to be able to operate reliably on the electricity market [7]. By using the forecast, it is also possible to optimise the operation of the plant, obtain information about future production, and, as a result, reduce the ageing of the batteries. Solar cells, also known as photovoltaics, are electronic devices that convert sunlight directly into electricity. Modern solar cells, as most people recognize them today, are found in panels mounted on homes and computers. Solar cells are currently one of the fastest growing renewable energy technologies and are poised to play a massive role in the future global electricity generation mix. There are a variety of approaches that can be taken to forecast the activity of the sun. There are two different strategies to choose from: physical and data-driven [8]. While data-driven approaches make primary use of historical data as their primary input for prediction, physical approaches rely on the knowledge that is derived from atmospheric science [9]. In order to choose an approach that is appropriate, you need to take into account the target forecasting horizon as well as the time-step, also known as the granularity. Both of these factors are determined by the anticipated use of the forecast [10]. The forecasts for the following day are the primary focus of this research (with a horizon of up to 6 h ahead) [11–14]. The use of numerical weather predictions is favoured for longer-term forecasts, while time series and sky images are preferred for more immediate forecasts [14]. Solar cells can be combined to supply electricity on a commercial basis or to connect electricity to small grids or to obtain electricity for personal use. Using solar cells is the best way to provide electricity to people living outside the grid. The cost of manufacturing panels equipped with solar cells has fallen dramatically over the past decades. For this reason it has become a viable form of electricity to use. Solar panels have a lifespan of about 25 years and come in different colours based on the materials used in manufacturing.

An artificial neural network, or ANN, is one that simulates the human brain natural capacity to recognise and remember certain patterns [15]. It is concluded in both of these reviews that these methods produce accurate forecast results. However, it is difficult to make direct comparisons between them because each forecast is based on a unique set of circumstances and geographic locations. When reviewing the most recent research on solar forecasting, comparability and reproducibility issues frequently arise in the literature. In order to avoid this, the ROPES guidelines for solar forecasting that are proposed in this document will be followed [16]. The authors in [17] provides a classification system for the various methods of weather forecasting based on the length of their forecasting horizons and the climatology of the local area. The RRMSE of the different methods ranges from 20% to 40% for temperate climate and intra-day forecasts, with the best performance coming from machine learning and cloud motion methods. For forecasts made one hour in the future using machine learning methods such as those described in [18], the error rate ranges between 20 and 25%.Cloud motion approaches have errors of approximately 28% and 10%, respectively, for one-hour forecasts When applied to forecasting horizons of one hour and six hours, this method produces error rates of 22.6 and 32.1%, respectively. Concentrated solar power (CSP) uses mirrors to concentrate the sun's rays. These rays heat the liquid. This heated liquid flows through the heat exchanger to form steam. The steam rotates the turbine to generate electricity. Concentrated solar energy is used to generate electricity in large-scale power plants.

Satellite images and real-time irradiance measurements are used as inputs to the forecast models in almost all of these studies. The forecast model must figure out how the weather will change over time, in addition to figuring out how to compute the irradiance from satellite images, in the case of the former. Both of these tasks are burdensome. In order to accomplish this, it is necessary to rely on data that is frequently unreliable or that is simply unavailable. A few examples of the types of installations that fall into this category include those that are small, have constrained budgets, are located in inaccessible areas, or have facilities that are difficult to maintain data acquisition systems. Other works in the corpus of research have attempted to address these limitations [19] developed a method for predicting irradiance that did not require the use of real-time measurements. This method relied on satellite images and a technique known as support vector regression (SVR). However, the SVR model must still be validated against the data that was collected. A concentrated solar power plant usually consists of a block of generators. These direct the sun's rays to a tall and condensing tower. One of the main advantages of such plants over power plants with panels containing solar cells is the presence of molten salt in them. Molten salt stores heat. This makes it possible to generate electricity even a few hours after the sun goes down. These models can be

trained and deployed in areas where there is no telemetry at all by making use of data from a select number of locations. Nonetheless, despite the fact that these two works make an effort to avoid the requirement of using measured irradiance, their models must still be trained using measured data.

2. Related Works

Neural networks have the inherent capacity (theoretically) to model any unambiguous function, regardless of how complicated the function may be (NNs). When trying to get a grasp on what neural networks are all about, Rosenblatt perceptron is a good place to begin. In the same way that there are many inputs in the brain, each of which has a unique electrical signal, these inputs are integrated, and whether or not a neuron fires are contingent on a threshold [20]. The input and the weights are multiplied together to generate a vector inner product, which is then used to determine whether or not the neuron will fire. Each individual node has a weight vector as well as a linear transformation associated with it. After that, the input is processed by non-linearity, which produces the distinctive signal characteristics that are associated with each node. An artificial neural network (ANN) is, as its name suggests, a collection of nodes that are interconnected with one another and that are capable of being trained to carry out a particular task [21]. To know the benefits of solar energy, we need to know what it is and what types of solar energy there are. First know what it is a renewable source of energy derived from the sun can generate heat and electricity for any use. Although it is a standard source, it is important to point out that it is not without its drawback, which also affects its purpose and use. It is derived directly from radiation reaching our planet from the Sun in the form of light, heat or ultraviolet rays. Depending on how solar energy is available, there are different types.

In supervised learning, the data that is used for training has a specific format that has been determined in advance. As a consequence of this, users are aware of the expected output that the function that connects input and output should produce when it comes to making predictions (be it classification or regression). In the same way that supervised learning works, we need to find a system that can learn a functional approximation based on a predefined structure that exists between the input and the output [22]. The most basic form of neural network, also known as a shallow neural network (SNN), has just one hidden layer of nodes sitting in between the network input and output. Shallow neural networks (SNNs) are the most common form of neural network. It is only capable of learning the most fundamental functions in a reasonable timeframe. Learning at a deep level is necessary in order to master more complicated functions. Deep learning refers to the process of stacking a neural network (NN) with more than one intermediate layer. When more layers are added to a network, it shortens the amount of time needed for the network to learn more complex functions. Stacking hidden layers can be done by adding new hidden layers to an existing hidden layer [23]. As its name suggests, it is a form of renewable and clean energy that uses the sun's energy to generate electricity. Unlike solar panels that use photoelectric energy to produce electricity from photons of light found in solar radiation, this energy uses this radiation to heat a liquid. When the sun's rays hit the liquid, it heats up, and this hot liquid can be used for various applications. To get a better idea, the energy consumption of a hospital, a hotel or a house corresponds to 20% of hot water use. With solar thermal energy we can heat water with the energy of the sun and use it so that we do not have to use fossil or other energy in this energy sector. Solar thermal energy contributes significantly to reducing energy costs, resulting in savings in energy and reducing CO_2 emissions that are responsible for global warming and climate change.

The number of parameters that can be learned and the efficiency with which this can be done are both determined by the connections that exist between the layers of a NN. Feed-forward neural networks make use of layers that are completely interconnected (NNs with a linear graph). Every one of the nodes in one layer is connected to every one of the nodes in the layer below it. This method begins with a linear transformation of the data and then transitions into non-linearity. This is necessary because each connection has a weight vector that corresponds to it and it presents a challenge when dealing with image data because nodes would need to be created for each individual pixel. In the case of an image with a resolution of one megabyte, for instance, each layer in an FCN would have a width of 0.106 [24].

2.1. Convolutional Neural Networks. There is a theory that the visual cortex of an animal functions as an intricately networked system of neurons that transmits a specific electrical signal from layer to layer, beginning with an image captured by the eye and ending with an understanding of what was captured by the brain. This theory is supported by a number of studies that have been conducted to test the hypothesis. When done in this manner, the first layer focuses on features that are considered more fundamental, such as colour gradients and lighting, before moving on to the next layer, which focuses on features that are considered more fundamental, such as textures and shadows (e.g. facial features) [25]. It uses heat thanks to solar collectors that receive the sun's rays and convert it into a working fluid. It is used to heat buildings and water, move turbines, and destroy dry grain or waste.

For instance, each layer is responsible for identifying an abstract feature, which in turn assists the subsequent layers in identifying additional abstract features. Because of this, the animal neurons are trained to respond to a variety of stimuli in a manner that is unconscious; as a result, the animal learns. This is precisely the purpose that convolution neural networks (CNNs) are meant to serve. Our artificial network is able to learn how to react to increasingly abstract features in the image data as it progresses through each successive layer. This enables the output layer to learn the geometry of a variety of different objects. However, because the network selects the abstract features it learns for each image classification task, this results in a loss of interpretability. The features, in their essence, are not something that can be written down

Figure 1: Proposed Model.

explicitly but are instead something that is learned by the machine through its imagination [26].

This is done rather than having every node in the subsequent layer connected to all of the other nodes in the layer below it. Due to the fact that CNNs were developed for the purpose of taking an image as their input, the linear transformation is represented by the convolution function that is present in each node. The comparison of this system to a biological network is apt. This idea is founded on the observation that the degree of correlation that exists between neighbouring pixels in an image weakens with increasing distance from the pixels that are being discussed in the image. This has the additional benefit that, instead of training a weight to be used between each pair of nodes in the convolutional network, the convolutional kernel is used for each node in the network [27]. The classification of images frequently makes use of CNNs that have multiple layers. As a direct consequence of this, the convolution function of CNNs handles shift invariance in an automatic fashion. CNNs are now programmed to learn about the geometric properties of features rather than the relative positions of pixels in images. Because the network looks for feature maps rather than particular pixel sequences, it is consequently much simpler to recognise objects in pictures as a consequence of this [28, 29].

3. Proposed Method

It is necessary to make a number of choices before defining the architecture of a CNN (with regard to the number of layers, activation functions, and so on). The selection of the model is done using the so-called NN model. Before making a final choice, it is common practise to calculate the performance achieved by some error metric when comparing the various model alternatives. This is done prior to making a decision. In order to accomplish this goal, the data from the previous two and a half years is divided into two distinct datasets. Figure 1 shows proposed model.

Additionally, available are the following three subsets of the model selection dataset shown in Figure 2:

(i) Training Data: Readings of the irradiance over the course of at least one year are required for the purposes of training. This is done to prevent the CNN from becoming over fit to the data. This data split contains roughly half of the total model selection data

(ii) Validation Data: Validation data is taken from irradiance measurements taken during a period of time that is distinct from the training period and is also shorter. Re-evaluating this data at a variety of points throughout the training process allows for the determination of whether or not the CNN has become overfit. When something like this takes place, a strategy for early stop is put into play so that a general solution to the problem can be found. In the training data for this dataset, the length of the night is reduced. This data split contains a quarter of the total data for the model selection process. Training and Validation The reference data consist of irradiance values measured during the same time period as the test data. These values are used to train and validate models

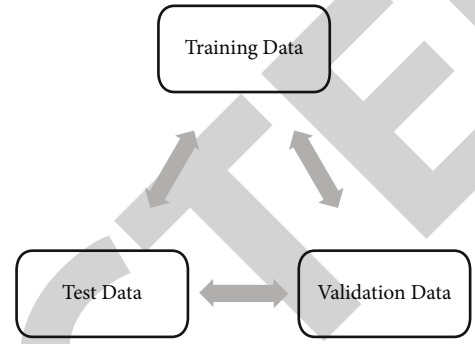

Figure 2: Subsets of the model selection dataset.

(iii) Test Data: The observations that had solar zenith angles that were greater than 80°, denoted by the notation $s > 80°$, have been removed from this set. This is because of the low levels of irradiance that are present in the early morning and early evening hours, which is a time when the readings from a pyranometer are less accurate. This includes the nights because it is impossible to provide accurate forecasts for any topology during the night-time hours. This dataset, which represents the final 25% of the model selection data, is used to evaluate and compare the effectiveness of the various model architectures

3.1. Non-Linear Model. Systems are considered nonlinear if they do not conform to the superposition principle, which can only be achieved by being nonlinear. Numerous applications based on real-world data have demonstrated that nonlinear models, when compared to linear ones in nonlinear models, can produce more accurate predictions than the former. The NARMAX model is versatile enough to be

applied to the simulation of a wide variety of nonlinear systems. It has been demonstrated that NARMAX is capable of modelling a wide variety of systems that exist in the real world. The following equation provides a graphical depiction of the mathematical representation of the NARMAX model. The output of the model is affected in various ways by factors such as historical values, random noise, and outside input.

It is important to make a distinction between mild and severe nonlinearity when discussing nonlinear systems. Modelling of many different engineering systems can be accomplished with the help of stable, mildly nonlinear systems like NARX or NARMAX models. Real-world systems, such as those pertaining to the stock market, oil prices, meteorological systems, and hydrological systems, are receiving a growing amount of attention as a direct result of the widespread use of system identification technologies. There is a possibility that polynomial NARX and NARMAX models will not be able to make accurate predictions regarding these nonlinear, complex, and non-stationary systems.

4. CNN for Prediction

The model that we will be using is a 13-layer convolutional neural network. The network is making use of LSTMs in order to model the function that transforms a H image of the Sun into a probability vector for each image containing a particular feature. If the features of an image are correctly learned by a neural network, then image classification can be made more accurate.

Between the input and the output of the system, the layers depicted in Figure 1 as cuboids are performing a significant number of large matrix computations. This process is repeated for each layer. The convolution kernels are made up of three 3x3 pixel squares, each of which was initially initialized by employing the HE initialization algorithm. To generate photovoltaic energy, it is necessary to capture photons of light held by solar radiation and convert it into electricity for use. This can be achieved through photovoltaic conversion process using solar panel. An important element of a solar panel is the photovoltaic cell. It is a semiconductor material (made of silicon) that requires no moving parts, no fuel, or noise. When this photovoltaic cell is continuously exposed to light, it absorbs the energy in the light's photons to generate energy, setting the electrons trapped by the internal electric field in motion. When this happens, the electrons collected on the surface of the photovoltaic cell generate a continuous current of electricity. In order for the network to learn which abstract features are being picked up by convolutions and which physical features they correspond to, it is the job of the optimizer to update the convolution kernel values while the network is being trained. A higher number of convolutions will be helpful in differentiating between these features.

The result of the convolution operation is then batch normalized after it has been processed. The equation provides a means of normalizing the convolution calculation relative to a batch mean (β) and standard deviation (γ). The network reliability can be improved with the help of this method as in Equation (1).

$$y = \gamma \frac{x - E[x]}{\sqrt{\sigma(x) + \epsilon}} + \beta \tag{1}$$

where.

x –output feature maps and.

y – feature maps,

ϵ - positive constant and.

σ –feature maps variance.

As a consequence of this, the dynamic range of the data is decreased, but the loss of two additional trainable parameters (β, γ) allows for the training process to be significantly sped up. It is possible to recover the true feature maps from the batch stabilized feature maps, as shown in Equation (1), if Equation (1) is manipulated while back-propagation is being performed. After the batch stabilization process is complete, the data is put through an activation function, which is a non-linear transformation. The output of the batch stabilization is shifted, and as a consequence, the signal that is being passed on to the subsequent layer has a different distribution. This particular function makes use of the rectified linear unit function as in equation (2).

$$\Phi(x) = \max(0, x). \tag{2}$$

This was chosen because of its ability to avoid gradient problem due to its sparse output. The reason for this ability is explained below. It is referred to as the vanishing gradient problem when the utilized gets stuck in the loss space due to decreasing gradients and back-propagation loss function gradients that are tending toward zero. It does not require extracting any static material to work. It produces very cheap energy, and its initial investment is easy to recover over several years. A major problem with renewable energy since its inception is the initial investment and its rate of return, although this is not thanks to the development of technology. A solar panel can have a useful life of 40 years. Using ReLUs allows one to circumvent this issue because the gradients of these models are invariably large as in Equation (3).

$$\mathrm{D}\phi \mathrm{d}x = H(x) \tag{3}$$

where.

$H(x)$–Heaviside function.

Since this results in less spatial information, over-fitting is reduced. For the purpose of this downsampling, the image is sectioned off into 2×2 grids of two-by-two-pixel segments so that the maximum amount of detail can be extracted from each individual segment. This indicates that in a downsampled image, a single pixel represents the original four-pixel block that the image was taken from.

Because each pixel in the input image represents more information from the original input, the network is able to learn more complex features by performing operations on a larger fraction of the original image (for example, four

pixels instead of one), which highlights larger, more complex features via the convolution operation. This allows the network to learn more complex features more quickly. It is possible to reduce over-fitting by 12tilized12 other methods such as average pooling, but maxpooling is the most widely used method because of the benefits it provides in reducing over-fitting. Other methods includes the fully-connected block and dropout 12tilized12ed12on are two of the most important concepts to understand in relation to this network. If there are N input nodes and M output nodes, then a linear transformation will result in $\mathrm{N} \times \mathrm{M}$ parameters that need to be changed for a layer to have a fully-connected topology. Dropout is a more recent development in the field of machine learning. In order for the network to train on an approximation of the actual structure of the network, it gives every node and connection an equal probability of being ignored while it is in the training phase. At the time of validation, an effective 12tilized12ed12on technique that reduces over-fitting while maintaining accuracy is to train the data set. The third fully-connected layer is what determines the classification of the images. In our model, the class labels are inferred based on the loss function that we choose to use, which also implicitly adds this last layer of activation.

4.1. Training. The training phase of a machine learning algorithm is by far the most difficult and significant part of the overall process. Training is the process by which a network learns which algorithm it should be approximating in order to achieve optimal performance. For the purpose of implementing this in the network, a feed-forward and back-propagation system are used. The number of epochs (full passes) of the feed-forward and back-propagation algorithm is another hyper-parameter, which means it is a parameter that the system does not learn and that needs to be tuned during training.

The images are being fed from input to output through the network, which is referred to as the network having a feed-forward nature. The way a NN is initially trained can have a significant effect on how well it performs. We use something that is known as He initialization rather than random or zero initialization of the weights because this allows us to reduce the number of epochs that are necessary for learning. Here, weights are selected at random from the normal distribution $N(0,\sigma)$, and the resulting matrix is 13utilized13ed as follows in Equation (4):

$$\sigma = \sqrt{\frac{2}{n_l}} \tag{4}$$

where.

n_l – total connections across layer l.

In order to obtain this result, the variance of the forward linear process of the neural network was 13tilized. First, as a result of this initialization, a machine learning algorithm was able to classify images more accurately than a human could.

To determine which category an image falls under, the network consults the weights it has been trained with after the feed-forward process is complete. After that, the process of back-propagation starts, in which each weight in the network gets updated so that the number of incorrect classifications gets lower the next time this process starts. This completely clean energy helps reduce your carbon footprint significantly. Thanks to its use we avoid the generation of greenhouse gases and we do not pollute either in its generation or in its use. There is very little pollution involved in the manufacturing of solar panels. Back-propagation optimization employs a technique known as stochastic gradient descent (SGD). The network perception of reality is compared to that perception using a function called the loss function, which measures the difference. Using a first-order gradient method, which is very simple to calculate mathematically, the weights can be easily and quickly updated as in Equation (5).

$$\Theta_{t+1} = \theta_t + \eta \nabla_\theta \mathrm{L}(x; \theta_t) \tag{5}$$

where.

θ_{t+1} –updated weight.

H –learning rate.

The learning rate refers to the process of calculating how much of a change in weight will take place in the loss space of the loss function. This hyper-parameter, which is the second of two that will be tested throughout the training, will also be examined. This method is very similar to standard SGD, but it also includes a velocity term that causes weight updates to accelerate over the course of multiple epochs. This velocity can then be added as follows as in Equation (6):

$$\theta_{t+1} = \theta_t + v_{t+1} = \theta_t + \mu v_t - \eta \nabla_\theta L(x; \theta_t + \mu v_t) \tag{6}$$

When the gradient is updated, the product of the momentum coefficient (μ) and the velocity (v_t) is also updated. This means that θ_{t+1} is not only updated by the gradient; it is also updated by the product of μ and v_t. When predictions are not accurate as a result of an argument in the gradient gradient argument, this feature enables a faster correction of the velocity term. If the product μv_t leads to inadequate weight updates, the optimizer may wish to try again in a different direction. Gradient functions have a tendency to become steeper when there are insufficient updates to the weights. With SGD and Nesterov momentum, we will not overshoot the target because the regions with flatter curvature are located closer to the minima. Because of this, we are able to move through the lost space at a faster rate.

Altering the values of the two other hyper-parameters enables a set of models to be trained. In order to reach general convergence, various problems require significantly varying numbers of epochs. The results cannot be reliable if there are not enough epochs because the model will be underfit if there are not enough of them. Overfitting can happen when the number of epochs is too high, and when this happens, the network may incorrectly classify data that it has never encountered before. Determining the optimal number of epochs is one way to avoid underfitting. However, overfitting should also be avoided at all costs. In addition, some of the training data can be used in the phase of validation rather than in the phase of training. Because of

this, for instance, it will be possible to monitor how the network reacts to unknown data because the validation data will have a predetermined category. However, the converse is also possible: the system may never get out of a bad local minimum, which will cause it to arrive at a solution that is suboptimal.

5. Results and Discussions

The performance of the suggested CNN models is evaluated with the help of a pyranometer for two different reasons. The selection of a model is the first step in determining the optimal structure that should be applied. The definitive findings will be reported once the model has been evaluated. In addition to this, the study investigates and quantifies the extent to which the accuracy of a forecast can be improved by the addition of additional datasets during the stage where the model is being evaluated. The results are 99.92% accurate with optimal hyper-parameters at the rate of $\eta = 5 \times 10^{-4}$, which we determined by training and validating across the hyper parameter ranges.

It is possible to draw the conclusion that our model has not successfully encapsulated all of the possible input-output mapping functions. Because it is difficult to find an image data classifier that is free of distortions and artefacts, which can cause misclassification, one should not underestimate how close this model comes to being perfect. Only discrete steps have been taken by us in the hyper-parameter space, which may result in a classification that is even more accurate.

Our model is contrasted with the persistence model, which acts as a benchmark for comparing other models to. This model is used because it is predicated on the assumption that there will be no change in the amount of radiation over the course of the forecast period. In addition to being called the root mean square error (RMSE), the mean absolute error is another name for it. In addition to this, it is used to determine the degree to which the forecasting model is an improvement on the reference persistence model. It is not possible to deduce from the classification percentage of a validation set whether or not our classifier has learned what we wanted it to base on the available statistical evidence. This can be caused by an uneven split in the validation set as well as by a classification task that has a strong bias. To solve this problem, our classifier makes use of something called a confusion matrix. In contrast to the classification determined by the network, the actual class of an image is reflected in this matrix.

Each class would have an equal amount of precision and recall. A deviation from one in the precision is produced whenever the instances is incorrectly classified. Every other class has a precision of one, which indicates that the network does not consider any images that do not contain these features to actually contain them even if they appear in the image. The only one of the recalls that is different from the others is an image that has an incorrect classification. This means that the network will never attribute a feature to any of those images that is not actually present in the image itself. This applies to each and every one of those images.

Table 1: Accuracy of Prediction.

Training samples	CNN	RCNN	U-net	Proposed
100	91.90767	92.44058	93.29245	94.16016
200	90.55034	91.07538	91.91467	92.76957
300	92.29715	92.83231	93.68779	94.55919
400	88.77206	89.28679	90.10959	90.94771
500	91.52316	92.05383	92.90214	93.76623
600	92.14522	92.67951	93.53358	94.40354
700	92.11339	92.64749	93.50127	94.37093
800	90.25394	90.77726	91.6138	92.4659
900	92.83424	93.37252	94.23298	95.10944
1000	90.4031	90.92728	91.76521	92.61872

Table 2: Precision.

Training samples	CNN	RCNN	U-net	Proposed
100	92.14559	92.67988	93.53396	94.40392
200	88.57739	89.09098	89.91199	90.74826
300	91.33169	91.86125	92.70778	93.57006
400	92.03151	92.56514	93.41815	94.28704
500	90.85801	91.38483	92.22697	93.08478
600	90.09833	90.62075	91.45585	92.30648
700	92.39287	92.9286	93.78496	94.65726
800	85.82268	86.3203	87.11577	87.92604
900	89.81567	90.33645	91.16893	92.01689
1000	92.16017	92.69454	93.54875	94.41885

The misunderstanding of our network does not bring about any detrimental effects to its functioning. Due to the fact that the margin of error is very small, we are confident that our network has learned the geometry of these features. It is essential to carry out both analyses because, if the deterioration in the forecast is deemed tolerable, there will be a reduction in the amount of money needed to implement the forecasting model. It is not necessary to leave a temporary pyranometer at the location of the target because a portable pyranometer can be used to collect training data and then moved to a different location.

Tables 1–4 demonstrates that, as was to be expected, the rRMSE obtained from real-world measurements is noticeably lower than that which was obtained through simulations. Nevertheless, there are a variety of other outcomes that could occur. Real-time irradiance feedback is of comparable or even slightly greater significance for the shorter-term predictions than it is for the longer-term forecast. However, it is important to note that forecasts that are not based on any actual data can still be useful in many different contexts. For time horizons of more than 30 minutes, all other models have a performance advantage over the persistent model. In point of fact, as the horizon gets higher, the influence of actual measurements on the quality of the forecast becomes less significant, while the advantage of using a clear-sky model grows. In conclusion, it can be observed

Table 3: Recall.

Training samples	CNN	RCNN	U-net	Proposed
100	92.60026	93.13718	93.99547	94.86973
200	90.52414	91.04903	91.88807	92.74273
300	90.47007	90.99464	91.83318	92.68733
400	92.14522	92.67951	93.53358	94.40354
500	88.19033	88.70169	89.5191	90.35172
600	88.54223	89.05562	89.8763	90.71224
700	92.02507	92.55866	93.41161	94.28044
800	90.64418	91.16976	92.00992	92.8657
900	88.34328	88.85552	89.67436	90.50842
1000	92.30929	92.84453	93.70012	94.57163

Table 4: F-measure.

Training samples	CNN	RCNN	U-net	Proposed
100	92.14559	92.67988	93.53396	94.40392
200	88.18804	88.69938	89.51677	90.34937
300	90.2786	90.80206	91.63883	92.49116
400	92.37265	92.90825	93.76443	94.63654
500	91.79955	92.33183	93.18269	94.04939
600	90.87638	91.40331	92.24562	93.1036
700	92.09863	92.63264	93.48628	94.3558
800	88.4745	88.9875	89.80755	90.64285
900	90.25739	90.78073	91.6173	92.46943
1000	91.86191	92.39456	93.246	94.11328

how the skill of the forecast begins to decrease with longer horizons, which exemplifies a limitation of satellite-based forecasts that is already well known.

6. Conclusions

Utilizing the DNN that was developed for the purpose of this study could make intraday forecasting of solar irradiance more accurate, thereby improving the controllability of power plants. The accuracy of the model has also been evaluated in light of the data sources that are at our disposal. In general, four different cases have been investigated. The DNN forecasting system uses a irradiance forecast for the future as a starting point. However, actual data from the target location can only be gathered during the training phase of the DNN. This data can only be used as a form of feedback to the forecasting system. According to the findings, the DNN is capable of making accurate predictions regarding solar radiation and, in every scenario, it outperforms the persistent algorithm. Even if there are no real-world observations available, the results of the proposed model outperform those of the current NWP forecasts for the same time horizon as the NWP forecasts. When making predictions for the short term, using actual data to reduce the margin of error can be helpful. When making predictions for the long term, however, weather information can be beneficial.

Data Availability

The data used to support the findings of this study are included within the article. Further data or information is available from the corresponding author upon request.

Conflicts of Interest

The authors declare that there is no conflict of interest regarding the publication of this article.

Funding

This research work is not funded from any organization.

Acknowledgments

The authors appreciate the supports from University of Gondar, Ethiopia. for providing help during the research and preparation of the manuscript.

References

[1] K. K. R. Samal, K. S. Babu, and S. K. Das, "Multi-directional temporal convolutional artificial neural network for PM2.5 forecasting with missing values: A deep learning approach," *Urban Climate*, vol. 36, article 100800, 2021.

[2] M. Shen, H. Zhang, Y. Cao, F. Yang, and Y. Wen, "Missing data imputation for solar yield prediction using temporal multi-modal Variational auto-encoder," in *Proceedings of the 29th ACM International Conference on Multimedia*, pp. 2558–2566, New York, 2021.

[3] H. Sun, K. J. Kuchenbecker, and G. Martius, "A soft thumb-sized vision-based sensor with accurate all-round force perception," *Nature Machine Intelligence*, vol. 4, no. 2, pp. 135–145, 2022.

[4] W. Li, Z. Shang, S. Qian, B. Zhang, J. Zhang, and M. Gao, "A novel intelligent fault diagnosis method of rotating machinery based on signal-to-image mapping and deep Gabor convolutional adaptive pooling network," *Expert Systems with Applications*, vol. 205, p. 117716, 2022.

[5] K. Yadav, M. Yadav, and S. Saini, "Stock values predictions using deep learning based hybrid models," *CAAI Transactions on Intelligence Technology*, vol. 7, no. 1, pp. 107–116, 2022.

[6] Y. Shen, Y. Ma, S. Deng, C. J. Huang, and P. H. Kuo, "An ensemble model based on deep learning and data preprocessing for short-term electrical load forecasting," *Sustainability*, vol. 13, no. 4, p. 1694, 2021.

[7] Y. Qian, Z. Huang, H. Fang, and Z. Zuo, "WGLFNets: Wavelet-based global-local filtering networks for image denoising with structure preservation," *Optik*, vol. 261, article 169089, 2022.

[8] X. J. Sun and J. C. W. Lin, "A target recognition algorithm of multi-source remote sensing image based on visual internet of things," *Mobile Networks and Applications*, vol. 27, no. 2, pp. 784–793, 2022.

[9] Y. Yuan, K. Dehghanpour, Z. Wang, and F. Bu, "A joint distribution system state estimation framework via deep actor-critic

Hindawi
International Journal of Photoenergy
Volume 2022, Article ID 7506237, 8 pages
https://doi.org/10.1155/2022/7506237

Research Article

An IOT Innovation of Smart Solar Energy Consumption Analysis and Control in Micro Grid

V. Anantha Krishnan,[1] A. Jeba Sheela,[2] B. Muthuraj,[3] U. Senthil Kumaran,[4] T. Vijay Muni,[5] Tirukoti Sudha Rani,[6] Ramesh N. S. V. S. C. Sripada,[7] Manzoor Hiu Siddique,[8] and Raja Raju[9]

[1]*School of Electrical Engineering, Vellore Institute of Technology, Chennai, Tamil Nadu 600127, India*
[2]*Department of Computer Science and Engineering, Easwari Engineering College, Chennai, Tamil Nadu 600089, India*
[3]*Department of Electrical and Electronics Engineering, Panimalar Engineering College, Chennai, Tamil Nadu 600123, India*
[4]*School of Information Technology, Vellore Institute of Technology, Vellore, Tamil Nadu, India*
[5]*Department of Electrical and Electronics Engineering, Koneru Lakshmaiah Education Foundation, Vaddeswaram, Andhra Pradesh 522302, India*
[6]*Department of Electronics and Communication Engineering, Aditya Engineering College, Surampalem, 533437 Andhra Pradesh, India*
[7]*Department of Computer Science and Engineering, Aditya College of Engineering & Technology, Surampalem, Andhra Pradesh, India*
[8]*Department of Chemistry, C. Abdul Hakeem College of Engineering & Technology, Melvisharam, 632509 Vellore, Tamil Nadu, India*
[9]*Department of Mechanical Engineering, St. Joseph University, Dar es Salaam, Tanzania*

Correspondence should be addressed to Raja Raju; raja.raju@sjuit.ac.tz

Received 27 July 2022; Revised 8 September 2022; Accepted 19 September 2022; Published 12 October 2022

Academic Editor: Br Ramesh Bapu

Solar energy consumption is a systematic study used to review the design of facilities, services, and equipment in an organization against specifications of solar panel. The solar panel energy consumption analysis is a work that should be done at the beginning of a solar energy. This way, potential changes can be highlighted before they affect the solar energy budget and schedule. The proposed model provides the IOT-based smart solar energy consumption analysis and control model by using solar photovoltaic micro grid. The proposed IOT design must meet product and process requirements. The solar panel energy should properly address important aspects of production processes. This should include risks related to product quality and safety. Finally, unacceptable risks must be minimized by design. In the solar energy consumption analysis process, the deliverables should be evaluated; customers should precheck the proposed design and identify problematic areas, if any. Solar energy consumption analysis reveals whether user requirements and features are sufficient to achieve the desired outcome. Likewise, there should be corrective actions for discrepancies found in design reviews.

1. Introduction

The visual inspection of tanks and vessels, which play an important role in oil and gas IOT devicesation, is a cornerstone of integrity assurance and is an important tool in detecting and quantifying defects and corrosion damage in general [1]. However, recent advances in accessibility technologies such as unmanned aerial nodes and remotely controlled nodes combined with imaging technology have begun to replace the human element in visual inspection [2]. Such remote monitoring services have provided significant benefits in preventing high-risk human interventions

in confined spaces and overworked or hazardous environments [3]. Quality assurance and quality control are two different processes that are used in different ways and for different purposes and have advantages in themselves [4]. Quality assurance inspections are process-oriented and focus on error prevention, while quality control inspections are product-oriented and focus on error detection [5]. Quality assurance is a set of activities to ensure quality in the processes by which products are made. Quality control is a series of steps taken to ensure quality in products [6]. Human survival and progress depend on the Earth's natural resources. So it is necessary to use them. Humans are dependent on resources for their survival. Human occupations are determined by the resources available in a place. Human economic activities vary from place to place according to resource availability. Nonrenewable resources should be handled with utmost care. Better research and development is necessary to make full use of renewable resources. These activities mainly focus on detecting defects in products. Quality assurance focuses on the process used to manufacture the product and in this way aims to prevent defects. So it is a proactive quality process [7]. Quality control aims to identify and correct defects in the finished product. So it is a reactive quality process. The purpose of quality assurance is to improve development and testing processes [8]. When this is done, defects do not occur during manufacturing. The purpose of quality control is to detect defects after a product has been developed, but before it is placed on the market [9]. In short, quality assurance is preferred to establish a good quality management system and assess its effectiveness in solar energy consumption analysis, while quality control is used to find and eliminate the sources of quality problems to meet customer requirements [10, 11]. As such, with quality assurance, it is a technique that attempts to prevent quality problems in planned and systematic activities including certification [12]. Quality control is the techniques used to obtain and maintain product quality. Solar energy consumption analysis can succeed in international trade to the extent that they can deliver the right products, at the right time, at the right price [13]. The sun is nature's greatest source of energy. Hundreds of different processes take place within this gaseous sphere every minute. Life on earth would be impossible without the sun, as it is the source of energy for all living things. All natural processes on earth are powered by solar energy. Without the sun, the planet's thermal regulation, photosynthesis, water cycle, and atmospheric circulation would be impossible. The use of solar energy on Earth is as common a phenomenon as inhalation and exhalation by humans. But it can give humanity more. It can be successfully used to obtain industrial energy, heat, or electricity. As global trade increases, the risk of not delivering products on time or not solar energy consumption analysis products of agreed quality is increasing [14]. Customers in different regions of the world need to ensure that the products, materials, and equipment ordered are equivalent to the requested specifications. In this regard, third-party authorized companies that provide independent and impartial service provide preshipment inspection services to ensure that products, materials, and equipment comply with contractual conditions [15, 16]. This way, quality is assured before shipment. Pre-export inspection services generally include the following types of services:

(i) Ensuring that products conform to predetermined specifications

(ii) Packaging control to ensure adequate protection of products during transit

(iii) Checks that loads are properly loaded and secured in the IOT devices nodes (stacking, lashing, and wedging control)

(iv) Verification that documents representing loads are complete

As a result, the report prepared by the authorized energy units as a result of the preshipment monitoring proves that the goods are ready for IOT devices in the ordered quality and quantity and are duly documented [17, 18]. Preshipment tracking services also reduce the risk of damage during transit. These services are offered to all solar energy consumption analysis regardless of the industry they operate in [19]. The development of using solar energy started in the twentieth century. Since then, hundreds of studies have been carried out by scientists from all over the world. They proved that the efficiency of using solar energy can be very, very high. This source can supply the entire planet with more energy than all other resources combined. Also, this type of energy is generally available and free.

With the development of computer and communication technologies, there has been significant growth in many fields throughout the world in recent years [20]. This rapid advancement increases the competition in the market. The quality of manufacturing energy unit's products is the most important factor in the success of the energy units' quality control function. Solar energy consumption analysis needs to evaluate, approve, and inspect materials and products from supplier companies or manufacturing companies to achieve their goals with quality assurance and quality control functions [21, 22]. Audits and evaluations of supplier companies have now become an indispensable process for solar energy consumption analysis in all sectors. Since production activities depend on the type and quality of the product supplied, raw materials are only formed into the actual final product or final product [23]. Therefore, it is important for an industry supplier of raw material to ensure that it is of good quality and standards and that the products it supplies meet all industry standards and policies. The final products must be of quality and reliability and quality that satisfy the customers. Evaluation of the quality program is a joint vendor and supplier activity [24]. The availability of natural resources that can provide energy to the earth is depleting every day. Therefore, active development of various ways of using solar energy is currently underway. This resource is a great alternative to traditional resources. Therefore, research in this area is incredibly important to society. The effectiveness of these energy units provides mutual benefit to all interested parties. With a vendor evaluation program,

the following are mainly evaluated: delivery time, product usage unit, quantity conformance, product delivery time competitiveness, accurate documentation, and response to emergency delivery conditions [25].

2. Literature Review

The most characteristic feature of IOT devices in the field of IOT is the ability to be flexible and responsive to customer needs, depending on the large increase in trade volumes and the need to maintain competitive advantages [1]. This trend is visible not only in local IOT devices chains but also in international IOT devices. This perspective pushes all supply chain organizations, where IOT device station plays a key role, to be more flexible [2]. Therefore, it is important to measure the effectiveness and efficiency of IOT device station activities and find and use suitable nodes. Through detailed analysis of the results obtained through various monitoring activities, solar energy consumption analysis develops appropriate strategies for appropriate infrastructure and technology improvements. IOT device station and IOT systems are strongly interrelated [3]. The performance of processes depends on each other. IOT hubs and container terminals play a very important role in integration. Solar energy consumption analysis operations are analyzed using several new methods for optimization and quality services [4]. There are many types of passive solar energy applications. Most of them are incredibly easy to use, but still very effective. There are also advanced options to help you get more value. For example, the first thing that comes to mind is the water storage container. If you paint it in a dark shade, in such a simple way, solar energy is converted into heat energy, and the water heats up. The next option cannot be done by an ordinary person on his own, as it requires a thorough analysis by an expert. This technology should be taken into account even at the design and construction stage of a house. Based on the climatic conditions, the building is designed to act as a solar collector. After that, materials are selected to maximize energy harvesting from the sun's rays.

The quality and reliability of solar energy consumption analysis operations depend on many factors, for example, distance to IOT devices, localization of distribution points and cargo IOT device station conditions, IOT devices nodes capacity, technical speed of nodes movement, technical deficiencies of cargo IOT devices, and systems and structural features of loading and unloading highways [5]. In addition, solar energy consumption analysis want to ensure that products are properly handled, that safe, IOT devices conditions meet all quality and safety requirements, and that goods are stored and IOT devices in accordance with good solar energy consumption analysis practices, regardless of the means of IOT devices used [6]. As a result, all the problems faced reduce the production efficiency in the energy units, cause waste of valuable materials, and increase operating costs. In some cases, it causes significant damage and threatens the health of employees. For solar energy consumption analysis to be successful, failure analysis must be part of all asset integrity management practices. The success of these studies depends on the use of appropriate analytical techniques [7]. Collectors are fundamental to the power supply principle. Such equipment absorbs energy and converts it into heat, with the help of which you can heat a house or heat water and convert solar energy into electrical energy. Collectors are widely used in industrial scale and private plots and agriculture. In addition to collectors, another equipment of the active system is panels with photocells. This device allows you to use solar energy in everyday life and on an industrial scale. Such panels are very simple, easy to maintain, and durable.

It is a well-known fact that coarse aggregate plays an important role in solar unit's construction. Coarse aggregate usually makes up about one-third of the volume of solar units. According to researches, coarse aggregate changes affect the strength and fracture properties of solar units. To accurately predict the behavior of solar units under loads, it is necessary to know the effects of aggregate type, size, and content [26]. This information can only be obtained through solar units and aggregate tests and observations. There is strong evidence that aggregate type is a serious factor in the strength of solar units. In high-strength solar units, high-strength coarse aggregates generally provide high compressive strength [27]. There are debates regarding the effects of coarse aggregate sizes on solar units, particularly on fracture energy. Understanding the effects of coarse aggregate has gained more importance with the use of high strength solar units [28].

In ordinary strength solar units, failure in compression is only related to cement bonding with aggregate particles. As the strength of the cement that makes up the solar units increases, the hardness and strength compatibility usually occur between the harder and stronger coarse aggregate and the surrounding mortar [29]. Therefore, microcracks in solar units are caused by aggregate particles. In this respect, aggregate strength becomes an important factor in high strength solar units. Therefore, solar units and aggregate tests performed in advanced laboratories are important [30]. Defects and safety incidents in machinery, pressurized equipment, and facilities cause health, safety, environmental, solar energy consumption analysis, and reputational damage in the oil and natural gas industry. Equipment failures occur without realizing how effective a facility's reliability programs are. Although not all failures are catastrophic, many failures are caused by gradual deterioration of features or excessive wear and tear, before the design life has expired and the components are no longer functional [31]. These negatives cost solar energy consumption analysis huge financial losses and downtime every year.

3. Proposed Model

Fault analysis is a study to determine why a broken system or component is not fulfilling its intended function. First, observations are made to identify the mechanical and human causes and hidden causes of the problem, and an engineering solution is implemented. Product specifications and user requirements must be clearly defined before starting a design review. At the end of solar energy consumption

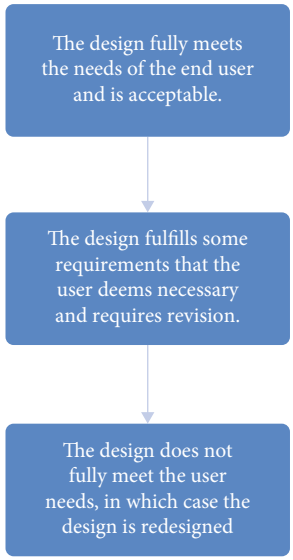

Figure 1: Possible outcomes of proposed model.

analysis studies, three possible outcomes emerge shown in Figure 1.

(i) The design fully meets the needs of the end user and is acceptable

(ii) The design fulfills some requirements that the user deems necessary and requires revision

(iii) The design does not fully meet the user needs, in which case the design is redesigned, another organizational design that meets the user needs, or the user needs are removed

The proposed provides solar energy consumption analysis and inspection services within the scope of services provided during design. Thanks to these services, solar energy consumption analysis can provide highly efficient, high-performance, and quality services that are secure, fast, and seamless. These methods have made it possible to create systems for harnessing solar energy, which are of two types:

(i) Active (photovoltaic systems, solar power plants and collectors)

(ii) Passive (selection of building materials and design of premises to maximize the use of solar energy)

By harnessing solar energy in this way, we have been able to harness an inexhaustible resource with greater productivity and return on investment. An energy unit's manager is a person with various skills such as

(i) Management

(ii) Leadership

(iii) Technical

(iv) Conflict management

(v) Client relations

Let us not forget that the sun already heats everything on Earth and your house is no exception. Therefore, the beneficial effect can be increased by making some corrections at the construction stage and using special techniques. Thus, you will get a house with very comfortable thermal regulation without much investment. In the past, different inspection and inspection strategies, inspection types, and inspection intervals were determined to reduce inspection costs. In these studies, different methods were used according to audit errors, audit amounts, and audit costs. Today, production monitoring and technical monitoring inspections are carried out for two purposes: evaluating compliance with design specifications and increasing product quality and reliability. Using solar energy to heat water is the easiest and cheapest way available to humans. Such equipment can be purchased at a reasonable price. At the same time, they can restore themselves quickly, significantly reducing the cost of centralized energy supply. Inspection controls, product quantity, product cost, and product monitoring study operational performance shown in Figure 2.

(i) Initiating

(ii) Planning

(iii) Executing

(iv) Controlling

(v) Monitoring

(vi) Completion

An energy unit is an activity with a start and end date, a transition, a unique and unknown element, and therefore a degree of risk. Energy units are usually created to solve a problem or take advantage of an opportunity. The day-to-day work normally undertaken by a solar energy consumption analysis is not an energy unit. The factor that determines whether an activity is an energy unit is its uniqueness. A successful energy unit's manager must simultaneously manage these four key elements of energy units shown in Figure 3.

(i) Solar panel energy construction resources

(ii) Optimization duration

(iii) Operational cost

(iv) Scope of the IOT devices

All these elements are interrelated, and each must be managed effectively. The most used resource in all energy units is the employees participating in the energy units. Energy unit's managers must ensure that the energy units works, that potential problems are resolved quickly, that the energy units is completed on time, and that the energy units quality and budget are acceptable. Energy unit managers are responsible for directing all activities necessary and that are shown in the following Figure 4.

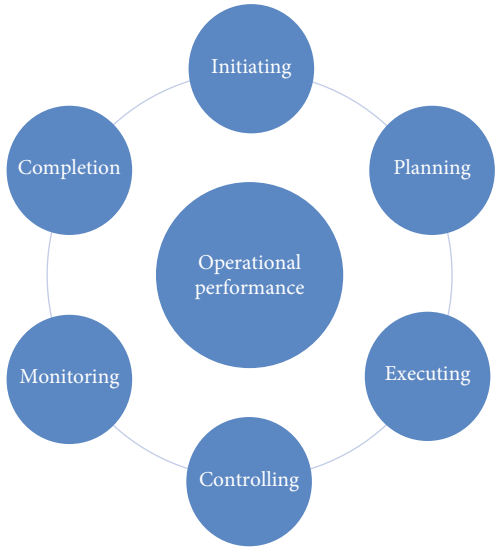

Figure 2: Operational performances.

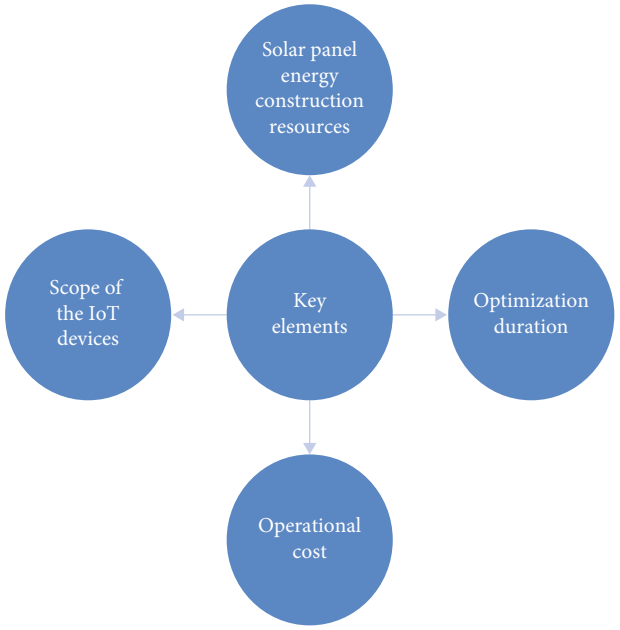

Figure 3: Key elements of energy units.

(i) Successfully achieve energy units goals

(ii) Performing risk management

(iii) Identifying and resolving potential problems before they occur

(iv) Recommending alternative approaches to emerging problems

(v) Reporting energy units progress

(vi) Planning is key to successful implementation

It is the easiest and cheapest way to use solar energy. Special devices that absorb solar radiation during the day and illuminate areas at night are very popular among owners of

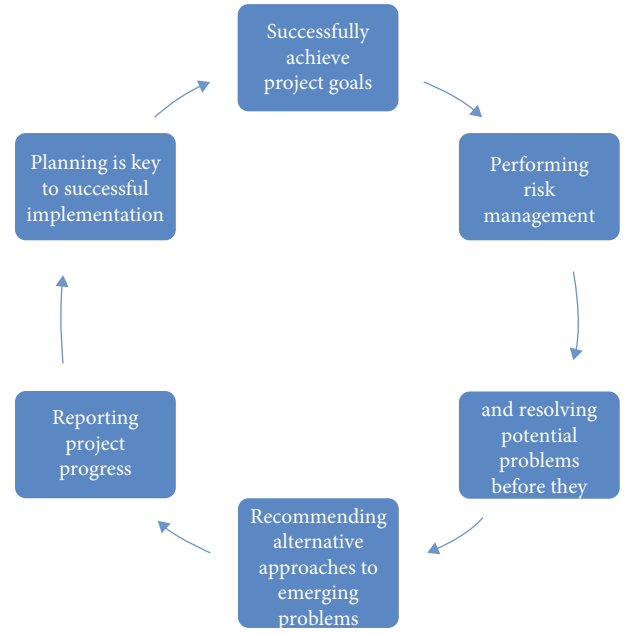

Figure 4: Energy directing activities.

private houses. Generally, production monitoring inspections focus on machine tool accuracy testing, part or product inspections, and process quality control. Additionally, solar energy consumption analysis should always check their product and process quality. These services provided by authorized organizations include monitoring of the manufacturing process, quality monitoring of end products, dimensional monitoring, packaging and loading monitoring, handling and storage monitoring, and source control. Therefore, failure and damage analysis should be performed to understand the root cause of problems, avoid recurrence, and reduce the cost of reliability. Technical solutions to understand malfunctions and their causes are incorporated at various stages, thus avoiding recurrence of malfunctions. This method uses a completely different system. A solar receiver looks like a multilayer structure. Its principle of operation looks like this. When passing through the glass, the rays strike the dark metal, which is known to absorb light well. Solar radiation heats the water under the iron plate. Then, everything happens as in the first method. Hot water can be used to heat space or generate electricity. True, the effectiveness of this method is not enough to be used everywhere.

4. Results and Discussions

The proposed solar energy consumption analysis model (SECAM) was compared with the existing organic photovoltaic energy harvesting system (OPEHS), a hybrid multimodal energy harvester (HMEH), improved metaheuristic-based clustering (IMBC), and Multi-Objective Optimization with Mayfly Algorithm (MOOMA).

4.1. Remote Monitoring. These services reduce solar energy consumption analysis' health and safety risks and increase

Table 1: Comparison of remote monitoring.

No of inputs	OPEHS	HMEH	IMBC	MOOMA	SECAM
250	59.23	60.68	59.00	71.48	87.17
500	59.12	60.70	58.83	71.21	86.67
750	59.10	61.58	59.56	71.51	86.79
1000	59.02	61.89	59.69	71.43	86.50
1250	58.96	62.34	59.97	71.45	86.31
1500	58.89	62.79	60.25	71.46	86.12
1750	58.83	63.24	60.53	71.48	85.93

Table 2: Comparison of quantitative analysis.

No of inputs	OPEHS	HMEH	IMBC	MOOMA	SECAM
250	59.02	61.89	59.69	71.43	86.50
500	58.95	62.34	59.97	71.44	86.31
750	58.89	62.79	60.25	71.46	86.12
1000	58.82	63.24	60.53	71.47	85.93
1250	58.76	63.69	60.81	71.49	85.74
1500	58.69	64.14	61.09	71.50	85.55
1750	58.62	64.59	61.37	71.51	85.36

resource utilization, thereby increasing efficiency in solar energy consumption analysis integrity. This remote monitoring was compared and demonstrated in the following Table 1.

In addition to quality control of energy units in the construction industry, an inspection of gas cylinders, pipelines, and storage tanks in the chemical industry and management of pipelines, chimneys, phase separators, and boilers in the oil and natural gas industry, nuclear power plants, wind turbines, solar panels, and dams are all included in remote monitoring services. It is preferred in inspecting accessible structures and enclosed areas or in the infrastructure investigation of viaducts, railways, and bridges.

4.2. Quantitative Analysis. Speeding up the process requires a detailed and quantitative analysis of the causes and effects along the critical path of a particular process. Depending on the operations of the solar energy consumption analysis, key processes include order status, inventory of equipment in stock, design verification, manufacturing progress, testing, packaging, solar energy consumption analysis, and distribution. This quantitative analysis was compared and demonstrated in the following Table 2.

Expediting the process ensures the efficiency and successful execution of procurement contracts involving unlimited goods and services, improves communication, helps avoid solar energy consumption analysis spillovers, and controls production delays. Process acceleration is one of the best quality assurance methods for energy units to be carried out within schedule and cost.

4.3. Process Acceleration. In short, process acceleration is an energy unit's management technique used as part of the procurement process based on ensuring the quality and timely delivery of materials and components. Solar energy consumption analysis must monitor and control the supplier's progress at the manufacturing facility to ensure that their products arrive at the agreed destination, at the agreed quality, and on the agreed contract delivery date. The expediting process is usually between the manufacturer and the supplier. This process acceleration was compared and demonstrated in the following Table 3.

Recognized companies provide efficient and cost-effective services in production planning and manufacturing processes for all major industry sectors and equipment. The proposed model provides process acceleration services within the scope of supplier services provided during equipment manufacturing. Thanks to these services, solar energy consumption analysis can provide highly efficient, high-performance, and quality services that are secure, fast, and seamless.

4.4. Acceptance Tests. Factory acceptance tests are an important way to ensure that purchased equipment and systems conform to agreed design specifications. These tests allow any problems to be corrected at the vendor's location or prior to production. Thanks to these tests, which require technical expertise and resources, any undesirable situation in the plant is prevented, and the overall quality of the product supplied is improved. This acceptance tests were compared and demonstrated in the following Table 4.

Although there are some general rules for factory acceptance testing in practice, the process is actually a customized process. Factory acceptance tests are very complex and depend on different factors. To succeed in factory acceptance testing, it is important to clarify expectations early and communicate effectively throughout the process. The processes of factory acceptance tests include planning, performing test operations, collecting test results, determining problems, and resolving problems when necessary.

4.5. Production Monitoring. It is an important method of evaluation that involves inspection, measurement, testing, and comparison of products or materials. An inspection process is to determine whether a material or material used in production is of appropriate size and condition or fits and conforms to specified requirements. Monitoring inspections at each stage of production is one of the main components of the quality management system in any energy units. Different selections are required at different stages of production to achieve the required quality. This production monitoring was compared and demonstrated in the following Table 5.

4.6. Planning Process. In the planning process, the tests to be performed, test criteria, protocols, required equipment, acceptable features, and responsibilities, as well as the personnel to participate in the tests are determined. Factory acceptance tests are coordinated and applied according to planned requirements, specifications, and contracts. This planning process was compared and demonstrated in the following Table 6.

Table 3: Comparison of process acceleration.

No of inputs	OPEHS	HMEH	IMBC	MOOMA	SECAM
250	62.20	64.41	62.90	75.02	90.02
500	63.40	65.73	63.63	76.34	90.40
750	64.01	66.56	64.52	76.88	90.97
1000	64.42	66.96	64.60	77.18	90.67
1250	65.32	68.03	65.41	78.11	91.14
1500	66.05	68.88	66.01	78.81	91.39
1750	66.77	69.73	66.61	79.51	91.64

Table 4: Comparison of acceptance tests.

No of inputs	OPEHS	HMEH	IMBC	MOOMA	SECAM
250	66.05	68.88	66.01	78.81	91.40
500	66.78	69.73	66.61	79.51	91.65
750	67.51	70.58	67.21	80.21	91.90
1000	68.24	71.43	67.81	80.91	92.15
1250	68.97	72.28	68.41	81.61	92.40
1500	69.70	73.13	69.01	82.31	92.65
1750	70.43	73.98	69.61	83.01	92.90

Table 5: Comparison of production monitoring.

No of inputs	OPEHS	HMEH	IMBC	MOOMA	SECAM
250	50.72	64.31	61.51	75.68	87.01
500	52.21	66.28	63.93	77.88	87.00
750	53.01	67.41	64.34	78.68	88.20
1000	54.27	69.10	66.09	80.41	88.59
1250	55.42	70.65	67.51	81.91	89.19
1500	56.56	72.20	68.92	83.41	89.78
1750	57.71	73.75	70.34	84.91	90.38

Table 6: Comparison of planning process.

No of inputs	OPEHS	HMEH	IMBC	MOOMA	SECAM
250	54.27	69.10	66.09	80.41	88.59
500	55.41	70.65	67.50	81.91	89.19
750	56.56	72.20	68.92	83.41	89.78
1000	57.70	73.75	70.33	84.91	90.38
1250	58.85	75.30	71.75	86.41	90.98
1500	59.99	76.85	73.16	87.91	91.57
1750	61.13	78.40	74.57	89.41	92.17

Briefly, factory acceptance testing is the process followed during and after the assembly process to verify that it conforms to design specifications and is functional. Thanks to these inspections, it is ensured that the components work properly according to the equipment's functionality.

5. Conclusion

Most of the companies provide remote visual inspection services to solar energy consumption analysis. Remote visual inspections and nondestructive inspection services are offered to solar energy consumption analysis from all sectors as a safe, flexible, and cost-effective alternative to traditional visual inspection methods. In this way, solar energy consumption analysis makes their operations faster, safer, and more cost-effective. The proposed solar energy consumption analysis model (SECAM) was compared with the existing organic photovoltaic energy harvesting system (OPEHS), a hybrid multimodal energy harvester (HMEH), improved metaheuristics-based clustering (IMBC), and Multi-Objective Optimization with Mayfly Algorithm (MOOMA). Solar energy consumption analysis strives to simplify and accelerate the integration of global operations. Speeding up processes is one of the key factors contributing to the successful implementation of large energy units. In this way, the solar energy consumption analysis ensures that its operations continue as planned and manages to minimize delays and costly product shortage issues.

Data Availability

The data used to support the findings of this study are included within the article. Further data or information is available from the corresponding author upon request.

Conflicts of Interest

The authors declare that there are no conflicts of interest regarding the publication of this paper.

Acknowledgments

The authors appreciate the supports from St. Joseph University, Dar es Salaam, Tanzania, for the research and preparation of the manuscript.

References

[1] A. M. Tairab, H. Wang, D. Hao, A. Azam, A. Ahmed, and Z. Zhang, "A hybrid multimodal energy harvester for self-powered wireless sensors in the railway," *Energy for Sustainable Development*, vol. 68, pp. 150–169, 2022.

[2] S. Zhang, N. Bristow, T. W. David, F. Elliott, J. O'Mahony, and J. Kettle, "Development of an organic photovoltaic energy harvesting system for wireless sensor networks; application to autonomous building information management systems and optimisation of OPV module sizes for future applications," *Solar Energy Materials and Solar Cells*, vol. 236, article 111550, 2022.

[3] A. Derdar, N. Bensiali, M. Adjabi et al., "Photovoltaic energy generation systems monitoring and performance optimization using wireless sensors network and metaheuristics," *Sustainable Computing: Informatics and Systems*, vol. 35, article 100684, 2022.

[4] G. C. Jagan and P. J. Jayarin, "Modern Resource Conservation Strategies to Develop Multifaceted Applications of Wireless Sensor Networks: A Review," in *2022 International Conference*

on Communication, Computing and Internet of Things (IC3IOT), pp. 1–4, Chennai, India, 2022, March.

[5] J. Raglend, G. Bhatti, J. Swaminathan, V. Herald-Wilson, J. B. Edward, and R. Sitharthan, "Perspectiva actual de las redes de sensoresinalámbricos para la captación de energía solar," *Revista Ingenio*, vol. 19, no. 1, pp. 16–21, 2022.

[6] S. Kosunalp and Y. Kaya, "IOT-TDMA: a performance evaluation of TDMA scheme for wireless sensor networks with internet of things," *Concurrency and Computation: Practice and Experience*, vol. 34, no. 21, 2022.

[7] A. E. Akin-Ponnle, F. S. Pereira, R. C. Madureira, and N. B. Carvalho, "From macro to micro: impact of smart turbine energy harvesters (STEH), on environmental sustainability and smart city automation," *Sustainability*, vol. 14, no. 3, article 1887, 2022.

[8] M. Sutharasan and J. Logeshwaran, "Design intelligence data gathering and incident response model for data security using honey pot system," *International Journal for Research & Development in Technology*, vol. 5, no. 5, pp. 310–314, 2016.

[9] S. Obilikpa, U. Onochie, C. Nweze et al., "The major mechanisms for efficient hybrid energy harvesting: overview and recent developments," *Asian Review of Mechanical Engineering*, vol. 10, no. 2, 2021.

[10] P. Mohan, N. Subramani, Y. Alotaibi, S. Alghamdi, O. I. Khalaf, and S. Ulaganathan, "Improved metaheuristics-based clustering with multihop routing protocol for underwater wireless sensor networks," *Sensors*, vol. 22, no. 4, article 1618, 2022.

[11] S. Mukase and K. Xia, "Multi-Objective Optimization with Mayfly Algorithm for periodic charging in wireless rechargeable sensor networks," *World Electric Vehicle Journal*, vol. 13, no. 7, p. 120, 2022.

[12] K. Goel and A. K. Bindal, "Regulated Energy Harvesting Scheme for Self-Sustaining WSN in Precision Agriculture," in *Proceedings of Data Analytics and Management*, pp. 367–385, Singapore, 2022.

[13] T. Zhang, F. Ma, C. Peng et al., "A very-short-term online PV power prediction model based on RAN with secondary dynamic adjustment," *IEEE Transactions on Artificial Intelligence*, vol. 2022, 2022.

[14] D. Anuradha, N. Subramani, O. I. Khalaf, Y. Alotaibi, S. Alghamdi, and M. Rajagopal, "Chaotic search-and-rescue-optimization-based multi-hop data transmission protocol for underwater wireless sensor networks," *Sensors*, vol. 22, no. 8, article 2867, 2022.

[15] N. Chouhan, "Artificial intelligence–based energy efficient clustering and routing in IOT assisted wireless sensor network," *Artificial Intelligence for Renewable Energy Systems*, vol. 2022, pp. 79–91, 2022.

[16] N. Subramani, P. Mohan, Y. Alotaibi, S. Alghamdi, and O. I. Khalaf, "An efficient metaheuristic-based clustering with routing protocol for underwater wireless sensor networks," *Sensors*, vol. 22, no. 2, p. 415, 2022.

[17] C. A. Marino, F. Chinelato, and M. Marufuzzaman, "AWS IoT analytics platform for microgrid operation management," *Computers & Industrial Engineering*, vol. 170, article 108331, 2022.

[18] C. Jamroen, N. Yonsiri, T. Odthon, N. Wisitthiwong, and S. Janreung, "A standalone photovoltaic/battery energy-powered water quality monitoring system based on narrowband internet of things for aquaculture: design and implementation," *Smart Agricultural Technology*, vol. 3, article 100072, 2023.

[19] T. Ahmad, R. Madonski, D. Zhang, C. Huang, and A. Mujeeb, "Data-driven probabilistic machine learning in sustainable smart energy/smart energy systems: key developments, challenges, and future research opportunities in the context of smart grid paradigm," *Renewable and Sustainable Energy Reviews*, vol. 160, article 112128, 2022.

[20] P. Sharma, Z. Said, A. Kumar et al., "Recent advances in machine learning research for nanofluid-based heat transfer in renewable energy system," *Energy & Fuels*, vol. 36, no. 13, pp. 6626–6658, 2022.

[21] B. Li, "Effective energy utilization through economic development for sustainable management in smart cities," *Energy Reports*, vol. 8, pp. 4975–4987, 2022.

[22] I. G. Sahebi, A. Mosayebi, B. Masoomi, and F. Marandi, "Modeling the enablers for blockchain technology adoption in renewable energy supply chain," *Technology in Society*, vol. 68, article 101871, 2022.

[23] M. S. Hossain, L. Kumar, M. E. H. Assad, and R. Alayi, "Advancements and future prospects of electric vehicle technologies: a comprehensive review," *Complexity*, vol. 2022, Article ID 3304796, 21 pages, 2022.

[24] G. M. Cabello, S. J. Navas, I. M. Vázquez, A. Iranzo, and F. J. Pino, "Renewable medium-small projects in Spain: past and present of microgrid development," *Renewable and Sustainable Energy Reviews*, vol. 165, article 112622, 2022.

[25] L. Richter, M. Lehna, S. Marchand et al., "Artificial intelligence for electricity supply chain automation," *Renewable and Sustainable Energy Reviews*, vol. 163, article 112459, 2022.

[26] Y. Xia, Y. Zhang, L. Dai, Y. Zhan, and Z. Guo, "A brief survey on recent advances in cloud control systems," *IEEE Transactions on Circuits and Systems II: Express Briefs*, vol. 69, no. 7, pp. 3108–3114, 2022.

[27] K. Saravanakumar and J. Logeshwaran, "Auto-theft prevention system for underwater sensor using lab view," *International Journal of Innovative Research in Computer and Communication Engineering*, vol. 4, no. 2, pp. 1750–1755, 2016.

[28] O. H. Abdalla and A. Mostafa, "Optimal number and locations of smart RMUs for self-healing distribution networks," *International Transactions on Electrical Energy Systems*, vol. 2022, article 4819129, pp. 1–14, 2022.

[29] W. T. Lin, G. Chen, and X. Zhou, "Distributed carbon-aware energy trading of virtual power plant under denial of service attacks: a passivity-based neurodynamic approach," *Energy*, vol. 257, article 124751, 2022.

[30] M. A. Benblidia, B. Brik, M. Esseghir, and L. Merghem-Boulahia, "Power allocation and energy cost minimization in cloud data centers microgrids: a two-stage optimization approach," *IEEE Access*, vol. 10, pp. 66213–66226, 2022.

[31] M. Z. Oskouei, H. Mehrjerdi, D. Babazadeh, P. T. Baboli, C. Becker, and P. Palensky, "Resilience-oriented operation of power systems: hierarchical partitioning- based approach," *Applied Energy*, vol. 312, article 118721, 2022.

Hindawi
International Journal of Photoenergy
Volume 2022, Article ID 5996061, 8 pages
https://doi.org/10.1155/2022/5996061

Review Article

Performance of Multilayered Nanocoated Cutting Tools in High-Speed Machining: A Review

S. Ganeshkumar,[1] **S. Venkatesh**,[1] **P. Paranthaman**,[2] **R. Arulmurugan**,[3] **J. Arunprakash**,[4] **M. Manickam**,[5] **S. Venkatesh**,[6] **and G. Rajendiran**[7]

[1]*Department of Mechanical Engineering, Sri Eshwar College of Engineering, Coimbatore, Tamil Nadu, India*
[2]*Department of Mechanical Engineering, Karpagam Academy of Higher Education, Coimbatore, Tamil Nadu, India*
[3]*Department of Mechanical Engineering, Karpagam College of Engineering, Coimbatore, Tamil Nadu, India*
[4]*Department of Aeronautical Engineering, Hindusthan Institute of Technology, Coimbatore, Tamil Nadu, India*
[5]*Department of Mechanical Engineering, Bharath Institute of Higher Education and Research, Chennai, Tamil Nadu, India*
[6]*School of Mechanical Engineering, Sathyabama Institute of Science and Technology, Chennai, Tamil Nadu, India*
[7]*Department of Motor Vehicle Engineering, Defence University, College of Engineering, Ethiopia*

Correspondence should be addressed to S. Ganeshkumar; ganeshkumar.s@sece.ac.in
and G. Rajendiran; rajendiran.gopal@dec.edu.et

Received 2 August 2022; Revised 1 September 2022; Accepted 20 September 2022; Published 11 October 2022

Academic Editor: BR Ramesh Bapu

In machining processes, cutting tools play a dominant role in producing quality products. The quality of finished goods is directly related to the cutting tool condition. Several types of research have been carried out in cutting tool condition monitoring. On the other hand, the manufacturing industries should be aware of the cutting tool selection, operating conditions, and performance of cutting tools. This article emphasizes the performance of coated cutting tools and tool materials for various machining operations. Nowadays, the nanocoating of CNC tool inserts increases the wear resistance, vibration emissions, metal removal rate, etc. These coating techniques influence the manufacturing industry to increase the productivity and quality of the finished goods and reduce the machining cost. The performance of thin film multilayered coatings such as TiN, TiAlN, AlTiN, Ti, and TiCN on plain silicon carbide tool inserts is revealed by the researchers to guide the manufacturing industry for proper tool selection and standard machining inputs for metal removal operation. The influence of coating material such as TiBN, TiN, TiAlN, and CrAlSiN in cutting tools leads to increase the life time of the cutting tools, which decreases the material sticking and cutting forces. Titanium carbo nitride is wear-resistant and corrosion-resistant. Compared to TiCN, TiAlN is harder due to the higher hardness of 32 GPa. This article concludes the material selection based on the work piece material which yields good metal removal with less cutting forces. The article concludes the cutting material selection based on the work piece for machining operations.

1. Introduction

In the manufacturing industry, the quality of components plays an essential role in satisfying the engineering needs. Precision and accuracy of components can be attained only by machining with appropriate machine tools and machining conditions. In engineering, steel is majorly used in automotive, aerospace, and other industrial applications. In general, machining processes such as drilling, turning, tapping, reaming, and hobbing are being used in manufacturing processes. Turning is the predominant operation among all the machining operations [1] after the machining process. In conventional lathe machines, instead of replacing the whole tool setup, to reduce the replacement cost, inserts are being used for replacement, in which tool inserts are being used in machine and worn out tool inserts are replaced by another insert. In the manufacturing of components, tool wear monitoring is essential, and it is the most challenging

one for the manufacturing industry to meet precision and accuracy. The precision and accuracy of the computer numerical control (CNC) lathe are more compared to the conventional lathe. In practice, after a prescribed period, the performance of machines was reduced due to the depreciation of tools and machine parts [2].

The reduction of machinability is due to the wear of cutting tools. The wear is classified as crater wear, flank wear, adhesive wear, polishing wear, corrosion wear, wear due to temperature, fretting wear, and cavitation damage. In several researches, crater wear and flank wear are taken into account due to the key role in material deterioration.

Several types of research are being carried out to increase machine life and tool life prediction using mathematics. Another predominant way of increasing the tool life is tool coating. In general, for machining of steels and ferrous alloys, silicon carbide materials have been widely used as coating materials. Tool inserts are coated with harder materials to increase the tool life [3]. Accordingly, materials are selected which are harder than base materials. Generally, tungsten, diamond, and carborundum materials are used as coating materials. These harder materials are coated with two different processes, i.e., physical vapor deposition and chemical vapor deposition methods. In most practical applications, the coating thickness is in the range of 0.0025 to 0.0005 μm [4].

Coating of inserts results in resisting the diffusion and shocks while machining, due to the higher hardness of coated inserts which has high wear resistance. Tool wear occurs in inserts due to the diffusion of atoms between the tool and chip material. If diffusion is arrested, then the crater wear rate can be reduced [5]. The present work reveals the technique of reducing tool wear by coating harder materials to control the crater wear and flank wear for ductile materials like steel. In general, predictors of wear are feed rate, depth of cut, and spindle speed. Based on the applications, machining processes for product demands were very high accuracy, surface finish, and precision. Predictors of tool wear are correlated, and the relation between the surface finish, accuracy, feed rate, depth of cut, and speed has been exhibited in the present work. Traditionally, Taylor's tool life equation $VT^n = C$, where V is the cutting speed, T is the tool life, C is the constant, and n is the material constant, is used to predict the tool life. The constant "C" for machining of high speed steel is 0.125, cemented carbide is 0.25, cast alloys is 0.50, and for ceramics is 0.6. In the conventional process, silicon carbide tool inserts are coated with more rigid ceramic materials, to obtain better machining characteristics and increased tool life for various machining operations. Carbide-based inserts play better performance for ferrous materials like steel, cast iron, iron, and stainless steel. Further, the reduction of tool wear rate will yield better accuracy and precision of components. Majorly, tool inserts are being manufactured with silicon carbide as the base material. [6, 7]. The coating thickness of 1-4 micrometers is achieved by magnetosputtering physical vapor deposition process for TiAlN and TiCN cutting tool inserts. The wear of TiN-coated tool inserts is 12% less than the uncoated silicon carbide tool inserts. TiN/Al_2O_3 showed the wear resistance which is 65% less than the uncoated tool inserts in machining of steels.

2. Cutting Tool Manufacturing Processes

The tool inserts are selected such that to withstand high temperature and heavy cutting forces at high cutting speeds, hence that the hardest materials make it in the world. A typical insert is made of 80% tungsten carbide, and 20% of the metal matrix binds the hard carbide together. Cobalt, titanium, and other ingredients are mixed in the milling room to reduce the particle size. The ingredient's particle sizes are reduced by mixing ethanol, water, and other organic binders [8]. The milling process is continued from 8 to 55 hours, depending upon the recipe. The slurry obtained in the milling process is pumped into a spray dryer, and hot nitrogen gas is sprayed to remove the moisture of ethanol and water content. After the drying process, spherical granules of identical sizes of ingredients are obtained. The mixed metal powders are pressed with 12 tons of pressure to manufacture the tool inserts. The binder added in the ball milling operation holds the powder together after pressing. The pressed inserts are very fragile and need to be hardened using a heated oven by sintering processes. The processes take place for 13 hours at approximately 1500°C. The inserts are sintered to make an extremely hardened product, almost the hardness of a diamond. After sintering processes, organic binders are incinerated, which leads to a shrink of approximately 50% of their original size. The cutting tool inserts are ground using grinding machines to make the insert with exact dimensions and tolerances. The excess carbide materials in the cutting fluids are recycled for the manufacturing of new inserts [9].

The majority of the tool inserts are coated either through chemical vapor deposition or physical vapor deposition techniques. The tool inserts are fixed in the fixture of the physical coating deposition machine, and a thin layer of coating material makes the tool insert harder. This coating technique also paves the way to get the specific color of the tool insert. The machining performance is influenced by the coating thickness, coating material, and nanostructure of the coating materials. CNC cemented carbide inserts are used for metal removal operations of steels, high-temperature alloys, and other nonferrous materials. In general, the cutting tips are attached to the tool holders [10]. A typical tool holder and tool insert is shown in Figure 1. The selection of inserts is based on the profile of machining and the materials to be machined. Tool inserts for internal and external turning involve high precision and accuracy of finished components. Sandvik Coromant cutting inserts, Kennametal, Mitsubishi, Hitachi, and Panasonic are the commercial machine tool insert manufacturers. These carbide tool inserts are capable of indexing while machining process to change the cutting edges. These tool inserts can be removed easily from the tool holder, which results in a good surface finish and more metal removal rate at higher cutting speeds [11].

3. Deposition Methods

There are two types of deposition methods used for different coating materials on the base material, i.e., physical vapor

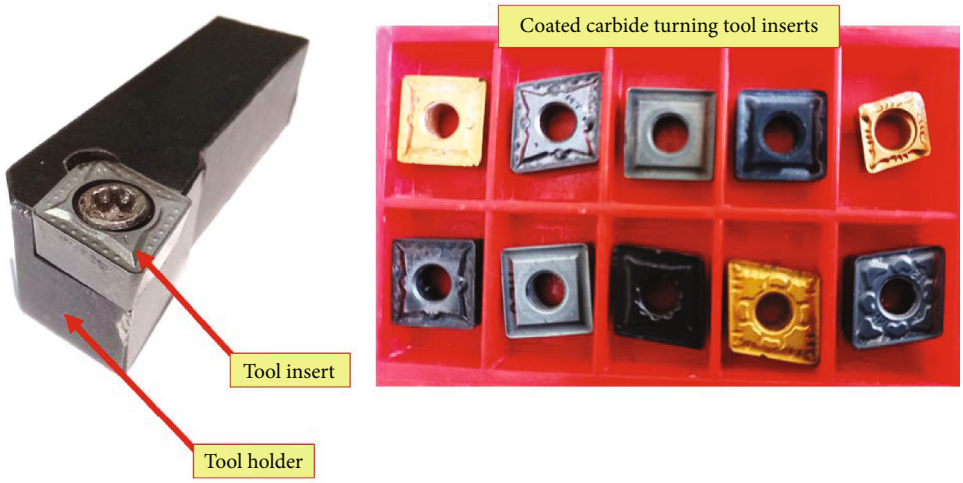

Figure 1: Tool insert, tool holder, and types of coated carbide tool inserts.

deposition methods and chemical vapor deposition methods. The physical vapor deposition method involves physical processes like heating and sputtering. The coating material vapor is evaporated from the chamber and forms a coating on the surfaces of the base material. Similar technologies are being used in the manufacturing of solar panels, semiconductor devices, electronic components, integrated circuits, etc. Commonly industries are using coating materials like titanium nitride, zirconium nitride, chromium nitride, and titanium aluminum nitride, while comparing the physical vapor deposition method and chemical vapor deposition method. PVD coatings are harder and possess good corrosion resistance, and it yields better results than electroplating. These coatings have very high thermal resistance and good impact strength [12]. While doing physical vapor deposition, the system requires a cooling water system. The cooling water system operates at a very high temperature, and it needs highly qualified personnel for operation. However, physical vapor deposition can fulfill the needs of complex geometries. In general, coating materials like TINALOX SN2, Hyperlox, ALOX SN2, HSN2, CC AluSpeed, SUPERSPEED, CCplus C, and CCplus D were widely used in research to improve the quality of machining. These materials are used in the machining of materials like steel, stainless steel, cast iron, nonferrous metals, graphite green compact materials, and Ti-Al alloys. Coated tool inserts increase tool life by increasing toughness, resistance to abrasion, resistance to thermal deformations, modulus of elasticity, and wear resistance, which results in achieving precision and accuracy in machining components [13]. Also, these coated tool inserts broaden the range of depth of cut, cutting speed, and other machining parameters and reduce the time of machining. Coating of tool inserts gives longer tool life and higher cutting parameters leading to reliable performance while machining. The coating process applies to turning, milling, drilling, tapping, and dry cutting operations with or without lubrication [14]. The PVD coated indexable Ti-coated tool inserts are often called as AloXSN^2. The coated machine tools of HSN2, CC AluSpeed, and SUPERSPEED are suitable for rough machining which increases 65% of life time compared to the uncoated tool inserts. The Sandvik Coromant, Mitsubishi, and Panasonic multilayer-coated tool inserts are used to machine the steels, alloys steels, brass, and aluminum alloys.

4. Performance of Coated Tool Inserts in Wear Resistance

The effect of grain size and hardness of wrought alloy 718 with cemented carbide tools is revealed in the turning operation. It is stated in the work that four different conditions of the same materials were studied. A large amount of grain size resulted in a deformed layer of the workpiece was clearly shown in this work. It was reported that transverse turning of discs was done with EMCO 635 CNC lathe with cutting fluids used [15]. It was stated that chip breakers were not used to investigate the morphology of chips and the hardness of the specimen. Uncoated standard cormorant tool inserts were used for experimentation purposes. It was inferred from the relationship between the hardness of the material and flank wear, i.e., flank wears strongly correlated with the hardness of the specimen. Grain size did not influence flank wear, and also, notch wear is associated with the formation of burr [16].

Antiwear resistance analysis in coating materials like chromium nitride and chromium carbonitride was carried out with multilayers. It was reported that chromium and chromium carbonitride coatings improved the quality of machining. TINA 900 M system cathodic evaporation techniques were employed in the research work [17]. The physical vapor deposition method was utilized in this work. Young's modulus, Poisson ratio, and stress were measured, and it was reported that antiwear multilayer coatings improved the quality of machining. Precipitation hardened stainless steels in dry turning using carbide tool inserts results in adhesion wear [18]. It was reported that, due to the adhesion process, diffusion of tool particles results in crater wear and abrasive wear. Tensile strength, yield strength, and hardness parameters were measured in the investigation. The microscopic structure was studied by a

digital microscopic system attached with a readout connected with processors and display units. Flank wear and cutting temperature were analyzed. Tool wear and quality of workpiece in a milling operation are investigated with chilled air flow [19]. It was shown that chilled airflow reduced the working temperature drastically and increased the lifetime of the milling tool. It was reported that chilled airflow increases the quality and surface finish. CFRP (carbon reinforced fiber plastic) material was used for the investigation, and it was shown that chilled air flow increased the quality even at high cutting speeds. Adhesive wear by the physical vapor deposition method was investigated in hot stamping production tools. It was stated that CrN-coated hot stamping or press hardening and stamping tools investigated through the physical vapor deposition method [20]. It was reported that AlcrN-coated tools adopted the same experimental procedure. Imaging confocal microscopic technology was used to view the microscopic pattern change of tool insert before coating and after coating. Topography and material thickness were analyzed by OLYMPUS stereoscopic lens. In drilling die-cast magnesium alloys with high-speed steel uncoated tool inserts, microanalysis of the tool was done to study the grain structure, and orientation of abrasive wear and adhesive wear was taken into account. It was concluded that a change in the trend of the flank face of the drill bit occurred after the drilling operation [21]. Flank wear dominated in drilling operation of die-cast magnesium alloys. Based on the scanning electron microscopic analysis, there were three types of wear reported, i.e., abrasive wear, adhesive wear, and diffusion wear. It was reported in the work that the diffusion process takes place from drilling tool to specimen, tool grains were diffused into the specimen, and the same was observed by microscopic analysis of chips [22]. As reported in work, adhesive wear occurs due to the adhesion force between the drilling tool and specimen, and it was reported that abrasive wear occurred due to the erosion of tool particles due to the cutting force given by the drilling tools [23].

The properties of the single crystal diamond (SCD) tool and polycrystalline diamond (PCD) tools during the machining of silicon and aluminum matrix composite materials are investigated. It was reported that there are many investigations were done on composite materials, ferrous alloys, and other alloys. It was reported that ultraprecision turning technique was introduced in this research. Chipping, peeling, and abrasive wear of SCD and PCD tool materials were observed by SEM analysis [24]. From the reported work, it was inferred that transferring silica particles into aluminum matrix composites results in wear behavior. It was reported that due to the high stiffness of the cutting system, stress relaxation in the cutting tool was observed. The graphitization of SCD tools was observed while machining copper and copper alloys [25]. The properties of coated carbide tools for milling operation are investigated with tool inserts coated with the chemical vapor deposition method. Ti and Cr were used for coating, and the adhesion of the material was tested by indentation adhesion test (Rockwell hardness "*C*" indentation test was carried out). The investigation was carried out with two different categories of coating materials, i.e., coating materials with pretreatment and without pretreatment). It was concluded that pretreated coating materials achieve high abrasion resistance, and tool life was increased. The quality of milling was improved by increasing high accuracy and precision. The surface coating of the cutting tools is achieved by the physical vapor deposition method by electrosputtering technique, chemical vapor deposition method, and LASER texturing techniques [26].

5. Wear Pattern with Diamond Tools

The wear pattern of the diamond tool while machining Al6061 and 1215 steel is revealed. The cutting force was measured in turning operation by a dynamometer, and three-axis transducers were used to measure cutting forces. In tool wear analysis, wear of edge radius, flank wear, and crater wear was taken into account, including the worn volume of inserts. It was reported that there are two categories of materials were used for machining in the investigation, namely, steel and aluminum alloy [27]. It was observed that cutting forces were lower for aluminum alloys than stainless steel. In the machining of AISI 1045 steel, the finite element modeling technique was used to apply the boundary conditions, governing equations were solved by software, and wear behavior was studied in AISI 1045 steel [28]. Cutting velocity, feed rate, and depth of cut were the parameters taken into account, and diffusive wear was observed predominantly at 700°C. Simulations were carried out by deform 3D simulation software. It was reported that 110,000 tetrahedral elements were used in the finite element model [29]. This method involves cost-effective and time-saving simulation processes. In all machining conditions, temperature places a predominant role [30]. In this investigation, temperature, pressure, and stress-induced in tool inserts were included. The study and improving the tool wear resistance property in stamping operations were carried out. Instead of the coating machine tools, die and punch tools were heat treated, and experiments were carried out for boundary lubrication conditions. To improve the wear property further, ceramic thin film AlCrN was coated on tool materials, and wear progressions were monitored [31].

6. Tool Wear Analysis in Turning Operation

The properties of Hastelloy C22HS evaluate tool life and study tool failure in the turning process. TiN, TiCN, and Al2 O3 were coated on the tool by both chemical vapor deposition and physical vapor deposition coating techniques. Results showed that the physical vapor deposition method performance was better than the chemical vapor deposition method. The relationship between the cutting force and process parameters was plotted. Flank wear, crater wear, adhesion wear, and abrasion wear were studied. A vertical machine center OKUMAMX45-VA was used for machining processes [32]. It was concluded that tool life decreases with increasing the depth of cut and feed rate. It was reported that axial depth and feed rate play a predominant role in tool life. It was observed that flank wear, cracking, chipping, adhesion, and abrasion were the failure modes

of tool inserts [33]. Tool life equations were developed from the turning test data and the machining properties of TiAlN coatings in the turning of a nickel-based specimen. Energy dispersive X-ray spectroscopy and SEM analysis have shown that, in nickel-based alloys, workpiece material adhered to tool insert rake face, flank wear, a crater on rake face, and notch in the depth of line were observed. The adhesion process was continuously monitored and observed that adhesion was in periodic formation by stacking and plucking [34]. It was reported that sticking of workpiece material in tool inserts affected the machinability of tool inserts and reduced the cutting forces and decreased accuracy and precision [35]. This investigation was carried out with predominant process parameters such as feed rate, depth of cut, and spindle speed. It was observed that plucking workpiece material adhered from the tool insert led to crater wear, and it was observed that transfer of grains of tool insert grains was into the workpiece. Experiments were carried out in wet conditions, and it was concluded that flank wear, crater wear, and adhesive wear were predominant parameters affecting the tool life in the machining of nickel-based alloys, and coated tool inserts increased the tool life, accuracy, and precision of machining components. CGI (compacted graphite iron) in the machining of cemented carbide milling tools coated with Al2O3 medium temperature chemical vapor deposition technique was utilized for coating. It was concluded that of workpiece material influenced tool life. Three types of materials were used for research and compared with each other [36]. It was shown that it proves cemented carbide cutting tools and Al2O3 coated milling tools performed in varied dimensions while machining with grey iron and compacted graphite iron (CGI). The microstructure of the milling tools (similar to our previous references) was as follows. Kristel dynamometer was used to measure the cutting force while machining. The white light interferometer was used to measure the surface roughness of the specimen. Scanning electron microscopy results showed that, if the microstructure is perpendicular to the cutting edge, it was reported. If that microstructure is perpendicular, it will give a better surface finish, accuracy, and precision in the workpiece [37]. A focused ion beam system observed microstructures with liquid gallium ion sources. FEI Quanta 3D FEG technique was used to fabricate the tool materials [38].

Hence, the microstructures were perpendicular, i.e., 90° to the rake face, and it was shown that it increases the lifetime of tool materials. The tool wear patterns in the machining of carbon steel were coated with cemented carbide inserts. This research involves the usage of lubricants in different conditions. AISI steel with 25 HRC was in milling operations with three types of lubrication: MQL, flooded, and minimum requirement of lubrications. It was concluded that the reduced flow rate of lubricants increased the quality of the workpiece compared to a flooded type of lubrication, and it was observed that adhesion and abrasive wear occurred in machine tools. The experimentation in tool failure and failure modes in forming of stainless steel were carried out. It was reported that the wear of forming tools leads to failure and inaccuracy of forming components. It was concluded that the increase of hardness of the forming tools led to an increase in galling resistance and increased the tool life [39–44].

The development of a new wear index by analyzing the mechanical properties of diamond tool inserts was also done through the petrographic study of diamond and calcium alkali-type rocks, i.e., ceramics. It was observed that the mechanical property table diamond plays an essential role in hardness [45]. Hence, it is used predominantly used in all cutting tools as coating materials. Silicon carbide tool inserts were more economical than diamond tools. Biotite, feldspar, quartz, plagioclase, and hornblende type ceramics were used as coatings. A conceptual design of new materials for coating turning tools was reported in this investigation by reference to the machining of granites and other ceramic specimens [46–49]. It was concluded that quartz and feldspar performed better, and it was widely used in the stone processing industry. The investigation has shown that ceramics like quartz and feldspar were used widely in the stone processing industry, and it was rarely used in turning and other machining purposes or not used commercially since hardness property cannot satisfy the machining of steel or other engineering components [50–54]. The work in TiAlN coatings for drilling operation was carried out. Effect of tool geometry on the wear of cemented carbide coated with TiAlN in the drilling of compact graphite iron was reported. It was concluded that adhesion mechanism was observed in TiAlN coated drill bits, and surface finish and accuracy were better while using drill bits coated with TiAlN in the machining of compact graphite iron (CGI) [54–59].

7. Conclusions

The recent advances in multilayered coating material for cutting tool inserts are reviewed in this article. The manufacturing techniques of cutting tool inserts from the slurry are discussed. The performance of coated tool inserts over uncoated silicon carbide inserts was discussed. The coating techniques, such as the physical vapor deposition method and chemical vapor deposition method, are revealed in this article. From the various researches, the coating material and thickness play the predominant role in wear pattern and tool life. The coating material is selected to withstand high cutting forces and temperature while machining. The wear resistance of the coating material depends on the pressure and temperature applied while manufacturing the tool inserts [60]. The single, bilayer, and multilayer coating of tool inserts leads to increasing wear resistance properties and metal removal ability. The recent advancements of nanolayered coatings lead to a reduction of ball sizes which increases the adhesive property [61, 62]. The increasing adhesive property reduces the adhesive wear of tool inserts. The performance level of multilayered coatings increases the performance level over conventional coating methods. The radial, feed force, and cutting force for the coated tool inserts are increased after the coating. The cutting force of TiN-coated high speed steels is 25% greater than uncoated silicon carbide tool inserts.

Data Availability

The raw/processed data required to reproduce these findings cannot be shared at this time as the data also forms part of an ongoing study.

Conflicts of Interest

The authors declare that they have no conflicts of interests.

References

[1] R. I. R. Abdullah, B. I. Redzuwan, M. S. Abdul Aziz, and M. S. Kasim, "Comparative study of tool wear in milling titanium alloy (Ti-6Al-4V) using PVD and CVD coated cutting tool," *Industrial Lubrication and Tribology*, vol. 69, no. 3, pp. 363–370, 2017.

[2] K. Abou-El-Hossein, O. Olufayo, and Z. Mkoko, "Diamond tool wear during ultra-high precision machining of rapidly solidified aluminium RSA 905," *Wear*, vol. 302, no. 1-2, pp. 1105–1112, 2013.

[3] V. Ageh, D. Choudhuri, and T. W. Scharf, "High frequency reciprocating sliding wear behavior and mechanisms of quaternary metal oxide coatings," *Wear*, vol. 330-331, pp. 390–399, 2015.

[4] M. M. Aguiar, A. E. Diniz, and R. Pederiva, "Correlating surface roughness, tool wear and tool vibration in the milling process of hardened steel using long slender tools," *International Journal of Machine Tools & Manufacture*, vol. 68, pp. 1–10, 2013.

[5] M. A. F. Ahmada, M. Z. Nuawia, S. Abdullaha, Z. Wahida, Z. Karimb, and M. J. P. E. Dirhamsyah, "Development of tool wear machining monitoring using novel statistical analysis method, I-kaz™," *Procedia Engineering*, vol. 101, pp. 355–362, 2015.

[6] J. Allebert, M. Jungedal, and P. Waara, "Wear on overlay welded HCWI vs. quenched and tempered low alloyed carbon steels evaluated with granite in a laboratory drum test machine," *Wear*, vol. 330-331, pp. 364–370, 2015.

[7] A. Alok and M. Das, "Multi-objective optimization of cutting parameters during sustainable dry hard turning of AISI 52100 steel with newly develop HSN^2-coated carbide insert," *Measurement: Journal of the International Measurement Confederation*, vol. 133, pp. 288–302, 2019.

[8] J. M. Arroyo, A. E. Diniz, M. Sergio, and F. de Limac, "Wear performance of laser precoating treated cemented carbide milling tools," *Wear*, vol. 268, no. 11-12, pp. 1329–1336, 2010.

[9] K. Aslantas, I. Ucunb, and A. C. Icekc, "Tool life and wear mechanism of coated and uncoated Al_2O_3/TiCN mixed ceramic tools in turning hardened alloy steel," *Wear*, vol. 274-275, pp. 442–451, 2012.

[10] M. Astrand, T. I. Selinder, F. Fietzke, and H. Klostermann, "PVD-Al_2O_3-coated cemented carbide cutting tools," *Surface and Coatings Technology*, vol. 188-189, p. 186, 2004.

[11] A. Attanasioa, E. Ceretti, A. Fiorentinoa, C. Cappellinia, and C. Giardinib, "Investigation and FEM-based simulation of tool wear in turning operations with uncoated carbide tools," *Wear*, vol. 344-350, pp. 344–350, 2010.

[12] A. Attanasioa, D. Umbrellob, C. Cappellinia, G. Rotellac, and R. M. Saoubid, "Tool wear effects on white and dark layer formation in hard turning of AISI 52100 steel," *Wear*, vol. 286-287, pp. 98–107, 2012.

[13] Y. Ayed, G. Germain, A. Ammara, and B. Furet, "Degradation modes and tool wear mechanisms in finish and rough machining of Ti17 titanium alloy under high-pressure water jet assistance," *Wear*, vol. 305, no. 1-2, pp. 228–237, 2013.

[14] S. Bahia, M. Nouaria, A. Moufkib, E. El Mansoric, and A. Molinarib, "Hybrid modelling of sliding-sticking zones at the tool-chip interface under dry machining and tool wear analysis," *Wear*, vol. 286-287, pp. 45–54, 2012.

[15] P. Bansa and I. S. Rajay Vedaraj, "Monitoring and analysis of vibration signal in machine tool structures," *International Journal of Engineering Development and Research*, vol. 2, pp. 2310–2317, 2014.

[16] B. D. Beake, J. F. Smith, A. Gray, G. S. Fox-Rabinovich, S. C. Veldhuis, and J. L. Endrino, "Investigating the correlation between nano-impact fracture resistance and hardness/modulus ratio from nanoindentation at 25-500 °C and the fracture resistance and lifetime of cutting tools with Ti_{1-x} Al_x N (x = 0.5 and 0.67) PVD coatings in milling operations," *Surface and Coatings Technology*, vol. 201, no. 8, pp. 4585–4593, 2007.

[17] A. Bedolla-Jacuinde, F. V. Guerra, M. Rainforth, I. Mejía, and C. Maldonado, "Sliding wear behavior of tempered ductile iron micro alloyed with boron," *Wear*, vol. 330, pp. 23–31, 2017.

[18] P. Bilek, P. Jurci, M. Novak, M. Hudakova, and L. Caplovic, "Tribological and mechanical properties of Cr_2N-11Ag- coatings deposited on Cr-V ledeburitic steel," *Wear*, vol. 340-341, pp. 47–52, 2015.

[19] C. Boher, S. LeRoux, L. Penazzi, and C. Dessain, "Experimental investigation of the tribological behavior and wear mechanisms of tool steel grades in hot stamping of a high-strength boron steel," *Wear*, vol. 294–295, pp. 286–295, 2012.

[20] M. E. R. Bonif Go and A. E. Diniz, "Correlating tool wear, tool life, surface roughness and tool vibration in finish turning with coated carbide tools," *Wear*, vol. 173, no. 1-2, pp. 137–144, 1994.

[21] M. C. Cakir, C. Ensarioglu, and I. Demirayak, "Mathematical modeling of surface roughness for evaluating the effects of cutting parameters and coating material," *Journal of Materials Processing Technology*, vol. 209, no. 1, pp. 102–109, 2009.

[22] J. L. Cantero, J. Díaz-Álvarez, M. H. Miguélez, and N. C. Marín, "Analysis of tool wear patterns in finishing turning of Inconel 718," *Wear*, vol. 297, no. 1-2, pp. 885–894, 2013.

[23] W. Chang, J. Sun, X. Luo, J. M. Ritchie, and C. Mack, "Investigation of microstructured milling tool for deferring tool wear," *Wear*, vol. 271, no. 9-10, pp. 2433–2437, 2011.

[24] V. V. Chayeuski, V. V. Zhylinski, P. V. Rudak, D. P. Rusalsky, N. Visniakov, and O. Cernasejus, "Characteristics of ZrC/Ni-UDD coatings for a tungsten carbide cutting tool," *Applied Surface Science*, vol. 446, pp. 18–26, 2018.

[25] S. Chinchanikar and S. K. Choudhury, "Wear behaviors of single-layer and multi-layer coated carbide inserts in high speed machining of hardened AISI 4340 steel," *Journal of Mechanical Science and Technology*, vol. 27, no. 5, pp. 1451–1459, 2013.

[26] Y. K. Chou and H. Song, "Tool nose radius effects on finish hard turning," *Journal of Materials Processing Technology*, vol. 148, no. 2, pp. 259–268, 2004.

[27] R. B. Da Silva, J. M. Vieira, R. N. Cardoso et al., "Tool wear analysis in milling of medium carbon steel with coated cemented carbide inserts using different machining lubrication/cooling systems," *Wear*, vol. 271, no. 9-10, pp. 2459–2465, 2011.

[28] W. W. Da Silvaa, M. P. Suarez, A. R. Machado, and H. L. Costa, "Effect of laser surface modification on the micro-

abrasive wear resistance of coated cemented carbide tools," *Wear*, vol. 302, no. 1-2, pp. 1230–1240, 2013.

[29] V. V. De Oliveiraa, P. A. De, C. Beltrãob, and G. Pintaudeb, "Effect of tool geometry on the wear of cemented carbide coated with TiAlN during drilling of compacted graphite iron," *Wear*, vol. 271, no. 9-10, pp. 2561–2569, 2011.

[30] N. R. Dhara and M. Kamruzzamanb, "Cutting temperature, tool wear, surface roughness and dimensional deviation in turning AISI-4037 steel under cryogenic condition," *International Journal of Machine Tools & Manufacture*, vol. 47, pp. 754–759, 2007.

[31] D. E. Dimla, "Sensor signals for tool-wear monitoring in metal cutting operations—a review of methods," *International Journal of Machine Tools & Manufacture*, vol. 40, pp. 1073–1098, 2002.

[32] D. Becker, "Wear of nanostructured composite tool coatings," *Wear*, vol. 304, no. 1-2, pp. 88–95, 2013.

[33] A. E. Diniz and R. Micaroni, "Cutting conditions for finish turning process aiming: the use of dry cutting," *International Journal of Machine Tools & Manufacture*, vol. 42, no. 8, pp. 899–904, 2002.

[34] L. A. Dobrzański and J. Mikuła, "The structure and functional properties of PVD and CVD coated Al_2O_3 + ZrO_2 oxide tool ceramics," *Journal of Materials Processing Technology*, vol. 167, no. 2-3, pp. 438–446, 2005.

[35] M. Dogra, V. S. Sharmab, and J. Durejac, "Effect of tool geometry variation on finish turning – a review," *Journal of Engineering Science and Technology Review*, vol. 4, no. 1, pp. 1–13, 2011.

[36] K. Edalati, M. Ashida, Z. Horita, T. Matsui, and H. Kato, "Wear resistance and tribological features of pure aluminum and Al- Al_2O_3 composites consolidated by high-pressure torsion," *Wear*, vol. 310, no. 1-2, pp. 83–89, 2014.

[37] A. Faraz, D. Biermann, and K. Weinert, "Cutting edge rounding: an innovative tool wear criterion in drilling CFRP composite laminates," *International Journal of Machine Tools & Manufacture*, vol. 49, no. 15, pp. 1185–1196, 2009.

[38] A. Fariasa, G. F. Batalha, E. F. Prados, R. Magnabosco, and S. Delijaicov, "Tool wear evaluations in friction stir processing of commercial titanium Ti-6Al-4V," *Wear*, vol. 302, no. 1-2, pp. 1327–1333, 2013.

[39] A. I. Fernandez-Abia, J. Barreiro, J. Fernández-Larrinoa, L. N. Lopez de Lacalle, A. Fernández-Valdivielso, and O. M. Pereira, "Behaviour of PVD coatings in the turning of austenitic stainless steels," *Procedia Engineering*, vol. 63, pp. 133–141, 2013.

[40] S. García-Rodrígueza, B. Torresa, A. Marotob, A. J. Lópeza, E. Oteroa, and J. Ramsa, "Dry sliding wear behavior of globular AZ91 magnesium alloy and AZ91/SiCp composites," *Wear*, vol. 390-391, pp. 1–10, 2017.

[41] S. F. Garcin, S. Fouvry, and S. Heredia, "A FEM fretting map modeling: effect of surface wear on crack nucleation," *Wear*, vol. 330-331, pp. 145–159, 2015.

[42] A. K. Ghani, I. A. Choudhury, and Husni, "Study of tool life, surface roughness and vibration in machining nodular cast iron with ceramic tool," *Journal of Materials Processing Technology*, vol. 127, no. 1, pp. 17–22, 2002.

[43] A. Gilewicza, B. Warcholinskia, P. Myslinskia, and W. Szymanskib, "Anti-wear multilayer coatings based on chromium nitride for wood machining tools," *Wear*, vol. 270, no. 1-2, pp. 32–38, 2010.

[44] S. Goel, X. Luo, R. L. Reuben, and H. Pen, "Influence of temperature and crystal orientation on tool wear during single point diamond turning of silicon," *Wear*, vol. 284-285, pp. 65–72, 2010.

[45] N. Gunes Yılmaza, R. M. Goktanb, and Y. Kibici, "An investigation of the petrographic and physico-mechanical properties of true granites influencing diamond tool wear performance, and development of a new wear index," *Wear*, vol. 271, no. 5-6, pp. 960–969, 2011.

[46] F. Haase, S. Lockwood, and F. D. Ford, "Vibration modelling of machine tool structures," *Transactions on Engineering Sciences*, vol. 34, pp. 137–146, 2001.

[47] B. Haddag and B. Nouari, "Tool wear and heat transfer analyses in dry machining based on multi-steps numerical modelling and experimental validation," *Wear*, vol. 302, no. 1-2, pp. 1158–1170, 2013.

[48] S. Hanke, M. Beyer, J. F. DosSantos, and A. Fischer, "Friction surfacing of a cold work tool steel–Microstructure and sliding wear behavior," *Wear*, vol. 308, no. 1-2, pp. 180–185, 2013.

[49] J. Hardell, S. H. S. Mozgovoy, L. P. C. Courbon, and B. Prakash, "Effect of oxide layers and near surface transformations on friction and wear during tool steel and boron steel interaction at high temperatures," *Wear*, vol. 330-331, pp. 223–229, 2015.

[50] S. Hernandez, J. Hardell, W. Winkelmann, M. Rodriguez Ripoll, and B. Prakash, "Influence of temperature on abrasive wear of boron steel and hot forming tool steels," *Wear*, vol. 338-339, pp. 27–35, 2015.

[51] X. Huang, I. Etsion, and T. Shao, "Effects of elastic modulus mismatch between coating and substrate on the friction and wear properties of TiN and TiAlN coating systems," *Wear*, vol. 338-339, pp. 54–61, 2015.

[52] A. Inspektor and P. A. Salvador, "Architecture of PVD coatings for metalcutting applications: A review," *Surface and Coatings Technology*, vol. 257, pp. 138–153, 2014.

[53] Y. Isik, "Tool life and performance comparison of coated tools in metal cutting," *International Journal of Materials and Product Technology*, vol. 39, no. 3/4, pp. 240–250, 2010.

[54] X. Wang and C. X. Feng, "Development of empirical models for surface roughness prediction in finish turning," *International Journal of Advanced Manufacturing Technology*, vol. 20, pp. 348–356, 2002.

[55] S. Venkatesh, S. P. Sivapirakasam, M. Sakthivel, S. Ganeshkumar, M. M. Prabhu, and M. Naveenkumar, "Experimental and numerical investigation in the series arrangement square cyclone separator," *Powder Technology*, vol. 383, pp. 93–103, 2021.

[56] S. Ganeshkumar, V. Thirunavukkarasu, R. Sureshkumar, S. Venkatesh, and T. Ramakrishnan, "Investigation of wear behaviour of silicon carbide tool inserts and titanium nitride coated tool inserts in machining of en8 steel," *International Journal of Mechanical Engineering and Technology*, vol. 10, no. 1, pp. 1862–1873, 2019.

[57] S. G. Kumar and V. Thirunavukkarasu, "Investigation of tool wear and optimization of process parameters in turning of EN8 and EN 36 steels," *Asian Journal of Research in Social Sciences and Humanities*, vol. 6, no. 11, pp. 237–243, 2016.

[58] S. Ganeshkumar, R. Sureshkumar, Y. Sureshbabu, and S. Balasubramani, "A review on cutting tool measurement in turning tools by cloud computing systems in industry 4.0 and IoT," *GIS science journal*, vol. 7, no. 8, pp. 1–7, 2020.

[59] S. Ganeshkumar, R. Sureshkumar, Y. Sureshbabu, and S. Balasubramani, "A numerical approach to cutting tool stress

in CNC turning of EN8 steel with silicon carbide tool insert," *International Journal of Scientific & Technology Research*, vol. 8, no. 12, pp. 3227–3231, 2019.

[60] G. Gokilakrishnan, S. Ganeshkumar, H. Anandakumar, and M. Vigneshkumar, "A Critical Review of Production Distribution Planning Models," in *2021 7th International Conference on Advanced Computing and Communication Systems (ICACCS)*, vol. 1, pp. 2047–2051, Coimbatore, India, 2021.

[61] S. Ganeshkumar and S. Venkatesh, "Manufacturing techniques and applications of multifunctional metal matrix composites," in *Functional Composite Materials: Manufacturing Technology and Experimental Application*, Bentham Science Publishers, 2022.

[62] S. Ganeshkumar, S. D. Kumar, U. Magarajan et al., "Investigation of tensile properties of different infill pattern structures of 3D-printed PLA polymers: analysis and validation using finite element analysis in ANSYS," *Materials*, vol. 15, no. 15, p. 5142, 2022.

Hindawi
International Journal of Photoenergy
Volume 2022, Article ID 1164613, 8 pages
https://doi.org/10.1155/2022/1164613

Research Article

Multicluster Analysis and Design of Hybrid Wireless Sensor Networks Using Solar Energy

T. Vino,[1] S. S. Sivaraju,[2] R. V. V. Krishna,[3] T. Karthikeyan,[4] Yogesh kumar Sharma,[5] K. G. S. Venkatesan,[6] G. Manikandan,[7] R. Selvameena,[8] and Mebratu Markos[9]

[1]*Department of ECE, Sathyabama Institute of Science and Technology, Chennai, Tamil Nadu, India*
[2]*Department of Electrical and Electronics Engineering, RVS College of Engineering and Technology, Coimbatore, Tamil Nadu, India*
[3]*Department of Electronics and Communication Engineering, Aditya College of Engineering & Technology, Aditya Nagar, ADB Road, Surampalem, 533437, East-Godavari District, Andhra Pradesh, India*
[4]*Department of Biomedical Engineering, Sona College of Technology, Salem, Tamil Nadu, India*
[5]*Department of Computer Science and Engineering, Koneru Lakshmaiah Education Foundation, Vaddeswaram, Guntur, Andhra Pradesh, India*
[6]*Department of Computer Science and Engineering, Megha Institute of Engineering and Technology for Women, Edulabad, 501301 Hyderabad, Telangana, India*
[7]*Department of Electronics and Communication Engineering, Saveetha School of Engineering, Saveetha Institute of Medical and Technical Sciences, Thandalam, Chennai, 602105 Tamil Nadu, India*
[8]*Department of Computer Science and Engineering, Dr. M.G.R Educational and Research Institute, Maduravoyal, 600095, Chennai, Tamil Nadu, India*
[9]*Department of Mechanical Engineering, College of Engineering, Wolaita Sodo University, Ethiopia*

Correspondence should be addressed to Mebratu Markos; mebratumarkos@wsu.edu.et

Received 26 July 2022; Revised 10 September 2022; Accepted 16 September 2022; Published 11 October 2022

Academic Editor: Br Ramesh Bapu

A wireless touch network is a distributed, self-organizing network of multiple sensors and actuators in combination with multiple sensors and a radio channel. Also, the security area of such a network can be several meters to several meters. The main difference between wireless sensor networks from traditional computer and telephone networks is the lack of a fixed infrastructure owned by a specific operator or provider. Each user terminal in a touch network is capable of acting as a terminal device only. Despite the long history of sensor networks, the concept of building a sensor network is not finally imposed and expressed in some software and hardware (platform) solutions. In this paper, the design and analysis of multicluster model of the sensor nodes in wireless sensor network with the help of solar energy. This proposed model provides the required energy to transmit the information between two end nodes in different cluster. The communication between the end to end clusters was increased based on this design. The implementation of sensory networks at the current stage depends largely on the specific needs of the industrial problem. The architecture, software, and hardware implementation technology is at an intensive development stage, attracting the attention of developers looking for a technological niche of future makers.

1. Introduction

One of the first prototypes of a touch network is considered to be a social system designed to detect and identify submarines [1]. Wireless sensor network technology has been developing intensively recently. However, only at the beginning, it was possible to produce a very cheap element base for devices such as the development of microelectronics [2]. Modern wireless networks are mainly based on the ZigBee standard [3]. A significant number of industries and market segments (manufacturing, various types of transportation, security, safety, security, safety, and security) are ready to implement sensor networks, and this volume is continuously increasing [4, 5]. This trend is related to

technological processes, the development of production, expanding the needs of individuals in the security sectors, expanding the needs of resource control, and the use of material-material values [6, 7]. Semiconductor technologies are developing new practical tasks and theoretical problems related to the applications of sensory networks in industrial and ethnic campuses [8]. The use of low-cost wireless sensor control devices opens up new areas to apply telemetry and control systems [9]. A liquid flow battery that is particularly suitable for large-scale long-term energy storage systems is provided with two chemical components dissolved in a liquid separated by a diaphragm. It is exposed in Figure 1.

(i) Directly identify possible failures of the means of execution on the control of such parameters, vibration, temperature, pressure, etc.

(ii) Real-time access control to remote monitoring object systems

(iii) Ensure the protection of museum values

(iv) Ensure accounting views

(v) Automatic censoring of views

(vi) Inspection and inspection of industrial properties

(vii) Management of commercial assets

(viii) Application as components in energy and resource saving technologies

(ix) Control environment environmental parameters

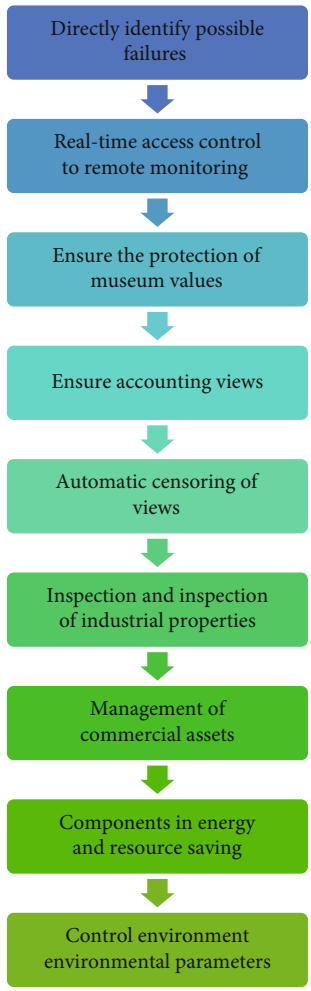

Figure 1: Objectives of low-cost wireless sensor control devices.

Trojan Battery is a lead-acid battery that discharges itself over time, even if it is not connected to a load and is charged to a very low level. This self-discharge rate changes with temperature, with higher temperatures increasing the rate of discharge, while lower temperatures decreasing the rate of discharge. Wireless sensor networks (WSN) are meds with miniature computing devices (temperature, pressure, light, illuminance, vibration levels, location, etc.) and signal transceivers operating in a specific radio scenario [10, 11]. The flexible configuration, cost reduction of installation is available. Intelligent sensors in other wireless and wireless data transfer interfaces allocate wireless networks, especially when it comes to the large number of devices connected to each other; the touch network allows you to connect up to 65,000 devices [12–14]. A constant reduction in the cost of wireless solutions and increasing their operational parameters allow you to gradually reorient through wired solutions in telemetry data collection systems, remote diagnostic information transfer [15]. "Sensor network" today is a well-established term, distributed, self-organizing, stable to the failure of individual components, a nonmaintained network, and does not require special installation of devices [16]. Each sensor network node may contain various sensors to control the external environment, a microcomputer, and a radio receiver [17]. They perform device measurements, perform initial data processing, and communicate with external information systems [18]. As with other lithium-ion batteries, lithium nickel manganese cobalt oxide (NMC) batteries do not require critical maintenance. A battery management system (BMS) monitors the battery's voltage, current, and temperature to ensure safety and service life. Excessive activity will reduce battery life, and the monitoring system will notify the warranty through battery management system (BMS) logs. Battery management system (BMS) shutdowns in any operating conditions where the system is not safe. The battery energy storage system uses lithium nickel manganese cobalt oxide (NMC) batteries manufactured by LGChem. A lithium nickel manganese cobalt oxide (NMC) battery can be used in winter as long as the safety temperature limit is confirmed.

Telecommunication 802.15.4/ZigBee is one of the modern directions for the development of "sensor networks" monitoring and self-regulation of resource management and process fault-tolerant distributed systems [19]. Today, the technology of wireless sensor networks is the only wireless technology through which you can monitor and control problems that are critical to the uptime of sensors [20]. Sensors integrated into a wireless sensor network form a regionally-distributed self-organizing system for collecting, processing, and transmitting information [21]. The main

application area is monitoring and monitoring of measured parameters of physical environments and objects. The adopted IEEE 802.15.4 standard describes wireless channel and access control for low-speed wireless private networks, which are the two lowest levels according to the OSI network model [22].

Usually, BCC is used to collect data from devices equipped with sensors: a temperature sensor, humidity, lighting, and monitoring. For example, miniature sensors could be used in medicine to monitor patients. Devices that the patient brings themselves can control the work of vital organs, in case of certain dangerous situations to inform the doctor [23]. The small dimensions of the devices allow not only "superficial" patient observations but also to examine the internal organs of a person. This is especially true for lead-acid batteries that are added to water, as when distilled water is added to fill the electrolyte level, the acidic liquid is exposed to the outside. We recommend that battery maintenance personnel wear safety glasses and gloves. If the customer requests external, then personnel complete this task in battery maintenance. Therefore, when gastroscopy is carried out in state hospitals, Polygynax uses a special device, a gastroscopic tube, but not all patients can swallow it. It is already available in the market in the form of tablets for conducting such studies [24]. These battery operated devices have a power supply, sufficient to work continuously for 24 hours, and send readings to another device that the patient has at this time. After that, the doctor can analyze the obtained results and make an accurate diagnosis. When using a battery in or near a living space, the basic part of the computer is chosen because the computer is an important guiding principle. The energy storage system uses lithium nickel manganese cobalt oxide (NMC) battery to monitor the battery management system. It is long lasting and very safe. This battery can store more electricity than other types of lithium-ion batteries by adding elements like nickel and manganese to the battery chemistry.

2. Related works

It can be used to automatically change the way a person enters a room to be used to manage any device (in a smart home system). Sometimes you have to follow the movement or destruction of any objects where it is difficult to find the cables. To do this, it is very profitable to apply touch networks again; the sensors are wireless because they provide an autonomous power supply [1]. Also, wireless sensor network technology can be used to transmit audio data—an intercom system and multimedia system with low power consumption. Based on wireless technology and telecommunication networks based on them, it has well-known advantages among flexible configuration and low installation costs [2]. Currently, wireless communication systems can account for the mass and most popular number of systems in the consumer market. Wi-Fi and Bluetooth. Each of them is characterized by range and transmission rate, operating frequency range, function and purpose, as well as other characteristics that determine the structure and structural features of remote telecommunication networks [3]. In the architectural aspect, the main difference between classical telecommunication radio networks and BSS is the use of a large number of supramundane intelligence sensors in the network that transmit small blocks of information over long distances (10-100 m) on average [4]. A zinc bromide liquid flow battery consists of a bromide salt dissolved in an electrolyte. The battery technology is slightly different from traditional bromide liquid flow cells, and its diaphragm is not cleaned or replaced. A liquid flow battery has an infinite charge and discharge cycle without performance degradation.

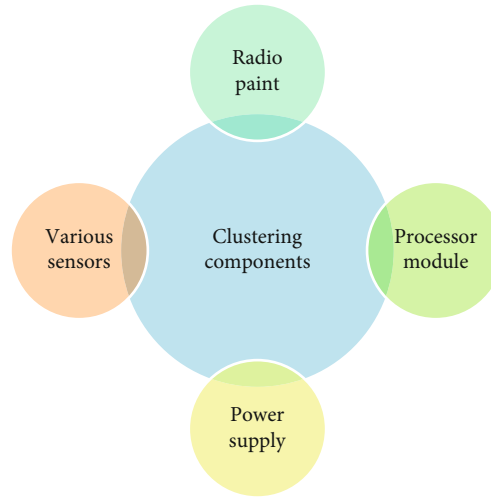

Figure 2: The proposed cluster formation requirements.

IEEE 802.15.4 provides two-way half-duplex data transfer while maintaining AES 128 encryption. The channel access policy is based on carrier sense collision avoidance multiple access (CSMA/CA) with restrictions on carrier and collisions. This is a network protocol, in which the principle of listening to the carrier frequency is used. The transmitting device that transmits data listens for the jam signal (content signal) and the ether [5]. The "someone else's 'jam signal transmitter'sleeps" for a random period, then repeats the frame attempts to initiate transmission. Thus, transmission may come from only one device, which improves network performance. In this case, data is sent in relatively small packages, which contain traffic and monitoring signals in the BSS. An important feature of the standard is the mandatory confirmation of the delivery of messages [6]. A liquid flow battery generally has little maintenance requirements. A liquid flow battery is similar to a fuel-powered lithium battery in that they are only equipped with an electronic device and an electrolytic cell.

A feature of devices connected to the IEEE 802.15.4 standard is low power consumption, which saves the connection in this mode because there is no dynamic data in the "fall" mode. While developing a standard, the main focus was on the speed of the configuration and reconfiguration processes [8]. Specifically, the transmission transition to the active state is about 10-15 ms. And new devices connect to the network in 30 ms. In this case, the duration of reconfiguration and connecting devices depends on the name "listening"

Figure 3: Functions of network coordinator.

by network routers [10]; the flow battery can be used in winter and can be installed in very cold conditions. It is best to monitor all used batteries throughout the day to ensure proper operation and proactively troubleshoot any potential on-site issues. This data can be provided to owners in real-time.

3. Proposed Model

Among the operational rules, the main distinguishing features of BSS are the requirements for stable operation in conditions of dynamic changes in the network topology due to sensors, autonomous power and power consumption, and significant restrictions of microprocessor memory. At the same time, the conditions for BSS operation are provided for the transfer of small amounts of information at low speeds. The "clustered" architecture of a touch network is based on a conventional terminal and the following components. Because the material is heavy, it should be installed in some ventilated area. At this point, their functions and maintenance requirements are well understood, so they are suitable for most solar + energy storage applications and should be stored in a moderately dry location. A lead-acid batteries terminal connection should be checked several times a year to make sure they do not loosen over time. The proposed cluster formation requirements are shown in the following Figure 2.

(i) Radio paint

(ii) Processor module

(iii) Power supply

(iv) Various sensors

The physical layer determines the data transfer method, communication system interface, hardware features, and parameters required to build a network. In practice, the physical state governs the operation of the transceiver, selecting channels, control signals, and transmission power level. The network coordinator (FFD: fully functional device) is shown in Figure 3. A typical node can be represented by three types of devices.

3.1. The Network Coordinator (FFD: Fully Functional Device)

(i) Enables global integration, configuration, and installation of network parameters

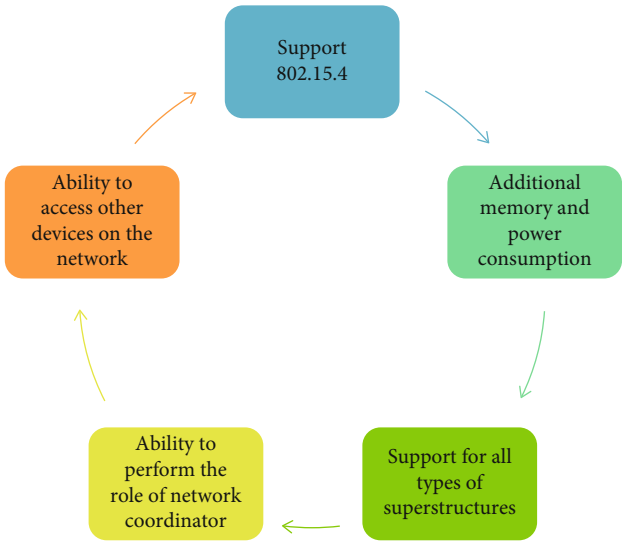

Figure 4: The performance parameters of fully functional device nodes.

(ii) The most demanding of the three types of devices are memory and power supply

Dedicated energy efficiency of network protocols for BSS is required to solve the task, which determines the resource of low power consumption node time during the autonomous power use of network nodes from batteries. A device with a full set of functions (FFD: fully functional device) and a liquid-filled lead-acid battery must be topped up regularly. Glass fiber separator (AGM) battery and gel lead-acid battery are sealed, so do not fill with electrolyte. If a lead-acid battery is not being used temporarily, it must be stored properly. The performance parameters of fully functional device nodes are shown in the following Figure 4.

(i) Support 802.15.4

(ii) Additional memory and power consumption allows the role of network coordinator

(iii) Support for all types of superstructures ("point-point", "star", "tree", and "mesh-free network")

(iv) Ability to perform the role of network coordinator

(v) Ability to access other devices on the network

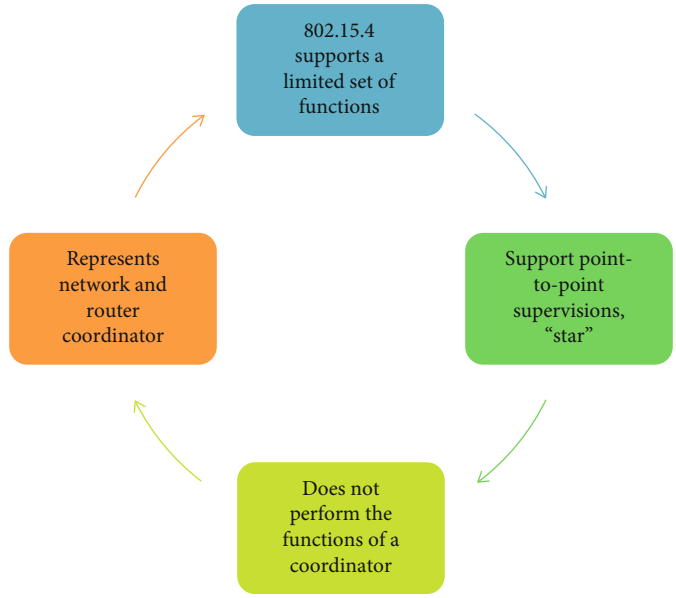

Figure 5: The performance parameters of reduced function device.

The performance parameters of reduced function device were shown in the following Figure 5.

(i) 802.15.4 supports a limited set of functions

(ii) Support point-to-point supervisions, "star"

(iii) Does not perform the functions of a coordinator

(iv) Represents network and router coordinator

The first version of 802.15.4 defined two physical levels with broadband characteristic through direct spectrum expansion DSSS (direct sequence spread spectrum).

(i) The first-868/915 MHz segment has a transmission rate of 20 and 40 Kbps, respectively

(ii) Second-2450 MHz band at 250 Kbps

Data transfer rates initially allowed on 868/915 MHz increased to 100 and 250 kbps. In addition, four health indicators were identified depending on the modeling method; while maintaining the broadband modulation of DSSS, 868/915 MHz can be used in the range of binary and quadruple phase manipulation (QPSK: quadrature phase shift keying). Since the version of the IEEE 802.15.4A standard, the number of physical dimensions increased to six due to the addition of an ultra-wide radiotechnology level ultra-wide band (UWB) for high-speed data transmission, radio technology with level specifications chirp spread spectrum (CSS), through linear frequency modulation method. In terms of broadening the frequency spectrum, the physical state UWB was defined by dedicated frequencies in three bands: 1 GHz, 3-5 GHz and 6-10 GHz, and five CSS. The spectrum in the 2450 MHz band is unlicensed, and the available frequency bands were expanded in the IEEE 802.15.4C and IEEE 802.15.4D versions. This specification is possible using at the physical level, quadrature phase manipulation or high-order phase manipulation (M-PSK) with a frequency of 780 MHz, and a frequency of 950 MHz-Gaussian frequency manipulation (Gaussian frequency-shift keying (GFSK)) or binary phase manipulation (binary phase-shift keeling (PSK)). The standard IEEE 802.15.4.4 specification defines mechanisms for coordinating network components at the physical level to ensure the generation of data fragments (frames), check and correct errors, and transmit frames at the network level. At the same time, the MAC sublayer (media access control) adjusts multiple accesses to a physical environment with a channel-level one-way separation, manages printing connections, and provides security.

4. Results and Discussion

The proposed multicluster analysis and design model (MCADM) was evaluated with the existing improved metaheuristics-based clustering (IMBC), multiobjective optimization with Mayfly algorithm (MOMA), artificial intelligence–based energy-efficient clustering (AIEEC), and the role of integrated structured cabling system (ISCS).

Network node management: the standard defines two types of network nodes: full-featured device FFD (fully functional device), which implements a function of integration and sets network parameters and operates in standard node mode as in Table 1 and Table 2. A device with a limited set of functions RFD (reduced function device) is only capable of communicating with fully featured devices. Any network must have at least one fully featured device.

It enables the coordinator function. Each device has a 64-bit identifier, but in some cases, the link may be used for a limited area of 16-bit connections. PAN (personal area network). The standard also supports the structured topology "star", in which the coordinator (fully functional device) network must be the central node of the created private

Table 1: Management of fully functional device nodes.

No of nodes	IMBC	MOMA	AIEEC	ISCS	MCADM
100	59.23	40.68	43.00	81.48	96.17
200	59.12	40.70	42.83	81.21	95.67
300	59.10	41.58	43.56	81.51	95.79
400	59.02	41.89	43.69	81.43	95.50
500	58.96	42.34	43.97	81.45	95.31
600	58.89	42.79	44.25	81.46	95.12
700	58.83	43.24	44.53	81.48	94.93

Table 2: Management of reduced function device nodes.

No of nodes	IMBC	MOMA	AIEEC	ISCS	MCADM
100	59.02	41.89	43.69	81.43	95.50
200	58.95	42.34	43.97	81.44	95.31
300	58.88	42.79	44.25	81.45	95.12
400	58.81	43.24	44.53	81.46	94.93
500	58.74	43.69	44.81	81.47	94.74
600	58.67	44.14	45.09	81.48	94.55
700	58.60	44.59	45.37	81.49	94.36

Table 3: Management of network topology.

No of nodes	IMBC	MOMA	AIEEC	ISCS	MCADM
100	58.89	42.79	44.25	81.46	95.12
200	58.82	43.24	44.53	81.47	94.93
300	58.75	43.69	44.81	81.48	94.74
400	58.68	44.14	45.09	81.49	94.55
500	58.61	44.59	45.37	81.50	94.36
600	58.54	45.04	45.65	81.51	94.17
700	58.47	45.49	45.93	81.52	93.98

Table 4: Management of autotuning clusters.

No of nodes	IMBC	MOMA	AIEEC	ISCS	MCADM
100	62.20	44.41	46.90	85.02	89.02
200	63.40	45.73	47.63	86.34	89.40
300	64.01	46.56	48.52	86.88	89.97
400	65.01	47.72	49.30	87.94	90.41
500	65.92	48.79	50.11	88.87	90.89
600	66.82	49.87	50.92	89.80	91.36
700	67.73	50.94	51.73	90.73	91.84

network with a unique identifier. After that, other devices can join the network, which is completely independent of other networks with similar locations.

Usually the network is of "cluster wood" type, and different types of devices (FFD and RFD.) are used in the network design phase. At the same time, most nodes have terminal devices, and as a result, within the radius of each of them, there must be at least one node router. It improves location of various classes of devices.

Network topology management: the channel-level and the IEEE 802.15.4 standard provide the general recommendations for network topology construction. As in Table 3, networks can be peer P2P (peer-to-peer, point-to-point); one has a "star" topology. Structurally P2P compounds are arbitrary structures that can only be defined by bounded ranges between pairs of nodes. Take this into account, there are different options for the topical structure of the BSS, especially the "wood" cluster "tree" RFD, the single connected "tree leaves" FFD, and most of the nodes in the network are FFD. Cellular network topology of each cluster has a local coordinator with a local coordinator. The cluster is formed "based on trees" with the coordinator.

Autotuning of clusters: many network clusters for building BCs use private technical solutions and their own layers of network protocols, which reduce power consumption by including solutions at component sizes. In addition to the technical characteristics of transceivers, microcontrollers and wireless modules for power consumption indicate the operational mode of network use and the intensity of data transmission. An allocation of modes of operations with an intensive work cycle and small transfer intensity are performed well as shown in Table 4.

Intensive operating cycle: in applications with an intensive operating cycle, the main share of power consumption is available on the radio interface-reception/transmission of packets, synchronization, and frequency autotuning. At the same time, in the case of propagation in the transport of long packets, the consumption of the transceiver dominates, and in the case of priority transmission of short packets, the consumption frequency autocalibration schemes by the consumption of radio frequency initialization schemes. In applications with a low intensity of transmission, low power methods of sensors, microcontrollers, and microcrystallization of transceivers play the role of indicators of presence and performance as in Table 5.

Table 5: Management of intensive operating cycle.

No of nodes	IMBC	MOMA	AIEEC	ISCS	MCADM
100	64.42	46.96	48.60	87.18	95.67
200	65.32	48.03	49.41	88.11	96.14
300	66.22	49.10	50.22	89.04	96.61
400	67.12	50.17	51.03	89.97	97.08
500	68.02	51.24	51.84	90.90	97.55
600	68.92	52.31	52.65	91.83	98.02
700	69.82	53.38	53.46	92.76	98.49

Perception subsystem management: as a rule, consists of an account, some statistics and analog-to-digital converter relief. The data processing subsystem consists of a central processor and memory, which is not only the data generated by the sensor but also service information that is essential for the proper and complete functioning of the communication subsystem. The monitoring subsystem allows the sensor to collect environmental data such as humidity, temperature, pressure, magnetic field, and chemical flight analysis. The

Table 6: Management of perception subsystem.

No of nodes	IMBC	MOMA	AIEEC	ISCS	MCADM
100	66.05	48.88	50.01	88.81	96.40
200	66.78	49.73	50.61	89.51	96.65
300	67.51	50.58	51.21	90.21	96.90
400	68.24	51.43	51.81	90.91	97.15
500	68.97	52.28	52.41	91.61	97.40
600	69.70	53.13	53.01	92.31	97.65
700	70.43	53.98	53.61	93.01	97.90

sensor can also be supplemented with a geoscope, an accelerometer, which can form a positioning system as in Table 6.

In the cut-off tip, the proposed model managed 95.50% of fully functional device nodes, 94.93% of reduced function device nodes, 94.55% of network topology, 90.41% of autotuning clusters, 97.08% of intensive operating cycle, and 97.15% of perception subsystem. This is because the proposed energy model directly searches the energy aware clusters, and then the available devices are earlier predicted by the proposed model. So the back-up devices are available to enhance the communication between the sensor nodes. Hence, the communication GAT was eliminated, and the lifetime of the network was increased.

5. Conclusion

Currently developing wireless sensor network technology. Wireless sensor networks are distributed self-regulating networks that are resistant to the failure of individual elements exchanging wireless communication information. Each network element has an autonomous power supply, a microcomputer, and a receiver/transmitter. The network coverage area can be from several meters to several meters, depending on the module and antenna type, as well as due to the ability to relay messages from one element to another. The proposed multicluster analysis and design model (MCADM) was evaluated with the existing improved metaheuristics-based clustering (IMBC), multiobjective optimization with Mayfly algorithm (MOMA), artificial intelligence–based energy-efficient clustering (AIEEC), and the role of integrated structured cabling system (ISCS). If the proposed model range of these devices does not allow their mutual detection, the data transfer between two end devices can be carried out by suspension. Therefore, devices with a small radius can communicate with each other using a system of repeaters.

Data Availability

The data used to support the findings of this study are included within the article. Further data or information is available from the corresponding author upon request.

Conflicts of Interest

The authors declare that there is no conflict of interest regarding the publication of this article.

Acknowledgments

The authors appreciate the supports from Wolaita Sodo University, Ethiopia for providing help during the research and preparation of the manuscript.

References

[1] P. Mohan, N. Subramani, Y. Alotaibi, S. Alghamdi, O. I. Khalaf, and S. Ulaganathan, "Improved metaheuristics-based clustering with multihop routing protocol for underwater wireless sensor networks," *Sensors*, vol. 22, no. 4, article 1618, 2022.

[2] S. Mukase and K. Xia, "Multi-objective optimization with mayfly algorithm for periodic charging in wireless rechargeable sensor networks," *World Electric Vehicle Journal*, vol. 13, no. 7, p. 120, 2022.

[3] D. Anuradha, N. Subramani, O. I. Khalaf, Y. Alotaibi, S. Alghamdi, and M. Rajagopal, "Chaotic search-and-rescue-optimization-based multi-hop data transmission protocol for underwater wireless sensor networks," *Sensors*, vol. 22, no. 8, article 2867, 2022.

[4] N. Chouhan, "Artificial intelligence–based energy-efficient clustering and routing in IoT-assisted wireless sensor network," *Artificial Intelligence for Renewable Energy Systems*, vol. 2022, pp. 79–91, 2022.

[5] N. Subramani, P. Mohan, Y. Alotaibi, S. Alghamdi, and O. I. Khalaf, "An efficient metaheuristic-based clustering with routing protocol for underwater wireless sensor networks," *Sensors*, vol. 22, no. 2, p. 415, 2022.

[6] J. Logeshwaran and S. Karthick, "A smart design of a multidimensional antenna to enhance the maximum signal clutch to the allowable standards in 5G communication networks," *ICTACT Journal on Microelectronics*, vol. 8, no. 1, pp. 1269–1274, 2022.

[7] S. K. Gupta and S. Singh, "Survey on energy efficient dynamic sink optimum routing for wireless sensor network and communication technologies," *International Journal of Communication Systems*, vol. 35, no. 11, 2022.

[8] Y. Yang, Y. Wu, H. Yuan, M. Khishe, and M. Mohammadi, "Nodes clustering and multi-hop routing protocol optimization using hybrid chimp optimization and hunger games search algorithms for sustainable energy efficient underwater wireless sensor networks," *Sustainable Computing: Informatics and Systems*, vol. 35, article 100731, 2022.

[9] D. Gurusamy and G. Diriba, "Sensor network and energy harvesting solutions towards water quality monitoring in developing countries," *Wireless Personal Communications*, vol. 2022, pp. 1–19, 2022.

[10] J. Logeshwaran, M. Ramkumar, T. Kiruthiga, and R. Sharanpravin, "The role of integrated structured cabling system (ISCS) for reliable bandwidth optimization in high-speed communication network," *ICTACT Journal on Communication Technology*, vol. 13, no. 1, pp. 2635–2639, 2022.

[11] N. M. Maroof and M. A. Waheed, "Autonomous scheduling and distributed graph routing algorithm (ASDGRA) for hybrid wireless sensor networks," in *In Inventive Communication and*

Computational Technologies, pp. 189–209, Springer, Singapore, 2022.

[12] H. T. Tran, M. T. Nguyen, G. Ala, and F. Viola, "Hybrid solar-RF energy harvesting mechanisms for remote sensing devices," *International Journal of Renewable Energy Research (IJRER)*, vol. 12, no. 1, pp. 294–304, 2022.

[13] C. Zhao, Q. Wu, D. Lin et al., "An energy-balanced unequal clustering approach for circular wireless sensor networks," *Ad Hoc Networks*, vol. 132, article 102872, 2022.

[14] E. A. Refaee and S. Shamsudheen, "Trust- and energy-aware cluster head selection in a UAV-based wireless sensor network using fit-FCM," *The Journal of Supercomputing*, vol. 78, no. 4, pp. 5610–5625, 2022.

[15] K. Saravanakumar and J. Logeshwaran, "Auto-theft prevention system for underwater sensor using lab view," *International Journal of Innovative Research in Computer and Communication Engineering*, vol. 4, no. 2, pp. 1750–1755, 2016.

[16] R. M. Maina, P. K. Lang'at, and P. K. Kihato, "Design and analysis of a multiple collaborative beamforming scheme in the realm of wireless sensor networks featuring 3-dimension node configuration," *Heliyon*, vol. 8, no. 5, article e09398, 2022.

[17] Z. U. A. Jaffri, M. Asif, W. U. Khan et al., "TEZEM: a new energy-efficient routing protocol for next-generation wireless sensor networks," *International Journal of Distributed Sensor Networks*, vol. 18, Article ID 155013292211072, 2022.

[18] R. Ahmad, R. Wazirali, and T. Abu-Ain, "Machine learning for wireless sensor networks security: an overview of challenges and issues," *Sensors*, vol. 22, no. 13, article 4730, 2022.

[19] K. Jaiswal and V. Anand, "FAGWO-H: a hybrid method towards fault-tolerant cluster-based routing in wireless sensor network for IoT applications," *The Journal of Supercomputing*, vol. 78, no. 8, pp. 11195–11227, 2022.

[20] H. Wu, X. Han, B. Yang, Y. Miao, and H. Zhu, "Fault-tolerant topology of agricultural wireless sensor networks based on a double price function," *Agronomy*, vol. 12, no. 4, p. 837, 2022.

[21] M. Sutharasan and J. Logeshwaran, "Design intelligence data gathering and incident response model for data security using honey pot system," *International Journal for Research & Development in Technology*, vol. 5, no. 5, pp. 310–314, 2016.

[22] J. Wan and J. Chen, "AHP based relay selection strategy for energy harvesting wireless sensor networks," *Future Generation Computer Systems*, vol. 128, pp. 36–44, 2022.

[23] M. A. Khan and A. A. Awan, "Intelligent on demand clustering routing protocol for wireless sensor networks," *Wireless Communications and Mobile Computing*, vol. 2022, Article ID 7356733, 10 pages, 2022.

[24] B. Han, F. Ran, J. Li, L. Yan, H. Shen, and A. Li, "A novel adaptive cluster based routing protocol for energy-harvesting wireless sensor networks," *Sensors*, vol. 22, no. 4, article 1564, 2022.

Hindawi
International Journal of Photoenergy
Volume 2022, Article ID 5767696, 8 pages
https://doi.org/10.1155/2022/5767696

Research Article

IoT-Based Solar Energy Measurement and Monitoring Model

L. Chitra,[1] N. Vasantha Gowri,[2] M. Maheswari,[3] Dipesh Uike,[4] N. R. Medikondu,[5] Essam A. Al-Ammar,[6] Ahmed Sayed Mohammed Metwally,[7] Ataul Islam,[8] and Abdi Diriba[9]

[1]*Department of Electrical and Electronics Engineering, Aarupadai Veedu Institute of Technology, Vinayaka Missions Research Foundation, Paiyanoor, Tamil Nadu 603104, India*
[2]*Department of Electrical and Electronics Engineering, Chaitanya Bharathi Institute of Technology (A), Hyderabad, Telangana 500075, India*
[3]*Department of Computer Science and Engineering, Panimalar Engineering College, Chennai, Tamil Nadu 600123, India*
[4]*Dr. Ambedkar Institute of Management Studies And Research, Nagpur, Maharashtra 440010, India*
[5]*Department of Mechanical Engineering, Koneru Lakshmaiah Education Foundation, Vaddeswaram, Andhra Pradesh 522302, India*
[6]*Department of Electrical Engineering, College of Engineering, King Saud University, P.O. Box 800 Riyadh 11421, Saudi Arabia*
[7]*Department of Mathematics, College of Science, King Saud University, Riyadh 11451, Saudi Arabia*
[8]*Faculty of Biology, Medicine and Health, University of Manchester, Manchester, UK*
[9]*Department of Mechanical Engineering, Mizan Tepi University, Ethiopia*

Correspondence should be addressed to Abdi Diriba; abdi@mtu.edu.et

Received 25 July 2022; Revised 28 August 2022; Accepted 1 September 2022; Published 4 October 2022

Academic Editor: BR Ramesh Bapu

In the early days, greenhouse energy did not pay much attention to coating inspections and new applications, spending more attention on repair solar energy projects instead. However, these attitudes have recently changed. Energy producers realize that preventing corrosion and deterioration is less expensive than solving the greenhouse problems when they occur. The proposed model also provides coating, paint control, and error analysis services within the scope of solar machinery and equipment-related services while the greenhouse equipment reached a low energy level. The greenhouse monitoring services ensure that a solar plant is economical, reliable, and of high quality, meets legal requirements, conforms to standards published by domestic and foreign organizations, and determines conditions that cause short circuits or power outages. In this context, with the help of cloud computing-based Internet of things (IOT), the industrial power stations, high-voltage substations, low-voltage networks, power stations that comply with legal regulations on safety from electricity, electrical installations for machinery, alarm systems, fire alarm systems, cathodic corrosion protection mechanisms in oil tanks and pipelines, emergency power supply installations, electrical installations in buildings, and gas alarm systems are inspected and documented.

1. Introduction

The biggest advantage of solar energy systems is that they do not have negative effects on the natural environment like renewable energy sources such as wind, hydraulic, and geothermal. The fuel of solar cells is solar energy and this energy costs nothing [1]. Also, it does not pollute the environment. In recent years, research has been done on solar-powered vehicles in the automotive industry and many other applications like solar still and so on [2]. Today, these cars have limited power; although they are single-seater vehicles, the speed of the vehicles is 40 kmph. However, it is still not suitable for daily use in today's traffic flow. Nevertheless, in today's conditions, developed and developing countries continue their research and development studies [3, 4]. A shared understanding of the significance of the social decisions society must make regarding energy sources, production, and environmental effects. The organization conducts vigorous

debates on global petroleum production and consumption patterns. Debates are now intensifying as to how long the world's crude oil reserves can be used and what alternatives can be used after they are exhausted. Scientists are devoted to finding alternative arrangements for future energy needs. In our country, research is being done on solar-powered vehicles, electronic devices for lighting, and heating devices. Electricity market regulation is enacted to increase the use of renewable energy sources [5]. This regulation regulates the principles and obligations for language practices in the electricity market. This framework also includes incentives for renewable energy sources [6]. Considering the increasing energy demand and solar energy potential of our country, it is necessary to accelerate efforts in this direction. Final Installation Inspection Energy Services for companies operating in the solar energy sector are inspections to prove that the installation and connections are in compliance with all requirements before commissioning solar energy facilities [7, 8]. The major problem with extracting oil from the Macal rocks is that it is not currently profitable if overcome. The energy it costs to extract it is more than what can be obtained from it. It is a situation where income is not met and expenditure is not met. Natural gas molecules are stuck to the rocks in the mantle layers. Only by squeezing them will they come to the surface. It is a complicated and costly process. As oil prices skyrocket, governments and oil companies are turning their attention back to methods previously abandoned as unaffordable. Interest in drilling oil wells on deep sea floors has increased. Since the discovery of oil in the North Sea region north of England, around 40 billion barrels of oil have been produced from oil wells there.

Solar energy is an energy source that does not pollute the environment, requires no external dependence, and is considered free. It is one of the leading renewable energy sources. Previously used in daily life and residences, solar energy has gradually expanded to agriculture, communication, industry, military services, and power generation [9]. Theoretically, solar radiation can be used in all areas of life. In a simple calculation, the amount of energy coming from the Sun in a year corresponds to 50 times the known coal reserves and 800 times the oil reserves [10]. In this respect, the solar energy source will occupy a very important place in the future. According to estimates, by 2050, 11 percent of the world's electricity generation will come from solar energy [11]. Currently, the amount of electrical energy obtained from solar energy is increasing by about 20 percent compared to that of the previous year. In this regard, countries like Germany, Italy, and Czech Republic are leading in production [12]. The share of these three countries reaches 70 percent. The good news is that our country has more solar energy potential than any other European country except Spain. In this regard, our country should adopt consistent and applicable policies for generating electricity using solar energy [13, 14]. At this point, manufacturing companies have a lot of work to do. Regardless of where they operate in the world, it is important to evaluate vendors and suppliers with an independent and unbiased perspective [15]. The ability of these companies to comply with the terms of the contract and meet certain standards and legal regulatory obligations can only be achieved through the work to be carried out by authorized companies [16]. There is an urgent need to find alternative sources of energy. Besides the increased cost, the impact on the environment is also a concern. Burning fossil fuels produces 21.3 billion metric tons of carbon dioxide annually. About half of it is occupied by plants and oceans. The remaining carbon dioxide is increasing the global warming and increasing the surface warming. Efforts are also underway to extract hydrogen gas from seawater and rocks. It is an ion that can provide energy without polluting the atmosphere.

Crude oil processed in refineries is approximately 43 percent gasoline, 18 percent fuel oil and diesel, 11 percent LPG (a mixture of liquefied petroleum gas, propane, or propane-butane), 9 percent jet fuel, 5 percent asphalt, and 14 percent other oil [17, 18]. Products are received. All these manufactured goods are transported by sea, road, and pipeline depending on the conditions [19, 20]. In the transportation of produced energy resources, disputes between the parties are likely to arise if the product does not conform to the terms of the contract or standards or is not accepted by the buyer for any other reason [21–30]. Energy resources are naturally occurring sources of energy for humans. It is a known fact that we need energy to do any work. We get the energy that we need to meet our daily needs from energy sources. Energy resources are generally divided into two broad categories, namely, renewable energy resources and nonrenewable energy resources. Renewable energy sources include solar, wind, hydro, geothermal, and biomass. Petroleum products, natural gas, coal, and fossil fuels are nonrenewable energy resources.

2. Literature Review

In parallel to the increase in human population, the world's demand for electrical energy is also increasing. For this reason, turning to renewable energy sources has become inevitable. Our country is completely foreign dependent for its energy needs [21]. As efforts are being made to use existing energy more efficiently, the search for new sources of energy continues. Among the renewable energy sources, solar energy is the most significant and widely used resource in recent years. Setting up solar farms or solar power plants are big projects [22]. For these installations carried out by the tender, the companies authorized by the tender offer support for the preparation, conduct certain tests and analysis, and negotiate the terms of the contract [23]. On the other hand, high levels of fossil fuel consumption, depletion of the ozone layer, effects of global warming, and the increase in greenhouse gases as current energy resources have reached a depleting state are forcing countries to seek new energy sources [24]. Renewable energy resources are resources that can be regenerated by the environment in a short period of time. These resources are obtained from natural sources like the Sun, wind, rain, and sea. From these sources energy can be drawn repeatedly at times of need. Renewable resources are abundant in nature. And when energy is obtained from these sources and used, they often do not harm the environment. For example, electricity is generated from the energy obtained from sunlight. In this way, the energy for our daily

needs is obtained from the resources of wind, geothermal energy, and wind and ocean waves.

As researchers work to make more efficient use of existing energy resources, the search for solutions for renewable energy sources continues [25]. Solar energy is one of the renewable energy sources and our country can be considered lucky in this regard. A lot of progress has been made in the world and in our country in getting electricity from solar energy [26]. Additionally, our nation has more solar energy potential than it can use to produce electricity. We are increasing public awareness of the issue and introducing new producer incentive programs [27]. Research on obtaining electrical energy from solar energy is progressing rapidly, but it is a fact that quality studies should not be neglected at the production stage. In this regard, the importance of unbiased and independent services provided in this direction by recognized organizations is high [28]. Nonrenewable energy resources are resources that cannot be regenerated by the environment in the short term. These resources are obtained from beneath the earth. These resources will disappear in fifty or sixty years. These cannot be renewed in a short period of time. Nonrenewable resources are limited to a certain amount. When we extract energy from these sources and use them, they emit large amounts of greenhouse gases. This causes environmental pollution.

3. Proposed Model

Semiconductor solar cells or photovoltaic cells are used to generate electricity from solar energy. Photovoltaic cells are also called solar cells. These batteries generate equal positive and negative charges from the photon energy that they reach and convert solar energy directly into usable electrical energy. Many different materials are used in the construction of solar cells. Semiconductor materials such as amorphous silicon, crystalline silicon, cadmium telluride, and gallium arsenide are often used. The most widely used of these is silicon, which is the most common in nature. Utilization of energy resources is essential as human survival and progress depend on the earth's energy resources. The extraction and use of energy from energy sources has serious effects on the environment. Therefore, energy should be used sparingly to reduce the impact of severe environmental impacts. And the dwindling nonrenewable resources must be conserved for the use of future generations. Better research and development are necessary to make full use of renewable resources.

The Sun's rays reaching the solar panel transfer electrons to the semiconductor technology in the batteries, resulting in electricity. Solar cells are durable, nonpolluting, and long-lasting devices. There is no electrical problem when they are working. Also, they do not require much maintenance. Batteries in the modular structure are connected to each other in series and parallel. Depending on the structure of the battery, solar energy is converted into electrical energy, which is currently 20 percent efficient. However, the batteries are enabled to follow the Sun, using methods such as maximum power monitoring based on sunrise and sunset times and methods such as temperature protection and air conditioning to try to achieve maximum efficiency. Unnecessary lights and fans can be turned off. This reduces electricity bills and indirectly prevents environmental pollution. Use of public vehicles can be used to reduce the use of private vehicles for transportation. Each of us will use energy resources sparingly where necessary to protect the environment and achieve economic self-sufficiency. Keeping track of production activities is important here. Authorized companies provide visual control services at production levels. After replacement or manipulations to increase the density of the electrolyte, a solution with a different indicator is installed in the solar photovoltaic cell banks. A gap in the range of 0.01 g/cu.cm is allowed. See, to equalize this value, that a corrective recharge is required. The essence of the method is to provide current for 1–2 hours while charging 2–3 times less than the nominal value. In the absence of a positive result, intensive rehabilitation methods are used. Charging is applied by devices equipped with regulators that provide a constant voltage at the input. The procedures for restoring density by corrective charging were shown in Figure 1:

(i) The solar photovoltaic cell is fully charged

(ii) At the moment of reaching the maximum charge when observing the boiling point of the electrolyte, the current strength decreases to 1–2 A

(iii) During the boiling process, the filtrate evaporates and the density of the liquid increases

(iv) For each individual case, the evaporation time may be different and sometimes reach 1 day

(v) As the density decreases below 1.25 g/cu.cm electrolyte which is added, the concentration is measured when the device cools down to 25°C

Renewable energy is energy that can be regenerated by the environment in the short term. This type of energy is obtained from natural sources like the Sun, wind, rain, sea, and earth. Renewable energy technology includes solar energy, hydroelectricity, wind energy, biomass energy, and biofuel energy. Renewable energy is often used for everyday activities such as electricity generation, water heating and cooling, and transportation. Renewable energy is derived from nonrenewable sources. And this kind of energy does not cause much harm to the environment. So, this type of energy is considered important these days. The Sun is the world's largest source of energy. Solar cells are used to generate electricity from the Sun without using any moving parts and without harming the natural environment; they silently convert the Sun's rays directly into electrical energy. Hence, it provides a clean source of energy. Solar cells last longer than other electrical energy-generating systems. When generating electricity from solar energy, photovoltaic systems are installed. In these systems, photovoltaic cells are connected in series or parallel to obtain high voltage, current, or power. Photovoltaic panels are numerous photovoltaic modules connected by electrical cables. Pipelines are generally used to economically transport liquids and gases

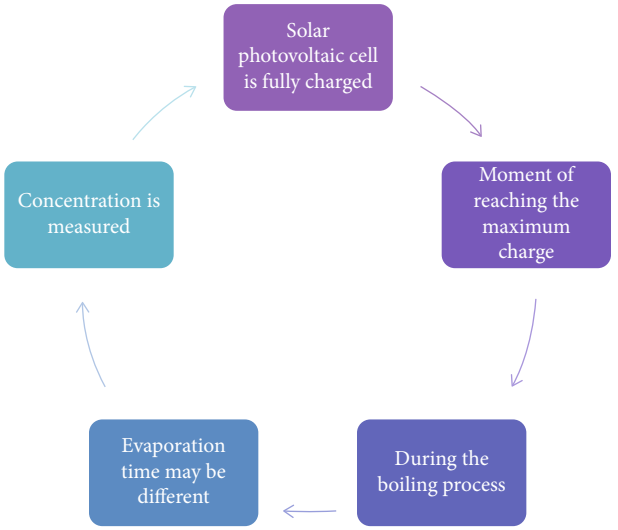

Figure 1: Procedures for restoring density by corrective charging.

over long distances. Generally, pipelines transport petroleum products such as crude oil, gasoline, diesel oil, and jet fuel and concentrated solids such as natural gas, sludge, and treated water. Pipelines were first built to transport oil from large oil fields. Today, it is mainly used to transport natural gas. The Sun is the source of many sources of renewable energy. Solar energy is the energy obtained directly from the Sun's light and heat. The Sun is the indirect source of energy for wind, water, and life. The energy obtained from the Sun is used directly to generate electricity and to heat and cool water. We use only a fraction of the energy that the Earth receives from the Sun for renewable energy. Although the first pipelines were made of wood, with the development of technologies over time, steel pipes started to be used. Today, pipes made of thinner but higher strength materials are used. The following procedures essential during pipeline construction were shown in Figure 2:

(i) Opening pipes

(ii) Placing pipes

(iii) Welding

(iv) Nondestructive testing

Welding is a very important process in pipeline construction. The safe and quality operation of the pipeline for many years depends on it. Control and inspection services of solar energy systems provided by recognized companies and postproduction, nondestructive testing services are also available. Nondestructive testing is a type of inspection performed without damaging the entire object or parts. The validity of this test is based on the results of previous destructive tests. The key here is nondestructive inspection of systems and equipment. Wind blows due to solar heating and Earth's circulation. The energy released when the wind blows is stored and generated by wind turbines. The method of storing and using wind energy is less polluting than the method of obtaining energy from

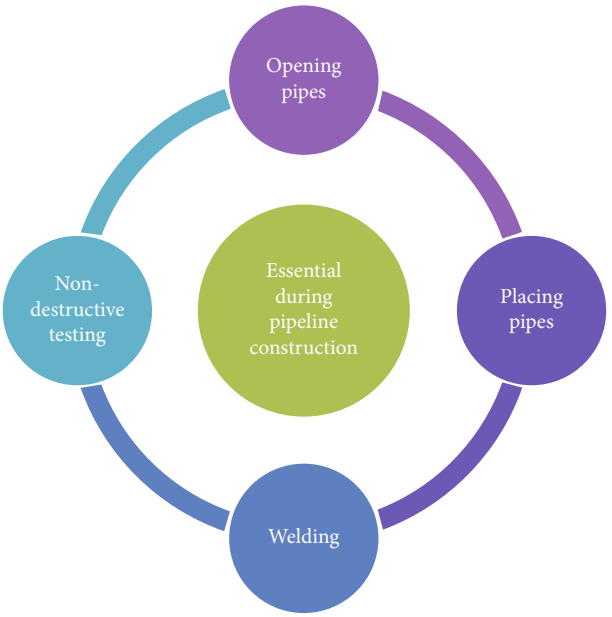

Figure 2: Essential during pipeline construction.

other energy sources. India ranks fourth in the world in generating electricity using wind energy. Before using correction electrolyte, it is necessary to implement the procedure shown in Figure 3:

(i) Some fluid is removed from the repaired cell

(ii) Now, it is necessary to add exactly the same amount of correction electrolyte, which will increase the density

(iii) Also, the photovoltaic solar cell is charged with a rated current by a constant device, which contributes to the mixing of fluids

(iv) After half an hour of charge, the solar PV cell should "rest" for 1–2 hours (this is necessary to equalize the density in the cell)

(v) The measurement is repeated, and if necessary, acid correction electrolyte is added again, but in smaller quantities

Hydroelectricity is the process of generating electricity using the kinetic energy of water due to the gravity of the earth. No solid waste or greenhouse gases are released in this energy generation process. Hence, hydropower occupies an important place in renewable energy. It is an extreme step when its resource is reduced to g/cu.cm by electrolyte and its resource is completely depleted. See that the steps are carried out in the following order shown in Figure 4:

(i) After preparation, the solar PV cells are completely removed from the solution from the cans using a pear

(ii) If the solar photovoltaic cell is turned on its side, it is necessary to drill holes with electrodes in the

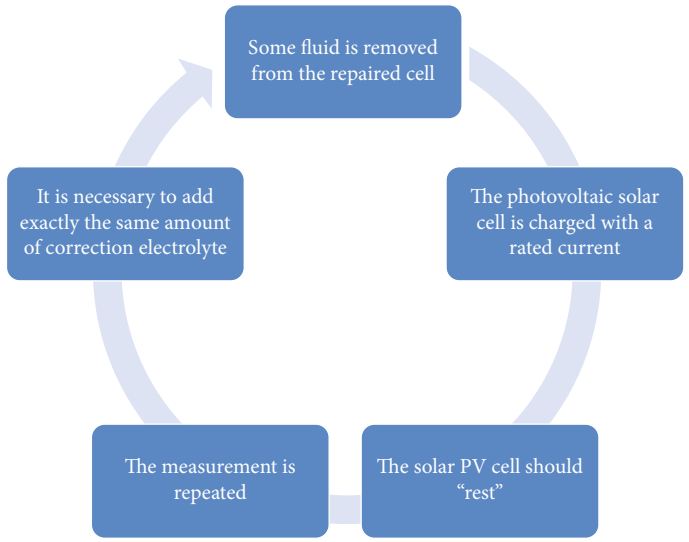

Figure 3: Necessary to implement the proposed procedures.

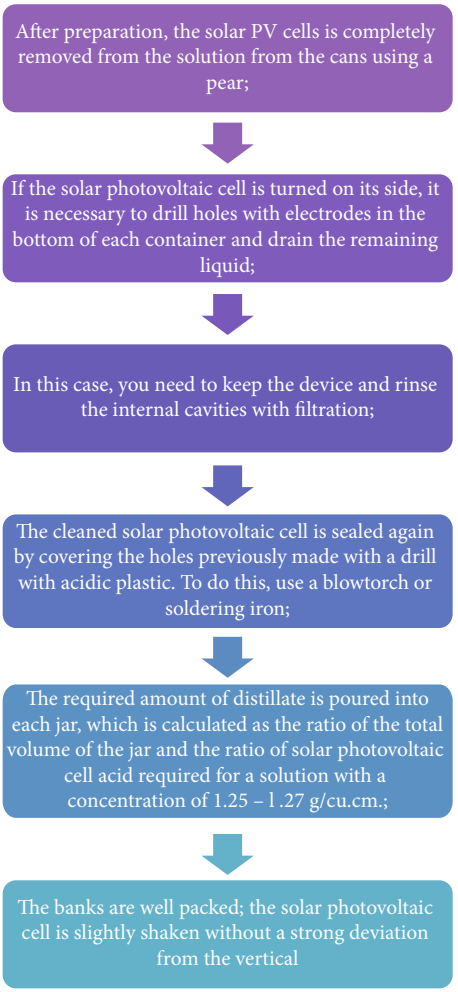

Figure 4: Reduced resource management.

bottom of each container and drain the remaining liquid

(iii) In this case, you need to keep the device and rinse the internal cavities with filtration

(iv) The cleaned solar photovoltaic cell is sealed again by covering the holes previously made with a drill with acidic plastic. To do this, use a blowtorch or soldering iron

(v) The required amount of distillate is poured into each jar, which is calculated as the ratio of the total volume of the jar and the ratio of solar photovoltaic cell acid required for a solution with a concentration of 1.25–1.27 g/cu.cm

(vi) The banks are well packed; the solar photovoltaic cell is slightly shaken without a strong deviation from the vertical

The solution must first be drained from each solar photovoltaic cell can. Then, fill with new liquid with a density of 1.25–1.27 g/cu.cm. After filling the jars to the "norm" mark, tightly close the lids and shake the solar photovoltaic cell a little. Do not turn the battery upside down. With such handling, pieces of lead salt can break off from the grid and move to the nearest electrode, causing the jar to close. After that, the damaged container becomes unusable. Concentration readings will prompt the need to repeat the electrolyte replacement procedure. If the indicator is below 1.25 g/cu.cm, see that the operation must be repeated until the desired result is obtained.

4. Results and Discussion

The proposed greenhouse solar energy monitoring (GHSEM) model was compared with the existing optimized

greenhouse environment and resource management (OGERS), demand side management of energy consumption (DSMEC), an optimization scheme for IoT (OSIOT), and photovoltaic spectrum performance analysis (PSPA).

4.1. Pipeline Integrity Tests. In this regard, pipeline integrity tests, i.e., insulation and cathodic tests and welder qualification tests carried out by recognized organizations, are of great importance. Welder qualification surveys are aimed at evaluating welder personnel of pipeline operators or supplier companies involved in pipeline construction. The comparison of pipeline integrity tests is demonstrated in Table 1.

Poor quality welding or incomplete or inappropriate welding procedures in pipes are the main reasons for the poor and unqualified welding process, premature failure, and unnecessary costs.

4.2. Design Review and Inspection. It is an engineering method performed by recognized organizations during design inspections of products. Design review is one of the most important steps in delivering a high-quality product. Basically, auditability is a design feature that expresses how easily an audit task can be created. Studies are studies that define how specific properties of a material are obtained according to the designed properties. In other words, the purpose of the investigation is to determine whether an operation has been performed or to make standard measurements or observations that will show whether the operation has been performed correctly. The comparison of design review and inspection is demonstrated in Table 2.

4.3. Design Life Cycle. Design concepts relate to different stages of the product life cycle but should be applied in the early design stages. Therefore, it affects various stages of the design life cycle such as design review, production, application, and support. In other words, information from these stages of production must be in the hands of the design team during the design of the product. At this stage, the product is simulated under actual usage conditions and sufficient information is obtained about the behavior of the product. The comparison of the design life cycle is demonstrated in Table 3.

The main purpose of design in the oil and gas industry is to meet the needs of stakeholders and at the same time reduce costs as much as possible. Shorter life cycles result in shorter time for businesses to enter the market. Conducting studies in the early stages of product development can provide design choice.

4.4. Fault Analysis. Industrial coatings play a very important role in protecting assets against deterioration on the one hand and projecting the brand and image of a business on the other. Plants, machinery and equipment, chimneys, and tanks in poor condition reflect the brand image poorly. For many industrial businesses, coatings are essential materials that require regular maintenance. Effective inspections and fault analysis and condition assessments are needed to keep chimneys, tanks, and pits in good condition. The comparison of fault analysis is demonstrated in Table 4.

Table 1: Comparison of pipeline integrity tests.

No. of inputs	OGERS	DSMEC	OSIOT	PSPA	GHSEM
100	49.53	54.49	88.94	74.73	93.68
200	48.24	53.74	84.32	71.33	93.58
300	48.49	53.77	84.32	71.69	93.51
400	47.71	53.28	81.24	69.54	93.42
500	47.19	52.92	78.93	68.02	93.34
600	46.67	52.56	76.62	66.50	93.25
700	46.15	52.20	74.31	64.98	93.17

Table 2: Comparison of design review and inspection.

No. of inputs	OGERS	DSMEC	OSIOT	PSPA	GHSEM
100	48.62	54.59	84.79	72.88	93.47
200	48.54	54.68	84.99	72.75	93.43
300	48.55	54.81	85.25	72.73	93.40
400	48.90	55.23	85.88	73.16	93.38
500	48.87	55.34	86.11	73.09	93.35
600	48.95	55.55	86.46	73.17	93.32
700	49.04	55.75	86.82	73.25	93.29

Table 3: Comparison of the design life cycle.

No. of inputs	OGERS	DSMEC	OSIOT	PSPA	GHSEM
100	48.67	53.43	85.61	71.41	93.69
200	48.17	53.43	84.52	71.15	93.58
300	47.42	52.60	83.38	70.58	93.52
400	47.42	53.33	83.74	71.72	93.47
500	46.80	52.92	82.63	71.31	93.39
600	46.35	52.80	81.95	71.34	93.31
700	45.90	52.69	81.28	71.38	93.24

Table 4: Comparison of fault analysis.

No. of inputs	OGERS	DSMEC	OSIOT	PSPA	GHSEM
100	48.47	54.44	85.27	72.74	93.43
200	48.75	54.84	85.91	72.98	93.40
300	48.03	54.27	85.33	72.33	93.38
400	47.98	54.35	85.56	72.27	93.35
500	47.76	54.26	85.59	72.07	93.33
600	47.54	54.18	85.62	71.86	93.30
700	47.32	54.09	85.65	71.66	93.28

4.5. Paint Inspections. A coating survey and paint test are done to gather information on how well the coating is performing, where there are weak spots and if any maintenance or repairs are needed to prevent corrosion and deterioration. Coating and paint controls ensure that safety gaps are identified and maintenance budgets are used only where necessary. The comparison of paint inspection is demonstrated in Table 5.

Table 5: Comparison of paint inspection.

No. of inputs	OGERS	DSMEC	OSIOT	PSPA	GHSEM
100	56.96	44.90	83.12	70.25	95.69
200	58.62	50.76	76.28	76.43	95.58
300	59.07	49.62	74.99	77.92	95.52
400	54.38	50.76	72.85	81.16	95.47
500	53.99	51.64	74.42	80.44	95.43
600	54.15	52.84	76.04	80.31	95.40
700	54.89	54.49	77.84	81.58	95.38

Coating and paint inspections are useful in predicting future maintenance needs and spotting current or potential problems. Coatings and paints need to be strong and effective to keep assets structurally sound and perform well. In a cutoff point, the proposed model achieved 93.42% of pipeline integrity test results, 93.38% of design review and inspections, 93.47% of design life cycle, 93.35% of fault analysis, and 95.47% of paint inspection results.

5. Conclusion

The main reason for this is, most often, a solar photovoltaic cell that is completely discharged within a few days. Trying to collect it in this case will not lead to a positive result. A similar problem is the result of a decrease in the density of the electrolyte poured into the solar photovoltaic cell banks. After all, this liquid is, in fact, a catalyst for the electrochemical process; without it, the solar photovoltaic cell is a plastic package that will not work. It consists of approximately 35% to 65%; this liquid has a specific density, which can decrease and increase depending on the charge. In this case, the density of the resulting solution is rarely checked. At the same time, when the amount of distilled water is sufficient, during recharging, the electrolyte boils with this liquid, which leads to a decrease in its density. Sooner or later, this indicator drops below a critical level and the starting solar panels will no longer work. In this case, it is necessary to increase this parameter of the solution in the solar photovoltaic cell, which will restore its performance.

Data Availability

The data used to support the findings of this study are included within the article. Further data or information is available from the corresponding author upon request.

Conflicts of Interest

The authors declare that there are no conflicts of interest regarding the publication of this paper.

Acknowledgments

The authors appreciate the support from Mizan Tepi University, Ethiopia, for the research and preparation of the manuscript. This work was funded by the Researchers Supporting Project No. (RSP-2021/363), King Saud University, Riyadh, Saudi Arabia.

References

[1] C. Maraveas, D. Piromalis, K. G. Arvanitis, T. Bartzanas, and D. Loukatos, "Applications of IoT for optimized greenhouse environment and resources management," *Computers and Electronics in Agriculture*, vol. 198, p. 106993, 2022.

[2] A. R. Prasad, R. Sathyamurthy, M. Sudhakar et al., "Effect of design parameters on fresh water produced from triangular basin and conventional basin solar still," *International Journal of Photoenergy*, vol. 2021, Article ID 6619138, 8 pages, 2021.

[3] A. Kumar, P. Singh, P. Raizada, and C. M. Hussain, "Impact of COVID-19 on greenhouse gases emissions: a critical review," *Science of the Total Environment*, vol. 806, Part 1, p. 150349, 2022.

[4] K. Zhang, J. Yu, and Y. Ren, "Demand side management of energy consumption in a photovoltaic integrated greenhouse," *International Journal of Electrical Power & Energy Systems*, vol. 134, p. 107433, 2022.

[5] X. Zhao, Z. Zhong, X. Lu, and Y. Yu, "Potential greenhouse gas risk led by renewable energy crowding out nuclear power," *Iscience*, vol. 25, no. 2, p. 103741, 2022.

[6] I. Ullah, M. Fayaz, M. Aman, and D. Kim, "An optimization scheme for IoT based smart greenhouse climate control with efficient energy consumption," *Computing*, vol. 104, no. 2, pp. 433–457, 2022.

[7] M. Sudhakar, R. Prasad, A. Ravinthiran, P. Dutt, and M. A. Chakaravarthi, "Performance improvement of trough concentrating photovoltaic thermal system: a review," *Materials Today: Proceedings*, vol. 16, no. 2, pp. 647–652, 2019.

[8] I. Ihoume, R. Tadili, N. Arbaoui et al., "Performance study of a sustainable solar heating system based on a copper coil water to air heat exchanger for greenhouse heating," *Solar Energy*, vol. 232, pp. 128–138, 2022.

[9] Q. Ma, Y. Zhang, G. Wu et al., "Photovoltaic/spectrum performance analysis of a multifunctional solid spectral splitting covering for passive solar greenhouse roof," *Energy Conversion and Management*, vol. 251, p. 114955, 2022.

[10] H. K. Kim, S. Y. Lee, J. K. Kwon, and Y. H. Kim, "Evaluating the effect of cover materials on greenhouse microclimates and thermal performance," *Agronomy*, vol. 12, no. 1, p. 143, 2022.

[11] S. Zhang, Y. Guo, S. Li et al., "Investigation on environment monitoring system for a combination of hydroponics and aquaculture in greenhouse," *Information Processing in Agriculture*, vol. 9, no. 1, pp. 123–134, 2022.

[12] Y. Natarajan, S. Kannan, and G. Dhiman, "Task scheduling in cloud using aco," *Recent Advances in Computer Science and Communications (Formerly: Recent Patents on Computer Science)*, vol. 15, no. 3, pp. 348–353, 2022.

[13] Y. Yuan, H. Fang, G. Wu et al., "Experimental investigation of full solar spectrum utilization based on nanofluid spectral splitter for greenhouse applications," *Energy Conversion and Management*, vol. 254, p. 115215, 2022.

[14] A. S. Alamoush, A. I. Ölçer, and F. Ballini, "Port greenhouse gas emission reduction: port and public authorities' implementation schemes," *Research in Transportation Business & Management*, vol. 43, p. 100708, 2022.

[15] J. Logeshwaran, M. J. Rex, T. Kiruthiga, and V. A. Rajan, "FPSMM: fuzzy probabilistic based semi Morkov model among the sensor nodes for realtime applications," in *2017 international conference on intelligent sustainable systems (ICISS)*, pp. 442–446, Palladam, India, 2017.

[16] P. Kalkal and A. R. Teja, "A sustainable business framework using solar and bio-energy to instate incessant power in rural India: optimal scheduling, smart metering, and economic viability," *IEEE Access*, vol. 10, pp. 11021–11035, 2022.

[17] A. Rabiu, W. H. Na, T. D. Akpenpuun et al., "Determination of overall heat transfer coefficient for greenhouse energy-saving screen using Trnsys and hotbox," *Biosystems Engineering*, vol. 217, pp. 83–101, 2022.

[18] E. Ravishankar, R. E. Booth, J. A. Hollingsworth et al., "Organic solar powered greenhouse performance optimization and global economic opportunity," *Energy & Environmental Science*, vol. 15, no. 4, pp. 1659–1671, 2022.

[19] K. Saravanakumar and J. Logeshwaran, "Auto-theft prevention system for underwater sensor using lab view," *International Journal of Innovative Research in Computer and Communication Engineering*, vol. 4, no. 2, pp. 1750–1755, 2016.

[20] W. Uddin, "Mobile and area sources of greenhouse gases and abatement strategies," in *Handbook of Climate Change Mitigation and Adaptation*, pp. 743–807, Springer International Publishing, Cham, 2022.

[21] F. Maureira, K. Rajagopalan, and C. O. Stöckle, "Evaluating tomato production in open-field and high-tech greenhouse systems," *Journal of Cleaner Production*, vol. 337, p. 130459, 2022.

[22] L. Jin, Y. H. Chang, M. Wang, X. Z. Zheng, J. X. Yang, and J. Gu, "The dynamics of CO2 emissions, energy consumption, and economic development: evidence from the top 28 greenhouse gas emitters," *Environmental Science and Pollution Research*, vol. 29, no. 24, pp. 36565–36574, 2022.

[23] M. Sutharasan and J. Logeshwaran, "Design intelligence data gathering and incident response model for data security using honey pot system," *International Journal for Research & Development in Technology*, vol. 5, no. 5, pp. 310–314, 2016.

[24] K. H. D. Tang, "Climate change policies of the four largest global emitters of greenhouse gases: their similarities, differences and way forward," *Journal of Energy Research and Reviews*, vol. 10, no. 2, pp. 19–35, 2022.

[25] L. Lu, M. E. Ya'acob, M. S. Anuar, and M. N. Mohtar, "Comprehensive review on the application of inorganic and organic photovoltaics as greenhouse shading materials," *Sustainable Energy Technologies and Assessments*, vol. 52, p. 102077, 2022.

[26] T. A. Kurniawan, X. Liang, D. Singh et al., "Harnessing landfill gas (LFG) for electricity: a strategy to mitigate greenhouse gas (GHG) emissions in Jakarta (Indonesia)," *Journal of Environmental Management*, vol. 301, p. 113882, 2022.

[27] S. H. Fatemi, A. Babapoor, D. Norozi Sarami, R. Heydarzade, and S. S. Sharifi, "A new look at the use of renewable energy in the agricultural industry," *Journal of Renewable and New Energy*, vol. 9, no. 1, pp. 29–39, 2022.

[28] Y. He, X. Li, P. Huang, and J. Wang, "Exploring the road toward environmental sustainability: natural resources, renewable energy consumption, economic growth, and greenhouse gas emissions," *Sustainability*, vol. 14, no. 3, p. 1579, 2022.

[29] S. Mikhailova, L. Mikhailov, G. Ismailova, N. Kenes, R. Yersaiyn, and R. Mahmutov, "Solar-powered smart window design with aerosol trap and greenhouse gardening," *Materials Today: Proceedings*, vol. 49, Part 6, pp. 2527–2531, 2022.

[30] B. Nagappan, Y. Devarajan, and E. Kariappan, "Performance analysis of sustainable solar energy operated ejector refrigeration system with the combined effect of Scheffler and parabolic trough collectors to lower greenhouse gases," *Environmental Science and Pollution Research*, vol. 2022, pp. 1–13, 2022.

Hindawi
International Journal of Photoenergy
Volume 2022, Article ID 2943386, 8 pages
https://doi.org/10.1155/2022/2943386

Research Article

Deep Learning-Based Smart Hybrid Solar Water Heater Erection Model to Extract Maximum Energy

Bharathi M L,[1] T. Sripriya,[2] B. Muthuraj,[3] D. Sateesh Kumar,[4] V. Venkatesh,[5] Badireddy Satya Sridevi,[6] Munaga Masthan Siva Krishna,[7] K. Rajan,[8] and Abdi Diriba[9]

[1]*Department of Electrical and Electronics Engineering, Sathyabama Institute of Science and Technology, Chennai, Tamil Nadu 600119, India*
[2]*Department of Electronics and Communication Engineering, Prince Shri Venkateshwara Padmavathy Engineering College, Chennai, Tamil Nadu 600127, India*
[3]*Department of Electrical and Electronics Engineering, Panimalar Engineering College, Chennai, Tamil Nadu 600123, India*
[4]*Department of Engineering Mathematics, College of Engineering, Koneru Lakshmaiah Education Foundation, Vaddeswaram, Andhra Pradesh 522302, India*
[5]*Department of Electrical and Electronics Engineering, Rajalakshmi Engineering College, Chennai, Tamil Nadu 602105, India*
[6]*Department of Electronics and Communication Engineering, Aditya Engineering College, Surampalem, Andhra Pradesh 533437, India*
[7]*Department of IT & MCA, Aditya College of Engineering & Technology, Surampalem, Andhra Pradesh 533291, India*
[8]*Department of Mechanical Engineering, Dr. M.G.R. Educational and Research Institute, Chennai, Tamil Nadu, India*
[9]*Department of Mechanical Engineering, Mizan-Tepi University, Ethiopia*

Correspondence should be addressed to Abdi Diriba; abdi@mtu.edu.et

Received 28 July 2022; Accepted 14 September 2022; Published 3 October 2022

Academic Editor: BR Ramesh Bapu

Currently, we are trying to get electricity in alternative ways. Many solar powered water heaters have come up to use water heaters. However, these tools are not 100 percent fully effective. The device we have manufactured is an automatic device that runs in the direction of sunlight. The device runs automatically in the morning facing east and in the evening facing west. In this instrument, the defective one-inch tube lamp and the three-quarter-inch tube lamp are put together and connected in series. In this paper, a smart deep learning model was proposed to improve the performance of the solar water heater. The gap between the tube lights is filled with methane gas, and the tube inside is filled with water. The water thus filled is heated by sunlight. Methane gas acts as a fast conductor of solar heat. An electronic control device is placed to determine the temperature of the hot water and to expel the hot water. This device can heat at least 10 liters of water in 15 minutes. Increasing the number of incandescent tube lights can heat up a large amount of water when this device is set up, or it can be designed by replacing tube lights with a series of large glass tubes using the same technology. This tool can be manufactured at low cost so that people from all walks of life can use it.

1. Introduction

The greatest gift of nature is solar energy. From the environment of living things to the photosynthesis of plants, nothing happens without the help of solar energy [1]. We have now achieved the development of converting solar energy into electrical energy and using electrical devices [2]. Many solar-powered products have been discovered. Water heaters are one of the most widely used home appliances [3]. Advances in the industry have led to the development of the new heat pump water heater. The existing smart connection allows you to control the water heater from anywhere [4]. It provides enough hot water for a house of three to five people. It helps to save a lot of money by reducing electricity usage. Many people say that drinking water in the sun gives you more energy and rejuvenates the body. But the other

truth is that water in bottled water has a negative effect when exposed to sunlight, say researchers [5–7]. This is because the plastic chemical BPA or bisphenol-A in the water bottle is harmful to the body. Although most plastic water bottles do not contain this chemical, PPA is often found in polycarbonate bottles [8]. Solar thermal energy contributes significantly to reducing costs, thereby saving energy and reducing CO_2 emissions that are responsible for global warming and climate change.

Another disadvantage is that the bacteria that can live in the sun increase its growth when exposed to sunlight in a water bottle [9]. The remaining DHW projects can be considered as compelling decisions dictated by circumstances, for example, saving in creating [10]. The researchers used plain bottled water and carbonated water. The bottled water was tested in sunlight for about 2, 6, and 10 days. There are no harmful aldehydes when placing the bed bottle with normal water in the sun. But chemical exposure to carbon dioxide when carbonated water is exposed to sunlight has been shown to contain harmful chemical molecules. When researchers further researched this, they studied the release of antimony at different temperatures [11, 12]. At the same time, the cost of developing and installing a water heater is low [13]. Inventors across the country have long used various installations to heat water. In the summer, when the temperature inside the car, such as closed rooms and garages, can reach 65 degrees Celsius, a toxic substance called antimony is formed inside the bed bottle [14, 15]. Thus this toxicity mixes with the water. Researchers have found that water bottles contain antimony. If the temperature is above 65 degrees Celsius in these two studies, the toxicity is likely to worsen [16]. They also insist that bottled water, like our groceries, be kept in a safe place out of direct sunlight. Whenever possible you should have copper, steel, and glass bottles instead of plastic water bottles [17, 18]. This will not harm us and will improve our health. Do not forget that it is better to drink water in a hygienic manner [19].

The population of the world is increasing day by day. Accordingly, the demand for electricity and fuel is rising [20]. As energy, diesel, petrol, and coal from crude oil are used. It is questionable how many more years the fuel will last for the millions of vehicles that run every minute around the world [21]. It is a boon that we get such unpolluted energy naturally from sunlight. At the same time, the need to use electricity sparingly is emphasized at various stages. Every drop of electricity that every individual saves cost [22]. Homes have new tools to prevent the water tank from overflowing. These can be fitted or a stop device can be used to accurately measure the water filling time [23, 24]. Instead of a 100 watt incandescent bulb, a 15 watt LED, low power bulb can be used. Use maximum sunlight during the day; avoid unnecessary lighting, lice, and AC operation. Street lights can use solar power in residential areas [25]. Sunlight transformers can be used to avoid lighting during the day. You can use sun-powered water heaters to get hot water. You can cook using solar cookers instead of electric cookers [26]. Many solar powered devices are currently on sale in the market. Using solar power in homes can save a lot of electricity [27].

The gas-heated boiler is installed only if the high power unit cannot be connected. This is a great and at the same time expensive option [28]. The power of the device directly determines its performance. An electric storage water heater is the easiest way to solve your hot water problem. Electricity is available almost everywhere [29]. Unlike gas appliances, this does not require any approvals or permits. Unlike direct flow, the storage water heater has a special tank equipped with heating elements and thermal insulation [30]. The water coming from the faucet enters the tank and then it enters the consumer through the drain fitting. This can occur under the influence of pressure and by gravity. In front of such a unit is installed a special thermometer, which allows you to determine the temperature of the water in the tank [31].

2. Literature Review

Solar energy refers to the simplest energy source we receive from the sun. By using solar panels, this energy is converted into electricity, which you can use for heating, cooling, or lighting. The best part about solar power is that it is clean and free from any pollution [1]. It is free, renewable, widely available, and used by many homeowners for a variety of purposes. Solar panels are one of the fastest growing energy sources and are used all over the world. It provides an alternative way to deliver energy to homes [2]. The sizes of panels vary to cover all homes, including large and small homes. Solar panels are also available for businesses used to generate electricity in office companies. When used for domestic purpose, the solar angle is installed on the roof at an optimal angle to receive sunlight [3]. This group captures sunlight and receives energy from it. This energy is then converted into electricity that you can use at home. Focusing your attention on the benefits of solar energy will always help you understand how installing a solar system in your home can benefit you [4]. Solar energy is stable and consistent throughout the year. This means that once you have solar power installed in your home you will never have a power shortage. Solar power can be easily used by home and business owners as the engine does not require advanced setup [5]. Solar energy is renewable in nature so you not only get electricity but also support a clean environment. The maintenance of the machine does not require special resources or expertise. You can own it without any professional experience [7]. For nearly half a century, the photovoltaic effect had no practical application for a simple reason—there was no technology to obtain materials with an unstable atomic structure. Opportunities for further research appeared only with the invention of semiconductors. The atoms of these materials have high electrons (n-conductivity) or lack thereof (p-conductivity). When using a two-layer system with an n-type layer (cathode) and a p-type layer (anode), the "explosion" of light photons strikes electrons from the atoms of the n-layer. Leaving their seats, they rush to the free orbits of the B-layer atoms and then return to their original positions by the attached load. As you all know, the movement of electrons in a closed circuit is electricity. But electrons can move electrons not because of the magnetic field,

but because of the flow of particles of solar radiation, not like electric generators [10]. When we talk about solar energy, the first thing we think of is solar panels. Photovoltaic solar energy is the most popular of all renewable energies, along with wind. However, another type of solar thermal energy is widely used in water heating.

Since the power of one photovoltaic module is not sufficient for electronic devices, a series connection of several cells is used to obtain the required voltage. In terms of current strength, this is increased by the parallel combination of a certain number of assemblies [11].The power generation in semiconductors is directly dependent on the amount of solar energy, so not only are the photocells installed outside, they also attempt to direct their surface perpendicular to the incident rays [12]. To protect the cells from mechanical damage and atmospheric impacts, they are mounted on a solid foundation and protected by glass from above. When in operation, solar panels do not make noise and do not contain harmful chemicals [13]. The first solar cell was based on selenium (Se), but the low efficiency (less than 1%), the rapid aging and high chemical activity of selenium solar cells forced them to look for other, cheaper, and more efficient materials [14]. And they were found on the crystalline silicon (Si) face. Since this element of the schedule is a dielectric, its conductivity is added from various rare earth metals. Depending on the production technology, there are many types of silicon photocells. Nevertheless, there are some reasons why not everyone uses this wonderful source of energy. Defects associated with solar energy must be overcome, which will only ensure its extensive use [21].

3. Proposed Model

The highest level of refining is made by cutting thin layers from silicon ingots. Externally, single-crystal-type photocells resemble plain dark blue glass plates with a pronounced electrode grid. Their efficiency reaches 19%, and the service life is up to 50 years. Although, the performance of panels made on the basis of monocrystals are demonstrated. The monocrystalline solar cells have the same dark color and cut corners. These features do not allow them to be confused with other solar cells. In the production of polycrystalline solar cells, less pure, but cheaper silicon is used. The simplification of technology affects the appearance of the plates—they are not a uniform shade, but a lighter method of creating borders of multiple crystals. The efficiency of such solar cells is slightly lower than that of monocrystalline—no more than 15% and the service life is up to 25 years. It should be noted that the decrease in key performance indicators did not affect the popularity of polycrystalline solar cells. They benefit from low cost, no strong dependence on external pollution, low cloud cover, and orientation towards the sun. It is a form of renewable and clean energy that uses the sun's energy to generate electricity. Unlike solar panels where photovoltaic energy is used to generate electricity from photons of light found in solar radiation, this energy uses this radiation to heat a liquid.

Polycrystalline solar cells have a light blue color and a random shape, which is the result of their structure being composed of many crystals. For solar cells made of amorphous Si, a crystalline structure is not used, but a very thin layer of silicon, which is encased in glass or polymer. Although this production method is inexpensive, such panels have a very short lifespan due to the combustion and decay of the amorphous layer in the sun. These types of photocells are not happy with its performance—their efficiency does not exceed 9% and decreases significantly during operation. The use of solar panels made of amorphous silicon is justified in deserts—higher solar activity sustains a drop in productivity, wider expansions make it possible to place solar power plants of any size in gradual decline, and batteries manufactured 40 years ago are still in operation, providing up to 80% of their original power. It has ability to spray silicone structure on any surface allowing you to create flexible solar panels. Further development of photovoltaic cell production technology is due to the need to reduce cost and improve performance. Film photocells today have the maximum performance and durability. The level management of proposed model is shown below in Figure 1.

(i) Limited water level, which will create difficulties

(ii) Excess water expenditure when discharging water from the cold tap in the faucet

(iii) Flow type or direct flow units—they heat the moving fluid and load it directly into the water supply system

(iv) Storage water heaters first supply the required water, followed by heating

(v) Flow-accumulation type units are an integrated option, which allows the use of a more convenient method depending on the need, if required

(vi) A good electric or gas water heater is based on both storage and flow type water heating. In the first case, the required amount enters the boiler and heats up after a while. If it is a flowing water heater, the water flow is sent through the heating element

(vii) In electricity, so-called induction water heaters differ in that they have an exclusively flow-through mechanism for heating water

Solar panels are always one step behind their factory counterparts and for many reasons. First, well-known manufacturers carefully select photocells, weeding out cells with unstable or reduced parameters. Second, in the manufacture of solar cells, special glass with increased light transmission and reduced reflection is used—this is almost impossible to find on sale. Third, before starting serial production, all parameters of industrial designs are tested using mathematical models. When the sun's rays hit the liquid, it heats up, and this hot liquid can be used for various applications. To get a better idea, the energy consumption of a hospital, a hotel, or a house corresponds to 20% of hot water use. With solar thermal energy, we can use the energy of the sun to heat water and thus we do not need to use fossil or other

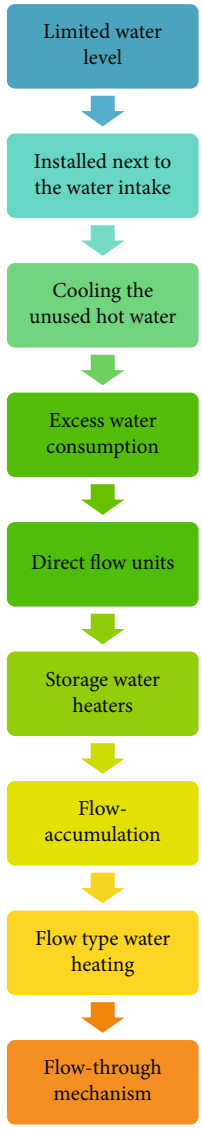

Figure 1: Proposed level management.

energy in this energy sector. As a result, the impact of cell heating on battery performance is minimized, the heat dissipation system is improved, the optimal cross-section connecting the phosphors is detected, and ways to reduce the decay rate of the photocells are explored. Such problems cannot be solved without a fitted laboratory and appropriate qualifications. The low cost of home-made solar panels allows you to create a plant that allows you to completely abandon the services of energy companies. Nevertheless, self-made solar panels show good performance results and are not far behind their industrial counterparts. In terms of price, here we have more than double the profit, i.e., at the same cost, home-made products will give twice as much more electricity consumed. Considering all of the above, a picture emerges of which solar cells are suitable for our conditions. Movies will disappear due to lack of sales and imageless—due to short service life and low performance. The crystalline silicon cells remain. I must say that it is better to use cheap "polycrystals" in the first home-made device. After activating the technology and "filling your hand", you should switch to single-crystal cells.

Inexpensive nonstandard photocells are ideal for running on technologies as well as high-quality devices that can be purchased at overseas trading sites. It is rare that there is no treasure chest with old radio components. But the diodes and transistors from older receivers and TVs are still the same semiconductors with p-n junctions, which, when illuminated by sunlight, generate current. Using these properties and combining several semiconductor devices, you can create a real solar battery. To make a low power solar battery, you can use the old element base of semiconductor devices. The attentive reader will immediately ask what c is. Why pay for factory-made mono or polycrystalline cells, if you use what is on your feet. As always, the devil is in the details. The truth is that the most powerful germanium transistors make it possible to obtain voltages not exceeding 0.2 V in bright sun at current strength measured in micro amps. To achieve the parameters that make up a flat silicon photocell, you will need several tens or hundreds of semiconductors. The battery made of old radio components is only good for charging the LED camping lamp or small mobile phone battery. Purchased solar cells are essential for the implementation of large projects. It is not uncommon for vendors to offer so-called damaged "B" class solar cells made of mono or polycrystalline solar panels. The lack of small chips, cracks, or corners practically does not affect the performance of the cells, but allows you to buy it at a very low price. For this reason they are best used in home-made solar panels. This is shown in Figure 2.

(i) Install a rubber gasket between the glass and the box

(ii) Dry run—to prevent overheating of the heating element if there is no water in the tank

(iii) Pressure control systems—power consumption is turned off when the fluid overheats

(iv) An integrated approach to security. The mechanical valve is filled by electronic sensors in the body or fitting

(v) In addition, there should be a power unit designed for 180-240 V voltage and not just standard 220 V

(vi) The boiler is fitted with a tap with a cold water supply and is additionally supplied to the outlet with a collector for hot water pipes to the consumption points. The main requirement for the body of a water heater is compression and adequate thermal insulation

(vii) Polyurethane foam is the most effective from this point of view. High quality thermal insulation is important for the efficient operation of the boiler without unnecessary costs for heat loss

The flow heater has a simple operating scheme. Water is supplied through a copper pipe. In the form of a spiral, the

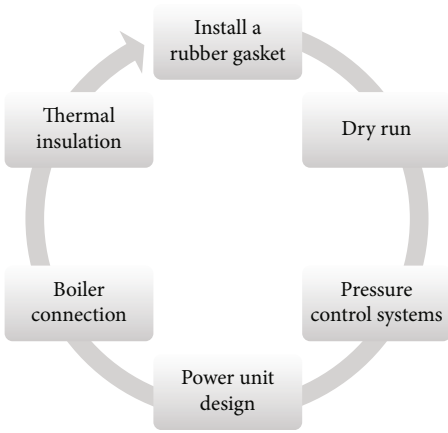

Figure 2: Proposed model flow.

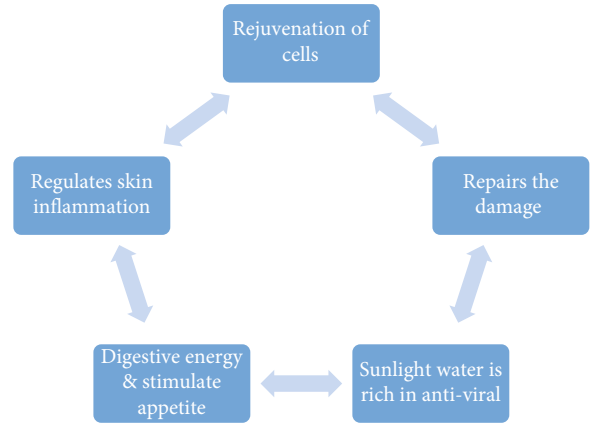

Figure 3: Enhanced energy of solar power.

tube itself revolves around an energy source: a gas burner or a heating element (in other words, a tube electric heater). An induction water heater uses the force of an alternating magnetic field, which acts on a material with a high resistance and heats it by the induction of an electric current. The current coming from the transformer is converted into high frequency current by the inverter and converted to a coil that generates an alternating magnetic field. The fluid pipe plays the role of center. Under the action of a magnetic field, the electricity excited in it heats it up and raises the temperature of the water. You will get enhanced energy if you drink water that has been dried in the sun.

(i) There will be rejuvenation in your body

(ii) It repairs the damage you have done to the cells

(iii) Sunlight water is rich in antiviral, antifungal, and antibacterial properties. It is ideal for cleansing the skin and rinsing the eyes

(iv) Sunlight drinking water has the power to improve your digestive energy and stimulate appetite. Destroys worms in the intestines and corrects problems like acidity and ulcers

(v) Regulates skin inflammation and cures itching. This, in turn, results in glowing skin

Figure 3 shows enhanced energy of solar power. In a storage heater, the water first enters the tank, where it is gradually heated to the desired temperature. Also, according to the laws of physics, the warmer layers gradually move to the top of the tank, and the colder ones sink to the bottom. Gas water heaters have open and closed combustion chambers for the release of waste energy products. A chimney or coaxial metal sleeve may be used. Electric columns can vary in the types of heating elements: tubular or dry. The most common tube is a metal tube, inside of which is placed a conductor with a high electrical resistance. The tube is heated by the conductor and gives heat to the water. In this case the dielectric is sand, which fills the space between the walls of the conductor and the pipe. The heating elements contribute to the buildup of volume, which reduces the efficiency of the heater. The so-called dry heating element is not a tube, but a special flask, inside of which contains special oil or quartz sand. It is also called ceramic with very few shapes on the walls of the flask, and this option is recognized as highly electrically safe. The waters of rivers, lakes, and reservoirs are exposed to solar radiation, although of course you would think that they are not heated. To take advantage of this solar radiation, a special installation is necessary to help heat the liquids so that they can be used later.

4. Results and Discussion

The proposed hybrid solar deep learning approach (HSDLA) was compared with the existing building integrated photovoltaic (BIPV) system, temperature-based machine learning models (TMLM), deep learning neural networks (DLNN), and solar power generation prediction (SPGP).

4.1. Flat-Blade Collector Management. Daily power consumption is easy to detect. To do this, look at the invoice sent by the energy sales organization and divide the number of kilowatts indicated there by the number of days in the month. A hose and insulation are included. For the absorbent layer, black copper sheet with excellent thermal conductivity is used, which is suitable for creating solar panels. It is necessary to take into account the fact that the solar panel produces electricity only during daylight hours, and up to 70% of production is carried out as shown in Table 1.

The hydraulic circuit is the pipes that make up the circuit, where we carry the heat transfer fluid that takes care of the operation we are going to do. The circuit is normally closed in most installations. Therefore, we are talking about one-way circuits, from the group, and return circuits, to the group. This circuit is like a kind of water boiler that contributes to the heating of a space.

4.2. Integrated Collector-Storage Systems Management. Light cloud or fog will reduce the efficiency of the current output of the solar installation by 2-3 times, while the sky covered by solid clouds will trigger a 15-20 times drop in productivity. Under ideal conditions, a solar panel with a capacity of

Table 1: Flat-blade collector management.

No. of inputs	BIPV	TMLM	DLNN	SPGP	HSDLA
500	77.85	70.86	75.00	82.83	90.73
1000	77.14	69.93	73.89	81.50	89.49
1500	75.84	68.93	73.19	80.63	89.38
2000	74.93	67.98	72.22	79.45	88.52
2500	73.93	67.01	71.31	78.35	87.84
3000	72.92	66.05	70.41	77.25	87.17
3500	71.92	65.08	69.50	76.15	86.49

Table 2: Integrated collector-storage systems management.

No. of inputs	BIPV	TMLM	DLNN	SPGP	HSDLA
500	81.71	74.86	78.92	87.36	92.43
1000	81.38	73.36	78.33	85.49	91.39
1500	80.04	72.25	77.35	84.66	91.26
2000	78.90	71.87	76.14	83.75	90.30
2500	78.07	70.57	75.36	82.40	89.72
3000	77.09	69.56	74.42	81.23	89.06
3500	76.11	68.55	73.49	80.07	88.41

Table 3: Exhaust-tube solar collectors.

No. of inputs	BIPV	TMLM	DLNN	SPGP	HSDLA
500	74.84	67.63	77.29	84.24	88.62
1000	73.54	66.63	76.59	83.16	88.46
1500	72.24	65.63	75.89	82.08	88.30
2000	70.94	64.63	75.19	81.00	88.14
2500	69.64	63.63	74.49	79.92	87.98
3000	68.34	62.63	73.79	78.84	87.82
3500	67.04	61.63	73.09	77.76	87.66

$11/7 = 1.6$ kW would be sufficient to generate 11 kWh of power. Taking into account the influence of natural factors, this parameter should be increased approximately 40-50%. In addition, there is another factor that should increase the size of the photocells used. First, do not forget that the battery does not work at night, which means that powerful batteries are required. Second, to run home appliances, you need 220 V current, so you need a powerful voltage converter (inverter). Experts say that the losses due to accumulation and conversion of electricity will take up to 20-30% of its total amount. Therefore, the actual power of the solar cell should be increased by 60-80% of the calculated value. Assuming an efficiency value of 70%, the nominal power of our solar panel would be equal to $1.6 + (1.6 \times 0.7) = 2.7$ kW as shown in Table 2.

The first thing to install is the collector or solar panel. This solar panel does not work like the well-known photovoltaic. It does not have a photovoltaic cell that collects photons of light to convert them into energy and circulate within them to allow us to capture solar radiation to start heating the liquid. There are different types of collectors and differences in their performance.

4.3. Exhaust-Tube Solar Collectors. The use of high-current lithium battery assemblies is a very elegant one, but by no means an inexpensive way to save solar power. To save electricity, you will need low voltage batteries rated at 12, 24, or 48 V. Their capacity should be designed for daily energy consumption and losses for change and conversion. In our case, an array of batteries designed to store $11 + (11 \times 0.3) = 14.3$ kWh of energy is required. If you use regular 12 V car batteries, you will need 14300 Wh/12 V = 1200 Ah built-in, six batteries each rated at 200 Ah as shown in Table 3.

They are responsible for transporting heat through the circuit. A heat exchanger transfers the energy captured by the sun to the water. They are usually external to the tank (called plate exchangers) or internal (coil).

4.4. Reservation of High Energy. As you can see, even providing electricity for the household needs of an average family requires intensive solar power installation. As for the use of home-made solar panels for heating, at this point such an effort does not reach the limit of self-sufficiency, not to mention the fact that anything can be saved. The size of the battery depends on the required power and dimensions of the current sources. When choosing the latter, you will definitely pay attention to the different types of photocells proposed as shown in Table 4.

As the demand for solar energy is not always the same as for photovoltaics, it requires some energy storage system. In this case, solar thermal energy is stored in accumulators. This accumulator stores hot water to make it available when we need it. They are tanks with capacity and necessary insulation to avoid energy losses and keep water hot at all times.

4.5. Flow Management. Electric direct flow water heater does not have a storage tank and has a large capacity. Power consumption can reach 30 kW. This is a small unit that allows you to install directly under the washbasin. The use of such a heater is possible only in homes designed for electric stoves. Prior to installation, it is important to consult an electrician regularly. Another type of electric direct flow water heater is called induction columns. Unlike units with heating elements, this type has the highest efficiency, up to 98 percent. Saving electricity with such a heater can be up to 30-50 percent. Except for the inner wall of the pipe through which the supply is carried, the heating element does not come into contact with water. The variable type magnetic field does not allow deposits to form and heats the entire volume of the liquid simultaneously, which saves time. The water heats up very quickly as shown in Table 5.

To move fluid from one place to another, pumps are needed to overcome pressure drops in circuits, as well as frictional and gravitational forces. For use in home-made devices, it is very convenient to choose medium-sized solar cells. For example, 3 × 6 inch polycrystalline panels are rated for 0.5 V output voltage and current up to 3 A. When producing a solar battery, they are connected in series in modules of 30 pieces, making it possible to obtain the voltage of 13-14 V required to charge a car battery (taking into account losses). The

Table 4: Reservation of high energy.

No. of inputs	BIPV	TMLM	DLNN	SPGP	HSDLA
500	76.60	69.57	79.54	86.49	89.39
1000	75.55	68.56	78.40	85.57	89.82
1500	74.50	67.55	77.26	84.65	90.25
2000	73.45	66.54	76.12	83.73	90.68
2500	72.40	65.53	74.98	82.81	91.11
3000	71.35	64.52	73.84	81.89	91.54
3500	70.30	63.51	72.70	80.97	91.97

Table 5: Reservation of high energy.

No. of inputs	BIPV	TMLM	DLNN	SPGP	HSDLA
500	79.41	72.56	82.32	90.10	91.52
1000	79.08	71.06	81.73	88.23	90.51
1500	77.74	69.95	80.75	87.40	90.35
2000	77.07	68.58	80.03	85.88	89.62
2500	76.24	67.28	79.25	84.53	89.04
3000	75.40	65.97	78.46	83.18	88.45
3500	74.57	64.67	77.68	81.83	87.87

maximum power of such a module is $15\,V \times 3\,A = 45\ W$. Based on this value, it is not difficult to calculate how many components are needed to build a solar panel of a given power and determine its dimensions. For example, to build a 180-watt solar electric collector would require 120 photovoltaic cells with a total area of 2160 square meters.

5. Conclusion

When the main heat is switched off in the summer, the usage of a heat exchanger becomes more problematic. It must modify and choose the boiler that will only function for the heat exchanger. The heat pump, like the water pump, expels heat. The heat of the sun heats the water. A pump fills the collection pipes with water, which is then heated to the proper temperature and discharged back into the common tank. Again, the solar collector warms up another component. Often, heat exchangers are installed just like electric heaters: the circuit between the pump and the pool. In some cases, it is better to use two heat exchangers at the same time. There is a vortex in the body of the heat exchanger. There is a space around, which should be filled with water from the pond. The boiling water passes through the vortex and due to the large contact area, the water from the pool heats up quickly. This is a very simple and popular method of raising the temperature in small pools, although an electric heater also has its drawbacks.

Data Availability

The data used to support the findings of this study are included within the article. Further data or information are available from the corresponding author upon request.

Conflicts of Interest

The authors declare that there are no conflicts of interest regarding the publication of this paper.

Acknowledgments

The authors appreciate the supports from Mizan-Tepi University, Ethiopia for the research and preparation of the manuscript.

References

[1] D. Assouline, N. Mohajeri, and J. L. Scartezzini, "Quantifying rooftop photovoltaic solar energy potential: a machine learning approach," *Solar Energy*, vol. 141, pp. 278–296, 2017.

[2] V. S. Nayagam, A. P. Jyothi, P. Abirami et al., "Deep learning model on energy management in grid-connected solar systems," *International Journal of Photoenergy*, vol. 2022, Article ID 6371182, 8 pages, 2022.

[3] S. SivaChandran, R. Venkatesh, S. Baskar, T. Maridurai, and R. Arivazhagan, "Experimental study of shell and tube heat exchanger," *AIP Conference Proceedings*, vol. 2473, article 020005, 2022.

[4] J. Mustafa, S. Alqaed, and M. Sharifpur, "Numerical study on performance of double-fluid parabolic trough solar collector occupied with hybrid non-Newtonian nanofluids: investigation of effects of helical absorber tube using deep learning," *Engineering Analysis with Boundary Elements*, vol. 140, pp. 562–580, 2022.

[5] A. Mosavi, M. Salimi, S. FaizollahzadehArdabili, T. Rabczuk, S. Shamshirband, and A. R. Varkonyi-Koczy, "State of the art of machine learning models in energy systems, a systematic review," *Energies*, vol. 12, no. 7, p. 1301, 2019.

[6] R. Kabilan, V. Chandran, J. Yogapriya et al., "Short-term power prediction of building integrated photovoltaic (BIPV) system based on machine learning algorithms," *International Journal of Photoenergy*, vol. 2021, Article ID 5582418, 11 pages, 2021.

[7] M. J. Dehghani, "Enhancing energo-exergo-economic performance of Kalina cycle for low- to high- grade waste heat recovery: design and optimization through deep learning methods," *Applied Thermal Engineering*, vol. 195, article 117221, 2021.

[8] J. A. Bellido-Jiménez, J. E. Gualda, and A. P. García-Marín, "Assessing new intra-daily temperature-based machine learning models to outperform solar radiation predictions in different conditions," *Applied Energy*, vol. 298, article 117211, 2021.

[9] R. Banos, F. Manzano-Agugliaro, F. G. Montoya, C. Gil, A. Alcayde, and J. Gómez, "Optimization methods applied to renewable and sustainable energy: a review," *Renewable and Sustainable Energy Reviews*, vol. 15, no. 4, pp. 1753–1766, 2011.

[10] Z. Sun, H. Jin, J. Gu et al., "Studies on the online intelligent diagnosis method of undercharging sub-health air source heat pump water heater," *Applied Thermal Engineering*, vol. 169, p. 114957, 2020.

[11] E. Almeshaiei, A. Al-Habaibeh, and B. Shakmak, "Rapid evaluation of micro-scale photovoltaic solar energy systems using empirical methods combined with deep learning neural networks to support systems' manufacturers," *Journal of Cleaner Production*, vol. 244, p. 118788, 2020.

[12] V. Chandran, C. K. Patil, A. M. Manoharan et al., "Wind power forecasting based on time series model using deep machine learning algorithms," *Materials Today: Proceedings*, vol. 47, pp. 115–126, 2021.

[13] A. Chiasson, J. Kelly Kissock, and A. Selvacanabady, "Lean Energy Buildings: Applications of Machine Learning, Optimal Central Chilled-Water Systems, and Hybrid Solar-Ground Source Heat Pump Systems," in *Advances in Sustainable Energy*, pp. 59–92, Springer, Cham, 2019.

[14] R. Chang, L. Bai, and C. H. Hsu, "Solar power generation prediction based on deep learning," *Sustainable Energy Technologies and Assessments*, vol. 47, p. 101354, 2021.

[15] Z. Wang, J. Liu, Y. Zhang, H. Yuan, R. Zhang, and R. S. Srinivasan, "Practical issues in implementing machine-learning models for building energy efficiency: moving beyond obstacles," *Renewable and Sustainable Energy Reviews*, vol. 143, p. 110929, 2021.

[16] M. Ali, R. Prasad, Y. Xiang et al., "Variational mode decomposition based random forest model for solar radiation forecasting: new emerging machine learning technology," *Energy Reports*, vol. 7, pp. 6700–6717, 2021.

[17] S. Al-Janabi, A. F. Alkaim, and Z. Adel, "An innovative synthesis of deep learning techniques (DCapsNet & DCOM) for generation electrical renewable energy from wind energy," *Soft Computing*, vol. 24, no. 14, pp. 10943–10962, 2020.

[18] F. Meng, Q. Zou, Z. Zhang et al., "An intelligent hybrid wavelet-adversarial deep model for accurate prediction of solar power generation," *Energy Reports*, vol. 7, pp. 2155–2164, 2021.

[19] M. E. Javanmard, S. F. Ghaderi, and M. Hoseinzadeh, "Data mining with 12 machine learning algorithms for predict costs and carbon dioxide emission in integrated energy-water optimization model in buildings," *Energy Conversion and Management*, vol. 238, article 114153, 2021.

[20] N. Kishor, M. K. Das, A. Narain, and V. P. Ranjan, "Fuzzy model representation of thermosyphon solar water heating system," *Solar Energy*, vol. 84, no. 6, pp. 948–955, 2010.

[21] N. Khan, F. U. M. Ullah, I. U. Haq, S. U. Khan, M. Y. Lee, and S. W. Baik, "AB-net: a novel deep learning assisted framework for renewable energy generation forecasting," *Mathematics*, vol. 9, no. 19, p. 2456, 2021.

[22] M. M. Rahman, M. Shakeri, S. K. Tiong et al., "Prospective methodologies in hybrid renewable energy systems for energy prediction using artificial neural networks," *Sustainability*, vol. 13, no. 4, p. 2393, 2021.

[23] M. A. Soleimanzade and M. Sadrzadeh, "Deep learning-based energy management of a hybrid photovoltaic-reverse osmosis-pressure retarded osmosis system," *Applied Energy*, vol. 293, p. 116959, 2021.

[24] J. Logeshwaran and R. N. Shanmugasundaram, "Enhancements of resource management for Device to Device (D2D) communication: a review," in *In 2019 third international conference on I-SMAC (IoT in social, Mobile, analytics and cloud)(I-SMAC)*, pp. 51–55, IEEE, Palladam, India, 2019.

[25] J. Logeshwaran, M. J. Rex, T. Kiruthiga, and V. A. Rajan, "FPSMM: fuzzy probabilistic based semi Morkov model among the sensor nodes for realtime applications," in *In 2017 international conference on intelligent sustainable systems (ICISS)*, pp. 442–446, IEEE, Palladam, India, 2017.

[26] X. S. Jiang, Z. X. Jing, Y. Z. Li, Q. H. Wu, and W. H. Tang, "Modelling and operation optimization of an integrated energy based direct district water-heating system," *Energy*, vol. 64, pp. 375–388, 2014.

[27] H. Zou, J. Tao, S. K. Elsayed, E. E. Elattar, A. Almalaq, and M. A. Mohamed, "Stochastic multi-carrier energy management in the smart islands using reinforcement learning and unscented transform," *International Journal of Electrical Power & Energy Systems*, vol. 130, p. 106988, 2021.

[28] S. Ghimire, R. C. Deo, N. Raj, and J. Mi, "Deep solar radiation forecasting with convolutional neural network and long short-term memory network algorithms," *Applied Energy*, vol. 253, p. 113541, 2019.

[29] S. Ghimire, R. C. Deo, N. Raj, and J. Mi, "Deep learning neural networks trained with MODIS satellite-derived predictors for long-term global solar radiation prediction," *Energies*, vol. 12, no. 12, p. 2407, 2019.

[30] P. Obstawski, T. Bakoń, and D. Czekalski, "Comparison of solar collector testing methods—theory and practice," *PRO*, vol. 8, no. 11, p. 1340, 2020.

[31] S. Seyedzadeh, F. P. Rahimian, S. Oliver, S. Rodriguez, and I. Glesk, "Machine learning modelling for predicting non-domestic buildings energy performance: a model to support deep energy retrofit decision-making," *Applied Energy*, vol. 279, article 115908, 2020.

Hindawi
International Journal of Photoenergy
Volume 2022, Article ID 5442304, 12 pages
https://doi.org/10.1155/2022/5442304

Research Article

Solar Power Generation in Smart Cities Using an Integrated Machine Learning and Statistical Analysis Methods

Ahmad Almadhor,[1] K. Mallikarjuna,[2] R. Rahul,[3] G. Chandra Shekara,[3] Rishu Bhatia,[4] Wesam Shishah,[5] V. Mohanavel,[6,7] S. Suresh Kumar,[8] and Sojan Palukaran Thimothy[9]

[1]*College of Computer and Information Sciences, Jouf University, Skaka, Aljouf 72388, Saudi Arabia*
[2]*Department of Mechanical Engineering, Government Polytechnic, Kudligi, 583135 Karnataka, India*
[3]*Department of Mathematics, BMS College of Engineering, Bangalore, Karnataka 560019, India*
[4]*Department of Electronics and Communication Engineering, Ganga Institute of Technology and Management, Kablana, Jhajjar, 124104 Haryana, India*
[5]*College of Computing and Informatics, Saudi Electronic University, Riyadh, Saudi Arabia*
[6]*Centre for Materials Engineering and Regenerative Medicine, Bharath Institute of Higher Education and Research, Chennai 600073, India*
[7]*Department of Mechanical Engineering, School of Technology, Glocal University, Delhi-Yamunotri Marg, Uttar Pradesh, 247121, India*
[8]*Department of General Engineering (MECH), Panimalar Engineering College Chennai City Campus, Chennai, Tamil Nadu, India*
[9]*Faculty of Mechanical Engineering, Arba Minch Institute of Technology (AMIT), Arba Minch University, Ethiopia*

Correspondence should be addressed to Sojan Palukaran Thimothy; sojan.palukaran@amu.edu.et

Received 21 July 2022; Revised 10 September 2022; Accepted 13 September 2022; Published 30 September 2022

Academic Editor: Br Ramesh Bapu

Presently, photovoltaic systems are an essential part of the development of renewable energy. Due to the inherent dependence of solar energy production on climate variations, forecasting power production using weather data has a number of financial advantages, including dependable proactive power trading and operation planning. Megacity electricity generation is regarded as a current research problem in the modern features of urban administration, particularly in developing nations such as Iran. Machine learning could be used to identify renewable resources like transformational participation (TP) and photovoltaic (PV) technology; based on resident motivational strategies, the smart city concept offers a revolutionary suggestion for supplying power in a metropolitan region. The sustainable development agenda is introduced at the same time as this approach. Therefore, the article's goals are to estimate Mashhad, Iran's electrical power needs using machine learning technologies and to make innovative suggestions for motivating people to generate renewable energy based on the expertise of experts. The potential of solar power over the course of a year is then assessed in our research study in Mashhad, Iran, using the solar photovoltaic modelling tool. The present idea in this research uses linear regression techniques to forecast utilising artificial neural networks (ANN). The most important factor in sizing the installation of solar power producing units is the daily mean sun irradiation. The amount of power that will be produced by solar panels can be estimated using the mean sun irradiance at a particular spot. A precise prediction can also be used to determine the complexity of the system, return on investment (ROI), and system load metrics. Several regression techniques and solar irradiance-related metrics have been combined to forecast the mean sun irradiation in terms of kilowatt hours per square metre. Azimuth and zenith factors considerably enhance the performance of the model, as demonstrated by the proposed method. The results of this study demonstrate 99.9% reliability rate for ANN model prediction of the electrical power usage during the summer and winter seasons. Thus, the maximum of power requirement during the hottest and coolest periods can be managed by using the photovoltaic system's renewable power projections.

1. Introduction

All modern nations face three major issues in the twenty-first century: social and economic development, environmental sustainability, and energy management. Additionally, one of the key elements of socioeconomic development for any nation in order to become developed is energy independence [1]. According to the International Energy Agency (IEA), energy production and consumption are currently the main man-made sources of air pollution, which kills 6.5 million people prematurely each year. Technology for reducing air pollution is now widely known, and maintaining clean air is crucial for preserving human health. Air pollution issues remain unresolved in many nations, despite the growing awareness of its importance, and in the coming decades, the hazards to world health will increase. PM2.5 refers to suspended particles with a diameter of 2.5 m or less that come from pollution sources. The small size of the pollution source's particles allows them to get through the lungs and into the alveoli, where they can affect the body's other organs [2]. In accordance with the majority of research, PM2.5 at or below 12 $\mu g/m^3$ is deemed healthy and poses little to no danger of exposure. The air is deemed harmful if the quantity reaches or exceeds 35 $\mu g/m^3$ over the course of a 24-hour period and can be problematic for persons who already have breathing conditions like asthma. As a result, managing and controlling urban air pollution is quite difficult. The ability to sense the climate and the surroundings around the city is essential for a smart city to build a smart environment and enhance the quality of life for its residents.

Among the most popular alternative energy sources being looked after to meet the rising demand for power while reducing carbon footprint and protecting fossil fuels and other environmental assets is photovoltaic technologies. The photovoltaic system uses highly conductive materials to convert solar radiation directly into electrical energy [3]. Every wealthy nation relies heavily on energy for economic growth, but using conventional energy sources pollutes cities more. As a result, the management of smart cities constantly suggests installing a renewable energy system to cut down urban pollution. In order to handle widespread urbanisation, cities must become smarter. They must also find innovative ways to manage energy, raise living standards, and protect the environment while doing so [4]. Solar cookers, solar collectors, solar water heaters and air, solar heat pumps, and solar dryers are just a few examples of the various devices that use SE to do beneficial tasks [5]. Because it allows for the load, or the device's power consumption, to be adjusted to correlate with the projected energy output, the concept of power neutrality provides a novel perspective on how devices ought to be constructed. This is due to the fact that power neutrality makes it possible. The term "energy neutral design" can also be used to refer to "environmentally powered electronics," in which electronic equipment either absorbs or harvests energy from their immediate surroundings and converts that energy into the electricity they need to function properly. Researchers have invested a lot of time in identifying various methods for energy modulation, whether through the scheduling of communications or the scheduling of the device's sensing and processing duties using predictions of energy production. Recent methods are especially pertinent for machine learning techniques since they use Internet-sourced public weather forecasts to feed solar electricity production predictions [6].

There are essentially three types of forecasting methods for PV power generation or solar insolation nowadays. Physical techniques fall under the first group because they can forecast future sun positions and the irradiance that outcomes without using any additional temperature data. Although the prediction of sun position can be important, this method is likely to ignore other pertinent meteorological circumstances. For instance, clouds or rain in the sky impede solar irradiation. Group 2 is analytical measurements, which can be further broken down into traditional approaches and contemporary methods that make use of statistical learning. Numerous trainings have embraced this data-driven strategy for creating PV forecast models as a result of the enormous advancements in analytical learning methods over the previous ten years. Last but not least, hybrid methods combine statistical methods with other techniques like signal processing or optimization algorithms [7]. The work involves evaluating solar radiation forecasting using a variety of machine learning regression models. Particularly, artificial neural networks (ANN) reach a very high level of accuracy. The second thing that we have contributed is the utilisation of sun angles (both azimuth and zenith) in conjunction with weather information. Both the solar azimuth and the solar zenith can be used to represent where the sun is located. The angle that is formed by measuring the direction of the sun counterclockwise from the horizon is known as the solar azimuth. The angle that is obtained by measuring the distance between the local zenith and the line of sight of the sun is known as the solar zenith. We demonstrate how these two perspectives enhance prediction accuracy. In particular, using the weather forecast, we attempt to calculate the mean daily solar energy W/m^2 that a solar plant at a specific site can consume. Figure 1 shows the solar zenith and azimuth angles [8].

A global grid generally uses technology to supply services and deal with urban concerns. Among other things, a smart city seeks to improve social services, encourage sustainability, and give its citizens a voice. Regarding what it means to be a "smarter city" as well as how to continue with that specific development, the emphasis of each "smart" urban design varies [9]. The system consists of solar PV modules (also known as solar cells), a power inverter, and a net metre, and they are fed into the power grid and used in metropolitan areas. Household appliances (23 percent), water heating (13 percent), lighting (11 percent), refrigerator (8 percent), space heating, and air conditioning (A/C) all use energy (45 percent). Industrial utilisation is shown in Figure 2 [10].

These are the main steps of the suggested study, in order. The first step is to collect the essential energy usage information from Mashhad, Iran's main electricity hub. The gathered data undergoes additional processing and analysis in order to uncover certain statistical tendencies. The second

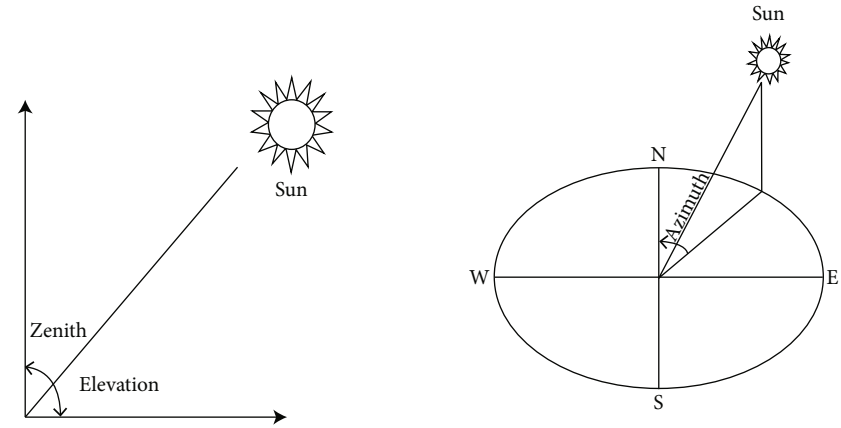

Figure 1: Solar zenith and azimuth angles.

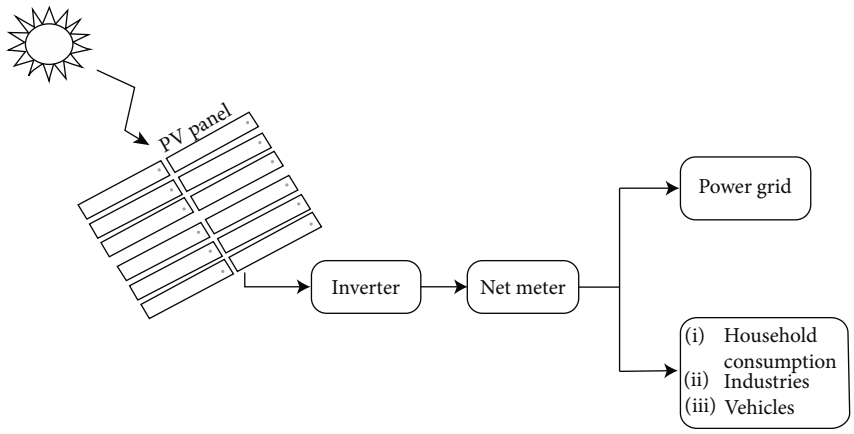

Figure 2: Smart city solar energy generation system.

stage entails running PV simulations using the application of gird PV systems. Then, final section emphasizes on developing a megacity incentive algorithm utilising the TP idea. In the fourth step, an ANN with linear regression appraisal is used for socioeconomic evaluations. To assess the approach for future energy management in urban areas, the fifth phase entails developing scenarios [11].

2. Related Works

Photovoltaic (PV) generation volatility has presented electric utilities with a number of management and operation issues. Grid operators should be aware of the performance of their asynchronous and synchronous generators in order to deliver power in a secure and reliable manner either a day or an hour in advance. During any unforeseen situations, it aids them in controlling the grid stability, frequency response, and inertia. This analysis makes an effort to offer both short- and long-term forecasts for renewable power generation based on machine learning. The researcher utilises Alice Springs, one of Australia's physically renewable power regions, and took into account a wide range of environmental factors. The study is aimed at analyzing a variety of machine learning approaches, such as long short-term memory with decision tree regression, polynomial regression, support vector regression, multilayer perceptron regression, and random forest regression. For both normal and unclear scenarios, several comprehensive comparative analyses were undertaken, and it was discovered that random forest regression performed significantly enhanced for database. Using a variety of performance criteria, the effect of data analysis on prediction accuracy is also examined. The work could assist grid operators in planning the time-ahead generation uncertainty and selecting a suitable PV power forecasting technique. Python is used for the forecasting along with a number of library functions like scikit-learn, Keras, pandas, and NumPy. Due to a lack of data, this study was unable to evaluate its performance using forecasted weather values, which could have negatively impacted predicting performance in real-world applications [12].

Utilising a variety of machine learning techniques, short-term solar power forecasting is frequently employed in sustainable energy integration and power source management. However, selecting the appropriate machine learning models and data properties can be challenging. This study develops a methodology for statistically evaluating several models and feature selection methods, and it identifies the best model and feature combination for forecasting short-term solar

power. More specifically, the methodologies use random forest, artificial neural network, and excessive gradient boosting (XGBoost), and the machine learning techniques use feature significance and principal component analysis (PCA). All potential combinations of these feature selection and machine learning algorithms are created and evaluated for solar power forecasting. For Hawaii, US, solar power forecasting, the ideal selection of characteristics and machine learning methods are discovered. The results of the tests indicate that the gradient boosted approach, with features chosen by the PCA method, is superior to the other strategies in terms of effectiveness. Building simpler (weaker) prediction models successively is how gradient boosting gets the job done. Each model in the sequence makes an attempt to anticipate the error that was caused by the model that came before it. Because of this, the algorithm has a propensity for quickly becoming overfit. The framework can be used to select the best machine learning approaches for relatively quick solar power prediction, using the simulation results as a baseline for comparison. Short-term solar activity forecasts have not commonly used the boost and spontaneous forest models [13].

Low-power electrical energy producing units can be connected to the grid by using solar energy and other renewable energy sources (wind, hydro, etc.). The opportunity to divide existing distribution networks into smaller units or microgrids that are self-sufficient and sustainable for shorter or longer periods is offered by the novel idea of distributed energy generation. Enhanced customer energy supply and effective energy use are both achievable in a setting with a smart grid, especially while the primary grid is down. The method to determine a rooftop PV system's potential power capacity in a smart city is presented in this study. Solar-powered generation units and the potential for serving existing loads will receive special consideration. The findings of a theoretical study on the promising applications of PV solar energy for the supply of power in several Serbian cities are provided as a case study. PV generation can lower electricity bills for PV system owners and dramatically lower CO_2 emissions from thermal power plants. A backup from the major public grid is necessary due to the unequal distribution of the electricity produced during the day and its sometimes limited availability during the winter [14]. Using clean, renewable solar power as your main source of energy and selling surplus power to the utility via net metering are just two of the many advantages of installing a grid-tied solar power system with battery backup, commonly known as a "hybrid solar system."

To meet the challenging goals for reducing greenhouse gases outlined in the 2015 Paris Agreement, the power generation industry must undergo a significant transformation. For the purpose of determining spot power prices, it is necessary to decrease uncertainty regarding supply and, in the case of renewable power, demand. In this work, a context-based approach for forecasting the production and consumption of energy in buildings is proposed and evaluated. It focuses on a home that has solar panels and an energy storage device. Evaluating the efficacy of stride predictors, Markov chains, and their incorporation into hybrid predictors is an additional step that must be taken in order to simulate the development of the relationship between the demand for and supply of energy. Markov chains are a useful tool for calculating the likelihood of a certain event taking place by modelling the event as a transition from one state to another state or as a transition from one state to the same state that it was in previously. Each of these techniques forecasts electrical power using historical data. The purpose is to identify the best approach and its ideal configuration that can be incorporated into an intelligent energy management system (perhaps based on hardware). Such a system's function is to coordinate and modify electricity production and consumption through forecasting in order to boost self-consumption and ease demand on the grid. Studies on real-world datasets have shown that a Markov chain with an electricity generation record of 150 values, a structure of single energy distribution value, and an intermission size of 1 is the highest reviewed predictor. Slow converging, instability, and vibration throughout training are some of its drawbacks [15].

The advanced energy domain is one of the trickiest areas of future study in smart urban. Important issues in optimization, the provision of intelligent, flexible networks, and sophisticated computational tools and approaches all call for additional study. When it comes to supporting future global growth in the face of resource depletion and climate change, renewable is a significant resource. In order to meet these higher criteria, artificial intelligence (AI) offers new rules for regulating the operations. In order to address the numerous challenges that will impede the sector's growth and resilience, it is required to improve the architecture of the power infrastructure as well as the deployment and production of RE. This study looks at the advantages of current advancements in the application of AI to the real estate industry in a European nation. The effectiveness of the transformation of RE from gross inland usage to final energy usage within the power sector, its effects on the composition of reliable energy by source (solar, wind, biomass, etc.), the productivity increases in the tertiary sectors especially in comparison to the economy at large as well as its similarity with infrastructure investment, and the possible ramifications of the implementation of AI for RE towards upcoming urban research were all examined by researchers. The establishment of a conceptual framework for appreciating the role of AI in the RE sector in Europe is the major goal of this research. A discussion of the consequences for possible future study on smart cities and proposed research goals is another audacious addition to this work. The broad use of RE still faces significant challenges. These relate not just to the required technology but also to the formulation of policies and factors that should be discussed in subsequent research [16].

Solar energy is produced worldwide using photovoltaic (PV) systems. Due to the intermittent output power of PV systems and their strong reliance on environmental conditions, solar power sources are erratic in nature. Irradiance, humidity, PV surface temperature, and wind speed are only a few of these variables. It is essential to properly foresee the renewable energy deployment highly uncertain in

photovoltaic systems. Forecasting solar energy is essential for an utility grid's supply chain management. Given that solar energy is climate-dependent and unpredictable, this forecast is extremely complex and difficult. In this study, it is addressed how various environmental conditions affect the output of the PV system. The effectiveness of artificial neural network- (ANN-) based multiple regression and prediction models is investigated with regard to certain parameters. Both the correlation-based feature selection (CSF) and the relief approaches are used in the decision-making process. Features that have a high correlation are more linearly dependent, and as a result, they virtually always have the same influence on the variable they are attempting to predict. In comparison to the ANN model, all other strategies that were discussed are inadequate. Because of how variable and unpredictable the weather is, it is challenging to forecast how much electricity solar PV systems will generate [17].

Monitoring monthly energy demand is necessary for metropolitan power systems to run smoothly. Various artificial intelligence-based forecasting models have been presented and have shown to work well, but they need a large enough training dataset. Because just one data point is produced per month in the case of monthly forecasting, it is difficult to gather enough data to build models. With the aid of transfer learning techniques, this data shortage can be reduced. This research proposes a novel transfer learning-based monthly electric demand forecasting method for a city or district utilising comparable data from other cities or regions. In order to do this, we gathered five kinds of monthly electric load data from 25 Seoul districts as well as numerous external data, including calendar, demographic, and weather information. Then, using the data acquired from the datasets and the information available for the target city or district, similar data were chosen by manipulative the coefficient correlation, and the chosen data were used to build a forecasting model. The model was then adjusted using the goal data. Through a number of studies, we thoroughly compared our model to other well-liked machine-learning strategies in order to show its efficacy. Some of the findings are reported. Compared to the basic DNN, the prediction performance increased while employing transfer learning [18].

3. Data Collection and Data Mining

A systematic approach for the Iranian city of Mashhad was completed as part of this programme. The studied region has commercial and touristic land uses and is Iran's second megacity. There are 3 million people living in the Iranian city of Mashhad, which is situated in the country's northeast. Throughout the analysis, MATLAB 2018 and SPSS 19 software were used to examine the fluctuations in electrical power consumption utilising data mining and statistical methodologies. For the year 2019, all data were acquired from the Mashhad Distribution Electrical Energy Company's consumption management division. The energy consumption discrepancies based on the energy utilisation regimes for the peak winter and peak summer consuming months (December and July, respectively), which are illustrated in Tables 1 and 2 with Figures 3 and 4, were examined using computational methods. For the trend analysis in the adopted mathematical techniques, machine learning systems that is multilayer perceptron artificial neural network and histogram methodologies are combined with descriptive statistics like histogram approaches and metrics like average, sample variance, mean, and frequency distribution. In relation to the winter season, summertime electrical power use has been higher. Principals must undertake an efficient power consumption peak management during the summer due to rising power consumption [11].

Table 1: Power consumption of Mashhad, Iran, in summer.

Bin	Freq	Cumulative value
40000	6	150%
35000	10	115%
30000	10	90%
25000	10	78%
20000	10	56%
15000	10	23%
10000	10	5%

4. Proposed System

The number of urban populations is expected to increase by 75% by 2050, driving up the cost of thoughtful, sustainable environments that offer residents a high quality of life. The emergence of smart cities is the result of this. A smart city will integrate technology, government, and society in order to improve particular elements, such as smart energy, smart economics, smart transportation, building automation, smart industry, sustainable cities, and representative democracy. The full dataset is first collected, and then, it is further processed using the ANN model shown in Figure 5. The present study estimated the amount of solar radiation coming from all around the globe by using ANN in combination with a technique called linear regression. You may determine whether or not there is a linear connection between the predictor, descriptive, or criteria variable and the response or outcome variable by using the technique of linear regression. The basic nature of linear regression makes it easy to grasp and explain, and it may be regularised to prevent overfitting. In addition, employing stochastic gradient descent to incorporate fresh data into linear models makes it simple to keep these models current. The parameters include location, longitude, elevation, and the day of the week. The duration, average outside temperature, stress at departmental levels, air velocity, and moisture levels. The prediction simply included one production: the expected global weekly sun radiation. Based on the lowest absolute percentage inaccuracy, the shortest RMS, and the highest linear correlation coefficient, the optimal approach and precise ANN model were chosen. Then, the relative error percentage rate for the present job was calculated and contrasted it with other similar mechanisms.

Table 2: Wintertime power use in Mashhad, Iran.

Bin	Freq	Cumulative value
40000	10	120%
35000	15	95%
30000	15	70%
25000	15	58%
20000	15	36%
15000	15	13%
10000	15	2%

Almost no studies have been done on the application of an energy production gathering system that focuses on the ANN-based linear regression model that captures economic circumstances, according to a complete assessment and critical evaluation of the studies that have been gathered. Given this gap in the state of the art, the following are the main goals of the current research, and Figure 6 illustrates the suggested system's flowchart. Data mining is used to identify patterns in the electrical energy use at homes in Mashhad, Iran. The construction of a drive mechanism for TP power generation in a contemporary metropolis, the modelling of a solar energy installation in the recipient's residence, and the use of scenario wizard were computed to assess the vulnerability of future outcomes.

4.1. Photovoltaic Simulations. The power generation was used to simulate photovoltaic platforms in residential energy consumptions, and the input data for the calculations described in overall results of experiments are shown. Modelling has been done using the meteorological data from Mashhad, Iran's mean irradiance. This image specifically depicts the irradiance that the panels received throughout the course of a day. The irradiation was evidently received from 8 AM to 6 PM, with the highest irradiation in Iran City happening at 12 PM. the possibility of obtaining sunshine from various horizons in Mashhad, Iran. According to the analysis's findings, between 11 AM and 12 PM, the 0° horizon receives the most sunshine on average. Furthermore, Mashhad, Iran's regular home use and its pattern of electricity usage. Particularly, current intensities and voltages that are approximately 10 A and 50 V have been used to achieve usage patterns for lamps, TVs, laptops, digital phone, and household solar panels. Whenever the output was larger than 2 kilowatt, it was demonstrated that the inverter's maximum effectiveness was almost 100%. To put it another way, as soon as the power hits 2 kilowatt, the efficiency of converting radiation to electrical signal begins to rise. The calculations for the electricity production in Mashhad, Iran, are finally displayed using the research approach based on the integration of ANN, photovoltaics, and regression analysis.

4.2. Implementation of ANN Using Linear Regression. The ANN model's construction is essential for determining the amount of solar radiation on a global scale because there is no radiation from the sun factors impacting in situ. This ANN model will enable the successful utilisation of a considerable amount of available ecological renewable power for a wide range of real applications. The ANN structure is composed on three tiers. Typically, there are 3 parts: one or more unseen units, an output neurons, and an input layer that accepts data from gathering sources that are beneficial for establishing connections between the receiver and transmitter layers via processed unit neurons. A design of a machine learning algorithm can calculate the value of a result after being trained on a given set of inputs. A feed-forward network ANN model with 3 layers with a quadratic output layer activation function and a tangent sigmoid hidden state activation function was built in MATLAB version 2018 for the current analysis. Out from the following nine factors, location, elevation, period, season, average atmospheric air temperature, mean station level pressure, mean wind velocity, and mean humidity levels, one, monthly average global solar irradiance, was predicted as an output. This provides a list of the training settings with each of the four methods used in the current study [19].

The disruptive innovation theory can be used to explain the developing technologies that are characterised by growing AI incorporation as new market leaders in the real estate sector. When faced with various kinds of technical and market change, dominant players' actions are elucidated by disrupting improvement as a management theory. A type of mathematical model known as an artificial neural network (ANN) mimics the function of a biological neuron. This technique for nonlinear modelling is effective. Multilayer perceptron (MLP), a neural network with a fully connected topology, is an early ANN architecture. In essence, MLP has a strong track record and is frequently used. Many brand-new ANN architectures are currently being developed. The primary architectural types used in this paper are ANNs with linear regression methods. Animal neurons' functionality serves as a model for artificial neural networks (ANN). A neuron is a type of processing unit that performs activation as well as output and input. Although there are other ANN versions, we employed the straightforward feed-forward neural network with back-propagation for this work. The ANN receives the weather characteristics as inputs and predicts the solar power as the output shown in Figure 7.

Regression, curve fitting, and prediction are just a few of the many tasks that artificial neural networks (ANNs) can perform. In this study, models for forecasting solar radiation are developed using artificial neural networks. A machine learning program's basic building element, the neurons, creates the response via a frequency response. Each input is multiplied by a weight, which serves as a link between the intake and the neuron and among the various layers of neurons. In the final stage, the neuron employs a frequency response to obtain the result. The benefit of ANN approaches is that they offer a concise solution for multivariable problems while requiring less computer work and no prior knowledge of mathematical calculations between the parameters.

4.3. Linear Regression. Linear regression is the most fundamental and well-liked regression approach (LR). The link

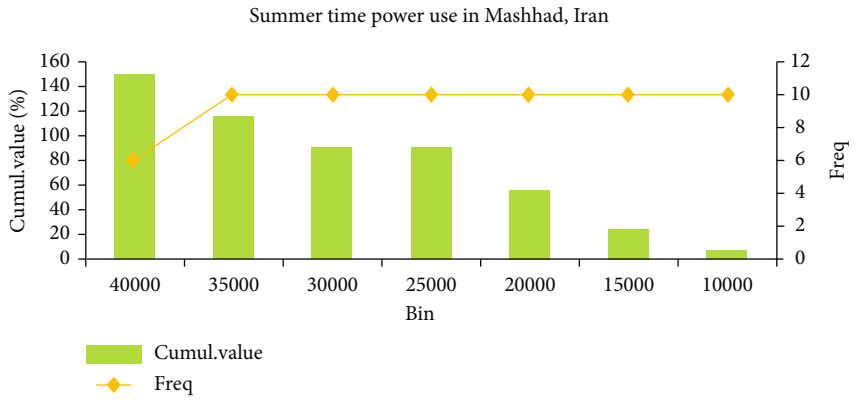

Figure 3: Summertime Mashhad city power consumption histogram.

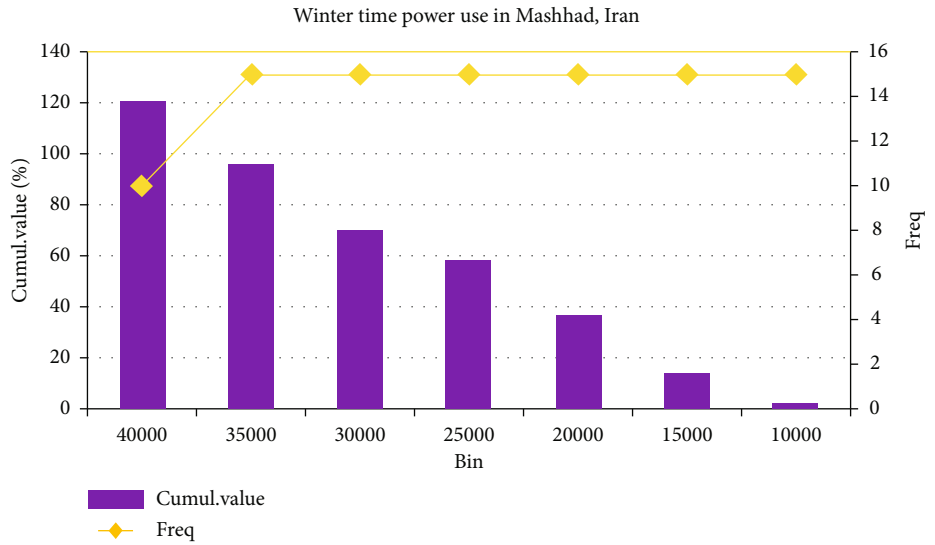

Figure 4: Wintertime Mashhad city power consumption histogram.

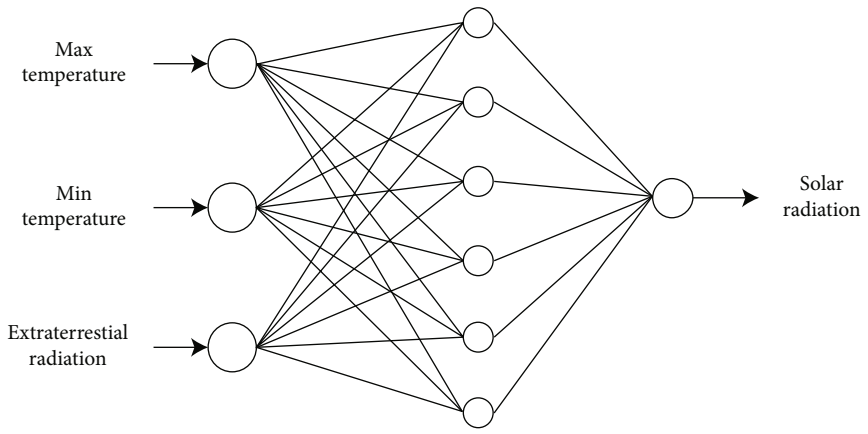

Figure 5: Diagrammatic representation of the ANN model used in this work.

between the dependent and independent variables is represented using future direction, and the unknown model parameters are estimated from the data using the statistical method. To estimate the parameter values, one can either solve a set of linear equations or utilise an iterative technique like linear regression. Regression analysis can be performed using a variety of techniques and algorithms, and applications can be made using specialised software like SPSS, SAS, SIMCA, STATISTICA, STATGRAPHICS, and NCSS. The least squares method is the most popular regression

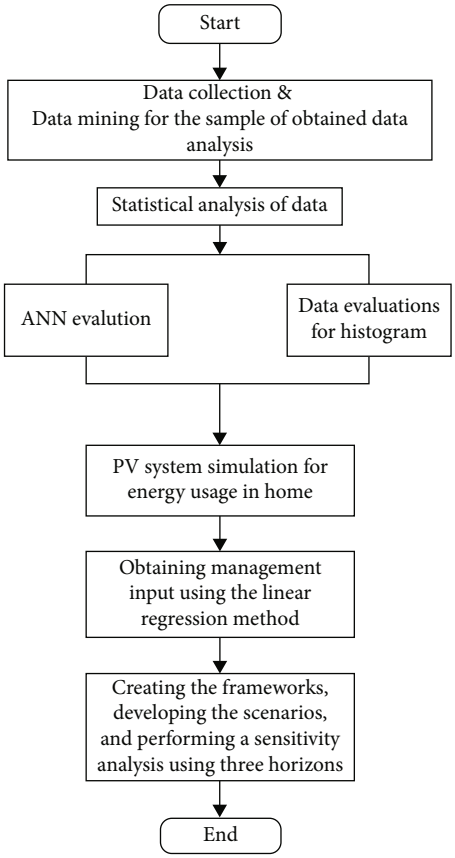

Figure 6: Flow chart of the proposed work.

analysis technique in building energy assessments. Linear regression can be used to identify a proper relationship (model or equation) between the forecast, descriptive, or target variable and the response or outcome variable. Regression analysis using only one dependent variables is known as univariate regression, and regression model using two or more response variables is known as multiple regressions.

For complicated systems like the power use of buildings, linear regression should indeed be viewed as an iterative process in which the outcomes are used to analyze, evaluate, criticise, and perhaps alter the inputs. The multivariate linear regression analysis tries to describe the relation among variables by fitting a linear expression to the dataset. When there are multiple predictor variables, the linear fitting is done while keeping all but one fixed. The presence of a link between a dependent variables and a regression coefficient does not suggest that the predictor variable is the cause of the response variable; rather, it just indicates that the two parameters have a high correlation. For instance, the temperature difference and the heat capacity of the walls both affect the heat flux through the walls, which is what causes the heat flow. In other words, the heat flux is not caused by the thermal conductivity of the walls, although it is strongly correlated with their heat capacity. Using simple linear regression as one of the regression analysis strategies depends on how complex the relationship between the variables is. The approaches for regression analysis are discussed in this section based on the classification in Table 3, which also includes a list of the equations relevant to the approach.

The inaccuracy to account for the discrepancy between the simulated values from Equation (1) and the identified data is represented by the equation of the linear regression form, in which Y is the primary predictor, X is the dependent variables, and α_0 and α_1 are the coefficient vectors or regression variables. In the estimated value form of Equation (1), X is the fitted or predicted value, and estimations of the coefficient of determination are provided. Estimated parameters can be determined for any collection of regression coefficient values that deviate from the observed data, which makes them different from regression coefficients in Equation (2).

$$X = \alpha_0 + \alpha_1 Y + \mathscr{E}, \tag{1}$$

$$\widehat{X} = \widehat{\alpha}_0 + \widehat{\alpha}_1. \tag{2}$$

The instance in which the variables utilised for the regression model correlate to one of the data instances of the actual observations used to identify is referred to as the fitted value.

To forecast solar intensity, first use a linear regression technique. Linear regression is a simple and popular technique for establishing the link between a reliant or responding variable, such as solar activity, and a collection of explanatory variables or forecasters. The regression attempts to minimise the sum of squared error variances between the observed solar radiation and the anticipated solar irradiance by applying a linear function of the prevailing climate metrics. To verify the precision of the forecasts in Table 3, utilise the experimental database for the remaining period of every year. Pay attention to the sun's cross identification root mean square and forecast frequency, which are 150 and 170 kilowatt hours, correspondingly. Figure 8 image illustrates how closely the model matches the projected solar intensity, albeit with minor deviations [20].

5. Results and Discussion

As per prosecution's findings, the annual energy use during the summertime is 1.32 higher than it is during the wintertime. The annual power usage in the summertime is between 25,000 and 30,000 $\mathrm{kW\,h^{-1}}$, according to histograms. All enhance the overall and scenario creation in the current study which are assessed in respect to the set restrictions (25,000–30,000 kWh). Throughout this research, Mashhad city's power consumption was projected using artificial neural network (ANN) time series that could be used to govern smart city initiatives. When compared to other classification and machine learning techniques from the viewpoints of data input and database design, the justification for choosing ANN for this inquiry is related to the versatility of this methodology for estimate of parametric variations over various timescales. In addition, the ANN system showed considerable accuracy for forecasting future energy demand in cities based on past research initiatives. By applying the ANN system for electrical energy data mining, the following objectives are attained:

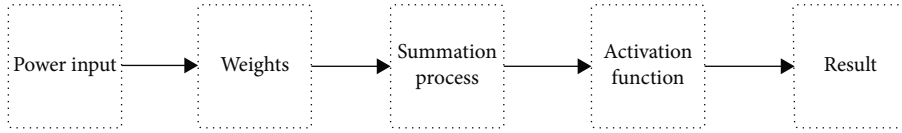

Figure 7: Architecture of ANN.

Table 3: Solar power intensity prediction using linear regression.

Observed	Linear regression
159	255
143	175
132	265
167	245
243	267
324	346
388	432
455	487
576	584
654	785

(i) Energy consumption forecasts for monitoring all Mashhad city electricity installations, including solar, methane, and hydropower ones, during peak demand and busy periods

(ii) On the basis of the predicted energy demand and the forces created by Mashhad's power plants, the energy crisis warning system was activated

(iii) Establishing a pattern for power utilisation and regulating it based on changes in the demand for electrical energy over time while also spotting abnormalities

The power consumption in each anticipated time step can also be linked to a summary of further data regarding the ANN time series characterizations for the machine learning procedure. A multilayer perceptron ANN, an intake ANN, was used to estimate the energy consumption in Mashhad city. The inputs were time-based factors, and the output took the city network's energy demand into account. There was an output layer, a hidden layer with two delays, and ten hidden neurons. An average of 70% of the data were used to train the model, 15% of the data were used to validate it, and 15% of the data were used to test it. It displays the results of calculating energy consumption during the summertime and wintertime, accordingly. The time period during which the full dataset is only once carried forward and reversed through the neural network, taking into account the fact that the created model seeks out the greatest match during the learning process, is referred to as an "epoch." The gradient descent method also necessitates that the model repeatedly pass the original dataset through this kind of neural network. This process is iterative; thus, numerous epochs can be observed. The 11th epoch in this inquiry is when the observed and predicted data are most closely matched. This shows that the eleventh epoch produces the lowest squared error (with a 99 percent accuracy).

The ANN forecasting model has the accurateness needed for the forecast of power requirement, according to the results. The created platform can be helpful for time-sensitive motivational activities and megacity management techniques. It is possible to construct motivating methods for solar energy use by utilising ANN time series prediction. It is possible to plan and evaluate energy use. Third, when approaching high periods of energy use, a set of predetermined motivational approaches may be assigned to each period. Households in Mashhad city use an average of 8.2 kW and 11.5 kW of electrical energy per day in the winter and summer, respectively, according to data obtained from the DEEC. Additionally, based on the information that is currently available, residences in Mashhad cities with renewable energy potential are anticipated to be about 90 square metres in size on average. The photovoltaic system model was used in the research to calculate the solar energy potential for 90 m^2. The flowchart shows the annual gains and losses in energy. This picture clearly shows how 21,195 kilowatt hours of renewable radiation are lost annually in a typical residential location. It is important to keep in mind that the dielectric breakdown cabling loss, which is associated with the resistance in the wires, lowers the system's efficiency. In contrast, the light-induced degradation is a capability loss that occurs within a few hours of being exposed to the sun and results in a decrease in performance. Power is lost as heat in the paper insulation of a cable when an electric field is created by the leakage current and the polarity reversal of current in an alternating current supply. This loss becomes more significant as the temperature rises. It has a direct impact on the way a cable functions in the system. Furthermore, it is clear from the simulation findings that the solar energy output is higher in the summer and spring than it is in the winter and fall. The DEEC may find that the study's findings are helpful in lowering peak energy demand given that May, June, July, August, and September frequently have the maximum solar energy potential. It is hard for the expected energy to completely meet the network's needs because solar energy production varies substantially from month to month.

When a PV system is installed in the yard or on the roof of a private residence, peak usage can still be controlled. The solar energy from the collection plane's global irradiation incident has accumulated on the panels. Global irradiation incidence is the term used to describe the solar panels' theoretical ability to absorb sun energy. The incentive algorithm for persuading people to generate solar power during peak hours was created as part of this study by speaking with 40 energy industry professionals. To establish the approach, energy sector experts took part in three sessions that

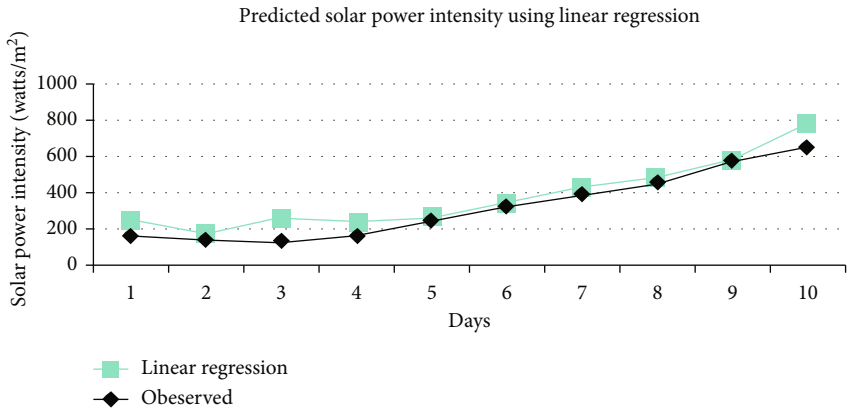

Figure 8: Solar power intensity prediction using linear regression.

Table 4: Solar power availability in Mashhad city.

Months	Temperature (degree Celsius)	Solar irradiation (kWh)
1	2	5540
2	6	9987
3	10	11345
4	16	16780
5	20	19657
6	24	23478
7	28	24456
8	26	21345
9	18	19880
10	14	14231
11	12	8764
12	8	5321

followed one another. Table 4 displays the results of their combined knowledge. At three meetings separated by a month, the announced committee assessed the agreement of the presented recommendations. Additionally, the permitted techniques were established through the linear revision process for the review and involvement of governmental authorities. The outcomes of each round and the TP items being authorized using the LR approach. It is crucial to remember that each approach was developed over the course of three time periods using the 3H technique (short-term, mid-term, and long-term). All approaches for the short (1H) time were built with financial incentives in mind based on the findings. Based on PV system and PV sol-online simulations, Figures 9 and 10 compare the amount of solar energy available and the amount of energy consumed in Mashhad city. The results show that, depending on the time period, Mashhad city's solar energy availability outstrips energy usage by a ratio of 10 or more.

However, the energy demand problem happens every year in several Iranian megacities, particularly Mashhad city, as a result of factors like the availability of water, the number of tourists, and the supply of gas for power plants. Additionally, with the use of particular motivating tactics as a TP in conjunction with optimised domestic energy efficiency, captured power can also be utilised for a variety of urban facilities in modern cities. Based on the findings of this investigation, some novel tendencies as well as some shared directions with prior studies may be seen. An innovative energy design, for instance, was provided to optimise energy use in smart cities. When solar cells and a triboelectric nanogenerator were used in tandem, power production performance improved from 9 megawatt to 28 megawatt per 130 millimetre to 24 millimetre solar panel area on a building's roof. While in the current study, the maximum power consumption in smart cities can be minimised by simply applying solar energy to home roofs and should be accomplished via TP. Furthermore, by implementing motivational citizenship programmes, energy consumption peaks can be managed. Some managers turn to technological solutions, while others place their faith on socioeconomic elements. Recent studies have shown that the second set of options could have more effectiveness in urban management. Various green power generation methods, including independent sustainable microgrids with rooftop solar arrays, micro-hydro turbines, biofuel central heating, aqua-electrolyzers, and power storage, were studied in a separate experiment. The salp swarm algorithm is the foundation of the controlling panel the authors supplied for energy management in urban centres. When electricity is not available, it can be provided by combining CHP with microgrid. On the other hand, by using ANN models to anticipate energy consumption and making modifications to citizen incentive programmes, the existing efforts could even be able to avert the shortage of energy that is now being experienced. The group developed a deep learning model based on LSTM in order to forecast the amount of electricity that would be generated by photovoltaic cells (long short-term memory recurrent neural network). Both the mean absolute error and the mean squared error of the predicted values have decreased as a result of the enhanced long-term memory network's implementation. This approach has the ability to produce short-term predictions of PV power and has the potential to lessen the influence that noise has on predictions of PV power. In this study, ANN computations allowed for the precise prediction of energy use. Additionally, compared to previous methodologies, which usually need time-consuming calculations, the proposed methodology could dramatically slow down computations [10].

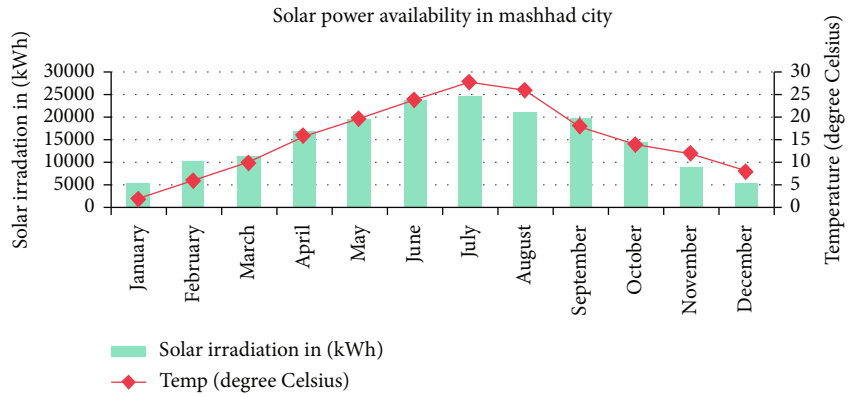

Figure 9: Solar power availability in Mashhad city.

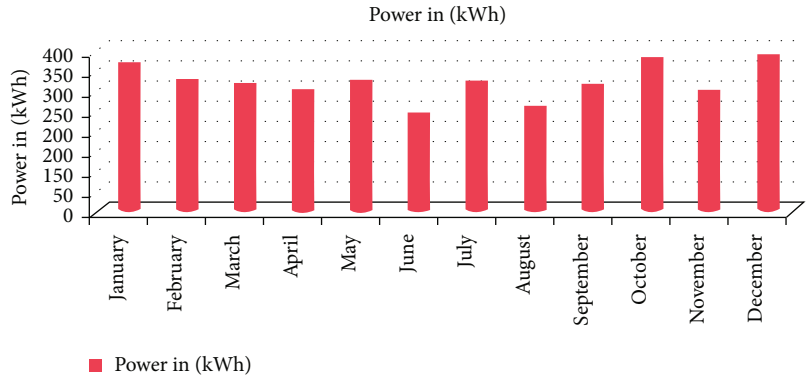

Figure 10: Power utilisation and the mean temperature in Mashhad city is 15.6 degrees Celsius, and the average size of a home is 100 square metres.

6. Conclusion

Energy recovery in metropolises is thought to be a critical concern, especially in developing countries. The amount of renewable energy could fill energy gaps and aid energy systems in managing maximum output in warm locations. Additionally, by using innovative urban organisations and solar energy collection, certain dangers can be transformed into possibilities. In the current work, linear regression was created as a smart system for anticipating energy demand, and machine learning and statistical models were utilised to evaluate Mashhad, Iran's usage of renewable energy. The PV system model was then employed for the research study of Mashhad, Iran, to replicate the distributed solar capacity and demonstrate its role in controlling power consumption requirements. Several implementation solutions for transformative participation (TP) in smart cities were proposed as a result of this study. The findings of this study demonstrated that neural network soft computing could properly predict more than 99 percent of the amount of electricity required to build the continuous surveillance system. The future of Iran's Mashhad city prospective for renewable energy then showed that solar radiations might be used to manage maximum power generation. The proposed model was linked to a photovoltaic system in order to use energy from the sun to fulfil the required energy. The created model also directly combined ANN and photovoltaic simulation, the former of which was used to supply solar resources and the former of which was used to determine electric power levels. The incentive algorithm for persuading people to generate solar power during peak hours was created as phase of this research by speaking with 45 experts in the energy fields. The specialists in the energy sector participated in three meetings that followed each other to design the plan. The approved strategies were created using the linear regression method for the government's review and input. Three temporal horizons were used for the creation of each approach and the LR evaluation. By accurately forecasting daily solar output using these diverse patterns, solar power firms may quickly make up for production deficits and avoid the expensive last-minute purchase of power from the market. This illustrates how machine learning regression approaches, in particular neural networks, can accurately and dependably estimate the average daily solar power. To boost the accuracy of such predictions, it is suggested and established that sun angles (azimuth and zenith) as well as weather and season-specific features be used. It was discovered that all tactics were created with financial incentives

in mind for the short-term timeframes. For the mid-term phases, the amount of cost factors was dropped. Over time, these solutions also started to apply to choices for citizenship and growth. It is hoped that these findings will benefit the concerned parties and ease energy management in smart cities. Due to the increasing need for power generation and the depletion of nonrenewable, renewable technologies have attracted the attention of individuals all over the globe. Therefore, thorough research should be done on various energy sources. According to the findings of this study, additional research is needed on some other alternative energy sources like wind energy, biogas, and incinerations. To build an integrated energy resource management framework that may help in accomplishing the aims of smart cities, all these approaches and factors need to be assessed and carefully examined. Considering that new forecasting technologies and machine learning methods are viable options for conducting additional study on achieving the goals of smart cities and can be used for efficient power management as a part of future studies is pointless.

Data Availability

The data used to support the findings of this study are included within the article. Further data or information is available from the corresponding author upon request.

Conflicts of Interest

The authors declare that there is no conflict of interest regarding the publication of this article.

Acknowledgments

The authors appreciate the supports from the Arba Minch University, Ethiopia, for providing help during the research and preparation of the manuscript.

References

[1] M. H. Maruf, M. A. u. Haq, S. K. Dey, A. Al Mansur, and A. S. M. Shihavuddin, "Adaptation for sustainable implementation of smart grid in developing countries like Bangladesh," *Energy Reports*, vol. 6, pp. 2520–2530, 2020.

[2] C.-J. Huang and P.-H. Kuo, "A deep CNN-LSTM model for particulate matter (PM2.5) forecasting in smart cities," *Sensors*, vol. 18, no. 7, article 2220, 2018.

[3] M. AlKandari and I. Ahmad, "Solar power generation forecasting using ensemble approach based on deep learning and statistical methods," *Applied Computing and Informatics*, vol. 2020, 2020.

[4] A. B. Kanase-Patil, A. P. Kaldate, S. D. Lokhande, H. Panchal, M. Suresh, and V. Priya, "A review of artificial intelligence-based optimization techniques for the sizing of integrated renewable energy systems in smart cities," *Environmental Technology Reviews*, vol. 9, no. 1, pp. 111–136, 2020.

[5] A. H. Elsheikh, S. W. Sharshir, M. Abd Elaziz, A. E. Kabeel, W. Guilan, and Z. Haiou, "Modeling of solar energy systems using artificial neural network: a comprehensive review," *Solar Energy*, vol. 180, pp. 622–639, 2019.

[6] S. Sahoo et al., "Artificial deep neural network in hybrid PV system forcontrolling the power management," *International Journal of Photoenergy*, vol. 2022, Article ID 9353470, 12 pages, 2022.

[7] S.-G. Kim, J.-Y. Jung, and M. Sim, "A two-step approach to solar power generation prediction based on weather data using machine learning," *Sustainability*, vol. 11, no. 5, p. 1501, 2019.

[8] T. M. Amirthalakshmi, S. Ramesh, R. T. Prabu et al., "A novel approach in hybrid energy storage system for maximizing solar PV energy penetration in microgrid," *International Journal of Photoenergy*, vol. 2022, Article ID 3559837, 7 pages, 2022.

[9] M. Azimi Nasab, M. Zand, M. Eskandari, P. Sanjeevikumar, and P. Siano, "Optimal planning of electrical appliance of residential units in a smart home network using cloud services," *Smart Cities*, vol. 4, no. 3, pp. 1173–1195, 2021.

[10] S. Maier, "Smart energy systems for smart city districts: case study Reininghaus District," *Energy, Sustainability and Society*, vol. 6, no. 1, p. 23, 2016.

[11] G. Ramkumar, S. Sahoo, T. M. Amirthalakshmi et al., "A short-term solar photovoltaic power optimized prediction interval model based on FOS-ELM algorithm," *International Journal of Photoenergy*, vol. 2021, Article ID 3981456, 12 pages, 2021.

[12] K. Mahmud, S. Azam, A. Karim, S. Zobaed, B. Shanmugam, and D. Mathur, "Machine learning based PV power generation forecasting in Alice Springs," *IEEE Access*, vol. 9, pp. 46117–46128, 2021.

[13] U. Munawar and Z. Wang, "A framework of using machine learning approaches for short-term solar power forecasting," *Journal of Electrical Engineering and Technology*, vol. 15, no. 2, pp. 561–569, 2020.

[14] A. Gellert, A. Florea, U. Fiore, F. Palmieri, and P. Zanetti, "A study on forecasting electricity production and consumption in smart cities and factories," *International Journal of Information Management*, vol. 49, pp. 546–556, 2019.

[15] A. C. Serban and M. D. Lytras, "Artificial intelligence for smart renewable energy sector in Europe—smart energy infrastructures for next generation smart cities," *IEEE Access*, vol. 8, pp. 77364–77377, 2020.

[16] D. Van Tai, "Solar photovoltaic power output forecasting using machine learning technique," *Journal of Physics Conference Series*, vol. 1327, no. 1, article 012051, 2019.

[17] S.-M. Jung, S. Park, S.-W. Jung, and E. Hwang, "Monthly electric load forecasting using transfer learning for smart cities," *Sustainability*, vol. 12, no. 16, p. 6364, 2020.

[18] N. Premalatha and A. Valan Arasu, "Prediction of solar radiation for solar systems by using ANN models with different back propagation algorithms," *Journal of Applied Research and Technology*, vol. 14, no. 3, pp. 206–214, 2016.

[19] N. Sharma, P. Sharma, D. Irwin, and P. Shenoy, "Predicting solar generation from weather forecasts using machine learning," in *2011 IEEE International Conference on Smart Grid Communications (SmartGridComm)*, pp. 528–533, Brussels, Belgium, Oct. 2011.

[20] C. Zurbrügg, S. Drescher, I. Rytz, A. H. M. M. Sinha, and I. Enayetullah, "Decentralised composting in Bangladesh, a win-win situation for all stakeholders," *Resources, Conservation and Recycling*, vol. 43, no. 3, pp. 281–292, 2005.

Hindawi
International Journal of Photoenergy
Volume 2022, Article ID 1048378, 8 pages
https://doi.org/10.1155/2022/1048378

Research Article

Deep Learning for an Innovative Photo Energy Model to Estimate the Energy Distribution in Smart Apartments

Komala C R,[1] S. Vimal,[2] G. Ravindra,[3] P. Hariramakrishnan,[4] Shaik Razia,[5] S. Geerthik,[6] K. Raja,[7] V. Mohanavel,[8,9] and Nedumaran Arappali[10]

[1]*Information Science and Engineering Department, HKBK College of Engineering, Bengaluru, Karnataka 560045, India*
[2]*Department of Computational Intelligence, School of Computing, SRM Institute of Science and Technology, Kattankulathur 603203, Tamilnadu, India*
[3]*Department of Electrical and Electronics Engineering, Sree Vidyanikethan Engineering College, Tirupati 517102, Andhra Pradesh, India*
[4]*Department of Electrical and Electronics Engineering, Panimalar Engineering College, Chennai 600123, Tamilnadu, India*
[5]*Department of Computer Science and Engineering, Koneru Lakshmaiah Education Foundation, Vaddeswaram, 522302, Andhra Pradesh, India*
[6]*Department of Information Technology, Agni College of Technology, Chennai, Tamilnadu, India*
[7]*Department of Mechanical Engineering, University College of Engineering Dindigul, Dindigul, 624622 Tamil Nadu, India*
[8]*Centre for Materials Engineering and Regenerative Medicine, Bharath Institute of Higher Education and Research, Chennai, 600073 Tamilnadu, India*
[9]*Department of Mechanical Engineering, School of Technology, Glocal University, Delhi-Yamunotri Marg, Uttar Pradesh, 247121, India*
[10]*School of Electrical and Computer Engineering, Kombolcha Institute of Technology, Wollo University, Ethiopia*

Correspondence should be addressed to Nedumaran Arappali; nedu.maran@kiot.edu.et

Received 27 July 2022; Revised 28 August 2022; Accepted 1 September 2022; Published 29 September 2022

Academic Editor: BR Ramesh Bapu

The outer surface of the building is the same size as its premises, with greater heat loss. Therefore, when building, renovating, or expanding apartment, if possible, avoid all kinds of spaces, ledges, and lodges in the walls. It makes sense to build unheated exterior buildings on the north side of the apartment. The storage rooms for garden tools and bicycles, technical buildings protect the warm part of the house from wind and cold. In the most common design of a private apartment, the energy consumption for heating is 110-130 kW per 1 m^2 per year. In this paper, an energy distribution model was proposed to estimate the photo energy with the help of deep learning model. A small apartment not only uses less energy but also requires lower construction costs. An energy-efficient apartment is a building with a low-energy consumption and comfortable microclimate. Energy savings in such homes can be up to 90%. Annual heat demand can be less than 15 kWh per square meter of energy-efficient home.

1. Introduction

In the context of strict energy consumption standards, heating systems for homes that meet new requirements play an important role in their storage [1]. For example, significant energy savings can be achieved by using self-regulating low-pressure systems that respond quickly to changes in room temperature [2]. When the rooms are heated by sunlight passing through the windows, the corresponding sensors can send a signal to the measurement valves. Accordingly, the boiler will work for less time, and gas consumption will be reduced [3]. In this case, a good service plate when heating your home can be provided by heating batteries and convectors with low recession. Heating with

floor heating and a tiled stove cannot operate quickly due to the large hot mass [4–7]. The availability of fuels including petroleum and coal is decreasing. Also, their use increases global warming and affects the environment. Therefore, renewable energy sources such as wind turbines and solar panels will meet the energy demand in the future. In this context, promotion of solar power generation can be a visionary and permanent solution. The use of coal and petroleum products continues to increase due to the industrial revolution and the proliferation of vehicles. The boiler must use efficient energy and comply with nonemissive standards of harmful substances in the atmosphere [8]. Nowadays, these requirements are met by condensing boilers running on liquid fuel or gas, as well as very efficient gas steam boilers [9]. Own home question arises to reduce power consumption if needed [10–12].

(i) The zero or very low typical energy consumption was achieved up to 10% [13]

(ii) Insulation should be at least 25-30 cm in one layer walls and 50 cm in attic bases

(iii) With a powerful, at least 40 cm insulation layer, all systems that use and recycle thermal energy are fitted so that it has almost no external energy losses

First, the thermal insulation of all elements of the house must be improved. Heating a well-insulated house requires a more compact and less powerful heating system, but is well-regulated as shown in Figure 1. It uses the energy of the sun, with windows facing south. In the energy supply, in addition to the phase energy, one or more alternating currents (wind generators and solar panels) are among the mandatory properties, such as a heat collector, daily energy saving device, recuperate for incoming air heating or cooling, and the use of ice to preheat the ventilated air in winter [14–18]. In summer, the same outside air on the floor is precooled with positive electrical balance. With a powerful, at least 40-cm insulation layer, all systems that use and recycle thermal energy are fitted so that it has almost no external energy losses [19]. Many sources of renewable alternative energy are fitted. Excess electricity can be sold to support outdoor buildings or to the public grid [20]. The technical specifications are passive and similar to that of an intelligent home. Energy derived from the grid, but mainly from its own sources, is used wisely, with the help of intelligent control [21]. The heating system provides seasonal energy storage, which heats the house during the hot season without the use of external energy resources [22]. Capacity is an economic concept with a certain set of minimum costs. Choose special care, high-quality, and durable insulation for the home. Insulation layer of walls and roofs of houses with minimum requirements minimum energy starts from 15 to 20 cm [23]. Walls, foundations, insulation materials, heating equipment, and pipes differ in their physical, mechanical, and chemical properties [24]. For example, it is better to insulate foundations with extruded polystyrene foam with high mechanical strength and practically zero hygroscopicity [25]. These insulation defects include high fire risk (toxicity

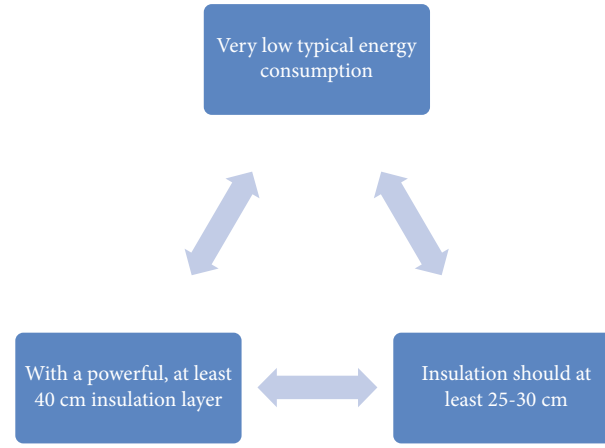

Figure 1: Powerful heating system.

of combustible materials) and sensitivity to ultraviolet light (protection from exposure) [26]. Due to the use of petroleum and coal, the environmental damage is severe. To solve all this, we are forced to use nonconventional and renewable energy. Among these, wind and solar energy play an important role. However, due to difficulties in generating and storing electricity from solar energy, there was initial reluctance to increase their use. However, the current modern technological development helps to remove these obstacles.

Of course, well-thought-out structured thermal insulation, minimal cold bridges, is one of the key components, but only from a distance [27]. A real energy-efficient house starts at the design stage and lays the foundation, which is well-insulated and waterproofed at the initial stage of construction [28]. There are no trivial things in such a house, and every element in the architectural look is thought out, the size of the house, its shape, the number of elongated elements, polishing, and looking at the sun. Roofing and wall insulation Brick, expanded clay concrete, foam concrete, aerated concrete, wood concrete, etc. are "breathable" materials used to construct wooden and stone homes. Due to its microscopic structure and antiseptic properties, it makes corrosion resistant and corrosive structures. Consequently, stone walls started to grow mold. Besides, it is durable, cheap, and fireproof [29]. However, there are many heaters, each of which has its own characteristics and characteristics that, accordingly, should be used for its intended purpose. With excellent thermal insulation and ceiling, the mandatory attributes of an energy-efficient home are a well-thought-out ventilation system (in older homes, it gives up to a third of the energy loss). An energy-efficient house, by definition, cannot heat the street rejected by hot air vents. The counter will solve the problem of heating the new incoming air through the counter-flow removed from the chamber [30]. A simple heat exchanger will solve the problem of preheating the incoming water using waste heat. To heat an energy-efficient house, it is necessary to use the energy of the sun, for which the building faces most of the windows to the south. Glass with two, three chambers glazed, glass with special film coating that transmits sunlight spectrum and reflects infrared radiation [31]. Heating is one of the most important components of an energy-efficient

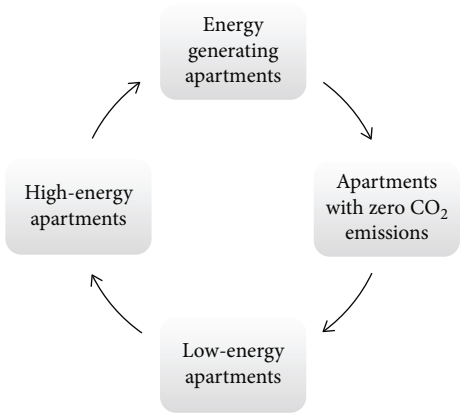

Figure 2: Different types of apartments.

home. It can be a core gas, electric, use the energy of the earth, wind, or sun, but it is also associated with an energy-saving device to remove peak loads. For example, there is a night charge for electricity with significant discounts in the area, and the basis for heating may be an electric boiler, with a tank of several tons of water. Heated water at night will cope with heating the house during the day. An alternative to water energy storage is in concrete screed floor which is huge. This will retain enough energy to keep the room at a comfortable daytime temperature.

2. Literature Review

One of the most important factors affecting the consumption of energy resources of the house is its location relative to the cardinal points. Most home windows should face south. At the same time, a deflection of up to 30 south of the azimuth slightly reduces the use of solar energy [1]. If the house is located differently, the walls and roof of the building should be more effectively insulated to compensate for the lack of heat entering the room from sunlight. About 90% of the light energy penetrates through the glass of the windows and heats the room [2]. Modern double-glazed windows are made with special coatings and inert gas filling. The coatings reflect the long wave infrared rays back into the room from the room, minimizing their loss through the windows [3]. Because of the large windows, the house will be much warmer in summer. This problem is solved by using another special glass coating, as well as automatic darkening systems, roof eves, and balconies [4]. They only allow direct sunlight to pass through the windows when the sun is low in winter. In summer, the windows on the sunny side of the house are shaded by trees. In winter, sunlight penetrates the house easily between the bare branches [5]. The use of nonconventional energy has become the imperative of the times. In particular, it is necessary to make full use of solar energy. As countries including India get more than 300 days of sunlight in a year, its use should be increased. This energy is not available at night, when it rains. Therefore, it is important to stock up when available. Current technology has solved these problems. Many countries have installed large-scale solar panels at sea to generate electricity from sunlight. The more solar thermal equipment is used, the lower the cost. Also, imports of petroleum crude oil can be drastically reduced. Similarly, the use of firewood and coal can be reduced and the forest can also be protected.

Most of the heat escapes from the house through its exterior tile. The greater the difference between indoor and outdoor temperatures creates the greater the heat loss. The amount of thermal insulation of a house is determined by the coefficients of resistance to heat transfer of its covering structures (floor, walls, windows, and roof). The higher it is, the better the insulation quality [6]. No creative and high-tech tricks will create comfort for residents without the equipment to regulate the energy processes in the home according to the given instructions. At night, for example, the temperature in the home should be lowered and ventilation reduced to create a more comfortable feeling [7]. A good trick to saving energy is to use both temperature regimes at home reduced to normal and minimum safe level. For the period when there are no tenants in the house, it is better to reduce the ventilation. Smart appliances can rationally regulate the operation of home appliances, controlling and minimizing energy consumption to a minimum [8]. Building an energy-efficient home will increase its cost by 7-15%, but even with less electricity, the reduced energy consumption will be up to 50%, which will provide many times more savings during operation. Good luck with your tireless struggle for energy efficiency at home, i.e., comfort and convenience in it [9]. Industrial establishments were provided with facilities to generate and use solar power during the day and use distributed power at night. Solar power generation is permitted only in factories having a capacity of approximately 3,000 and 4,000 KW and having a separate power feeder. Due to this, a large number of factories are unable to generate solar power. Companies that were producing 300, 400, and 500 kilowatts of solar power had to stop producing solar power [10].

3. Proposed Model

A "passive" house is a house with excellent thermal insulation, minimal electricity, and thermal energy. It mainly maintains a comfortable microclimate with human heat, solar energy, and household appliances such as kettles and stoves. Passive home technologies (buildings with very low-energy consumption and no traditional heating system) are efficient and have already been tried and tested in harsh climates. There are practically no heat losses in such homes shown in Figure 2.

3.1. Low-Energy Apartments. Uses at least 50% less energy than standard buildings built to current energy standards. Generally, when electricity is carried through wires, about 20 percent is wasted. This is why the electricity board gets high compensation. Only 5 percent of global electricity is compensated. By reducing the wastage of electricity through modern technological methods, the losses can be recovered. In this way, thousands of crores of rupees can be saved. Also, the manpower capacity of the power board should be increased. The workforce needs to be upgraded to fully handle modern technologies.

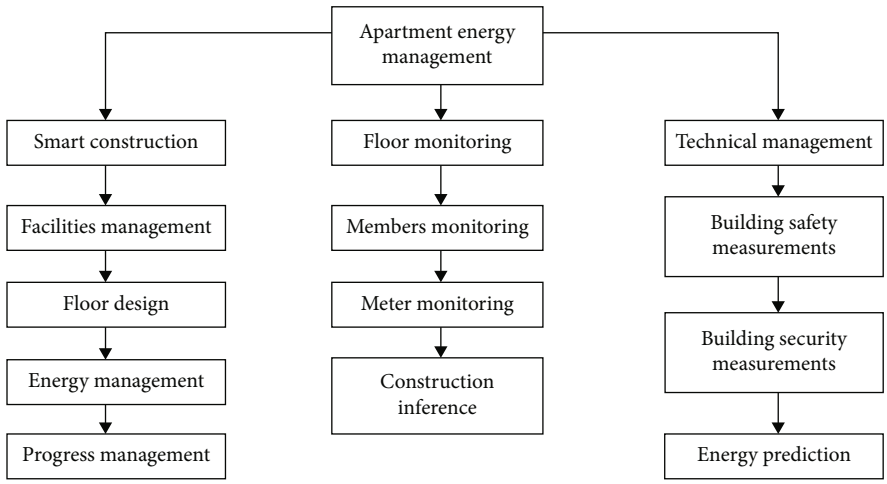

Figure 3: Apartment energy management.

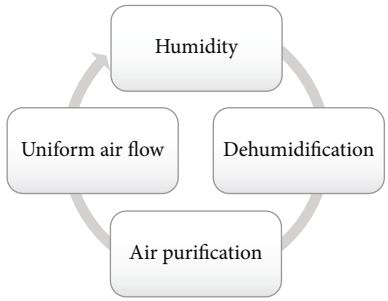

Figure 4: Construction of energy-efficient apartment.

3.2. High-Energy Apartments. They are 70-90% less energy consuming than ordinary buildings of ultra-low-energy homes with clearly defined requirements. The pioneer in the construction of such houses was the dormant house (dormant house), which is generally accepted as a "dormant" building if it meets the requirements created for dormant buildings.

3.3. Energy-Generating Apartments. These are buildings that generate electricity for their own needs. In some cases, the surplus energy can be sold to an energy company in the summer and repurchased in the winter. Good thermal insulation, innovative design, and use of renewable energy sources (solar panels and floor heat pumps) make these homes pioneers of modern home construction. The power can be obtained directly from the sun. But it can get little power when it is surrounded by rain. Solar energy is used all over the world. Also, the use of solar energy to generate electricity or heat and convert seawater into fresh water is becoming increasingly popular.

3.4. Apartments with Zero CO_2 Emissions. This house does not emit CO_2. This means self-sufficient energy from home renewable sources, including space heating/cooling, hot water supply, ventilation, lighting, cooking, and electrical appliances.

The apartment energy management system is demonstrated in Figure 3. Initially the smart construction plans are listened and prepared as per the specifications. Then, the facilities are listed, and the list of services is demonstrated. Then, the floor design and energy management equipments are mounted as the construction plan was proposed by the specified supervisor. Now, it is the time to list the energy equipments of the apartment. The energy equipments are listed, and the suitable devices are mounted in the floor. These mounted equipments are started progression. This progress management was very efficient. The interior is the only part of the sun that generates significant amounts of heat through fusion. In fact, 99% of the energy produced by the sun takes place within 24% of the sun's radius. By 30% radius, fusion has almost completely ceased. The remainder of the sun is transferred from the interior through successive layers, eventually reaching the heliosphere and escaping into space as sunlight or particle kinetic energy. The following parameters are important in the construction of energy-efficient apartment, and it is shown in Figure 4.

3.4.1. Humidity. The device can provide optimal performance -50% humidity at a temperature of 22 degrees. The built-in element of the outdoor unit extracts moisture from the air masses and distributes it evenly throughout the room.

3.4.2. Dehumidification. The device removes excess moisture from the room without lowering the temperature, which is especially important in the fall and spring. On hot summer days with high humidity, you can dry and cool the air masses in the room using a slip system. The two-stage of air purifications are in outdoor and indoor units. Installing a phytocatalytic filter allows not only the removal of dust and small insects from the air masses, but also the removal of formaldehyde, viruses, and mold; ensuring uniform air flow, wide-angle dampers can be operated downwards or upwards so that air masses are "spread" around the room. Solar energy is the conversion of sunlight into electricity. Sunlight can be directly converted into electricity using photovoltaic cells or indirectly through fully integrated solar power (ISP). Generally, water is boiled by concentrating

Table 1: Exterior thickness management.

No of inputs	LVRMM	DLCA	ADSM	FPSMM	EDDLM
100	62.95	71.19	83.98	86.23	95.43
200	61.46	69.22	81.56	84.03	93.01
300	59.97	67.25	79.14	81.83	91.02
400	58.48	65.28	76.72	79.63	89.03
500	56.99	63.31	74.3	77.43	87.04
600	55.5	61.34	71.88	75.23	85.05
700	54.01	59.37	69.46	73.03	83.06

Table 2: Noise protection management.

No of inputs	LVRMM	DLCA	ADSM	FPSMM	EDDLM
100	60.66	68.09	81.15	83.23	91.81
200	58.36	66.96	79.55	82.56	91.33
300	56.06	65.83	77.95	81.89	90.85
400	53.76	64.7	76.35	81.22	90.37
500	51.46	63.57	74.75	80.55	89.89
600	49.16	62.44	73.15	79.88	89.41
700	46.86	61.31	71.55	79.21	88.93

Table 3: Climate change management.

No of inputs	LVRMM	DLCA	ADSM	FPSMM	EDDLM
100	57.32	66.51	77.23	81.13	89.90
200	56.68	65.06	75.98	80.04	89.74
300	56.02	64.58	73.25	79.56	87.97
400	55.37	63.45	71.51	78.67	87.27
500	54.72	62.49	69.52	77.89	86.31
600	54.07	61.52	67.53	77.10	85.34
700	53.42	60.56	65.54	76.32	84.38

Table 4: Heat loss and cold bridges management.

No of inputs	LVRMM	DLCA	ADSM	FPSMM	EDDLM
100	52.15	76.65	74.46	82.70	96.13
200	52.26	77.15	74.46	83.79	96.39
300	52.32	77.9	75.29	84.93	96.96
400	52.41	78.48	75.57	86.04	97.32
500	52.50	79.11	75.98	87.15	97.74
600	52.58	79.73	76.40	88.27	98.15
700	52.67	80.36	76.81	89.38	98.57

the sun's energy into the water. Electricity is produced by this method.

Determine the magnitude of the exhaust or supply flow using

$$F_A = S * A, \tag{1}$$

Table 5: Thermal insulation management.

No of inputs	LVRMM	DLCA	ADSM	FPSMM	EDDLM
100	52.37	77.9	74.56	84.57	95.82
200	52.41	76.85	73.45	83.04	94.80
300	52.45	75.8	72.34	81.51	93.78
400	52.49	74.75	71.23	79.98	92.76
500	52.53	73.70	70.12	78.45	91.74
600	52.57	72.65	69.01	76.92	90.72
700	52.61	71.60	67.90	75.39	89.70

where F_A is the desired value of the air flow, S is the size of the room, and A is the number of air updates per hour.

For example, an apartment is 65 square meters. And a ceiling height of 2.5 m, with an optimal air flow (65 ∗ 2.5)/2 =81.25 cubic meters/h.

Calculate the airflow using the following equation

$$S = \frac{L}{(W * 3600)} \tag{2}$$

where $W = 1\ m/s$ and the value is used to connect the 3600 time units. Therefore, $S = 81.25/3600 = 0.02257\ sq.m.$

Scientists believe it started when a cloud collapsed under its own gravity, a term known as the cloud theory. It not only created a great ball of light at the center of our solar system, but also triggered a process. Through this, the nitrogen collected in the center began to combine to generate solar energy. The process, technically known as nuclear fusion, releases incredible amounts of energy in the form of light and heat. But getting that energy from the core of our sun out to Earth and beyond involves some important steps. Ultimately, these all come down to layers of the sun, and each has a role to play in ensuring that solar energy gets to where it helps create and sustain life. Convert the value obtained according to the formula to the value of the radius in

$$R = \frac{\sqrt{S}}{\pi}. \tag{3}$$

According to the example, the pipe radius is .00.02257/3.4 = 0.085 m or 8.5 cm. The diameter should be taken with rounding up about 20 cm. The inner part of the sun extends from its center to about 20–25% of the solar radius. It is in the interior that energy is produced by the conversion of hydrogen atoms (H) to helium (He) molecules. This is possible due to the extreme pressure and temperature in the interior, which are estimated to be equivalent to 250 billion atmospheres (25.33 trillion KPa) and 15.7 million Kelvin, respectively. Two positrons are released from this process, as well as two neutrinos (which convert two electrons into negative electrons) and energy.

4. Results and Discussion

The proposed energy distribution deep learning model (EDDLM) was compared with the existing low-voltage

Table 6: Solar energy management.

No of inputs	LVRMM	DLCA	ADSM	FPSMM	EDDLM
100	52.44	76.57	73.05	82.40	94.56
200	52.46	77.29	73.62	82.98	95.21
300	52.48	78.01	74.19	83.56	95.86
400	52.50	78.73	74.76	84.14	96.51
500	52.52	79.45	75.33	84.72	97.16
600	52.54	80.17	75.90	85.30	97.81
700	52.56	80.89	76.47	85.88	98.46

Table 7: Heat supply management.

No of inputs	LVRMM	DLCA	ADSM	FPSMM	EDDLM
100	55.62	84.35	72.52	79.89	89.87
200	58.04	86.55	74.51	81.38	91.84
300	58.45	87.35	75.71	82.18	92.97
400	60.20	89.08	77.44	83.44	94.66
500	61.62	90.58	79.03	84.59	96.21
600	63.03	92.08	80.63	85.73	97.76
700	64.45	93.58	82.22	86.88	99.31

Table 8: Energy efficiency management.

No of inputs	LVRMM	DLCA	ADSM	FPSMM	EDDLM
100	60.05	88.02	76.19	84.51	94.18
200	62.37	89.45	77.62	85.52	94.55
300	63.62	90.54	77.78	86.16	96.08
400	66.35	91.02	78.55	86.82	96.58
500	68.14	92.28	79.35	87.65	97.53
600	70.15	93.29	80.07	88.40	98.40
700	72.17	94.30	80.79	89.16	99.28

residential micro-grids management (LVRMM), decentralized load control architecture (DLCA), autonomous demand-side management (ADSM), and fuzzy probabilistic based semi-Morkov model (FPSMM).

4.1. Exterior Thickness. Table 1 shows the comparison of exterior thickness management. The size of the future living space in the house directly depends on the thickness of the exterior walls. If the walls are thick, say 38.5 cm, rather than 32 cm. Living space will decrease significantly. So, in a house with an area of 10×11 m with walls of a certain thickness, its living area will lose 2.73 meters at each site. This means more houses per square meter! With a wall thickness of 49 cm, the living area on each floor is reduced to about 8 m^2.

4.2. Noise Protection. The sound insulation of the walls and structures of a house directly depends on the density and texture of the material from which they are made. When designing a home, it is important to focus on isolating yourself from shock and noise. Solid (without windows and doors) walls, for example, made of fiber-reinforced concrete with a thickness of 250 mm, fully meet the requirements of comfort. Sound insulation of walls with more than 25% partial windows is no longer as effective: In this case, a significant portion of the noise penetrates through the windows. Here, first of all, special measures for sound insulation will be required. Table 2 shows the comparison of noise protection management.

4.3. Climate Change Management. The concept of "comfort at home" has many different meanings. Some believe that a house made of baked clay bricks is more comfortable, while others prefer silicate bricks, while others prefer wood over a frame system. A comfortable microclimate is a balanced combination of all these elements in the construction of a house. Table 3 shows the comparison of climate change management.

4.4. Heat Loss and Cold Bridges. When insulating a house, special attention should be paid to areas that have lost heat or are known as "cold bridges." In these places, the heat goes out more intensely than the others. An example is balconies with roofs in the form of a solid slab and window slopes or joints between exterior walls and basement. To minimize heat loss and avoid possible damage to structures (e.g., mold formation on them due to perspiration), it is important to take this into account even during the design and construction phase of the house. Particular attention should be paid to sealing joints in windows, doors, roofs, and installation of roller shutter housings. Table 4 shows the comparison of heat loss and cold bridges management.

4.5. Thermal Insulation. If previously it was believed that insulation with a thickness of 10 cm (mineral fiber mats or polyurethane foam sheets) is sufficient for roof insulation, now more stringent standards apply to roof insulation. For roofs of energy-efficient ("heated") houses, the resistance to heat transfer should be at least 6 W/m^2,i.e., the thermal conductivity coefficient of 0.04 W/m^2K (at equilibrium humidity) and thermal insulation thickness of a material made of at least 24 cm. However, the most effective and greatest comfort is the heating system with infrared film heaters, whose efficiency is 92-97%. Table 5 shows the comparison of thermal insulation management.

4.6. Passive and Active Solar Energy. Table 6 shows the comparisons of solar energy management. The use of double-glazed windows with low heat transfer coefficient allows to save energy resources. The modern market offers double-glazed windows even with $K_t = 1.3 - 1.1\ W/(m^2 - K)$. Double-glazed windows and luxury class $(0.9 - 0.8\ W/(m^2 - K))$, but they are more expensive. With energy savings, double-glazed windows create comfort in the premises. Or the use of a glass unit with a heat transfer coefficient of 1.11 W/m^2-K does not lead to a sharp increase in the price of the window, for example, unlike the use of glued angora pine wood frames.

4.7. Heat Supply. Passive house is a heated house with minimal consumption of heating medium. Your home will be heated by an integrated system, which includes a gas dual

circuit boiler and a heat pump. The heat pump requires a submersible drainage sump pump. Double steel pipe weave is reduced to a depth of 100 m. The upper half of the pipes' thermal insulation. The heat pump is driven through the tube by the liquid mixture antifreeze type. At depth, the mixture heats up and provides heat inside the house. The heat is pumped through the cooling system by the pumps. A solid fuel boiler is installed to heat the water. It is heated by waste and wood waste. Energy saving dual cycle boiler burns waste without leaving any smoke. Table 7 shows the heat supply management.

4.8. Energy Efficiency. Based on the most recent technological advancements, energy represents the achievement of economically sensible use of energy resources. This does not mean reducing anything or losing anything. The goal of achieving maximum energy efficiency in the home is achieved primarily by minimizing heat loss thermal energy in all energy processes without affecting the end result of rational use. Table 8 shows the comparison of energy efficiency management.

5. Conclusion

Generally, forced ventilation in the apartment provides for its maintenance, for which the interior surfaces and filters should be cleaned once or twice a year, depending on the intensity and frequency of use. In the process, you will remove the built-ups on the grills and visors with a vacuum cleaner or other suitable method. It is necessary to wipe the damping surfaces of the housing and device using a damp cloth. Supply and exhaust ventilation in the apartment, home or office will improve the quality of human life. After all, fresh air is essential for the normal functioning of the brain. For proper well-being, having fresh air in the apartment is the most important point. $3\,m^3$ of fresh air should be supplied to $1\,m^2$ of covered area. There is a rule for an adult who needs $30\,m^3$ of air per hour. Due to the fact that the fan is powered by current, it is necessary to check the condition of the power cable and connections. If the operation is irregular, the equipment should be operated for 5 or 10 minutes, once a quarter. If forced ventilation is installed in an apartment with your own hands, it must comply with the requirements of the SNiP, and the use of additional devices such as controllers, controllers, timers, and sensors will improve energy costs and extend their life.

Data Availability

The data used to support the findings of this study are included within the article. Further data or information is available from the corresponding author upon request.

Conflicts of Interest

The authors declare that there are no conflicts of interest regarding the publication of this paper.

Acknowledgments

The authors appreciate the supports from Wollo University, Ethiopia, for the research and preparation of the manuscript.

References

[1] F. Ahmad, M. S. Alam, I. S. Alsaidan, and S. M. Shariff, "Battery swapping station for electric vehicles: opportunities and challenges," *IET Smart Grid*, vol. 3, no. 3, pp. 280–286, 2020.

[2] P. Balakrishna and K. S. Swarup, "A method of low voltage residential micro-grids management using AMI/GIS systems and its application benefits," *Renew Energy Focus*, vol. 32, pp. 1–9, 2020.

[3] B. Bibak and H. Tekiner-Moğulkoç, "A comprehensive analysis of vehicle to grid (V2G) systems and scholarly literature on the application of such systems," *Renew Energy Focus*, vol. 36, pp. 1–20, 2021.

[4] A. N. Arularasan, M. Manoj, M. Sudhakar et al., "A holistic framework for environment conscious based material selection and experimental assessment using digraph-based expert system," *Scientific Programing*, vol. 2022, article 2112683, 10 pages, 2022.

[5] D. Croce, F. Giuliano, M. Bonomolo, G. Leone, R. Musca, and I. Tinnirello, "A decentralized load control architecture for smart energy consumption in small islands," *Sustainable Cities and Society*, vol. 53, p. 101902, 2020.

[6] F. Elghitani and W. Zhuang, "Aggregating a large number of residential appliances for demand response applications," *IEEE Transactions on Smart Grid*, vol. 9, no. 5, pp. 5092–5100, 2018.

[7] S. Favuzza, M. Ippolito, F. Massaro, R. Musca, G. Schillaci, and G. Zizzo, "Building automation and control systems and electrical distribution grids: a study on the effects of loads control logics on power losses and peaks," *Energies*, vol. 11, no. 3, p. 667, 2018.

[8] R. Ford, M. Pritoni, A. Sanguinetti, and B. Karlin, "Categories and functionality of smart home technology for energy management," *Building and Environment*, vol. 123, pp. 543–554, 2017.

[9] A. Mohsenian-Rad, V. W. S. Wong, J. Jatskevich, R. Schober, and A. Leon-Garcia, "Autonomous demand-side management based on game-theoretic energy consumption scheduling for the future smart grid," *IEEE Transactions on Smart Grid*, vol. 1, no. 3, pp. 320–331, 2010.

[10] R. Jena and B. Pradhan, "Earthquake vulnerability assessment using expert-based approach in GIS," in *2019 6th International Conference on Space Science and Communication (IconSpace)*, pp. 53–56, Johor Bahru, Malaysia, 2019.

[11] D. RavishankarSathyamurthy, B. Mageshbabu, A. Madhu, A. R. MuthuManokar, and M. S. Prasad, "Influence of fins on the absorber plate of tubular solar still-an experimental study," *Materials Today: Proceedings*, vol. 46, no. 9, pp. 3270–3274, 2021.

[12] R. Terracciano, V. Galdi, V. Calderaro, D. Pappalardo, G. Ceneri, and A. O. Pití, "Demand side management services for smart buildings with the use of second generation smart meter and the chain-2 of E-distribuzione," in *2020 IEEE International Conference on Environment and Electrical Engineering and 2020 IEEE Industrial and*

Commercial Power Systems Europe (EEEIC / I&CPS Europe), Madrid, Spain, 2020.

[13] S. Paul and N. P. Padhy, "Real-time bilevel energy management of smart residential apartment building," *IEEE Transactions on Industrial Informatics*, vol. 16, no. 6, pp. 3708–3720, 2020.

[14] D. Geer, "In brief: grid-based modeling technique furthers earthquake risk prediction," *IEEE Distributed Systems Online*, vol. 7, no. 2, pp. 5–5, 2006.

[15] O. Özel and A. R. Boynuegri, "Thermal modelling and energy management of a smart home with renewable energy sources," in *2020 6th International Conference on Electric Power and Energy Conversion Systems (EPECS)*, pp. 97–102, Istanbul, Turkey, 2020.

[16] M. F. A. Azis, F. Darari, and M. R. Septyandy, "Time series analysis on earthquakes using EDA and machine learning," in *2020 International Conference on Advanced Computer Science and Information Systems (ICACSIS)*, pp. 405–412, Depok, Indonesia, 2020.

[17] J. Logeshwaran, M. J. Rex, T. Kiruthiga, and V. A. Rajan, "FPSMM: fuzzy probabilistic based semi morkov model among the sensor nodes for realtime applications," in *2017 International Conference on Intelligent Sustainable Systems (ICISS)*, pp. 442–446, Palladam, India, 2017.

[18] E. Oral and C. Satriano, "Future magnitude 7.5 earthquake offshore Martinique: spotlight on the main source features controlling ground motion prediction," *Geophysical Journal International*, vol. 227, no. 2, pp. 1076–1093, 2021.

[19] J. D. Zechar and J. Zhuang, "Risk and return: evaluating reverse tracing of precursors earthquake predictions," *Geophysical Journal International*, vol. 182, no. 3, pp. 1319–1326, 2010.

[20] D. Valeriy, B. Inna, S. Maryna, and H. Maksym, "Evaluation of differentiated impact of apartment building occupants' behavior on energy consumption," in *2020 IEEE 7th International Conference on Energy Smart Systems (ESS)*, pp. 196–200, Kyiv, Ukraine, 2020.

[21] Z. Foroozandeh, S. Ramos, J. Soares, and Z. Vale, "Optimal contract power and battery energy storage system capacity for smart buildings," in *2021 IEEE PES Innovative Smart Grid Technologies Europe (ISGT Europe)*, pp. 1–5, Espoo, Finland, 2021.

[22] J. Logeshwaran, "The control and communication management for ultra dense cloud system using fast Fourier algorithm," *ICTACT Journal on Data Science and Machine Learning*, vol. 3, no. 2, pp. 281–284, 2022.

[23] Z. Foroozandeh, S. Ramos, J. Soares, and Z. Vale, "Goal programming approach for energy management of smart building," *IEEE Access*, vol. 10, pp. 25341–25348, 2022.

[24] M. R. M. Rilfi and J. D. Kanchana, "IoT and Machine Learning Based Efficient Garbage Management System for Apartment Complex and Shopping Malls," in *2021 6th International Conference on Information Technology Research (ICITR)*, Moratuwa, Sri Lanka, 2021.

[25] J. Zhuang, "Gambling scores for earthquake predictions and forecasts," *Geophysical Journal International*, vol. 181, no. 1, pp. 382–390, 2010.

[26] J. Logeshwaran, M. Ramkumar, T. Kiruthiga, and R. Sharanpravin, "The role of integrated structured cabling system (ISCS) for reliable bandwidth optimization in high-speed communication network," *ICTACT Journal on Communication Technology*, vol. 13, no. 1, pp. 2635–2639, 2022.

[27] Y. Su and Z. Jin, "Building service oriented applications for disaster management - an earthquake assessment example," in *2009 Fourth International Conference on Cooperation and Promotion of Information Resources in Science and Technology*, pp. 3–8, Beijing, China, 2009.

[28] J. Logeshwaran and R. N. Shanmugasundaram, "Enhancements of resource management for device to device (D2D) communication: a review," in *2019 Third International conference on I-SMAC (IoT in Social, Mobile, Analytics and Cloud)(I-SMAC)*, pp. 51–55, Palladam, India, 2019.

[29] S. Nimkar and M. M. Khanapurkar, "Edge computing for IoT: a use case in smart city governance," in *2021 International Conference on Computational Intelligence and Computing Applications (ICCICA)*, pp. 1–5, Nagpur, India, 2021.

[30] Y. I. Soluyanov, A. I. Fedotov, A. R. Akhmetshin, and V. I. Soluyanov, "Calculation of new electrical loads for public premises included in multi-apartment residential buildings," in *2022 4th International Youth Conference on Radio Electronics, Electrical and Power Engineering (REEPE)*, pp. 1–5, Moscow, Russian Federation, 2022.

[31] R. Alisic, M. Molinari, P. E. Paré, and H. Sandberg, "Ensuring privacy of occupancy changes in smart buildings," in *2020 IEEE Conference on Control Technology and Applications (CCTA)*, pp. 871–876, Montreal, QC, Canada, 2020.

Hindawi
International Journal of Photoenergy
Volume 2022, Article ID 7902301, 11 pages
https://doi.org/10.1155/2022/7902301

Research Article

Estimation of Groundwater Quality in Arid Region or Semiarid Region by Using Statistical Methods and Geographical Information System Technique

Ahmed A. S. Alothman,[1] Mohamed Saad Ahmed,[2] S. Radjarejesri,[3] G. Ramkumar,[4] Ram Prasad,[5] Panuganti Lakshmi,[6] Mika Sillanpaa,[7] and Subash Thanappan[8]

[1]*Department of Agricultural Engineering, College of Food and Agricultural Sciences, King Saud University, P.O. Box 2460, Riyadh 11451, Saudi Arabia*
[2]*Department of Geology and Geophysics, College of Science, King Saud University, Riyadh 11451, Saudi Arabia*
[3]*Department of Chemistry, Sona College of Technology, Salem, 636005 Tamil Nadu, India*
[4]*Department of Electronics and Communication Engineering, Saveetha School of Engineering, SIMATS, Chennai, Tamil Nadu, India*
[5]*Department of Electronics and Communication Engineering, Mahatma Gandhi Central University, Motihari, India*
[6]*Department of Civil Engineering, Aditya Engineering College, Surampalem, 533437 Andhra Pradesh, India*
[7]*Department of Biological and Chemical Engineering, Aarhus University, Norrebrogade 44, 8000 Aarhus C, Denmark*
[8]*Department of Civil Engineering, Ambo University, Ambo, Ethiopia*

Correspondence should be addressed to Subash Thanappan; subash.thanappan@ambou.edu.et

Received 21 May 2022; Revised 13 August 2022; Accepted 20 August 2022; Published 29 September 2022

Academic Editor: Br Ramesh Bapu

This study takes place in year of 2021 during the premonsoon and postmonsoon seasons and twenty water samples were collected. Chemical factors like chloride, fluoride, sulphate, nitrate, and phosphate were measured in water samples. There is a significant difference in anion dominance between pre- and postmonsoonal (PRM and POM) water samples. The following anions are $HCO_3 > TDS > Cl^- > SO_4^{2-} > TH > NO_3 > F^- > PO_4$ and $TDS > HCO_3^- > SO_4^{2-} > Cl^- > TH > NO_3^- > F^- > PO_4^-$. In both seasons, particular way of cations is $Na^+ > Ca^{2+} > Mg^{2+} > K^+$. SAR, Kelly's ratio, residual sodium carbonate, potential salinity, permeability index, and sodium percentage were used to evaluate the irrigation water quality. To investigate the geochemical regulation and hydrogeochemistry of groundwater, two approaches were used: according to the findings, groundwater in various parts of the investigation was determined to be unfit for human consumption.

1. Introduction

Most rural and urban residents depend on groundwater as their prime supply of drinking water when the monsoons fail and surface water is sparse [1]. The use of agricultural fertilizer, which adds to groundwater contamination, increases as the population expands. Because of the sluggish movement of the aquifer's cycle, groundwater aquifer poisoning can last for decades. Groundwater's suitability for drinking and irrigation is influenced by soluble salts and many other factors [2–4]. There are many factors that influence the amount of soluble salts in a rock, such as the mineral content, the type of soil, the climate, and the drainage properties of the soil. Quality irrigation water is extremely important to agriculture [5]. Poor irrigation water has a negative impact on plant development and productivity, as well as the soil's condition [6–8]. When irrigation water quality is examined, groundwater resources are better to be managed for recharging and properly utilization as shown in Figure 1 [9].

Figure 1: Methods to recharge ground water.

The physical, chemical, and biological properties of groundwater must be assessed before it may be used for drinking, irrigation, or industrial reasons [10–12]. A semiarid climate with annual rainfall ranging from 724 to 913 mm characterizes the study area furthermore [13, 14]. Rainwater harvesting for both domestic and agricultural use is insufficient. Borewell water is the primary source of supplies for the community's needs, including drinking, irrigation, and industrial applications [15, 16]. It was looked into if groundwater could be used for drinking, irrigation, or industrial uses. Numerous studies investigating the quality of the groundwater and the presence of important ions have been conducted [17–20].

2. Methodology

Around the industrial area, twenty areas were chosen to be sampled. During both seasons, water samples are gathered in 2 litres polypropylene beakers at premonsoon (PRM) and postmonsoon (POM) sites. The sampling sites are placed six kilometers apart, i.e., one station is six kilometers from the next. The samples were examined in accordance with APHA's normal procedures.

2.1. Index of Water Quality (WQI). WQI provides the parameters for household water quality [21] and suggested a WQI computation that contains four phases.

(i) Metrics are given weights (w) based on how important they are to one's health

(ii) The second step is used equation (1) to determine the relative reputation of each constraint

$$W_i = \frac{w_i}{\sum_{i=1}^{n} w_i}. \tag{1}$$

In which, w_i is the weight assigned to i^{th} parameter. W_i is the relative weight of i^{th} parameter, and n denotes the number of parameters.

(i) The (q_i) scale of quality evaluation is calculated in the following equation

$$q_i = \left(\frac{C_i}{S_i}\right) \times 100, \tag{2}$$

where q_i is the quality rating scale of i^{th} parameter. C_i is the concentration of i^{th} parameter. S_i is the desirable limit of i^{th} parameter given by WHO.

(i) Suffix index (SI) is computed for the i^{th} parameter and is in the following equation

$$\text{SI}_i = Wi \times q_i \text{ and } \text{WQI} = \Sigma \text{SI}_i. \tag{3}$$

2.2. Water Quality in Irrigation. Water quality measures were analyzed using the sodium adsorption ratio (SAR), potential saltiness (PS), permeability index (PI), magnesium hazard ratio (MHR), redox stability constant (RSC), Kelly's ratio, and corrosive ratio. The experiment was carried out in millilitres per litre and is shown in the following equations.

$$\begin{aligned}
\text{SAR} &= \frac{\text{Na}^+}{\sqrt{(\text{Ca}^{2+} + \text{Mg}^{2+})/2}},\\
\%\text{Na} &= \frac{\text{Na}}{\left(\text{Ca}^{2+} + \text{Mg}^{2+} + \text{Na}^{+}\right)},\\
\text{RSC} &= \left(\text{HCO}_3^- + \text{CO}_3^{2-}\right) - \left(\text{Ca}^{2+} + \text{Mg}^{2+}\right),\\
\text{MHR} &= \frac{Mg^{2+}}{\left(\text{Ca}^{2+} + \text{Mg}^{2+}\right)} \times 100,\\
\text{KI} &= \frac{\text{Na}^+}{\left(\text{Ca}^{2+} + \text{Mg}^{2+}\right)},\\
\text{PI} &= \frac{(\text{Na}^+ + \text{K}^+) + \sqrt{\text{HCO}_3^-}}{\text{Ca}^{2+} + \text{Mg}^{2+} + \text{Na}^+ + \text{K}} \times 100,\\
\text{PS} &= \text{Cl}^- + \left(\frac{1}{2}\right)\text{SO}_4^{2-},\\
\text{PI} &= \frac{\left(\text{Cl}^- + \text{SO}_4^{2-}\right)}{2\left(\text{HCO}_3^- + \text{CO}_3^{2-}\right)}.
\end{aligned} \tag{4}$$

Table 1: EC, TDS, chloride, fluoride, and TH readings are used to classify groundwater samples.

Range	Class	The number of samples		Station number on a sliding scale		%	
		PRM	POM	PRM	POM	PRM	POM
EC Wilcox							
<250	Outstanding	0	0	0	0	0	0
250-750	Good	1	1	19	18	5	5
750-2000	Allowable	10	13	13, 9, 15, 7, 18, 14, 2, 17, 1, 3	9, 11, 15, 0, 17, 19, 7, 1, 3, 14, 16, 6	45	50
182000-5000	Unsure	8	6	8, 6, 5, 16, 10, 2, 12, 13, 12, 4	8, 5, 10, 12, 2, 4, 13	40	30
>5000	Unfitting	0	0	0	0	0	0
TDS (mg/L) classification Davis and Dewiest							
<500	Suitable for consumption	1	2	11, 19	18, 11, 9	8	13
500-1000	Allowable to consume alcohol	8	9	15, 9, 18, 7, 14, 0, 17, 1, 3	15, 1, 17, 7, 19, 3, 1, 14, 16, 6	40	45
1000-3000	Irrigation-friendly	8	6	8, 6, 5, 16, 10, 2, 12, 13, 4	8, 5, 10, 12, 13, 2, 4	40	30
>3000	Drinking water and irrigation are both unsafe	0	0	0	0	0	0
Stuyfz and classification of chlorides							
<5	Actual oligohaline	0	0	0	0	0	0
5–30	Oligohaline	1	0	18	0	4	0
30–150	Fresh	4	4	11, 1, 7, 14, 9	7, 9, 18, 7, 17	20	20
150–300	Fresh-brackish	4	6	18, 17, 12, 17, 8	19, 0, 15, 14, 12, 3, 16	20	30
$300–10^3$	Brackish	8	7	3, 0, 2, 6, 7, 14, 4, 13, 10	8, 6, 11, 5, 3, 4, 13, 10	40	35
$10^{3\text{-}104}$	Brackish-salt	0	0	0	0	0	0
$10^4 - 2 \times 104$	Salt	0	0	0	0	0	0
$>2 \times 10^4$	Hyperhaline	0	0	0	0	0	0
Total hardness classification							
0–75	Soft	5	5	4, 3, 7, 19, 1, 11	4, 7, 19, 18, 1, 17	25	25
75–150	Abstemiously tough	7	10	8, 17, 14, 10, 5, 18, 0	9, 0, 8, 14, 16, 11, 15, 2, 3, 5, 6	30	50
150–300	Tough	5	2	5, 12, 3, 16, 13, 6	12, 13, 10	25	10
>300	Very tough	1	0	10	0	5	0
Chaturvedi fluoride classification							
<0.5	Caries in the teeth	5	6	18, 5, 15, 3, 0, 6	10, 5, 18, 19, 9, 11, 17	25	20
0.5–1	Maximum permissible limit	1	10	10, 19	3, 6, 0, 8, 7, 14, 16, 15, 13, 4, 12	5	50
1–3	Fluorosis of the teeth	5	1	17, 16, 7, 9, 14, 8	2, 1	25	5
3–4	Bones that are stiff	3	0	1, 11, 12, 13	0	15	0
>4	Knee deformities are a common occurrence.	1	0	2,4	0	5	0
>10	Skeletal fluorosis	0	0	0	0	0	0

3. Results and Discussion

Table 1 lists the highest, smallest, and average concentrations of several water quality parameters for PRM and POM conditions. There are many classifications for electrical conductivity in addition to total dissolved solids, chloride, fluoride, and also overall hardness.

3.1. Drinking Water Quality Parameters. Premonsoon pH values range from 7.0 to 8.5, whereas postmonsoon pH values range starts 6.97 to 7.72. Premonsoon EC values range starts 360 to 3910μS/cm, and POM EC values range starts 650 to 3910μS/cm, respectively. PRM TDS concentrations range starts 218 to 1685 mg/L, while POM concentrations range starts 347 to 1760 mg/L. Prior to the monsoon,

Table 2: The coefficients of correlation (r) between several water quality metric premonsoon.

	pH	EC	TDS	Cl^-	TH	Ca^{2+}	Mg^{2+}	HCO_3^-	SO_4^{2-}	F^-	NO_3^-	PO_4	Na	K
pH	1													
EC	-0.014	1												
TDS	0.014	1. 016	1											
Cl^-	0.078	0.583	10.578	1										
TH	0.452	0.049	0.083	0.458	1									
Ca^{2+}	0.368	-0.007	0.124	0.059	0.821	1								
Mg^{2+}	0.321	0.092	0.124	0.283	0.783	0.358	1							
HCO_3^-	0.052	0.0412	0.386	0.093	-0.029	-0.021	-0.051	1						
SO_4^{2-}	-0.030	0.364	0.345	-0.042	-0.048	-0.052	-0.016	0.019	1					
F^-	0.296	0.223	0.183	-0.049	0.114	0.257	-0.019	0.458	0.082	1				
NO_3^-	-0.054	0.183	0.189	0.172	-0.546	-0.041	-0.048	0.148	-0.039	-0.049	1			
PO_4	0.049	-0.026	-0.029	-0.04	-0.058	-0.042	-0.052	0.052	-0.061	0.162	-0.040	1		
Na	0.009	0.243	0.243	0.008	0.003	0.049	0.018	0.048	0.269	0.178	0.008	0.002	1	
K	0.098	0.021	0.019	0	0.031	0	0.104	0	0.058	0.039	0.007	0.029	0.016	1

Table 3: The coefficients of correlation (r) between several water quality metric postmonsoon.

pH	1													
EC	0.019	1												
TDS	0.025	0.982	1											
Cl^-	0.009	0.660	0.568	1										
TH	0.188	0.261	0.212	0.430	1									
Ca^{2+}	0.242	0.152	0.118	0.290	0.430	1								
Mg^{2+}	0.216	0.159	0.132	0.282	0.862	0.241	1							
HCO_3^-	0.058	0.552	0.548	0.284	0.036	0	0.008	1						
SO_4^{2-}	0	0.288	0.368	0.042	0.032	0.006	0.024	0.124	1					
F^-	0.318	0.249	0.302	0.018	0	0.048	0.007	0.332	0.140	1				
NO_3^-	0.001	0.031	0.041	0.024	0	0	0.016	0.002	0.146	0.006	1			
PO_4	0.002	0.130	0.118	0.36	0.251	0.192	0.0182	0.026	0.002	0.004	0.006	1		
Na	0.058	0.334	0.314	0.091	0.128	0.023	0.072	0.105	0.232	0.243	0.026	0.003	1	
K	0.002	0	0.002	0	0.031	0	0.023	0.003	0.039	0.015	0.004	0.003	0.014	1

Table 4: Diverse water quality characteristics weight and relative weight.

A chemical metric	Weight (wi)	Weighted average (Wi)	WHO (2004) S
pH	4	0.072	9.6
TDS (mg/L)	6	0.118	1100
Cl^- (mg/L)	6	0.118	225
TH (mg/L)	3	0.046	500
Ca^{2+} (mg/L)	4	0.072	80
Mg^{2+} (mg/L)	4	0.072	35
HCO_3^- (mg/L)	4	0.072	360
Na (mg/L)	6	0.012	210
K (mg/L)	3	0.046	25
SO_4 (mg/L)	6	0.012	210
F (mg/L)	6	0.012	1
NO_3^-	4	0.03	60
	$\Sigma w_i = 56$	$\Sigma W_i = 0.682$	

fluoride concentrations range from 0 mg/L to 8.78 mg/L. Each of the 20 samples was analyzed and found to be under the permitted limit, with 40% of them falling inside the limit [22, 23]. Fluoride levels in the environment are high due to weathering of rocks, as well as the use of fertilizers, pyrotechnics, and match manufacturing. Nearly 90% of samples show a significant decrease in fluoride concentration following the postmonsoon rains [24–26]. Fluoride levels in postmonsoon water are low because precipitation dilutes groundwater. Premonsoon levels of nitrate in most Southeast Asian towns and cities are less than 1 mg/L. Postmonsoon season saw a considerable decrease of mosquito populations in the northern areas. The regional distribution of fluoride exceeding the BIS allowed limit is depicted in the premonsoon plot. Dental fluorosis affects 30% of PRM and 10% of POM seasons, according to [27, 28]. There is a correlation between low level calcium and high-level bicarbonate alkalinity in groundwater, according to [29]. One of the most fluoride (8.78 mg/L) and the second-highest amount

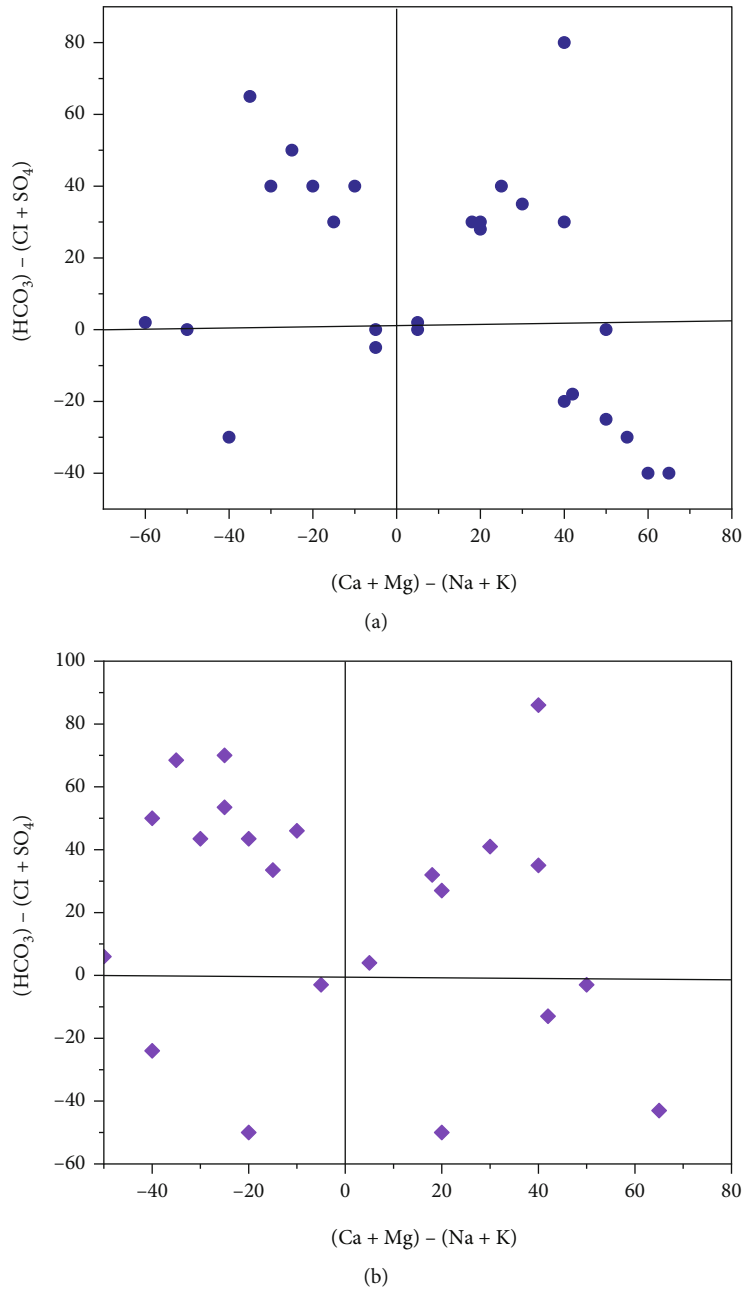

Figure 2: Diagram of Chadha. (a) Premonsoon. (b) Monsoon.

(4.96 mg/L). The PRM ranges from 214 mg/L to 2112 mg/L in alkalinity, while the POM extends from 230 mg/L to 1600 mg/L; in both cases, 92% of samples exceed 380 mg/L. In comparison to the PRM season, water samples taken after the monsoon show a decreased concentration of bicarbonate. The PRM and POM values for sulphate vary from 4 to 1278 mg/L, respectively. Only 38% and 8% of PRM and POM water samples, respectively, exceeded the BIS acceptable sulphate limit (200 mg/L). The aerobic nitrification process, which transforms fertilizer ammonium sulphate into nitrate, gives it a high monetary worth. There are a wide range of values between 1 and 30 mg/L during the postmonsoon period [30]. After the postmonsoon, nitrate concentrations are low because rainwater dilutes it. A higher concentration of phosphate is found in the POM period than in the premonsoon period. Run-off detergents and sewage discharge are a couple of possible causes. Groundwater samples from PRM and POM periods show a range of 8 to 72 mg/L of calcium [31]. A total of all samples follows both WHO (121 mg/L) and the BIS (204 mg/L) standards. Magnesium across the spectrum from 2 to 35 mg/L before and after the monsoon, respectively. Premonsoon samples have a magnesium concentration of 10% higher than the BIS-acceptable level of 30 mg/L. The salt contents in the water varied between 8 and 94 mg/L during PRM and 7 to 78 mg/L after monsoon. In the last two seasons, there have

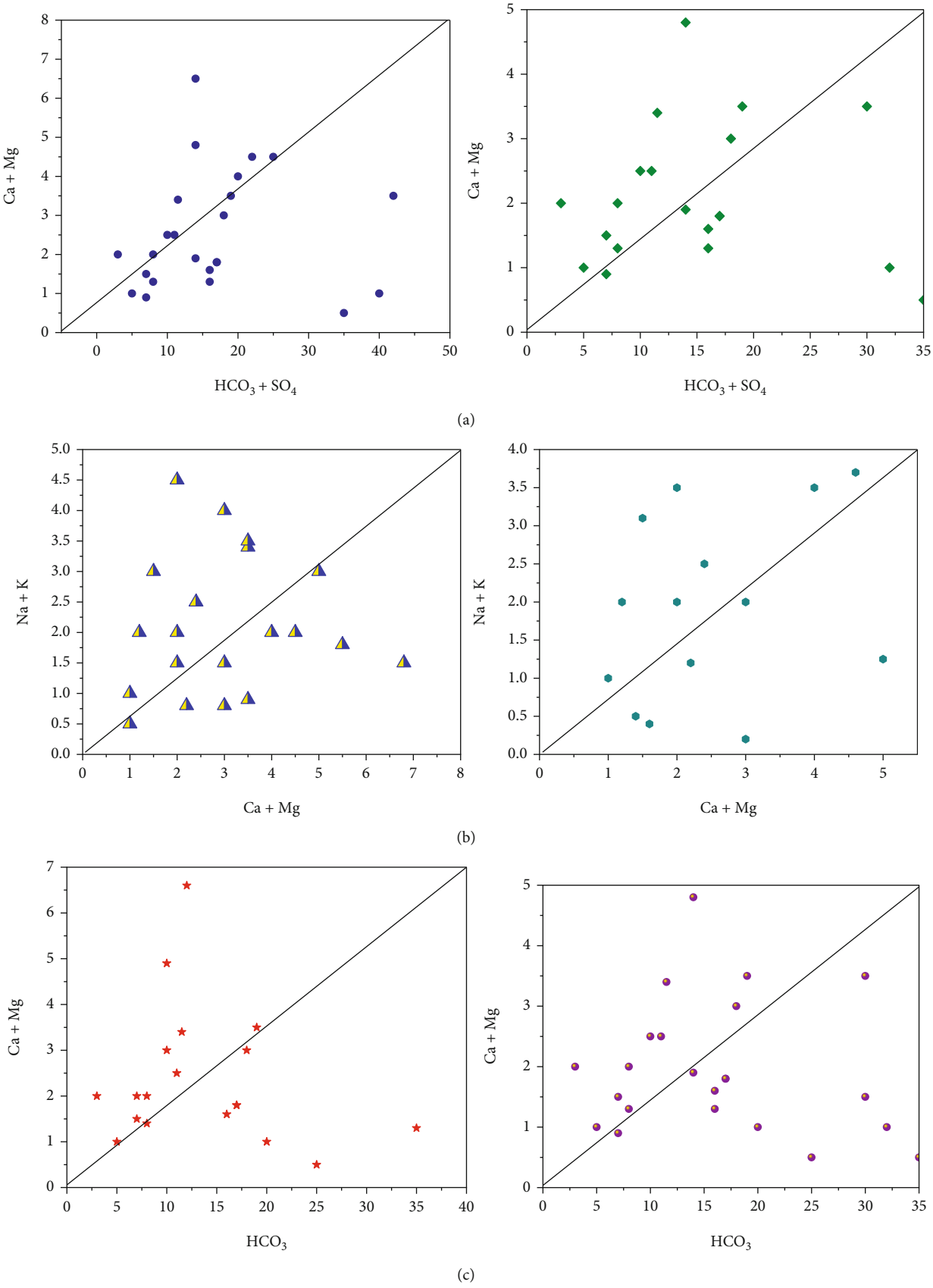

Figure 3: Scatter diagram. (a) $HCO_3 + SO_4$ vs.Ca + Mg. (b) Ca + Mg vs.Na + K. (c) HCO_3 vs.Ca + Mg.

Table 5: Piper tri-linear and Chadha diagram were used to characterise groundwater.

Water type characteristics		Sample percentage	
		PRM	POM
Piper diagram subdivision			
1	Alkalies (Na + k) outnumber alkaline earth (Ca + Mg).	55	70
2	Alkalies are more abundant than alkaline earths.	35	20
3	Weak acids (CO3 + HCO3) outnumber strong acids (SO4 + Cl).	50	60
4	Strong acids are more powerful than weak acids.	40	30
5	Type of magnesium bicarbonate	20	45
6	Type of calcium chloride	5	0
7	Type of sodium chloride	10	10
8	Type sodium-bicarbonate	0	0
9	Types are mixed	55	35

been no infractions of the 200 mg/L restriction. Potassium concentrations range from 5 mg/L to 48 mg/L prior to the monsoon, while POM levels range from 3 mg/L to 32 mg/L.

3.2. Analysis of Correlation. Water quality metrics can be linked using correlation analysis. The relationship is perfect linear if correlation coefficient is closer 1.Among +0.8 and +1.0, there is an extremely significant correlation between the two variables. There is a moderate link between the "*r*" values of +0.5 to 0.8 and -0.5 to -0.8. If "*r*" is between -0.5 and +0.5, then, there is little connection between the two variables. Water quality metrics were correlated using correlation coefficients. $R > 8$ was considered in the linear regression equation.

3.3. Index of Water Quality (WQI). The Water Quality Index is a statistic for assessing a body of water's health. Tables 2, 3, and 4 show the WQI water categorization used in this investigation. WQI values in the range of 112–212 were discovered in 40% of PRM samples and 10% of POM samples, indicating that they were unfit for drinking. During the PRM season, 11% of the samples exhibit water quality concerns, making them unfit for consumption [32]. Rainwater mixing lowers the WQI values of all samples during the monsoon season, causing them to be lower than PRM.

3.4. Wilcox Plot. In the Wilcox plot, the data findings are plotted using the EC and SAR data. Before and after the monsoon, the majority of samples fell into the C3S1 zone. More than half of the PRM and POM samples contained the C3S1 zone, indicating high salinity and little sodium threat. A wide range of soil types can be irrigated using this type of water sample [33]. There was an extremely high salinity and low sodium hazard zone in samples from 30% of PRM samples and 25% of POM samples (C4S1). Plants with a high salt tolerance should be irrigated with C4S1 water. In both seasons, 5% of the samples are classified as belonging to the C2S1 zone. The remaining premonsoon samples were collected in the zones C4S2 and C3S2 (5%). In fine-grained soils with limited drainage, hydrating plants with C4S2 and C3S2 water are impossible.

3.5. Chadha Diagram. The hydrogeochemistry and water kinds are depicted in Chadha's diagram. It was listed the proportion of water found in each of the fields described by [34]. Recharging waters make up 20% of the water samples collected in field 5 Ca^{2+}-Mg^{2+}-HCO_3^-. There is a 50% rise in the POM period. The concentration of moderate acidic anions (as opposed to strong acidic anions) is higher in the POM period than in the PRM period. They have a short-term hardness due to the presence of dissolved CO_3^- in the form of bicarbonate in these types of water. Approximately 35% of the samples collected prior to the monsoon are in the sixth field and include water of the type, Ca-2+, Mg-2+, Cl-. The dominant Cl-type or Cl-dominant, Ca-2+, Mg-2+ type of water was found. When it comes to the postmonsoon season, however, this field receives only 25% of the total rain. In this sector, sodium is dissolved in water and then adsorbs onto mineral surfaces, which may explain why, $Na^+ + K^+$ is in excess to $Ca^{2+} + Mg^{2+}$. Pre- and postmonsoon samples from field seven include 14 and 9% of the Na-+ and Cl-water type, respectively. 30% of water samples are field 8 in premonsoon conditions, with mild acidic anions greatly outnumbering strong acidic anions. It does, however, drop to 20% in the postmonsoon season. Figure 2 shows the diagram of Chadha is one of the most well-known in the field: (a) premonsoon and (b) monsoon.

3.6. Scatter Plot. Na^+ and Cl^- were plotted against each other to create the scatter plot you see here. The graph illustrates which process predominate in the research area: mineral weathering, ion exchange, or halite dissolution [35]. In pre- and postmonsoon, 45 and 40% of sample concentrations are lower than the equiline, respectively. The fact that the molar ratio is greater than one indicates that Na^+ has been liberated during the weathering of silicate (feldspar). Carbonate acid reacts with feldspar minerals, causing them to break down in water when silicate weathering occurs. There is halite dissolution if the ratio is equal to one. Carbonate weathering is responsible for 66% of PRM and 55% of POM samples falling a reading over the line that indicates high calcium and magnesium in the scatter diagram, $(HCO_3^- + SO_4^{2-})$ vs. $(Ca^{2+} + Mg^{2+})$. The reverse ion exchange mechanism in the shale bed exchanges water's,

Table 6: Parameters used to classify groundwater.

Parameter	Range	The water's quality	Total number of samples		(%)	
			PRM	POM	PRM	POM
Ratio of sodium adsorption (in meql-1)	<10	Excellent	15	15	95	95
	10-20	Good	0	0	0	0
	20-28	Doubtful	0	0	0	0
	>28	Unsuitable	0	0	0	0
Kelly's ratio (KR) is a mathematical formula (in meql-1)	<1	Suitable	12	16	62	82
	1-3	Marginal	4	2	22	14
	>3	Unsuitable	3	2	11	6
RSC stands for residual sodium carbonate (in meql-1)	<1.25	Safe	0	0	0	0
	1.25-2.25	Marginal	2	4	6	16
	>2.25	Unsuitable	20	18	96	85
PS stands for potential salinity (in meql-1)	<6	Excellent to good	7	6	32	25
	6-12	Good to injurious	7	7	32	32
	>12	Injurious to unsatisfactory	9	10	42	46
The permeability index (PI) is a measure of how permeable a material is (in meql-1)	>80	Excellent	20	20	95	90
	30-80	Good	2	2	6	6
	<30	Unsuitable	0	0	0	0
Sodium percentage (SP) is a measure of how much sodium is present in a given amount (in meql-1)	<25	Excellent	3	4	12	15
	25-45	Good	8	8	35	30
	45-65	Permissible	7	8	32	35
	65-85	Doubtful	6	4	25	16
	>85	Unsuitable	0	0	0	0
The magnesium ratio (MR) is a measure of how much magnesium is present in a given amount of (in meql-1)	<30	Suitable	7	6	45	20
	>30	Unsuitable	13	16	65	80
Corrosive ratio (CR)	>1.5	Eroding	4	2	15	6
	<1.5	Harmless	18	20	85	100
Index of water quality (WQI)	<45	Excellent	2	5	6	25
	45-95	Good	10	14	45	70
	95-190	Poor	9	4	45	20
	190-290	Very poor	3	0	12	0
	>290	Undesirable for drinking	0	0	0	0

Na^+ for Ca^{2+} and Mg^{2+}. Ionexchange dominates silicate weathering in PRM (35%) and postmonsoon (45%) samples, which are both below a line. 48% of the samples fall below and above the scatter plot's line. Figure 3 shows the scatter diagram (a) $HCO_3 + SO_4$ vs.Ca + Mg, (b) Ca + Mg vs.Na + K, and (c) HCO_3 vs.Ca + Mg.

3.7. Irrigation Water Quality. As a result, all samples from the PRM and POM periods are suitable for irrigation in this study since the SAR value is less than 10 [36]. The higher-than-10 SAR values indicate that when water shrinks and expands, soil permeability in clayey soil diminishes. The groundwater can be divided into three categories according to Kelly's ratio. Some of them are appropriate (less than 1) while others (between 1 and 2) are just marginally suitable for irrigation. A total of 10% and 5% of PRM and POM water samples, respectively, were discovered to be unfit for irrigation, using Kelley's ratio. This classification was devised by [37] based on the residual sodium carbonate (RSC). Water samples are deemed dangerous during the PRM and

Table 7: Guidelines for interpreting the quality of irrigation water.

Water constraint	Normal irrigation water ranking	Range during PRM	POM
Sodium absorption ratio (SAR)	0-10	0.4-5.0	0.3-4.0
Magnesium (Mg^{2+})	0-6	0.17-2.90	0.40-2.50
Bicarbonate (CO_3^{2-})	0-12	3.5-35.0	3.7-27.2
Calcium (Ca^{2+})	0-25	0.6-3.60	0.50-2.50
Sodium (Na^+)	0-45	0.35-4.10	0.35-3.75
Sulphate (SO_4^{2-})	0-25	0.2-27.4	0.2-16.5
Electrical conductivity (EC)	<2100	370-3920	655-3600
Chloride (cl^-)	0-35	0.5-20.0	1.8-19.0
Acid/base (pH)	6.2-8.7	7.2-8.4	7-7.75
Potassium (K^+)	0-0.050	0.15-1.20	0.05-0.95

POM periods. During the PRM, only 6% of water samples in the western section of the research region were of questionable quality. The majority of the remaining samples are those that cannot be irrigated. Because of their high salt concentration, 15% of the POM samples were mediocre, and the rest 85% are not suited for irrigation.

Tables 5 and 6 show the calculated potential salinity (PS). Water samples taken before the monsoon season had a salinity range of 0.5 to 24.2 $meql^{-1}$, with a mean value of 9.6 meql-1. At postmonsoon period is an average 9.3 $meql^{-1}$ ranging from 2.0 to 20.7. Water samples are categorized into three kinds based on their potential saltiness. Only 30% and 25% of PRM and POM water samples are of outstanding to good quality, respectively, during these seasons. There were 28% good to damaging samples, and the rest were unsuitable for irrigation in both seasons. Water samples have PI levels ranging from 60 to 260 meql-1 before the monsoon and PI values ranging from 74 to 240 $meql^{-1}$ at monsoon. PI was used to classify the irrigation water by [38]. The vast majority of specimens in table are opted for monsoon irrigation with only 5% being unsuitable. In both seasons, the samples are completely impermeable. The SP value varies from 15 to 78 $meql^{-1}$ before the monsoon and from 10 to 69 meql-1 after the monsoon. In one-quarter of the cases, water samples obtained before and after the monsoon are unfit for irrigation. Magnesium ratios in water samples ranged from 30 to 82 meql-1 during the pre- and post-POM phases. PRM and POM water samples with magnesium ratios less than 50% and 25%, respectively, fall into the "safe" group. As a result of pollution, none of the irrigation water samples left are valid at this time. Between 0.2 and 2.9 is the typical premonsoon calcium-to-magnesium ratio. Samples with Ca : Mg ratios of less than 1 comprise 60% of the samples, whereas those with ratios larger than 1 comprise 40%. A postmonsoon range of 0.3 to 3.1 is seen, with an average value of 0.78. Samples that include a Ca : Mg ratio of less than one makes up 70% while samples with a ratio larger than one make up 30%. Most samples (60% and 70%, respectively) have a ratio less than 1 in both seasons, the findings show. It has been shown that soil structure and agricultural productivity are negatively impacted by an increase in SAR. Useful for industrial uses, the corrosion ratio (CR) measures the corrosiveness of water. Before the rainy season, 85% of the water samples had a CR value less than 1, while after it, 95% of the samples had a CR value lower than 1. Table 7 provides irrigation water suitability guidelines. According to it, EC, K, and HCO3 exceed the parameter levels in all seasons, whereas sulphate surpasses the guideline value in PRM season. Water samples collected before and during the monsoon season are ideal for irrigation.

4. Conclusion

(i) As the monsoon season approaches, the order of anion dominance in water samples changes from $HCO_3 > TDS^- > Cl^- > SO_4^{2-} > TH > NO_3 > F^> > PO_4^3$ to $TDS > HCO_3 > SO_4^{2-} > Cl^- > TH > NO_3^- > F > PO_4^-$. In both seasons, and cations are dominant in the following order: $Na^+ > Ca^{2+} > Mg^{2+} > K^+$. TDS, chloride, sulphate, and phosphate are all terms for total hardness. In both seasons, the majority of water samples had calcium, magnesium, sodium, and potassium levels that were within acceptable limits

(ii) Samples polluted by alkalinity make up 80% of the total. Fluoride and nitrate are found in premonsoon and postmonsoon water samples, respectively, however, they are not found in postmonsoon water samples. According the Water Quality Index, 50% of pre- and postmonsoon water tests are safe for consumption

(iii) The water samples' SAR, KR, PS, PI, and Na % readings suggest that they can be used for irrigation, according to the researchers

Data Availability

The data used to support the findings of this study are included within the article. Further data or information is available from the corresponding author upon request.

Conflicts of Interest

The authors declare that there is no conflicts of interest regarding the publication of this article.

Acknowledgments

The authors appreciate the supports from Ambo University, Ethiopia, for providing help during the research and preparation of the manuscript. The authors would like to acknowledge the Researchers Supporting Project Number (RSP2022R455), King Saud University, Riyadh, Saudi Arabia.

References

[1] G. Alagumuthu and M. Rajan, "Chemometric studies of water quality parameters of Sankarankovil block of Tirunelveli,

Tamilnadu," *Journal of Environmental Biology*, vol. 31, no. 5, pp. 581–586, 2010.

[2] P. Li, D. Karunanidhi, T. Subramani, and K. Srinivasamoorthy, "Sources and consequences of groundwater contamination," *Archives of Environmental Contamination and Toxicology*, vol. 80, no. 1, pp. 1–10, 2021.

[3] S. M. Avvannavar and S. Shrihari, "Evaluation of water quality index for drinking purposes for river Netravathi, Mangalore, South India," *Environmental Monitoring and Assessment*, vol. 143, no. 1–3, pp. 279–290, 2008.

[4] D. M. Joshi, A. Kumar, and N. Agrawal, "Assessment of the irrigation water quality of river ganga in Haridwar district," *Rasayan Journal of Chemistry*, vol. 2, no. 2, pp. 285–292, 2009.

[5] A. K. Chaturvedi, K. P. Yadava, K. C. Pathak, and V. N. Singh, "Defluoridation of water by adsorption on fly ash," *Water, Air, and Soil Pollution*, vol. 49, no. 1–2, pp. 51–61, 1990.

[6] S. Chidambaram, M. Bala Krishna Prasad, R. Manivannan et al., "Environmental hydrogeochemistry and genesis of fluoride in groundwaters of Dindigul district, Tamilnadu (India)," *Environment and Earth Science*, vol. 68, no. 2, pp. 333–342, 2013.

[7] S. N. Davis and R. J. M. De Wiest, *Hydrogeology*, Wiley, New York, 1966.

[8] S. M. Deshpande and K. R. Aher, "Evaluation of groundwater quality and its suitability for drinking and agriculture use in parts of Vaijapur, district Aurangabad, MS, India," *Research Journal of Chemical Sciences*, vol. 2, no. 1, pp. 25–31, 2012.

[9] S. B. Megdal, "Invisible water: the importance of good groundwater governance and management," *Npj Clean Water*, vol. 1, article 15, 2018.

[10] D. K. Tank and C. P. S. Chandel, "Analysis of the major ion constituents in groundwater of Jaipur city," *Natural Science*, vol. 8, no. 10, pp. 1–7, 2010.

[11] S. Dixit, S. K. Gupta, and S. Tiwari, "Nutrient overloading of Fresh Water lake of Bhopal, India," *Electronic Green Journal*, vol. 1, no. 21, 2005.

[12] L. D. Doneen, *Notes on water quality in agriculture*, Notes Water Qual. Agric, 1964.

[13] F. M. Eaton, "Significance of carbonates in irrigation waters," *Soil Science*, vol. 69, no. 2, pp. 123–134, 1950.

[14] C. Gajendran, S. Jayapriya, Y. Diana, V. Oshin, and J. Christina, "Assessment of groundwater quality in Tirunelveli District, Tamil Nadu, India," *International Journal of Environmental Sciences*, vol. 3, no. 6, pp. 1847–1880, 2013.

[15] E. T. Glover, T. T. Akiti, and S. Osae, "Major ion chemistry and identification of hydrogeochemical processes of ground water in the Accra Plains," *Geoscience*, vol. 50, pp. 10279–10288, 2012.

[16] J. D. Hem, *Study and interpretation of the chemical characteristics of natural water*, Department of the Interior, US Geological Survey, 1985.

[17] S. M. Hill, K. G. McQueen, and K. A. Foster, "Regolith carbonate accumulations in Western and Central NSW: characteristics and potential as an exploration sampling medium," *State of the Regolith, Proceedings of Regolith*, vol. 98, pp. 191–208, 1999.

[18] J. Y. Hwang, S. Park, H. K. Kim et al., "Hydrochemistry for the assessment of groundwater quality in Korea," *Journal of Agricultural Chemistry and Environment*, vol. 6, no. 1, pp. 1–29, 2017.

[19] A. Jafar Ahamed, K. Loganathan, and S. Ananthakrishnan, "A comparative evaluation of groundwater suitability for drinking and irrigation purposes in Pugalur area, Karur district, Tamilnadu, India," *Archives of Applied Science Research*, vol. 5, no. 1, pp. 213–223, 2013.

[20] M. Jalali, "Effect of sodium and magnesium on kinetics of potassium release in some calcareous soils of western Iran," *Geoderma*, vol. 145, no. 3–4, pp. 207–215, 2008.

[21] A. N. Jerry, *Basic environmental technology (water supply, waste disposal and pollution control)*, Wiley, New York, 1986.

[22] K. R. Karanth, *Hydrogeology*, Tata McGraw-Hill Publishing Company, 1989.

[23] U. Karmegam, S. Chidamabram, P. Sasidhar, R. Manivannan, S. Manikandan, and P. Anandhan, "Geochemical characterization of groundwater's of shallow coastal aquifer in and around Kalpakkam, South India," *Research Journal of Environmental and Earth Sciences*, vol. 2, no. 4, pp. 170–177, 2010.

[24] A. Karthik and G. Brindha, "Green revolution conversion of offline education to online education," *International Journal of Pharmacy and Technology*, vol. 8, no. 3, pp. 15393–15407, 2016.

[25] N. Karthikeyan, A. Saranya, and M. C. Sashikkumar, "Spatial analysis of groundwater quality for Virudhunagar District, Tamil Nadu using GIS," *International Journal of Remote Sensing and Geoscience*, vol. 2, no. 4, pp. 23–30, 2013.

[26] W. P. Kelley, "Permissible composition and concentration of irrigation waters," *Proceedings of the American Society of Civil Engineers*, vol. 66, pp. 607–613, 1940.

[27] P. Meena, P. Jain, and K. Meena, "Assessment of ground water quality and its suitability for drinking and domestic uses by using WQI and statistical analysis in river basin area in Jahzpur tehsil, Bhilwara district (Rajasthan, India)," *International Journal of Current Microbiology and Applied Sciences*, vol. 5, no. 3, pp. 415–427, 2016.

[28] M. Meybeck, "Global chemical weathering of surficial rocks estimated from river dissolved loads," *American Journal of Science*, vol. 287, no. 5, pp. 401–428, 1987.

[29] P. C. Mishra and R. K. Patel, "Study of the pollution load in the drinking water of Rairangpur, a small tribal dominated town of North Orissa," *Indian Journal of Environment and Ecoplanning*, vol. 5, no. 2, pp. 293–298, 2001.

[30] N. S. Magesh and N. Chandrasekar, "Evaluation of spatial variations in groundwater quality by WQI and GIS technique: a case study of Virudunagar District, Tamil Nadu, India," *Arabian Journal of Geosciences*, vol. 6, no. 6, pp. 1883–1898, 2013.

[31] K. Pandian and K. Sankar, "Hydrogeochemistry and groundwater quality in the Vaippar River basin, Tamil Nadu," *Journal of the Geological Society of India*, vol. 69, no. 5, pp. 970–982, 2007.

[32] P. Ravikumar, M. Aneesul Mehmood, and R. K. Somashekar, "Water quality index to determine the surface water quality of Sankey tank and Mallathahalli lake, Bangalore urban district, Karnataka, India," *Applied Water Science*, vol. 3, no. 1, pp. 247–261, 2013.

[33] A. Saleh, F. Al-Ruwaih, and M. Shehata, "Hydrogeochemical processes operating within the main aquifers of Kuwait," *Journal of Arid Environments*, vol. 42, no. 3, pp. 195–209, 1999.

[34] S. D. Boominathan, S. Palanisamy, S. Kanagaraj, and G. Munusamy, "Mapping of ground water quality for Ramanathapuram Taluk of Tamil Nadu using geographical information system," *Cloud Publications International Journal of*

Advanced Remote Sensing and GIS, vol. 4, no. 1, pp. 953–959, 2015.

[35] R. Shyam and G. S. Kalwania, "Health risk assessment of fluoride with other parameters in ground water of Sikar city (India)," *Environment and Earth Science*, vol. 65, no. 4, pp. 1275–1282, 2012.

[36] R. Singh, T. H. Syed, S. Kumar, M. Kumar, and A. S. Venkatesh, "Hydrogeochemical assessment of surface and groundwater resources of Korba coalfield, Central India: environmental implications," *Arabian Journal of Geosciences*, vol. 10, no. 14, 2017.

[37] V. Sivasankar, T. Ramachandramoorthy, and A. Chandramohan, "Deterioration of coastal groundwater quality in island and mainland regions of Ramanathapuram District, Southern India," *Environmental Monitoring and Assessment*, vol. 185, no. 1, pp. 931–944, 2013.

[38] I. Szabolcs and C. Darab, "The influence of irrigation water of high sodium carbonate content of soils," *Proceedings of 8th International Congress of ISSS*, vol. 2, pp. 803–812, 1964.

Hindawi
International Journal of Photoenergy
Volume 2022, Article ID 7228470, 13 pages
https://doi.org/10.1155/2022/7228470

Research Article

Performance Evaluation and Estimation of Energy Measures of Grid-Connected PV Module

R. Srimathi,[1] **J. Meenakshi**,[1] **R. Vijayabhasker**,[2] **and Semagn Shifere Belay**[3]

[1]*School of Electrical Engineering, Vellore Institute of Technology, Chennai, 600127 Tamil Nadu, India*
[2]*Department of Electronics and Communication Engineering, Regional Campus, Anna University, Coimbatore 641046, India*
[3]*School of Computing, Woldia Institute of Technology, Woldia University, Ethiopia*

Correspondence should be addressed to Semagn Shifere Belay; semagn.s@wldu.edu.et

Received 5 July 2022; Revised 15 September 2022; Accepted 17 September 2022; Published 28 September 2022

Academic Editor: BR Ramesh Bapu

In this paper, the effectiveness of two grid-connected photovoltaic (PV) techniques up of copper indium selenium (CIS) and monocrystalline silicon (m-Si) arrays has been examined. In order to determine whether the technology is suitable for the actual winter and summer climatic conditions in Thoothukudi, Tamil Nadu, the observed and calculated performances have been compared. The final yield, photovoltaic (PV) effectiveness, array yield, performance ratio, and capacity utilisation factor seem to be the variables used to evaluate performance. Using recorded meteorological data at the selected location, PVsyst software predicts both PV systems' year-round performances. These predictions are then contrasted to the outcomes of the actual measurements. The outcome showed that with a maximal observed performance ratio, both PV systems function marginally better in the winters than those in the summers. The performance indicators of the PV mechanisms are contrary with those of other PV systems with comparable capacities that are located in different places.

1. Introduction

The quantities of energy utilized globally have substantially increased over the past few decades. It increases from 6131 TWh in 1973 to 23816 TWh in 2014, and it is predicted that this increase will improve quality of life by enabling advanced technology. By 2040, it is anticipated that 56 percent of the world's energy would be consumed. Two significant obstacles stand in the way of the rising demand for electricity: the scarcity of common resources and the environmental issues brought on by emissions from the excessive usage of fossil fuels [1]. The rapid depletion of fossil fuel resources around the world increases the power price hikes, concerns about energy security, and environmental issues [2]. In all of these circumstances, one of the prospective power sources to substitute nonrenewable energy sources was environmentally friendly and sustainable energy sources, like solar energy [3].

India has a lot of potential for solar energy production. The geographical area, which experiences solar energy equivalent to 3000 hours of sunshine annually, is the explanation. This is more than 5000 quadrillion kW hours. India almost universally receives 4–7 kilowatt hr of solar radiation per square metre. Under the National Solar Mission, India has the bold ambition to construct massive power grid connected solar power facilities designed to work in conjunction capacity of 20,000 MegaWatt by 2020. Understanding how well solar PV systems function under various climatic conditions is necessary for a successful deployment [4].

A significant sustainable energy source that generates electricity using photovoltaic (PV) power grids with no fossil fuel usage or emissions [5]. Semiconductor materials are used in photovoltaic cells or panels, which enable the direct conversion of solar energy to electrical energy. For a very long period, these modules can offer you a source of electricity that is secure, trustworthy, maintenance-free, and ecologically sustainable [6]. Although PV systems are more pricey than other alternatives for power generation, this technology has been encouraged because of its significant gains, which can be categorized into three: benefits for customers, benefits for electric utilities, and benefits for the environment [7]. When using PV modules in solar projects, it is important

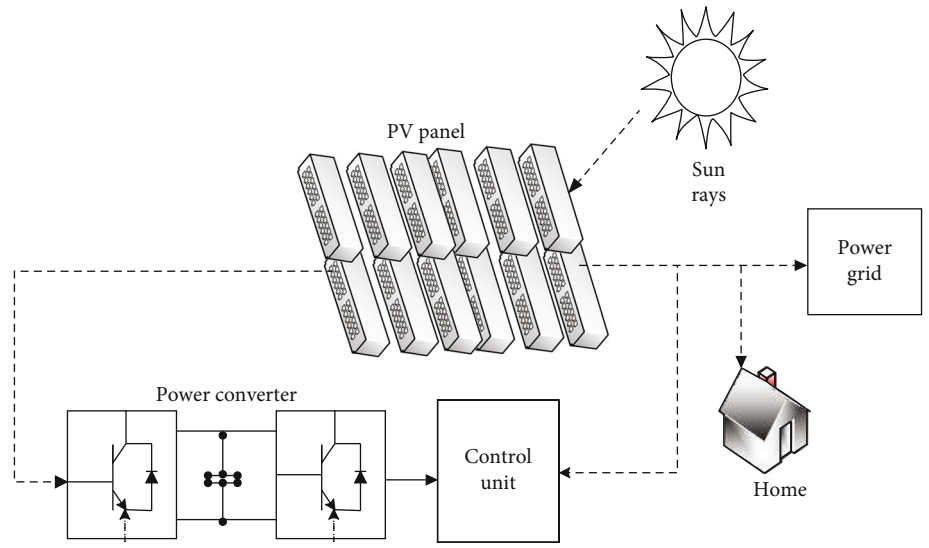

Figure 1: Grid-connected PV module's configuration.

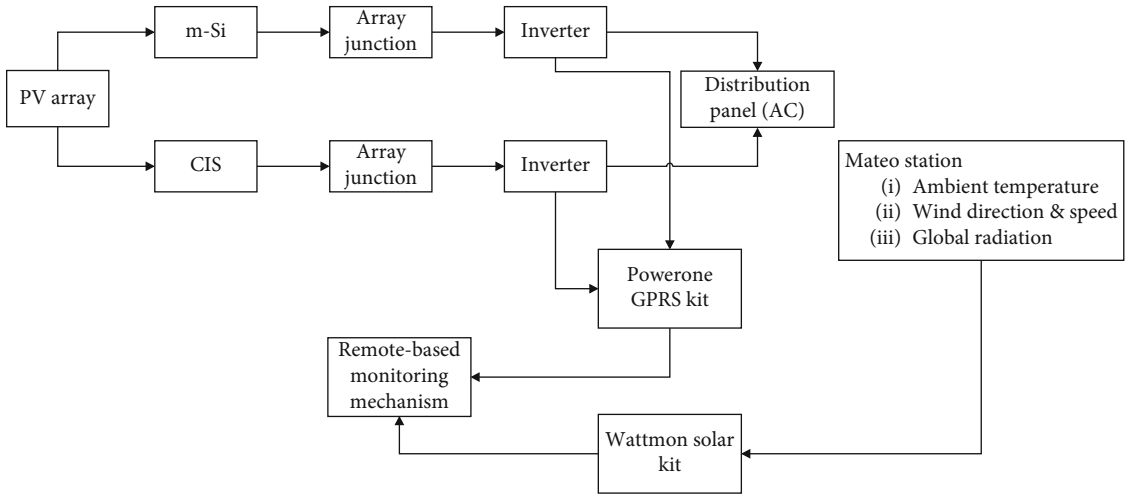

Figure 2: Presented grid-connected PV module's schematic diagram.

to understand how they operate and how they will behave in various climatic situations. The standard condition test (STC) is typically conducted indoors or in an air mass (AM) of 1.5, an intensity of 1 kilowatt/m2, and a cell temperature of 25°C. Thus, it is essential to assess the actual efficiency of PV systems in outside conditions using trustworthy tools in predicting in a particular geographic area [8].

In the recent times, various studies have been carried out to enhance every aspect of photovoltaic (PV) systems. The behaviour of PVs in this environment, including temperature, irradiance, and cell temperature, must be taken into consideration while maximising production [9]. For academics, PV installers, and stakeholders, performance evaluations of various PV systems for a chosen site with its meteorological parameters are more straightforward to derive important conclusions. The outdoor performance of thin-film and monocrystalline(m-Si) photovoltaic systems that have been coupled to the grid was presented in this paper [2]. Solar panels made from monocrystalline silicon have cells that are each carved from a single ingot of monocrystalline silicon. Due to the fact that each cell is crafted from a singular piece of silicon, the composition of these cells is more refined. As a direct consequence of this, mono panels have a little higher efficiency level than poly panels. The goal is to determine practical PV technology's long- and short-term viability and effectiveness for places with comparable environmental circumstances. Under hot temperatures in south India, the real effectiveness of grid-connected PV modules with a copper indium selenium (CIS) PV array and monocrystalline (m-Si) system are contrasted. With specific input parameters relevant to the local latitude and longitude, the PVsyst software also predicts the performances of both PV systems. The proposal's objective is to evaluate the energy efficiency of thin film PV technology and crystalline silicon in real-world climatic circumstances in Thoothukudi, Tamil Nadu, in southern India. A methodical process is developed to conduct the

Table 1: PV systems' technical specifications.

Parameter	CIS	m-Si
MNM (watt)	180	210
V_{mp} (V)	88.5	39.62
I_{mp} (A)	2.4	6.8
V_{oc} (V)	115	48.15
TCOP (%/K)	-0.35	-0.41
I_{sc} (A)	2.45	5.65
Inverter (kVA)	1.7	1.4
Rated power (kWp)	1.62	1.3
NMS	4	1
Azimuth angle (degree)	180	180
NM	10	5
Module tilt (degree)	10	10

Note: MNM: module nominal Power, V_{mp}: module current at maximum power, I_{mp}: module voltage at maximum power, V_{oc}: module open circuit voltage, TCOP: temperature coefficient of power, I_{sc}: module short circuit current, NMS: number of module string, NM: number of modules.

Table 2: Sensor's technical specifications in weather station [15].

Instrument	Accuracy	Range
WSS WS120	±4%	0-75 m/s
SRS (PYRA 300 V2)	±6%	0-1800 W/m^2
MTS(RTD Pt1000Ω)	±0.6°C	0-100°C
WDS	±4°	0-360°
ATS (RTD Pt1000Ω class A)	±0.4°C	0-100°C

Note: WSS: wind speed sensor, SRS: solar radiation sensor, MTS: module temperature sensor, WDS: wind direction sensor, ATS: ambient temperature sensor.

analysis, and the approach used for this study is described below. They are shown in Figure 1.

2. Related Works

In this work, he presents a brand-new model design, simulation analysis, and test validation for the connected PV grid system. The simulation of a PV system has connected to a solar generator with a 3.2 Kwp rated power and a single stage grid coupled to an inverter uses this technique. Before the PV system is described by a single diode lumped circuit, its key parameters, which are a part of the overall PV model, are assessed. Testing was done by doing external I-V feature estimations, which confirmed the findings for the PV module's characteristics. In order to account for power conversion efficiency, the AC power output is compared to the DC input power after being applied to an effective second-order model with the parameters of interest. The MATLAB/Simulink environment produces the simulation results. Results demonstrate successful data compatibility for I-V signals or for the full operating system. To demonstrate how accurately the prediction analysis shows electricity generation in a PV system, indicators of severe error are provided [10].

Renewable energy sources are increasingly being used in energy systems. The distribution of decision makers for photovoltaic (PV) decisions is becoming more and more dependent on economic analysis. Energy production and heat data from PV systems installed in Istanbul, Turkey in 2009 were analysed to determine the potential for solar power generation. Along with measurement, commercial factors were used. This study takes into account a number of taxes, including utility and supply taxes. The necessity for economic analysis to inform decision makers' choices about photovoltaic (PV) distribution is growing. The PV systems that will be implemented in Istanbul, Turkey, are examined in this article. Tests were conducted using signals like power interruptions that were gathered in PV modules and tiny stations as part of an ongoing experiment. The consequences of employing photovoltaic systems on annual expenses as well as other taxes, including utility and food taxes, were taken into account. According to the findings, users can install solar PV systems to cut the electricity costs by more than 40%. Although solar PV systems have substantial upfront costs, subsequent price drops in PV modules and cost savings measures all help to bring down energy bills. Additionally, the price of electricity per kW-hour is less than the Turkish solar energy industry's guaranteed price. The solar PV system's capacity to fulfil summer's increased demand is one of its advantages. The utilisation of a PV system will be even more profitable if a utility company utilises a taxation system with seasonal operation intervals. This is because the efficiency of the PV system will be increased. The scope of the study is going to be expanded so that it can monitor the production of solar energy. This is because having reliable information about expected solar production is necessary in order to regulate the demand side. Solar forecasting is essentially a method that gives grid operators with a technique to predict and balance the amount of energy generation and consumption. Assuming the grid operator has access to a variety of generating assets, reliable solar forecasting enables the grid operator to optimise the method in which they deploy their controllable units in the most effective manner possible. Future initiatives will also address difficulties with power system implementation and quality enhancement, like cost reduction through the use of PV Integral Battery Storage systems [7].

Grid-connected photovoltaic (PV) system analysis, which may vary in terms of construction, technique, or location, is made easier by the use of relevant performance metrics. The four performance parameters that determine the overall system effectiveness regarding energy output, solar service, and the overall impact of system loss are reference yield, performance rating, final PV system yield, and PVUSA rating. These frameworks are examined for their capacity to offer the required insights into the development of the PV system and performance testing. They are replicated in a wide range of technologies, styles, and spatial situations. Also presented are techniques for calculating the system's AC power measurements during the design stage utilising multiples created from the performance metrics that were actually measured. It has been found that using the led to the reduction factor as a whole produces results that are

Table 3: Evaluation metrics for assessment.

Sl. No	Parameters	Symbol	Equation	Eqn. No
1	Final yield	Y_F	$\frac{E_{AC}}{P_{PV,rated}}$	(1)
2.	Monthly energy output	$E_{AC,M}$	$\sum_{d=1}^{n} E_{AC,d}$	(2)
3.	Efficiency of PV module	η_{PV}	$\frac{E_{DC,d}}{A_a H_t}$	(3)
4.	Array yield	Y_A	$\frac{E_{DC}}{P_{PV,rated}}$	(4)
5.	System efficiency	η_{sy}	$\left(\frac{E_{AC,d}}{A_a H_t}\right) \times 100\%$	(5)
6.	Capacity utilization factor	CUF	$\frac{E_{AC}}{8760 \times P_{PV,rated}}$	(6)
7.	System loss	L_S	$Y_A - Y_F$	(7)
8.	Reference yield	Y_R	$\frac{H_t}{H_r}$	(8)
9.	Temperature loss	L_T	$E_{DC} \times \left(\frac{(25 - T_M)\gamma}{1 + \gamma(T_M - 25)}\right)$	(9)
10.	Performance ratio	PR	$\left(\frac{Y_F}{Y_R}\right) \times 100\%$	(10)
11.	Array capture loss	L_{ACap}	$Y_R - Y_A$	(11)

Symbols definition: n: number of days in a month; $P_{PV,rated}$: PV array's nominal power (kWp), $E_{DC,d}$: energy output of daily DC from the array (kWh/kWp); $E_{AC,d}$: energy output of daily AC (kWh/kWp); γ: module's temperature coefficient of power; H_t: global-in-plane solar irradiation (kWh/m^2/day); A_a: array area of PV (m^2); T_M: temperature of PV module ($^\circ$C); H_r: in-plane reference irradiation of array (kWh/m^2/day).

Table 4: Energy parameters.

Sl. No.	EM	Eqn.	Eqn. No	Unit
1.	LCCE	$\frac{(T_L \times E_{\text{out}}) - E_{\text{in}}}{T_L \times E_{sol}}$	(12)	Years
2.	EPF	$T_L \times \left(\frac{E_{\text{out}}}{E_{\text{in}}}\right)$	(13)	—
3.	EPBT	$\frac{E_{\text{in}}}{E_{\text{out}}}$	(14)	%

more similar to those of the PVUSA technique; however, a greater knowledge of the issues and reduce factor can give rise to tighter agreement and reveal opportunities for improving system performance [11]. To adjust for lower output in actual operating conditions contrasted to the conditions in which the PV panel was rated, a scaling factor known as the photovoltaic (PV) derating factor is applied to the power output of the PV array.

The issue of electrical security has become more pressing due to rising electricity consumption in developing nations. To make use of the unused energy from renewable resources, this has become required. Due to their grid connectivity, PV systems have emerged as the most effective source of renewable energy on a broad scale. The design, operation, and integration of new grid-connected systems can be aided by performance analysis of these plants that are connected to the power. One of the largest auxiliary solar power plants, a 10 MW photovoltaic power grid attached to Ramagundam, receives a fair quantity of 4.97 kiloWatt hr/m2/day per year and the mean temperature is about 27.3 degrees centigrade. The business is geared for seasonal activities. This study goes into detail into the characteristics of solar PV architecture and its annual performance. Performance rating is determined by measuring various power losses (such as those caused by temperature, internal networks, electronics power, associated grids, etc.). The findings of plant performance tests are also contrasted with simulation results from PV system and PV-GIS software. The crop's final yield ranges from 1.96 to 5.07 hours each day, with a yearly performance rate of 86.12 percent. It generates 15,798,192 MWh or 17.68 percent of CUF power annually. Monitoring data and operating details for a Photovoltaic system can be used for significant initiatives in the future [4].

It is necessary to perform research to meet the load rather than the effects of the distributed generation (DG) grid as a result of the Net Plus-energy Buildings (NPEB) plan. This document is an imitation of the EnergyPlus software application, which is based on NPEB and works with four Brazilian city areas. Analysis covers grid interaction, loads matching indications, and photovoltaic (PV) efficiency limits (LMGI). There are new grid effect indicators available to research how DG affects the electrical grid. The investigation of economic elements is done in the second phase with the aid of net metering. The years are displayed in the

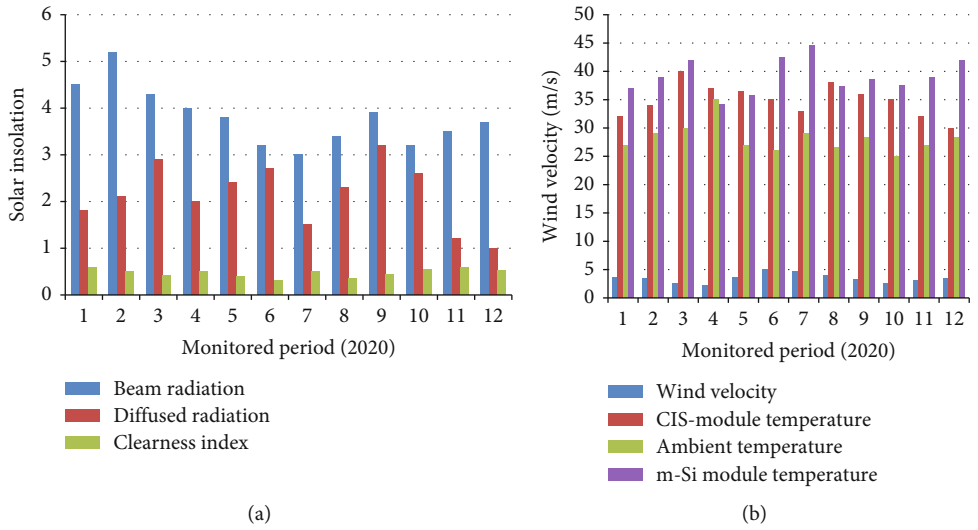

Figure 3: Monthly meteorological data. (a) Clearness index and mean global solar-radiation and (b) variations in module temperature, wind velocity, and ambient temperature.

Table 5: Solar-radiation and clearness index.

Monitored period (month)	Beam radiation (kWh/m^2/d)	Diffused radiation (kWh/m^2/d)	Clearness index
Jan	4.5	1.8	0.6
Feb	5.2	2.1	0.5
Mar	4.3	2.9	0.42
Apr	4	2	0.5
May	3.8	2.4	0.4
Jun	3.2	2.7	0.3
Jul	3	1.5	0.5
Aug	3.4	2.3	0.35
Sep	3.9	3.2	0.43
Oct	3.21	2.6	0.55
Nov	3.5	1.2	0.6
Dec	3.7	1	0.52

results. The yearly electricity supply loads vary from 20 to 36 percent depending on the climatic variables of the photovoltaic load relative and power generation levels exported to Brazil's high grid by yearly basis power peak position around 0.7 but it can exceed 0.8 in extremely sunny conditions. When PV production is high and temperature control capacity is high, solar energy can supply up to 51% of the electricity requirement. The building achieves grid equity between 6 and 18 percent of discount rates, according to the economy, and payment terms are offered under various conditions for investment expenses, discount rates, and power bills. Investment expenses and loan discount rates, among other non-technical and unpredictable factors, have a substantial effect. It is difficult to attain grid equity, thus political backing and financial incentives are still required. According to studies, local economic situations fluctuate based on the price of power and the real discount rates [12].

In this paper, analysis and modelling of a grid are presented to help evaluate the interaction behaviour of its nodes and to help control performance during system development (GCPS). Maintenance costs are low. Most of the power comes from the sun, therefore it helps save money on electricity. In addition, setting it up is a breeze. Grid-connected PV systems have a short gestation period. Its natural characteristics are easily imitated using basic specification data and a straightforward solar array circuit model. Comprehensive power control and GCPS security are provided by user-defined and constructed modules and power circuits to account for the passage of normal and defective situations, which are controlled by its dynamic power control. In PSCAD/EMTDC, a temporary power system software package, the model is referred to and used. To confirm that the suggested simulation model is successful in assessing the GCPS detection and protection performance in accordance with the temporary magnetic field analysis, comprehensive simulation results are provided and analysed. This approach may offer a practical tool for managing the creation and assessment of GCPS effectiveness [13].

There are numerous issues with integrated photovoltaic (PV) systems that result in an average loss of 20–25 percent in power production. There are many different factors, including temperature impacts, variances in the position and inclination of solar panels, partial loss, and partial shading, and due to production methods, PV module current-voltage (V) properties can vary. By employing the proper electrical systems, these losses can be minimised. The idea of a smart photovoltaic module, a low-cost dc-dc converter having high point-tracking capabilities (MPPT), a controller, and a power supply cable (PLC) are all introduced in this work. This study also looks at the intermediate, cable, and modular topologies for grid-connected PV system construction. The suggested system, a smart PV module, belongs to this last category. The boost dc-dc converter's topology and operating principles are being examined. Additionally, MPPT approach comparisons are carried out, which

Table 6: Variations in module temperature, wind velocity, and ambient temperature.

Monitored period (month)	Wind velocity (m/s)	CIS-module temperature (°C)	AT (°C)	m-Si MT (°C)
Jan	3.7	32	27	37
Feb	3.4	34	29	39
Mar	2.6	40	30	42
Apr	2.2	37	35	34.2
May	3.6	36.5	27	35.7
Jun	5.1	35	26	42.4
Jul	4.6	33	29	44.5
Aug	4	38	26.5	37.4
Sep	3.2	36	28.4	38.6
Oct	2.6	35	25	37.5
Nov	3.1	32	27	39
Dec	3.5	30	28.4	42

Note: AT: ambient temperature, MT: module temperature.

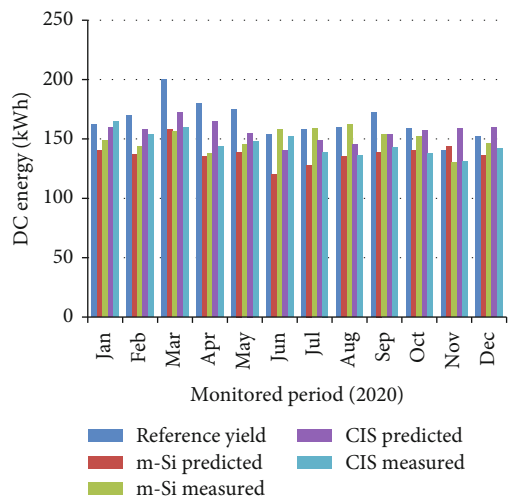

Figure 4: CIS and m-Si PV array's predicted and measured array yield comparison.

demonstrate the greatest outcomes of the growing performance. The PLC in every photovoltaic modules and its capability for grid-connected PV power are taken into consideration and studied in this article with regard to communications. A smart PV module (with dc-dc converter) prototype has undergone testing utilising the PV system testing platform to confirm its full performance. This paper explains this extremely potent instrument created to test all types of PV systems. By implementing a smart failure detection system, users will be able to create PV plant repair procedures based on specific data [14].

The proposed (PCGSS) with bidirectional flows would enable residual energy to be brought to the power system in whole or in part, depending on its requirements, while in a critical working environment, the grid would then directly supply loads. A photovoltaic (PV) system's charging time would be reduced as a result, increasing its viability for commercial use. A completely new management method is proposed to achieve this goal, improve the power produced, and allow the system to function as a scattered resource inside the utility grid. New alternatives are constrained: in the first, all of the power from the dispersed network is consumed by the grid, and in the second, power is added to the grid as needed. In order for the system to function according to the routes employing management algorithms with either Max Power Points (MPP) or Limited Power Points (LPP) applications, requirements must be met. The maximum power point, also known as the MPP, is the point on the current-voltage curve of an illuminated solar module that corresponds to the point at which the product of that module's current and voltage is at its highest value. LPP is carried out using a modified Perturbation and Observation approach. For continued power delivery and to maintain system performance, the battery system has been connected to the PV system. There are limits to a system's capacity to deliver the best loads. [1].

In accounting for differences, input variables and failure rates based on the state of vital components, including PV modules, inverters, and capacitors, this study offers a systematic approach for assessing the dependability of large-scale power systems connected to a solar grid (PV). In order to examine PV systems connected to the actual grid, state calculations are used. The key PV system components' failure levels based on ambient conditions are constructed and taken into account in the reliability study. To gauge the dependability performance of PV systems, a number of indication of the strength are defined. Considering the state of critical components like inverters, PV modules, and capacitors, as well as input parameters and failures, this study offers a methodical approach for assessing the dependability of high-power applications connected to a solar grid (PV). In order to examine photovoltaic panels connected to the actual grid, state calculations are used. The key photovoltaic systems components' failure levels based on ambient conditions are constructed and taken into account in the durability study. To gauge the dependability performance of PV systems, a number of reliability indicators are defined [5].

In developed countries, the deployment of energy photovoltaic systems (GCPVS) in urban structures is very widespread. International multilateral projects are being developed by many nations to hasten the installation of photovoltaic as a significant, long-lasting source of renewable energy. The prior approach, which relies on sensory networks (ANNs), is made to function with PV module electrical properties. This technique might create PV modules with crystalline V-I curves of any temperature and irradiance. The outcomes showed that the suggested ANN provided a good, precise prediction of the functionality of the crystallized PV modules. This technology, which is based on ANNs, will now be used to determine the fair value of the power that is supplied for PV installations. It is essential to determine the greatest amount of energy that can be harvested from a photovoltaic panel in order to maximise the amount of power that can be generated by a solar

Table 7: CIS and m-Si PV modules' measured and predicted final yield.

Monitored period (2020)	Reference yield	m-Si predicted	m-Si measured	CIS predicted	CIS measured
Jan	162	140	149	160	165
Feb	170	137	144	158	154
Mar	200	158	156	172	160
Apr	180	135	138	165	144
May	175	139	145	155	148
Jun	154	120	158	140	152
Jul	158	128	159	149	139
Aug	160	135	162	145	136
Sep	172	139	154	154	143
Oct	159	140	152	157	138
Nov	140	144	130	159	131
Dec	152	136	146	160	142

Units of measurements: monitored periods are in months; measured and predicted yield is in kWh/kWp; and reference yield is in kWh/m^2.

Table 8: Temperature loss, PV efficiency, and array yield's monthly variation for PV modules.

Monitored period (2020)	CIS				m-Si			
	L_T	Y_A	T_M (°C)	η_{PV}	L_T	Y_A	T_M (°C)	η_{PV}
Jan	0.24	4.4	35	12.5	0.25	4.6	40	13
Feb	0.23	4.5	34	13	0.27	4.8	35	14
Mar	0.22	4.8	31	12.56	0.25	5.0	33	14.6
Apr	0.224	5.2	30	13.1	0.236	4.8	32	15
May	0.24	4.54	33	13.5	0.17	4.24	34	14.5
Jun	0.28	4.32	36	14	0.25	4.25	35	14
Jul	0.32	4.21	39	13.2	0.3	4.12	37	14.2
Aug	0.21	4.5	32	13.7	0.27	4.75	35	14.7
Sep	0.23	5.1	37	13.6	0.26	5.25	38	14.6
Oct	0.25	4.25	38	12.32	0.24	4.75	40	15.2
Nov	0.29	4.12	32	14	0.22	4.5	39	16
Dec	0.121	4.64	37	13.8	0.26	4.72	42	15.8

photovoltaic system. A comparison is made between the performance of a conventional MPPT method and one that is based on an artificial neural network (ANN). Since the modules used in these functions are identical to those used in this solar generator, this method will be utilised in particular to determine the power supplied for a given installation, the "Unver Generator". Prices for PV modules are not rated when being compared [6].

3. Methodology

The development's goal is to evaluate the thin film photovoltaic (PV) systems and crystalline silicon's energy efficiency in real-world climatic circumstances in Thoothukudi, Tamil Nadu, in Southern India. A methodical process is developed to conduct the assessment. In order to assess the effectiveness of colocated monocrystalline Silicon (m-Si) and copper indium selenium (CIS) PV systems, the PV plants were initially developed employing PVsyst software. Grid-tied PV systems and a remote monitoring technology were deployed on the rooftop to conduct the exploratory method. The meteorological station that was set up at the location provides data on the ambient temperatures, wind speed, and sun radiation over horizontal substrates. The measured variables, like PV array's surface temperature, current, and output voltage, have been used to study the array yield, PV, energy output, final yield, and system efficiencies. This research looks at the PV technology's capacity utilisation factor (CUF) and performance ratio (PR). The computed energy losses include system loss, temperature loss, and array capture loss. Moreover, with the simulated results calculated from the PVsyst optimization technique, the PV systems' year-round performance is contrasted to and evaluated against the actual outside climatic constraints. In the end, energy measurements such as energy production factor (EPF), life cycle conversion efficiency (LCCE), and energy payback time (EPBT) have been assessed in order to estimate the whole energy performance of the PV systems. The efficiency of photovoltaic solar panels can be evaluated by measuring the relationship between the panels' voltage and current and therefore their power output under a variety of climatic variables, such as total sun irradiance. This will give an idea of how well the panels are functioning.

3.1. PV System Description. The rooftop has been installed with the grid-tied PV frameworks using p-Si and CIS technologies that were used for the performance evaluation. Tamil Nadu does have a tropical climate with small seasonal variations in winter and summer temperatures. The coldest season, which lasts from November to February, has an average temperature of 28°C while the warmest season, which lasts from March to June, has an average temperature that reaches 40°C. The PV plants are made up of 10 CIS modules and 5 m-Si modules, with operational capacities of 1.62 kWp, and 1.3 kWp, correspondingly. The PV module's north-south orientation faces directly south, and they are inclined at a 10° fixed angle.

Temperatures of the photovoltaic (PV) modules of the system as well as the ambient temperature, global radiation,

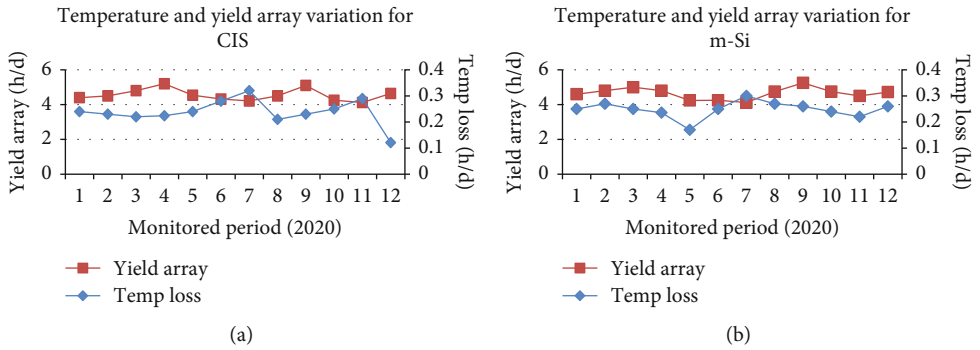

Figure 5: Temp loss and yield array for (a) CIS and (b) m-Si.

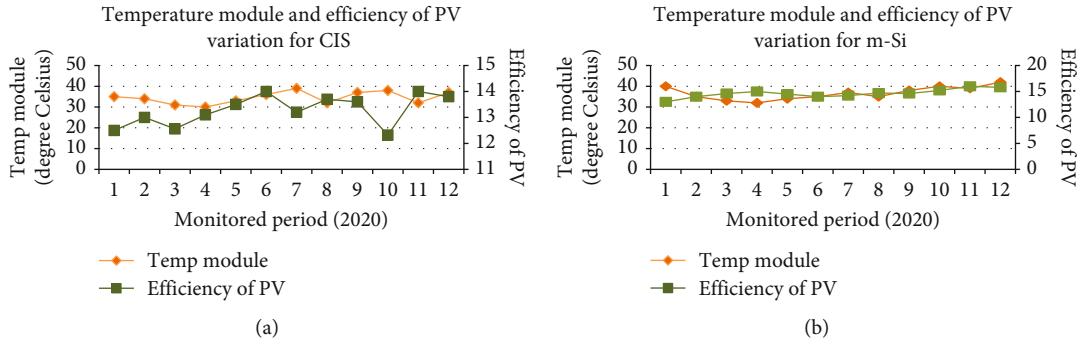

Figure 6: PV efficiency and temp module for (a) CIS and (b) m-Si.

Table 9: System loss, final yield, system efficiency, and capture losses monthly variation for PV modules.

Monitored period (2020)	m-Si				CIS			
	L_S	Y_F	η_{sy}	L_{ACap}	L_S	Y_F	η_{sy}	L_{ACap}
Jan	0.25	4.5	13	1.2	0.24	5.0	11.5	0.52
Feb	0.75	4.8	12.7	1.63	0.21	5.28	11.3	0.64
Mar	0.04	4.9	12	1.54	0.21	5.29	11.8	0.43
Apr	0.02	4.4	11.6	1.26	0.14	4.9	11.4	0.36
May	0.06	4.2	11.8	1.34	0.12	4.5	12.2	0.21
Jun	0.5	3.75	13.2	1.1	0.28	4.25	12.5	0.34
Jul	0.25	4.0	13.4	1.4	0.24	4.29	11.9	0.45
Aug	0.52	4.25	13	1.6	0.21	4.6	12.6	0.47
Sep	0.34	4.9	13.3	1.59	0.19	4.8	12.7	0.38
Oct	0.25	4.75	13.7	1.48	0.15	5.2	11.82	0.27
Nov	0.001	4.2	13.5	1.05	0.02	5.5	12.9	0.25
Dec	0.002	4.5	13.9	1.36	0.005	4.9	13.2	0.22

direction, wind speed, and diffused radiation are continuously measured by the Wattmon solar kit, which is a component of the weather station at the location. Wattmon is a web-based application that allows you to log data, monitor, and control the devices you use. The system's Alternating Current (AC) power output is connected to the electric grid using PowerOne single phase 250 V solar inverters with 1.4 kW and 1.7 kW capacities for m-Si and CIS units, correspondingly. Every six minutes, a real-time gathering mechanism is set up using a PowerOne GPRS kit to monitor the AC and Direct Current (DC) outputs from the PV plants. The presented grid-connected PV module's schematic diagram is depicted in Figure 2. The employed PV technologies detailed specifications are represented in Table 1 and the utilized sensor's technical specifications in the meteorological/weather station are depicted in Table 2.

4. Performance Parameters

4.1. Analysing Performance Metrics. The PV systems' performance is studied in this research using the effectiveness metrics established by the IEC standard 61724 [16] and International Energy Agency (IEA). Reference yield, system losses, final yield, array yield and array, system and PV efficiencies, PR, and CUF are some of the evaluation metrics, and they are all shown in Table 3. The exact energy yields from array could be standardised to the system's regarded power (i.e., 1.3k Wp) [17]. The applicability of these normalised performance measures offers a foundation for comparing PV installations under diverse operating environment. Losses that diminish the effectiveness of the system are caused by radiation and convection heat transfer, both of which are utilised in the generation of power in PV modules. Convective heat transfer occurs in photovoltaic modules as a result of the movement of air across the surface of the module. Radiation is the final means through which heat can be transferred from the PV module to the environment around it. The array capture loss, cell temperature loss, and system loss were the more noticeable losses [18]. Per degree Celsius increase in module temperature over typical test

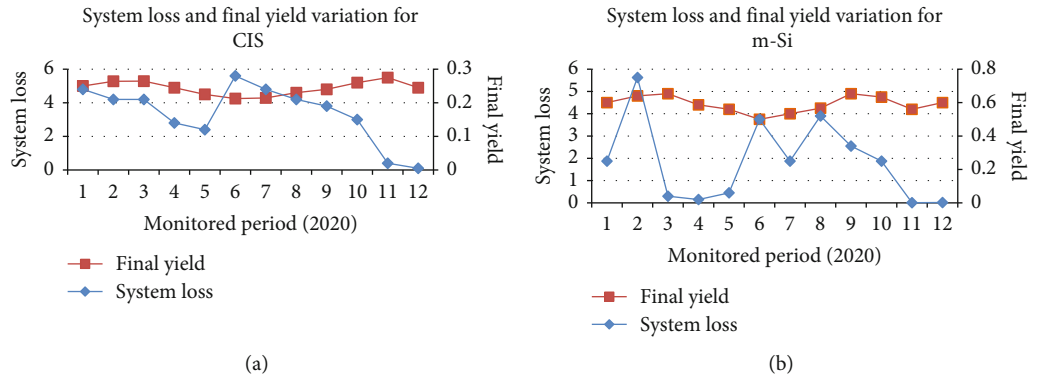

Figure 7: Final yield and system loss of (a) CIS and (b) m-Si.

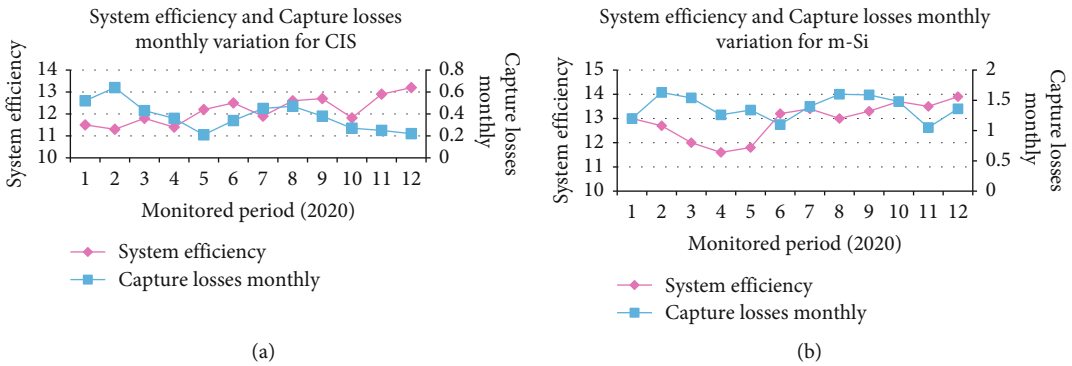

Figure 8: Capture loss and system efficiency of (a) CIS and (b) m-Si.

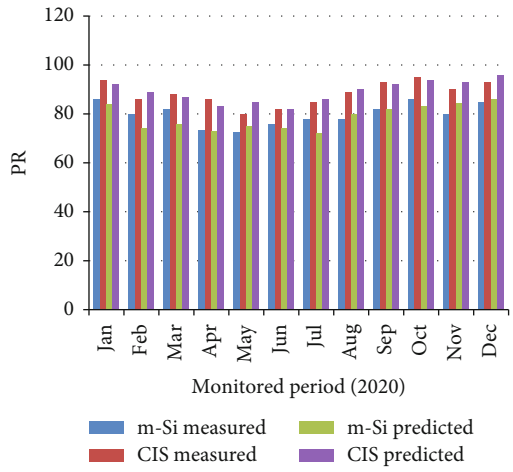

Figure 9: CIS and m-Si PV array's predicted and measured PR comparison.

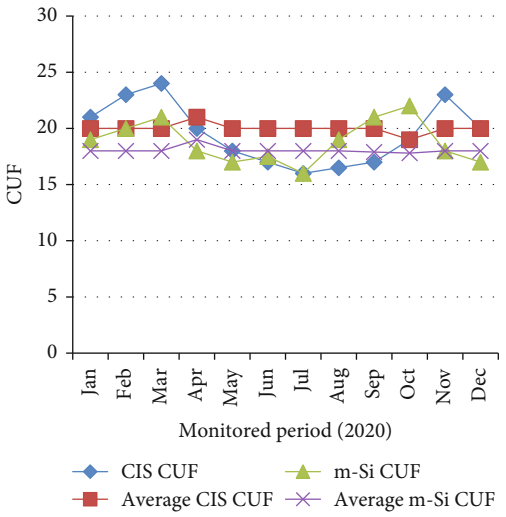

Figure 10: Monthly mean CUF for measured period.

circumstances, the PV module's energy production drops from 0.3 to 0.4 percent [19]. The temperature of the PV system relates to the temperature-related loss. A rise in the external temperature causes the panel temperature to rise, which reduces the amount of power produced.

4.2. Energy Metrics and Embodied Energy. The overall amount of energy needed for all the steps in a producing process, such as installation, fabrication, raw materials, and maintenance, is known as embodied energy E_{em}. To evaluate whether the system either adds to or reduces global warming and also to ascertain the PV system's performance, this assessment is crucial. Three fundamental energy measures are used to calculate a PV system's performance. Table 4 shows their representations as energy production factor (EPF), life cycle conversion efficiency (LCCE), and energy payback time (EPBT). The embodied energy's breakup for

Table 10: Performance comparison.

System's location	Module technique	Power (kWp)	PR	References
Brazil	Polycrystalline silicon (p-Si)	2.2	82.9	[20]
New Zealand	p-Si	10	78	[21]
Spain	m-Si	4.3	69.8	[22]
India	m-Si	3000	60	[23]
Ireland	m-Si	1.72	81.5	[24]

Table 11: Embodied energy's breakup.

Sl. No.	Materials	Embodied energy (kWh)	
		CIS	m-Si
1	M.S. support structure	632.82	575.91
2	Inverter	485.40	264.00
3	PV module	5191.01	460.30
4	Electronic components, maintenance, operation, and cables	653.50	653.50
	Total	6762.73	1952.71

Table 12: PV system's energy metrics.

PV array	EPF	LCCE	EPBT
CIS	1.04	0.1312	0.998
m-Si	0.221	0.1211	4.321

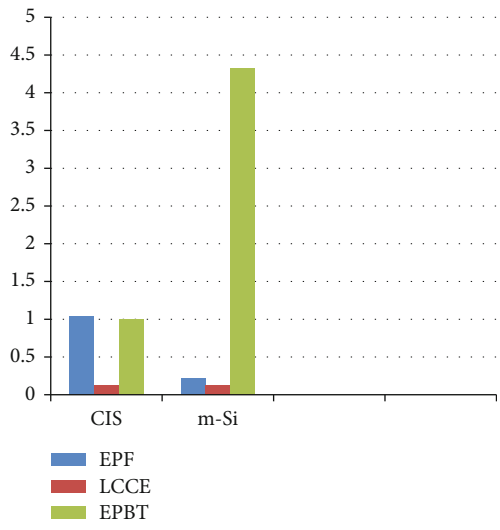

Figure 11: PV equipment's energy metrics.

the CSI and m-Si PV plants was evaluated as 1692.28 kWh and 6865.73 kWh, respectively.where E_{out} is PV system's overall energy generation (kWh/year), T_L is PV system's overall lifetime (years), E_{in} is total energy involved in PV system's installation and fabrication (kWh), E_{sol} is the input of annual solar radiation (kWh), and EM is energy metrics.

5. Results and Discussion

5.1. Meteorological Database. From January to December 2020, the CIS and m-Si PV module's efficiency has been assessed continuously. Figures 3(a) and 3(b) collect and graph the various variables, including diffused radiation, global radiation, wind velocity, clearness index, module surface temperature, and ambient temperature.

The beam radiation were ranges from 5.2 kWh/m^2/d to 3 kWh/m^2/d; the diffused radiation were ranges from 1 kWh/m^2/d to 3.2 kWh/m^2/d; and the clearness index from the months January to December ranges from 0.3 to 0.6. Moreover, the wind velocity were ranges from 2.2 m/s to 4.6 m/s for the monitored period 2020; the ambient temperature ranges from 25°C to 35°C; the m-Si module temperature ranges from 34.2°C to 44.5°C; and the CSI module temperature ranges from 30°C to 40°C. The solar insolation of the CIS and m-Si power plant has been represented in Table 5 and the variations in module temperature, wind velocity, and ambient temperature are depicted in Table 6.

5.2. Energy Yields Analysis. The test site's CIS and m-Si PV plants' evaluated output was contrasted with the findings of the PVsyst simulation, which are shown in Figure 4. In order to minimize the uncertainties, the simulations incorporate the test site's latitude, longitude, and altitude as well as observed climate databases (ambient temperature, worldwide solar radiation, and wind speed). The graph demonstrates that the projected and observed array yields for CIS and m-Si PV technologies followed the similar pattern. It turns out that for both PV systems, the array yield anticipated by the algorithms and the actual observed values correspond very closely. Table 7 illustrates the measured and predicted final yield for CIS and m-Si PV modules.

However, because of the lower in-plane incoming radiation in December compared to the expected amount in August, the observed array yield for both CIS and m-Si PV systems was the lowest. Additionally, it has been found that in the majority of climatic situations, CIS technology outperformed m-Si technology. Furthermore, because the ambient temperature was relatively less during the summer season and the dispersed element of light was larger in incoming

radiation, the CIS technology had observed a substantial yield above the projected value.

5.3. System Efficiency, PV, and Energy Losses Analysis. System loss, array capture loss, and temperature loss seem to be the energy losses taken into account in this research and should be given the appropriate attention. The module temperature was recorded at 44°C and 40°C, correspondingly, which significantly reduces the DC energy yield. In April, temperature losses for CIS and m-Si PV modules were reported to be as 0.224 h/day and 0.236 h/day. The system temperatures' monthly average takes into account daylight hours or from 6 a.m. to 7 p.m. The modules' temperatures for m-Si and CIS PV modules were 39°C and 32°C, correspondingly, during the cold months of November through January because of the decreased temperature losses, which are measured as 0.121 h/day and 0.26 h/day in December. Despite the clear skies and greater mean incident solar insolation in March month, the array's DC energy yield was found to be significantly higher despite high-temperature depreciation. Additionally, a modest increase in DC energy generation is seen from June to September, along with minor changes in temperature degradation for CIS and m-Si PV modules. In any case, India seems to be in a warm, humid region, and because the temperature changes are never negative, the PV array experiences no gains rather than losses. The effectiveness of a PV method is highly influenced by both the module and irradiance temperature. For CIS and m-Si technologies, the mean monthly PV performance ranges from a low of 12.56 percent and 12.32 percent in April to a high of 15.8 percent and 14.6 percent in January. Throughout the year, the CIS technology's mean module temperature is 4°C less than the m-Si technique. The PV effectiveness for both techniques is significantly lower in the hot than it is in the cold leading to increased module temperatures. Month-wise comparison is shown in Table 8. Figures 5(a) and 5(b) shows the temperature loss and yield array for CIS and m-Si. Figures 6(a) and 6(b) shows the PV efficiency and temp module for CIS and m-Si.

However, due to massive wind velocities that lower the module temperatures, a modest gain in PV effectiveness is seen for both PV modules in June and July. Through the year, the effectiveness of CIS PV system is practically on par with that of m-Si innovation. It demonstrates that the CIS system is operating equally well in regards to energy production as that of the m-Si plant underneath the real warm and wet weather conditions of southern India. The m-Si and CIS systems show the greatest L_{ACap} values of 1.63 h/day and 1.05 h/day as well as the lowest values of 0.64 h/day and 0.25 h/day, respectively. Table 9 shows the system loss, final yield, system efficiency, and capture losses monthly variation for PV modules. Figures 7(a) and 7(b) show the final yield and system loss for CIS and m-Si. Figures 8(a) and 8(b) show the capture loss and system efficiency for CIS and m-Si.

5.4. Annual and Monthly Performance Variation. The measurement values at the location for a full year are typically used to comprehensively examine the solar PV installations energy performance. The monthly overall in-plane-solar radiation ranged from 136.25 kWh in December 2020 during cold months to 194.54 kWh in March 2020 while summer months, even during evaluation period (January-December 2020) in this research. The lowest and highest values for standardized monthly energy production for m-Si and CIS PV systems, correspondingly, were 104.15 kWh and 115.25 kWh in December and 148.42 kWh and 162.64 kWh in March, including both. According to the recorded monthly mean energy production for the CIS and m-Si silicon power plants, the three most important environmental elements that determine energy production are the irradiance of the sun, the velocity of the wind, and the temperature of the surrounding environment. Despite all of the advancements, the performance of solar cells is still affected by a wide variety of environmental parameters. Some of these factors include temperature, humidity, wind velocity, light intensity, altitude, and air pressure. The PV array's discharge current gradually increases as the radiation frequency increases, as is obvious. The irradiance has a linear relationship with the DC power that the PV systems produce. However, because of the opposing influence of the system temperature, there is a drop in the effectiveness of solar PV modules.

5.5. CUF and System PR Analysis. The performance ratio (PR) was among the most important factors to consider when evaluating an SPV system's effectiveness. Since PR is a measurement of a PV system's efficiency regardless of where it is installed, it is also known as the "quality factor." Figure 9 displays the simulation of observed PR that was attained during the observation time. It should be remembered that plants function slightly better in the cold than they do in the summertime. This is due to substantial energy inefficiencies in the summer caused by increasing PV module heating at comparatively small wind speeds. For the m-Si plant, the observed monthly PR values were nearly identical to those predicted by the software, however, for the CIS plant, the observed PR values are greater for the majority of the months in 2020.

This explains an improvement of roughly 8% in the CIS system's yearly mean daily PR when contrasted to the m-Si plant. Although CIS technique has a lesser STC conversion effectiveness than m-Si modules, it offers greater performance all year long. Since dispersed light's short waves fractions seem to be more concentrated in the spectrum's ultraviolet and blue end, CIS technique is better able to transform these frequencies into useful energy than m-Si technologies.

There has been no absorbance loss for CIS in the wavelength's lower wavelength region less than 520 nm, which led to an enhancement in the short-circuit power intensity. The solar PV system's cell efficiency and GHI determine the specific location's CUF for the deployed PV system. According to the system's final yield, the CUF eventually fluctuates with the AC power produced. During the maximum summertime in March 2020, the monthly mean CUF is at its highest, reaching 20.16 percent for m-Si systems and 23.09 percent for CIS systems, correspondingly. Both

PV systems' CUF is considerably lower than the mean CUF of the majority of rooftop SPV modules when compared. Moreover, the monthly mean CUF for measured period is shown in Figure 10. Moreover, the presented PV system comparison with other systems is shown in Table 10.

5.6. Analysis of Energy Metrics. For the PV system's real outdoor effectiveness under study, the EPF, EPBT, and LCCE were estimated. Table 11 provides the calculated embodied energy for the PV modules. The m-Si and CIS PV devices' corresponding total embodied energies are calculated to be 6762.73 kWh and 1952.71 kWh. Table 12 and Figure 11 provide information on the PV equipment' energy metrics.

6. Conclusions

In the current study, two colocated smaller scale roof-top PV plants on the campus had their performance compared. The monocrystalline silicon (m-Si) and copper indium selenium (CIS) technology, with capacities of 1.3kWp and 1.62kWp, correspondingly, are the foundations of the grid-connected PV installations. The PV system's behaviour in the winter and muggy climate of southern Tamil Nadu, India, has been represented by the external evaluation. The monthly and yearly performance metrics are evaluated and contrasted with predicted outcomes. The incident solar irradiation and ambient temperature have a significant impact on the module's temperature, which in turn affects the output power. For practically identical incident solar irradiance on the early days used for the study in heat and cold, the CIS PV module produces more power than the m-Si technology. By using the observed site variables as inputs to the modelling programme, the year-round efficiency forecast of the CIS and m-Si PV technologies is in reasonable accordance with the annual energy's observed values injected to the grid with an ambiguity.

Data Availability

The data used to support the findings of this study are included within the article.

Conflicts of Interest

The authors declare that there is no conflict of interest regarding the publication of this article.

Acknowledgments

The authors would like to express their gratitude towards Vellore Institute of Technology, Chennai for providing the necessary infrastructure to carry out this work successfully.

References

[1] A. Guichi, A. Talha, E. M. Berkouk, and S. Mekhilef, "Energy management and performance evaluation of grid connected PV-battery hybrid system with inherent control scheme," *Sustainable Cities and Society*, vol. 41, pp. 490–504, 2018.

[2] F. Perera, "Pollution from Fossil-Fuel Combustion is the Leading Environmental Threat to Global Pediatric Health and Equity: Solutions Exist," *International Journal of Environmental Research and Public Health*, vol. 15, no. 1, p. 16, 2017.

[3] F. Hussain, M. Y. H. Othman, K. Sopian, B. Yatim, H. Ruslan, and H. Othman, "Design development and performance evaluation of photovoltaic/thermal (PV/T) air base solar collector," *Renewable and Sustainable Energy Reviews*, vol. 25, pp. 431–441, 2013.

[4] B. Shiva Kumar and K. Sudhakar, "Performance evaluation of 10 MW grid connected solar photovoltaic power plant in India," *Energy Reports*, vol. 1, pp. 184–192, 2015.

[5] S. Ramesh, J. Seetha, G. Ramkumar et al., "Optimization of solar hybrid power generation using conductance-fuzzy dual-mode control method," *International Journal of Photoenergy*, vol. 2022, Article ID 7756261, 10 pages, 2022.

[6] F. Almonacid, C. Rus, P. J. Pérez, and L. Hontoria, "Estimation of the energy of a PV generator using artificial neural network," *Renewable Energy*, vol. 34, no. 12, pp. 2743–2750, 2009.

[7] A. Batman, F. G. Bagriyanik, Z. E. Aygen, Ö. Gül, and M. Bagriyanik, "A feasibility study of grid - connected photovoltaic systems in Istanbul, Turkey," *Renewable and Sustainable Energy Reviews*, vol. 16, no. 8, pp. 5678–5686, 2012.

[8] T. M. Amirthalakshmi, P. Ramesh, R. Thandaiah, G. Ramkumar, S. Sahoo, and P. Thomas, "A novel approach in hybrid energy storage system for maximizing solar PV energy penetration in microgrid," *International Journal of Photoenergy*, vol. 2022, Article ID 3559837, 7 pages, 2022.

[9] A. El Mouatamid, R. Ouladsine, M. Bakhouya et al., "Modeling and Performance Evaluation of Photovoltaic Systems," in *2017 International renewable and sustainable energy conference (IRSEC)*, pp. 1–7, Tangier, 2017.

[10] A. Chouder, S. Silvestre, N. Sadaoui, and L. Rahmani, "Modeling and simulation of a grid connected PV system based on the evaluation of main PV module parameters," *Simulation Modelling Practice and Theory*, vol. 20, no. 1, pp. 46–58, 2012.

[11] B. Marion, J. Adelstein, K. Boyle et al., "Performance parameters for grid-connected PV systems," in *Conference Record of the Thirty-first IEEE Photovoltaic Specialists Conference, 2005*, pp. 1601–1606, Lake buena Vista, FL, USA, 2005.

[12] G. A. Dávi, E. Caamaño-Martín, R. Rüther, and J. Solano, "Energy performance evaluation of a net plus-energy residential building with grid-connected photovoltaic system in Brazil," *Energy and Buildings*, vol. 120, pp. 19–29, 2016.

[13] S.-K. Kim, J.-H. Jeon, C.-H. Cho, E.-S. Kim, and J.-B. Ahn, "Modeling and simulation of a grid-connected PV generation system for electromagnetic transient analysis," *Solar Energy*, vol. 83, no. 5, pp. 664–678, 2009.

[14] E. Roman, R. Alonso, P. Ibanez, S. Elorduizapatarietxe, and D. Goitia, "Intelligent PV module for grid-connected PV systems," *IEEE Transactions on Industrial Electronics*, vol. 53, no. 4, pp. 1066–1073, 2006.

[15] R. P. Kalidasa, K. Murugavel, and A. Karthick, "Performance analysis and energy metrics of grid-connected photovoltaic systems," *Energy for Sustainable Development*, vol. 52, pp. 104–115, 2019.

[16] I E Commission, *Photovoltaic system performance monitoring-guidelines for measurement, data exchange and analysis*, IEC 61724, 1998.

[17] V. Sharma, A. Kumar, O. S. Sastry, and S. S. Chandel, "Performance assessment of different solar photovoltaic technologies

under similar outdoor conditions," *Energy*, vol. 58, pp. 511–518, 2013.

[18] S. K. Yadav and U. Bajpai, "Performance evaluation of a rooftop solar photovoltaic power plant in Northern India," *Energy for Sustainable Development*, vol. 43, pp. 130–138, 2018.

[19] F. Tahri, A. Tahri, and T. Oozeki, "Performance evaluation of grid-connected photovoltaic systems based on two photovoltaic module technologies under tropical climate conditions," *Energy Conversion and Management*, vol. 165, pp. 244–252, 2018.

[20] L. C. de Lima, L. de Araújo Ferreira, and F. H. B. de Lima Morais, "Performance analysis of a grid connected photovoltaic system in northeastern Brazil," *Energy for Sustainable Development*, vol. 37, pp. 79–85, 2017.

[21] M. Emmanuel, D. Akinyele, and R. Rayudu, "Techno-economic analysis of a 10 kWp utility interactive photovoltaic system at Maungaraki school, Wellington, New Zealand," *Energy*, vol. 120, pp. 573–583, 2017.

[22] A. De Miguel, J. Bilbao, J. Cazorro, and C. Martín, *Performance Analysis of a Grid-Connected PV System in a Rural Site in the Northwest of Spain*, Elsevier Science Ltd, 2002.

[23] K. Padmavathi and S. A. Daniel, "Performance analysis of a 3 MW_p grid connected solar photovoltaic power plant in India," *Energy for Sustainable Development*, vol. 17, no. 6, pp. 615–625, 2013.

[24] L. M. Ayompe, A. Duffy, S. J. McCormack, and M. Conlon, "Measured performance of a 1.72 kW rooftop grid connected photovoltaic system in Ireland," *Energy Conversion and Management*, vol. 52, no. 2, pp. 816–825, 2011.

Hindawi
International Journal of Photoenergy
Volume 2022, Article ID 2845755, 9 pages
https://doi.org/10.1155/2022/2845755

Research Article

A Machine Learning-Based Novel Energy Optimization Algorithm in a Photovoltaic Solar Power System

Kalapala Prasad,[1] J. Samson Isaac,[2] P. Ponsudha,[3] N. Nithya,[4] Santaji Krishna Shinde,[5] S. Raja Gopal,[6] Atul Sarojwal,[7] K. Karthikumar,[8] and Kibrom Menasbo Hadish[9]

[1]*Department of Mechanical Engineering, University College of Engineering Kakinada, JNTUK, Kakinada, Andhra Pradesh 533003, India*
[2]*Department of Biomedical Engineering, Surgical and Critical Care Equipment Laboratory, Karunya Institute of Technology and Sciences, Coimbatore, Tamil Nadu 641114, India*
[3]*Department of Electronics and Communication Engineering, Velammal Engineering College, Chennai, Tamil Nadu 600066, India*
[4]*Department of Electronics and Communication Engineering, Panimalar Engineering College, Chennai, Tamil Nadu 600123, India*
[5]*Computer Engineering Department, Vidya Pratishthan's Kamalnayan Bajaj Institute of Engineering & Technology, Baramati, Maharashtra 413133, India*
[6]*Department of Electronics & Communications Engineering, Koneru Lakshmaiah Education Foundation, Vaddeswaram, Andhra Pradesh 522502, India*
[7]*Department of Electrical Engineering, FET, MJP Rohilkhand University, Bareilly, Uttar Pradesh 243006, India*
[8]*Department of Electrical and Electronics Engineering, Vel Tech Rangarajan Dr. Sagunthala R&D Institute of Science and Technology, Avadi, Chennai, Tamil Nadu 600062, India*
[9]*Faculty of Mechanical Engineering, Arba Minch University, Arba Minch, Ethiopia*

Correspondence should be addressed to Kibrom Menasbo Hadish; kibrom.menasbo@amu.edu.et

Received 4 June 2022; Revised 2 September 2022; Accepted 8 September 2022; Published 28 September 2022

Academic Editor: BR Ramesh Bapu

Performance, cost, and aesthetics are all difficult to beat in today's expanding distributed rooftop solar sector, and flat-plate PV is no exception. Photovoltaics will be able to take advantage of some of their most significant advantages as a result of this marketplace, including the elimination of transmission losses and the generation of power at the point of sale. Concentrated photovoltaic (CPV) technology, on the other hand, represents a viable alternative in the quest for ever-lower normalised energy costs and ever-shorter energy payback times. Material, components, and manufacturing techniques from allied sectors, particularly the power electronics industry, have been adapted to lower system costs and time-to-market for the system under development. The LFR is less than 30 mm wide to maximise thermal efficiency, and a densely packed cell array has been used to maximise electrical output. The Matlab simulations show that the proposed machine learning-based LFR technique has a greater concentration rate than the present LFR method, as demonstrated by the results.

1. Introduction

The usage of distributed energy resources (DERs) including solar power and wind has increased dramatically around the world in recent years [1, 2]. Furthermore, solar energy is a completely free, easily accessible, and scalable renewable resource that may be used in a variety of applications and shown in Figure 1 [3]. The utilisation of solar panels to generate considerable amounts of electricity without the use of fossil fuels will enable the world to transition to a clean energy economy. Several international rules and financial incentives have been implemented to increase solar energy share in the smart grid [4]. It will be difficult for photovoltaic (PV) power plants to expand on a large scale if there is

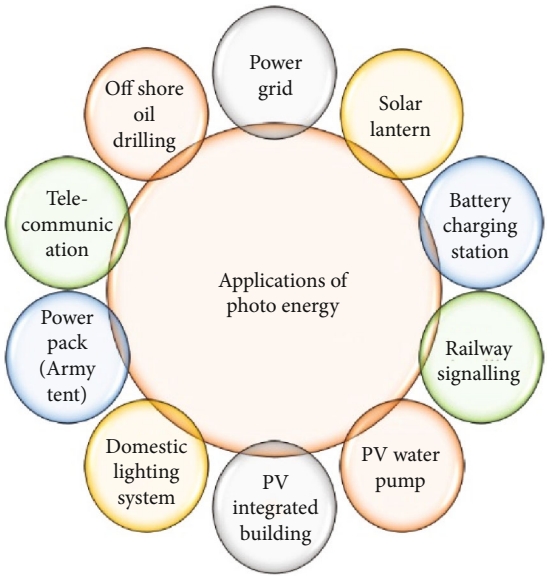

Figure 1: Shows applications of photo energy.

uncertainty in the real-time control and economic benefits they provide. To mitigate the negative effects of PV power on the overall power system and to improve system stability, it has become more important to employ reliable forecasting methods for precisely anticipating PV power [5, 6]. The utilisation of more detailed source data can be utilised to develop more advanced forecasting models, which can then be used to attain an increased average accuracy rate of PV power forecasts using the current power grid smart electricity metres [7].

It was impossible to design a high-efficiency solar energy conversion system long ago while keeping costs down. Using normal methods, it is difficult to evaluate and predict the heat transfer and storage characteristics of a typical solar energy conversion device, such as a solar water heater (SWH) [8]. For the high-performance SWH design, it is vital to be familiar with the relationships that exist between external settings and thermal performance coefficients (CTP). On the other hand, some relationships are challenging to understand for a number of reasons, including [9]. Measurements take time, control experiments are found difficult for conducting, and currently, no model adequately integrates external settings with inherent SWH properties. Methods for assessing energy system attributes [10, 11] and enhancing system performance [12–15] are currently at the forefront of technological development. Although there are certain exceptions to this rule, there are a few. Due to these challenges, as well as cost constraints, the logical design of high-performance SWHs is significantly hampered.

The fact that machine learning assists us in precisely determining the values of CTP with only a few easily measured independent variables is fortunate for us. Using a nonlinear fitting approach and a machine learning technique with proper algorithms, assuming the database is large enough to learn from the correlations in the data, this can be accomplished with relative ease. Using this technique, we can obtain a prediction from the predictive model without having to determine the unique physical models for each CTP. As these research findings illustrate, machine learning technologies have a great deal of potential in the field of energy systems. Power systems are complex, dynamic networks of electrical components that operate in a dynamic environment. The evolution of electricity systems has occurred over several decades. Economic, technological, environmental, and political motivations have all played a role in bringing about these transformations [1–3]. In a smart grid system [4, 5], both energy and information are sent back and forth amongst the numerous stakeholders, allowing for bidirectional energy flow as well as bidirectional information flow. Several factors have contributed to the disruption of the energy system. As a starting point, the rising reliance on renewable energy sources by the power system introduces greater uncertainty. Identifying solutions that allow for the adoption of distributed energy resources in a deregulated electricity market becomes more difficult as customers become more involved in the market [6, 7].

To address these concerns, effective grid planning and operating procedures are required. As a result of the ongoing grid changes [8, 9], both commercial transactions and the physical flow of electricity are becoming increasingly complex. Because of the abundance of data and the instability of information, decision-making has become more difficult than it used to be [10, 11]. Future smart grids will consequently necessitate the development of systems that can continuously monitor, predict, and schedule energy consumption and output in real-time, as well as learn and make decisions.

2. Related Works

Many power system challenges can be broken down into a set of sequential decisions that must be made one after another. Traditional methods include things like programming, convex optimization, and heuristic approaches, to name a few. The advantages and disadvantages of these methods can be better understood by contrasting them with optimisation algorithms on a qualitative level [16, 17]. The mathematical approach known as Lyapunov optimization is an example of a classical mathematical approach [18]. There are several advantages to this strategy, including exact mathematics and real-time management. Because it is based on explicit objective functional expressions, it cannot be used to abstract away many real-world optimization option scenarios from the optimization problem [19]. The validity of the Lyapunov criterion in complicated, high-dimensional settings is also in doubt, according to some researchers.

For any programming style, such as mixed-integer programming, dynamic programming, or stochastic programming, there are a variety of options to choose from. These strategies can be used for a variety of problems, including sequence optimization problems [20–25]. Despite this, it is required to start over with each iteration of this strategy because the results are so complex. Aside from that, the expense of computation makes real-time decision-making impractical in some circumstances. It is difficult to effectively

predict renewable energy generation and demand in real-world situations using computer-aided forecasting techniques [26–30]. In the field of heuristic techniques, particle swarm optimization (PSO) [31, 32] and genetic algorithms (GA) [33, 34] are two examples. The application of a heuristic technique to address optimization problems, particularly nonconvex optimization problems, is effective in dealing with the challenge of large data sets and complex situations. However, because they cannot be quantitatively verified, these procedures are less dependable than other alternatives [35]. It is not necessary to have an exact objective function when using machine learning techniques, as is the case with convex optimization approaches. For its part, machine learning examines the decision-making process in the context of the data that is fed into it. While convex optimization approaches have problems dealing with huge datasets, machine learning does not have this problem. The major importance of the proposed machine learning-based approach is to produce the solar power optimization in the automatic. Hence, there is the result, and computational accuracy was increased. If these attributes get higher values, then, the results are getting huge. So the machine learning model was introduced in power optimization. The current status of the system indicates that machine learning generates online decisions in real time rather than relying on a set of rules that have been established in advance. Machine learning, in contrast to heuristic methods, is more stable and better suited for decision-making tasks than these methods.

3. Background

To focus sunlight onto a stationary absorber, Fresnel reflectors with long, thin segments use a shared focal point. Using a secondary concentrator, the beams are reflected within the accepted angle of incidence. The absorber is responsible for converting this concentrated energy into the thermic fluid. Power or other commercial reasons can be generated through the use of a heat exchanger. The LFRSC modular components can be joined together to form a bigger system, depending on the application being addressed. A rooftop collector is built with Fresnel mirrors and a secondary concentrator with CPCs, which we used in conjunction with the linear Fresnel reflecting mirrors. The PRO-e Package is used to represent the collector assembly and the components that make up the assembly. Radiation from the beam is focused on a stationary receiver employing Fresnel reflectors. The receiver is made up of two absorber tubes made of stainless steel. Secondary CPC reflectors on receivers direct beam radiation to the absorber tube, which serves as the receiver receiving element. A thick pane of glass protects the entire optical system from exposure to the outside environment.

Its dimensions are 2.2 metres in length, 1.383% in width, and 0.351% in height, and it weighs 0.351 kilogrammes. Each mirror array in the CPC system is made up of ten mirrors, which is the maximum number allowed. The sunlight is focused onto two parallel tubes of absorber by a total of twenty mirrors with similar widths. The receiver is made up of two absorber tubes made of stainless steel with a diameter of 25 mm. When it comes to optical design, the angle of incidence of the reflecting mirror is considered crucial. Thin mirrors are often utilised to focus on the absorber at the shared focal point of the reflector and the reflector absorber. Reflected radiation from the neighbouring mirrors should not be hindered by the space between them if they are placed close together. As a result, there is no mirror placed beneath the absorber to prevent the shadow generated by this device and the secondary concentrator. When estimating the radii of tube absorbers, the perpendicular drop lengths from point f on reflector rays are taken into consideration. To design the LFRSC, the tubular absorber served as a starting point for the process [1]. The tubular absorber radius can be approximated as half the width of the mirror element [2] divided by its radius. In this case, the first mirror is located $0.5W + f \tan(\xi_0)$ distance from the planes, whereas the second mirror is located at $0.5W$ distance. Values larger than one-half the length of the mirror should be avoided at all costs. As a result, shading will not be provided. The study refers to the first mirror element as Q_1 in Equation (1) for the time being.

$$Q_1 = R + f \tan(\xi_0), \tag{1}$$

where Q_1 is the first mirror location, R is the absorber radius, and f is the focal distance.

The first mirror element inclination is shown below:

$$\theta_1 = 0.5\left[\frac{(Q_1 + (0.5W)\cos\theta_1)}{(f - (0.5W)\sin\theta_1)}\right]. \tag{2}$$

Upon impacting the second mirror element, its positioning and tilt concerning the aperture plane are adjusted to ensure that it will arrive at its focal point in the proper position. As a result, the first and second mirrors require some more breathing room. As a result, the second mirror shift is referred to as the shift. The second mirror is beginning to shift as in the following equation:

$$S_2 = W \sin\theta_1 \tan(2\theta_2 + \xi_0). \tag{3}$$

The position and tilt of the second mirror w.r.t the aperture plane are critical factors as in the following equation:

$$\left(XX'\right) \text{ is } Q_2 = Q_1 + W\cos\theta_1 + S_2. \tag{4}$$

Generalized equations for the location of shift (S) and its tilt of the n^{th} mirror are obtained using geometrical considerations that are similar to those used in the previous formulations in the following equations:

$$\begin{aligned} Q_n &= Q_{n-1} + W\cos\theta_{n-1} + S_n, \\ S_n &= W\sin\theta_{n-1}\tan(2\theta_n + \xi_0), \\ \theta_n &= 0.5\left[\frac{(Q_n + (0.5W)\cos\theta_n)}{(f - (0.5W)\sin\theta_n)}\right], \end{aligned} \tag{5}$$

With $S_1 = 0$, $\theta_1 = 0$, and $Q_1 = 0.5\,\mathrm{W} + f\ \tan(\xi_0)$ are considered as the initial values for the optimisation process, and the value of n varies between 1 and K, where K is the number of mirrors elements found at either half of the parabolic concentrators. Shift, tilt, and location can be calculated using the iteration method by calculating the equations above for each mirror element. A total of 20 mirror components are required for a complete module with two absorbers. The secondary concentrator profile is designed based on the relationships shown in the following equations:

$$\begin{aligned} R &= \frac{2f}{(1-\cos\phi)}, \\ z &= R\cos(\phi - \theta_{\max}), \\ r &= R\sin(\phi - \theta_{\max}) - a', \\ f_l &= a'(1-\cos(90+\theta_{\max})), \\ 2a' &= \frac{2f}{(1-\cos(90+\theta_{\max}))}, \end{aligned} \tag{6}$$

where f_l is the parabola, $\theta_{\max}$ is the focal length, $2a^{'}$ is the acceptance angle, z is the spherical coordinate, and r is the absorber radius.

4. Proposed Method

With a linear Fresnel reflector (LFR) tracking in the north-south direction, it was thought that the reflector would be able to produce a level of performance that would be acceptable. Because the collector design is the primary focus of this study, it is critical to determine the maximum power output that can be achieved for a certain operational surface temperature of the absorber pipe. The machine learning was supported for automation predictions and optimization. Hence, the reduction of human level was possible. So the optimization will get accurate results while the manual calculations. The proposed model operates on the Carnot cycle. The Carnot cycle eliminates the need to make assumptions regarding piping configuration, flow rate, or the heat engine or heat transfer fluid that would be required to model a complete plant. Even though the energy approach has significant disadvantages, it is still extensively employed in the solar literature, despite the thought taking into account specific applications. The TMY hourly average of energy per unit area (in $\mathrm{W/m^2}$ of the total mirror area of the collector) for an LFR is calculated as follows:

$$E_{x,\mathrm{out}} = Q\left(1 - \frac{T_a}{T_r}\right), \tag{7}$$

where Q is the net transferred heat to external surface of target receiver as in Equation (8) and T_r is temperature.

$$Q = Q_{\mathrm{in}}{}^{*} - Q_{\mathrm{Loss}}, \tag{8}$$

where Q_{Loss} is the term used to describe the heat loss to temperature T_a and it changes based on the receiver setups. In the solar literature, the insulated pipes of nonevacuated with evacuated and cover glazing tubes are the two most common types of receivers to be encountered. The amount of heat that can be delivered to a receiver $Q_{\mathrm{in}}{}^{*}$ from a solar collector total mirror area is determined by three factors: direct sun radiation (DNI) on the mirror area A_m and the normal incidence $\eta_0(0=\theta)$ of the collector. The losses incurred by collectors are not taken into consideration in this computation as in the following equation:

$$Q_{\mathrm{in}}{}^{*} = \mathrm{DNI}.A_m\eta_0(0=\theta).\mathrm{IAM}. \tag{9}$$

In the calculation of optical efficiency and IAM, the following parameters are taken into consideration: reflectance, transmission, absorbance, intercept factor, shadowing, and blocking. Aspects such as the effective mirror aperture area and incidence cosines are also taken into consideration. In order to approximate the elevation of individual mirror elements, the following parameters must be known: the corresponding width (W), slope angle (θ_n), and shift (S_n) of the mirrors that are in operation and this helps in eliminating the shadowing es_n shown in the following equation:

$$es_n = \frac{W}{2}(\sin\theta_n + \sin\theta_{n+1}) - S_n\mathrm{Tan}\theta_p. \tag{10}$$

The height of the sun is often defined by the profile angle, denoted by p, which is the angle θ_p between the plane and sun vector that consists of the rotation axes of each mirror. It is important to note that this plane is perpendicular to the tracking axis of the mirror. The computations of the Sun-Earth geometry are not provided in this document. It is required to use an iterative procedure to estimate the correct slope angle when the elevation varies. Depending on the LFR design, a small separation between mirrors can cause reflected rays from surrounding mirrors to be obstructed. It is proposed that the following steps should be taken to remove blocking, and the equation is shown in the following:

$$eb_n = \frac{W}{2}(\sin\theta_{n+1} + \sin\theta_n) - \frac{S_n h}{(Q_{n+1} + (W/2)\mathrm{Cos}\theta_{n+1} + S_n)}, \tag{11}$$

where h is the receiver height and Q_n is the horizontal distance between the receiver tower and mirror element.

The LFR is biaxially dependent on the angle of direct sunlight incidence when viewed from different directions. Therefore, the transversal and longitudinal planes IAM (θ_t, θ_l) were employed in this work as angle modifiers for rays travelling in IAM(θ_t), which is the considered vertical plane and is found perpendicular to the axis of rotation, and IAM(θ_l), which is perpendicular to the rotation axes. When calculating biaxial IAMs, ray-tracing is frequently employed. IAM(θ_t) and IAM(θ_l) are used to compute the overall optical efficiency, which is the total of the transversal and longitudinal incidence angles of the sunbeams. IAM(θ_t) and IAM(θ_l) are used to determine the overall optical efficiency. The estimation of hourly stagnation temperatures, $T_{r,\max}$, is

made possible by an optical efficiency that is dependent on the incidence angle. The temperature reaches equilibrium when the amount of heat lost to the environment equals the amount of heat absorbed by the atmosphere and shown in the following equation.

$$T_{r,\max} = T_a + \frac{\mathrm{DNI}.\eta_0(\theta = 0).\mathrm{IAM}.A_m}{U_L A_r}, \tag{12}$$

where U_L is the coefficient of heat loss and A_r is the receiver area.

The heat loss coefficient is denoted by UL, while the receiver area is denoted by Ar. The captured radiation would be squandered if the stagnation temperature dropped below the desired operating temperature, as we anticipated. As a result, the collector has been rendered inoperable. Heat loss was estimated using a correlation of the parallel plate, which takes into account both convection and radiation heat losses from the receiver's bottom, together with conduction from the insulated sidewalls. Parallel plate correlation was used to estimate the heat loss. This results in a loss of the form Q_{Loss} equal to the following equation:

$$Q_{\mathrm{Loss}} = A_r U_L (T_r - T_a). \tag{13}$$

4.1. Classifier. An input layer I with a two-dimensional representation is followed by hidden convolution and pooling layers, as well as an output layer that is totally connected. Each convolution layer neuron has nonlinear kernels, which divide input into receptive fields as it passes through the layer. Following the completion of convolution at the k^{th} kernel in the l^{th} convolution layer, we can compute the following results in the following equation:

$$f_l^k(p, q) = \sum_c \sum_{x,y} i_c(x, y) e_l^k(u, v), \tag{14}$$

where $i_c(x, y) - (x, y)^{\mathrm{th}}$ is the element of channel c for I and $e_l^k(u, v) - (u, v)^{\mathrm{th}}$ is the element of kernel k for layer l.

Using a sweeping average or maximum function across tiny patches of convolution output, it is possible to avoid overfitting on the training set, resulting in an even lower dimension of the returned features. Finally, the fully connected layer establishes a connection between the collected features and the target label of the underlying classification or regression operation. The classifier is the circuit which produces the different heat source classification. Each convolution layer neuron has nonlinear kernels, which divide input into receptive fields as it passes through the layer. Based on this classification, the proposed model provides the quality optimization while compared with the existing models. In applications where local spatial and temporal correlations of data are important, the convolution and pooling layers of the CNN achieve state-of-the-art performance because they process their local input patches at the same time, a feature known as parallel processing. As a result, in real-world applications, our model outperforms SAE, ANNs, and LSTM models. By using a densely packed cell array to maximise electrical output, the LFR is less than 30 mm wide, which helps to maximise thermal efficiency. To maximise electrical output, the LFR is less than 30 mm broad. In addition to the kernel-based CNN utilised in the previous study, recent research has developed spectral graph convolutions to capture spatial patterns in graph-structured power system datasets. The convolution operation of the graph CNN is computed for an N-node graph with D -dimensional features $X \in R^{N \times D}$, adjacency matrix A, and degree matrix D in the following equation:

$$f(X, A) = \sigma\left(D^{-0.5} A D^{-0.5} X W\right), \tag{15}$$

where W is the weighted matrix at the convolution layer.

The linear Fresnel reflector was constructed and produces the quality solar tracking in the north-south direction. So the solar light energy optimization will increase due to these activities. There is also no mirror placed beneath the absorber to prevent the shadow generated by this device and the secondary concentrator.

5. Results and Discussions

The results of the proposed LRF with existing models are shown between Figures 2–5. The Analytical Hierarchy Process (AHP) was used to handle the issue of assigning importance to client needs in QFD research, which was previously addressed by other methods (AHP). For concept design modifications to be evaluated against consumer and technical criteria as well as their priorities while using an AHP framework, the addition of a Pugh matrix must be made to the framework. It is a difficult technique to execute an AHP, QFD, and Pugh matrix combination because of their interdependence. When used together, QFD and AHP are complementary strategies that can be utilised to aid in the prioritisation of technical difficulties. This will not be accomplished just through the use of the Pugh matrix. As a result, the more difficult technique was able to discern between the different notions. The researchers emphasised that they had a 15% preference for the Elevation Linear Fresnel Reflector (ELFR) design over the circular method in their study. Here, the Matlab is the simulation tool used to compute the performance of the proposed model. This tool is used to gather the results and help to compare the proposed model with the existing models. An often-heard criticism of quantitative factor analysis and adaptive hypothesis testing is that the results can be highly dependent on the criteria that are used in the procedure. As a result of this selection, various models emerge as the greatest. To address this issue, thorough technical and economic research, as well as comparisons with existing LFR designs, has been carried out.

The improved performance of the LFR can be observed immediately after installation. The LFR increases energy consumption by 13%, adds 274 additional operating hours per year, and reduces land use by 17% by keeping the working temperature at 300°C all year. The H-variable arrangement, which is a layout of horizontal mirror spacing specified for shadowing at a sun transverse angle of 45°, is an improvement when compared to the present

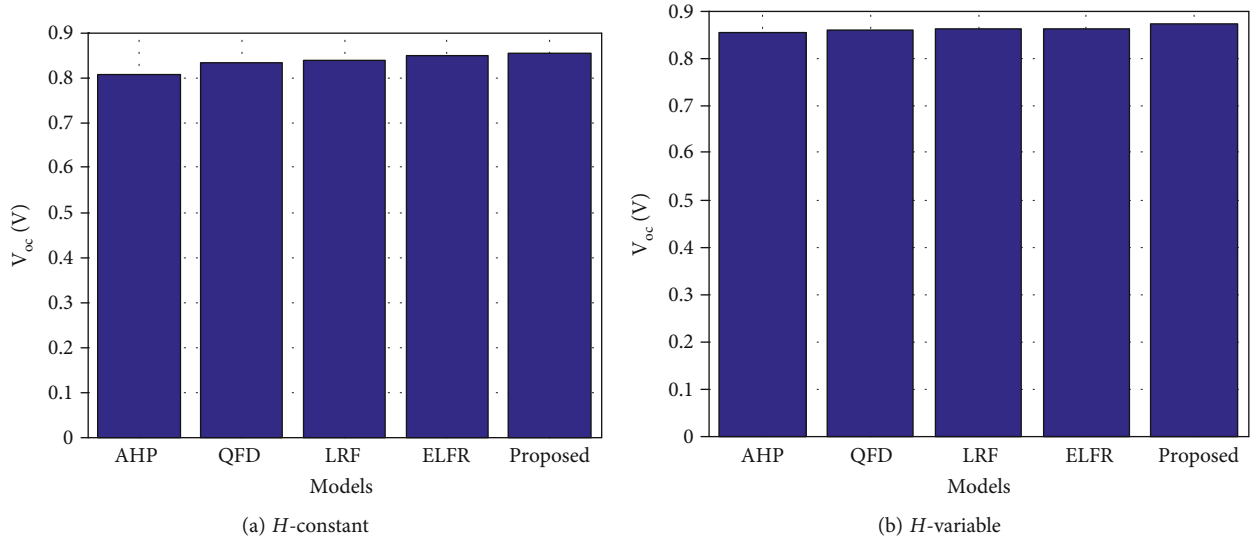

(a) *H*-constant (b) *H*-variable

Figure 2: Variances in open-circuit voltage.

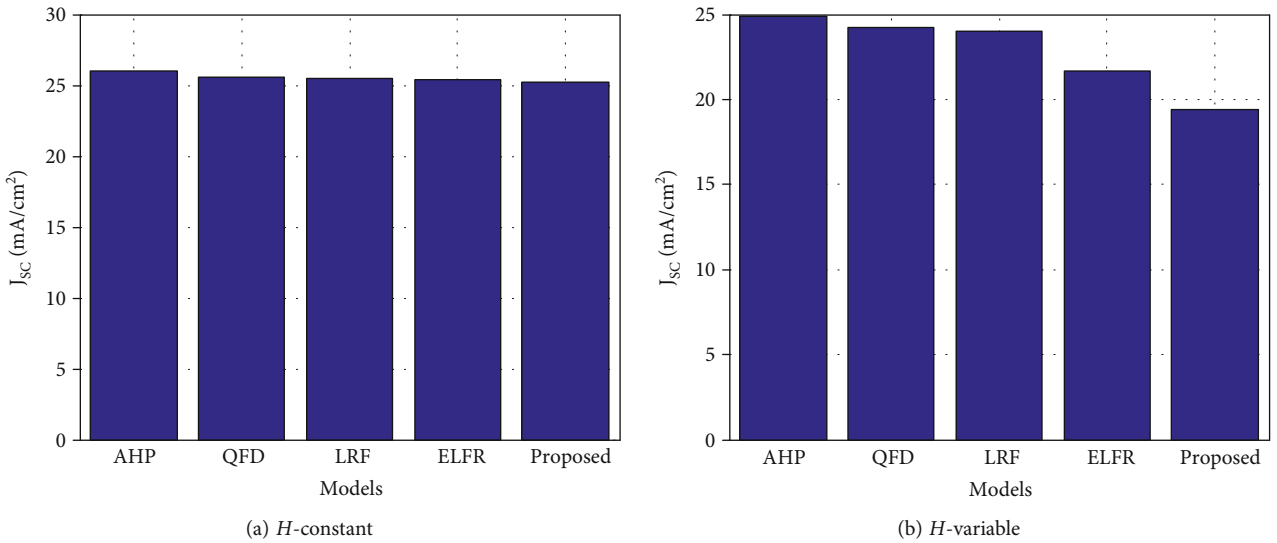

(a) *H*-constant (b) *H*-variable

Figure 3: Short circuit current.

arrangement. The energy increase over a standard narrow constant horizontal mirror spacing configuration, denoted by the *H*-constant, is predicted to be 23%. The annual optical efficiency of the LFR is expected to be 49%, compared to 39% for the H-constant models. These figures are equal when compared to the annual optical efficiency of the Fresdemo LFR, which is 43% every year. Even though the LFR has certain potential financial drawbacks, it is still worth investigating. The cost per unit of energy increases by 2% and 6% for *H* -constant due to the cost associated with elevating components. In a scenario with high land costs, the cost per unit of energy for the LFR would be reduced by 60% if component costs were reduced by 60% compared to the *H*-constant.

The design that is most appropriate for a given situation will be dictated by the priorities that have been established. The LFR has the potential to be extremely beneficial, when additional factors are taken into consideration, effective land use becomes even more advantageous. Solar thermal power plants will benefit from higher temperatures for longer periods during the day, increasing the number of full load hours and the amount of storage available. Major modifications are required for an electricity-producing plant that uses ELFRs to overcome the system's rising capital costs and increasing complexity. The utilisation of more detailed source data can be utilised to develop more advanced forecasting models, which can then be used to attain an increased average accuracy rate of PV power forecasts. This was improving the use of minimum utilisation while the power forecasting was dry. The constraints of the LFR must be addressed, and the cost-effectiveness of the technology must be enhanced. To keep the cost and complexity of the prototype as low as possible, the team developed serial

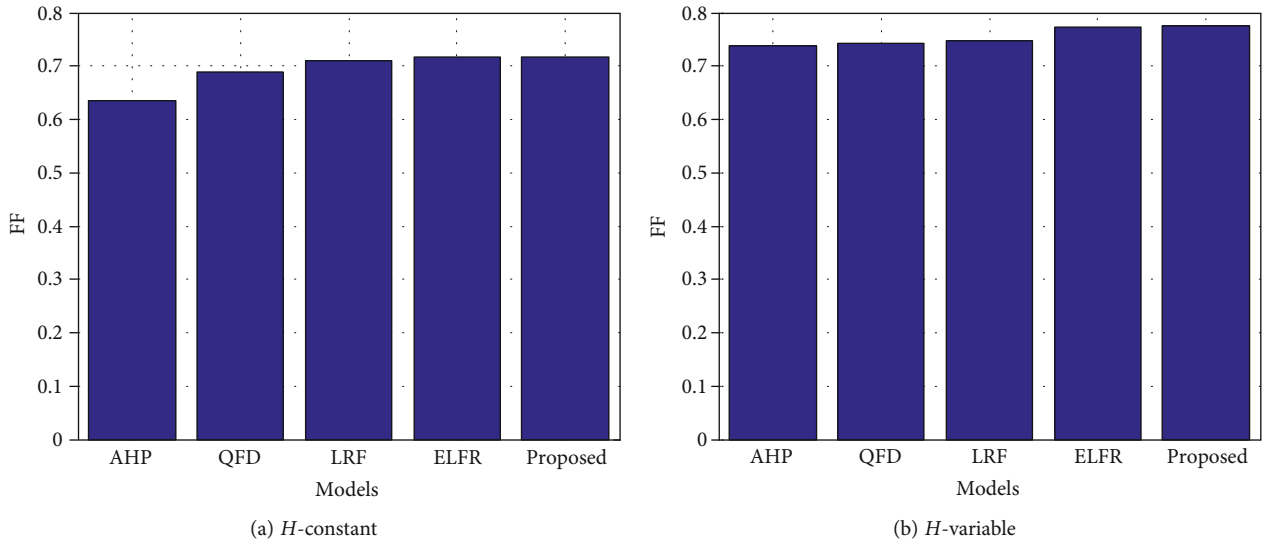

(a) H-constant (b) H-variable

Figure 4: Fill factor.

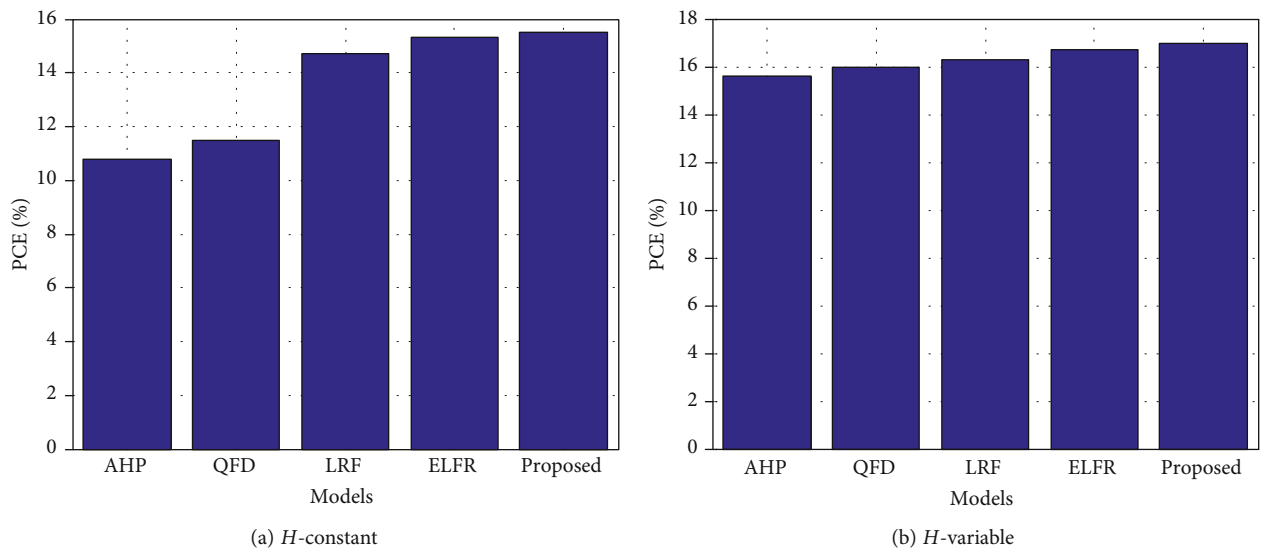

(a) H-constant (b) H-variable

Figure 5: Power conversion efficiency.

communication boards that ease control while minimising cabling and auxiliary power demands. The adoption of embedded control systems in large-scale installations would be advantageous because it would make things even easier to manage. The tracking of solar lights was too important to optimize the power in various proposed methods. The computation of the different methods getting the motor rotation on solar light tracking is slightly less than the proposed model predictions. The proposed model analyzes the high power location and time in the smart machine leaning method. So the proposed model gets more results compared with the other existing models.

6. Conclusions

In this paper, we study the distributed rooftop solar, i.e., LFR performance. LFR can take advantage of some of their most significant advantages, such as the removal of transmission losses and the generation of electricity at the point of sale. Concentrated solar power technology, on the other hand, is a realistic option when it comes to achieving ever-lower normalised energy costs and ever-shorter energy payback times. For CPV applications, materials, components, and manufacturing techniques from the power electronics sector, in particular, have been adapted to lower system costs and time to market, as well as to improve system performance and reliability. As a result of using a densely packed cell array to maximise electrical output, the LFR is less than 30 mm wide, which helps to maximise thermal efficiency. To maximise electrical output, the LFR is less than 30 mm broad. The Matlab simulations suggest that the proposed machine learning-based LFR technique has a higher concentration rate than the current LFR technique, which is supported by the results of the experiment.

Data Availability

The data used to support the findings of this study are included within the article. Further data or information is available from the corresponding author upon request.

Conflicts of Interest

The authors declare that there are no conflicts of interest regarding the publication of this paper.

Acknowledgments

The authors appreciate the supports from Arba Minch University, Ethiopia, for the research and preparation of the manuscript. The authors thank Velammal Engineering College, MJP Rohilkhand University, and Vel Tech Rengarajan Dr. Sagunthala R&D Institute of Science and Technology for providing assistance to this work.

References

[1] O. Erixno, N. Abd Rahim, F. Ramadhani, and N. N. Adzman, "Energy management of renewable energy-based combined heat and power systems: a review," *Sustainable Energy Technologies and Assessments*, vol. 51, article 101944, 2022.

[2] E. W. Ramde, E. T. Tchao, Y. A. K. Fiagbe, J. J. Kponyo, and A. S. Atuah, "Pilot low-cost concentrating solar power systems deployment in sub-Saharan Africa: a case study of implementation challenges," *Sustainability*, vol. 12, no. 15, p. 6223, 2020.

[3] M. E. Zayed, J. Zhao, A. H. Elsheikh, W. Li, S. Sadek, and M. M. Aboelmaaref, "A comprehensive review on dish/Stirling concentrated solar power systems: design, optical and geometrical analyses, thermal performance assessment, and applications," *Journal of Cleaner Production*, vol. 283, article 124664, 2021.

[4] S. Wu, C. Wang, and R. Tang, "Optical efficiency and performance optimization of a two-stage secondary reflection hyperbolic solar concentrator using machine learning," *Renewable Energy*, vol. 188, pp. 437–449, 2022.

[5] A. Latif, S. S. Hussain, D. C. Das, and T. S. Ustun, "State-of-the-art of controllers and soft computing techniques for regulated load frequency management of single/multi-area traditional and renewable energy based power systems," *Applied Energy*, vol. 266, article 114858, 2020.

[6] R. Uthirasamy, V. Kumar Chinnaiyan, S. Vishnukumar et al., "Design of boosted multilevel DC-DC converter for solar photovoltaic system," *International Journal of Photoenergy*, vol. 2022, Article ID 1648474, 23 pages, 2022.

[7] Z. D. Cheng, X. R. Zhao, Y. L. He, and Y. Qiu, "A novel optical optimization model for linear Fresnel reflector concentrators," *Renewable Energy*, vol. 129, pp. 486–499, 2018.

[8] H. S. Dhiman and D. Deb, "Fuzzy TOPSIS and fuzzy COPRAS based multi-criteria decision making for hybrid wind farms," *Energy*, vol. 202, article 117755, 2020.

[9] Z. Zeng, D. Ni, and G. Xiao, "Real-time heliostat field aiming strategy optimization based on reinforcement learning," *Applied Energy*, vol. 307, article 118224, 2022.

[10] A. Khosravi, M. Malekan, J. J. G. Pabon, X. Zhao, and M. E. H. Assad, "Design parameter modelling of solar power tower system using adaptive neuro- fuzzy inference system optimized with a combination of genetic algorithm and teaching learning-based optimization algorithm," *Journal of Cleaner Production*, vol. 244, article 118904, 2020.

[11] A. P. Gonzalo, A. P. Marugán, and F. P. G. Márquez, "Survey of maintenance management for photovoltaic power systems," *Renewable and Sustainable Energy Reviews*, vol. 134, article 110347, 2020.

[12] H. A. Maddah, M. Bassyouni, M. H. Abdel-Aziz, M. S. Zoromba, and A. F. Al-Hossainy, "Performance estimation of a mini-passive solar still _via_ machine learning," *Renewable Energy*, vol. 162, pp. 489–503, 2020.

[13] C. Liu, Q. Ma, Z. J. Luo et al., "A programmable diffractive deep neural network based on a digital-coding metasurface array," *Nature Electronics*, vol. 5, no. 2, pp. 113–122, 2022.

[14] X. Fu, Y. Zhou, F. Yang et al., "A review of key technologies and trends in the development of integrated heating and power systems in agriculture," *Entropy*, vol. 23, no. 2, p. 260, 2021.

[15] R. Pirayeshshirazinezhad, S. G. Biedron, J. A. D. Cruz, S. S. Guitron, and M. Martínez-Ramón, "Designing Monte Carlo simulation and an optimal machine learning to optimize and model space missions," *Access*, vol. 10, pp. 45643–45662, 2022.

[16] N. Yuvaraj, K. Praghash, R. A. Raja, and T. Karthikeyan, "An investigation of garbage disposal electric vehicles (GDEVs) integrated with deep neural networking (DNN) and intelligent transportation system (ITS) in smart city management system (SCMS)," *Wireless Personal Communications*, vol. 123, no. 2, pp. 1733–1752, 2022.

[17] M. Hasan, M. Warburton, W. C. Agboh et al., "Human-like planning for reaching in cluttered environments," in *2020 IEEE International Conference on Robotics and Automation (ICRA)*, pp. 7784–7790, Paris, France, 2020, May.

[18] Z. Tong, J. Cai, J. Mei, K. Li, and K. Li, "Dynamic energy-saving offloading strategy guided by Lyapunov optimization for IoT devices," *IEEE Internet of Things Journal*, 2022.

[19] A. Kumar, G. Wu, M. Z. Ali, R. Mallipeddi, P. N. Suganthan, and S. Das, "A test-suite of non-convex constrained optimization problems from the real- world and some baseline results," *Swarm and Evolutionary Computation*, vol. 56, article 100693, 2020.

[20] S. Ghimire, R. C. Deo, H. Wang, M. S. Al-Musaylh, D. Casillas-Pérez, and S. Salcedo-Sanz, "Stacked LSTM sequence-to-sequence autoencoder with feature selection for daily solar radiation prediction: a review and new modeling results," *Energies*, vol. 15, no. 3, p. 1061, 2022.

[21] A. Peloni, A. V. Rao, and M. Ceriotti, "Automated trajectory optimizer for solar sailing (atoss)," *Aerospace Science and Technology*, vol. 72, pp. 465–475, 2018.

[22] C. Feng, J. Zhang, W. Zhang, and B. M. Hodge, "Convolutional neural networks for intra-hour solar forecasting based on sky image sequences," *Applied Energy*, vol. 310, article 118438, 2022.

[23] M. Premkumar, P. Jangir, C. Ramakrishnan, G. Nalinipriya, H. H. Alhelou, and B. S. Kumar, "Identification of solar photovoltaic model parameters using an improved gradient-based optimization algorithm with chaotic drifts," *IEEE Access*, vol. 9, pp. 62347–62379, 2021.

[24] B. Gobinathan, M. A. Mukunthan, S. Surendran et al., "A novel method to solve real time security issues in software industry using advanced cryptographic techniques," *Scientific Programming*, vol. 2021, Article ID 3611182, 9 pages, 2021.

[25] Z. L. Li, P. Li, Z. P. Yuan, J. Xia, and D. Tian, "Optimized utilization of distributed renewable energies for island microgrid clusters considering solar-wind correlation," *Electric Power Systems Research*, vol. 206, article 107822, 2022.

[26] X. Xu, Z. Wei, Q. Ji, C. Wang, and G. Gao, "Global renewable energy development: influencing factors, trend predictions and countermeasures," *Resources Policy*, vol. 63, article 101470, 2019.

[27] N. Yuvaraj, K. Praghash, and T. Karthikeyan, "Data privacy preservation and trade-off balance between privacy and utility using deep adaptive clustering and elliptic curve digital signature algorithm," *Wireless Personal Communications*, vol. 2021, article 3611182, pp. 1–16, 2021.

[28] J. Gao, H. Wang, and H. Shen, "Smartly handling renewable energy instability in supporting a cloud datacenter," in *2020 IEEE international parallel and distributed processing symposium (IPDPS)*, pp. 769–778, IEEE, 2020.

[29] L. L. Li, S. Y. Wen, M. L. Tseng, and C. S. Wang, "Renewable energy prediction: a novel short-term prediction model of photovoltaic output power," *Journal of Cleaner Production*, vol. 228, pp. 359–375, 2019.

[30] F. Rodríguez, A. Fleetwood, A. Galarza, and L. Fontán, "Predicting solar energy generation through artificial neural networks using weather forecasts for microgrid control," *Renewable Energy*, vol. 126, pp. 855–864, 2018.

[31] M. Sharif, J. Amin, M. Raza, M. Yasmin, and S. C. Satapathy, "An integrated design of particle swarm optimization (PSO) with fusion of features for detection of brain tumor," *Pattern Recognition Letters*, vol. 129, pp. 150–157, 2020.

[32] S. S. Band, S. Janizadeh, S. Chandra Pal et al., "Novel ensemble approach of deep learning neural network (DLNN) model and particle swarm optimization (PSO) algorithm for prediction of gully erosion susceptibility," *Sensors*, vol. 20, no. 19, p. 5609, 2020.

[33] C. K. H. Lee, "A review of applications of genetic algorithms in operations management," *Engineering Applications of Artificial Intelligence*, vol. 76, pp. 1–12, 2018.

[34] T. Harada and E. Alba, "Parallel genetic Algorithms," *ACM Computing Surveys (CSUR)*, vol. 53, no. 4, pp. 1–39, 2021.

[35] S. Alseekh, A. Aharoni, Y. Brotman et al., "Mass spectrometry-based metabolomics: a guide for annotation, quantification and best reporting practices," *Nature Methods*, vol. 18, no. 7, pp. 747–756, 2021.

Hindawi
International Journal of Photoenergy
Volume 2022, Article ID 4931922, 8 pages
https://doi.org/10.1155/2022/4931922

Research Article

Flexible Polymer Solar Cells with High Efficiency and Good Mechanical Stability

I. Kathir,[1] Santaji Krishna Shinde,[2] C. Parswajinan,[3] Sudheer Hanumanthakari,[2,4] K. Loganathan,[5] S. Madhavarao,[6] A. H. Seikh,[7] M. H. Siddique,[8] and Manikandan Ganesan[9]

[1]*Department of Electrical & Electronics Engineering, V.S.B. Engineering College, Karur, 639111 Tamil Nadu, India*
[2]*Department of Computer Engineering, Vidya Pratishthan's Kamalnayan Bajaj Institute of Engineering & Technology, Baramati, Pune, 413133 Maharashtra, India*
[3]*Department of Mechanical Engineering, Sri Sairam Engineering College, Chennai, 600044 Tamil Nadu, India*
[4]*Department of Data Science and Artificial Intelligence, Faculty of Science and Technology, ICFAI Foundation for Higher Education, Hyderabad, India*
[5]*Department of Mechanical Engineering, Rajalakshmi Engineering College, Chennai, 602105 Tamil Nadu, India*
[6]*Department of Mechanical Engineering, Sagi Rama Krishnam Raju Engineering College, Bhimavaram, 534204 Andhra Pradesh, India*
[7]*Mechanical Engineering Department, College of Engineering, King Saud University, P.O. Box 800, Al-Riyadh 11421, Saudi Arabia*
[8]*Intelligent Construction Automation Centre, Kyungpook National University, Daegu, Republic of Korea*
[9]*Department of Electromechanical Engineering, Faculty of Manufacturing, Institute of Technology, Hawassa University, Ethiopia*

Correspondence should be addressed to Manikandan Ganesan; mani301090@hu.edu.et

Received 24 June 2022; Revised 6 August 2022; Accepted 9 August 2022; Published 22 September 2022

Academic Editor: Br Ramesh Bapu

Single-junction polymer solar cells have demonstrated exceptional power conversion efficiency. Interlayer adhesion will be critical in building flexible polymer solar cells since inorganic conveyance layers would surely break. Aluminium-doped zinc oxide modified by polydopamine has emerged as a viable electron transportation layer in polymer solar cells, enhancing mechanical qualities by offering a high degree of flexibility and adhesion to the active layer. Power conversion efficiency of 12.7% is achieved in nonfullerene polymer solar cells built on PBDB-T2F:IT-4F with aluminium-doped zinc oxide 1.5% polydopamine electron transporting layer. Furthermore, the device based on Ag-mesh wire-wound electrodes has a power conversion efficiency of 11.5% and retains more than 90% of original power conversion efficiency afterward 1500 cycles of bending. For implantable and adaptable polymer solar cells for wide areas, roll-to-roll fabrication of inorganic electron transport layers is advantageous because of their mechanical resilience and thickness insensitivity.

1. Introduction

Polymer solar cells [1] have studied extensively as attractive substitute to development of the sustainable photovoltaic technology because of their ability to be manufactured by vast chemical functionalization whereas the sustaining capabilities such as low density, stretchability, and programmable visibility [2, 3]. Power conversion efficiency (PCE) of more than 14% has been obtained in laboratory size using polymer solar cells (PSCs) [4] so far. Flexible, long-lasting, and low-cost electronic components are essential to making flexible and wearable over a vast area PSCs a reality in the manufacturing process [5]. Additionally, many papers have concentrated on the fabrication of superior photoelectric, substrate lack of sensitivity, and mechanical characteristics in actively and interface materials [6] in addition to those generating stretchy transparent conductive electrodes [7, 8]. Recently, the idea of a metal oxide transport layer has been floated around a replacement for the

hygroscopic and acidic PEDOT: PSS hole transporting layer (HTL), as well as the fullerene derivative electron transport layer that has an amalgamation problem [9–14]. There are numerous advantages of using ZnO as an electron transport layer material [15] including low cost, easy accessibility, environmental friendliness, excellent stability, and photochromic capabilities, and the applications of solar cells are shown in Figure 1 [16].

As a result, the commonly used sol-gel-derived ZnO exhibits surface flaws that can be linked to interstitial zinc or adsorbed oxygen. Due to ZnO's relatively poor conductivity, it would not be applicable to large wrap printing since it does not create thick layers [17–20]. There are numerous ways to passivate ZnO's surface imperfections and increase its conductivity, such as using aluminium-doped ZnO [21–23]. However, in a prior study, we developed AZO nanoparticles (NPs) that are highly conductive and surfactant-stable, allowing for outstanding a thick adhesive improves both storage stability and performance characteristics of more than 80 nm [24–26]. For flexible and wearable polymer solar cell applications, inorganic AZO's intrinsic brittleness and low stickiness limit its use. For this reason, in polymer solar cells, AZO electron transport layer shattering and operative layer interparticle deformation are inevitable [27–29]. This can have a significant impact on charge transit and extraction. As far as we are aware, there has been no official report on the subject matter. Polyvinylphenol (PVP), an insulating polymer, can be doped into an indium oxide (In_2O_3) a preterminology approach and processed at 225°C to produce polycrystalline films [30–35]. These works shows that thermal annealing temperatures are too high for flexible PSCs made of PET, which has a lower glass transition temperature than other plastic substrates [36]. Thus, our aim is to produce polymer solar cells that can be bendable with consistent solar behavior and roll-to-roll printing for huge area production, inorganic electron transport layers with such width lack of compassion, mechanical durability, and interfacial adhesion qualities. PDA has been added to crucifix nanostructures with AZO to create electron transport layer with adhesiveness in situ in order to achieve a bendable electron transport layer.

2. Methodology and Materials

Inorganic material long-term stability would be substantially harmed by the high PVP doping concentration. It is still possible to use an inorganic carrying layer in flexible polymer solar cells with good mechanical properties, though, thanks to this approach. A unique bendable AZO derivative was used as an electron transport layer in flexible PSCs that were produced in situ by adding low-content PDA to AZO. Intense hydrogen-bonding connections between molecular constituents are established. Because of the PDA modification, the AZO exhibits outstanding mechanical properties, including strong electron mobility at low temperatures and good adhesiveness between organic active layer and the interfacial area. When using PBDBT-2F:IT-4F with aluminium-doped zinc oxide:1.5% polydopamine (PDA) electron transport layer, nonfullerene PSCs can achieve power conversion efficiency of 12.7%. The fully flexible polymer solar cells have also achieved a significant power conversion efficiency of around 11.5%. According to our knowledge, this is the most efficient flexible PSC on the market. After 1500 bending cycles, the flexible gadget retains more than 90% of its initial power conversion efficiency. After peeling 3M tape ten times, the AZO active layer is perfectly formed. Just a slit of PDA is visible, demonstrating excellent interlayer adhesion. Fully flexible polymer solar cells can now take use of the improved mechanical qualities of modified AZO electron transport layers. For mass manufacture of solar modules, it is even more favorable because of its protracted durability and depth insensitivity (up to 80 nm).

3. Result and Discussion

The optical characteristics of AZO and the PDA-modified AZO have been studied using transmittance and photoluminescence (PL) measurements inserting insulated PDAs in order to study it. PDA-modified AZO films showed improved flexibility more than 90% in the range of specific wavelength of 450–850 nm, making them suitable for use as electron transport layers in inverted photovoltaic cells (PCs).

As shown in Figures 2(a)–2(d), the oxygen deficiency and the ZnO bond O_2 ions show up in the O 1s XPS spectra at 530.1 and 531.15 eV, respectively. A drop in the strength of the second peak at 531.5 eV indicates that the PDA has effectively movement that occurs and traps in the PDA-modified AZO. Because of the N-Zn bond interaction between AZO and PDA, the X-ray photoelectron spectroscopy spectra of aluminium-doped zinc oxide and the polydopamine-changed AZO exhibit a modest change in the peak location of N 1s toward a low specific term. AZO and polydopamine-modified aluminium-doped zinc oxide 2p X-ray photoelectron spectroscopy spectra are also shown. Aluminium-doped zinc oxide and polydopamine interact via the N-Zn link, as seen by the shifting at the top of zinc 2p 3/2 for the polydopamine-modified compound.

Using this method of AZO and AZO changed by PDA, the signal intensity of UV photoelectron spectroscopy has been examined (UPS). Figure 2 shows that the equivalent zones of conductivity for aluminium-doped zinc oxide, AZO:1.0% polydopamine, AZO:1.5% PDA, and AZO:2.0 percent PDA are -4.30, -4.24, -4.11, and -4.17 eV, respectively; for AZOA, better frequency syncing with lowest unoccupied molecular orbital is seen for AZO:1.5 percent PDA when used as electron transporting layer in polymer solar cells, which is commensurate with the higher photocurrent. The XRD pattern measurement of aluminium-doped zinc oxide and the polydopamine-modified aluminium-doped zinc oxide demonstrates showing that the crystalline nature of AZO is unaffected by the insertion of PDA, while revealing a typical wurtzite crystal structure [30]. In light of the data presented herein, we can say with confidence that using AZO in PDA improves ohm contact with the active layer while simultaneously reducing flaws, making it a perfect electron transport layer to increase performance of the component. As far as we can determine, the majority of electron transport layers are used in high-performance PSCs that are less than 2–10 nanometers thick because of their low conductivity.

As a result, new electron transport layer materials with great charge mobility have been developed recently in order

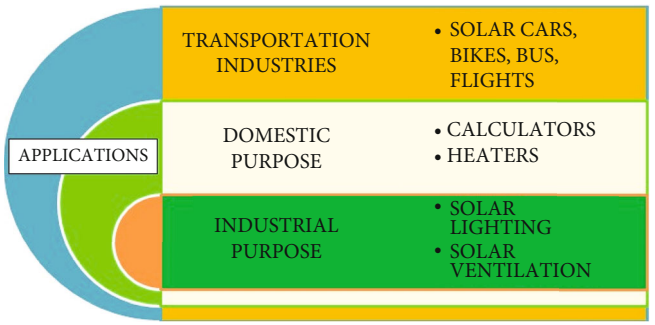

Figure 1: Applications of solar cell.

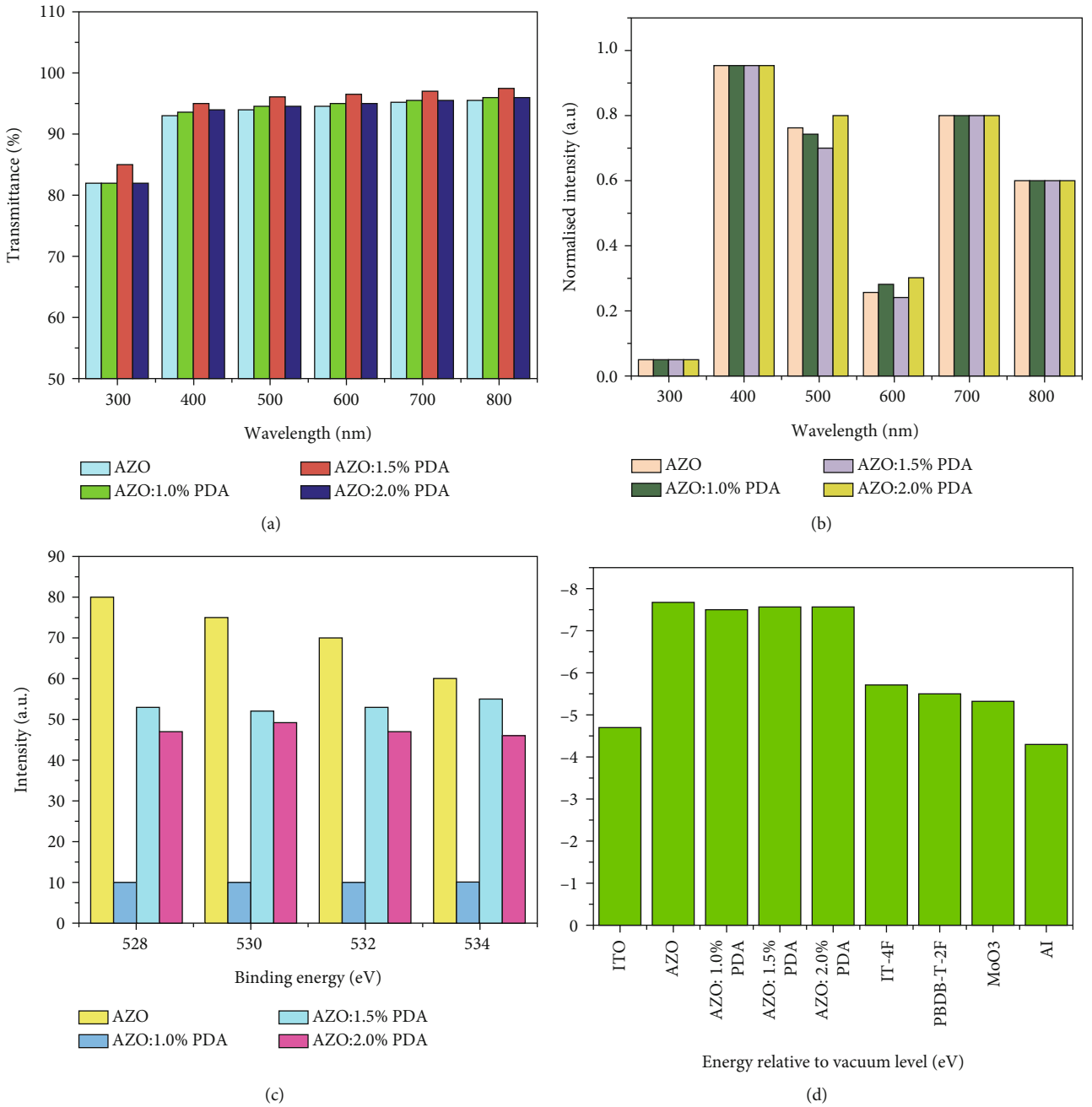

Figure 2: AZO performance in terms of (a) transmission spectra, (b) room temperature excitation of 315 nm excitation PL, (c) X-ray photoelectron spectroscopy, and (d) energy levels in existence of additive PDA.

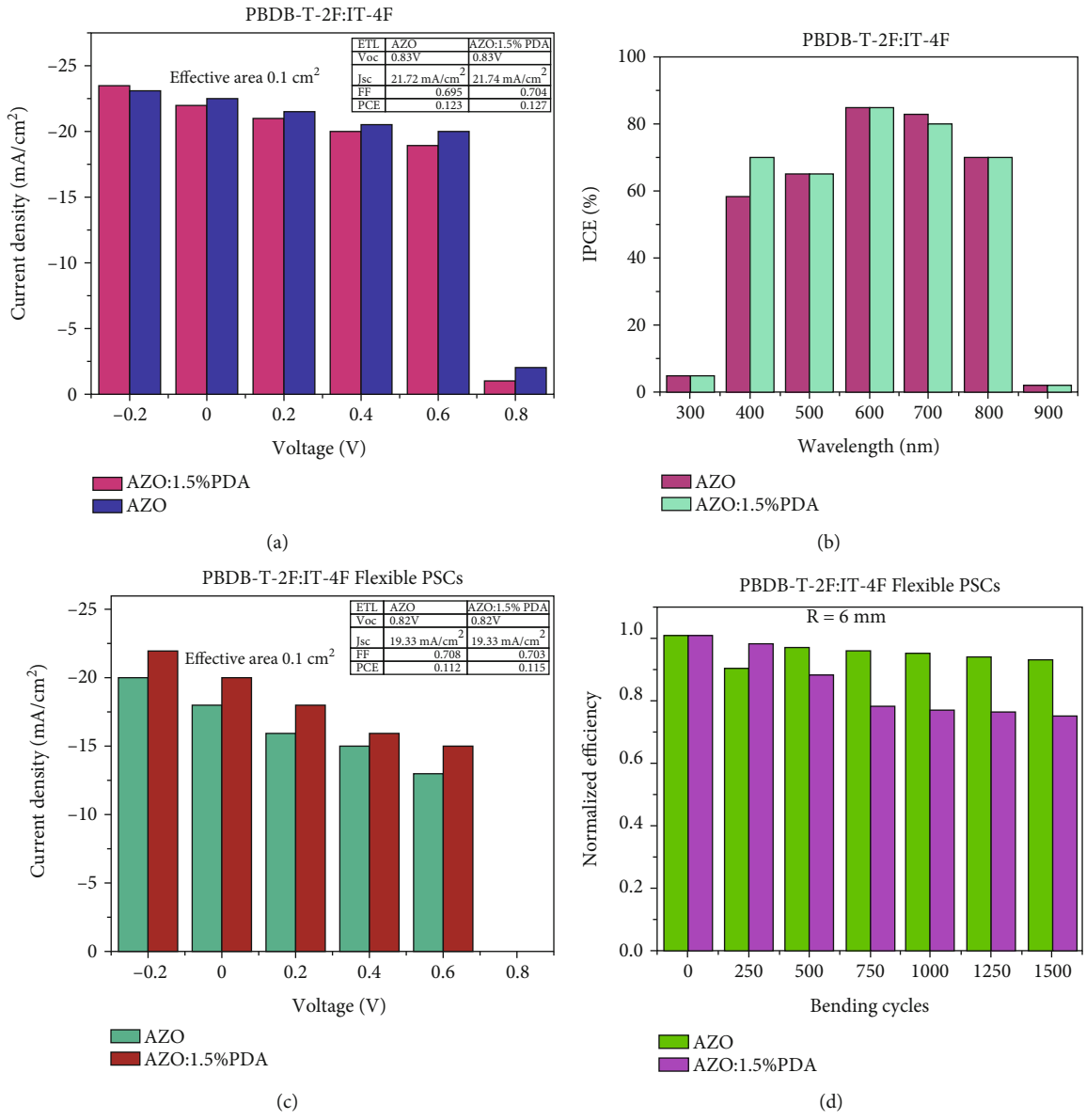

Figure 3: Device characteristics. (a) J–V curves. (b) IPCE spectra of inverted PSCs. (c) J–V curves of flexible devices. (d) Normalized average PCE of flexible PSCs.

to perform more effectively under thicker electron transport layers. Thick film (80 nm) electron mobility measurements show that AZO- and PDA-modified AZO are highly sensitive to the thickness of the plate electron transport layers in this study. Furthermore, it should be mentioned that both films were processed at 140°C for 20 minutes. Thick AZO films have a unique nanoripple pattern, which shows the atomic force microscopy images of the thicker films have a more textured surface. Because of this feature, the active layer has a greater area of contact, which facilitates charge transfer and collecting. PDA has been found to alter the electron transport properties of AZO electron transport layers, so in order to better understand this effect, two configurations of electron-only sensors have been introduced, one of which reveals the electron mobility of the whole device, while the other reveals the conductivities of the modified material, which is aluminium-doped zinc oxide or aluminium-doped zinc oxide: polydopamine electron transporting layer/PBDB-T:ITIC/aluminium. There were three inverted PSCs tested for their photovoltaic performance, each with its own unique active layer material. The incident photon-to-current efficiency (IPCE) spectra and the current density-voltage (J-V) curves are in excellent agreement. PBDB-T:ITIC PSCs based on 1.5% PDA (80 nm) and a current density of 16.57 mA cm^{-2}, a voltage of 0.886 V, and an overall fill factor of 67.4% obtained a power conversion efficiency of 10.3 percent.

For devices with electron transporting layers of aluminium-doped zinc oxide, AZO:1.0% PDA, AZO:1.5 percent PDA, and AZO:2.0 percent polydopamine, the integrated Jsc values obtained from IPCE spectra and the J–V curves (4% misfit) are in excellent agreement. PSC inversions based on PBDB-T:ITIC and aluminium-doped zinc oxide or AZO/

Table 1: Device properties of inverted PSCs with PBDB-T-2F and IT-4F layers.

Device type	BH	J_{sc}^{a} (mAcm^{-2})	V_{oC} (V)	FF (%)	PCE (%)
AZO-PSCs	PBDB-T-2F:IT-4F	21.61 ± 0.11[20.75][b)]	0.830 ± 0.002	69.2 ± 0.3	12.1 ± 0.2[12.3][a)]
AZO:1.5% PDA-PSCs	PBDB-T-2F:IT-4F	21.62 ± 0.12[20.81][b)]	0.830 ± 0.004	70.1 ± 0.3	12.5 ± 0.2[12.7][a)]
AZO-flexible PSCs	PBDB-T-2F:IT-4F	19.15 ± 0.18	0.820 ± 0.003	70.6 ± 0.2	11.0 ± 0.2[11.2][a)]
AZO:1.5% PDA-flexible PSCs	PBDB-T-2F:IT-4F	19.82 ± 0.15	0.820 ± 0.003	70.0 ± 0.3	11.3 ± 0.2[11.5][a)]
AZO-flexible PSCs	PBDB-T:ITIC	14.89 ± 0.19	0.89 ± 0.002	67.9 ± 0.3	9.0 ± 0.2[9.2][a)]
AZO:1.5% PDA-flexible PSCs	PBDB-T:ITIC	16.09 ± 0.16	0.89 ± 0.002	66.9 ± 0.2	9.4 ± 0.2[9.6][a)]

PDA electron transport layers were tested for long-term stability. Power conversion efficiency deteriorates over time in a glove box filled with nitrogen. After 30 days of storage, the power conversion efficiency value of the AZO:1.5% PDA electron transport layer-based encapsulated PSCs is still >85 percent higher than the original power conversion efficiency value. AZO:PDA and active layer have strong interfacial contact, resulting in a high level of stability. On both plastic and glass substrates, the PBDB-T-2F:IT-4F dynamic material is utilised to illustrate the ubiquity of the polydopamine-modified AZO electron transport layer. Power conversion efficiency is 13.1 percent by a Jsc of 22.84 mA cm^{-2}, and the FF is 70.4%.

This power conversion efficiency value is more than the aluminium-doped zinc oxide electron transport layer when compared to the PSC device (12.3%). A Jsc value of 20.75 cm^{-2} for the AZO and the AZO:1.5% PDA is consistent with the J–V curves as shown in Figure 2(b). Power conversion efficiency of 11.5 percent can still be attained with the PET/Ag mesh-based flexible electrode, even with its lower Jsc of 19.97 mA cm^{2} and higher Voc of 0.79 V and FF of 69.3% for the aluminium-doped zinc oxide: 1.5% polydopamine-based device. Insensitive to thickness and bendable PSCs with AZO:1.5 percent polydopamine electron transporting layer have been claimed to have the greatest power conversion efficiency of any flexible polymer solar cells to date. The AZO:-power PDA's conversion efficiency was normalized. As a function of six-millimeter bend cycles, the device was measured to verify the bendability of the device. Over the course of 1600 bending cycles, the AZO:1.5% fully flexible PDAs maintain more than 90% of their original power conversion efficiency. The PBDB-T:ITIC-based flexible polymer solar cells showed a similar outcome. Flexible devices' outstanding mechanical capabilities are mostly due to the addition of PDA to AZO, which promotes the interfacial interaction among the active layer and the AZO:PDA electron transport layer during the bending process and increases the bending durability and is shown in Figures 3(a)–3(d).

Because of its intrinsic brittleness, inorganic AZO cannot be used for flexible or wearable PSCs. The first time this difficulty has been addressed, AZO electron transport layers have been able to bend. In ITIC films AZO and AZO/PBDB-T, after 60 cycles of bending, there are evident cracks; however, the aluminium-doped zinc oxide:1.5% polydopamine and aluminium-doped zinc oxide:1.5% polydopamine/PBDB-T:ITIC films do not. Even after 250 bending cycles, ITIC retains its initial homogeneous shape. An increase in AZO nanocrystals' mechanical stability when bent can be achieved by using PDA as a flexible elastomer binder between the nanocrystals, according to this study. The AFM peak-force model shows that the AZO:PDA composite has a greater ductility than the pure AZO (255 MPa), indicating a better flexural endurance. For both AZO and the Young's modulus analysis, there is no noticeable difference in transmittance.

PDA 1.5% and AZO 1.5% are substantially stiffer than PDA:1.5 percent and AZO:1.5 percent after bending. We note that the PDA elasticized AZO exhibits superior transparency than the pure AZO, which may be explained by flaws being suppressed and heterogeneous nanocrystals being uniformly improved in uniformity. The bendable aluminium-doped zinc oxide:1.5, as shown in Table 1, percent PDA decreased the intensity of UV absorption of the PBDB-T:ITIC active layer more significantly than the bendable AZO:ITIC active layer, as shown in Figure 3.

4. Mechanical Stability

The adhesion between functional layers in a polymer solar cells is another important component in determining the mechanical properties of the device. Peeling perovskite layers from ZnO with scotch tape is a comparable method employed in this study to examine the interfacial adhesion of the 3M tape. Tablet machines were used to apply 0.5 MPa of force on 3 M tape with a layer of current collector, and the results were excellent. Next, a universal testing machine is used to perform a peeling test on the sample. The layer that is currently being used was easily pulled off after peeling five times due to low attachment of the absorber region to the AZO layer. Because of the attractive force contacts among polydopamine functional groups and natural at present layer, some well central to the effective on aluminium-doped zinc oxide:1.5% polydopamine is scarcely shed off until the 10 reapplications. After peeling procedure, a UV–vis absorption measurement was conducted to establish that the active layer's absorption intensity changed. Because the PDA-modified AZO is so sticky, the active layer maintains its uniformity and integrity under peeling, indicating that the active layer's absorption intensity is not diminished.

Due to PDA and organic active layer intermolecular interactions, devices' adhesion and mechanical properties have been improved. It was necessary to conduct a Fourier transform infrared spectroscopy (FTIR) measurement in order to verify the mechanism of contact. Notably, PTB7-Th:PC71BM was used to enhance visualization of intermolecular interactions

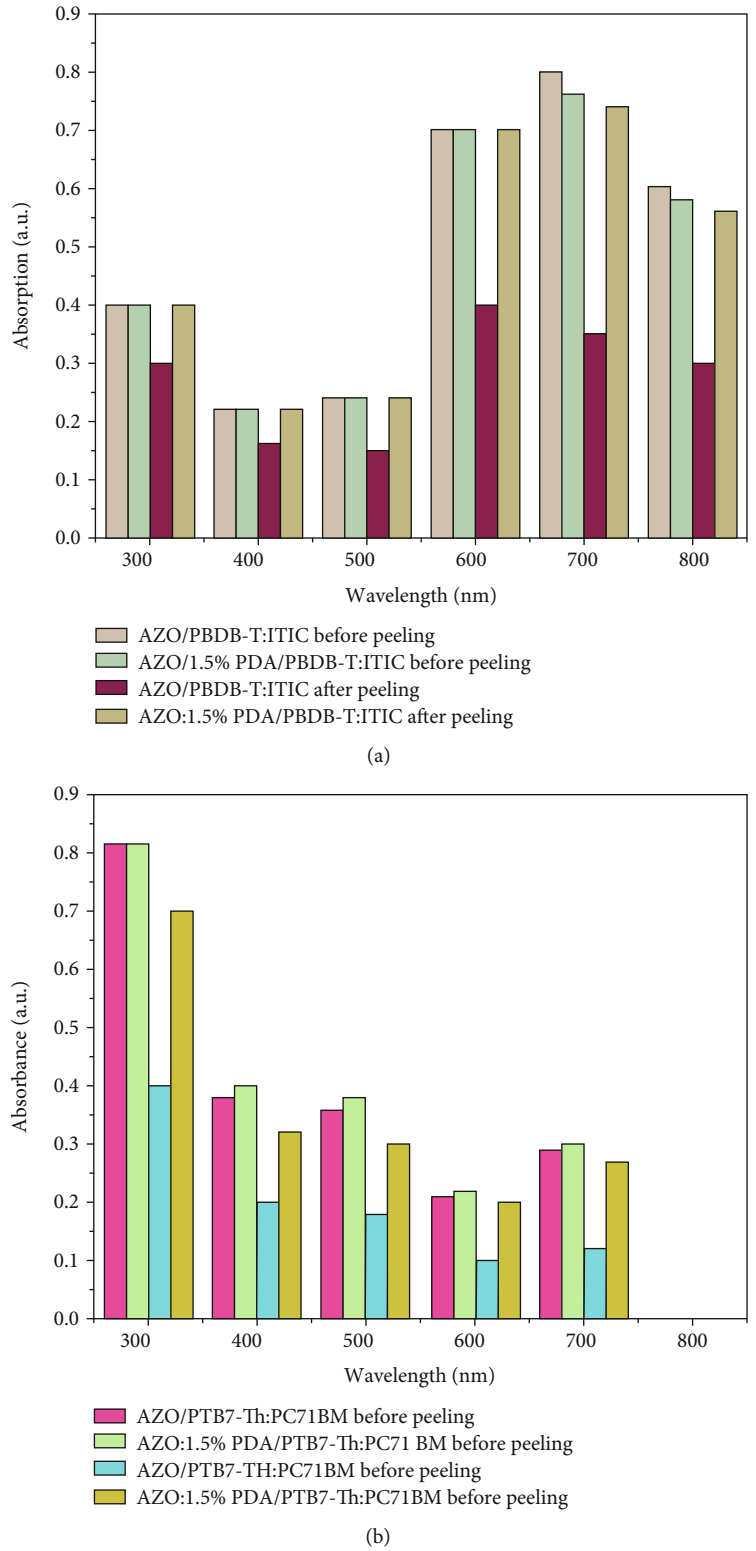

Figure 4: (a) UV–absorption spectra of AZO/PBDB-T:ITIC. (b) AZO:1.5% PDA/PTB7.

in the large-content PDA. Intricately symmetric tremors of NH and OH (v(NH) and (OH)) and CO (v(CO)) in PDA were ascribed to the 3000–3500 cm^{-1} and 1750 cm^{-1} peaks, respectively. To demonstrate the establishment of a hydrogen bond, the PTB7-Th:PC71BM:PDA mix film had a broader and more powerful NH and OH than the pure PDA film. Stretching vibrations of CO (v(CO)) have been found to shift toward a short wavenumber in agreement with this behavior. This can be attributed to the newly created hydrogen bond as well as shown in Figures 4(a) and 4(b).

The active layer systems PBDB-T:ITIC:PDA and PBDB-T-2F:IT-4F: polydopamine both used a similar method. AZO:PDA interfacial layer's NH and OH groups can establish hydrogen bonds with PTB7-Th:O PC71BM's and CO, which could improve the enhancing mechanical adhesion and durability by enhancing among the activated layer and the substrate and the interfacial layer. Since the PDA-elasticized AZO electron transport layers have such good properties, like bendability and interfacial adhesion, they provide a new way to make PSCs that are accessible and versatile and that perform reliably.

5. Conclusion

The PDA-integrated AZO has a number of advantages including the following:

(i) Ultrahigh optical and electrical conductivities and the ability to be used as an electron transport layer without regard to thickness

(ii) Optimizing inorganic electron transport layer flexural endurance, which improves the flexibility of polymer solar cell devices. Natural absorber layer adherence to the artificial electron transport layer, which contributes to the device's long-term performance

(iii) With an interlayer thickness of 80 nm, the best power conversion efficiency of 12.7% has been attained using the AZO:1.5% PDA electron transport layer and even in that case to the power conversion efficiency of component-like dense interlayers that have been reported

(iv) Furthermore, a power conversion efficiency of 11.5% has been achieved for totally versatile polymer solar cells focused on PET mesh electrodes, and the equipment is capable of storing greater than 92% of starting power conversion efficiency next bending for 1500 cycles

Data Availability

The data used to support the findings of this study are included within the article. Further data or information is available from the corresponding author upon request.

Conflicts of Interest

The authors declare that there is no conflict of interest regarding the publication of this article.

Acknowledgments

The authors appreciate the supports from Hawassa University, Ethiopia, for providing help during the research and preparation of the manuscript. The authors thank V.S.B. Engineering College, Vidya Pratishthan's Kamalnayan Bajaj Institute of Engineering and Technology, and Sri Sairam Engineering College for providing assistance to this work. The authors would like to acknowledge the Researchers Supporting Project Number (RSP-2021/373), King Saud University, Riyadh, Saudi Arabia.

References

[1] V. Shrotriya, "Polymer power," *Nature Photonics*, vol. 3, no. 8, pp. 447–449, 2009.

[2] S. Baskar, T. Maridurai, R. Arivazhagan, S. SivaChandran, and R. Venkatesh, "Thermal management of solar thermoelectric power generation," *AIP Conference Proceedings*, vol. 2473, article 020010, 2022.

[3] J. Chen, G. Li, Q. Zhu et al., "Highly efficient near-infrared and semitransparent polymer solar cells based on an ultra-narrow bandgap nonfullerene acceptor," *Journal of Materials Chemistry A*, vol. 7, no. 8, pp. 3745–3751, 2019.

[4] S. Li, L. Ye, W. Zhao et al., "A wide band gap polymer with a deep highest occupied molecular orbital level enables 14.2% efficiency in polymer solar cells," *Journal of the American Chemical Society*, vol. 140, no. 23, pp. 7159–7167, 2018.

[5] X. Yang, X. Hu, Q. Wang et al., "Large-scale stretchable semi-embedded copper nanowire transparent conductive films by an electrospinning template," *ACS Applied Materials & Interfaces*, vol. 9, no. 31, pp. 26468–26475, 2017.

[6] G. Ji, Y. Wang, Q. Luo et al., "Fully coated semitransparent organic solar cells with a doctor-blade-coated composite anode buffer layer of phosphomolybdic acid and PEDOT:PSS and a spray-coated silver nanowire top electrode," *ACS Applied Materials & Interfaces*, vol. 10, no. 1, pp. 943–954, 2018.

[7] X. Liu, L. Ye, W. Zhao et al., "Morphology control enables thickness-insensitive efficient nonfullerene polymer solar cells," *Materials Chemistry Frontiers*, vol. 1, no. 10, pp. 2057–2064, 2017.

[8] Y. Cui, B. Xu, B. Yang, H. Yao, S. Li, and J. Hou, "A novel pH neutral self-doped polymer for anode interfacial layer in efficient polymer solar cells," *Macromolecules*, vol. 49, no. 21, pp. 8126–8133, 2016.

[9] Y. W. Lee, K. Pak, S. Y. Park et al., "Regioisomeric polythiophene derivatives: synthesis and structure-property relationships for organic electronic devices," *Macromolecular Research*, vol. 28, no. 8, pp. 772–781, 2020.

[10] Z. Zhang, Z. Zhang, Y. Yu et al., "Non-conjugated polymers as thickness-insensitive electron transport materials in high-performance inverted organic solar cells," *Journal of Energy Chemistry*, vol. 47, pp. 196–202, 2020.

[11] F. Tian, H. Chen, Y. du et al., "Rational molecular design for isoindigo-based polymer semiconductors with high ductility and high electrical performance," *Journal of Materials Chemistry C*, vol. 7, no. 37, pp. 11639–11649, 2019.

[12] T. Sekitani, Y. Noguchi, K. Hata, T. Fukushima, T. Aida, and T. Someya, "A rubberlike stretchable active matrix using elastic conductors," *Science*, vol. 321, no. 5895, pp. 1468–1472, 2008.

[13] Z. Wu, C. Sun, S. Dong et al., "n-Type water/alcohol-soluble naphthalene diimide-based conjugated polymers for high-performance polymer solar cells," *Journal of the American Chemical Society*, vol. 138, no. 6, pp. 2004–2013, 2016.

[14] S. Berny, N. Blouin, A. Distler et al., "Solar trees: first Large-Scale demonstration of fully solution coated, semitransparent,

flexible organic photovoltaic modules," *Advancement of Science*, vol. 3, no. 5, p. 1500342, 2016.

[15] S. Hong, H. Kang, G. Kim et al., "A series connection architecture for large-area organic photovoltaic modules with a 7.5% module efficiency," *Nature Communications*, vol. 7, no. 1, pp. 1–6, 2016.

[16] Q. Guo, J. Lin, H. Liu et al., "Asymmetrically noncovalently fused-ring acceptor for high-efficiency organic solar cells with reduced voltage loss and excellent thermal stability," *Nano Energy*, vol. 74, article 104861, 2020.

[17] D. Baran, R. S. Ashraf, D. A. Hanifi et al., "Reducing the efficiency-stability-cost gap of organic photovoltaics with highly efficient and stable small molecule acceptor ternary solar cells," *Nature Materials*, vol. 16, no. 3, pp. 363–369, 2017.

[18] M. P. De Jong, L. J. Van Ijzendoorn, and M. J. A. De Voigt, "Stability of the interface between indium-tin-oxide and poly(3,4-ethylenedioxythiophene)/poly(styrenesulfonate) in polymer light-emitting diodes," *Applied Physics Letters*, vol. 77, no. 14, pp. 2255–2257, 2000.

[19] G. Angelini, P. de Maria, A. Fontana et al., "Study of the aggregation properties of a novel amphiphilic C_{60} fullerene derivative," *Langmuir*, vol. 17, no. 21, pp. 6404–6407, 2001.

[20] Q. Chen, H. Ding, Y. Wu et al., "Passivation of surface states in the ZnO nanowire with thermally evaporated copper phthalocyanine for hybrid photodetectors," *Nanoscale*, vol. 5, no. 10, pp. 4162–4165, 2013.

[21] B. S. Bendre and S. Mahamuni, "Luminescence in ZnO quantum particles," *Journal of Materials Research*, vol. 19, no. 3, pp. 737–740, 2004.

[22] L. E. Greene, M. Law, B. D. Yuhas, and P. Yang, "ZnO–TiO_2 core–shell nanorod/P3HT solar cells," *Journal of Physical Chemistry C*, vol. 111, no. 50, pp. 18451–18456, 2007.

[23] L. K. Jagadamma, M. al-Senani, A. el-Labban et al., "Polymer solar cells with efficiency >10% enabled via a facile solution-processed Al-doped ZnO electron transporting layer," *Advanced Energy Materials*, vol. 5, no. 12, p. 1500204, 2015.

[24] Y. Zhu, L. Zhao, Z. du et al., "P-type tetrathiafulvalene derivative as the interface modification layer in non-fullerene organic solar cells with high performance," *Synthetic Metals*, vol. 282, article 116946, 2021.

[25] Y. Wang, Z. Peng, S. Xiao et al., "Highly stable Al-doped ZnO by ligand-free synthesis as general thickness-insensitive interlayers for organic solar cells," *Science China. Chemistry*, vol. 61, no. 1, pp. 127–134, 2018.

[26] L. Petti, P. Pattanasattayavong, Y. H. Lin et al., "Solution-processed p-type copper(I) thiocyanate (CuSCN) for low-voltage flexible thin-film transistors and integrated inverter circuits," *Applied Physics Letters*, vol. 110, no. 11, article 113504, 2017.

[27] Y. Li, G. Xu, C. Cui, and Y. Li, "Flexible and semitransparent organic solar cells," *Advanced Energy Materials*, vol. 8, no. 7, p. 1701791, 2018.

[28] L. Zuo, S. Zhang, M. Shi, H. Li, and H. Chen, "Design of charge transporting grids for efficient ITO-free flexible up-scaled organic photovoltaics," *Materials Chemistry Frontiers*, vol. 1, no. 2, pp. 304–309, 2017.

[29] W. Liu, S. Liu, N. K. Zawacka et al., "Roll-coating fabrication of flexible large area small molecule solar cells with power conversion efficiency exceeding 1%," *Journal of Materials Chemistry A*, vol. 2, no. 46, pp. 19809–19814, 2014.

[30] L. Chen, J. Zhang, X. Zhang, F. Liu, and X. Wang, "Optical properties of trivalent europium doped ZnO:Zn phosphor under indirect excitation of near-UV lightn," *Optics Express*, vol. 16, no. 16, pp. 11795–11801, 2008.

[31] D. Gao, J. Zhang, G. Yang et al., "Ferromagnetism in ZnO nanoparticles induced by doping of a nonmagnetic element: Al," *Journal of Physical Chemistry C*, vol. 114, no. 32, pp. 13477–13481, 2010.

[32] L. Nian, W. Zhang, N. Zhu et al., "Photoconductive cathode interlayer for highly efficient inverted polymer solar cells," *Journal of the American Chemical Society*, vol. 137, no. 22, pp. 6995–6998, 2015.

[33] H.-Y. Park, D. Lim, K.-D. Kim, and S.-Y. Jang, "Performance optimization of low-temperature-annealed solution-processable ZnO buffer layers for inverted polymer solar cells," *Journal of Materials Chemistry A*, vol. 1, no. 21, pp. 6327–6334, 2013.

[34] D. H. Sin, S. B. Jo, S. G. Lee et al., "Enhancing the durability and carrier selectivity of perovskite solar cells using a blend interlayer," *ACS Applied Materials & Interfaces*, vol. 9, no. 21, pp. 18103–18112, 2017.

[35] P. M. Pihko, "Activation of carbonyl compounds by double hydrogen bonding: an emerging tool in asymmetric catalysis," *Angewandte Chemie International Edition*, vol. 43, no. 16, pp. 2062–2064, 2004.

[36] B. C. Thompson and J. M. J. Fréchet, "Polymer–fullerene composite solar cells," *Angewandte chemie international edition*, vol. 47, no. 1, pp. 58–77, 2008.

Hindawi
International Journal of Photoenergy
Volume 2022, Article ID 4713869, 9 pages
https://doi.org/10.1155/2022/4713869

Research Article

Demonstrating and Investigating the Mechanical Strength of Solar Cells

V. Ravi Raj,[1] R. Krishna Priya,[2] K. V. Bindu,[3] N. Prabhu,[4] S. Madhavarao,[5] G. Ramkumar,[6] A. H. Seikh,[7] M. H. Siddique,[8] and Endalkachew Mergia Anbese[9]

[1]*Department of Mechanical Engineering, Sri Sairam Engineering College, Chennai, 600044 Tamil Nadu, India*
[2]*Deanship of PG and Research, National University of Science and Technology, Muscat, Oman*
[3]*Department of Electrical & Electronics Engineering, RMK College of Engineering and Technology, Chennai, India*
[4]*Department of Mechanical Engineering, PSN Engineering College, Melathediyoor, Tirunelveli, 627152 Tamil Nadu, India*
[5]*Department of Mechanical Engineering, Sagi Ramakrishnam Raju Engineering College, Bhimavaram, 534204 Andhra Pradesh, India*
[6]*Department of Electronics and Communication Engineering, Saveetha School of Engineering, SIMATS, Chennai, Tamil Nadu, India*
[7]*Mechanical Engineering Department, College of Engineering, King Saud University, Saudi Arabia*
[8]*Department of Industrial Engineering, Yonsei University, Seoul, Republic of Korea*
[9]*Department of Civil Engineering, Ambo University, Ambo, Ethiopia*

Correspondence should be addressed to Endalkachew Mergia Anbese; endalkachew.mergia@ambou.edu.et

Received 14 June 2022; Revised 6 August 2022; Accepted 10 August 2022; Published 19 September 2022

Academic Editor: B.R. Ramesh Bapu

This study reports on the silicon photovoltaic cells with such an alumina metallization. The photovoltaic cell's silicon component was subjected to an effective stress studied using a simulation model built with this information. In order to evaluate the efficiency of photovoltaic cells on both sides, as well as in two distinct orientations, a four-point bending experiment analysis was carried out using the model. The side and direction of loading have a significant impact on both strength and fracture. There is tensile stress going perpendicularly along the busbars; the back side of the test specimen had the lowest measured strength.

1. Introduction

In the collection and management of solar power systems, mechanical integrity is critical [1]. There is a lot of interest in fractures in modules because mechanical or thermal stress can drastically affect the module's electrical efficiency and reliability [2]. According to the loads, the tipping point or ultimate strength for the solar cell fracture must be evaluated, despite the fact that there are several factors that contribute to cell breakdown, but they are only one of them [3]. This strength is further characterized by the specific fault structure that emerges during the production methodology for cells, which begins the silicon wafering process [4]. However, defects in silicon wafers and the tensile strength solar cells have been extensively studied. The interfacial fracture behaviour of photovoltaic cells determines how quickly photoelectric array's cells break down [5, 6], with little attention to solar panel quality consideration. Si, Al, and Ag [7] are all components that can be found in current silicon solar cells; analyzing each layer's contribution to cell strength is necessary [8, 9], and the uses of solar cells are shown in Figure 1.

Due to the overlap in the metallization structure between the two paste components (AgAl and Al), fire procedures can have a substantial impact on cell strength. Fracture testing revealed that cracks formed in the AgAl/Al overlap zone, causing local stress concentrations that eventually led to fracture at reduced stress levels. Strength tests on typical

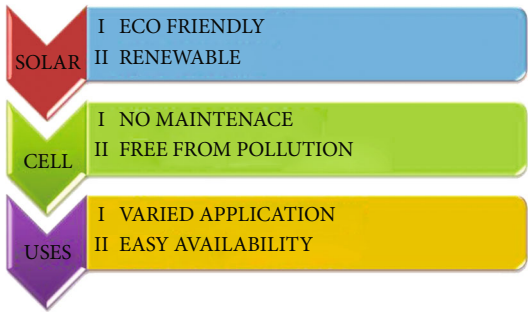

Figure 1: Uses of solar cell.

solar cells were carried out by [10] using 4-point bending and an analytical stress evaluation. Higher drying and lower firing temperatures could be proven to reduce the back-side tensile strength of the solar cell. Aluminium back contact has also been tested for its mechanical qualities [11]. In order to anticipate the maximum deflection of solar cells after discharge, [12] devised this model. Mori–Tanaka homogenization [13] was used to estimate the Al layer's mechanical reaction. Although mechanical models of a solar cell are still lacking, stress 4-point bending tests can be done to examine them [14].

Solar cell strength is determined using a mechanical model that mimics the current standard idea using the H-pattern, Al-BSF [15, 16]. Mechanical homogenization methods are used to examine several aspects of the solar cell layer system, including Al, Si, and Al thin film deposition on the back side [17]. In order to analyze and characterize the bending behaviour and stress fields in solar cells, finite element analysis [18] is utilized, taking into account the different material layers. Al-BSF and the H-pattern solar cells are tested [19] in 4-point bending with varying loads using the FE model and the Weibull analysis [20]. A simulation model constructed using this information was used to study the effective stress on the silicon component of a photovoltaic cell.

2. Material and Methods

2.1. Samples. Solar cells with a diameter of 160 mm, 160 mm, and 220 mm (TTV: 30 mm) were employed for the strength evaluations. Al-BSF, H-pattern, and three busbars were used for the standard concept cells. Material consistency is ensured because all cells come from the same batch. Continuous Ag-busbars with a width of 4 mm and a length of 130 mm created the back-side contact. On the sunny side of the busbars, an alkali perforated coating with an antireflection layer was also found (width 2 mm, length 160 mm) (front side). Table 1 contains more details on the simulation model's material properties.

2.2. Strength Testing. Silicon solar cells can be tested using the same methods as silicon wafers. However, in the literature, it is most commonly used to quantify the strength of wafers. Uniaxial bending moments evenly distribute the stress across a vast surface area, including the sample's edges and surface. A consistent flexural stress is applied to the sample's lower portion. With an outer span of 120 mm, the four-point bend configurations in this study used inner rollers that had a diameter of 60 mm. Steel rollers with a diameter of 12 mm are used in the machine. Among the rollers and the cells, PTFE foils are utilized to improve contact behaviour and reduce friction [21]. When comparing the busbars to the rollers, at the busbars, the rolls feature little slots. During examination, the cell and roller are not separated by foils in the grooves. Table 2 shows the four distinct testing configurations that were carried out.

Ductile tension is applied to the rear and front sides of the solar panels, with the busbars parallel and perpendicular to the rollers. Each design was tested with 60 solar cells. The universal testing equipment was used to conduct all of the tests with a 1 kN load cell. The machine's position was used to determine the sample's deflection. It was decided that the load speed would be 0.1 mm/s. During testing, each sample's power and bending were recorded. A force of 0.5 N was applied to the photovoltaic array before it was broken. To prevent the cells from breaking during 4-point bending testing, strips of sticky tape were applied diagonally to the rollers. A mechanical prototype is utilized to compute the rupture stress during the four-point bending test. To put it another way, the Weibull modulus is a measure of how much the fracture stress values vary over time. This method was used to determine the Weibull parameters using maximum likelihood estimation (MLE).

3. Modeling

3.1. Layer Properties. Different layers are depicted in Figure 2 as part of the solar cell's structure. For the solar cell concept studied here, contact metallizations include screen-printed silver pastes (busbars and fingers) and aluminium pastes (back contact). While burning, aluminium diffused into silicon, creating the eutectic and the back surface field (BSF). AlSi particles that are weakly linked are found in the bulk porous Al layer after fire. Alumina covers these particles. The crystal structure of the silicon in the cell is cubic, whereas the BSF has an Al-doped zone. Doped regions are expected to have identical mechanical properties. Still, the Ag solution used for transmission lines and fingers has a more homogeneous microstructure than the Al layer on the backside. Researchers employed the Mori–Tanaka approach to conduct theoretical mechanical studies on eutectic and Al pastes to homogenize the elastic modulus. According to the theoretical calculations, AlSi has a Young's modulus of 74 GPa in its eutectic layer.

Modeling silicon relies on continuous elastic properties, whereas other levels are represented as brittle materials that can be deformed. Ag paste's optimal rigidity and production stresses were found to be at 41.5 MPa for Al paste. We can see how the Al paste fractures on the interface among the elements and the glass by using a spherical particle as an example. Furthermore, the weak interparticle forces are thought to be a result of the porous structure. Thus, it is hypothesized that the solar cell's stress behaviour in compression is predominantly influenced by the porous Al,

Table 1: The mechanical model's material parameters.

Layer	Material	Young's modulus E (GPa)	Poisson's ratio ν	Thickness of layer $t(\mu m)$
Front-side busbars	Silver	8	0.41	12
Silicon	Silicon	$C_{11} = 172.6$, $C_{12} = 64.86$, $C_{44} = 81.24$	0.29	≈215
Eutectic layer	Aluminium silicon	76	0.42	4
Back-side Al paste	Por. Al	7	0.40	30
Busbars on back side	Silver	8	0.41	30

Table 2: Solar cell strength testing in four-point bending is performed using batches and configurations of samples.

Name	Side in tensile stress	Position rollers to busbars	Cell numbers	Direction of tensile stress to busbars
SP	Sunny side	Lateral	60	Transverse
SC	Sunny side	Transverse	60	Lateral
BP	Back side	Lateral	60	Transverse
BC	Back side	Transverse	60	Lateral

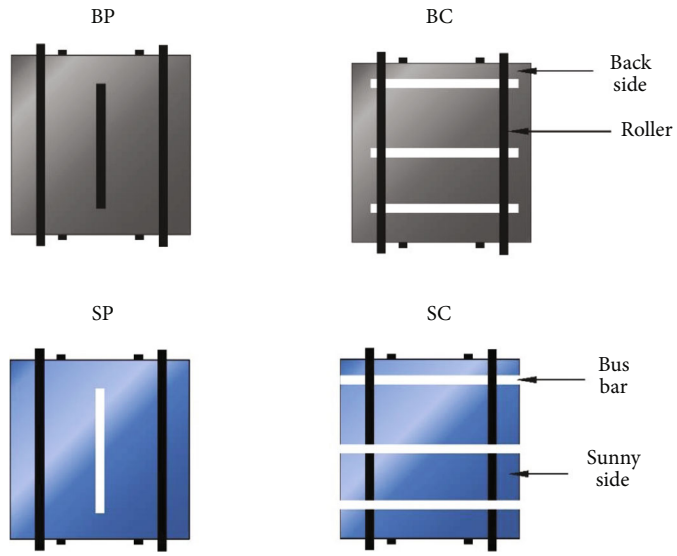

Figure 2: Detailed diagrams of all of the configurations used for strength testing.

while the cell's stress behaviour in tension is more susceptible to failure. As the system compresses, the AlSi particles may contribute a little amount of stiffness. To determine cell breakage, it has been assumed that the silicon layer breaks. As a failure criterion, the highest possible primary stress is employed. Further, it is thought that flaws on the silicon layer's surface cause fracture at the silicon layer. As a result, the solar cell's fracture is not due to another layer in the solar cell.

3.2. Mechanical Model. Displacements and the photovoltaic panels under frustration were calculated using the FE casing structure that was constructed in the ANSYS finite element (FE) programme and shown in Figure 3. Silicon's mechanical properties are not affected by the BSF; hence, it is not shown as a solitary framework. Because the anti-reflective coating on the top side is so thin, it is not taken into account. Small grids of Ag on the solar cell's upper surface are also ignored because of their inconsequential impact on the cell's stiffness and stress distribution. This simulation model does not take into account residual stresses after thermal processing, the values of which are taken to remain constant throughout all samples. The calculated stress fields can then be superimposed with these new stresses. There are nodes, and the photovoltaic cell's levels are partitioned in the FE model's shell elements. Silicon, on the other hand, is regarded as a linear elastic isotropic material. As shown in Table 1, the elastic constants of silicon are represented using Voigt's notation for anisotropic linear elastic behaviour (f100g crystal orientation). Ductile layers' plastic material behaviour was ignored since stress levels in the ductile layers did not exceed yield stresses. The simulation prototype additionally accounts for nonlinearities as well as massive deflection contact and friction among the rollers of the four-point bending test system. To get the best results, choose a coefficient of friction equal to 0.18.

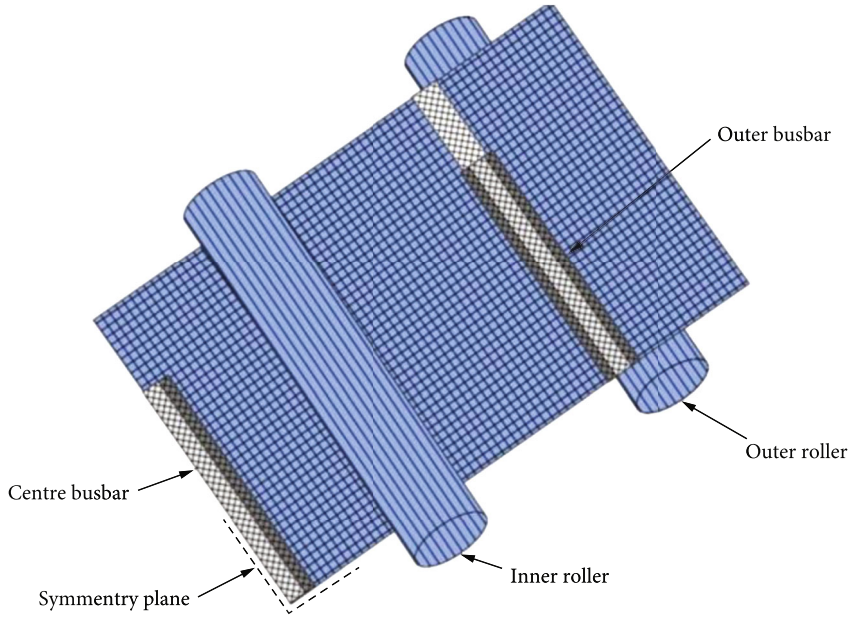

Figure 3: FEM model in quarter symmetry with mesh shell elements and different sections for different layers with busbars parallel to the roller.

4. Results

4.1. Resulting Numbers from Simulation. Deflection, which characterizes the solar cell's structural behaviour, serves as the model's load parameter. If you compare the same pattern of pure silicon substrate on a silicon wafer as a silicon layer within a cell, a 10 mm deflection exhibits the maximum stress (first major stress on the ductile side of the silicon layer) and as an example of where a silicon wafer's loading force compares to a pure silicon substrate. The stiffness (force) of silicon among a wafer and a cell is reduced by <3%. There is just a small amount of stress in the surrounding metallization layers that affects the maximum stress in the silicon. When it comes to stress concentrations at metallization–silicon interfaces, however, the shell model cannot account for them. Despite this, simulations can be used to predict whether a photovoltaic works using the same assumptions as for pure silicon wafers. In this case, the fracture stresses were calculated using the mechanical solar cell model, which took into account the number of cosystem's consequences. The roller force vs. deformation curves from study were analyzed to those from the simulated world in order to verify the quantitative instances of 4-point bending tests. The experiment's nonlinear curve progression can be characterized via simulation, as can be seen. Experimental results and computer simulations show that the pastes in Table 2 have a satisfactory overall stiffness. 0.5 N was the starting point for the experiment's experimental curve because of the initial force used.

4.2. The Results of Testing for Strength. Deformation constraints were calculated using a simulation framework on the fracture's power and diversion. Weibull criteria for the four topologies illustrated in Table 3 were determined using these stressors. Fault stresses are sprinkled by the Weibull

Table 3: Weibull parameters of strength with 90% confidence bounds were obtained by four-point bending experiments using solar cells in various configurations.

Tensile stress side	Busbar roller positions	m	σ_θ (MPa)
Sunny side	Transverse	15	201
Sunny side	Lateral	16	204
Back side	Transverse	15	246
Back side	Lateral	18	172

modulus, which was not significantly different in any of the varied designs. Defects are evenly distributed among all samples as a result of this. Neither significant difference between layouts across or parallel to busbars when tensile stress is applied to the sunny side. To put it another way, rollers perpendicular to busbars have a higher typical fracture stress than rollers parallel to the busbars. Since the metallization layers are taken into consideration, these fracture stress values can be used to evaluate the absolute strength of the use of photovoltaics (neglecting residual stress states). Examination of shattered cells led to the use of optical tools to inspect the cells. The back-side metallization connects each cell even if the sunny side is checked. EL is more difficult to conduct on the underside of the solar cell, which shatters more quickly. In the preferred cleavage planes (112) or (113) of silicon, all cracks propagate in a 460 degree angle. Many minor cracks were found in a region of continual flexure (among the red lines) during testing on the sunny side. If you look closely, you will find two distinct lines of cracks running in opposite directions on the surface of the busbars, which is where the cracks originate. For SP design, a single break can spread across the cell's thickness. The origin is more difficult to find if the back side is examined, as large regions are not electrically connected. Back-side testing shows that cracks

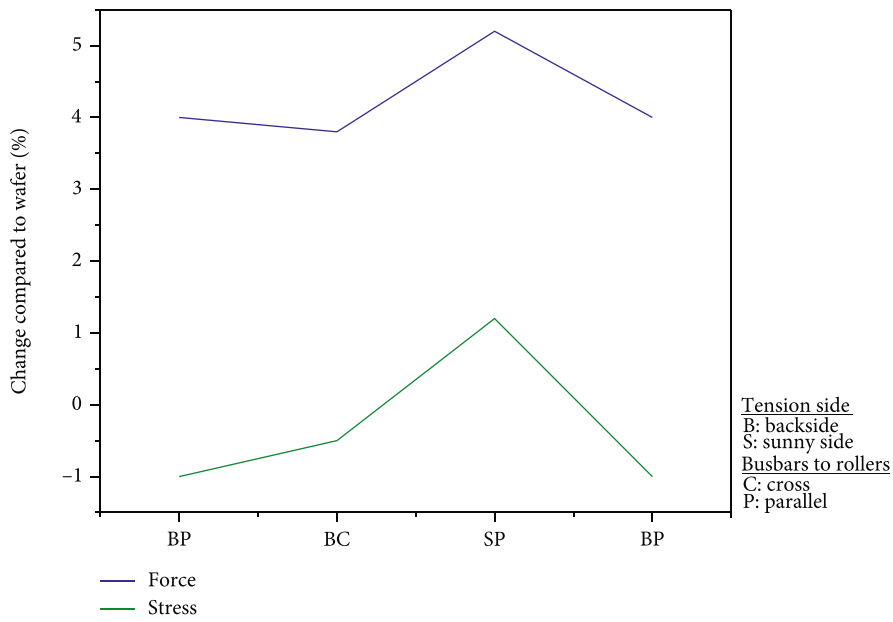

Figure 4: Rollers of variant solar cell designs at 10 mm bending have the highest first primary stress and response force of pure silicon (wafer) of the same thickness.

commonly spread in two directions from busbars for the optical inspection, indicating that the transmission lines and the pore structure are where the cracks begin. As observed in the EL photos, back-side testing results in a lesser number of cracks than sunny-side testing.

5. Elaboration

5.1. Loading Direction Affects the Strength of a Load. Figure 4 shows that the rollers of variant solar cell designs at 10 mm bending have the highest first primary stress and response force of pure silicon (wafer) of the same thickness. For perforated polycrystalline silicon because of defects in the silicon, they are unusable in the resin coating form, since the durability of the sunshine end of solar cells is irrespective of the beam axis. On the other hand, the loading direction has a significant impact on the strength of the back side. The creation of a eutectic layer, however, does not change the busbar's direction dependency, despite the fact that the flaws on the surface have been altered. Figure 5 shows the rollers' force vs. displacement curves. The comparison of the (a) SP configuration specimen in simulation and experiment and (b) all configurations in the experiment.

Figure 6 shows that the local stress concentrations in 3D models cannot explain the disparity in BC and BP strength. Busbars and Al paste appear to be controlled by their metallization mechanism. Finding similar statistics on the maximum load orientation contributes to the effectiveness of solar cells being not possible. Four-point bending tests on typical solar cells just for the back and front sides were conducted as in Table 3. They [6] evaluated a variety of ring–on–ring test configurations of metallizations. It is not possible to directly compare axisymmetric stress to biaxial stress in this test because of the nature of the 4-point bending test. They [22] discovered that the strength of an aluminium busbar differs depending on whether it is perpendicular or parallel to the aluminium back paste [23]. Cracks can be found in the overlap area between the Al and Ag pastes in the BC configuration. It was tested on a smaller sample of solar cells and busbars in the BC arrangement. These samples were shattered into two pieces during shipping. The back-side paste and busbars were discovered to be the source of the cracks in these samples. Cracks caused by stress concentrations in the delamination of material layers were also found to be similar. These cracks are more likely to form at high-stress circumstances, as is the case with the BC framework in 4-point bending. These overlap cracks, however, may be affected by the composition of the busbar and rear contact adhesive.

So far, the mechanical model has ignored the effects of manufacturing residual stresses. Tensile stresses from the front side of silicon and flexural rigidity stresses on the rear are expected as a result of heat treatment shear strength. The rear side might have a substantially minor crack stress, whereas the front end could take a greater relative crack stress. Peripheral shear forces, such as those caused by overlying anodization layers, might have an effect on the direction of the residual stress components in a component design. Consider these points in greater detail. Cell breakage is more pronounced when the same loads are applied parallel to the busbars. Although soldering and lamination in modules may have an impact on failure mechanisms, this is not a certainty. Because modules put the entire cell under tensile stress, it is impossible to compare them.

5.2. Fracture Behaviour Influenced by Layering. Associated to the back end in tensile stress, the sunny side of the cell reveals a lot more cracks that do not separate the complete thickness of the cell, which includes the metal. Cracks were also seen on the back side of the board when it was arranged in parallel rather than perpendicular orientation. For example,

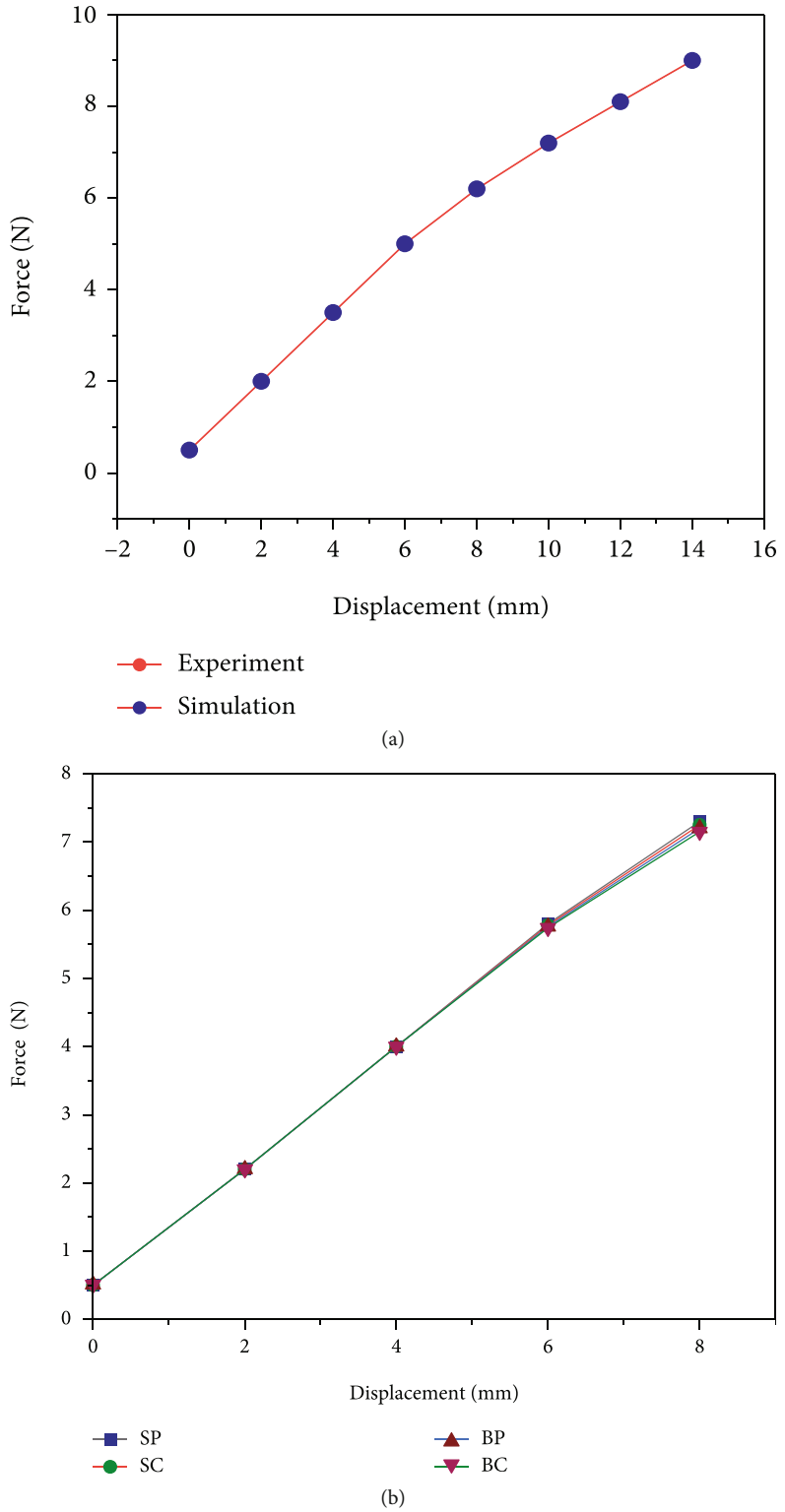

Figure 5: The rollers' force vs. displacement curves. The comparison of the (a) SP configuration specimen in simulation and experiment and (b) all configurations in the experiment.

the elastic energy in a solar cell could explain how a crack branching or many crack origins can occur. As a result, energy can be employed to propagate multiple cracks in materials tested on the sunny side. Back-side tests break the cell, causing elastic energy to be lost because the silicon pieces are no longer connected. As a result of the higher energy available, additional branched cracks will form on the back side in parallel formation. Cracks appeared close and corresponding to the busbar in all 4-point bending configurations other than the SP configuration. If the fracture travels in cleavage planes of

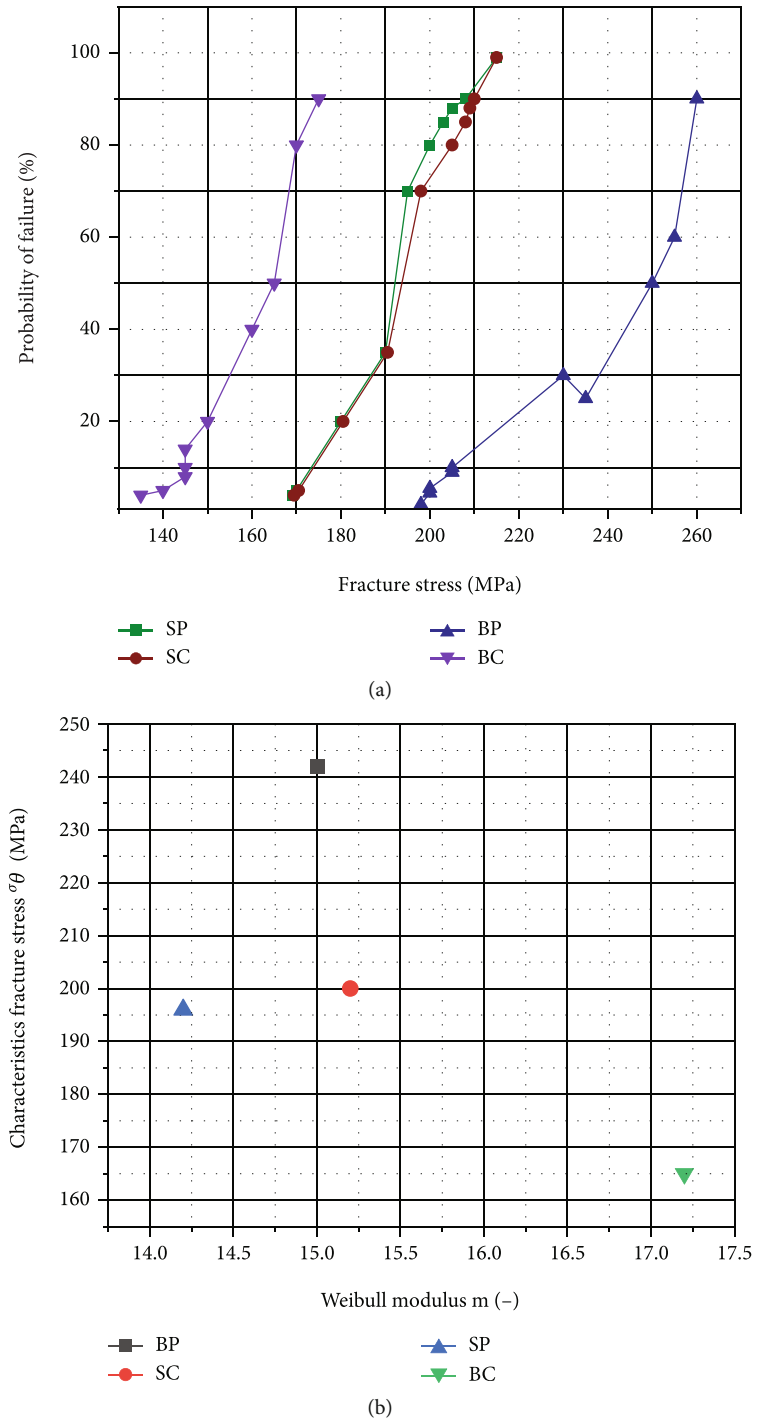

Figure 6: Analysis of four-point bending tests using solar cell in various parameters. MLE (a) Weibull drawing and (b) Weibull constraints with 95% assurance intervals are provided.

silicon, a fault or remaining stress near the busbar is likely to be the cause of this particular crack propagation. Despite the huge crack near the busbar, the two front-side layouts are indistinguishable in terms of their structural integrity. The occurrence of two fractures on the back-side arrangement indicates that a crack originated near the busbars. These cracks do not propagate similar to busbars, unlike the SP design.

6. Conclusions

The layered structure can be considered in this study; however, it has only a little influence on the stiffness and stress distribution of the solar cell. The model, on the other hand, may be used to correctly and precisely estimate the fracture stress of solar cells. This model may also be used to

investigate different metallization processes on various solar cell designs:

(i) Square crystalline silicon solar cells were exposed to four-point bending examinations with rear and sunny sides under tensile stress in order to determine their tensile strength

(ii) The Weibull modulus of all configurations was the same, which can be taken as a similar defect distribution for all of them. If the rollers are parallel or perpendicular to busbars, the characteristic fracture stress is not much different

(iii) Tensile stress on back side of perpendicular rollers is stronger than that on parallel ones. To put it another way, the metallization structure of solar cells appears to have a direct impact on the cell's strength

(iv) The loading direction in the current standard solar cells is unaffected by the direction of the sun. Because of this, the strength of the back side varies depending on which way it is being loaded

(v) In future efforts, the Al and Ag pastes overlapping can be investigated further. Breakage of photovoltaic modules can be studied by bending the modules to examine the cracking of solar cells in modules

Data Availability

The data used to support the findings of this study are included within the article. Further data or information is available from the corresponding author upon request.

Conflicts of Interest

The authors declare that there is no conflict of interest regarding the publication of this article.

Acknowledgments

The authors appreciate the support from Ambo University, Ethiopia, for providing help during the research and preparation of the manuscript. The authors thank Sri Sairam Engineering College, RMK College of Engineering and Technology, for providing assistance to this work. The authors would like to acknowledge the Researchers Supporting Project number (RSP-2021/373), King Saud University, Riyadh, Saudi Arabia.

References

[1] A. Veera Kumar, T. V. Arjunan, D. Seenivasan, R. Venkatramanan, and S. Vijayan, "Thermal performance of an evacuated tube solar collector with inserted baffles for air heating applications," *Solar Energy*, vol. 215, pp. 131–143, 2021.

[2] M. Köntges, I. Kunze, S. Kajari-Schröder, X. Breitenmoser, and B. Bjørneklett, "The risk of power loss in crystalline silicon based photovoltaic modules due to micro-cracks," *Solar Energy Materials & Solar Cells*, vol. 95, no. 4, pp. 1131–1137, 2011.

[3] K. Wasmer, A. Bidiville, F. Jeanneret et al., "Effects of Edge Defects Induced by Multi-Wire Sawing on the Wafer Strength," in *23rd European Photovoltaic Solar Energy Conference*, pp. 1305–1310, Valencia, 2008.

[4] A. Bohne, S. Schoenfelder, C. Hagendorf, D. Schmidt, and J. Bagdahn, "The influence of the wire sawing process on mono-and multicrystalline silicon wafers," in *Proceedings of 23rd PVSEC*, pp. 1780–1784, Spain, 2008.

[5] B. Klusemann, H. J. Böhm, and B. Svendsen, "Homogenization methods for multi-phase elastic composites with non-elliptical reinforcements: comparisons and benchmarks," *European Journal of Mechanics-A/Solids*, vol. 34, pp. 21–37, 2012.

[6] C. Kohn, T. Faber, R. Kübler et al., "Analyses of Warpage Effects Induced by Passivation and Electrode Coatings in Silicon Solar Cells," in *22nd European Photovoltaic Solar Energy Conference and Exhibition*, pp. 1–10, Milan, Italy, 2007.

[7] T. Behm, W. Fütterer, C. Funke et al., "Challenges of the wire saw wafering process," *Photovoltaics International*, vol. 11, pp. 36–47, 2011.

[8] A. Grün, A. Lawerenz, R. Porytskyy, and O. Anspach, "Investigation of wafer surfaces with space-resolved breaking strength tests and corresponding analysis of the crack depth," in *26th EU PVSEC*, pp. 2116–2119, Hamburg, 2011.

[9] H. Wu, S. N. Melkote, and S. Danyluk, "Mechanical strength of silicon wafers cut by loose abrasive slurry and fixed abrasive diamond wire sawing," *Advanced Engineering Materials*, vol. 14, no. 5, pp. 342–348, 2012.

[10] F. Kaule, W. Wang, and S. Schoenfelder, "Modeling and testing the mechanical strength of solar cells," *Solar Energy Materials & Solar Cells*, vol. 120, pp. 441–447, 2014.

[11] C. Kohn, R. Kübler, M. Krappitz et al., "Influence of the metallization process on the strength of silicon solar cells," in *24th European Photovoltaic Solar Energy Conference*, p. 25, Hamburg, Germany, 2009.

[12] V. A. Popovich, M. Janssen, J. Bennett, and I. M. Richardson, "Breakage issues in silicon solar wafers and cells," *Photovoltaics International*, vol. 12, pp. 49–57, 2011.

[13] V. A. Popovich, M. Janssen, I. M. Richardson, T. Van Amstel, and I. J. Bennett, "Microstructure and mechanical properties of aluminum back contact layers," *Solar Energy Materials & Solar Cells*, vol. 95, no. 1, pp. 93–96, 2011.

[14] T. Van Amstel, V. A. Popovich, P. C. de Jong, and I. J. Bennett, "A Multiscale Model of the Aluminium Layer at the Rear Side of a Solar Cell," in *Proceedings of the 23rd European Photovoltaic Solar Energy Conference*, pp. 1–12, Hamburg, Germany, 2009.

[15] A. Veera Kumar, T. Arjunan, D. Seenivasan, R. Venkatramanan, and S. Vijayan, "Techno-economic evaluation of an evacuated tube solar air collector with inserted baffles," *Proceedings of the Institution of Mechanical Engineers, Part E: Journal of Process Mechanical Engineering.*, vol. 235, no. 4, pp. 1027–1038, 2021.

[16] W. Weibull, "A statistical distribution function of wide applicability," *Journal of Applied Mechanics*, vol. 18, no. 3, pp. 293–297, 1951.

[17] S. Schoenfelder, A. Bohne, and J. Bagdahn, "Comparison of test methods for strength characterization of thin solar wafer," *Proceedings of the 22nd European Photovoltaic Solar Energy Conference*, vol. 1, pp. 1636–1640, 2007.

[18] E. Din, *843-2 Hochleistungskeramik–Mechanische Eigenschaften monolithischer Keramik bei Raumtemperatur–Teil 2:*

Bestimmung des Elastizitätsmoduls, Schubmoduls und der Poissonzahl, 2007.

[19] J. Krause, R. Woehl, M. Rauer, C. Schmiga, J. Wilde, and D. Biro, "Microstructural and electrical properties of different-sized aluminum-alloyed contacts and their layer system on silicon surfaces," *Solar Energy Materials & Solar Cells*, vol. 95, no. 8, pp. 2151–2160, 2011.

[20] V. A. Popovich, N. Van Der Pers, M. Janssen et al., "Residual and bending stress measurements by X-ray diffraction and synchrotron diffraction analysis in silicon solar cells," in *2012 38th IEEE Photovoltaic Specialists Conference*, pp. 442–447, Austin, TX, USA, 2012.

[21] M. Pander, *Mechanische Untersuchungen an Solarzellen in PV-Modulen mittels Finite-Elemente-Modellierung*, Hochschule für Tech, Wirtschaft und Kul, Leipzig, Germany, 2010.

[22] J. J. Hall, "Electronic effects in the elastic constants of n-type silicon," *Physics Review*, vol. 161, no. 3, pp. 756–761, 1967.

[23] M. Sander, S. Dietrich, M. Pander, M. Ebert, and J. Bagdahn, "Systematic investigation of cracks in encapsulated solar cells after mechanical loading," *Solar Energy Materials & Solar Cells*, vol. 111, pp. 82–89, 2013.

Hindawi
International Journal of Photoenergy
Volume 2022, Article ID 3690635, 12 pages
https://doi.org/10.1155/2022/3690635

Research Article

Optimization of Oil Yield from the Macro Algae Spirogyra by Solvent Extraction Process Using RSM and ANN

S. Aravind[1], **Debabrata Barik**[2] **and Nagaraj Ashok**[3]

[1]*Research Scholar, Department of Mechanical Engineering, Karpagam Academy of Higher Education, Coimbatore 641021, India*
[2]*Department of Mechanical Engineering, Karpagam Academy of Higher Education, Coimbatore 641021, India*
[3]*Faculty of Mechanical Engineering, Jimma Institute of Technology, Jimma University, Jimma, Ethiopia 378*

Correspondence should be addressed to Debabrata Barik; debabrata93@gmail.com and Nagaraj Ashok; nagaraj.ashok@ju.edu.et

Received 13 June 2022; Revised 27 July 2022; Accepted 18 August 2022; Published 19 September 2022

Academic Editor: BR Ramesh Bapu

The present work was done to optimize the process parameters of the oil extraction from the algae species spirogyra by using n-hexane as the solvent using the Soxhlet apparatus. The response surface methodology (RSM) and artificial neural network (ANN) were employed to optimize the particle size of the algae powder, dryness level of the algae powder, solid to solvent ratio, reaction time, and extraction temperature of the oil extraction process. Also, the physiochemical properties of the extracted oil were investigated. The comparative evaluation was done between the RSM and ANN models to select the more precise and accurate model. The coefficient of determination, R^2 of 98.92%, and the mean absolute percentage deviation (MAPD) of 0.492% for ANN revealed that the current model created with a network topology of 3 : 11 : 1 with tansig (hyperbolic tangent sigmoid) transfer function in the input layer and purelin (pure linear) transfer function in the output layer trained with trainlm (Levenberg–Marquardt) algorithm found to provide the optimal solution with better accuracy in prediction of the output. The physicochemical properties investigated, such as heating value, flashpoint, density, viscosity, iodine number, acid value, saponification value, and cetane index, showed that the extracted oil from the algae spirogyra species can be used as an alternative fuel.

1. Introduction

The advancement of technology in the fields of different energy-dependent sectors resulted in heavy energy consumption. The world's demand for energy to be met has started increasing drastically. All these paved the path for finding an alternative and renewable energy source. The use of fossil fuels is a major reason for the emission of greenhouse gases, which leads to the global warming effect. To avoid such cases, biomass-based energy is welcomed internationally [1]. Various biomass-based energy sources are available in that biofuels play a major role in replacing mineral fuels. Biomass is a renewable source, and it utilizes CO_2 for its growth through the photosynthetic effect. Compared to various biomasses available, the algae seem to have a higher level of photosynthetic effect. They can be grown in large quantities effectively in a controlled environmental condition. Some of the algae species contain high lipid content, and around 15,000 gallons of oil for one acre of land for one complete year can be produced from such a source globally [2, 3]. Yuvarani et al. [4] extracted oil from the algae species *Cladophora glomerate* using various solvents like n-hexane, toluene, chloroform, methanol, isopropanol, and co-solvent mixtures of chloroform/methanol, hexane/isopropanol and they found that the oil yield for hexane was highest compared to other types of solvents. For hexane, the oil production was around 11.7 w/wt% for 100 g of the biomass at an extraction temperature of 65 °C and extraction time of 3.5 hours. Another group of researchers, Halim et al. [5], used n-hexane as a solvent to extract oil from the algae species *Chlorococcum*. They found that with four grams of *Chlorococcum* sp. and 300 ml of hexane in a Soxhlet apparatus for an extraction time of 7.5 hours; the oil yield was around 5.5 w/wt%. Abdullah et al. [6] studied the effect of operating parameters like extraction temperature, extraction time, and mixing rate of the solvent for extracting oil from

the algae species *chlorella vulgaris* using heptane as solvent. Their study revealed that the optimum parameters were 65°C of extraction temperature and 5 hours of extraction time, resulting in an oil yield of 61.27%. Hidalco et al. [7] carried out a solvent extraction process on the algae species *Botryococcus braunii* with polar and nonpolar solvents and mixtures of them. They found that the oil yield of 19.8 w/wt% by using chloroform/Methanol in the ratio of 1 : 3. When compared to other solvents, the mixture of polar and nonpolar solvents showed more oil yield. Attach et al. [8] performed the Soxhlet method to extract oil from pumpkin, melon, oil bean, and rubber seeds using solvents with different dielectric constants. They also exhibited that the dielectric constant of the solvent had a noticeable effect on the oil extraction rate. The dielectric constant was low for a nonpolar solvent, whereas for the polar solvents, it was high. Dasari et al. [9, 10] used the nonpolar solvent n-hexane to extract the oil from castor seeds using the Soxhlet method. The oil yield was around 52.8% for a solvent ratio of 1 : 3 for an extraction time of 13 hours. Lohani et al. [11] carried out the solvent extraction process using n-hexane and ethyl acetate as a solvent on various oil-bearing seeds like camelina, flax, mustard, and canola by considering three levels of process parameters such as extraction time and extraction temperature with constant solid to solvent ratio of 1 : 4. They documented that the oil yield was maximum for canola which was in the range of 21-36% for n-hexane solvent.

Apart from the production of oil from the algae and conversion of the same into biodiesel, the effect of various process parameters affecting the production rate of bio-oil from biomass sources was studied, and researchers optimized the parameters. The application of response surface methodology (RSM) and artificial neural network (ANN) techniques for optimizing the process seems to be commonly used in many areas of research work. The ability to optimize the process with a minimum number of experimental runs made RSM and ANN popular tools for optimization. The optimization of oil extraction parameters was carried out in several works with a combination of factorial designs.

Ajala et al. [12] optimized the process of extracting shea butter from their kernels by using the Box-Behnken response surface methodology. The significance of the process parameters was also studied with analysis of variation (ANOVA). The optimized oil extraction of 67% of shea butter from the kernel was obtained for 30 g of kernels, 346 ml of n-hexane, and an extraction time of 40 minutes as optimal process parameters. Selvan et al. [13] employed the central composite design (CCD) for RSM with a second-order polynomial equation and found the optimal conditions for extracting oil from Aegle marmelos. They also employed ANN for the prediction of optimal parameters. Their results showed that the coefficient of determination was higher for ANN (0.998) than for RSM (0.976). Bokhari et al. [14] found the optimal conditions for extracting the oil from crude rubber seed oils by solvent extraction method using CCD RSM. The optimal conditions were found to be the seed to solvent ratio of 1 : 40, extraction temperature of 60°C, the reaction time of 4.5 hours, and ventilation time for the seeds of 3 hours. Okeleye et al. [15] conducted extensive work in optimizing the oil extraction from the Kariya seeds by solvent extraction method using D-optimal RSM and ANN. Their result showed that the prediction level was higher for ANN when compared to RSM. Osman et al. [16] used different optimization techniques to optimize the process parameters for extracting the oil from the sesame seeds using various solvents in the solvent extraction method. Their results showed that the ANN model showed very consistent performance compared to RSM and other modelling techniques. Ajala et al. [17] optimized the process parameters using D-optimal RSM and ANN for extracting oil from the yellow oleander seed by solvent extraction method. The optimized value obtained by both techniques was the same, but the level of fit and coefficient of determination was better for the ANN model.

Table 1: Levels of the input parameters.

			Coded level		
Input parameter		Unit	−1	0	+1
Particle size	θ_1	μm	0.366	0.462	0.641
Dryness level	θ_2	%	50	75	100
Solid to solvent ratio	θ_3	g/ml	1 : 5	1 : 10	1 : 15
Reaction time	θ_4	Hours	1	2	3
Reaction temperature	θ_5	°C	65	70	75

Abdissa [18] implemented the RSM technique to optimize the oil yield from the algae sludge using various solvents like methanol, ethanol, and hexane. The optimization result showed that the solvent hexane showed 61% of oil yield compared to other solvents. Aygün et al. [19] optimized Dyacrodes edulis seed oil extraction using polar and nonpolar solvents using RSM and ANN models. The optimization results showed better results using both techniques. Venkatesan et al. [20] used RSM and ANN models to optimize and predict the oil extraction from the C. innophyllum. The optimized biodiesel as 98.1% is derived with 0.94 volume to volume ratio of methanol to oil molar ratio, 0.98% by weight of potassium hydroxide catalyst loading, and 1 hour 20 minutes of reaction time with 70°C constant reaction temperature as predicted by Kriging model. Kenechi et al. [21] used the RSM model to predict the oil extraction of the luffa seed oil. The RSM model showed significant results with an R^2 value of around 84.7% and with a mean square error in the range of 0.55. The RSM indicated the temperature as the major factor influencing oil extraction from the luffa seed. Gul et al. [22], in their investigation, used wet microalgae Chlorella pyrenoidosa to extract the biodiesel by using the RSM model as the optimization technique. They used factors such as time, temperature, solvent-to-wet biomass ratio, and hydrochloric acid concentration with varying ranges. They identified that the RSM model showed temperature as the significant factor with a low p value and highest f value.

In the present work, algae oil was produced from spirogyra species using the Soxhlet apparatus with n-hexane as solvent. The process parameters involved during the oil

Table 2: The CCD arrived with Design-Expert factorial design and the response values.

Exp. no	Particle size θ_1 μm	Dryness level θ_2 %	Solid to solvent ratio θ_3 g/ml	Reaction time θ_4 Hours	Extraction temperature θ_5 ˚C	Oil yield % Experimental value	Predicted value RSM	Predicted value ANN
1	−1	-1	+1	−1	−1	22.13	22.42	22.15
2	−1	+1	−1	+1	−1	20.97	21.44	20.98
3	−1	-1	+1	+1	−1	23.05	23.06	22.95
4	−1	+1	+1	−1	−1	22.61	22.90	22.64
5	−1	+1	−1	−1	1	21.56	21.71	21.59
6	−1	+1	−1	−1	−1	20.05	20.22	19.86
7	−1	+1	−1	+1	+1	23.19	22.98	23.46
8	−1	−1	+1	−1	+1	23.58	23.30	23.60
9	−1	+1	+1	−1	+1	23.48	23.52	23.52
10	−1	−1	+1	+1	+1	23.53	24.00	23.54
11	−1	−1	−1	+1	−1	20.49	20.81	20.53
12	−1	+1	+1	+1	−1	23.53	23.56	23.55
13	−1	−1	−1	−1	+1	21.03	21.36	21.06
14	−1	0	0	0	0	23.63	24.31	23.65
15	−1	−1	−1	+1	+1	22.71	22.62	22.75
16	−1	−1	−1	−1	−1	19.57	19.61	19.73
17	−1	+1	+1	+1	+1	23.59	24.23	23.61
18	0	0	0	0	−1	23.26	22.87	23.27
19	0	0	0	−1	0	23.98	24.78	24.00
20	0	0	0	0	0	24.78	25.42	25.20
21	0	0	−1	0	0	24.04	24.48	24.07
22	0	0	0	+1	0	26.10	25.80	26.12
23	0	0	+1	0	0	26.58	26.65	26.54
24	0	0	0	0	0	25.23	25.42	25.20
25	0	0	0	0	0	25.58	25.42	25.20
26	0	−1	0	0	0	24.41	25.11	24.44
27	0	0	0	0	0	25.70	25.42	25.20
28	0	0	0	0	0	24.83	25.42	25.20
29	0	0	0	0	0	24.90	25.42	25.20
30	0	+1	0	0	0	25.72	25.52	25.75
31	0	0	0	0	0	25.35	25.42	25.20
32	0	0	0	0	+1	23.46	24.30	23.48
33	0	0	0	0	0	25.41	25.42	25.20
34	+1	+1	+1	−1	+1	22.82	22.80	22.83
35	+1	−1	+1	+1	+1	23.44	23.44	23.44
36	+1	+1	−1	−1	−1	18.81	18.80	18.89
37	+1	−1	−1	+1	−1	19.25	19.56	19.27
38	+1	+1	+1	+1	−1	22.29	22.55	22.32
39	+1	+1	−1	+1	+1	21.96	22.11	21.97
40	+1	−1	+1	−1	−1	20.89	21.31	20.91
41	+1	−1	+1	+1	−1	21.81	22.08	21.83
42	+1	+1	−1	+1	−1	19.72	20.15	19.74
43	+1	−1	−1	−1	−1	18.34	18.22	18.38
44	+1	+1	+1	−1	−1	21.35	21.75	21.38
45	+1	+1	+1	+1	+1	23.34	23.64	23.35
46	+1	−1	1	−1	+1	22.34	22.61	22.44

Table 2: Continued.

Exp. no	Particle size θ_1	Dryness level θ_2	Solid to solvent ratio θ_3	Reaction time θ_4	Extraction temperature θ_5	Oil yield %		
						Experimental value	Predicted value	
	μm	%	g/ml	Hours	˚C		RSM	ANN
47	+1	−1	−1	+1	+1	21.47	21.77	21.48
48	+1	0	0	0	0	23.54	23.32	23.65
49	+1	+1	−1	−1	+1	20.26	20.71	20.28
50	+1	−1	−1	−1	+1	20.37	20.38	19.88

production process were the solid to solvent ratio, reaction temperature, reaction time, the particle size of algae powder, and the dryness level of the algae powder which were considered and analyzed. The effect of these parameters on the yield of oil was computed using RSM and ANN. The combined analysis by RSM and ANN gives optimized process parameters for more oil yield. Also, a physiochemical analysis for the produced oil was undergone to find the suitable application of the produced algae oil.

2. Materials and Methodology

2.1. Materials. The algae *spirogyra* species algae were cultivated in a water tank at Karpagam Academy of Higher Education. Then, the collected algae were sun-dried and ground to a fine powder using a mechanical grinder. The algae were harvested with the help of a round metal mesh of a grid size of 1 mm. From 30 micron mesh, the powder obtained had an average size of 0.366 μm. Similarly, from a 40-micron mesh, the average powder size was 0.462 μm, and from a 60-micron mesh, the average powder size obtained was 0.641 μm. The n-hexane used for the experiments was purchased from the local dealer, and it specifies to the standard.

2.2. Methodology. The Soxhlet apparatus was loaded with the algae powder in the thimble fitted with the filter paper. The round bottom flask was filled with n-hexane in the quantity of 750 ml, and the process was carried out as per the experimental design [6–8]. At the completion of each experiment, the oil was extracted from the oil-solvent mixture through the distillation process by heating them to a temperature of 75 ˚C (boiling range of n-hexane). The oil yield is calculated using the following equation:

$$\text{Oil yield (\%)} = \frac{\text{Mass of extracted algae oil}}{\text{Mass of the total oil content present in 50g of algal powder used}} \times 100\%. \quad (1)$$

3. Experimental Design and RSM Modelling

The response surface methodology (RSM) can be abridged as defining the collaboration between the independent variables, modelling the system under design mathematically, and it saves time and cost by reducing the number of trials. With these advantages of RSM, a central composite design (CCD) factorial design with five input parameters and a second-order polynomial equation was employed to represent the oil yield (output parameter) [23]. The solid to solvent ratio, reaction temperature, reaction time, the powder's particle size, and the algae powder's dryness level were considered the input parameters for the modelling. The reason for selecting the input parameter for the optimization process is purely based on the factors influencing the extraction of the oil content from the algae. The factors which majorly influencing the oil extraction was found to be solid to solvent ratio, reaction temperature, reaction time, particle size of the powder, and the dryness level of the algae powder. The levels for the input parameters are given in Table 1. The level codes are given as −1 low, 0 middle, and +1 upper. For RSM modelling, a second-order polynomial was chosen as given in the following equation:

$$\begin{aligned} Y = {} & \beta_0 + \beta_1\theta_1 + \beta_2\theta_2 + \beta_3\theta_3 + \beta_4\theta_4 + \beta_5\theta_5 + \beta_{12}\theta_1\theta_2 \\ & + \beta_{13}\theta_1\theta_3 + \beta_{14}\theta_1\theta_4 + \beta_{15}\theta_1\theta_5 + \beta_{23}\theta_2\theta_3 + \beta_{24}\theta_2\theta_4 \\ & + \beta_{25}\theta_2\theta_5 + \beta_{34}\theta_3\theta_4 + \beta_{35}\theta_3\theta_5 + \beta_{45}\theta_4\theta_5 + \beta_{11}{\theta_1}^2 \\ & + \beta_{22}{\theta_2}^2 + \beta_{33}{\theta_3}^2 + \beta_{44}{\theta_4}^2 + \beta_{55}{\theta_5}^2, \end{aligned} \quad (2)$$

where Y represents the output variable (i.e., oil yield) and θ_1 to θ_5 represents the design factors. β_0 denotes the regression coefficient, and β_1 to β_{55} denotes the linear, interactive, and quadratic regression coefficients, respectively. According to the CCD factorial design, the number of experimental runs was found to be 50. All the experiments were carried out, and the coefficients of the second order polynomial equation were fitted through regression analysis. The significance of the statistical model was evaluated by using ANOVA. The Design-Expert (version 11.0) was used to

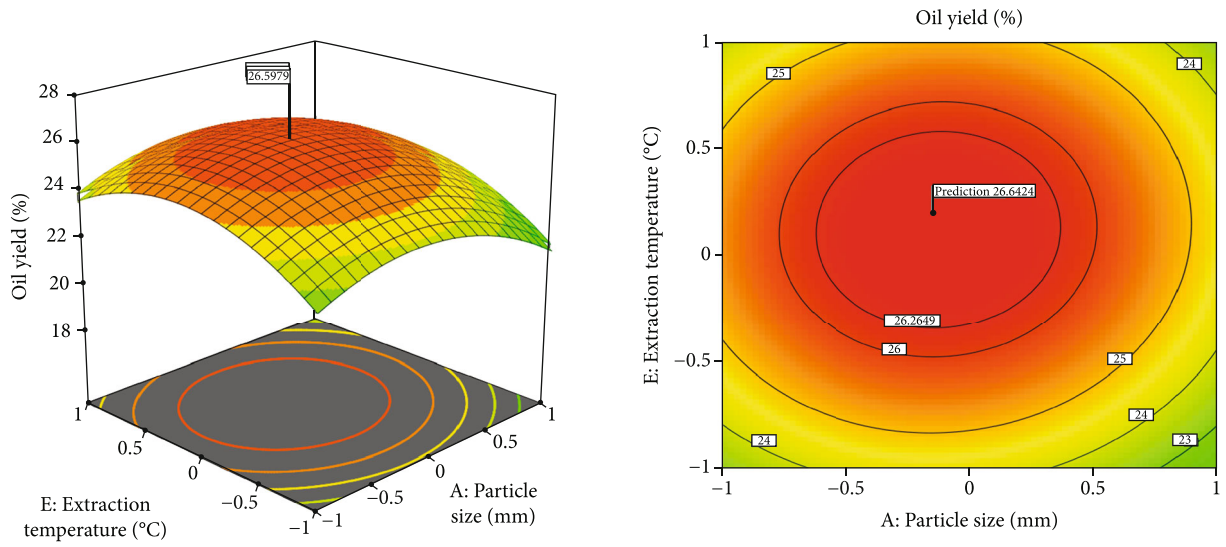

(a)

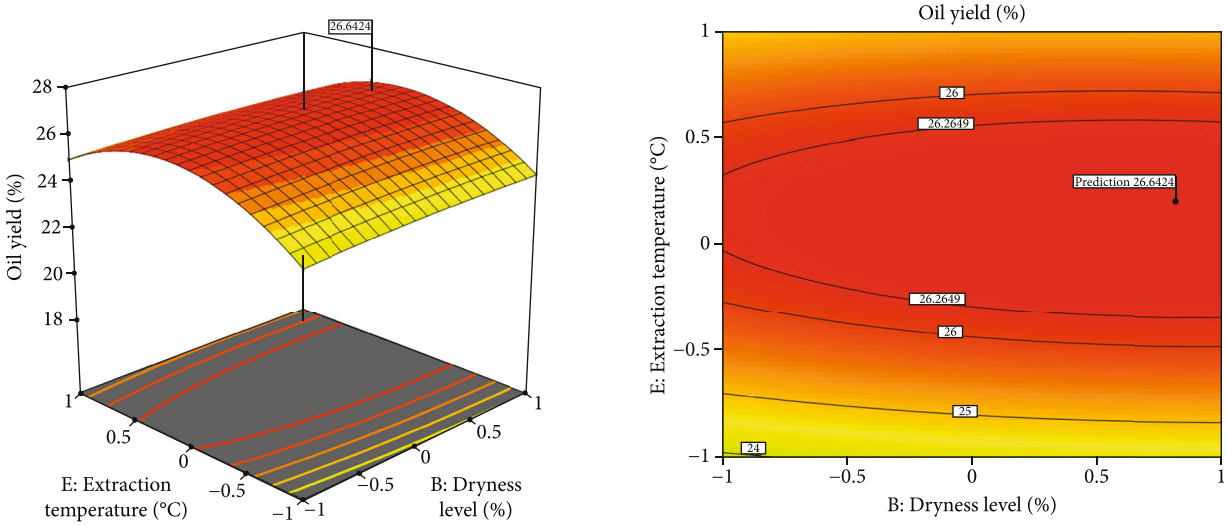

(b)

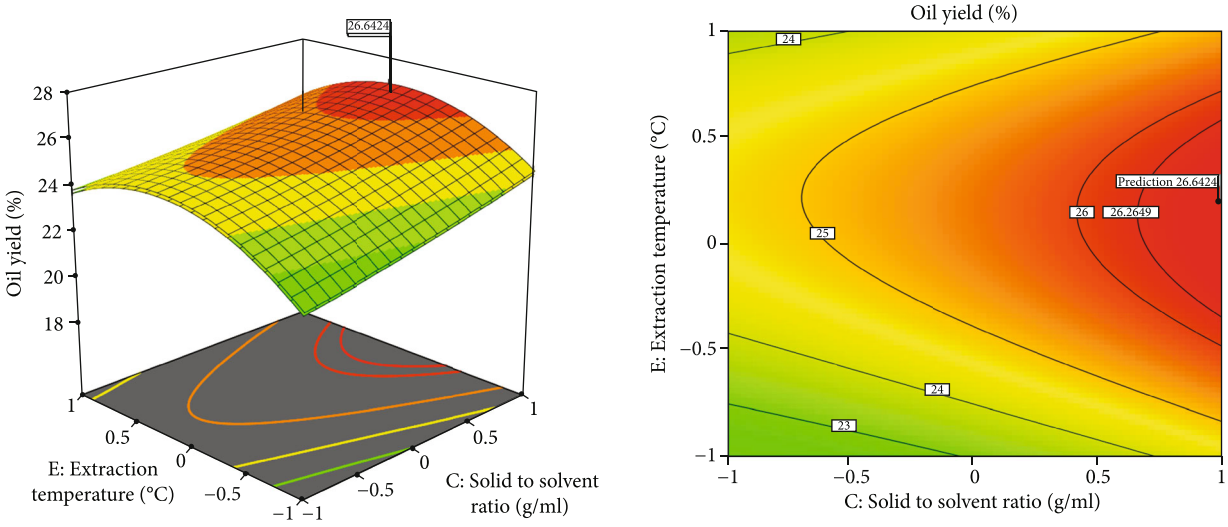

(c)

Figure 1: Continued.

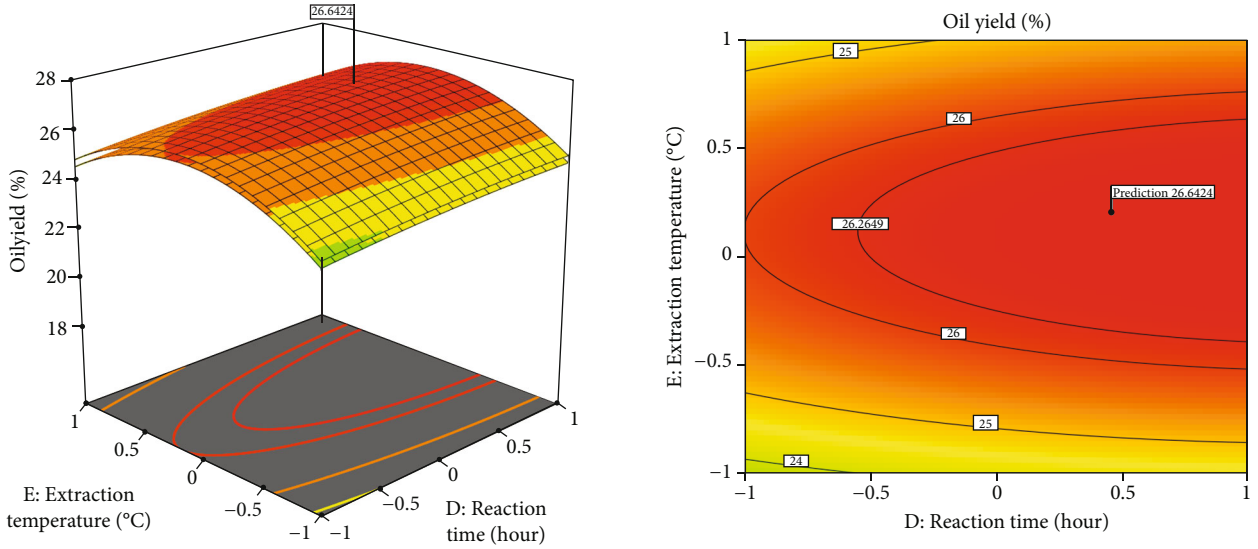

(d)

Figure 1: (a), (b), (c), (d) 3D surface plot and contour plot of the effect of oil yield % with the design factors.

conduct the statistical analysis. The coded levels using CCD with the help of the Design-Expert factorial design and the corresponding response values are shown in Table 2.

4. ANN Modelling

The artificial neural network (ANN) model can learn by itself with a limited set of input data and has high accuracy in predicting the output data. Also, the input data are stored in their database and have not been considered a separate data set, which is another benefit. This nature of ANN helps avoid the loss of data that does not work effectively in the model. Hence, based on these advantages, an ANN model was created using MATLAB R2009a version with neural network toolbox. The experimental data were normalized to avoid surfeiting the data set due to low to high variations. This normalization enhances the training of the prediction model. The standardization is done using the following equation [23]:

$$\text{standardization} = \left[\frac{2(\alpha_{\text{actual}} - \alpha_{\text{min}})}{(\alpha_{\text{maxi}} - \alpha_{\text{min}})}\right] - 1, \quad (3)$$

where α_{actual}, α_{min}, and α_{max} are the experimental data's actual, minimum and maximum values. The standardization process produces data from − 1 to +1. The performance of the ANN model relies on the number of the input layer, the number of neurons in the hidden layer and the number of output layers with different transfer functions and training algorithms. The $x - y - z$ topology was followed, where x denotes the number of the input layers, y represents the number of neurons in the hidden layer, and z denotes the number of the output layer. A three-layer ($x = 3$) feed-forward network with transig as a transfer function in the hidden layer, with the number of neurons ranging from $y = 5$ to 20, was studied by taking different transfer functions in the output layer ($z = 1$). The ANN model was trained using different training algorithms, and the model with the best coefficient of determination (R^2) and mean square error (MSE) was selected as the best prediction model.

5. Model Validation

The RSM and ANN models were validated to check for their efficiency in predicting the optimal values of the process parameters. This validation can be done by comparing the experimental data set with the predicted data set by the two models. In order to help this validation process, statistical formulas can be employed. Equations (4), (5), (6), (7), (8), and (9) represent the coefficient of determination, adjusted R^2, mean absolute error, root mean square error, standard error prediction, and the mean absolute percentage deviation, respectively [15, 17, 23–25]:

$$\text{coefficient of determination, } R^2 = 1 - \frac{\sum_{j=1}^{m}\left(z_{j,p} - z_{j,e}\right)^2}{\sum_{j=1}^{m}\left(z_{j,p} - z_{e,\text{avg}}\right)^2}, \quad (4)$$

$$\text{adjusted}R^2 = 1 - \left[\left(1 - R^2\right) \times \frac{m - 1}{m - k - 1}\right], \quad (5)$$

$$\text{Mean absolute error, MAE} = \sqrt{\frac{\sum_{j=1}^{m}\left|\left(z_{j,e} - z_{j,p}\right)\right|}{m}}, \quad (6)$$

$$\text{Root mean square error, RMSE} = \sqrt{\frac{\sum_{j=1}^{m}\left(z_{j,e} - z_{j,p}\right)^2}{m}}, \quad (7)$$

Table 3: ANOVA analysis.

Source	SS	Df	MS	F value	p value	
Model	199.75	20	9.99	62.85	< 0.0001	Significant
$\theta_1 - \theta_1$	8.19	1	8.19	51.53	< 0.0001	
$\theta_2 - \theta_2$	1.38	1	1.38	8.68	0.0063	
$\theta_3 - \theta_3$	39.30	1	39.30	247.30	< 0.0001	
$\theta_4 - \theta_4$	8.76	1	8.76	55.13	< 0.0001	
$\theta_5 - \theta_5$	16.92	1	16.92	106.47	< 0.0001	
$\theta_1\theta_2$	0.0018	1	0.0018	0.0111	0.9169	
$\theta_1\theta_3$	0.1504	1	0.1504	0.9462	0.3387	
$\theta_1\theta_4$	0.0358	1	0.0358	0.2255	0.6385	
$\theta_1\theta_5$	0.3365	1	0.3365	2.12	0.1563	
$\theta_2\theta_3$	0.0351	1	0.0351	0.2206	0.6421	
$\theta_2\theta_4$	0.0006	1	0.0006	0.0035	0.9533	
$\theta_2\theta_5$	0.1349	1	0.1349	0.8490	0.3644	
$\theta_3\theta_4$	0.6062	1	0.6062	3.81	0.0605	
$\theta_3\theta_5$	1.47	1	1.47	9.22	0.0050	
$\theta_4\theta_5$	0.0053	1	0.0053	0.0332	0.8567	
θ_1^2	6.27	1	6.27	39.44	< 0.0001	
θ_2^2	0.0300	1	0.0300	0.1888	0.6671	
θ_3^2	0.0411	1	0.0411	0.2585	0.6150	
θ_4^2	0.0459	1	0.0459	0.2887	0.5952	
θ_5^2	8.20	1	8.20	51.58	< 0.0001	
Residual	4.61	29	0.1589			
Lack of fit	3.75	22	0.1704	1.39	0.3440	Not significant
Pure error	0.8595	7	0.1228			
Cor total	204.36	49				
R^2	0.9854		Adj R^2	0.9752		
C. V %	1.76					

$$\text{Standard error prediction, SEP} = \frac{\text{RMSE}}{z_{\text{avg,e}}} \times 100, \quad (8)$$

$$\text{Mean absolute percentage deviation, MAPD} = \frac{100}{m}\sum_{j=1}^{m}\frac{\left|\left(z_{j,e} - z_{j,p}\right)\right|}{\left|\left(z_{j,e}\right)\right|}, \quad (9)$$

where $z_{j,p}$ denotes the predicted response, $z_{j,e}$ denotes the experimental value, $z_{e,avg}$ is the average of the total experimental data, m is the total number of experiments conducted, and k is the total number of design factors.

6. Results and Discussion

6.1. Results Obtained from the RSM. The experimental design based on CCD for full factorial was created, and the 50 sets of experiments were carried out. The results are shown in Table 2. The range of oil yield was found to be around 18.34 to 26.58%. The regression analysis was performed, and the regression of the second order polynomial equation was found to be

$$\begin{aligned} Y\,(\text{oil yield}) = {} & +25.2 - 0.4907\,\theta_1 + 0.2013\,\theta_2 + 1.0751\,\theta_3 \\ & + 0.5076\,\theta_4 + 0.7054\,\theta_5 - 0.0074\,\theta_1\theta_2 \\ & + 0.0685\,\theta_1\theta_3 + 0.0334\,\theta_1\theta_4 + 0.1025\,\theta_1\theta_5 \\ & - 0.0331\,\theta_2\theta_3 + 0.0042\,\theta_2\theta_4 - 0.0649\,\theta_2\theta_5 \\ & - 0.1376\,\theta_3\theta_4 - 0.2140\,\theta_3\theta_5 + 0.0128\,\theta_4\theta_5 \\ & - 1.5918\,\theta_1^2 - 0.1102\,\theta_2^2 + 0.1289\,\theta_3^2 \\ & - 0.1362\,\theta_4^2 - 1.8205\,\theta_5^2. \end{aligned} \quad (10)$$

The optimal process parameters were found using the regression equation (Equation (10)). On solving this equation, for an optimal oil yield of 26.62%, the optimal parameters were found to be 0.336 μm of particle size, 98.2% of dryness level, 1 : 14.9 solid to solvent ratio, 1.75 hours of reaction time, and 70.98 °C of extraction temperature. To confirm the above predicted optimal values

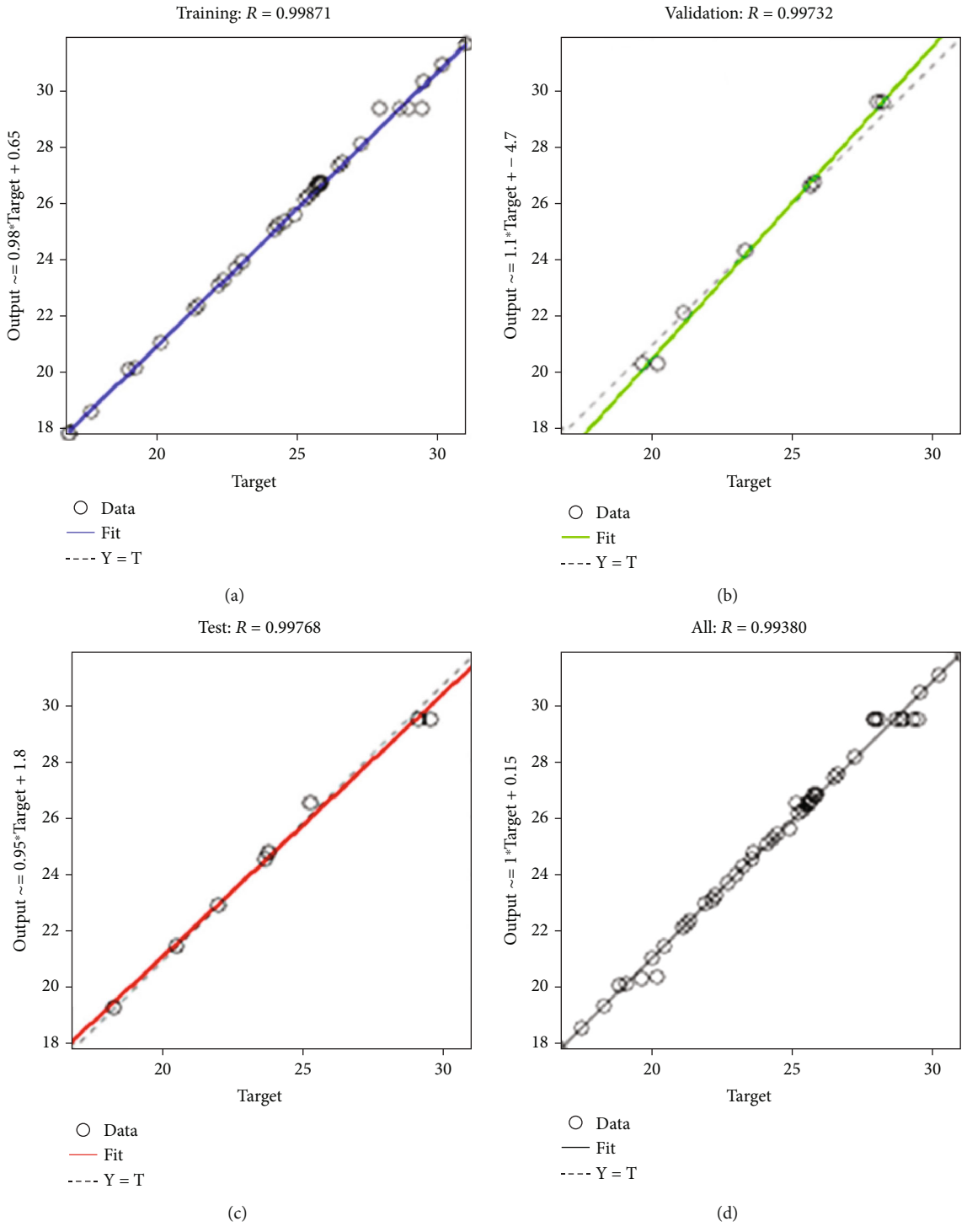

Figure 2: (a) Training data, (b) validation data, (c) test data, and (d) relation between predicted and experimental data set of the optimal ANN model.

using a regression equation, an experimental run was conducted, and the oil yield was found to be 26.34%. Figure 1 shows the interaction of different process parameters with the oil yield in the form of 3D surfaces and contour surfaces. All the contours showed that smaller particle size, maximum dryness level, maximum solid to solvent ratio, intermediate reaction time, and extraction temperature of

Table 4: Evaluated results of RSM and ANN model.

Performance parameters	R^2	Adj R^2	MAE	RMSE	SEP %	MAPD %
RSM	0.9854	0.9752	0.8524	0.4892	1.4251	1.3054
ANN	0.9892	0.9887	0.3057	0.1973	0.8365	0.4092

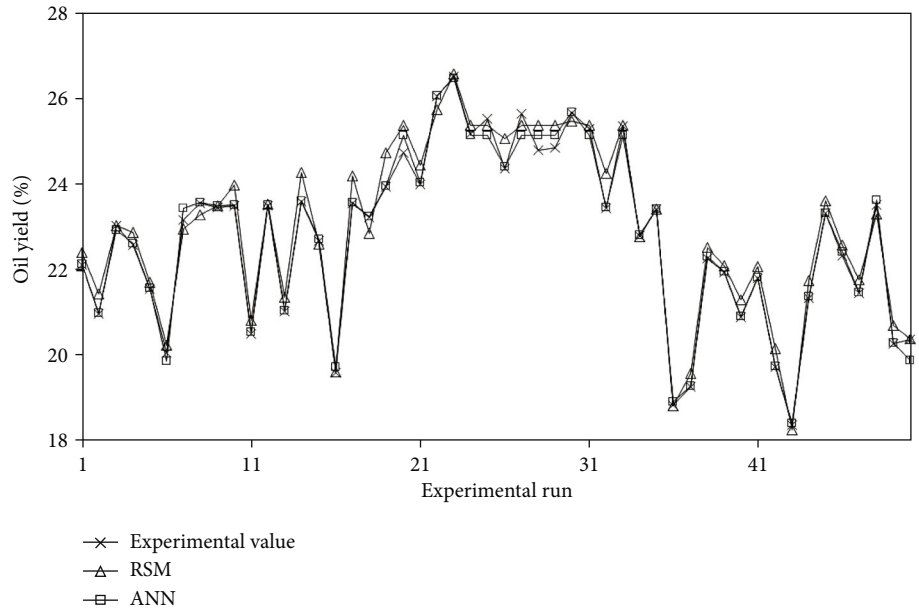

Figure 3: Comparison of experimental, predicted values of RSM and ANN.

the solvent resulted in the maximum oil yield from the algae spirogyra species. In order to know the significance of this model, an ANOVA analysis is given in Table 3. The p value less than 0.05 is considered to be significant; in this present RSM model, the interaction levels of the design factors θ_1 to θ_5, $\theta_3\theta_4$, ${\theta_1}^2$, and ${\theta_5}^2$ were less than 0.05. The R^2 of this present model is 0.9854, and the adj R^2 is 0.9752, which is in reasonable agreement and thus makes the model significantly. The lack of fit F value of 1.39 implies that the lack of fit is not significant relative to the pure error. There is a 34.40% chance of a lack of fit F value. This large F value could have occurred due to noise. Nonsignificant lack of fit is good [24, 26]. Also, the C.V of this model is 1.76, which is less than 5%, which shows that the model's reproducibility is good.

6.2. Results of ANN Model. The ANN model built for this present study was investigated by considering three layers ($x = 1$) of input factors of feed-forward type, the hidden layer withstanding transfer function with neurons ranging from $y = 5$ to 20 and the output layer of $z = 1$ for various training algorithms like Traingda, Traingdm, Traingdx, Trainlm, Trainrp, and Trainseg. The experimental data set was segregated into 70% of data for training remaining 30% of data for testing and validation [24]. The network model was run for various topologies, and the optimal topology was found with the model's best R^2 value and MSE. It was found that the optimal network topology was 3 : 11 : 1 with transig as transfer function in the input layer and purelin as transfer function in the output layer for Levenberg–Marquardt training algorithm [15, 17, 24]. The optimal network is showcased in Figures 2(a)–2(d) with R values for training, validation, testing, and overall, as 0.9987, 0.9973, 0.9976 and 0.9938, respectively. These R values confirm the degree of better correlation with the experimental and predicted data. The coefficient of determination for the optimal network topology was 0.9892 and MAE of 0.012; this shows that the prediction accuracy of the optimal model is very high. The oil yield values predicted by this model are equivalence to the experimental oil yield values [27, 28].

6.3. Evaluation of the RSM and ANN Model. The precision and accuracy of the developed RSM and ANN models were evaluated by calculating the performance parameters like R^2, adj R^2, MAE, RMSE, SEP, and MAPD using the Equations (4) to (9). The values calculated are shown in Table 4. The R^2 value for the RSM and ANN model seems to be nearby, making both the models better for optimizing the oil yield parameters. But the MAPD for RSM is higher than the ANN, which makes the ANN model reliable and consistent. Figure 3 compares the predicted values of RSM and ANN with the experimental values. It can be seen that the predicted values of the ANN model were very close to the experimental value when compared to the RSM predicted values. The capability of the ANN model for nonlinear data evaluation is more precise than the second-order polynomial model of RSM. Hence, the ANN model efficacy is better than the RSM model for optimization and modelling of this present study [24, 26].

6.4. Physiochemical Properties of the Extracted Oil. The various physicochemical properties of the extracted oil were compared with standard algae oil, diesel, biodiesel, algae oil from other species, and biomass using the solvent extraction method, shown in Table 5 [29]. The heating value of the extracted oil was found to be 32.57 MJ/kg, comparable to diesel biodiesel standard [28, 30]. The flash point of the extracted oil was around 79 °C, which is in range with the standard value. The density and the kinematic viscosity of the extracted oil were less than the standard values, which shows that the oil extracted can be used as an alternative fuel source in IC engines. The saponification value shows the

Table 5: Physio chemical properties of various biomass compared with standard values of diesel and biodiesel with the present study.

Type of biomass	Solvent used	Density kg/m^3	Specific gravity	Kinematic viscosity, mm^2/s	Acid value, mg KOH/g oil	Iodine value, g I_2/100 g oil	Saponification value, mg KOH/g oil	Calorific value, MJ/kg	Cetane number	Flash point, °C	Ref. no
ASTM standards		4052-91	D5355	D445	D1980-87	D96	D221	D240	D613	D664	
Diesel	—	837	0.835	3.96				44.8	45-50	72	
Standard biodiesel	—	860-900	0.903 -0.921	1.9-6.0	0.8	120	—	37.27	47	130	[30]
Spirogyra sp. (present study)	n-Hexane	858	0.852	3.72	2.142	67	174.56	32.57	32.7	79	
Cladophora glomerata	n-Hexane	892	0.892	3.8	0.935	76.24	244.1	33.6	55.82	110	[31]
Chlorella sp.	n-Hexane/ethanol	912	0.912	4.73	0.37	97.12	—	37.86	—	179	[30]
Chlorophyta sp	n-Hexane	887	0.887	—	1.24	81.27	256	—	—	108	[27]
Dunalliela sp.	n-Hexane/methanol	864	0.864	4.13	0.835	48	196	34.53	—	168	[28]
Acutodesmus obliquus	Ethanol/n-hexane	945	0.945	3.33	7.4	156.4	165.66	36.54	31.82	127	[32]
Castor oil	n-Hexane	958	0.958	4.5	3.2	84.6	378.6	35.45	38.1	112	[33]
Calophyllum seed oil	n-Hexane -methanol (1 : 1)	885	0.885	2.6	13	126.8	152	—	—	—	[32]
Sandbox seed oil	n-Hexane	941	0.941	4.18	1.878	186.28	242.63		26.25		[34]
Kariya seed oil	n-Hexane	903	0.903	7.149	2.12	55.78	249.76	41.36	—	140	[35]

amount of potassium hydroxide required to form soap from one gram of lipid content. For the present study, the value found was 174.56 mg KOH/g of oil, which is within the standard value [30]. The free fatty acids present in the oil have saturated and unsaturated parts. The amount of unsaturated fatty acids present in the oil can be identified with the iodine value of that particular oil. Higher the values of iodine number, the higher the presence of double bonds of C = C in the oil. The iodine value of the algae oil in this study is in the range, which shows that the oil can be a better alternative energy source. The acid value illustrates the damaging effect of the oil-used material. The higher the acid value, the higher the damaging effects. In this present study, the acid value for the extracted oil was found to be 67 g I_2/100 g of oil, which is in the permissible range [28]. The cetane index of the extracted oil was found to be 32.7, which is a better value and shows that it can be used as fuel in CI engines [30]. In comparison, it can be shown that the algae oil obtained from the *Spirogyra* can be used as an alternative fuel.

7. Conclusion

The present work represents the modelling of the solvent extraction process by the Soxhlet apparatus to extract oil from the algae species spirogyra. The optimization models were created using RSM and ANN to find the optimal process parameters for oil extraction from the algae. The optimal conditions were found to be 0.336 μm of particle size, 98.2% of dryness level, 1 : 14.9 solid to solvent ratio, 1.75 hours of reaction time, and 70.98 °C of extraction temperature for an optimum oil yield of 26.62%. The ANN model was found to be the best model when compared with the RSM model with improved performance parameters. The physiochemical properties were determined as per ASTM standards for the extracted oil, and the results showed that the extracted oil from the spirogyra species could be a better alternative energy source. Further, the extracted oil from the algae spirogyra species can be produced in large quantity by cultivating them in large tanks. And this extracted oil can be mixed with the mineral fuels in certain ratio and used as an alternative fuel in the diesel engine.

Data Availability

The data used to support the findings of this study are included within the article.

Conflicts of Interest

The authors declare that there is no conflict of interest regarding the publication of this article.

Acknowledgments

The authors sincerely thank the Karpagam Academy of Higher Education (KAHE), Coimbatore, India, and appreciate the support from Jimma Institute of Technology, Jimma University, Jimma, Ethiopia, for the research and preparation of the manuscript.

References

[1] L. Gouveia and A. C. Oliveira, "Microalgae as a raw material for biofuels production," *Journal of Industrial Microbiology & Biotechnology*, vol. 36, no. 2, pp. 269–274, 2009.

[2] H. Chen, D. Zhou, G. Luo, S. Zhang, and J. Chen, "Macroalgae for biofuels production: progress and perspectives," *Renewable and Sustainable Energy Reviews*, vol. 47, pp. 427–437, 2015.

[3] T. M. Mata, A. A. Martins, and N. S. Caetano, "Microalgae for biodiesel production and other applications: a review," *Renewable and Sustainable Energy Reviews*, vol. 14, no. 1, pp. 217–232, 2010.

[4] M. Yuvarani, D. Kubendran, A. R. Salma Aathika et al., "Extraction and characterization of oil from macroalgae Cladophora glomerata," *Energy Sources, Part A: Recovery, Utilization, and Environmental Effects*, vol. 39, no. 23, pp. 2133–2139, 2017.

[5] R. Halim, B. Gladman, M. K. Danquah, and P. A. Webley, "Oil extraction from microalgae for biodiesel production," *Bioresource Technology*, vol. 102, no. 1, pp. 178–185, 2011.

[6] N. Abdullah, N. A. Amran, and N. H. M. Yasin, "Algae oil extraction from freshwater microalgae Chlorella vulgaris," *Malaysian Journal of Analytical Sciences*, vol. 21, no. 3, pp. 735–744, 2017.

[7] P. Hidalgo, G. Ciudad, and R. Navia, "Evaluation of different solvent mixtures in esterifiable lipids extraction from microalgae Botryococcusbraunii for biodiesel production," *Bioresource Technology*, vol. 201, pp. 360–364, 2016.

[8] J. C. Attah and J. A. Ibemesi, "Solvent extraction of the oils of rubber, melon, pumpkin and oilbean seeds," *Journal of the American Oil Chemists Society*, vol. 67, no. 1, pp. 25–27, 1990.

[9] S. R. Dasari and V. V. Goud, "Effect of pre-treatment on solvents extraction and physico-chemical properties of castor seed oil," *Journal of Renewable and Sustainable Energy*, vol. 6, no. 6, article 063108, 2014.

[10] S. R. Dasari and V. V. Goud, "Comparative extraction of castor seed oil using polar and non polar solvents," *International Journal of Current Engineering and Technology*, vol. 1, pp. 121–123, 2013.

[11] U. C. Lohani, P. Fallahi, and K. Muthukumarappan, "Comparison of ethyl acetate with hexane for oil extraction from various oilseeds," *Journal of the American Oil Chemists' Society*, vol. 92, no. 5, pp. 743–754, 2015.

[12] E. O. Ajala, F. Aberuagba, A. M. Olaniyan, and K. R. Onifade, "Optimization of solvent extraction of shea butter (Vitellaria paradoxa) using response surface methodology and its characterization," *Journal of Food Science and Technology*, vol. 53, no. 1, pp. 730–738, 2016.

[13] S. S. Selvan, P. S. Pandian, A. Subathira, and S. Saravanan, "Comparison of response surface methodology (RSM) and artificial neural network (ANN) in optimization of Aegle marmelos oil extraction for biodiesel production," *Arabian Journal for Science and Engineering*, vol. 43, no. 11, pp. 6119–6131, 2018.

[14] S. Kumar, S. Jain, and H. Kumar, "Prediction of jatropha-algae biodiesel blend oil yield with the application of artificial neural networks technique," *Energy Sources, Part A: Recovery, Utilization, and Environmental Effects*, vol. 41, no. 11, pp. 1285–1295, 2019.

[15] A. A. Okeleye and E. Betiku, "Kariya (Hildegardiabarteri) seed oil extraction: comparative evaluation of solvents, modeling, and optimization techniques," *Chemical Engineering Communications*, vol. 206, no. 9, pp. 1181–1198, 2019.

[16] H. Osman, I. Shigidi, and A. Arabi, "Multiple modeling techniques for assessing sesame oil extraction under various operating conditions and solvents," *Food*, vol. 8, no. 4, p. 142, 2019.

[17] S. O. Ajala and E. Betiku, "Yellow oleander seed oil extraction modeling and process parameters optimization: performance evaluation of artificial neural network and response surface methodology," *Journal of Food Processing and Preservation*, vol. 39, no. 6, pp. 1466–1474, 2015.

[18] D. Abdissa, "Optimization of oil extraction process from blended sludge and algae for biodiesel production," *Production Engineering Archives*, vol. 27, no. 3, pp. 203–211, 2021.

[19] T. Aygün and O. Topuz, "Optimization of extraction parameters and effect of different solvent systems on the omega-3 fatty acids content of algal oil (Nannochloropsis sp.). Eurasian," *Journal of Food Science and Technology*, vol. 5, no. 2, pp. 174–189, 2021.

[20] M. Morshed, K. Ferdous, M. R. Khan, M. S. I. Mazumder, M. A. Islam, and M. T. Uddin, "Rubber seed oil as a potential source for biodiesel production in Bangladesh," *Fuel*, vol. 90, no. 10, pp. 2981–2986, 2011.

[21] K. Nwosu-Obieogu, G. W. Dzarma, C. B. Ugwuodo, L. I. Chiemenem, and K. N. Akatobi, "Luffa seed oil extraction: response surface and neuro-fuzzy modelling performance evaluation and optimization," *Process Integration and Optimization for Sustainability*, vol. 6, no. 1, pp. 175–188, 2022.

[22] G. Muhammad, A. D. P. Ngatcha, Y. Lv et al., "Enhanced biodiesel production from wet microalgae biomass optimized via response surface methodology and artificial neural network," *Renewable Energy*, vol. 184, pp. 753–764, 2022.

[23] A. M. Akintunde, S. O. Ajala, and E. Betiku, "Optimization of Bauhinia monandra seed oil extraction via artificial neural network and response surface methodology: a potential biofuel candidate," *Industrial Crops and Products*, vol. 67, pp. 387–394, 2015.

[24] S. Mani, S. Jaya, and R. Vadivambal, "Optimization of solvent extraction of Moringa (Moringa oleifera) seed kernel oil using response surface methodology," *Food and Bioproducts Processing*, vol. 85, no. 4, pp. 328–335, 2007.

[25] R. M. Joshi and M. J. Pegg, "Flow properties of biodiesel fuel blends at low temperatures," *Fuel*, vol. 86, no. 1-2, pp. 143–151, 2007.

[26] B. O. Ighose, I. A. Adeleke, M. Damos, H. A. Junaid, K. E. Okpalaeke, and E. Betiku, "Optimization of biodiesel production from Thevetia peruviana seed oil by adaptive neuro-fuzzy inference system coupled with genetic algorithm and response surface methodology," *Energy Conversion and Management*, vol. 132, pp. 231–240, 2017.

[27] A. S. Yusuff, "Extraction, optimization, and characterization of oil from green microalgae *Chlorophyta* species," *Energy Sources, Part A: Recovery, Utilization, and Environmental Effects*, pp. 1–12, 2019.

[28] A. Zonouzi, M. Auli, M. J. Dakheli, and M. A. Hejazi, "Oil extraction from microalgae Dunalliela sp. by polar and non-polar solvents. International Journal of Agricultural and Biosystems," *Engineering*, vol. 10, no. 10, pp. 642–645, 2016.

[29] S. Aravind, D. Barik, P. Ragupathi, and G. Vignesh, "Investigation on algae oil extraction from algae Spirogyra by Soxhlet extraction method," *Materials Today: Proceedings*, vol. 43, pp. 308–313, 2021.

[30] S. Deshmukh, R. Kumar, and K. Bala, "Microalgae biodiesel: a review on oil extraction, fatty acid composition, properties and effect on engine performance and emissions," *Fuel Processing Technology*, vol. 191, pp. 232–247, 2019.

[31] A. M. Escorsim, G. da Rocha, J. V. Vargas et al., "Extraction of Acutodesmus obliquus lipids using a mixture of ethanol and hexane as solvent," *Biomass and Bioenergy*, vol. 108, pp. 470–478, 2018.

[32] A. P. Ibrahim, R. O. Omilakin, and E. Betiku, "Optimization of microwave-assisted solvent extraction of non-edible sandbox (Huracrepitans) seed oil: A potential biodiesel feedstock," *Renewable Energy*, vol. 141, pp. 349–358, 2019.

[33] I. A. Kartika, M. Cerny, V. Vandenbossche et al., "Direct Calophyllum oil extraction and resin separation with a binary solvent of n-hexane and methanol mixture," *Fuel*, vol. 221, pp. 159–164, 2018.

[34] O. Akaranta and A. C. I. Anusiem, "A bioresource solvent for extraction of castor oil," *Industrial Crops and Products*, vol. 5, no. 4, pp. 273–277, 1996.

[35] A. W. Adebayo, B. S. Ogunsina, and O. S. Gbadamosi, "The effect of cold-pressing and solvent extraction on some characteristics of kariya (Hildergadiabarteri) seed oil," *Nutrition & Food Science*, vol. 45, no. 4, pp. 625–633, 2015.

Hindawi
International Journal of Photoenergy
Volume 2022, Article ID 3437364, 8 pages
https://doi.org/10.1155/2022/3437364

Research Article

Artificial Intelligence-Based Deep Learning Model for the Performance Enhancement of Photovoltaic Panels in Solar Energy Systems

Radhey Shyam Meena,[1] Anoop Singh,[2] Shilpa Urhekar,[3] RohitBhakar,[4] Neeraj Kumar Garg,[5] Mohammad Israr,[6] D. P. Kothari,[7] C. Chiranjeevi,[8] and Prasath Srinivasan[9]

[1]*Ministry of New and Renewable Energy, New Delhi, India*
[2]*Department of Industrial & Management Engineering, Indian Institute of Technology, Kanpur, Uttar Pradesh 208016, India*
[3]*University of Petroleum and Energy Studies, Dehradun, Uttarakhand 248007, India*
[4]*Department of Electrical Engineering/Centre for Energy, Malaviya National Institute of Technology, Jaipur, Rajasthan 302017, India*
[5]*Department of Electrical Engineering, Engineering College, Jhalrapatan, Rajasthan 326023, India*
[6]*Maryam Abacha American University of Nigeria, Renewable Energy Society of India, New Delhi, India*
[7]*VNIT, Nagpur, Renewable Energy Society of India, New Delhi, India*
[8]*School of Mechanical Engineering, Vellore Institute of Technology, Vellore, Tamil Nadu 632014, India*
[9]*Department of Mechanical Engineering, College of Engineering and Technology, Mizan Tepi University, Ethiopia*

Correspondence should be addressed to Prasath Srinivasan; prasathsrinivasan@mtu.edu.et

Received 20 June 2022; Revised 20 August 2022; Accepted 24 August 2022; Published 17 September 2022

Academic Editor: B. R. Ramesh Bapu

This study looks into artificial intelligence methods for scaling solar power systems, such as standalone, grid-connected, and hybrid systems, in order to lessen environmental effect. When all essential information is provided, conventional sizing methods may be a feasible alternative. It is impossible to apply typical procedures in instances where data is unavailable. The new suggested artificial intelligence model employing multilayered perceptrons is employed for sizing solar systems, and this model functions on current photovoltaic modules that incorporate hybrid-sizing models; so, they should not be rejected entirely. In this work, the convergence speed of the proposed model for single diode, two diodes, and three diodes are the comparison factors to estimate the performance of the proposed model.

1. Introduction

As a result of the global energy crisis, many scientists and engineers are focusing their attention on renewable energy sources [1]. As a result of these findings, researchers were compelled to investigate new methods and materials [2] and tactics for converting sunlight into electrical energy or some form of energy. The conversion of solar radiation into electrical energy is accomplished through the use of photovoltaic (PV) systems. The difficulty in implementing solar systems is the high cost of their installation. There is a lot of literature devoted to figuring out how to make these systems more successful while also being less expensive. It has been demonstrated that artificial intelligence (AI) algorithms have a substantial impact on the performance of PV systems [3]. In photovoltaic systems, artificial intelligence algorithms can be utilized for modelling, sizing, control, fault diagnostics, and output estimation. It compares artificial intelligence algorithms with classical algorithms for each type of application [4]. Figure 1 shows the AI applications in solar panel.

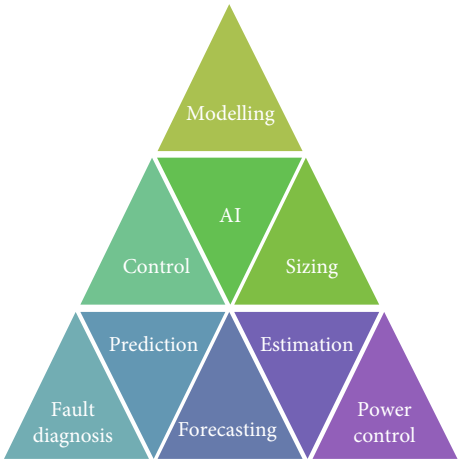

Figure 1: AI applications in solar panel.

Figure 2: Photovoltaic applications.

The slicing is the task to separate the information about the previous predictions. This was helpful to the deep learning model to predict the output details to construct the solar panel outputs. The control unit is the module to control the solar tracking and energy management modules. Research into photovoltaic systems is strongly reliant on the accurate modelling of solar cells, and the various applications of PV system are shown in schematic in Figure 2. To model a PV system, it is necessary to first determine the parameters of the system numerically. The solar cell circuits with a single diode and two diodes are both equivalent circuits in terms of performance [5]. Each of the five properties of the single-diode model is represented by a single value: diode saturation current, series resistance, shunt resistance, and photo generated current [6]. There are seven parameters in the double-diode model. The modelling and sizing of PV systems are dependent on obtaining accurate estimates of these attributes. To determine the parameters of solar cells, several standard procedures have been published and are available online [7].

An analytic-numerical technique for the five-parameter single-diode model is described above [8]. Initially, the analytic part acts as a jumping-off point for the numerical answer to be constructed. A pattern search approach [9] for single diode, two-dimensional diodes, and photovoltaic modules is described. Traditionally used methodologies, on the other hand, are unable to precisely predict the properties of solar-electricity-generating modules. Many scientists have turned to AI technologies for parameter detection as a result of this [10–15]. The synergy between artificial intelligence and other technologies can be used to build extremely powerful computer systems. The attempt to make up for flaws in traditional processes is a frequent theme in various alternate techniques. When designing computing systems, the goal is to make them better, more efficient, and more effective in certain situations. It is possible that the ability to learn and extrapolate from current knowledge will be required to achieve this goal. With the right application of intelligent technologies, it is possible to develop usable systems that are superior to those developed using traditional methodologies.

Many wealthy countries have also instituted particular strategies to encourage the use of renewable resources. Renewable energy (RE) technologies such as photovoltaic (PV) technology are among the promising of the current production. The importance of the artificial intelligence and other technologies can be used to build extremely powerful computer systems. It is possible to calculate the output of a unit by adding up all of the values. The deep learning provides the prediction about the earlier performance and is helpful to change the necessary actions in the lagging locations. The major contribution of this paper is to enhance the energy levels of the photovoltaic panel's capacity. These improvement predictions are performed with the help of artificial intelligence-based smart deep learning approach. So, the energy generations and management activates are performed as per the artificial mode. The results of the proposed model were getting higher level.

2. Related Works

An ANN is made up of a collection of small, interconnected processing units. Essentially, these components act as channels for the transmission of information. It is possible to attach both an input and a weight to the data of an incoming connection. It is possible to calculate the output of a unit by adding up all of the values. Even though ANNs are implemented using computers, there are no preprogrammed jobs associated with them. Instead, through training, they are trained to recognize patterns in the datasets that are used as inputs to the machine learning algorithms. It is possible to submit new patterns to them for prediction or categorization after they have been taught. Artificial neural networks [16–20] can be trained using a variety of methods, including computer programmes, physical models, and real-world systems. It is feasible to utilize an ANN to process a large number of inputs and produce outputs that can be used by using a large number of inputs and creating outcomes that can be used by designers. To develop artificial neural networks, it is necessary to have a thorough understanding of the human brain and neurological systems. It is necessary to connect processing units with links of various weights to generate a black box representation of systems.

In an artificial neural network, the neurons in each layer are connected to those in the layer above them by a network of connections known as a neural network. Data is fed into the neural network through the input layer, while the network response to the data is stored in the output layer. There may be extra layers between input and output in addition to the input and output layers. It is necessary to process the sum of the weights of each input and output to acquire a result in all hidden and output neurons [21–26], which is accomplished through the use of a nonlinear transfer function.

Even in the absence of predefined rules, a neural network is capable of processing massive volumes of data, and it can do so even when the input is skewed or otherwise inaccurate. Up to this point, traditional symbolic or logic-based strategies have been ineffective at dealing with these capabilities [27–30]. Conventional computer systems and artificial intelligence techniques will soon realize that neural computing can be used as an alternative or as a compliment. Once the network has been trained, neural computing has the potential to provide a significant speed advantage over classical computing. When it comes to implementing changes, the capacity of a system to be educated using datasets rather than written codes may be more cost-effective and convenient than writing codes. ANN interconnects the weights and that is altered as a means of gaining knowledge about the system. Many artificial neural networks (ANNs) are employed in the solution of issues such as pattern matching and data compression. As a promising and rising technology, artificial neural networks (ANNs) have emerged as a popular tool for forecasting and prediction [31, 32].

Fuzzy techniques can be incorporated into neural networks to improve their performance. A possible solution would be to allow a neural network for processing ambiguous input. Fuzzifying crisp input data before it goes through fuzzy neural processing is yet another way [33] that has been proposed. Modified neurons are the possibility in nodes at every layer of the network that translates fuzziness in the input to crispness in the output. Weights connecting the node to other nodes in the preceding layer have fuzzy values in the input vector, as do the weights connecting the node to other nodes in the preceding layer. Both the input data and the weights that are presented by the membership functions are defined as follows: a total of two membership functions are needed to complete the computation, one that reflects the weight of the fuzzy inputs using an updated summation method, and another that represents the original weighted integration using an additional membership function. The output of the node can then be determined using a crisp value by conducting a centered operation on the result and comparing the results [34, 35].

3. Proposed Method

Research and development on genetic and neurological systems have seen a significant surge in recent years, particularly since the late 1980s. Recent research [15–20] has focused on the application of evolutionary algorithms to improve the operation and design of neural networks. The use of genetic algorithms, artificial neural networks, and problem-solving methodologies is also being investigated in another project. New evolutionary computing approaches can be used to make neural networks easier to tune and design. Genetic algorithms can also be used to improve the performance of neural learning methods. The single-diode model consists of the four properties represented by a single value: they are the single-diode saturation current, single-diode series resistance, single-diode shunt resistance, and single-diode photogenerated current. Sizing renewable energy power systems is a complicated procedure due to the difficulty of achieving coordination between renewable energy resources, generators, energy storage, and loads.

The components of a PV power system include an array of solar cells, an energy storage component, and additional accessories. The photovoltaic (PV) array is a device that uses solar energy and converts it to direct current electricity. PV modules are connected to make an array. Electrical energy is stored in the storage component (which is typically a battery) and can be accessed at a later time as needed. The components of the system are in charge of regulating the system's operation. This includes a PV array tracker to maximize the quantity of the energy received from the solar panels. With the help of a powerful processor, the photovoltaic array output can be converted into a form that can be used by the end-user. Figure 3(a) shows the flowchart for estimating the sizing parameters based on MLP.

Because fuel consumption and maintenance costs are minimized when the null time of the engine-generator is reduced and the engine operates at its peak efficiency, it is possible to reduce fuel consumption and maintenance expenses. Renewable energy sources, energy storage components, and engine generators must all work together to ensure the system's stability, which requires careful coordination. The generic algorithms are very useful to understand the artificial neural networks and problem-solving methodologies. This will create the better understanding about the solar panel power production management and energy optimization systems. For their operation to be successful, grid-connected systems must be powered by electricity generated by a utility provider. In these configurations, the utility grid acts as both the system storage and backup power supply. To comply with utility power quality regulations for these systems, DC–AC inverters must be employed. The sizing renewable energy power systems is a complicated procedure due to the difficulty of achieving coordination between renewable energy resources, generators, energy storage, and loads.

According to Figure 3(a), MLP can be used to estimate the size parameters by estimating the size parameters. The model receives as inputs the location latitude and longitude, and as outputs, it returns two hybrid-sizing parameters based on the inputs (f, u). The block diagram of the model is depicted in Figure 3(b). The number of important sizing parameters has been determined by the results of the hybrid-sizing approach. Based on the information, it is concluded that the relative error does not surpass 6%.

The hybrid slicing is the function to manage the different entity-based or requirement-based slicing. This is used to separate the data type-based slicing modules. These techniques can be incorporated into neural networks to improve

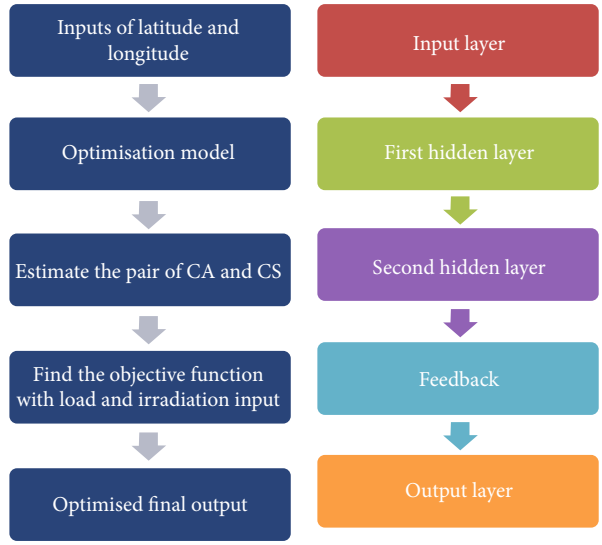

Figure 3: (a) Flowchart for estimating the sizing parameters based on MLP. (b) MLP block diagram.

their performance. A possible solution would be to allow a neural network for processing ambiguous input. Predictions made by the model include classifications based on which dataset is used as a training set. Based on the results of fine-tuned hyperparameter studies, the proposed MLP design includes a hidden layer with 16 neurons and an output layer with 16 neurons.

To study the effect of increasing the number of neurons in one hidden layer from 2 to 128 on performance, each one is multiplied by the previous number twice, for a total of four times. Whenever the study discovered the optimal number of neurons (let us say k), the study begins by adding layers of hidden neurons (let us say k per hidden layer) to examine how the prediction accuracy changes as the number of hidden layers increases. In these proposed configurations, the power utility and grid-based solar power plants act as both sides the system energy storage and backup power supply monitor. To comply with utility power quality regulations for these systems, direct and alternative current inverters must be employed. For prediction tasks, the sigmoid function is employed in MLP models that perform binary classification and thus perform binary classification. When it comes to deep learning architectures, the sigmoid function is widely used in its output layers. In the domain of IR, input values are transformed into output values in the range [0,1]. As a result, the sigmoid function is used to compress all input values between -1 and -1 to the sigmoid function, and this is also known as squash. In our shift to gradient learning, the sigmoid is considered the option because it approximates a thresholding unit in a smooth and differentiable manner. The sigmoid function can be represented mathematically in

$$\text{sigmoid}\,(x) = \frac{1}{1+e^{-x}}, \tag{1}$$

where x is the data computed by MLP layer.

With the softmax function and k-classes, we can classify scenarios that require multiple classifications. It is possible to transform a value into the vector using a probability distribution that consists of a total sum and therefore, it is normalized as follows.

$$\text{softmax}\,(x_i) = \frac{e^{x_i}}{\sum_{j=1}^{k} e^{x_j}}. \tag{2}$$

ReLU or the activation function is also implemented in our approach to some extent. Here is the ReLU formula in its most basic form as in

$$f(x) = \max\,(0, x). \tag{3}$$

In deep learning systems, ReLU has been the most frequently used activation function, and it has been responsible for some of the most cutting-edge discoveries that have been made available to researchers to date. In contrast to the sigmoid and tanh activation functions, the ReLU activation function assists models in deep learning in providing improved performance and generalization. Because the gradient-descent activation function represents a nearly linear function, linear models are easier to optimize with this method. The output of the previous hidden neural layer is changed by ReLU, which also serves as an activation function for the current hidden neural layer. Using ReLU, neural networks can be improved by accelerating their training, which in turn enhances their overall performance. The positive component of the ReLU is lower than the gradients of the logistic and hyperbolic tangent models, while the negative component of the ReLU is lower still.

Since training progresses at a faster rate than in previous years, the positive element of the score is updated more frequently. To eliminate overfitting concerns, we are exploring employing the Early Stopping technique with a five-day

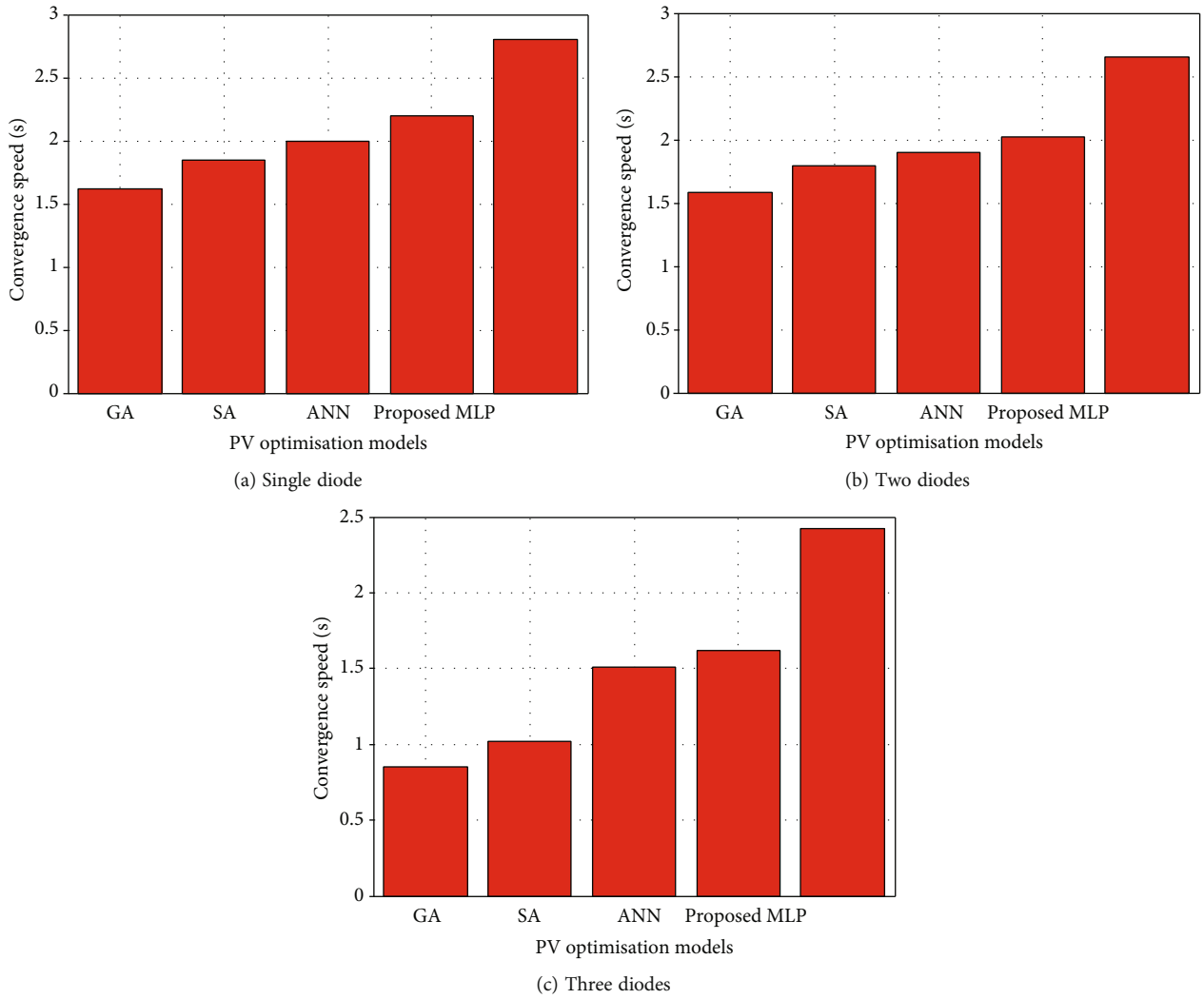

Figure 4: Convergence speed of various diodes.

patience period as an alternative. The learning process will be terminated as a result of this after five consecutive epochs of failure. To avoid this, the learning process must be terminated after 10 epochs, unless otherwise specified. In the network implementation with the Adam optimizer function, 100 batches are used with a learning rate of 0.001.

4. Results and Discussions

The PC utilized to conduct this investigation has the following specifications: an Intel (R) Core (TM) M380 CPU running at 2.53 GHz, 2 GB of RAM, and a 64-bit operating system. To validate the MLP-based PV model, a polycrystalline KC200GT PV module is used. As inputs to this MLP technique, information such as PV module datasheets, whale counts, and iterations are all submitted to the algorithm. The findings should be available in a few days. Initially, the MLP generates a random sample in the domain of interest to get things started. The entire number of solutions in this study is equal to the search agents that are assigned as 30. Figure 4 shows the convergence speed.

The study is used to determine the fitness function for each position. After that, the best fitness function is determined by trial and error. According to the individual fitness functions of each whale, a value of 2–0 is chosen for parameter a, which is then used to compute the values of two other parameters, A and C; the location of each neuron is changed in response to this value. The value of the parameter p controls whether the MLP moves in a spiral or a circular fashion. The previous stages are performed indefinitely until a termination threshold is reached. For the sake of this inquiry, the MLP was ended after 500 iterations of the procedure. As illustrated in Figure 4 where it takes around 2.8 s, the advantage of the MLP's rapid convergence speed is obvious. The algorithm code is developed using the Matlab programming language. According to MLP, a single-diode PV model yields the best optimal values, a double-diode PV model yields the next best optimal values, and a three-diode PV model yields the next best optimal values, according to MLP.

When compared to models constructed using iterations and the GA technique, the MLP-based single-diode PV

Table 1: Electrical specifications considered for the PV module under STC.

Parameters	Value
I_{sc}	8.2241 A
V_{oc}	32.934 V
I_{mp}	7.6115 A
V_{mp}	26.153 V
P_{max}	200.054 W
K_v	-0.121 V/°C
K_i	0.00324 A/°C
N_s	54.15

Table 2: Performance evaluation of single-diode PV MLP model.

Parameters	Value
I_{pv} (A)	8.292
I_o (A)	8.5514×10^{-8}
R_s (Ω)	0.291
R_p (Ω)	424.262
$\propto$	1.297

Table 3: Performance evaluation of double-diode PV MLP model.

Parameters	Value
I_{o1} (A)	1.921×10^{-8}
I_{o2} (A)	3.735×10^{-10}
R_s (Ω)	0.282
R_p (Ω)	291.415
$\propto_1$	1.214
$\propto_2$	1.134
I_{pv} (A)	8.151

Table 4: Performance evaluation of three-diode PV MLP model.

Parameters	Value
I_{pv} (A)	8.045
$\propto_3$	0.999
$\propto_2$	1.208
$\propto_1$	1.290
R_p (Ω)	333.680
R_s (Ω)	0.334
I_{o3} (A)	4.816×10^{-10}
I_{o2} (A)	4.572×10^{-10}
I_{o1} (A)	2.512×10^{-8}

model provided in this research performs significantly better. This work was carried out using the Matlab Optimization Toolbox, which is an integrated part of Matlab, to optimize the fitness function of a three-diode PV model using GA and SA techniques, with the results to demonstrate the outcomes of the Matlab Optimization Toolbox. MLP-based optimization is competitive when compared to other heuristic optimization strategies. Based on these findings, we may conclude that the MLP-derived PV model parameter values are within a suitable range and are equivalent to those obtained using other optimization methods such as genetic algorithms. Upon further examination of the curves under various temperatures and levels of irradiation, it was discovered that the PV model with a three-diode is accurate in all circumstances and the performance results are shown from Tables 1–4.

5. Conclusions

As a result of these applications, it is necessary to emphasize the importance of using artificial intelligence for PV system sizing. Artificial intelligence techniques have demonstrated that it is feasible to properly and successfully size photovoltaic systems. In general, artificial intelligence techniques have demonstrated the ability to precisely and successfully size PV systems based on certain readily available data. It is undeniable that artificial intelligence-based solutions for PV system sizing are becoming increasingly popular, particularly in rural areas. It is possible to employ AI as a design tool to assist in determining the proper size of solar PV systems. There has been no attempt made to depict every possible application of AI, and the examples offered here are by no means exhaustive in their scope. This research investigates several AI solutions for scaling PV power systems, including standalone, grid-connected, and hybrid systems, to reduce their environmental impact. When all of the relevant information is available, conventional methods of sizing may be a viable option. It is impossible to use traditional approaches in situations where the data is not available to them. Thus, this work showed that the proposed model provides the best results while compared with existing models.

Data Availability

The data used to support the findings of this study are included within the article. Further data or information is available from the corresponding author upon request.

Conflicts of Interest

The authors declare that there are no conflicts of interest regarding the publication of this paper.

Acknowledgments

The authors appreciate the supports from the Mizan Tepi University, Ethiopia, for the research and preparation of the manuscript.

References

[1] F. Touati, A. Khandakar, M. E. Chowdhury, S. P. Antonio Jr., C. K. Sorino, and K. Benhmed, "Photo-Voltaic (PV) Monitoring System, Performance Analysis and Power Prediction Models in Doha, Qatar," in *In Renewable Energy-Technologies and Applications*, IntechOpen, 2020.

[2] T. Maridurai, R. Arivazhagan, S. SivaChandran, R. Venkatesh, and S. Baskar, "Review on direct steam generation using concentrated solar collectors," in *AIP Conference Proceedings*, vol. 2473, p. 020008, Chennai, India, 2022.

[3] S. K. Srivastava, "Application of Artificial Intelligence in Renewable Energy," in *In 2020 International Conference on Computational Performance Evaluation (ComPE)*, pp. 327–331, Shillong, India, July 2020.

[4] S. Rao, S. Katoch, V. Narayanaswamy et al., "Machine learning for solar array monitoring, optimization, and control," *Synthesis Lectures on Power Electronics*, vol. 7, no. 1, pp. 1–91, 2020.

[5] N. Yuvaraj, K. Praghash, R. A. Raja, and T. Karthikeyan, "An investigation of garbage disposal electric vehicles (GDEVs) integrated with deep neural networking (DNN) and intelligent transportation system (ITS) in smart city management system (SCMS)," *Wireless Personal Communications*, vol. 123, no. 2, pp. 1733–1752, 2022.

[6] P. D. Muthusamy, G. Velusamy, S. Thandavan, B. R. Govindasamy, and N. Savarimuthu, "Industrial Internet of things-based solar photo voltaic cell waste management in next generation industries," *Environmental Science and Pollution Research*, vol. 29, no. 24, pp. 35542–35556, 2022.

[7] B. Gobinathan, M. A. Mukunthan, S. Surendran et al., "A novel method to solve real time security issues in software industry using advanced cryptographic techniques," *Scientific Programming*, vol. 2021, Article ID 3611182, 9 pages, 2021.

[8] M. A. Rodriguez Licea, "Fault tolerant boost converter with multiple serial inputs and output voltage regulation for vehicle-to-aid services," *Energies*, vol. 13, no. 7, p. 1694, 2020.

[9] E. Cardelli, A. Faba, M. Pompei, and S. Quondam Antonio, "Pattern search approach to ferromagnetic material modelling," *International Journal of Numerical Modelling: Electronic Networks, Devices and Fields*, vol. 32, no. 4, p. e2271, 2019.

[10] A. N. Akkewar, "Statistical analysis of hybrid renewable energy systems by using artificial intelligence," *Journal of Next Generation Technology (ISSN: 2583-021X)*, vol. 1, no. 2, 2021.

[11] N. Elizabeth Michael, M. Mishra, S. Hasan, and A. Al-Durra, "Short-term solar power predicting model based on multi-step CNN stacked LSTM technique," *Energies*, vol. 15, no. 6, p. 2150, 2022.

[12] A. M. Kuriakose, D. P. Kariyalil, M. Augusthy, S. Sarath, J. Jacob, and N. R. Antony, "Comparison of Artificial Neural Network, Linear Regression and Support Vector Machine for Prediction of Solar PV Power," in *In 2020 IEEE Pune Section International Conference (PuneCon)*, pp. 1–6, Pune, India, December 2020.

[13] L. Abualigah, R. A. Zitar, K. H. Almotairi et al., "Wind, solar, and photovoltaic renewable energy systems with and without energy storage optimization: a survey of advanced machine learning and deep learning techniques," *Energies*, vol. 15, no. 2, p. 578, 2022.

[14] I. Moukhtar, A. Z. El Dein, A. A. Elbaset, and Y. Mitani, *Solar Energy: Technologies, Design, Modeling, and Economics*, Springer Nature, 2020.

[15] G. de Freitas Viscondi and S. N. Alves-Souza, "Solar irradiance prediction with machine learning algorithms: a Brazilian case study on photovoltaic electricity generation," *Energies*, vol. 14, no. 18, p. 5657, 2021.

[16] G. R. Yang and X. J. Wang, "Artificial neural networks for neuroscientists: a primer," *Neuron*, vol. 107, no. 6, pp. 1048–1070, 2020.

[17] A. Xu, H. Chang, Y. Xu, R. Li, X. Li, and Y. Zhao, "Applying artificial neural networks (ANNs) to solve solid waste-related issues: a critical review," *Waste Management*, vol. 124, pp. 385–402, 2021.

[18] B. Li, C. Delpha, D. Diallo, and A. Migan-Dubois, "Application of artificial neural networks to photovoltaic fault detection and diagnosis: a review," *Renewable and Sustainable Energy Reviews*, vol. 138, p. 110512, 2021.

[19] S. Chung and L. F. Abbott, "Neural population geometry: an approach for understanding biological and artificial neural networks," *Current Opinion in Neurobiology*, vol. 70, pp. 137–144, 2021.

[20] G. Goh, N. Cammarata, C. Voss et al., "Multimodal neurons in artificial neural networks," *Distill*, vol. 6, no. 3, p. e30, 2021.

[21] S. Mangini, F. Tacchino, D. Gerace, D. Bajoni, and C. Macchiavello, "Quantum computing models for artificial neural networks," *EPL (Europhysics Letters)*, vol. 134, no. 1, p. 10002, 2021.

[22] P. M. Kumar, R. Saravanakumar, A. Karthick, and V. Mohanavel, "Artificial neural network-based output power prediction of grid-connected semitransparent photovoltaic system," *Environmental Science and Pollution Research*, vol. 29, no. 7, pp. 10173–10182, 2022.

[23] F. Masi, I. Stefanou, P. Vannucci, and V. Maffi-Berthier, "Thermodynamics-based artificial neural networks for constitutive modeling," *Journal of the Mechanics and Physics of Solids*, vol. 147, p. 104277, 2021.

[24] A. B. Çolak, "An experimental study on the comparative analysis of the effect of the number of data on the error rates of artificial neural networks," *International Journal of Energy Research*, vol. 45, no. 1, pp. 478–500, 2021.

[25] G. Di Franco and M. Santurro, "Machine learning, artificial neural networks and social research," *Quality & Quantity*, vol. 55, no. 3, pp. 1007–1025, 2021.

[26] J. A. Jeffrey, S. S. Kumar, P. Vaidyaa, A. Nicho, A. Chrish, and J. Joshith, "Effect of turning parameters in cylindricity and circularity for o1 steel using ANN," *Materials Today: Proceedings*, vol. 59, no. 2, pp. 1291–1294, 2022.

[27] G. Ciatto, R. Calegari, and A. Omicini, "2P-Kt: a logic-based ecosystem for symbolic AI," *SoftwareX*, vol. 16, p. 100817, 2021.

[28] R. Mehta, "Performance analysis of fuzzy logic-based digital library architecture using n-ary Huffman coding, regression and fairness measures," *SN Computer Science*, vol. 3, no. 2, pp. 1–18, 2022.

[29] S. Ferilli and D. Redavid, "Experiences on the improvement of logic-based anaphora resolution in English texts," *Electronics*, vol. 11, no. 3, p. 372, 2022.

[30] A. K. Pandey, V. Singh, and S. Jain, "Fuzzy Logic Based Maximum Power Point Tracking Scheme for PV System Using PV and IV Characteristics," in *In 2021 IEEE 4th International Conference on Computing, Power and Communication Technologies (GUCON)*, pp. 1–6, Kuala Lumpur, Malaysia, September 2021.

[31] D. Patel, S. Patel, P. Patel, and M. Shah, "Solar radiation and solar energy estimation using ANN and fuzzy logic concept: a comprehensive and systematic study," *Environmental Science and Pollution Research*, vol. 29, no. 22, pp. 32428–32442, 2022.

[32] Ü. Ağbulut, A. E. Gürel, and Y. Biçen, "Prediction of daily global solar radiation using different machine learning algorithms: evaluation and comparison," *Renewable and Sustainable Energy Reviews*, vol. 135, p. 110114, 2021.

[33] W. Dong, Q. Yang, X. Fang, and W. Ruan, "Adaptive optimal fuzzy logic based energy management in multi-energy microgrid considering operational uncertainties," *Applied Soft Computing*, vol. 98, p. 106882, 2021.

[34] S. Mishra, S. K. Dash, P. K. Ray, and P. S. Puhan, "Analysis and experimental evaluation of novel hybrid fuzzy-based sliding mode control strategy for performance enhancement of PV fed DSTATCOM," *International Transactions on Electrical Energy Systems*, vol. 31, no. 10, p. e12815, 2021.

[35] D. Zeltner, B. Schmid, G. Csiszár, and O. Csiszár, "Squashing activation functions in benchmark tests: towards a more explainable artificial intelligence using continuous-valued logic," *Knowledge-Based Systems*, vol. 218, p. 106779, 2021.

Hindawi
International Journal of Photoenergy
Volume 2022, Article ID 2131583, 12 pages
https://doi.org/10.1155/2022/2131583

Review Article

Role of Microbes and Nanomaterials in the Removal of Pesticides from Wastewater

Arpita Roy[1], **Madhura Roy**[2], **Saad Alghamdi**[3], **Anas S. Dablool**[4], **Angham Ahmed Almakki**[5], **Ismat H. Ali**[6], **Krishna Kumar Yadav**[7], **Md. Rabiul Islam**[8], **and Marina M. S. Cabral-Pinto**[9]

[1]*Department of Biotechnology, School of Engineering & Technology, Sharda University, Greater Noida, India*
[2]*Centre for Translational and Clinical Research, School of Chemical and Life Sciences, Jamia Hamdard University, India*
[3]*Laboratory Medicine Department, Faculty of Applied Medical Sciences, Umm Al-Qura University, Makkah, Saudi Arabia*
[4]*Department of Public Health, Health Sciences College at Al-Leith, Umm Al-Qura University, Makkah, Saudi Arabia*
[5]*Department of Laboratory and Blood Bank, Security Forces Hospital, Makkah, Saudi Arabia*
[6]*Department of Chemistry, College of Science, King Khalid University, P.O. Box 9004, Abha 61413, Saudi Arabia*
[7]*Faculty of Science and Technology, Madhyanchal Professional University, Ratibad, Bhopal 462044, India*
[8]*Department of Pharmacy, University of Asia Pacific, Dhaka, Bangladesh*
[9]*Geobiotec Research Centre, Department of Geosciences, University of Aveiro, 3810-193 Aveiro, Portugal*

Correspondence should be addressed to Arpita Roy; arpita.roy@sharda.ac.in and Md. Rabiul Islam; robi.ayaan@gmail.com

Received 15 April 2022; Accepted 25 May 2022; Published 8 June 2022

Academic Editor: B. R. Ramesh Bapu

Pesticides are a class of xenobiotic compounds that are recalcitrant and show persistence in the environment for a longer period of time. Research studies have linked their potential for mutagenicity, teratogenicity, and carcinogenicity. The accumulation of pesticides in water sources due to runoff from agricultural lands has posed a serious threat to the biota of the water ecosystem as well as to the human population. Long-term exposure to pesticides can cause neurological disorders, reproductive complications, cancer, immunological, and pulmonary diseases. The use of pesticides has dramatically surged in agricultural as well as nonagricultural practices. Tons of pesticides are applied in the fields, but a limited amount reaches to the target organism while the rest is wasted and gets accumulated in soil or ends up in water sources like groundwater or river, which results in eradication of nontarget organisms. A variety of pesticides are used for pest management, such as organochlorine (DDT), carbamates (carbaryl), organophosphates (malathion), and pyrethroids (pyrethrins). These chemicals are highly toxic to flora and fauna because of their nonbiodegradable and persistence nature. Biomagnification of pesticides usually leads to cause various problems in human beings. Organochlorines like DDT have been banned in many developed countries due to these reasons. Therefore, the removal of pesticides from wastewater and natural water sources is of utmost importance. Conventional methods possess various limitations; therefore, there is a requirement of an alternative method which can efficiently remove these pollutants from the wastewater. In this review, environmental impacts and health-related complications of pesticides and microbial remediation approaches and use of different nanomaterials in the pesticide removal have been discussed.

1. Introduction

In agriculture, crops are attacked by various pests which include organisms such as insects, fungi, bacteria, unwanted crops (weeds), and some animals. If the pests remain uncontrolled, they would destroy and damage the crop and thus lead to substantial economic loss for the agronomist. Pesticides have come to aid in the agricultural practices as they are able to eliminate, repel, mitigate, and control the pests attacking the crops. There is a diverse range of synthetic as

well as natural compounds which fall under pesticides, and depending upon the target organism, they fall under insecticides, herbicides, etc. The largest demand of pesticides is generated by agriculture which accounts for 85% of the whole production worldwide, and the rest is used for other purposes like control of seasonal vector-borne diseases and pest removal in domestic settings as well as for industrial setups [1]. A huge growth in the human population worldwide has tempted the excessive use of pesticides to produce the large appetite for food crops, but compromising the quality of the product due to the toxicity of pesticides and their detrimental effects on human health. Since the Indian economy is highly dependent on agriculture, the consumption of pesticides in India is the highest among South Asian countries [2].

Pesticides consist of a broad range of synthetic and natural compounds that are widely used for pest control. These are organochlorines, organophosphorus, phenoxy derivatives, pyrethrins and pyrethroids, triazines, carbamates, dipyridyl derivatives, glycine derivatives, chloroacetanilide, dithiocarbamates, benzimidazoles, and other miscellaneous compounds. The composition of some pesticides with their exposure and health effects is elaborated in Table 1.

Conventional methods of removal of pesticides have some limitations, like that they are suitable for only some specific substrates, they are highly dependent on chemical properties such as charge, hydrophobicity, size, and molecular weight of the chemical compound, which limits their selectivity, higher machinery cost, and difficult in situ remediation, and also, process of removal requires energy input and other chemicals, making it worse for the environment as well. Microbial remediation does not possess this kind of limitations as microbes can be acclimatized to a number of chemicals by various means. Microbial remediation is cheaper if done in situ and one microbe can be used for different pesticide removal, thus increasing the range of chemicals which can be removed. Therefore, in this review, a discussion of the effects of pesticides on human health as well as the environment has been done. Further various conventional methods, their limitations, and microbial remediation approach for removal of pesticides have been discussed.

Nanotechnology is one of the most emerging and widely studied fields because of its extensive applications. Nanoparticles (NPs) are the most basic constituents of nanotechnology. The size of NPs varies between 1 and 100 nanometers (nm). NPs are usually made up of metal or metal oxides, carbon, and other organic substances [3]. NPs demonstrate distinctive biological, physical, and chemical characteristics as compared to the relative bulk particles, due to the increased mechanical strength, and the enhanced ratio of surface area to volume, and they also demonstrate better stability or reactivity in a chemical reaction. As a result of the aforementioned characteristics of NPs, they have varied applications. NPs exist in different shapes, sizes, and dimensions [4]. The different types of dimensions of NPs are (a) zero-dimensional: like nanodots, length, breadth, and height have a specified single point; (b) one-dimensional: these types of NPs have only a single parameter, like graphene; (c) two-dimensional: in such NPs, they possess both length and breadth, like carbon nanotubes; (d) three-dimensional: these types of NP possess length, breadth, and height, as in gold NPs.

NPs can be of different shapes and forms such as conical, spherical, hollow, tubular, spiral, cylindrical, and flat. They can have a regular or uneven surface. Various NPs can be either crystalline or amorphous with unbound or clustered single or multicrystal solids [5]. Various methods are employed for the synthesis of NPs in order to either develop or enhance their characteristics and make their production cost-effective. Few methods are altered to enhance the mechanical, chemical, optical, and physical characteristics of NPs [4]. Thus, NPs are widely used in biotechnology and pharmaceuticals, electronics and communication, automobiles and machinery, agriculture, chemical processes, and environmental testing. Nanotechnology provides the potential for a future that is both clean and renewable.

2. Environmental Impacts of Pesticides

The application of pesticides has been associated with merits as well as demerits. They increase crop production as well as yield by eradicating the pests feeding on the crops. Without pesticides, crop production would decrease by 40% worldwide due to the pest attacks. They also help in the reduction of insect-mediated aflatoxin contamination of crops which is a carcinogenic leading to liver cancer, reduction in immune response, and lesser growth in children. They also help in prevention of disease outbreaks (e.g., malaria), protect the farm land and forests from invasive pests, and help in controlling the population of bugs. Despite all these benefits associated with them, their production and use in many countries have been banned because of many complications associated with them.

An ideal pesticide should only mediate killing of its target pest, but nontarget organisms usually get affected by them as well. Pesticides after their application can be taken up by the target organisms or they might get dissipated into the groundwater which could ended up in the surface water bodies such as rivers, lakes, or ponds, volatilize into atmosphere, or taken up by the soil and finally reach to nontarget organisms. Their usage poses a serious threat to flora and fauna biodiversity, disturbs the food webs, and has a serious implication on the ecosystem. Usually, pesticides are applied by sprayer in the form of volatilized material which evaporates into the air, increasing the area in which it could spread and, in this way, they can affect nontarget organisms as well. Herbicides, insecticides, etc. are applied in this way, and thus, they cause more harm to nontarget organisms than to target organisms. A variety of aquatic as well as terrestrial animals and plants are under serious threat due to the unrestricted use of pesticides. Some exotic species such as the bald eagle, osprey, and peregrine falcon have experienced survival threats due to overconsumption of pesticides [6]. Moreover, soil, air, and water are subjected to pollution and toxicity as they are the end point where these chemicals ultimately runoff. The bioaccumulation of pesticides in the case of lipophilic pesticides and the seepage of pesticides into groundwater indicate a major issue of their removal from

Table 1: Pesticides with their composition, health effects, and associated properties.

Pesticide	Composition	Exposure	Effects on human health	Physical and chemical properties
Organophosphorus	Organic carbonaceous and phosphoric acid derivative	Easily absorb by the skin, lungs, gastrointestinal tract (GI), and conjunctiva and metabolized by cytochrome P450 in the liver	Muscarinic syndrome, nicotine syndrome, effects on the CNS, teratogenic and carcinogenic	Most are polar, highly stable, and water soluble
Organochlorines	Organic carbonaceous compound with cyclodiene ring	Absorption via skin, GI tract, and lungs, ingestion of contaminated food, and inhalation	It has been linked to diabetes, cancer, asthma, and growth disorder in children	Lipophilic, polar, and show high persistence with long half-life
Carbamates	Organic compound with general chemical formula RHNCOOR, a derivative of carbamic acid	Absorption through the gastrointestinal tract, lungs, and skin	Lesser CNS symptoms, abdominal pain, behavioral change, diarrhea, vomiting, urinary incontinence, dyspnea, bronchospasm, bradycardia, hypoxemia, etc.	Polar compound, water-soluble, and have potential chemical reactivity
Pyrethrins and pyrethroids	Natural compounds extracted from *Chrysanthemum cinerariaefolium* and pyrethroids are synthetic derivatives of pyrethrins, chemical structure contains an acidic and alcohol moiety and an ester bond in the center	Show little cytotoxicity but hyperexcitablity, target voltage-gated chloride, sodium and calcium channels, nicotinic receptors, GABA-gated chloride channels, metabolized by CYP450	They have known to cause asthma and rhinitis (act as an allergen to respiratory system) as well as contact dermatitis	Readily degradable in the presence of light (pyrethrins)
Triazines	Derivatives of a six-membered heterocyclic compound (s-triazine) with substitution at positions 2, 4, and 6.	—	Human poisoning is rare and might produce local irritation	—
Dithiocarbamates	Synthetic derivatives of S-containing dithiocarbamates (either dimethyldithiocarbamate or ethylenebisdithiocarbamate) in conjugation with metallic salts of manganese, ferric, or zinc	Absorption is slow	Exposure for longer period might produce adverse effects; metabolites are carcinogenic	Less phytotoxic and have more stability
Phenoxy derivatives	Consist of an aliphatic carboxylic acid group in conjugation with either an aromatic ring (methyl substituted) or chloride	Absorption in GI tract, lungs, negligible in skin	CNS damage, teratogenic, shows hepatotoxicity and carcinogenicity, renal failure, hyperthermia, birth defect, etc.	Half-life is less (1-3 days), are easily hydrolyzed and decomposed
Dipyridyl derivatives	Dipyridylium quaternary ammonium derivatives	Tissue damage in the lungs, liver, and kidneys	Induction of pulmonary injury, hypoxemia, and edema hemorrhage, necrosis in the GI tract, liver, kidney tubules, and lungs	Highly toxic, exposure results in the production of radicals which damage lipid membranes.

these sources, as ultimately the human race would face the consequences of this pollution.

Because of the lower biodegradability and more stability of these chemicals, they usually tend to accumulate in the ecosystem as well as in the food webs posing a daunting hazard for the higher-order organisms in the food webs, i.e., predators. The aquatic ecosystem has suffered a lot of damage due to the excessive use of these chemicals. Pesticides usually end up in the aquatic ecosystem by drift or leaching through the soil, contaminating ground water or by direct application into the water source like to control waterborne pests. Fish and aquatic plants are affected due to the toxicity of these chemicals, as well as the dissolved oxygen level is decreased, leading to oxygen stress. Exposure of these chemicals could occur by three [6]: dermally (absorption through skin), orally (entry via mouth), and breathing (entry via gills). The runoff of herbicides in rivers causes the eradication of aquatic plant life, which is solely responsible for 80% of the oxygen supply in this ecosystem, leading to the death of various fish and animals [6]. Atrazine, a triazine

derivative, is highly toxic to some species of fish, and it has been observed that it might also secondarily affect the immune system in amphibians. Loss of reproductive potential [6], habitat loss for various amphibians, high mortality of aquatic organisms, and changes in abundance and composition of planktons are some of the potential impacts of pesticides.

Terrestrial biodiversity is also under threat due to the overconsumption of pesticides. Nontarget plants are the worst affected by the sprayed herbicides. Plants exposed to glyphosate has increased vulnerability to diseases and also poor quality of seeds. Reduction in the productivity of nontarget plants, wildlife, and forest plants has been observed even at lower doses of sulphonamides, imidazolinones, and sulfonylureas [7]. Broad-spectrum pesticides such as organophosphates, pyrethroids, and carbamates have affected the population of beneficial insects such as beetles and bees that are crucial for growth in plants and pollination. Insecticides like neonicotinoids have resulted in a decline in demography of honey bees leading to lesser crop production as well as a sharp decline in the production of honey and bees wax which is consumed commercially in various cosmetic products. Consumption of pesticides like DDT, organophosphates, has led to accumulation of these chemicals and its metabolites in birds resulting in high mortality as well as reproductive loss in them. Plants act as a source of food for humans and are the consumer of carbon dioxide, and as the draining of pesticides in the soil affects plant production as well as the microbiota of the soil, which is essential for the requirement of plant nutrients, there are serious complications associated with this. The reduction of soil fertility and degradation of soil quality due to the shrinking population of soil-dwelling microbes is an important environmental impact of pesticides.

Fungicides like dinitrophenyl and chlorothalonil have been reported to obstruct the nitrification and denitrification process done by microbes. Symbiotic or cooperative relationship among mycorhizal fungi and plants roots are also inhibited by pesticides [8]. The friend of the farmer, earthworms have also seen a huge decline due to the pore water of pesticides in the contaminated soil. The neurotoxic effects of some fungicides and insecticides have not spared earthworms, and there has been a substantial loss of soil fertility due to a smaller population of earthworms in farmland soils [9]. It has been observed that neonicotinoids could accumulate in the soil and destroy the population of earthworms such as *Eisenia foetida* from the soil.

Pesticides have also found to trigger or cause bronchial hyperactivity or asthma. These xenobiotics may cause inflammation, irritation, endocrine disruption, or immunosuppression leading to exacerbation of asthma in exposed individuals. An investigative research by Raanan et al. [10] concluded that organophosphates exposure in early life could lead to childhood asthma [10]. Herbicide pendimethalin and insecticide aldicarb were reported to positively worsen the asthma in active patients.

Farmers in Iran reported having a substantial high risk of developing acute leukemia due to exposure to pesticides. Prenatal exposure or exposure in pregnancy to household pesticides was found to be positively linked to development of childhood leukemia. Risk of neurobehavioral defects or cognitive effects were reported to be higher (3 fold increase) in individuals who had these three metabolites hexachlorobenzene, transnonachlor, and p,p′-DDE in their plasma [11]. Other effects of pesticides such as organophosphorous could be impairment of male reproductive system and reduction in fertility by inhibition of spermatogenesis, decreasing sperm count, density and reduction in sperm motility or viability, mass reduction in testis, DNA damage in sperm, and morphological abnormality in sperm.

3. Conventional Methods of Pesticide Removal

Pesticide removal is the process by which the contaminated soil or water is purified in which these chemicals are degraded or filtered or extracted out. In conventional methods, chemical oxidation, ozonation, Fenton oxidation, photocatalytic degradation, photochemical degradation (such as UV radiation), coagulation and flocculation, electrocoagulation, incineration, electrooxidation, reverse osmosis, adsorption, nanofiltration, membrane distillation, and electrodialysis are used.

Advanced oxidation process (AOP) or chemical oxidation process takes advantage of highly reactive hydroxyl radical for pesticide degradation. The hydrogen is extracted from the organic substrates by the free hydroxyl radicals or in case of double-bond electrophilic addition takes place [12]. There is another reaction of free radicals with the oxygen molecule to form a peroxyl radical, which ultimately leads to complete mineralization of the pesticide by undergoing various stepwise oxidative degradation reactions. Moreover, phenols substituted with halogens could also be attacked by hydroxyl radicals.

Ozonation deploys ozone gas to oxidize and degrade xenobiotics. Ozone is a strong oxidizing agent that attacks an organic substance at low pH, or it can also be used to generate hydroxyl radicals by modifying pH, and thus, hydroxyl radicals can do their part [12]. A recent study on the removal of pesticide residues from rice grains reported that residues of deltamethrin (92.7% removal) and bifenthrin (91.1% removal) residues were effectively removed from stored rice grains using ozone as a degrading agent [13].

Hydroxyl radicals can also be produced for the oxidation of organic pesticides at acidic pH using *Fenton's reagent*, which represents a mixture of hydrogen peroxide and ferrous or ferric ions [12]. Fenton oxidation was investigated to remove methyl parathion, and various parameters (mentioned them) were studied to identify their role in degradation [14]. Fenton oxidation was reported to be able to remove 74-92% of methyl parathion.

Photocatalytic process deals with the use of a catalyst such as TiO_2, Fe_2O_3, ZnO, ZnS, and CdS, which gets activated by absorption of photon and further helps in oxidation of organic compounds. Heterogeneous TiO_2 in combination with UV has been mostly studied for its degradative potential. Phenoxy derivatives 2,4-dichlorophenoxyacetic acid and 2,4-dichlorophenoxypropanoic acid were reported to be effectively degraded using heterogeneous TiO_2/UV at

283 nm, and degradative potential was observed to be directly proportional to the concentration of Ti in pillared clay [15]. Mepiquat chloride was reported to be completely degraded by using heterogeneous TiO_2P-25 where UVA was at pH 3, and degradation rates were higher as compared to homogeneous photocatalytic process.

Coagulation is a destabilization process in which a coagulant is added such that it destabilizes a stable charged particle.

Flocculation is the subsequent step of mixing that promotes accumulation of microflocs leading to the sedimentation of coagulated particles. In a study, four pesticides (dieldrin, aldrin, bentazon, and atrazine) were taken, and their removal by coagulation-flocculation was investigated using different concentrations of aluminum sulphate as a coagulant. Removal of pesticides was below 50% for all the investigated doses, and hydrophobicity of organic compound was observed to be directly related to the removal efficiency of treatment. A combinatorial approach of coagulation and fenton oxidation was reported to be more effective in wastewater treatment of nonbiodegradable pesticides. Polyferric chloride was deployed as the coagulant which was used as the first step of treatment, resulting in removal of 58% chemical oxygen demand and also lesser hydrogen peroxide requirement in the consecutive fenton oxidation step [16].

Electrocoagulation is a modified coagulation process in which an electrocoagulation cell (like an electrochemical cell) is used to destabilize an emulsified, suspended, or dissolved contaminants in wastewater by passing an electric current into it. In this process, electrodes of aluminum or iron are used, and wastewater acts as an electrolyte. Hydrolysis of water takes place at cathode resulting into the formation of molecular hydrogen and hydroxyl groups, and simultaneously, dissolution of metal from the anode takes place to produce coagulant in situ [17]. Released metal ions initiated the coagulation by neutralizing surface charges on the suspended solids [17]. The electric field also helps in electrolysis, ionization, hydrolysis, and free radical formation which also helps in decontamination of pollutants.

Reverse osmosis (RO) technology has been used for ground water treatment contaminated with organochlorines. Membranes used were of RO98pHt polyamide, and removal rate was observed to be 98.4-99.7% for pesticides, and dissolved solids were reduced from 1.35 g/dm^3 to less than 0.05 g/dm^3 [18]. Coupling of electrodialysis to desalinate wastewater and nanofiltration could improve the retention of pesticides on NF membranes [19]. Other conventional methods like electrooxidation and membrane distillation are also used for the removal of pesticides.

4. Microbial Remediation of Pesticides

Despite the advances in the conventional approach, researchers are discovering other means to degrade the pesticides in the environment. Microbial remediation uses microorganisms to eradicate these compounds from the contaminated source. Certain bacterial species and their strains, actinomycetes, fungi, and algae, have been documented to show degradation of pesticides. Microorganisms utilize these chemicals as a source of their energy by metabolizing them and directing their intermediates into energy generation pathways like Krebs cycle. These microbial strains have been enriched, cultured, isolated, and screened from various rivers, sewage, and soil [20]. For degradation of endosulfan, Kafilzadeh et al., [21] isolated bacterial strains from water samples, and they found five bacterial genus *Acinetobacter*, *Alcaligenes*, *Klebsiella*, *Bacillus*, and *Flavobacterium* capable of degrading endosulfan [21]. Various bacteria show the ability to degrade pesticides, which include *Pseudomonas*, *Bacillus*, *Alcaligenes*, *Flavobacterium*, *Klebsiella*, *Thiobacillus*, *Escherichia coli*, *Bacillus licheniformis*, and *Clostridium*. Various algae that are capable to degrade pesticides include Diatoms, *Chlamydomomas*, green algae, and microalgae, and fungi include *Anthracophyllum*, *Cladosporium*, *Rhizopus*, *Aspergillus fumigatus*, *Aspergillus*, *Penicillium*, *Mucor*, *Fusarium*, *Mortierella* sp., and *Trichoderma* sp. [20].

Bacteria are in the forefront for bioremediation purposes, as they are highly adaptive and liable to undergo mutation rapidly, thus acclimatizing themselves according to the demand of the vicinity environment. Pesticides are used as a nutrient by microbes and go through enzymatic reactions to produce carbon dioxide and water. These chemicals are first taken up by the microbes, followed by sequential attacks of metabolic enzymes, and they are completely degraded into lesser toxic or nontoxic compounds. These enzymatic reactions involve oxidation (epoxidation, N/P/S-oxidation, hydroxylation reactions on aromatic ring, aliphatic chain, or N-hydroxylation, oxidative dehalogenation, oxidative deamination, and oxidative dealkylation), reduction (reductive dehalogenation, and reduction of nitro or quinone), hydrolysis of ester bonds, condensation, decarboxylation, dehalogenation, dehydrogenation, and others [22].

Microbes could perform mineralization of compounds or cometabolism for degradation. Mineralization refers to the conversion of organic compounds into inorganic one by microbial enzymatic systems. For a molecule to undergo mineralization, it should have resemblance to the natural ligand (should be analog to the natural compound) against which the microbes have enzymes to act upon it [20]. Microbes use this analog as the nutrient and convert them into nontoxic inorganic compound, carbon dioxide, and water. As most pesticides do not resemble the natural compound metabolized by the microbes, they could not undergo mineralization. Another degradative strategy is cometabolism in which an organic compound which could be used as a primary energy source is provided along with the compound to be degraded which helps in the degradation of pesticides. Enzymes or cofactors used for the consumption of energy yielding substrate help in the metabolism of pesticides.

The bioremediation of pesticides depends on environmental factors, as well as some intrinsic factors related to microbes or pesticide chemical structure. These factors include the following:

(i) Metabolic activity and adaptability capacity of the microbial strain

(ii) Molecular weight, substitution type, location and frequency, and spatial structure determine the rate and efficiency of pesticide degradation. Polymeric compounds are resistant to degradation. The bioavailability of pesticides is also an important factor in bioremediation

(iii) Environmental conditions such as temperature, pH, salinity, humidity, available nutrients, required concentration of substrate, surfactant availability, carbon dioxide, and aerobic or anaerobic conditions are some of the factors that influence the remediation process carried out by microbes

Bioremediation can take place in situ (biostimulation, composting, biosparging, bioventing, and liquid delivery systems) as well as ex situ (biofilters, bioreactors, and land farming). The microbes residing in the contaminated soil can be used for bioremediation by stimulating them with nutrient or electron donors. Microbes can be added intentionally to break down the pesticides if the native microbes are not capable of bioremediation of these chemicals.

5. Bacterial Remediation of Pesticides

Organochlorines have been shown to undergo bioremediation by bacterial genus *Bacillus*, *Micrococcus*, *Arthrobacter*, and *Pseudomonas*. The CS5 strain of *Achromobacter xylosoxidans*, which was isolated form activated sludge, was reported for its capability to degrade α-endosulfan and β-endosulfan by more than 0.0248 g/L and 0.0105 g/L, respectively, after eight days of incubation [23]. Hexachlorobenzene was observed to be anaerobically dechlorinated by *Dehalococcoides* sp., and the trichlorobenzene reductive dehalogenase enzyme was reported to be crucial in degradation which was the product of the *cbrA* gene [24]. Two closely related species of *Citrobacter amalonaticus* were isolated, and their genome was sequenced by Chaussonnerie et al. [25], and they reported their potential of biotransformation and remediation of chlordecone by these two isolates [25]. Ozdal et al. [26] reported five bacterial species (*Pseudomonas aeruginosa*, *Acinetobacter lwoffii*, *Stenotrophomonas maltophilia*, *Citrobacter amalonaticus*, and *Bacillus atrophaeus*) that were isolated from cockroaches that resides in pesticide contaminated zones and reported that endosulfan bioremediation by these isolates was found to be 88.5, 80.2, 85.5, 56.7, and 64.4%, respectively [26]. Anaerobic mineralization of pentachlorphenol by various bacterial strains was studied by Li et al. [27]. They reported various dechlorinators (*Sulfospirillum Dehalobacter, Desulfovibrio*, and *Deslfitobacterium* spp.) and phenol degraders (*Syntrophus* and *Cryptanerobacter* spp.) and determined the responsible functional genes; *cprA* (chlorphenol reductive dehalogenase), *bamA* (benzoyl-CoA reductase), and seven variants of nitrogenase reductase genes ([27]).

More than 90% of chlorpyrifos has been reported to be degraded by *P. putida* MAS-1 in minimal salt concentration [28]. Several strains of microbes were able to remediate chlorpyrifos such as *Providencia stuartii*, *B. cereus*, *Actinobacteria* sp., *Xanthomonas* sp. *4R3-M3*, and *Pseudomonas* sp. *4H1-M3*. Sharma et al. [29] reported that a *Bacillus* sp. G2 was able to remediate cypermethrin, and a novel mechanism was discussed in which intermediates such as 4-propylbenzoate, phenol M-tert-butyl, 4-propylbenzaldehyde, and 1-dodecanol were produced [29]. In a study, *Pseudomonas stutzeri* SMK strain, under controlled conditions, was able to degrade dichlorvos effectively [2].

The treatment of acetamiprid by *Rhodococcus* sp. strain BCH2 and the explanation of its degradative mechanism were also found [30]. Madhuban et al. [31] reported the remediation of imidacloprid and metribuzin by the *Burkholderia cepacia* strain CH-9 (aerobic) and showed 69 and 86% removal of imidacloprid and metribuzin, respectively, after 20 days [31].

Carbofuran hydrolase (a product of the *mcd* gene) enzyme has been reported for carbamate degradation by hydrolyzing the methylcarbamate linkage in various microbial genera such as *Bacillus*, *Pseudomonas*, *Ralstonia*, *Mesorhizobium*, *Ochrobactrum*, and *Rhodococcus*. Shin et al. [32] reported various carbamate degrading bacteria which included *Spingomonas*, *Rhodococcus*, *Spingobium*, *Microbacterium*, and *Bosea* [32]. Using carbaryl as the main source of carbon and nitrogen, *Corynebacterium*, *Bacillus*, and *Morganella* were able to degrade carbaryl by 48.8%, 94.6%, and 87.3%, respectively [33].

Fuentes et al. [34] reported that some actinomycetes genera (*Streptomyces* and *Micromonospora*) were capable of degrading organochlorines (lindane, chlordane, or methoxychlor). *Streptomyces* have also been studied for removal of chlorpyrifos and pentachlorophenol [35]. It was reported that chlorpyrifos was effectively removed by *Streptomyces* sp. M7 (99.2%). In bioremediation of cypermethrin, two enzymes estearses and phosphatases were involved in the degradation of pesticide [36].

6. Fungal Remediation of Pesticides

Xiao et al. [37] conducted a study to evaluate fungal species capable of degrading heptachlor and its epoxide. The remediation of heptachlor was observed to be 71, 74, and 90% by *P. tremellosa*, *P. brevispora*, and *P. acanthocystis*, respectively, after incubating them for two weeks. The heptachlor was metabolized to heptachlor epoxide, 1-hydroxy-2, 3-epoxy-chlordene, and 1-hydroxychlordene, and the removal of heptachlor epoxide after 2 weeks was found to be 25, 22, 16, and 16% by *P. aurea*, *P. lindtneri*, *P. brevispora*, and *P. acanthocystis*, respectively [37]. The *lin* gene was found to be responsible for the uptake and metabolism of hexachlorocyclohexane in *Spingobium francense*, *Spingobium japonicum*, and *Spingobium indicum* [38]. Remediation of acetamiperid and thiacloprid by *Rhodotorula mucilaginosa* strain IM-2 was reported by [39]. *Aspergillus niger* has been reported to produce hydrolase for the hydrolysis of carbamates [40].

A. niger was investigated for its capability to degrade endosulfan, and it was observed that the culture was able to tolerate 400 g/L of technical grade endosulfan, and endosulfan was completely eliminated after 12 days of incubation

[41]. Likewise, white rot fungus *Trametes hirsuta* was also observed to degrade endosulfan and endosulfan sulfate via hydrolytic pathways [42]. *Lecanicillium saksenae*, *Fusarium oxysporum*, *Penicillium brevicompactum*, *Aspergillus oryzae*, and *Lentinula edodes* were shown to be able to degrade difenoconazole, pendimethalin (99.5% removal by *L. saksenae*), and terbuthylazine (maximum 80% removal by *A. oryzae*) [43].

7. Types of Nanoparticles

NPs are categorized into various types on the basis of size, shape, morphology, and chemical properties [44].

8. Carbon-Based Nanoparticles

The carbon-based NPs mainly include fullerenes and carbon nanotubes (CNTs).

8.1. Graphene. It is an allotrope of carbon and a 2D planar and hexagonal complex of honeycomb-like lattices. Graphene sheets generally have a thickness of 1 nm [45].

8.2. Fullerenes. They are composed of carbon atoms that are bonded to each other by sp2 hybridization, forming spherical molecules of carbon (C60). Fullerenes are composed of about 28-1500 atoms of carbon, the single layers have a diameter of 8.2 nm, and the multilayered ones have a diameter of about 4 to 36 nm [46].

8.3. Carbon Nanotubes (CNT). They are formed by the graphene nanofoil that has a honeycomb-like network of atoms that are embedded into hollow coils, resulting in CNTs. The single-layered carbon nanotubes are about 0.7 nm, and the multilayered ones are 100 nm. The size of CNTs can vary from several micrometers to a few millimeters. They have hollow ends or can be enclosed by half fullerene molecules [47]. CNTs can have a relatively same shape as rolled graphite [48]. The rolled sheets can be single-walled carbon nanotubes, double-walled carbon nanotubes, or multiwalled carbon nanotubes [49].

8.4. Carbon Black. They are spherical amorphous carbon substances and have a diameter that varies between 20 and 70 nm. Since the particles bound instantly, they form a clustered shape, and approximately 500 nm clusters are formed [50].

8.5. Carbon Nanofiber. They are formed in a similar manner to CNTs and nanofoils of graphene, except that they are coiled into a cone-shaped structure rather than cylindrical tubes [51].

9. Metal NPs

They are produced from metals by using constructive or destructive procedures at the nanoscale level. NPs can be generated from most of the metals [52, 53]. Some of the metals that are often used for the production of NPs are zinc, aluminum, copper, lead, cobalt, gold, cadmium, silver, and iron [52, 54, 55]. NPs have unique surface properties, such as a high ratio of surface area to volume, spherical structure, reactivity, pore size, color, surface charge density, sensitivity, and sizes varying between 10 and 100 nm [56, 57].

9.1. Metal-Oxide NPs. Several metal-oxide NPs have been synthesized for the electrochemical determination of biological compounds. Some of the examples include Fe_2O_3, ZnO, Co_3O_4, MnO_2, NiO, and TiO_2 [58]. Moreover, mixed metal oxides have been of great interest due to such characteristics. The CuO nanoparticles have distinct features, because of which they have multiple applications like sensors, catalysts, antibacterial, and superstrong materials [59, 60]. Metal-oxide NPs have the ability to interact with other NPs due to the high surface area to volume ratio [61, 62].

9.2. Ceramics NPs. They are inorganic and nonmetallic substances that are synthesized by heating and cooling. Ceramic NPs exist in several morphologies and sizes; they can be hollow, dense, amorphous, porous, and polycrystalline. Thus, they have various applications in imaging, catalysis, photocatalysis, and photodegradation of dyes [63, 64].

9.3. Semiconductor NPs. They demonstrate a broad variety of applications since they exhibit characteristics of both metals and nonmetals [65]. Since these NPs exhibit larger bandgaps, bandgap tuning causes important modifications in their characteristics. Consequently, they demonstrate significant applications in photooptics, electronic devices, and photocatalysis [66, 67].

9.4. Polymeric NPs. These are organic nanoparticles [68, 69]. Generally, they exist in the form of a capsule or sphere. The former is a solid mass that is enclosed in the particle, and the latter is a matrix substance with a solid mass [70]. Lipid nanotechnology is one of the emerging fields for the production of lipid NPs that have important applications in drug delivery and cancer treatment [71, 72].

10. Role of Nanomaterials in Pesticide Remediation

10.1. Cerium Oxide (CeO2). The CeO2 nanofibers are synthesized from the metal-oxide frameworks of the Ce(1,3,5-benzenetricarboxylate) (H2O)6 (Ce-BTC), and they have been extensively studied for their uses in the adsorption of pesticides from water bodies [73]. The metal-organic frameworks of Ce-BTC were formed by using the hydrothermal procedure, and the CeO2 nanofibers are synthesized using the calcination procedure from Ce-BTC NPs at 650 degrees Celsius for 3 hours. 2,4-Dichlorophenoxyacetic acid (2,4-D) was adsorbed from water using CeO2 nanofibers using a batch system at 308 K with the q_{max} value of 95.78 mg g^{-1}. 2,4-D was adsorbed into CeO2 by diffusion into the particle and the boundary layer on the basis of isothermal and kinetic studies.

10.2. Magnesium Ferrite (MgFe2O4). The mesoporous MgFe2O4 is magnetically retrievable and has been investigated for the adsorption of chlorpyrifos from wastewater containing pesticides [74]. MgFe2O4 having a high surface

area of 170 $m^2 \cdot g^{-1}$ was synthesized by employing benign initiating substances and urea as binary purpose intercessors in a single-step solvothermal procedure. Chlorpyrifos was significantly adsorbed on the MgFe2O4 adsorbent at a pH > 9 , as exhibited by the batch adsorption studies. Similarly, chemisorption was observed when the hydroxylated magnesium ferrite surface having electronegative atoms such as sulfur, oxygen, and chlorine reacted with the aromatic ring of chlorpyrifos, which caused degradation into small organic molecules. This experiment demonstrated that the mesoporous magnesium ferrite with effective adsorption properties can be used for the treatment of wastewater.

10.3. Activated Carbon. Several investigations were conducted to study the removal of pesticides from the water bodies by employing activated carbons, like paclobutrazol [75], carbendazim and linuron [76], 11 pesticides [77], 2,4-dichlorophenoxyacetic acid (2,4-D) [78], iodosulfuron [79], and carbendazim (T. [80]). There are 2 types of activated carbon that are commercially available (GAB; $V_{Mic} = 0.27$ c $m^3 \cdot g^{-1}$, $S_{Mic} = 580\ m^2 \cdot g^{-1}$, $pH_{PZC} = 7.46$ and CBP; $V_{Mic} = 0.04\ cm^3 \cdot g^{-1}$, $S_{Mic} = 99\ m^2 \cdot g^{-1}$, $pH_{pzc} = 4.76$) and were used for the adsorption of 2,4-dichlorophenoxyacetic acid (2,4-D; pKa = 2.73) and 4-chloro-2-methylphenoxyacetic acid (MCPA; pKa = 3.07) from aqueous solutions [81]. The microporous GAB demonstrated better adsorption abilities ($q_{max} = 367.15\ mg \cdot g^{-1}$) than CBP ($q_{max} = 273.07\ mg \cdot g^{-1}$). The data of the assessment of adsorption exhibited that pH and ionic strength were important parameters for analyzing the rate of adsorption, which was increased for both types of pesticides by enhancing the ionic strength. As per the pesticides pKa and the pH_{PZC} of activated carbons, removal of 2,4-D and MCPA was decreased with an increase in pH (pH > 4.76). The results concluded that the mechanism of adsorption was determined by the electrostatic interaction between the surface of the activated carbon and pesticides.

10.4. Graphene-Based NMs. Lazarevic-Pasti et al. [82] studied the impact of graphene-based materials on the removal of dimethoate and chlorpyrifos from the aqueous medium. The outcomes demonstrated that the adsorption of the pesticides on the adsorbents based on graphene was significantly dependent on the structural characteristics of the sorbent and sorbate, and the surface area was not the primary determinant for the pesticide elimination capability. The chlorpyrifos was specifically eliminated with aromatic moiety in the graphene basal plane, which contains the p electron system and high structural order, while adsorption of the aliphatic dimethoate onto hydrophilic oxidized graphene surfaces took place. Both chlorpyrifos and dimethoate were eliminated due to the moderate proportion of oxygen functional groups on the surface of graphene-based adsorbent.

10.5. Carbon Nanotubes (CNTs). The CNTs that were produced from plastic wastes were used as an efficient adsorbent for the removal of diuron from the water bodies [83]. This study demonstrated that the CNTs that were produced from plastic wastes, with $q_{max} = 103.73\ mg \cdot g^{-1}$ can be applied as a significant adsorbent for the treatment of water bodies. The multiwalled CNT was synthesized using particle size varying between 10 and 40 nm of the compound Ni/MgO, having a surface area of 9.10 $m^2 \cdot g^{-1}$ [84]. The effective elimination of about 90.5% diuron from water was carried out using multiwalled CNT ($q_{max} = 132.5\ mg \cdot g^{-1}$) under specific conditions ($C_{diuron} = 100\ \mu g \cdot L^{-1}$, time = 60 minutes, pH = 7.0, temperature = 25°C, CMWCT = 2.0 $g \cdot L^{-1}$). The statistical adsorption results indicated instant exothermic adsorption into the multiwalled CNTs. Modeling readings and computing the energy and binding affinity of diuron with multiwalled CNTs were used to identify the supramolecular adsorption process. The bonding between multiwalled CNT and diuron includes p-p T-shaped bonds, p-donor hydrogen bonds, p-p stacked, and p-alkyl bonds. These findings revealed that 16 hydrophobic interactions and 2 hydrogen bonds were involved in diuron physical adsorption and the formation of the multiwalled CNT-diuron compound.

10.6. Titanium Dioxide (TiO_2) NPs. $TiO_2(s)/H_2O_2/UV$ and $TiO_2(c)/H_2O_2/UV$ systems were investigated for the disintegration of insecticides as a function of the irradiation time. $TiO_2(s)/H_2O_2/UV$ system demonstrated the most efficient disintegration rate of the insecticides. 100% disintegration of the insecticides was accomplished after irradiation for 320 minutes by the $TiO_2(s)/H_2O_2/UV$ system. The half-life values of the insecticides were 36.28 and 43.86 for methomyl and dimethoate under the $TiO_2(s)/H_2O_2/UV$ system. But the half-life values of the insecticides were 19.52 and 27.72 minutes for methomyl and dimethoate under the TiO2 (s)/ H2O2/UV system, respectively. In comparison to light settings, the disintegration of the pesticides examined in the dark utilizing the various techniques was minimal. Under dark conditions, the disintegration percentages of the studied pesticides using the various techniques ranged from 0.30 to 1.6 percent [85].

10.7. Nanopesticides. Various pesticides can be enclosed or adsorbed in multiple nanomatrices such as lipid NP, polymers, CNT, silica, or graphene oxides [86]. The nanopesticides have several advantages; they enhance the solubility of the barely soluble components, avoid early disintegration of pesticides, enhance the solubility of barely soluble components, and cause stimulated production of the active constituents [87, 88]. Silver NPs (Ag) were synthesized using the extract of the stem of the cotton plant (*Gossypium hirsutum*) and demonstrated effective antibacterial functions against pathogenic bacteria (*Xanthomonas campestris pv. campestris* and *Xanthomonas axonopodis pv. malvacearum*) that invade the crops of *Brassicaceae* and *Malvaceae* [89]. Ag-based chitosan nanocomposites exhibit better fungicidal activities compared to conventional fungicides [90].

11. Challenges and Future Prospects

Population worldwide is increasing rapidly, so as to deliver the food requirements of this burgeoning population, pesticides have been integrated in the modern lifestyle. Overconsumption of pesticides have resulted in buildup of resistance

(acquired resistance) in the targeted pests. Excessive consumption of pesticides has led to clearance of normal susceptible population but providing a selective advantage to resistant pests leading to increase in their population. The control of important pests in crop, livestock parasites, household pests, and vector-borne diseases has become extremely challenging due to the developed resistance in them. Another issue with pesticides is reappearance of a large number of pest populations after the application of a pesticide known as pest resurgence. Pest resurgence has been associated with killing of natural enemies, increase in reproductivity, and feeding of insect pests, by using pesticides at less lethal dosages, and sometimes, secondary pests become primary pests because of eradication of the primary pest. Elimination of nontarget organisms like pollinators and earthworms has a huge impact on agricultural output. Pollinator populations have seen a major reduction due to the application of pesticides which translates into the reduction of crop production. Soil fertility is highly dependent upon the earthworms present in the soil. Indiscriminate use of xenobiotics has reduced the population of earthworms in the soil, and thus, more fertilizers are required to maintain soil nutrient quality [91]. Pesticides disturb the balance in ecosystem and have serious implications on the environment and human health; most of them are nonbiodegradable and highly toxic, led to bioaccumulation and biomagnification, and cause pollution of air, water, and soil which are some other challenges offered by the use of pesticides.

Bacterial and fungal remediation as well as use of nanomaterials are the future of pesticides removal from the environment. It has been reported for various pesticides but extensive research is necessary to increase the range of chemicals it could remediate as well as to know about the mechanism behind the remediation process. Genetic engineering could be used for production of superbugs with various genes combined for a range of pesticides removal. Coexpression of mixed plasmids with different set of genes for elimination of pesticides is the new approach which is possible due to genetic engineering, and in the upcoming years, it may be used for environmental clearance of pesticides.

12. Conclusion

The bioremediation of pesticides is urgent as it affects the environment and human population. Conventional methods could be used for its removal but their inherent problems like cost and time have discouraged their use. Microbial remediation is a good alternative for conventional methods. Microbes isolated from contaminated environments like water, soil, or sewage have been shown to possess enzyme systems to degrade these chemicals. Persistent organic pollutants like DDT can be utilized and metabolized by these microorganisms. Bacteria and fungi are the most studied, and various enzymes and pathways have been reported for the remediation of pesticides. For efficient removal of pesticides, conventional and microbial treatment could be coupled to increase the efficiency of elimination. Apart from microbial remediation of pesticides, use of nanomaterials for the removal of pesticides is another potential method that can be utilized. Different conventional methods could be integrated, or different microbial genes could be coupled by novel techniques offered by genetic engineering to enhance the efficiency of remediation treatment. Similarly, different nanomaterials can be used along with microbes to enhance the remediation efficiency. Thus, microbial and nanoremediation is the future for removal of pesticides.

Data Availability

The data used to support the findings of this study are included within the article.

Conflicts of Interest

The authors declare that they have no conflicts of interest.

Acknowledgments

The author (AR) is grateful to the Sharda University for Seed Fund-4 2001 (SUSF2001/12).

References

[1] K.-H. Kim, E. Kabir, and S. A. Jahan, "Exposure to pesticides and the associated human health effects," *Science of the Total Environment*, vol. 575, pp. 525–535, 2017.

[2] S. G. Parte, A. S. Kharat, and A. D. Mohekar, "Isolation and characterization of dichlorvos degrading bacterial strain *Pseudomonas stutzeri* smk," *Research Journal of Life Sciences, Bioinformatics, Pharmaceutical and Chemical Sciences*, vol. 2, no. 5, pp. 283–288, 2017.

[3] S. Hasan, "A review on nanoparticles: their synthesis and types biosynthesis: mechanism 4 9–11 assessment R 2007 nanoparticles in the environment," *Research Journal of Recent Sciences*, vol. 2277, p. 2502, 2015.

[4] E. J. Cho, H. Holback, K. C. Liu, S. A. Abouelmagd, J. Park, and Y. Yeo, "Nanoparticle characterization: state of the art , challenges, and emerging technologies," *Molecular pharmaceutics*, vol. 10, no. 6, pp. 2093–2110, 2013.

[5] S. Machado, J. G. Pacheco, H. P. A. Nouws, J. T. Albergaria, and C. Delerue-Matos, "Characterization of green zero-valent iron nanoparticles produced with tree leaf extracts," *Science of the total environment*, vol. 533, pp. 76–81, 2015.

[6] L. A. Helfrich, D. L. Weigmann, P. A. Hipkins, and E. R. Stinson, *Pesticides and aquatic animals: a guide to reducing impacts on aquatic systems*, Virginia Cooperative Extension, 2009.

[7] R. Mishra, R. Lone, D. Manzoor, and R. Shuab, "Imbalance due to Pesticide Contamination in Different Ecosystems," *International Journal of Theoretical and Applied Sciences*, vol. 10, pp. 239–246, 2018.

[8] K. Hage-Ahmed, K. Rosner, and S. Steinkellner, "Arbuscular mycorrhizal fungi and their response to pesticides," *Pest Management Science*, vol. 75, no. 3, pp. 583–590, 2019.

[9] R. Miglani and S. S. Bisht, "World of earthworms with pesticides and insecticides," *Interdisciplinary Toxicology*, vol. 12, no. 2, pp. 71–82, 2019.

[10] R. Raanan, K. G. Harley, J. R. Balmes, A. Bradman, M. Lipsett, and B. Eskenazi, "Early-life exposure to organophosphate

pesticides and pediatric respiratory symptoms in the CHAMACOS cohort," *Environmental Health Perspectives*, vol. 123, no. 2, pp. 179–185, 2015.

[11] D.-H. Lee, P. Monica Lind, D. R. Jacobs, S. S. Jr, B. van Bavel, and L. Lind, "Association between background exposure to organochlorine pesticides and the risk of cognitive impairment: a prospective study that accounts for weight change," *Environment International*, vol. 89-90, pp. 179–184, 2016.

[12] S. Chiron, A. Fernandez-Alba, A. Rodriguez, and E. Garcia-Calvo, "Pesticide chemical oxidation: state-of-the-art," *Water Research*, vol. 34, no. 2, pp. 366–377, 2000.

[13] M. B. R. de Ávila, L. R. A. Faroni, F. F. Heleno, M. E. L. R. de Queiroz, and L. P. Costa, "Ozone as degradation agent of pesticide residues in stored rice grains," *Journal of food science and technology*, vol. 54, no. 12, pp. 4092–4099, 2017.

[14] R. Saini, M. K. Mondal, and P. Kumar, "Fenton oxidation of pesticide methyl parathion in aqueous solution: kinetic study of the degradation," *Environmental Progress & Sustainable Energy*, vol. 36, no. 2, pp. 420–427, 2017.

[15] M. Abdennouri, M. Baâlala, A. Galadi et al., "Photocatalytic degradation of pesticides by titanium dioxide and titanium pillared purified clays," *Arabian Journal of Chemistry*, vol. 9, pp. S313–S318, 2016.

[16] G. Pliego, J. A. Zazo, M. I. Pariente et al., "Treatment of a wastewater from a pesticide manufacture by combined coagulation and Fenton oxidation," *Environmental Science and Pollution Research*, vol. 21, no. 21, pp. 12129–12134, 2014.

[17] S. M. Islam, "Electrocoagulation (EC) technology for wastewater treatment and pollutants removal," *Water Resources Management*, vol. 5, no. 1, pp. 359–380, 2019.

[18] M. A. R. E. Šír, M. Podhola, T. Patočka et al., "Removal of pesticides and inorganic pollutants by reverse osmosis," *Environment Protection Engineering*, vol. 41, no. 2, 2015.

[19] L. D. Nguyen, S. Gassara, M. Q. Bui, F. Zaviska, P. Sistat, and A. Deratani, "Desalination and removal of pesticides from surface water in Mekong Delta by coupling electrodialysis and nanofiltration," *Environmental Science and Pollution Research*, vol. 26, no. 32, pp. 32687–32697, 2019.

[20] Y. Huang, L. Xiao, F. Li et al., "Microbial degradation of pesticide residues and an emphasis on the degradation of cypermethrin and 3-phenoxy benzoic acid: a review," *Molecules*, vol. 23, no. 9, p. 2313, 2018.

[21] F. Kafilzadeh, M. Ebrahimnezhad, and Y. Tahery, "Isolation and identification of endosulfan-degrading bacteria and evaluation of their bioremediation in Kor River, Iran," *Osong Public Health and Research Perspectives*, vol. 6, no. 1, pp. 39–46, 2015.

[22] R. Prabha, D. P. Singh, and M. K. Verma, "Microbial interactions and perspectives for bioremediation of pesticides in the soils," in *Plant-Microbe Interactions in Agro-Ecological Perspectives*, pp. 649–671, Springer, Singapore, 2017.

[23] W. Li, Y. Dai, B. Xue et al., "Biodegradation and detoxification of endosulfan in aqueous medium and soil by *Achromobacter xylosoxidans* strain CS5," *Journal of Hazardous Materials*, vol. 167, no. 1-3, pp. 209–216, 2009.

[24] N. Taş, M. H. A. van Eekert, A. Wagner, G. Schraa, W. M. de Vos, and H. Smidt, "Role of "*Dehalococcoides*" spp. in the Anaerobic Transformation of Hexachlorobenzene in European Rivers," *Applied and environmental microbiology*, vol. 77, no. 13, pp. 4437–4445, 2011.

[25] S. Chaussonnerie, P.-L. Saaidi, E. Ugarte et al., "Microbial degradation of a recalcitrant pesticide: chlordecone," *Frontiers in microbiology*, vol. 7, p. 2025, 2016.

[26] M. Ozdal, "Isolation and characterization of α-endosulfan degrading bacteria from the microflora of cockroaches," *Polish Journal of Microbiology*, vol. 65, no. 1, pp. 63–68, 2016.

[27] Z.-L. Li, J. Nan, C. Huang et al., "Spatial abundance and distribution of potential microbes and functional genes associated with anaerobic mineralization of pentachlorophenol in a cylindrical reactor," *Scientific reports*, vol. 6, no. 1, article 19015, 2016.

[28] M. Ajaz, S. A. Rasool, S. Khan Sherwani, and T. A. Ali, "High profile chlorpyrifos degrading Pseudomonas putida MAS-1 from indigenous soil: gas chromatographic analysis and molecular characterization," *International Journal of Basic Medical Sciences and Pharmacy (IJBMSP)*, vol. 2, no. 2, 2012.

[29] A. Sharma, S. Gangola, P. Khati, G. Kumar, and A. Srivastava, "Novel pathway of cypermethrin biodegradation in a *Bacillus* sp. strain SG2 isolated from cypermethrin-contaminated agriculture field," *3 Biotech*, vol. 6, no. 1, 2016.

[30] S. S. Phugare and J. P. Jadhav, "Biodegradation of acetamiprid by isolated bacterial StrainRhodococcussp. BCH2 and toxicological analysis of its metabolites in silkworm (*Bombax mori*)," *Clean–Soil, Air, Water*, vol. 43, no. 2, pp. 296–304, 2015.

[31] M. Gopal, D. Dutta, S. K. Jha, S. Kalra, S. Bandyopadhyay, and S. K. Das, "Biodegradation of imidacloprid and metribuzin by *Burkholderia cepacia* strain CH9," *Pesticide Research Journal*, vol. 23, no. 1, pp. 36–40, 2011.

[32] D.-H. Shin, D.-U. Kim, C.-N. Seong, H.-G. Song, and J.-O. Ka, "Genetic and phenotypic diversity of carbofuran-degrading bacteria isolated from agricultural soils," *Journal of Microbiology and Biotechnology*, vol. 22, no. 4, pp. 448–456, 2012.

[33] M. Hamada, A. Matar, and A. Bashir, "Carbaryl degradation by bacterial isolates from a soil ecosystem of the Gaza Strip," *Brazilian Journal of Microbiology*, vol. 46, no. 4, pp. 1087–1091, 2015.

[34] M. S. Fuentes, C. S. Benimeli, S. A. Cuozzo, and M. J. Amoroso, "Isolation of pesticide-degrading actinomycetes from a contaminated site: bacterial growth, removal and dechlorination of organochlorine pesticides," *International Biodeterioration & Biodegradation*, vol. 64, no. 6, pp. 434–441, 2010.

[35] M. S. Fuentes, G. E. Briceño, J. M. Saez, C. S. Benimeli, M. C. Diez, and M. J. Amoroso, "Enhanced removal of a pesticides mixture by single cultures and consortia of free and immobilized *Streptomyces* strains," *BioMed Research International*, vol. 2013, Article ID 392573, 9 pages, 2013.

[36] V. K. Vaze, "Biodegradation of pesticide cypermethrin by phosphatase and esterase enzymes produced by actinomycetes," *Research Journal of Pharmacy and Technology*, vol. 10, no. 2, pp. 445–448, 2017.

[37] P. Xiao, T. Mori, I. Kamei, and R. Kondo, "Metabolism of organochlorine pesticide heptachlor and its metabolite heptachlor epoxide by white rot fungi, belonging to genus *Phlebia*," *FEMS Microbiology Letters*, vol. 314, no. 2, pp. 140–146, 2011.

[38] R. Pal, S. Bala, M. Dadhwal et al., "Hexachlorocyclohexane-degrading bacterial strains Sphingomonas paucimobilis B90A, UT26 and Sp+, having similar lin genes, represent three distinct species, Sphingobium indicum sp. nov., Sphingobium japonicum sp. nov. and Sphingobium francense sp. nov., and reclassification of [Sphingomonas] chungbukensis as Sphingobium chungbukense comb. nov," *International journal of*

systematic and evolutionary microbiology, vol. 55, no. 5, pp. 1965–1972, 2005.

[39] Y.-J. Dai, W.-W. Ji, T. Chen et al., "Metabolism of the neonicotinoid insecticides acetamiprid and thiacloprid by the yeast *Rhodotorula mucilaginosa* strain IM-2," *Journal of Agricultural and Food Chemistry*, vol. 58, no. 4, pp. 2419–2425, 2010.

[40] Z. Qing, L. Yang, and L. Yu-Huan, "Purification and characterization of a novel carbaryl hydrolase from *Aspergillus niger* PY168," *FEMS Microbiology Letters*, vol. 228, no. 1, pp. 39–44, 2003.

[41] T. S. Bhalerao and P. R. Puranik, "Biodegradation of organochlorine pesticide, endosulfan, by a fungal soil isolate, Aspergillus niger," *International Biodeterioration & Biodegradation*, vol. 59, no. 4, pp. 315–321, 2007.

[42] I. Kamei, K. Takagi, and R. Kondo, "Degradation of endosulfan and endosulfan sulfate by white-rot fungus *Trametes hirsuta*," *Journal of Wood Science*, vol. 57, no. 4, pp. 317–322, 2011.

[43] A. P. Pinto, C. Serrano, T. Pires et al., "Degradation of terbuthylazine, difenoconazole and pendimethalin pesticides by selected fungi cultures," *Science of the Total Environment*, vol. 435-436, pp. 402–410, 2012.

[44] I. Khan, K. Saeed, and I. Khan, "Nanoparticles: properties, applications and toxicities," *Arabian Journal of Chemistry*, vol. 12, no. 7, pp. 908–931, 2019.

[45] A. Bandyopadhyay and D. Jana, "A review on role of tetrarings in graphene systems and their possible applications," *Reports on Progress in Physics*, vol. 83, no. 5, article 056501, 2020.

[46] K. D. Patel, R. K. Singh, and H.-W. Kim, "Carbon-based nanomaterials as an emerging platform for theranostics," *Materials Horizons*, vol. 6, no. 3, pp. 434–469, 2019.

[47] S. Jana, A. Bandyopadhyay, S. Datta, D. Bhattacharya, and J. Debnarayan, "Emerging properties of carbon based 2D material beyond graphene," *Journal of Physics: Condensed Matter*, vol. 34, article 053001, 2022.

[48] R. Song, Q. Wang, B. Mao et al., "Flexible graphite films with high conductivity for radio-frequency antennas," *Carbon*, vol. 130, pp. 164–169, 2018.

[49] A. E.-M. A. Mohamed and M. A. Mohamed, "Carbon nanotubes: synthesis, characterization, and applications," in *Carbon Nanomaterials for Agri-Food and Environmental Applications*, pp. 21–32, Elsevier, 2020.

[50] O. Mkhari, T. D. Ntuli, N. J. Coville, E. N. Nxumalo, and M. S. Maubane-Nkadimeng, "A comparison of fluorescent N-doped carbon dots supported on the surface of hollow and solid carbon spheres, and solid silica spheres," *Diamond and Related Materials*, vol. 118, p. 108500, 2021.

[51] L. K. Foong, M. M. Foroughi, A. F. Mirhosseini et al., "Applications of nano-materials in diverse dentistry regimes," *RSC Advances*, vol. 10, no. 26, pp. 15430–15460, 2020.

[52] I. Ijaz, E. Gilani, A. Nazir, and A. Bukhari, "Detail review on chemical, physical and green synthesis, classification, characterizations and applications of nanoparticles," *Green Chemistry Letters and Reviews*, vol. 13, no. 3, pp. 223–245, 2020.

[53] H. E. M. Abdelmoneim, M. A. Wassel, A. S. Elfeky et al., "Multiple applications of CdS/TiO_2 nanocomposites synthesized via microwave-assisted sol–gel," *Journal of Cluster Science*, vol. 33, pp. 1119–1128, 2022.

[54] J. A. Kumar, T. Krithiga, S. Manigandan et al., "A focus to green synthesis of metal/metal based oxide nanoparticles: various mechanisms and applications towards ecological approach," *Journal of Cleaner Production*, vol. 324, article 129198, 2021.

[55] S. S. Salem, E. F. El-Belely, G. Niedbała et al., "Bactericidal and in-vitro cytotoxic efficacy of silver nanoparticles (Ag-NPs) fabricated by endophytic actinomycetes and their use as coating for the textile fabrics," *Nanomaterials*, vol. 10, no. 10, pp. 1–20, 2020.

[56] V. Singh, P. Yadav, and V. Mishra, *Recent advances on classification, properties, synthesis, and characterization of nanomaterials*, pp. 83–97, Green Synthesis of Nanomaterials for Bioenergy Applications, 2020.

[57] R. K. Kankala, Y. H. Han, J. Na et al., "Nanoarchitectured structure and surface biofunctionality of mesoporous silica nanoparticles," *Advanced Materials*, vol. 32, no. 23, article 1907035, 2020.

[58] A. Roy, S. Datta, M. Roy et al., "Nanomaterials and bioactive compounds against SARS-CoV-2," *Journal of Nanomaterials*, vol. 2022, Article ID 4568443, 13 pages, 2022.

[59] C. Pandit, A. Roy, S. Ghotekar et al., "Biological agents for synthesis of nanoparticles and their applications," *Journal of King Saud University-Science*, vol. 34, no. 3, article 101869, 2022.

[60] M. F. Al-Hakkani, "Biogenic copper nanoparticles and their applications: a review," *SN Applied Sciences*, vol. 2, no. 3, pp. 1–20, 2020.

[61] A. Roy, A. Sharma, S. Yadav, L. T. Jule, and R. Krishnaraj, "Nanomaterials for remediation of environmental pollutants," *Bioinorganic Chemistry and Applications*, vol. 2021, Article ID 1764647, 16 pages, 2021.

[62] M. Hasanin, M. A. Al Abboud, M. M. Alawlaqi, T. M. Abdelghany, and A. H. Hashem, "Ecofriendly synthesis of biosynthesized copper nanoparticles with starch-based nanocomposite: antimicrobial, antioxidant, and anticancer activities," *Biological Trace Element Research*, vol. 200, pp. 2099–2112, 2022.

[63] X. Zeng, E. Li, G. Xia et al., "Silica-based ceramics toward electromagnetic microwave absorption," *Journal of the European Ceramic Society*, vol. 41, no. 15, pp. 7381–7403, 2021.

[64] T. Ayode Otitoju, P. Ugochukwu Okoye, G. Chen, Y. Li, M. Onyeka Okoye, and S. Li, "Advanced ceramic components: materials, fabrication, and applications," *Journal of Industrial and Engineering Chemistry*, vol. 85, pp. 34–65, 2020.

[65] A. D. Terna, E. E. Elemike, J. I. Mbonu, O. E. Osafile, and R. O. Ezeani, "The future of semiconductors nanoparticles: synthesis, properties and applications," *Materials Science and Engineering: B*, vol. 272, article 115363, 2021.

[66] B. J. Abdullah, "Size effect of band gap in semiconductor nanocrystals and nanostructures from density functional theory within HSE06," *Materials Science in Semiconductor Processing*, vol. 137, article 106214, 2022.

[67] J. Fang, Z. Zhou, M. Xiao, Z. Lou, Z. Wei, and G. Shen, "Recent advances in low-dimensional semiconductor nanomaterials and their applications in high-performance photodetectors," *InfoMat*, vol. 2, no. 2, pp. 291–317, 2020.

[68] L. H. Madkour, "Examples of nanomaterials with various morphologies," in *Nanoelectronic Materials: Fundamentals and Applications*, L. H. Madkour, Ed., pp. 141–164, Springer International Publishing, Cham, 2019.

[69] S. Dacrory, A. H. Hashem, and M. Hasanin, "Synthesis of cellulose based amino acid functionalized nano-biocomplex: characterization, antifungal activity, molecular docking and

hemocompatibility," *Environmental Nanotechnology, Monitoring & Management*, vol. 15, article 100453, 2021.

[70] M. Saifullah, M. R. I. Shishir, R. Ferdowsi, M. R. Tanver Rahman, and Q. Van Vuong, "Micro and nano encapsulation, retention and controlled release of flavor and aroma compounds: a critical review," *Trends in Food Science & Technology*, vol. 86, pp. 230–251, 2019.

[71] S. Noore, N. K. Rastogi, C. O'Donnell, and B. Tiwari, "Novel bioactive extraction and nano-encapsulation," *Encyclopedia*, vol. 1, no. 3, pp. 632–664, 2021.

[72] A. Husen, "Chapter 1 - Introduction and techniques in nanomaterials formulation," in *Nanomaterials for Agriculture and Forestry Applications*, A. Husen and M. Jawaid, Eds., pp. 1–14, Elsevier, 2020.

[73] E. Abdelillah Ali Elhussein, S. Şahin, and Ş. S. Bayazit, "Preparation of CeO_2 nanofibers derived from Ce-BTC metal-organic frameworks and its application on pesticide adsorption," *Journal of Molecular Liquids*, vol. 255, pp. 10–17, 2018.

[74] L. Sharma and R. Kakkar, "Magnetically retrievable one-pot fabrication of mesoporous magnesium ferrite ($MgFe_2O_4$) for the remediation of chlorpyrifos and real pesticide wastewater," *Journal of Environmental Chemical Engineering*, vol. 6, no. 6, pp. 6891–6903, 2018.

[75] G. A. Grant, P. R. Fisher, J. E. Barrett, and P. C. Wilson, "Removal of paclobutrazol from irrigation water using granular-activated carbon," *Irrigation Science*, vol. 36, no. 3, pp. 159–166, 2018.

[76] A. Hgeig, M. Novakovic, and I. Mihajlovic, "Sorption of carbendazim and linuron from aqueous solutions with activated carbon produced from spent coffee grounds: equilibrium, kinetic and thermodynamic approach," *Journal of Environmental Science and Health, Part B*, vol. 54, no. 4, pp. 226–236, 2019.

[77] G. A. Grant, P. R. Fisher, J. E. Barrett, and P. C. Wilson, "Removal of agrichemicals from water using granular activated carbon filtration," *Water, Air, & Soil Pollution*, vol. 230, no. 1, p. 7, 2019.

[78] M. J. Amiri, R. Roohi, M. Arshadi, and A. Abbaspourrad, "2,4-D adsorption from agricultural subsurface drainage by canola stalk-derived activated carbon: insight into the adsorption kinetics models under batch and column conditions," *Environmental Science and Pollution Research*, vol. 27, no. 14, pp. 16983–16997, 2020.

[79] K. S. Ahmad, "Adsorption evaluation of herbicide iodosulfuron followed by *cedrus deodora* sawdust-derived activated carbon removal," *Soil and Sediment Contamination: An International Journal*, vol. 28, no. 1, pp. 65–80, 2019.

[80] T. Wang, Z. Zhang, H. Zhang et al., "Sorption of carbendazim on activated carbons derived from rape straw and its mechanism," *RSC Advances*, vol. 9, no. 71, pp. 41745–41754, 2019.

[81] A. Spaltro, M. Pila, S. Simonetti et al., "Adsorption and removal of phenoxy acetic herbicides from water by using commercial activated carbons: experimental and computational studies," *Journal of Contaminant Hydrology*, vol. 218, pp. 84–93, 2018.

[82] T. Lazarevic-Pasti, V. Anicijevic, M. Baljozovic et al., "The impact of the structure of graphene-based materials on the removal of organophosphorus pesticides from water," *Environmental Science. Nano*, vol. 5, no. 6, pp. 1482–1494, 2018.

[83] S. K. Deokar, G. S. Bajad, P. Bhonde, R. P. Vijayakumar, and S. A. Mandavgane, "Adsorptive removal of diuron herbicide on carbon nanotubes synthesized from plastic waste," *Journal of Polymers and the Environment*, vol. 25, no. 2, pp. 165–175, 2017.

[84] N. H. Al-Shaalan, I. Ali, Z. A. ALOthman, L. H. Al-Wahaibi, and H. Alabdulmonem, "High performance removal and simulation studies of diuron pesticide in water on MWCNTs," *Journal of Molecular Liquids*, vol. 289, article 111039, 2019.

[85] A. Massoud, A. Derbalah, I. El-Mehasseb et al., "Photocatalytic detoxification of some insecticides in aqueous media using TiO_2 nanocatalyst," *International journal of environmental research and public health*, vol. 18, no. 17, p. 9278, 2021.

[86] M. Kah, R. S. Kookana, A. Gogos, and T. D. Bucheli, "A critical evaluation of nanopesticides and nanofertilizers against their conventional analogues," *Nature Nanotechnology*, vol. 13, no. 8, pp. 677–684, 2018.

[87] P. C. Balaure, D. Gudovan, and I. Gudovan, "Nanopesticides: a new paradigm in crop protection," in *New Pesticides and Soil Sensors*, pp. 129–192, Academic Press, 2017.

[88] C. G. Athanassiou, N. G. Kavallieratos, G. Benelli, D. Losic, P. U. Rani, and N. Desneux, "Nanoparticles for pest control: current status and future perspectives," *Journal of Pest Science*, vol. 91, no. 1, pp. 1–15, 2018.

[89] G. L. Vanti, V. B. Nargund, R. Vanarchi et al., "Synthesis of *Gossypium hirsutum*-derived silver nanoparticles and their antibacterial efficacy against plant pathogens," *Applied Organometallic Chemistry*, vol. 33, no. 1, article e4630, 2019.

[90] V. T. Le, L. G. Bach, T. T. Pham et al., "Synthesis and antifungal activity of chitosan-silver nanocomposite synergize fungicide against *Phytophthora capsici*," *Journal of Macromolecular Science, Part A*, vol. 56, no. 6, pp. 522–528, 2019.

[91] C. Pelosi, S. Barot, Y. Capowiez, M. Hedde, and F. Vandenbulcke, "Pesticides and earthworms. A review," *Agronomy for Sustainable Development*, vol. 34, no. 1, pp. 199–228, 2014.